SUPERCRITIAL FLUID EXTRACTION - SUPERCRITICAL FLUID CHROMATOGRAPHY - MASS SPECTROMETRY (SFE-SFC-MS) METHOD DEVELOPMENT FOR ONLINE EXTRACTION OF COMPLEX BIOLOGICAL AND ENVIRONMENTAL MATRICES

by

BLAIR KRISTEN BERGER

DISSERTATION

Submitted in partial fulfillment of the requirements
for the degree of Doctor of Philosophy at
The University of Texas at Arlington
August, 2021

Arlington, Texas

Supervising Committee:

Kevin A. Schug, Supervising Professor
Daniel W. Armstrong
He Dong
Saiful M. Chowdhury

ACKNOWLEDGEMENTS

This work was supported by a research support agreement with Shimadzu Scientific Instruments, Inc. And would like to thank the Shimadzu service and applications chemists for their ongoing support of the instrument during the duration of this work. I would like to express my appreciation to my Supervising Committee, Dr. Daniel Armstrong, Dr. He Dong, and Dr. Saiful Chowdhury, thank you for your willingness to serve on my committee and your , your time, patience, and thoughtful feed-back.

I would like to extend my deepest gratitude to my Supervising Professor, Dr. Kevin Schug for all of his guidance, advice, and unrelenting support. Thank you for always being there, no matter how big or small, and your trust in me. Thank you for taking the time to meet me in Brussels, giving me the opportunity to be a part of your lab and welcoming me into your research family that is Schug Group.

My sincere appreciation to Dr. Paige Wicker for her invaluable insights and guidance, her continual encouragement and support, but most importantly for your friendship.

SFC Crew. I would also like to thank the rest of the SFC research team for their collaborative effort during sample collection and data collection. Especially the hard work of Emily Preuss, for all of her long hours of dedicated involvement in the development of the micro-blood sampling technique and all other matters that in a large part allowed this work to come to light. Ayat Omar for her many hours of cryomilling, Brady Drennan and Alex Kaplitz, for always being available to help. Thank you all for your many hours of hard work. Rob Magnuson for being available to lend a helping hand when needed the most. Tiffany Liden, Jaime York and Haillee Anderson for words of advice and encouragement, as well as all other members of Schug Group, .

Rick Wickfors and Kimber Fogelman for their seemingly endless patience and willingness to explain not just how or what, but why, thank you for your mentorship during the time at Aurora, your encouragement during and in the years past, and for your intellectual contribution to my development as a scientist.

DEDICATION

To my Father, Terry Berger.

Who taught me to love to wonder what things are made of,

How do you cite a lifetime of tutorials on viewing the world thru a scientific eye and to love every minute of it.

Thank you for being my teacher, my mentor, my professor, and most of all my Papa Dukes.

To both my parents, Leslie and Terry, for their unwavering support through all my endeavors.

your endless love, encouragement and dedicated partnership for success in my life.

To my husband, Jasper, who has been a constant

source of support and encouragement during the challenges of life.

Jij bent mijn steen.

TABLE OF CONTENTS

ABSTRACT

Supercritical Fluid Extraction – Supercritical Fluid Chromatography – Mass Spectrometry (SFE-SFC-MS) Method Development for Online Extraction of Complex Biological and Environmental Matrices

Blair Kristen Berger, Ph.D.

The University of Texas at Arlington, 2021

Supervising Professor: Kevin A. Schug

A systematic approach to the rapid development of hyphenated online methods for supercritical fluid extraction-supercritical fluid chromatography-mass spectrometry (SFE-SFC-MS) was established for the analysis of complex biological and environmental samples with limited sample sizes. Extensive sample preparation and cleanup is incompatible with small sample sizes. Hyphenated online extractions offer major advantages desirable where sample quantity is limited. By minimizing sample preparation and handling, online extractions provide higher throughput, and minimizes the opportunity for sample contamination or loss. However, hyphenated methods have been difficult to develop since each step has its own requirements, which has slowed penetration into many areas which it should be ideally suited. Recent instrument advances provide new opportunity in online extraction with hyphenated SFE-SFC-MS. The first step involved synergistically optimizing MS-detection, SFC-separation, and SFE-extraction. Reference materials and quality controls (QCs) were developed using two separate complex matrices: A micro-dried blood spot (DBS) coring technique for antidoping analysis, and microplastics (μPs) reference materials from cryomilled plastic pellets, for environmental pollutants polycyclic

aromatic hydrocarbons (PAHs). A micro-DBS coring technique was established for the for anti-doping analysis was established for direct applicability to with application to androgenic anabolic steroids (AAS) to reflect method validity for evaluation of real/field samples, For DBS: methods were optimized in a stepwise process for the separation and extraction of androgenic anabolic steroids (AAS) were applied to micro-DBS made with human and bovine blood and final method optimizations were performed with focus for Anti-doping analysis. µP Field samples: Pre-optimized methods for the online extraction and separation of environmentally persistent organic pollutants (ePOPs) were applied to marine-exposed µPs and final method optimizations were performed with focus for the targeted analysis of PAHs. The goal was to contribute alternative solutions for blood-based anti-doping testing to current techniques and broaden the accessibility of online SFE-SFC to the scientific community.

CHAPTER 1

HYPHENATED INSTRUMENTATION (SFE-SFC-MS) THEORY OF OPERATION

CHAPTER 1

HYPHENATED INSTRUMENTATION (SFE-SFC-MS)

THEORY OF OPERATION

1.1. Supercritical Fluid Chromatography (SFC)

1.1.1. What is SFC?

Supercritical fluid chromatography (SFC) is a separation technique similar to high performance liquid chromatography (HPLC), but uses dense carbon dioxide (CO_2), to replace the majority of the mobile phase.[1] SFC is usually a normal phase technique where the stationary phase is more polar than the mobile phase. Pure CO_2 is non-polar, with a solvent strength much like hexane. Therefore, polar organic solvents (most commonly an alcohol, like methanol [MeOH]) are used as cosolvents to modify the polarity of the mobile phase. SFC also uses packed columns similar to those used in HPLC. In SFC, progressively more polar solutes require progressively more polar mobile phases and stationary phases.

Mobile Phase (MP). Carbon dioxide is almost universally the main MP component in SFC, but it is an effective solvent only at relatively high densities, and only for relatively non-polar solutes. In modern SFC, 100% CO_2 is almost never used. The addition of cosolvents allows a wide range of MP polarities.[2] The most commonly used cosolvent is MeOH, which is the most polar common solvent completely miscible with CO_2. Other common cosolvents include ethanol (EtOH), isopropyl alcohol (IPA), and acetonitrile (ACN), plus others (**Figure 1; top blue bars, *MP***). More polar additives are often needed to improve peak shapes (normally a base for basic solutes and an acid for acidic solutes). Additives, such as formic acid (FA), triethylamine (TEA), ammonium formate (AmFo), and many others, are added to the cosolvent (< 0.1% typically). Cosolvents and additives are LC grade.

Stationary Phase (SP). Traditional SFC phases include: octadecylsilane (C18), cyano (CN), silica (Sil), amino (NH_2), diol, and ethylpyridine (EP) (**Figure 1; bottom orange bars, *SP***). In recent years, a plethora of new phases

have been developed specifically for SFC, and in the pharmaceutical industry, where most compounds are basic, the ethylpyridine phase is probably the most commonly used.

SFC uses much of the same hardware and software as HPLC, with a few important additions to maintain a single phase through the system. The CO_2 is typically supplied as a gas in equilibrium with a liquid at cylinder pressure of 5 MPa (~50 bar). A chiller is required to liquefy the CO_2 to permit pumping. The pumps use higher compressibility compensation compared to HPLC. The second SFC-specific instrument component is a back-pressure regulator (BPR), which precisely controls the (post-column) outlet pressure of the system. SFC uses the same detectors as HPLC, being compatible with UV, MS and ELSD detectors.

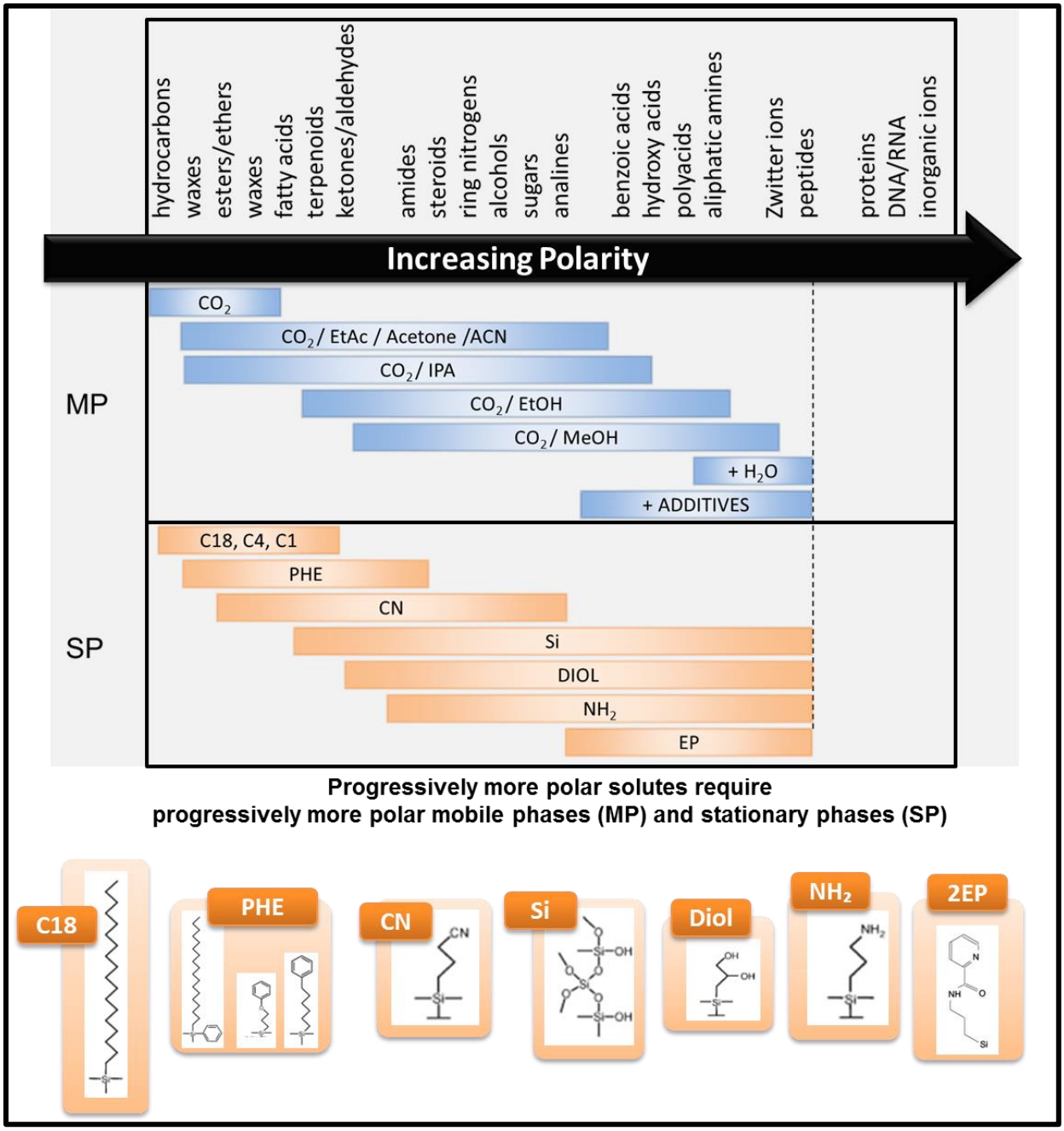

Figure 1. Mobile Phases ([MP], top blue bars) and Stationary Phases ([SP], bottom orange bars) Traditionally Used in SFC; showing range of polarity from left to right (black arrow) and comparing to applicable analyte classes successfully demonstrated in SFC separations (classes shown above arrow). **Mobile Phases (MP, top to bottom) include:** [CO_2] carbon dioxide alone, [CO_2/EtAc/ACE/ACN] CO_2 modified with EtAc (ethylacetate), ACE (acetone) or ACN (acetonitrile); [CO_2/IPA] CO_2 modified with IPA (isopropyl alcohol); [CO_2/EtOH] CO_2 modified with EtOH (ethanol); [CO_2/MeOH] CO_2 modified with MeOH (methanol); [+H_2O] CO_2 modified with less than 10% H_2O (water); and [+ADDITIVES] CO_2 modified with any of the above MP combinations with additive (such as an acid or a base). **Stationary phases ([SP], bottom orange bars), include (top-to-bottom):** [C18, C4, C1] Octyl-decyl silica with carbon chain lengths of 18, 4 and 1; [PHE] phenyl-type; [CN] cyano-type; [Si] bare silica; [DIOL] diol-type; [NH_2] amino-type; and [EP] ethyl pyridine-type, functional groups. *Left panel showing structures for traditional phases.* ***Figure adapted from Berger 1995 and 2015.***[1],[3]

1.1.2. SFC and Phase Diagrams.

A phase diagram showing typical operating ranges of common chromatographic techniques is shown in **Figure 2.** Highlighted in green is the region in which SFC tends to operate. Anywhere CO_2 can exist as a dense solvent, without the necessity for super high pressures and/or super low temperatures is the most commonly used region for SFC. Anywhere below 70 °C will only require modest pressure (> 10 MPa [100 bar]) to achieve this. Therefore, defined states (i.e., 'super-critical' versus 'sub'-critical) do not exclusively define the most common operating range of SFC.

The majority of SFCs operating range lies outside the definition of 'supercritical fluid' and instead in the defined 'liquid region' of CO_2 phase diagrams (often called "subcritical"). For modern SFC, phase diagrams are only useful to show why the name 'Supercritical fluid chromatography' was a poor name for the technique. Sadly, the use of phase diagrams with the emphasis on the defined 'super' versus 'sub'-critical has led to misconceptions and caused ongoing confusion (especially for new users of the technique). Many attempts at changing the name over the years, have unfortunately just added to the confusion.

Therefore, it has been suggested that the most appropriate definition of SFC as: all the situations where a gas (almost exclusively CO_2) is used as a dense solvent as part of a chromatographic mobile phase. Without emphasis on the definition of 'sub' or 'super-critical', as this implies there is a distinct difference between the two. In reality, the changes in density and viscosity are near-linear across these 'definition' boundaries, and there is no sudden change in retention, efficiency or linear velocity regardless of the 'super'/'sub'-critical nature of the fluid (this debate was laid to rest in the late 1980's). This means SFC (in its most commonly used form) could be considered a form of LC, but provides characteristics of interest that are intrinsic to using a gas. Since a gas, even as a dense fluid, inherently retains many of the properties of a gas (e.g., lower viscosity and higher diffusion coefficients) when compared to normal liquids. This leads to practical advantages in SFC over LC; using 3-5 times higher flow rates than LC without loss in efficiency or resolution, and having much lower pressure drops (~1/3 to 1/5th that of LC) allowing the use of smaller particles and or longer columns without ultra-high pressures.[3]

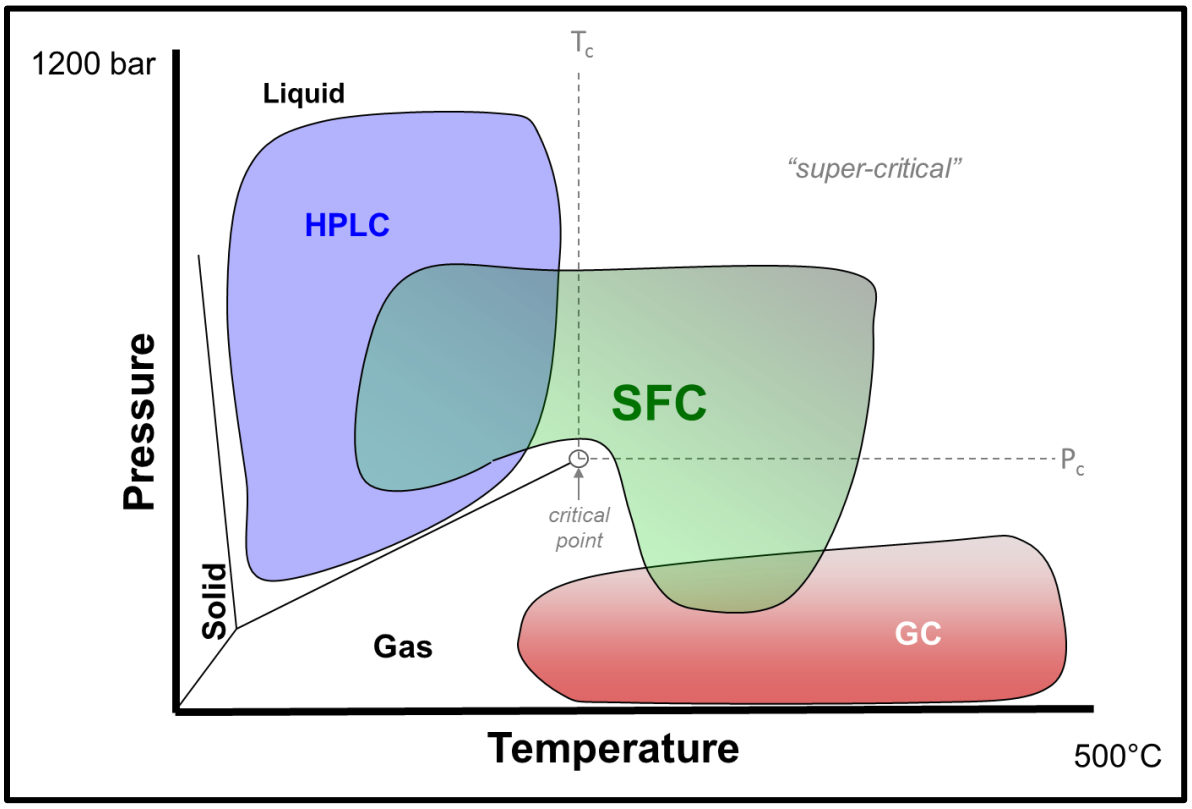

Figure 2. Phase Diagram showing Typical Operating Ranges of Common Chromatographic Techniques: Supercritical Fluid Chromatography (SFC, green) versus High Performance Liquid Chromatography (HPLC, blue) and Gas Chromatography (GC, red). **Solid black lines** indicate **phase boundaries** between physical states of matter (solid, liquid, and gas physical states). Phase boundaries are equilibrium lines, where two phases exist in equilibrium. Crossing one of these lines is accompanied by a dramatic change between states, and directly on the solid line two phases exist at once, but away from these lines only one phase exists. Note that the operating range of all three chromatography techniques avoid crossing the solid phase boundaries lines, as phase transitions during operation would have dramatic negative impacts on performance. The **critical point** defined by the **critical pressure (Pc)** and **critical temperature (Tc**) above which only one phase can exist (i.e., the end of the equilibrium line). Alternatively the **dotted gray lines** extending out from the critical point, indicate **ambiguous 'definition boundaries'** of the "super-critical" region. Definition boundaries (gray dotted lines) are NOT phase boundaries and crossing them has no dramatic effect on physical state and no phase transition. Crossing the Pc dotted line ($< P_c$) the definition of the fluid changes from 'supercritical fluid' to a 'gas' and crossing the Tc dotted line ($< T_c$) the definition of the fluid changes from 'supercritical fluid' to a 'liquid'. SFC takes advantage of the critical point (i.e., wrapping around) stretching across all three ranges. ***(Figure adapted from lecture given by visiting scientist Dr. Terry A Berger, at University of Texas at Arlington in 2020).***[9]

1.1.3. Benefits of SFC (why use it?).

Although SFC is similar to HPLC, there are some practical benefits of SFC that make it a highly competitive technique to HPLC and these benefits ultimately make SFC an important member of the analytical chemists toolbox. CO_2 is a gas at room temperature and atmospheric pressure, due to the inherently weak intermolecular interactions between CO_2 molecules. Compressing CO_2 molecules together results in a dense fluid. Even though at higher density, where CO_2 acts as a solvent, the intermolecular forces are still weak. Therefore, CO_2, even as a dense fluid, retains higher solute diffusion coefficients and lower viscosity when compared to normal liquids.

Higher diffusion coefficients - lower viscosity. In chromatography, the separation speed is dictated by the diffusion coefficient of the solutes in the mobile phase, and the distances the solute molecules must diffuse in the mobile phase. Diffusion coefficients are inversely proportional to the viscosity of the fluid in which the fluid diffuses. Pure CO_2 has viscosity ≈ $1/20^{th}$ the viscosity of water, but it is non-polar. To elute and separate polar solutes polar organic solvents (i.e., normal liquids) are mixed with the CO_2. Their inherently higher viscosity slows the chromatography when mixed with CO_2. Even at the highest typical modifier concentration (≈ 40%), SFC is still considered 3 to 5 times faster than HPLC on the same sized column. The pressure drop in modern packed columns further degrades mobile phase viscosity and speed, but pressure drops remain $1/3^{rd}$ to $1/5^{th}$ those in HPLC.

SFC is Orthogonal to reversed phase HPLC. Orthogonality of SFC to standard methods makes SFC an indispensable tool in the analytical lab. Orthogonality means the elution order is not expected to be the same, nor is it expected to be opposite; it is expected to be different. This means that using SFC in combination with other separation techniques can allow for resolution capabilities not possible with other techniques alone. This is especially beneficial in applications such as trace contaminants, discovery and/or purification.

SFC is Green. SFC uses dramatically lower amounts of organic solvents (between 2 – 50% modifier), compared to HPLC. Less solvent results in much lower organic waste generation. Furthermore, the CO_2 utilized in SFC (making up the remaining 50 - 98% of the MP) is recycled from other industrial processes. This results in much lower generation of toxic wastes and lower operating costs for SFC.

SFC has been shown to be superior in many isomeric separations.[4] Over the past 15 years, SFC has become a validated technique that in many cases overcomes the limitations and surpasses the capabilities of gas chromatography (GC) and HPLC.[5]

1.1.4. Analyte classes separated by SFC.

Any solute soluble in MeOH (or less polar organic solvent) will elute using CO_2-based MPs. Although small peptides (up to 40mer) can be separated, solutes requiring an aqueous, buffered environment (i.e., large biomolecules, like proteins) will not elute and are not a good match for SFC.[1] SFC is especially ideal for isomers. In the pharma industry, where more than 80% of all small drug-like molecules are pure enantiomers, SFC has largely replaced HPLC for chiral and other isomeric separations based on differences in structure only.[4]

As a general rule, solutes with a mass up to 25,000 Da can be separated with CO_2 based fluids. Applicable analyte classes successfully demonstrated in SFC separations are shown at the top of **Figure 1.** Generally, SFC is ideal for relatively non-polar molecule too large for GC to quite polar small drug-like molecules, and has been demonstrated on an applicable range of compounds that represents over 80% of these types of molecules. Being successfully applied to compounds with LogP between -1 and 7 (**Figure 3**), SFCs range coincides with the majority of commercially produced drugs.

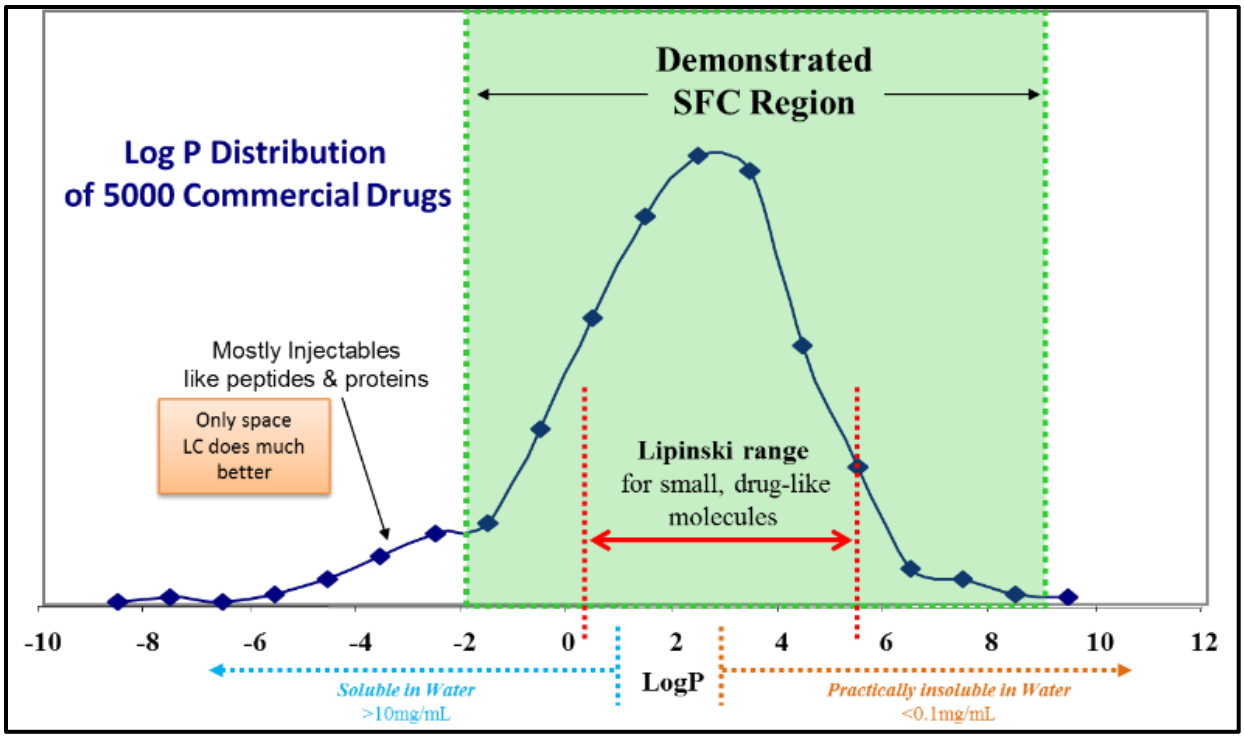

Figure 3. Demonstrated SFC Region Overlaid over LogP distribution of 5,000 Commercially available Drugs (plotted by log of the partition coefficient between octanol and water [LogP; Blue]). Showing the demonstrated SFC range [green] and the Lipinski range for small, drug-like molecules [Red]. Figure adapted from Berger (2015).[1]

1.1.5. Who uses SFC?

Primarily industries use SFC. It is especially popular among the pharmaceutical industry. Pfizer, Merck , Lilly , GSK, & Sanofi, all use SFC as the primary method for chiral analysis, and is also important for purification.[6],[7],[8] Although rapidly changing, not many schools teach SFC, especially not in practical training (as in instrument use). SFC can be found in the analytical labs of some professors in the US and especially in Europe.

1.1.6. Retention Controls in SFC.

Modifier concentration is the primary control variable for controlling retention, just as in LC, but SFC has the added benefit of additional controls over retention and selectivity in secondary instrument parameters (e.g., column temperature and system outlet pressure). Flow rate is also a secondary control variable through its effect on average pressure in the column. Each variable has a different typical effects on retention and selectivity.

Primary Control variables.

Modifier concentration is the most powerful tool in changing retention. Solvent strength is very non-linear. The first 1% methanol has an effect as much as one would expect with 10% on retention. The addition of modifier shortens retention As a rule of thumb, doubling modifier concentration halves retention.

Flow Rate. The efficiency vs. flow rate curves (vanDeemter or Knox plots) appear to be are very flat in SFC compared to HPLC. Generally, flow rate is used to simply speed up separations trading modest efficiency for speed, or alternatively, since SFC is 3-4 times faster than LC, some of this extra speed can be traded for a boost in efficiency and resolution by increasing column length.

Secondary Control Variables.

Column Temperature. Temperature has little effect on overall retention and is considered a secondary control variable. However, temperature can have a large effect on selectivity, resulting in an analyte-specific effect on retention. Normally higher temperature will produce lower efficiency, this decrease in efficiency is slight within the recommended operating ranges of most instruments (max 60 °C). But higher temperatures, although not recommended, can be used (e.g., 70 °C), but then one should watch for any degradation in peak shapes. The most useful aspect of column temperatures involves modest changes in temperature that can at times have large effect on selectivity (with little effect on retention) and can be used as a powerful tool to improve an SFC separation during method development.

System Outlet Pressure. Outlet pressure is considered a secondary control variable, as it has little effect on retention, resolution, and/or selectivity. Although there are some analytes where changes in outlet pressure can effect selectivity, this is much less common than with column temperature. This is most apparent at low modifier concentration. Thus, outlet pressure is mostly regarded as a secondary control variable and will normally be expected to produce flat horizontal graphs when retention time is plotted versus pressure.

Identifying changes in Selectivity in Retention Plots. This effect can be shown by plotting retention time (for a group of analytes) versus a range of settings for a specific secondary parameter. Nearly flat graphs indicate little change in retention. But any relative change in slope of the plot (between different analytes), indicates a compound-specific change in retention (i.e., a change in selectivity). For example, on the bottom of **Figure 4**, are graphs plotting retention of three groups of analytes using a range of outlet pressures (between 100 – 200 bar [10 – 20 MPa]) showing the typical effect of change in outlet pressure on retention. The graphs are nearly flat (indicating little change in retention) and parallel (indicating no relative change in retention, or selectivity), these types of graphs are commonly produced by changes in outlet pressure. Alternatively, on the top of **Figure 4**, are graphs plotting retention using different column temperatures (ranging between 30 and 60 °C). Note the nearly flat (i.e., little change in retention), non-parallel graphs, indicating a compound specific effect on retention (i.e., change in selectivity). Changes in column temperature will commonly produce these types of graphs, which can be

used to identify useful ranges to improve an SFC separation and to increase resolution of co-eluting analytes and/or at times decrease runtimes.

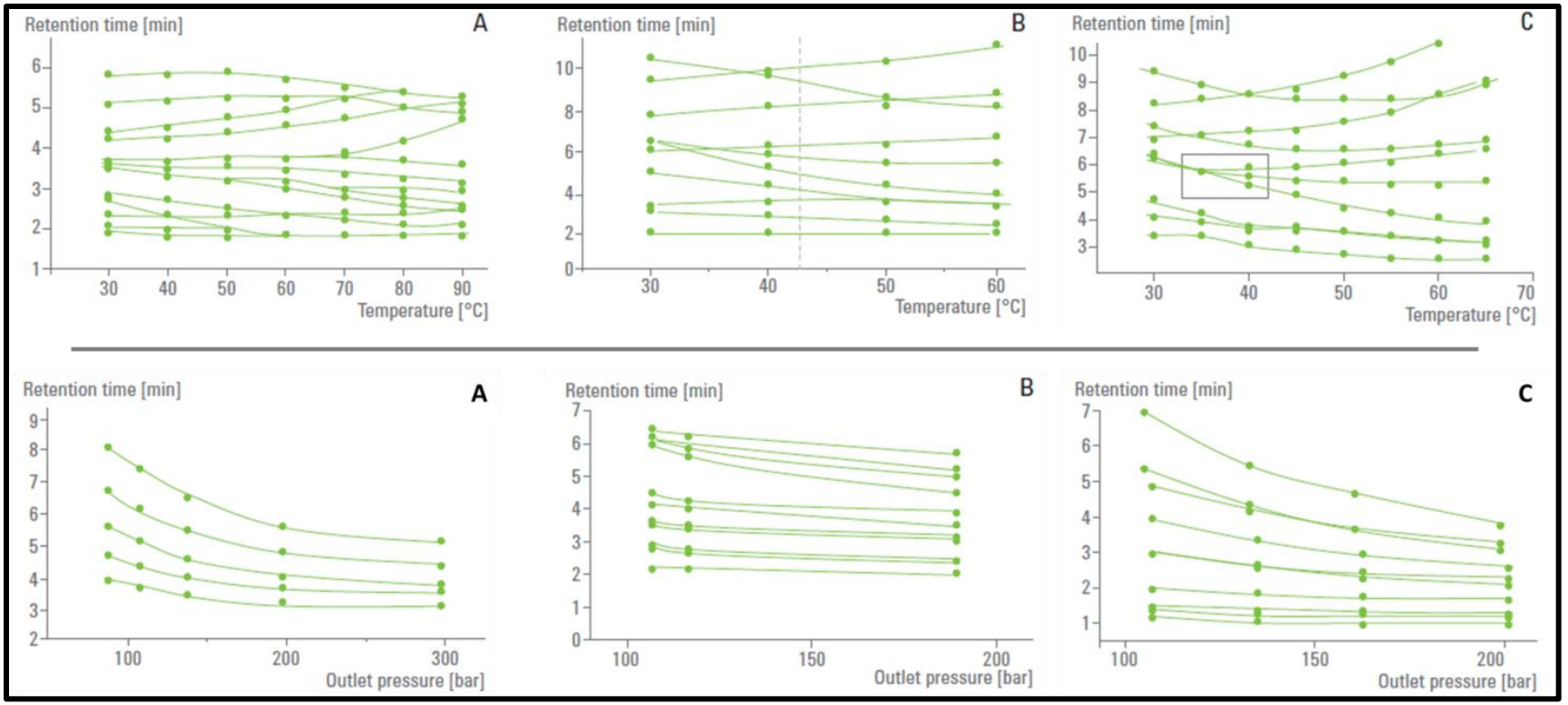

Figure 4. Retention Time Graphs for Secondary Parameters; showing effect of [top] Column Temperature and [bottom] Outlet Pressure on retention for groups of [A] Stimulants; [B] Antidepressants; [C] Antipsycotics *(top)*/Herbicides *(bottom)*. *(Figure adapted from Berger 2015).*[1]

1.2. Mass Spectrometry (MS) Detection.

A triple quadrupole mass spectrometer was used in MRM-mode for Detection. The basic parts of an MS that are important for detection are the Source, Analyzer, and Detector (**Figure 5**).

- ***Inlet*** (**Figure 5; left, pink**): connects the outlet of the chromatographic system to the MS source. SFC or SFE-SFC effluent is delivered to the MS, post-column.
- ***Source*** (**Figure 5; left orange**)**:** In the MS source, the solvent is removed, and the analyte is ionized, resulting in charged gas phase ions. Two different sources were used: for steroids the source was electrospray ionization (ESI) and for pollutants atmospheric pressure chemical ionization (APCI).
- ***Analyzer*** (**Figure 5; left green**)**:** The MS analyzer is responsible for the sorting of Ions for Detection and uses an electric and/or magnetic field to separate and sort ions. The analyzer used in this work was always a triple-quadrupole mass analyzer.
- ***Detector*** (**Figure 5; left blue**): Ions are measured via the ion current, which is recorded by the data system.

Basic Principle used in Multiple Reaction Monitoring (MRM). Gas phase ions are delivered in vacuum to the first stage quadrupole (Q1) from the source and the ions are sorted/selected according to their m/z [MS1]. In the second stage ions are fragmented via collision with an inert gas. The third quadrupole (Q3) is used to separate and sort the resulting fragment ions for detection according to their m/z [MS2].

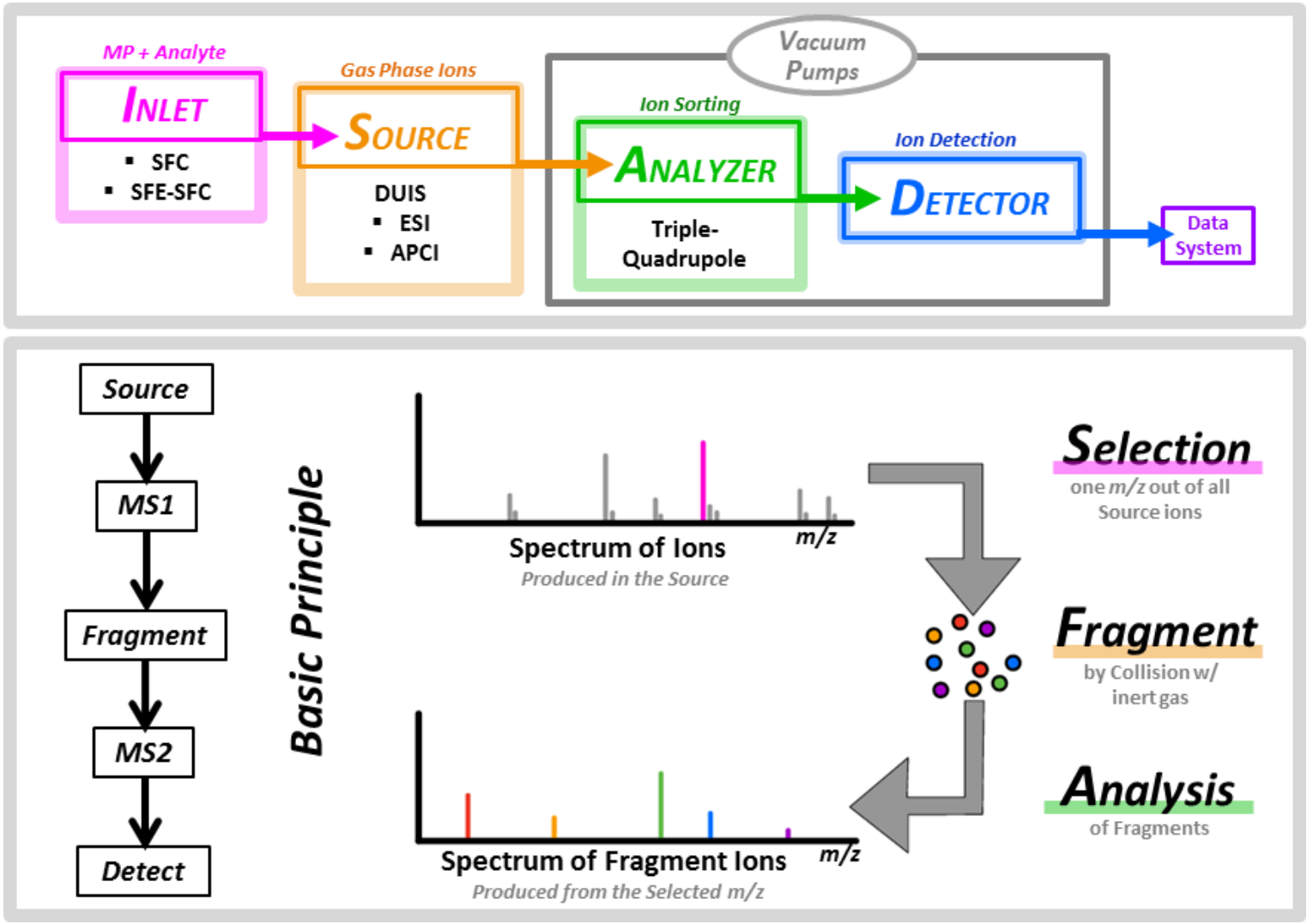

Figure 5. Basic Mass Spectrometry Principle and Ion Flow in Instrument. [Left] Basic anatomy of a Mass Spectrometer and [right] Basic Principle of Ion selection, fragmentation and Analysis used for multiple reaction monitoring. *(Figure modified from course notes from Chemistry course CHEM 5324: Lectured 2020 by Dr. Chowdhury)* [10]

1.2.1. Source: Electrospray Ionization (ESI).

Electrospray ionization (ESI) is an ambient pressure ionization technique. Complete desolvation is necessary before the vacuum to the MS. In positive ionization mode, ESI utilizes an intense electric filed between two electrodes: the spray needle (**Figure 6; Top, red**) acts as the positive [+] electrode and the spray shield (**Figure 6; bottom, yellow**) acts as the counter (negative [-]) electrode. The sample is introduced thru the spray needle and an aerosol is generated. Negative ions are stripped and positive ions are enriched at the positively charged needle tip. The electrospray process generally involves: [A] droplet formation; [B] droplet shrinkage (evaporation); and [C] desolvation (desorption of gaseous ions).

Aerosol Generation (droplet formation). Sample is introduced via the spray needle (pneumatic nebulizer). At the needle tip, the spray creates droplets mainly via two forces - the strong shear forces produced by a sheath gas (**Figure 6; blue**) and the strong electrostatic field formed by the high voltage potential applied between the needle tip and the spray shield (**Figure 6; orange**). The needle tip acts as the positive (+) electrode and the spray shield as the counter, negative (-) electrode. Positive ions accumulate at the positively charged needle tip (**Figure 6; pink**). When the applied energy is just greater than zero the solvent begins to bulge, forming a cone at the tip of the needle. As the energy increases the solvent begins to stretch (Taylor cone), and once the onset energy is exceeded, a plume/mist of highly charged droplets is generated.

Evaporation (droplet shrinkage). Evaporation leads to droplet shrinkage, building charge density on the droplet surface. As the Rayleigh limit is reached, Coulombic repulsions promote further droplet breakup (fission), creating smaller and smaller droplets.

Desolvation. Coulombic repulsions create smaller and smaller charged droplets. Once the charge density reaches ~10 V/cm, ion evaporation (i.e., desolvation) occurs and droplet desorption to the gas phase produces sample ions. The desolvation process is dependent on the applied potential voltage (potential energy), the capillary size/diameter, the flowrate and on solvent characteristics.

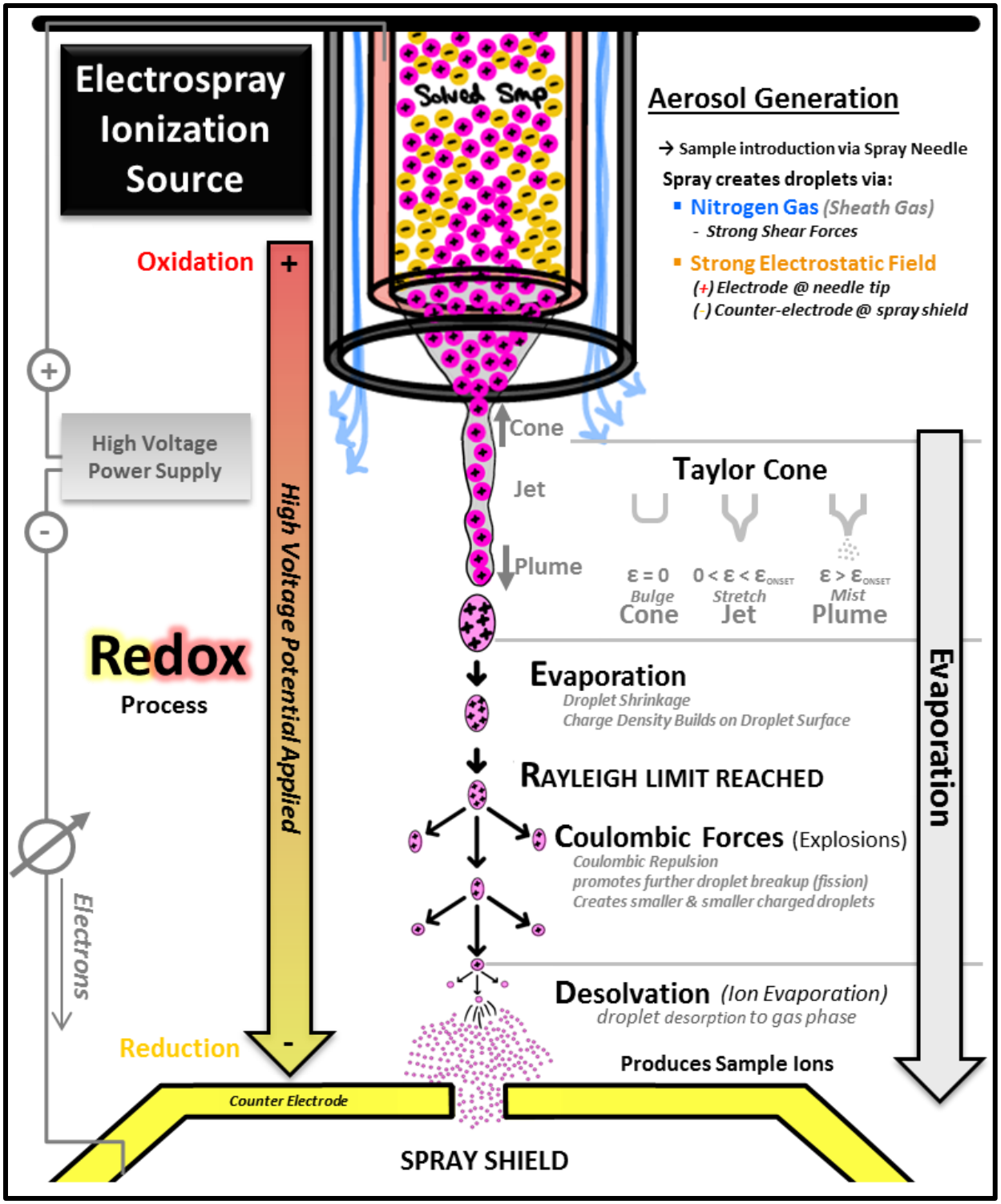

Figure 6. **Electrospray Ionization (ESI) Source showing spray generation of Spray, Desolvation and production of Gas Phase Sample Ions.** *(Figure modified from course notes from Chemistry course CHEM 5324: Lectured 2020 by Dr. Chowdhury)*[11]

1.2.2. Source: Atmospheric Pressure Chemical Ionization (APCI) (Figure 7).

Sample is delivered to the MS inlet via SFC effluent at atmospheric pressure. Nebulizer gas facilitates the spray which is predominantly mobile phase (MP).

Corona Discharge. The spray comes in contact with the corona needle where a high electrical potential has been applied (~ 2 - 5 kV). The current flows from a high potential electrode to a neutral fluid (usually air) which ionizes the fluid (Nitrogen [N_2] and Oxygen [O_2] in the air), and creates charged gas molecules. This results in a neutral mix of electrons (e^-) and cations (+ ions; N^{2+}, H_2O^+). In other words, a region of plasma around the electrode is formed. Eventually the charged gas molecules (cations and electrons), pass charge to nearby areas of lower potential, via charge transfer to the MP (methanol [CH_3OH]), resulting in charged mobile phase clusters [$H^+(CH_3OH)_2$]. Finally, proton transfer from the MP charge clusters to the analyte results in analyte ions (e.g., $[M+H]^+$). These charged Ions pass thru the sampling cone to the next stages (under vacuum) for sorting and detection.

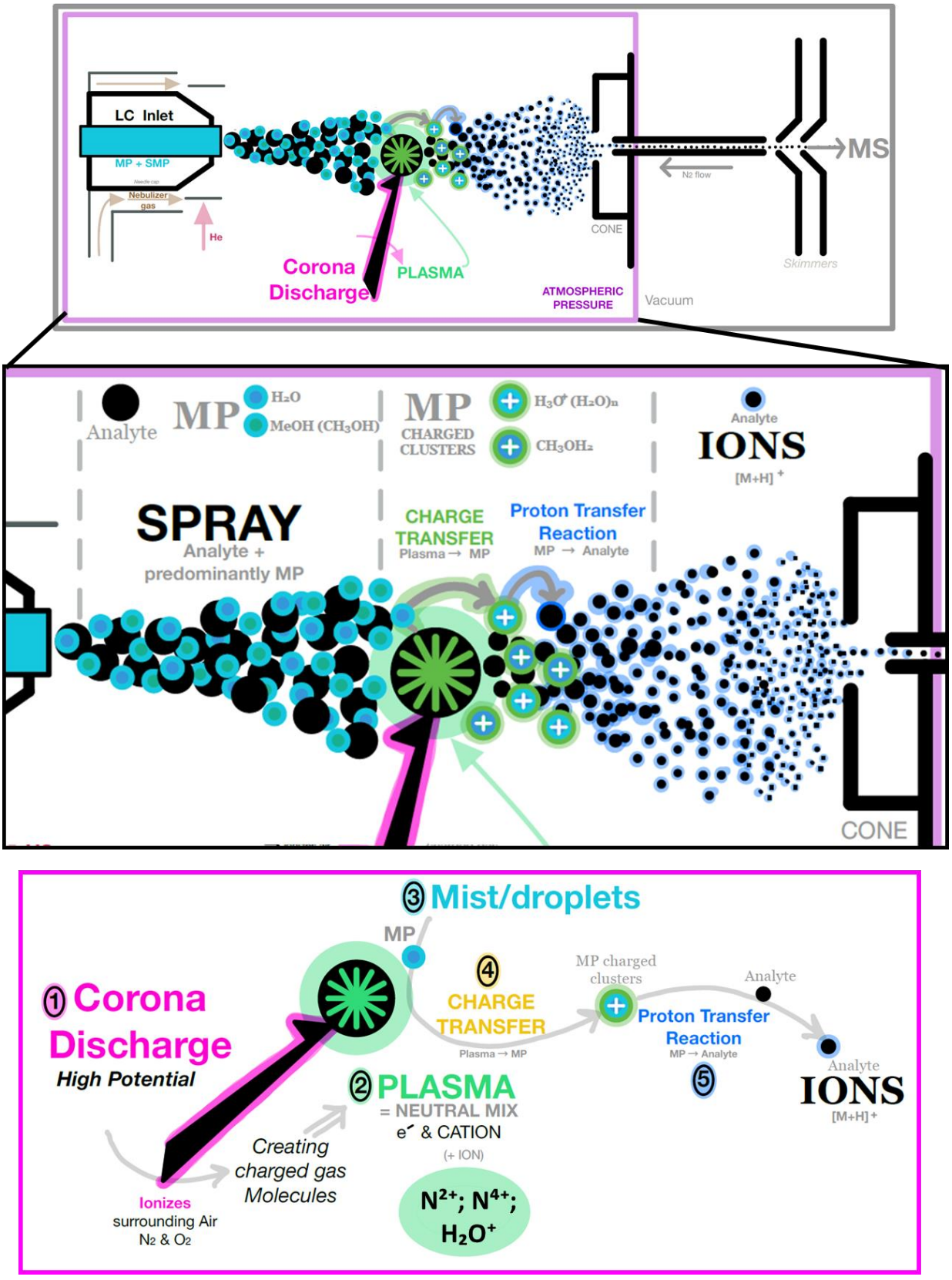

Figure 7. Atmospheric Pressure Chemical Ionization (APCI) Source: showing Corona Discharge and Ion Formation. *(Figure modified from course notes from Chemistry course CHEM 5324: Lectured 2020 by Dr. Chowdhury)*[12]

1.2.3. Quadrupole Mass Analyzer (ion sorting)

Quadrupole. A quadrupole is made up of four metal rods in a hyperbolic orientation (positioned in a perfectly parallel 'square array'). Oscillating electric fields (using DC and RF voltages) are applied to the rods and used to separate ions of particular mass to charge ratios (m/z). The stability of ion trajectories within the oscillating electric field separates ions according to m/z. A positive (+) ion that enters the space between the rods, will be drawn towards a negative (-) rod. If the potential then changes sign before the ion discharges itself by hitting the rod, the direction of the ion changes. Under a defined set of DC and RF fields; an ion with a specific m/z will pass through the rods.

Electric Fields. One pair of rods (**Figure 8; red**) receives a positive (+) and the second pair (**Figure 8; blue**) receives a negative (-) DC potential and a time dependent oscillating RF voltage is applied (180° apart). Ions are attracted or repulsed by the poles depending on charge and smaller ions move faster than larger slower moving ions. Each mass has its own stability region. A specific set of DC and RF fields result in stable (i.e., non-collisional) trajectories for a range of m/z of ions that will eventually make it through. Ions outside the range move closer and closer to the poles on an unstable (i.e., collisional) trajectory, and eventually are lost thru collision with a pole, or are drawn away by the vacuum. Only ions with stable trajectories (i.e., stable oscillation in the x- and y-directions simultaneously) make it through to the detector.

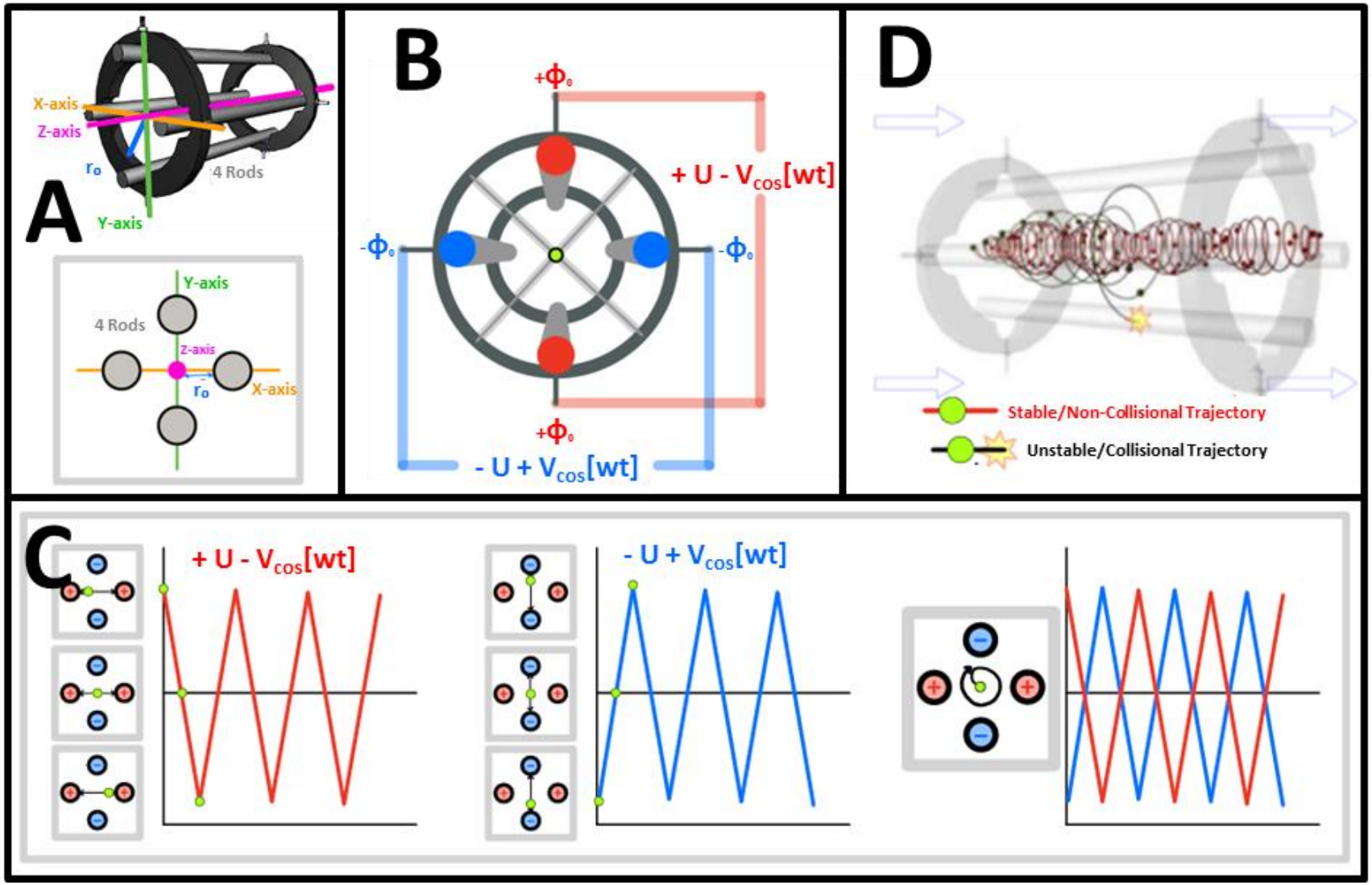

Figure 8. **Quadrupole Mass Analyzer showing basic principle of ion trajectories resulting from applied oscillating electric fields.** ***(Figure modified from course notes from Chemistry course CHEM 5324: Lectured 2020 by Dr. Chowdhury).***[13]

1.2.4. Triple-Quad: Multiple Reaction Monitoring (MRM)

Multiple reaction monitoring (MRM) refers to a type of quantitation strategy utilizing a triple quadrupole (triple-quad) mass spectrometer. A triple-quad is a tandem-MS instrument, incorporating three sequential quadrupole mass analyzers (Q1, q2, and Q3). Sample ions are sorted and a single (precursor) ion is selected, then fragmented. The resulting fragment ions are sorted again and multiple fragments (product ions) are selected for detection (**Figure 9**).

Triple Quad Setup. In the first stage (quadrupole 1 **[Q1]**) sample ions are sorted and selected according to m/z. For MRMs a single ion is selected (precursor ion) for each analyte. Only selected ions are allowed to enter the next stage (quadrupole 2 **[q2]**) to be fragmented. Fragmentation occurs via collision induced dissociation (CID), where the ions are made to collide with an inert gas. Fragments are then sorted in the third stage (quadrupole 3 **[Q3]**), and only selected fragment ions are allowed to pass thru to the detector.

Multiple reaction monitoring (MRM) provide highly selective and sensitive mass spectrometric detection. ions that make it thru to detection have been sorted twice (one specific precursor selected [Q1] → fragmented → then one specific fragment is selected as product [Q3]). One (or more) fragments can be selected for a single precursor and allows for both qualitative and quantitative analysis. Each selected fragment represents a single 'transition' (i.e., ion produced from the fragmentation of a single precursor), and therefore a single MRM-transition. A qualitative comparison can be made by overlaying each MRM-transition for all selected fragments for a single analyte and comparing peak intensities between the different ions (**Figure 9; right bottom, *Qualitative***). As different analytes may provide isomeric information related to fragmentation patterns from differences in ion ratios which can be helpful in identification. MRMs also allow for quantitative analysis, by selecting a single fragment (**Figure 9; right top, *Quantitative***), the amount of analyte present can be determined (via calibration) of the integrated peak area under the curve. Lastly, an MRM-TIC represents a sort of total ion chromatogram (MRM-TIC) which combines the signals for all fragments (all MRM-transitions) from a single precursor ion (ideally, specific to a single targeted analyte). Since an MRM-TIC normally represent a single

analyte, when overlaid with other MRM-TICs, allows an overview chromatogram of multiple analytes (this is the most commonly displayed type of chromatogram).

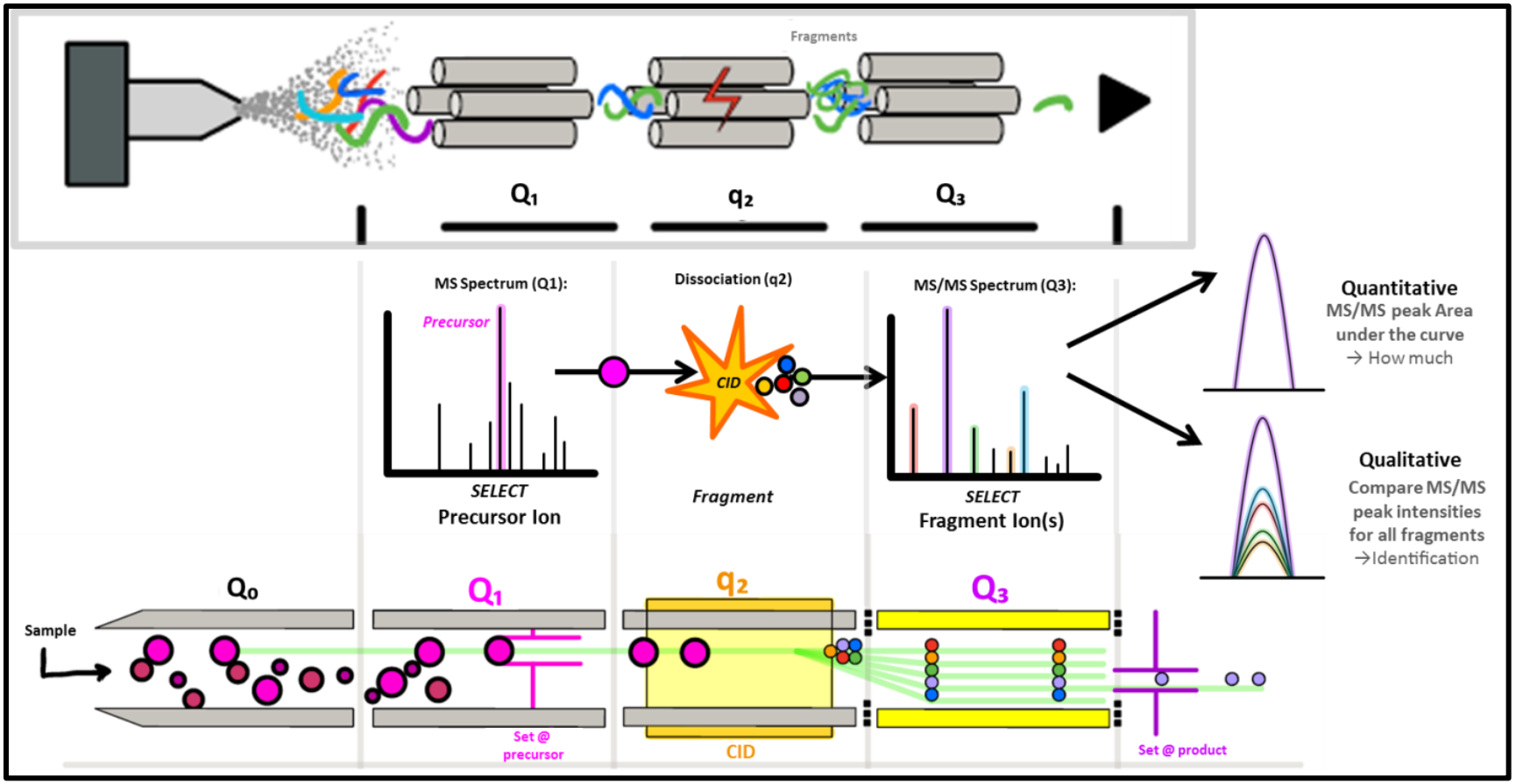

Figure 9. Triple Quadrupole Mass Spectrometer; showing Basic Three Stage Triple-Quad Setup and general concept of Multiple reaction monitoring (MRM) for Quantitative and Qualitative MS Detection. *(Figure modified from course notes from University of Texas at Arlington; Chemistry course CHEM 5324: Lecture given in 2020 by Dr. Chowdhury).*[13]

1.3. Online Extraction Methods

1.3.1. Benefits of SFE hyphenation

Supercritical fluid extraction (SFE) also uses compressed CO_2 as the main solvent. This provides a green, environmentally friendly alternative to traditional techniques by reducing the use of organic solvents. SFE is well suited for the extraction of many small drug-like molecules. Offline-SFE has been more dominantly adopted, in large-scale industrial applications, but online-SFE offers many advantages, including limited sample handling, direct analysis, and shorter prep time. Online-SFE is especially beneficial where sensitive and/or restricted quantity sample are the main focus.[14]

Online SFE/SFC applications. Analytical SFE-hyphenation has been reported as early as the late 1980's, having been coupled with HPLC, GC, and SFC. Literature in the early 2010s showed increased interest in a variety of areas.[15] Due to the availability of a new era of commercial instrumentation, the past five years has seen resurgence, with applications in biological, food, and soil samples.[16]

1.3.2. Benefits of hyphenated methods

Offline extraction requires large solvent volumes, multi-step assays, derivatizations, and other elaborate procedures that can have secondary complications that yield limitations non-conducive to small sampling sizes. Hyphenated online extractions offer major advantages desirable where sample quantity is limited or restricted. By minimizing sample handling and simplifying sample prep, online extractions provide higher throughput, enabling rapid development of relevant methodology.[14] Recent instrumental advances provide new opportunity in online extraction with hyphenated supercritical fluid extraction – supercritical fluid chromatography –mass spectrometry (SFE-SFC-MS), but continued difficulties in development of hyphenated methods slow its penetration into many arenas in which it is ideally suited to provide solutions for many difficult sample considerations.

1.3.3. The Hyphenation Hoedown (planning for hyphenated methods)

Continued difficulties in the development of hyphenated methods continue to slow penetration into fields where SFE-SFC-MS should be ideally suited to provide solutions for many difficult sample considerations. Recent advancements using multivariate optimization provide a better understanding to the synergistic relations between the hyphenated extraction and separation processes.[17] Little information is available to new users to guide method development (especially limited is info for the use of 0.2-mL extraction vessels). The availability of systematic examples of observed effects, should provide a multitude of information to help guide development of novel methods.

1.3.4. The Hyphenated Method Development Two-Step (Figure 10).

This process can be involved, since once one set of parameters are optimized, complications found during hyphenation with the next technique requires you to go back and re-optimize. This circle of re-optimizations can be time consuming, and synergistic effects between instrument parameters can make determining the source of an undesirable effect difficult. This makes the hyphenated method development process feel as if making progress one step forward, often requires two steps back (for re-optimizations).

MS-based Detection Optimization. For detection optimization, multiple reaction monitoring (MRM) transitions are used to take advantage of the increased selectivity of the MS/MS triple quadrupole mass spectrometer. MRM-optimization is performed to select precursor and product ions, voltages, and collision energies for each analyte. Resulting MRM-transitions are utilized to identify critical groups of analytes, which due to structural similarities will require chromatographic separation.

SFC-based Separation Optimization starts with stationary phase screening. Best performing columns are used to screen modifiers and evaluate the need for additives to improve peak shapes. MS re-optimizations are performed as necessary to compensate for any changes in detection due to mobile phase (MP) changes. Once an optimal column and MP composition is chosen, a final SFC-optimization is performed, where flow rate, modifier concentration, and secondary parameters are investigated for effects on retention, resolution and selectivity. A

final modifier gradient optimization and MS parameter optimization, results in a final SFC-MS method for further development (for future use in hyphenation with online extraction).

SFE-based Extraction Optimization. Next, SFE-specific parameters are screened to optimize for extraction of the target analytes; important parameters include modifier concentration and duration of the different extraction modes, as well as extraction vessel temperatures and outlet pressures during extraction. This is the first time that the sample matrix composition becomes a focus, and thus, requires the development of blank materials and controls appropriate for direct comparison to final samples. It is important to note that when coupling SFE to SFC, in the event that the chosen phase is not capable of sufficiently retaining the 'extraction plug', it would be necessary to re-start at the SFC column screening step.

Application Specific Matrix Optimizations. A preliminary matrix evaluation is performed, ideally using a model quality control, which ensures method validity for application to final real samples. The final hyphenated method is developed by performing matrix-specific optimizations. A series of extractions, using quality controls, are performed to evaluate the contribution from the sampling materials, looking for any interferences and/or analyte-matrix interactions, and re-optimizations are performed as necessary. Most commonly this would include gradient changes to move target analytes away from interfering signals, and/or MS-based optimizations to try to compensate for suppression effects due to analyte-matrix interactions. The final method is evaluated for reproducibility and extraction performance compared between spiked blank materials and spiked sample matrix.

Method Validation. The optimized hyphenated method is evaluated for linearity, precision and accuracy, stability, and robustness. Finally, the final SFE-SFC-MS method is applied to real samples. Specifically in this work, optimized methods were applied to two separate complex matrices - one for environmental-type samples and one for biological-type samples.

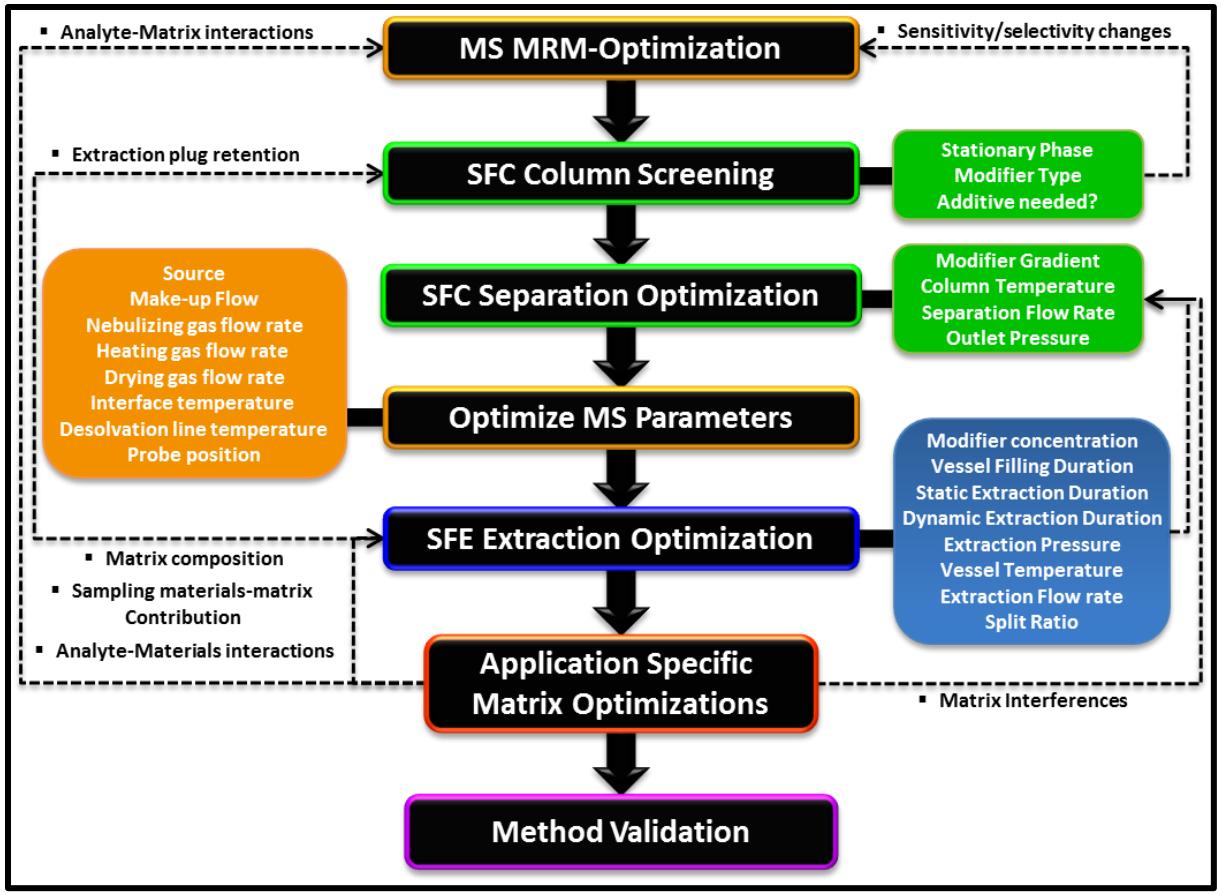

Figure 10. Online SFE-SFC-MS Method Development Flow Chart; showing important instrument parameters for each development step and showing possible re-optimization pathways that could be required, during: MS-based detection optimization [orange]; SFC-based separation optimization [green]; SFE-based Extraction optimization [blue]; application-specific matrix optimizations [red]; and Method validation [purple]. Adapted from **Wicker et. al. 2020.**[12]

1.3.5. Online SFE-SFC-MS Method Development Process (Figure 11).

Online method development in its most simple form consists of five main steps: 1. MS-detection optimization; 2. SFC-Separation optimization; 3. SFE-Extraction optimization; and 4. Matrix-Specific Optimizations.

MS-Detection Optimizations consists of three Main Sub-Sections: **1. Q3 Scans** are performed to determine optimal precursors from characteristic Ionization patterns for each compound. Optimal solutions concentrations for further MS-optimization is are also chosen in this step; **2. MRM-Optimizations.** Multiple reaction monitoring (MRM) optimizations are performed for each of the target compounds to choose optimal product ions, and associated collision energies and voltages; **3. Identification of Critical Pair Groups.** MRM-transitions and Q3 scans are used to identify critical pair groups, (i.e., compounds that cannot be separated by MS-alone).

SFC-Separation optimizations for SFE-SFC-MS analysis is the second step in method development for online methods, and can be broken down into three main steps: 1. **Column Selection**. Column screening is normally performed with a generic method for rapid comparison between phases. Comparing the resolution of critical groups to help evaluate phases, a column is chosen for further development. **2. Separation Optimization**. Best performing column is used to develop a separation method by evaluating mobile phase compositions and the effect of instrument parameters on retention, resolution and selectivity, and a final gradient optimization is performed. **3. Final method evalua**tion for reproducibility of peak areas and retention times.

SFE-Extraction Optimizations Online extractions are hyphenated with the pre-developed SFC-MS method to screen SFE extraction parameters, including: duration and modifier concentration for each extraction step, vessel temperature, extraction pressure, and flow rate during extraction.

Matrix specific optimizations with quality controls are application specific and the final method is applied to real samples.

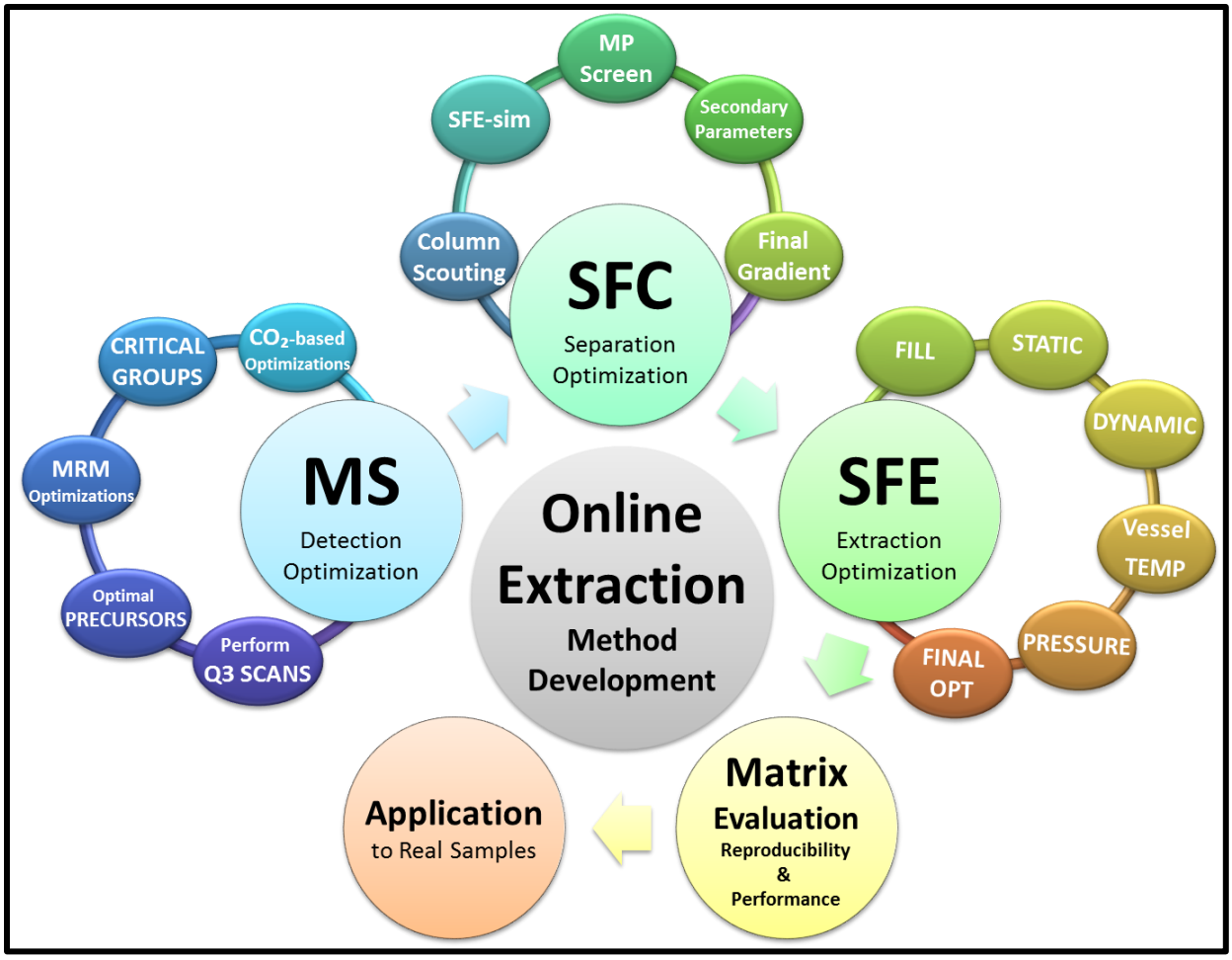

Figure 11. **Online SFE-SFC-MS Method Development Process Steps.**

1.4. Instrument Configurations

The Shimadzu Nexera UC^{TM} Online SFE-SFC-MS System (**Figure 12**) is a hyphenated instrument combining:

- The detection sensitivity of triple quadrupole mass spectrometer (triple-quad MS)
- Separation specificity of a supercritical fluid chromatograph (SFC)
- Convenience of online extraction via supercritical fluid extraction unit (SFE) with automated sampling.

The system shares a solvent delivery system (**Figure 12; Red**). Similarly to LC, two pumps are used to meter and deliver the system mobile phase (MP) at a user specified flow rate and composition. For SFC one of these pumps is specifically for the preconditioning and pumping of carbon dioxide (CO_2). Liquid CO_2 is supplied via a dip tube at cylinder pressure from a standard 50 lbs gas cylinder. A chiller reduces the temperature to 5 °C and two binary pistons meter and deliver CO_2 as a dense fluid. The second pump delivers degassed solvent to modify the polarity of the CO_2, and the two are mixed prior to sample introduction.

Detection. An additional solvent pump for makeup flow to facilitate delivery of the effluent for detection by a triple-quad mass spectrometer (**Figure 12; Orange**). A photodiode array ultra-violet (UV) detector is also available for the system, but was not utilized in the current work.

Other SFC-specific modules. The system is equipped with a stirred air column oven and a back pressure regulator [BPR_A] controls the system outlet pressure (**Figure 12; Green**).

Sample introduction is via an extraction loop or liquid injector (**Figure 12; Blue & Purple**). The liquid injector is used for MS-optimization and SFC-only modes. The extraction loop is used for online extractions.

The injector is equipped with a 5.0-µL external sample loop, and can be used with 'full' or 'partial' loop injections. During sample loading, the loop is bypassed (by an injection valve). A metering pump draws a specified volume of a liquid sample (the 'sample plug'), which is then pushed onto the loop while the injection valve is in the 'load' position. At the time of injection, the valve switches to the 'inject' position. The sample loop is now in the flow

path of the instrument and the sample plug is carried by the mobile phase to the column. The injection valve switching, indicates the start of analysis, and the delay between injection and t_o (delay/void volume; time it takes for the 'injection plug' to reach the column), depends on the flow rate and the length and diameter of tubing between the injection valve and the head of the column.

Alternatively, during online extraction, a solid sample is placed inside a small chamber (the 'extraction vessel'), extracted online, and the resulting extract delivered via the extraction loop. The Extraction loop is facilitated by two valves. These 2-position (6-port) valves work in unison to divert the system flow either to 'bypass', to 'fill', or to flow thru the extraction vessel. In online extractions, the introduction of the extract is done during one of the extraction steps, via a continuous flow over the column. Therefore, the introduction of the 'extract plug' to the column is performed previous to the start of the analysis and must be retained at the column head for a duration of time before analysis starts (t_{start}). This 'plug retention' becomes an important part of method development for online extractions, and at times a second BPR (BPR_B) is required to facilitate this process.

General Instrument Configurations. To facilitate rapid method development, different instrument configurations are used to isolate only the required modules for the analysis-type. These configurations can be broken down into four main setups: 1. FIA-MS Optimization configuration; 2. SFC-optimization configuration; 3. Instrument setup for online extractions; and 4. SFE-simulation configuration.

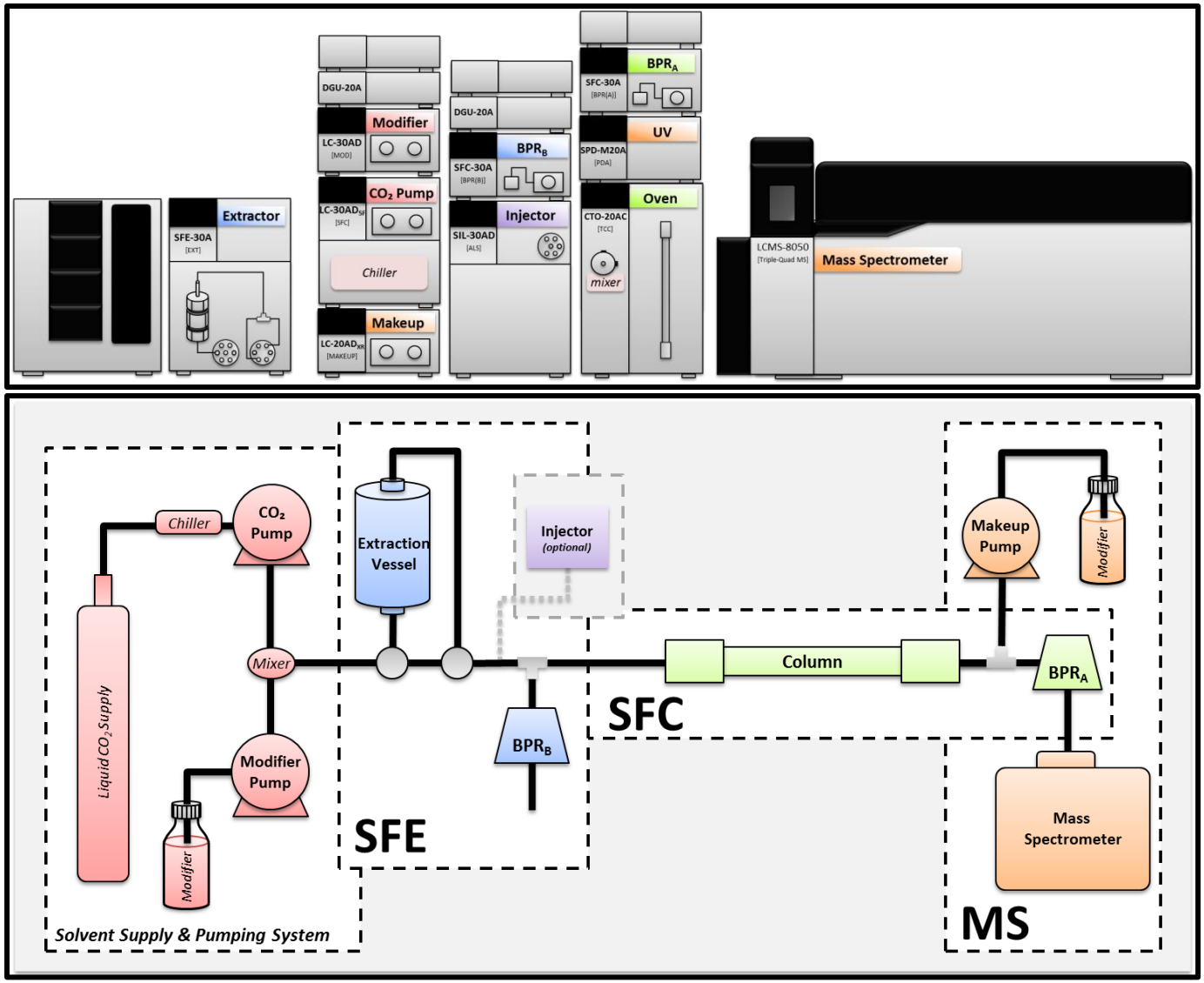

Figure 12. Nexera UC™ SFE-SFC-MS Instrument Setup. [Top] Instrument diagram identifying individual modules; [bottom] Instrument Schematic showing typical system tubing connections between modules.

1.4.1. FIA-MS Optimization Configuration.

Flow Injection analysis (FIA)-mode is used specifically for MS optimizations. This configuration is meant to reduce the time for each run to enable rapid MS method screening. For flow injection analysis (**Figure 13**), only the modifier pump, injector and mass spec are used. All modules associated with gas pre-conditioning (chilling and pumping), and pressure maintenance (back pressure regulators) are not connected/turn off. No column is installed. The extraction loop is bypassed and sample is introduced by the liquid injector. Makeup flow is optional, but when used is plumbed post injector. Makeup flow is only used if a different composition is required to facilitate ionization (e.g., An alternative additive is required to be present than the main MP [*this would only become apparent in late stages of SFC-MS method development and likely would be used for mid or final re-optimizations*]). Modifier solvent is supplied (via degasser) and pumped by the quaternary infusion pump to deliver 100% organic solvent as the main system MP. Tubing is minimized between all instrument modules to reduce run times.

The pump outlet is connected directly to the injection valve. Injections are made via the 5.0-µL external loop. The injector outlet is connected directly to the MS interface. In this configuration using 100% modifier (at flow rate of 240 µL/min), average runtime is approximately 0.5 min. This allows rapid injection cycles for MRM precursor and product ion searches, and automated optimal voltages and collision energy optimizations.

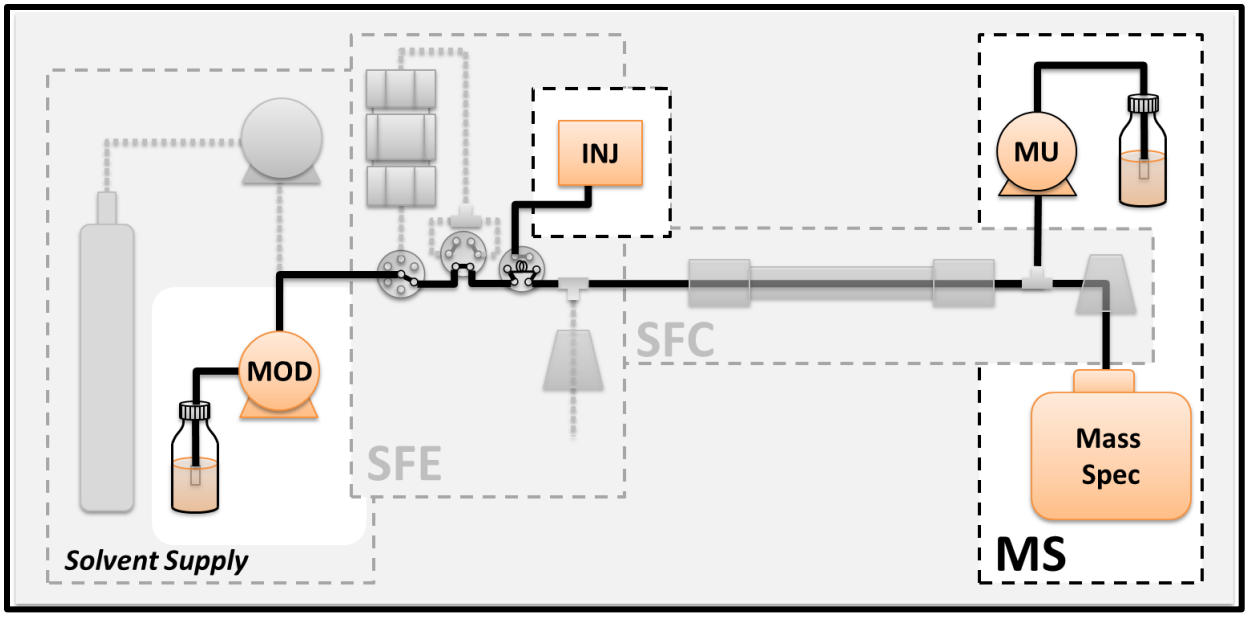

Figure 13. Nexera UC™ Instrument Setup During Flow Injection Analysis (FIA)-MS Optimizations: showing modules utilized for MS Detection Optimizations using FIA-Analysis with 100% modifier and overall flow path between modules. Modules utilized during FIA-MS analysis included: **[MOD]** Modifier pump (*quaternary modifier infusion pump*); **[INJ]** Injector (*automatted liquid injector*); **[MU]** Makeup Pump (*binary modifier infusion pump*); and **[Mass Spec]** Triple-quadrupole mass spectrometer.

1.4.2. Configuration used for SFC Optimizations.

The general SFC-only configuration (**Figure 14**) is utilized for a wide variety of analysis modes. This configuration was used when MS-based optimizations for detection required CO_2 to be present in the MP [CO_2-MS Optimization Mode], as well as during all SFC-type method development phases, e.g., column screening and SFC-based method optimizations [SFC-Separation Optimization mode].

CO_2-MS Optimization Mode. MS-optimizations that require CO_2 to be present in the MP, are similar to flow injection analysis where the goal is to reduce the time for each run as much as possible to enable rapid injections for mass spec based method screening. Therefore, just as in FIA-MS optimizations tubing is minimized between modules to reduce run times. The biggest difference from liquid-based FIA injections is that the majority of the mobile phase will now be a gas. Therefore, in order to incorporate CO_2 in the MP, not only is the use of the CO_2 pump and BPR required (to maintain a dense fluid throughout the system), but additionally a restrictor (column or small diameter tubing) is also required. This restriction is necessary to produce a delta pressure between the pumps and the BPR to effectively meter and deliver the MP. Without a delta pressure to buffer system pressure pulses (between the compression/delivery strokes of the pumps and the adjustments of the BPR), the BPR would be in constant flux trying to maintain a stable set outlet pressure. This inherently would cause high noise as well as many other undesirable issues, resulting in non-ideal instrument conditions.

Ideally, the column would be replaced by a short section of tubing (at least 120 µm ID) with fittings and zero-dead volume unions on each end (**Figure 14; Top**). Using a restrictor should produce shorter runtimes that would mimic more the FIA-mode analysis times of 0.5-1.0 min runs. In the current work, the majority of CO_2-MS optimization injections were performed with a restrictor unless specified otherwise.

Therefore, if a 'restrictor' cannot be utilized, a column must be installed for MS-optimization, even if injecting individual standards (**Figure 14; Bottom**). This of course results in longer runtimes, which would depend on compound specific retention. Although runtimes could be reduced with higher modifier concentrations, if no information is available on the effect of SFC-based MP composition on the ionization behavior of targeted

analytes, caution should be taken that low versus high modifier concentrations may have significant differences in the effects on the ionization and fragmentation of various analytes.

SFC-Separation Optimization Mode. (**Figure 14; BOTTOM**) This configuration is meant to reduce the time for each run to enable rapid SFC-method screening and optimizations (as in effect of modifier concentration, flow rate and secondary parameters [column temperature and outlet pressure] on retention and resolution). Generally, anytime online extraction was not required, SFC-only mode would be utilized to minimize runtimes and to reduce effects of background matrix effects. Important factors in SFC-based method screening include, the stationary phase, the mobile phase composition (including modifiers and additives), as well as effect of instrument parameters on resolution; flow rate, modifier concentration, column temperature and outlet pressure.

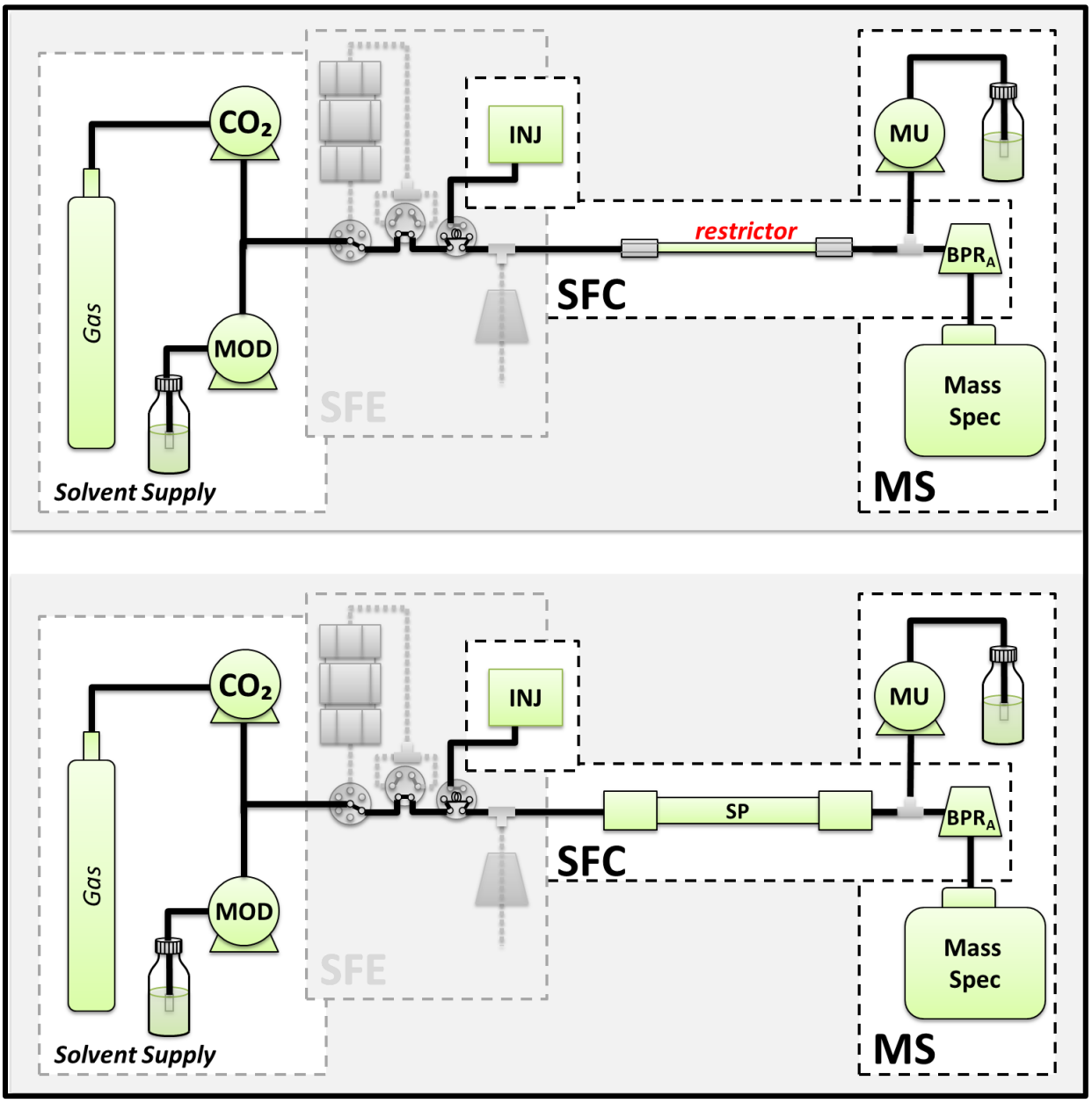

Figure 14. Nexera UC™ SFC-MS Instrument Setup During SFC-Optimizations: [Top] CO_2-MS Optimization Mode (with restrictor installed) and [Bottom] SFC-Separation Optimization Mode with column installed, showing modules utilized for CO_2-MS optimization mode, SFC column screening and SFC-based method development using CO_2 as the main component of the MP modified with organic solvent and overall flow path between modules while utilizing the injector for sample introduction. Modules utilized during SFC-MS optimizations included: **[Gas]** carbon dioxide cylinder with dip tube; **[CO_2]** CO_2 pump (*carbon dioxide delivery unit*); **[MOD]** Modifier pump (*quaternary modifier infusion pump*); **[INJ]** Injector (*automatted liquid injector*); **[SP]** chromatographic stationary phase (*column, shown on bottom*) or alternatively **[restrictor]** short narrow diameter tubing *(shown on top for MS optimizations, not requiring chromatographic separation);* **[MU]** Makeup Pump (*binary modifier infusion pump*); **[BPR_A]** Back pressure regulator, post-column (*outlet pressure*); and **[Mass Spec]** Triple-quadrupole mass spectrometer.

1.4.3. General Instrument setup for Online Extractions.

Online extraction utilizes the majority of the instrument modules (**Figure 15**). This configuration is similar to the SFC-only configuration but bypasses the liquid injector and instead utilizes the extraction loop for sample introduction (see sample introduction above). Online SFE-SFC at times requires a second BPR in order to split the system flow. In this case, the dual back pressure regulators (BPR_A and BPR_B) work in sync to 'split' the system flow and to deliver appropriate volumes of an 'extraction plug' to the head of the column. Extraction modes and the extraction process are detailed in the following section.

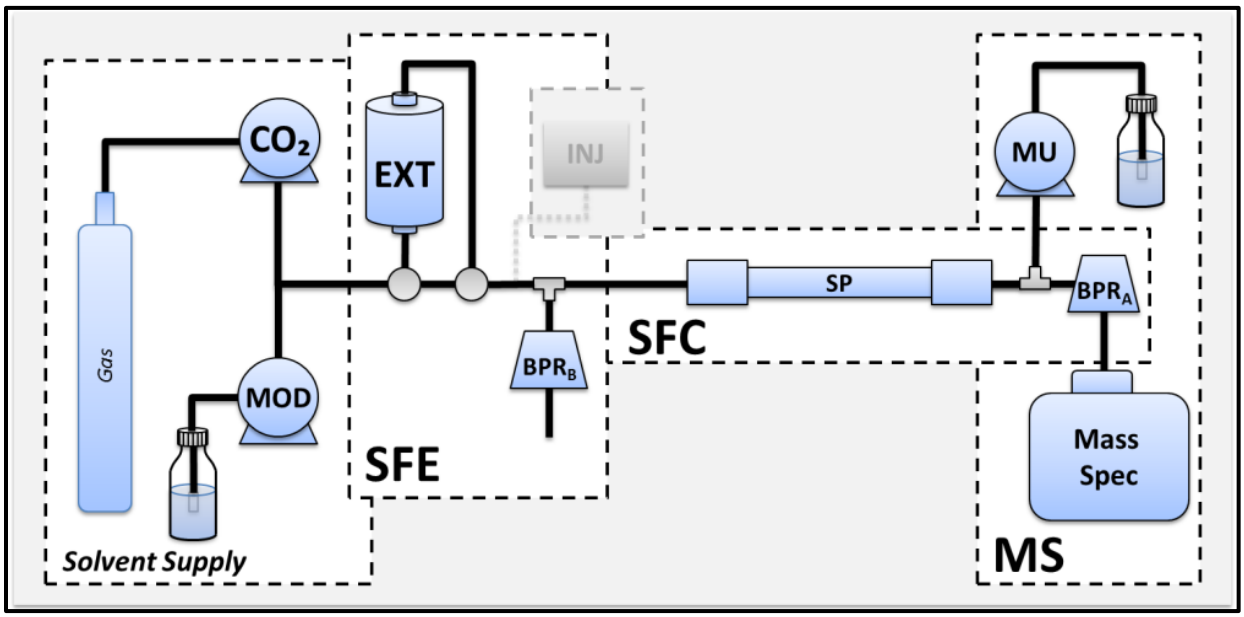

Figure 15. Nexera UC™ SFE-SFC-MS Generic Instrument Setup for Online Extractions: showing modules utilized for online extraction utilizing the extraction loop for sample introduction and overall flow path between modules. This configuration uses carbon dioxide (CO_2) as the main mobile phase component modified with organic solvent. Modules involved in online extractions: **[Gas]** carbon dioxide cylinder with dip tube; **[CO_2]** CO_2 pump (*carbon dioxide delivery unit*); **[MOD]** Modifier pump (*quaternary modifier infusion pump*); **[EXT]** supercritical fluid extraction unit (*showing Extraction vessel and loop only*); **[BPR_B]** back pressure regulator, pre-column (*potential splitter*); **[SP]** chromatographic stationary phase (*column*); **[MU]** Makeup Pump (*binary modifier infusion pump*); **[BPR_A]** back pressure regulator, post-column (*outlet pressure*); and **[Mass Spec]** Triple-quadrupole mass spectrometer.

1.5. Online Extraction Mode

1.5.1. Automated sampling for online extractions (Figure 16; A).

The extraction unit can be equipped with a rack changer to allow for the automatic processing of up to 48 samples. Samples are loaded directly into vessels with or without an additional filler. Vessel racks hold 4 vessels which are moved from the thermostatted rack drawers to the extractor via an automated arm. Once placed in the extractor, a needle placed at the top of the vessel completes the extraction loop.

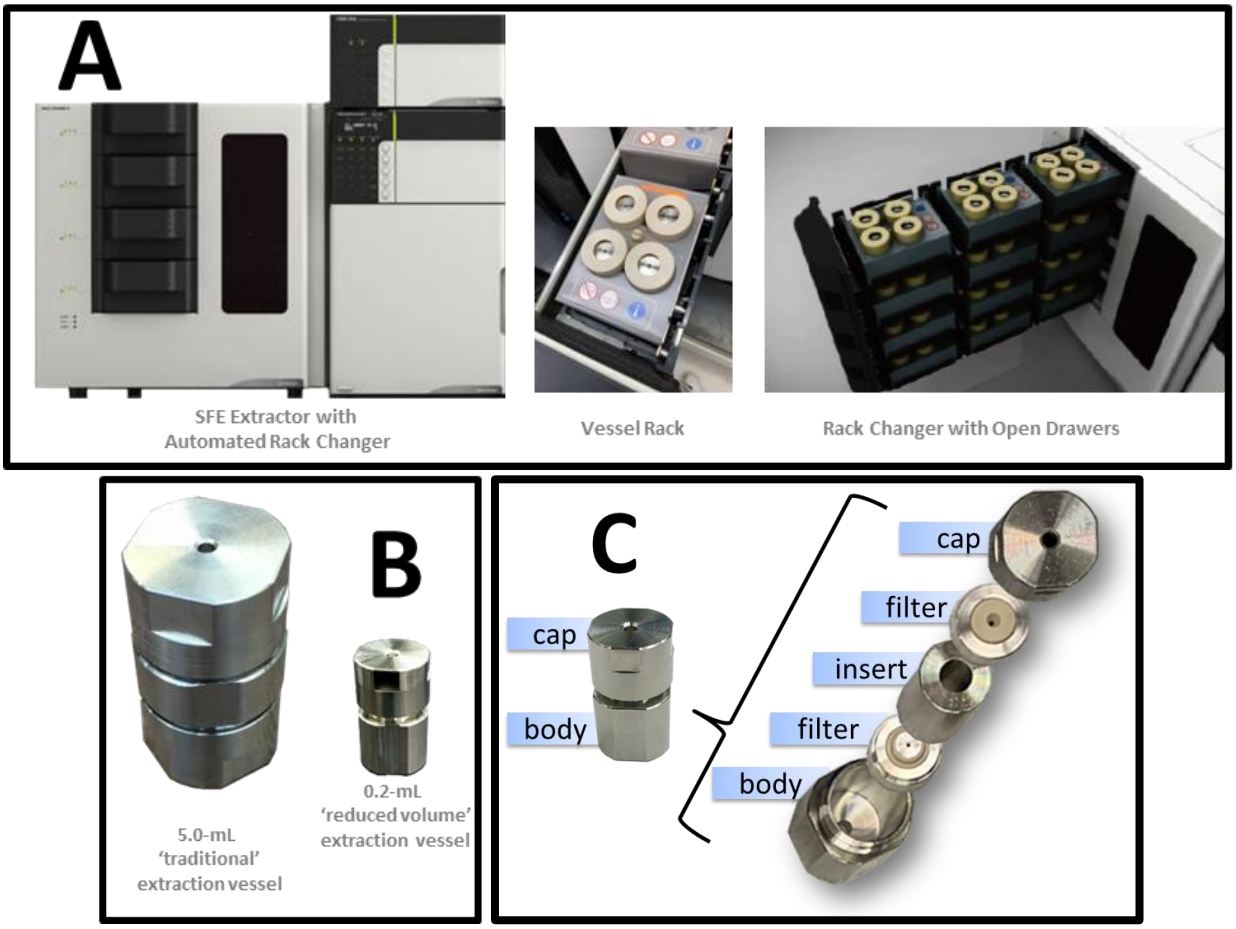

Figure 16. Online Extraction [A] Modules specific for the Automation of Online Extractions using [B] 0.2-mL (right) or 5.0-mL (left) Extraction Vessels and [C] Breakout view of the internal parts of a 0.2-mL extraction Vessel.

1.5.2. Extraction Vessel Sizes: 5.0-mL versus 0.2-mL vessels.

Online extractions using the Shimadzu Nexera UC are performed using an extraction chamber/vessel. There are two sizes of vessels: 5.0-mL or 0.2-mL vessels (**Figure 16**; **B**). The larger volume (5.0-mL) vessels, are the most commonly used and are meant for large sample volumes (~1 gram of starting materials). The use of a packing material is often required with this type of vessel. A dehydrant (an inert, cellulose based powder) is normally used. One to 1.5 grams of dehydrant is mixed with the sample before the mixture is loaded into the extraction vessel. Larger sample volumes of course result in larger extract volumes. These large volume 'extract plugs' represent a larger mass of analytes, where if the entire volume was loaded, would overload the analytical column resulting in poor retention of the 'extract plug'. In order to reduce the volume of extract introduced to the column (i.e., introduction rate), a system split is utilized. This 'split' comes with complications and is not well defined. Alternatively, 0.2-mL vessels are intended for use with small sample sizes and provide a variety of benefits for these types of samples. The smaller volume means no filler is required and results in a more concentrated extract in a smaller volume of extraction solvent. This smaller, more concentrated "extraction plug", more closely resembles the concentrations that would be found in an 'injection plug' from the autosampler. The entire 'extraction plug' can be loaded onto the analytical column without fear of overloading the analytical-scale phase. This means that the system can be operated in a 'splitless-mode' extraction configuration. Splitless-mode of course circumvents the ambiguity of the split-ratio, as the entire system flow goes thru the column and out to the detector.

Practical considerations for the use of 0.2-mL vessels. Two additional important notes for the proper use of the smaller vessels are merited. Both being of practical matters, as they are different than when using the more common 5.0-mL vessels. First, vessels require the use of a torque wrench to avoid overtightening during closing. Using the appropriate closing tool is of utmost importance as overtightening quickly leads to damage of the SS threads (e.g., cross threading) and/or damage to the vessel filters (e.g., cracking). The standard torque wrenches used for 5.0-mL vessels (with 4 N-m torque) are not compatible and will cause damage to 0.2-mL vessels. The closing tool appropriate for use with 0.2-mL vessels has a torque of **1.5 N-m**. Second, vessel end filters are a

standard part of the main body of a vessel (**Figure 16**; **C**). Vessel filters are the only impedance to stop larger particulates from extractions from exiting the vessel (and therefore entering the rest of the chromatographic instrument system). For 5.0-mL vessels there is one filter-type (standard for 5.0-mL), and these are 'sinter'-type filters being compatible for samples with small particles (i.e., small gauge filter, blocks particulates from entering the chromatographic system). For 0.2-mL vessels there are two filters types: 'Screen-type' and 'Sinter-type' filters (**S_Figure 1**). 'Screen'-type filters are standard for 0.2-mL vessels, but these types of filters need to be used with caution, as they have a very large gauge, and therefore will allow particulates to leave the extraction chamber. These filters are not compatible with samples like dried blood spots (a paper core). Alternatively, sinter-type filters (compatible with particulate type samples) can be purchased separately.

1.5.3. Extraction Process

The extraction process consists of four main steps which are automated by the system. The four major steps of an online SFE-SFC-MS method are shown in **Figure 17,** and include: 1. Vessel filling; 2. Static extraction; 3. Dynamic Extraction; and 4. Analysis. Immediately after the analysis, the system completes a wash of the extraction loop, before resetting for the next run. The proportion of the system flow going thru the column during extractions depends on if a split or split-less configuration is used. Care should be taken in regard to system flow rates to ensure compatibility with individual column specifications.

Vessel Filling. System flow is split between the extraction loop and the online SFC system. Mobile phase enters the extraction loop, and fills the vessel containing the sample. The extraction chamber is deadheaded, and excess flow is diverted over the column and BPR_A stabilizes system wide pressure (to the set outlet pressure).

Static 'Passive' Extraction. The flow path does not change from vessel loading. The sample (now exposed to fill solvent), is left for a duration of time, for passive extraction, while system effluent continues to flow through the column out thru BPR_A.

Dynamic 'Active' Extraction. The extraction valve directs the system flow directly thru the extraction vessel. As solvent flows thru, it actively extracts from the sample, the 'extract plug' is delivered to the column, and system flow continues.

Analysis. Both switching valves bypass the extraction loop directing all system flow on-column. This is the end of the extraction process and the chromatographic method is started.

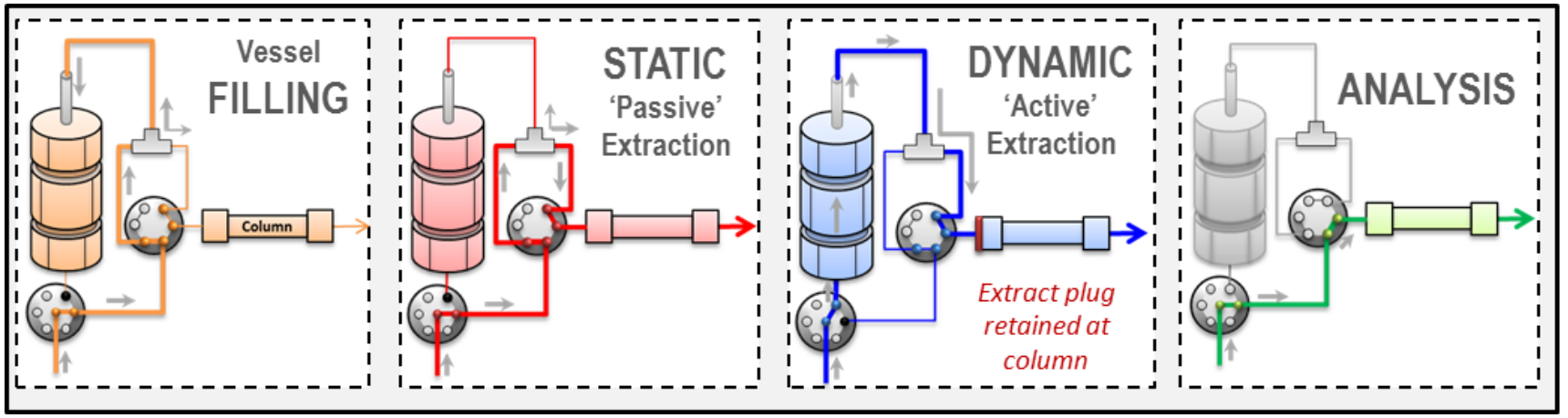

Figure 17. General Process for Online SFE-SFC-MS Extractions

1.5.4. 'Split' versus 'Splitless' Extraction Modes.

Online SFE-SFC at times requires two BPRs in order to split the system flow. Located post-column, BPR_A, always serves to regulate the system outlet pressure (to MS). Alternatively, located pre-column, a tee splits some of the system flow, to a second regulator, BPR_B.

BPR_B (pre-column) when necessary, this regulator acts as a diversion valve to bypass the column, forcing the majority of the system flow out to waste. This is called 'Split-mode' extractions and is sometimes utilized to facilitate the delivery of an appropriate volume of extract as an 'extraction plug' to the column.

BPR_A (post-column) always serves as the main system outlet pressure regulator and acts as the main control in order to maintain a set pressure. In the current work, all text references to the system outlet pressure refers to the setting for BPR_A. The use of BPR_A follows the traditional ideals applied during SFC-type analyses for the system outlet pressure, and the recommended range is typically between 10 and 25 MPa (100 – 250 bar).

'Splitless-mode' Extractions **(Figure 18; Top).** When only one of the BPRs are used, the system is operated in 'Splitless-mode'. BPR_B is either bypassed or "closed" (i.e., shut; set to 40 MPa [400 bar]). Shutting BPR_B pushes a piston tightly against a diagram, closing the alternative flowpath, and ultimately forces all the system flow through BPR_A. Therefore in 'splitless-mode' the system is operated with no difference from SFC-only mode (utilizing only one of the BPRs).

'Split-mode' Extractions **(Figure 18; Bottom).** When both BPRs are utilized, the system is operated in 'Split-mode'. In 'Split-mode' operation, the mobile phase is split by a differential in pressure between the two BPRs (BPR_A versus BPR_B). The majority (≥ 90%) of the system flow is diverted out to waste (thru BPR_B), while an 'extraction plug' is delivered to the head of the column (carried in the remaining ≤ 10% of the total system flow, pushed thru to BPR_A). Although determining the split ratio can be quite challenging, and small changes in the split can have secondary effects on nearly the entire system, studies have been performed to investigate the

parameters which have an effect of the split ratio. The introduction rate of analytes is directly related to the split ratio, which is affected by MP flow rate, system backpressure (BPR_A), and modifier concentration.[14]

Bamba et al. characterized the split ratio via studies on differential BPR pressures ($\Delta P_{BPR[B]}$), using injections of pesticides on a modified instrument. When the system is operated in a 'Full Split', both BPRs have the same pressure setting ($BPR_A = BPR_B$; $\Delta P_{BPR[B]} = 0$), and results in the largest split ratio (pushing the maximum percentage of the flow towards the column). $\Delta P_{BPR[B]}$ is increased by increasing the BPR_B setting. At a given **BPR_A** setting, a larger split (i.e., larger $\Delta P_{BPR[B]}$) pushes less flow out to waste (i.e., more flow on column). Large split ratios are harder to reproduce and produce higher %RSDs. So for example, (using an arbitrary setting for BPR_A = 15 MPa [150 bar]), common $\Delta P_{BPR[B]}$ are between 0.1 (ex. BPR_B = 15.1 MPa [151 bar]) and 1.0 (ex. BPR_B = 16.0 MPa [160 bar]). Using $\Delta P_{BPR[B]}$ = 0.1, would be expected to produce more reproducible results, but would be expected to push up to 98% of the total flow out to waste.

'Split' versus 'Splitless'. Although 'Split-mode' extractions are required when using 5.0-mL vessels, where large sample volumes (~ 1 gram of starting materials), produce too large a volume of extract, ultimately overloading the analytical column. For use with these larger vessels, applications where sample availability is not an issue, the advantages of split-mode extractions outweigh any negative effect on reproducibility. And these advantages would do not extend to applications where sample volumes are limited. Alternatively, using 0.2-mL vessels requires significantly less sample volume when compared to 5.0-mL vessels, and does not require system splitting. Splitless-mode provides many advantages, as the entire system flow is delivered to the column, reducing any negative effects on reproducibility and maximizing introduction rates.

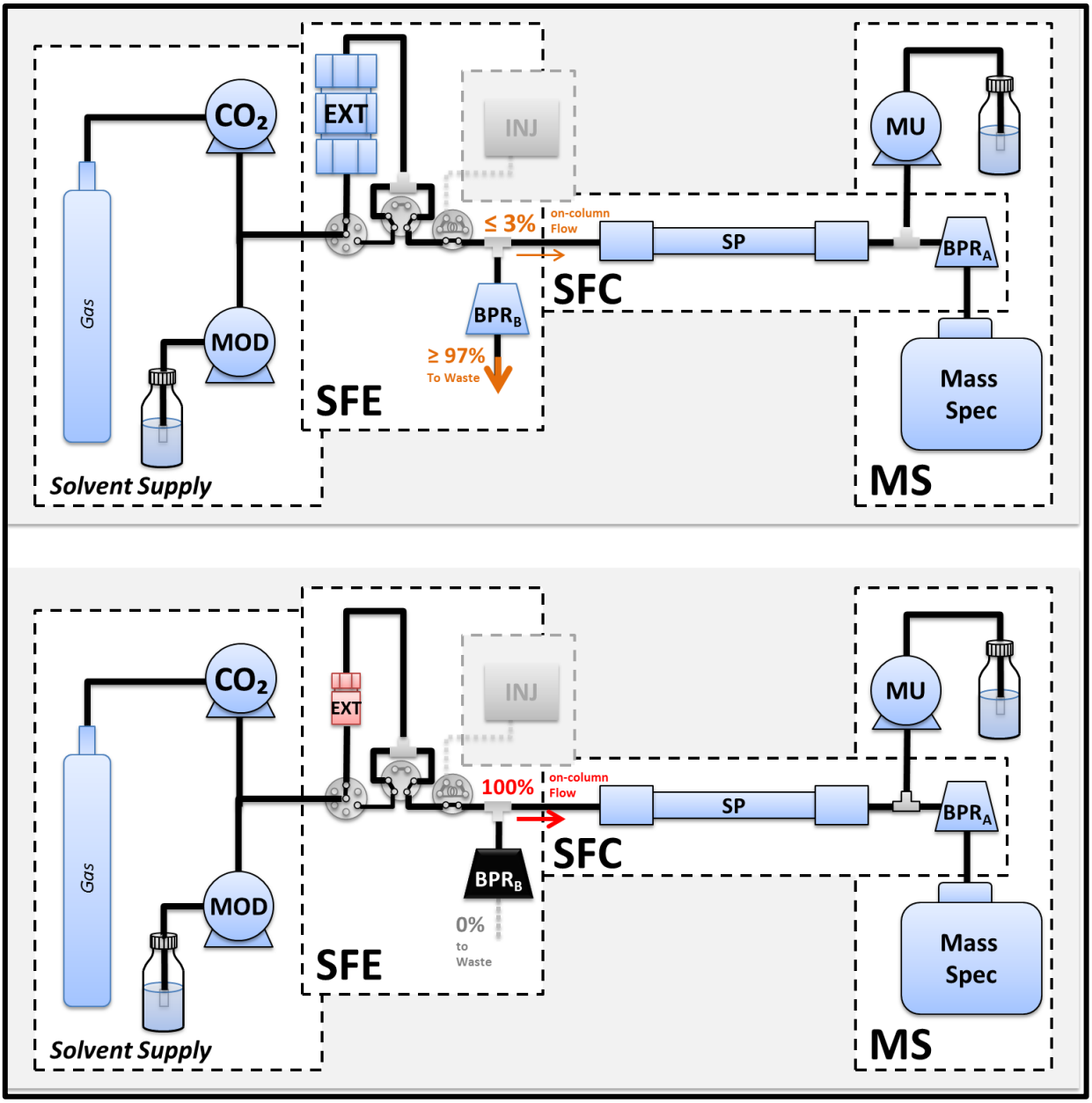

Figure 18. Nexera UC™ SFE-SFC-MS Instrument Setup for Online Extractions utilizing [Top] 5.0-mL extraction vessels in Split-mode and [Bottom] 0.2-mL vessels in Splitless-mode: showing modules utilized for online extractions. Using CO_2 as the main component of the MP modified with organic solvent and overall flow path between modules while utilizing the extraction loop for sample introduction. Modules involved in online extractions: **[Gas]** carbon dioxide cylinder with dip tube; **[CO_2]** liquid carbon dioxide delivery unit (*CO_2 pump*); **[MOD]** quaternary modifier infusion pump (*modifier pump*); **[EXT]** supercritical fluid extraction unit (*showing Extraction vessel and loop only*); **[BPR_B]** back pressure regulator, pre-column (*potential splitter*); **[SP]** chromatographic stationary phase (*column*); **[MU]** binary modifier infusion pump (*makeup flow*); **[BPR_A]** back pressure regulator, post-column (*outlet pressure*); and **[Mass Spec]** Triple-quadrupole mass spectrometer.

1.6. SFE-Simulation Configuration.

The SFE-Simulation configuration is utilized during the SFC column screening step of method development. This simulation is utilized to provide information at an early method development stage, allowing a more informed decision during the column selection process. Since the ultimate goal is to hyphenate the method with online extraction, the chromatographic resolution is not the only concern. Ultimately, the phase chosen also needs to retain a 'plug' at the head of the column. So even at this very early stage, performing an initial evaluation of each phases ability to accomplish this would be highly beneficial, to avoid wasting large amounts of time, by avoiding the need to re-start method development at later stages.

Many factors can have an effect on plug retention, and ultimately it would be impossible to simulate all factors involved. But the extraction steps involved in the creation and delivery of the 'extract plug' arguably have the largest effect on 'plug' integrity. So, in theory, a generic simulation of these two steps should give an idea of how a phase will perform. To accomplish this the system is setup in the SFC-only configuration, and SFC injections are performed while the system is operated as if the extraction loop was being utilized. This is performed both with (**Figure 19; Top**) and without (**Figure 19; Bottom**) a split (using BPR_B) to at least partially simulate the pressure conditions that would occur during an online extraction. This simulation allows a rapid initial evaluation of each columns ability to retain a plug at the column head for analysis.

1.7. General Sample Preparation workflows.

Using SFE-SFC-MS to minimize sample preparation is one of the ultimate goals; therefore, as little pre-processing of the sample as possible is beneficial. Typically, a nearly unprocessed sample is placed directly inside an extraction vessel, closed and loaded into the rack changer for online analysis. Since minimal preparation of the sample is ideal, method development inherently entails an emphasis on matrix evaluations for not only the sample but must also include controls for evaluation of the sampling materials. Therefore, quality controls and blanks for final matrix-specific optimizations should be developed that complement the application and allow true evaluation of developed methods.

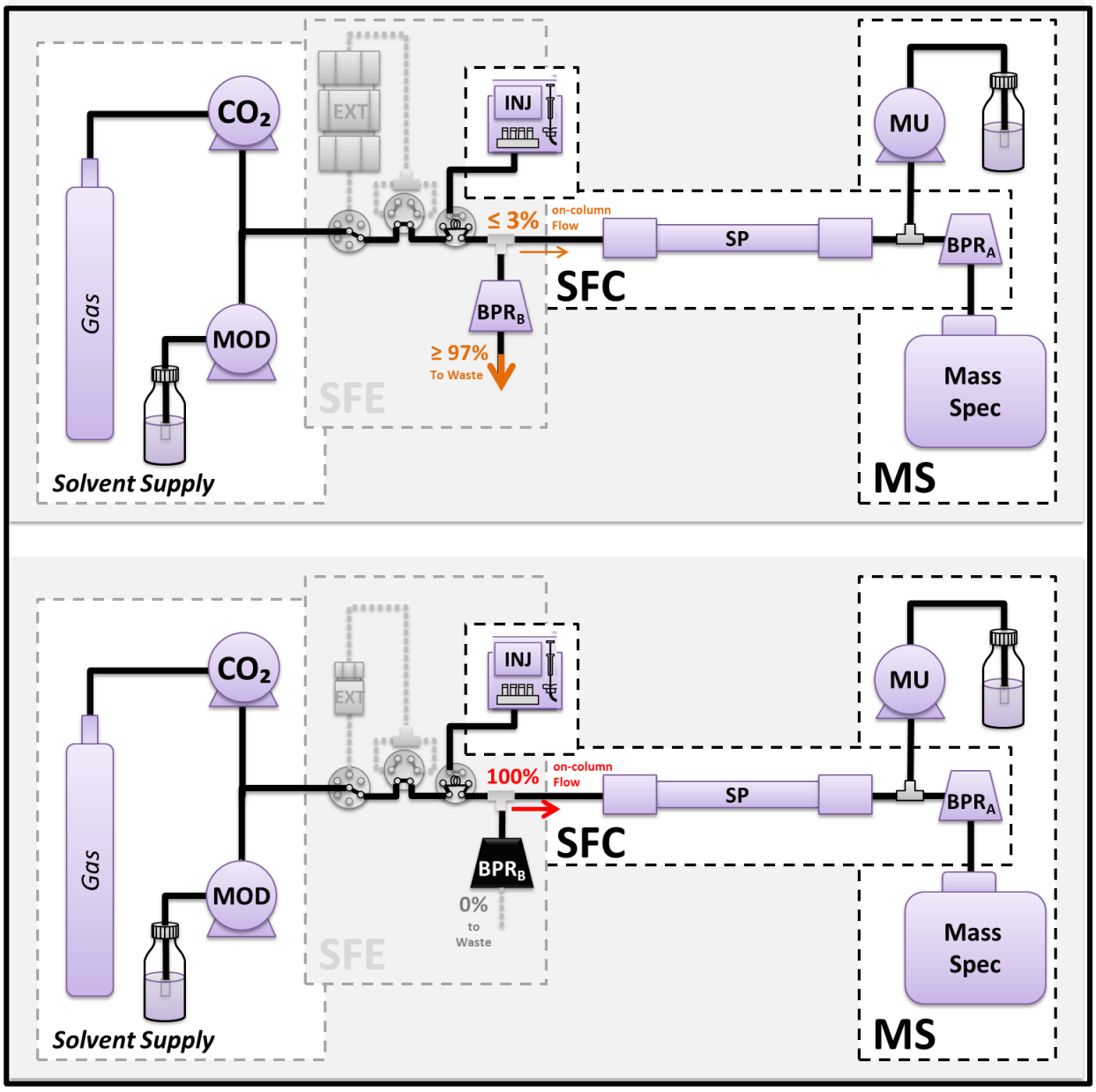

Figure 19. Nexera UC™ Instrument Setup for Simulation of Online Extractions During Column Selection: showing modules utilized for sample plug loading simulations. Using CO_2 as the main component of the MP modified with organic solvent and overall flow path between modules while utilizing the injector for sample introduction. [Top] utilizing split-mode (simulating extractions from 5.0-mL vessels) and [Bottom] splitless mode (simulating extractions from 0.2-mL vessels), during plug loading. Modules involved in online extractions: **[Gas]** carbon dioxide cylinder with dip tube; **[CO_2]** liquid carbon dioxide delivery unit (*CO_2 pump*); **[MOD]** quaternary modifier infusion pump (*modifier pump*); **[INJ]** automated liquid injector; **[BPR_B]** back pressure regulator, pre-column (*potential splitter*); **[SP]** chromatographic stationary phase (*column*); **[MU]** binary modifier infusion pump (*makeup flow*); **[BPR_A]** back pressure regulator, post-column (*outlet pressure*); and **[Mass Spec]** Triple-quadrupole mass spectrometer.

1.8. Summary

The Nexera UC is a hyphenated instrument, incorporating online SFE extractions with SFC analysis and MS detection. Online extractions provide many benefits especially in regard to minimizing sample preparation and handling. These benefits are especially pronounced for the extraction and analysis of samples with limited availability/small sample sizes, or those that contain target analytes that are susceptible to oxidation in air. However, hyphenated method development has its own set of challenges and re-optimizations are at times necessary making building robust methods time consuming. Many instrument configurations are possible and the instrument is easily plumbed to facilitate the shortest possible runtimes to speed up different stages of method development.

Literature Cited:

[1] Berger TA. (2015). "Supercritical fluid chromatography" Primer series; publication number 5991-5509EN; Agilent Technologies, USA. https://www.agilent.com/cs/library/applications/5991-8554EN_SFC_appcompendium_LR.pdf

[2] Berger TA. (1991). "Density of Methanol-Carbon Dioxide Mixtures at Three temperatures: Comparison with Vapor Liquid Equilibria Measurements and Results obtained from Chromatography." *Journal of High Resolution Chromatography.* **14**(5): p312–316. https://doi.org/10.1002/JHRC.1240140504

[3] Berger TA. (1995). "Packed Column SFC." *RCS Chromatography Monographs Series*; R. M. Smith (Eds.).; The Royal Society of Chemistry: Cambridge, UK. ISBN: 0-85404-500-7

[4] Bolanos B, Greig M, Ventura M, Farrell W, Aurigemma CM, Li H, Quenzer TL, Tivel K, Bylund JMR, Tran P, Pham C, Phillipson D. (2004). "SFC/MS in drug discovery at Pfizer, La Jolla." *International Journal of Mass Spectrometry.* **238**(2): p85-97. https://doi.org/10.1016/j.ijms.2003.11.021

[5] Tarafder A. (2016). "Metamorphosis of supercritical fluid chromatography to SFC: An Overview." *Trends in Analytical Chemistry.* **81**: p3–10. http://dx.doi.org/10.1016/j.trac.2016.01.002

[6] Maftouh M, Granier-Loyaux C, Chavana E, Marini J, Pradines A, Vander Heyden Y, Picard C. (2005). "Screening approach for chiral separation of pharmaceuticals Part III. Supercritical fluid chromatography for analysis and purification in drug discovery." *Journal of Chromatography A.* **1088**(1-2): p67-81. https://doi.org/10.1016/j.chroma.2004.12.038

[7] White C. (2005). "Integration of supercritical fluid chromatography into drug discovery as a routine support tool Part I. Fast chiral screening and purification." *Journal of Chromatography A.* **1074**(1-2): p163-173. https://doi.org/10.1016/j.chroma.2005.03.073

[8] Berger TA, Berger BK, Fogelman K. (2012). "8.18 Chromatographic Separations and Analysis: Supercritical Fluid Chromatography for Chiral Analysis and Semi-Preparative Purification." In: E.M. Carreira & H. Yamamoto (Eds.). Comprehensive Chirality (pp.354-392). Elsevier: Amsterdam, Netherlands. https://doi.org/10.1016/B978-0-08-095167-6.00836-3

[9] Berger, TA. Guest Speaker Lecture on Introduction to Packed Column Supercritical Fluid Chromatography (SFC). Presented at University of Texas at Arlington, Arlington, TX, USA, September 20, 2020.

[10] Chowdhury, SM. CHEM 5324 Lecture on Mass Spectrometry (MS) Background. Presented at University of Texas at Arlington, Arlington, TX, USA, January 22, 2020.

[11] Chowdhury, SM. CHEM 5324 Lecture on Mass Spectrometry; Sources; Electrospray Ionization (ESI). Presented at University of Texas at Arlington, Arlington, TX, USA, February 7, 2020.

[12] Chowdhury, SM. CHEM 5324 Lecture on Mass Spectrometry; Sources; Atmospheric Pressure Chemical Ionization (APCI). Presented at University of Texas at Arlington, Arlington, TX, USA, February 5, 2020.

[13] Chowdhury, SM. CHEM 5324 Lecture on Mass Spectrometry; Analyzers; Quadrupole Mass Analyzers. Presented at University of Texas at Arlington, Arlington, TX, USA, February 26, 2020.

[14] del Pilar Sanchez-Camargo A, Parada-Alfonso F, Ibanez E, Cifuentes A. (2017). "On-line coupling of supercritical fluid extraction and chromatographic techniques." *Journal of Separation Sciences.* **40**(1): p213–227. https://doi.org/10.1002/jssc.201601040

[15] Taylor LT. (2013). "Analytical Supercritical Fluid Extraction Goes Back to the Future." *LC/GC special Issues*. **31**(11): p10–13.

[16] del Pilar Sanchez-Camargo A, Parada-Alfonso F, Ibanez A, Cifuentes A. (2019). "Recent applications of on-line supercritical fluid extraction coupled to advanced analytical techniques for compounds extraction and identification." *Journal of Separation Sciences.* **42**(1)**:** p243–257. https://doi.org/10.1002/jssc.201800729

[17] Wicker AP, Tanaka K, Nishimura M, Chen V, Ogura T, Hedgepeth W, Schug KA. (2020). "Multivariate approach to on-line supercritical fluid extraction - supercritical fluid chromatography - mass spectrometry method development." *Analytica Chimica Acta*. **1127**: p282-294. https://doi.org/10.1016/j.aca.2020.04.068

[18] Sakai M, Hayakawa Y, Funada Y, Ando T, Fukusaki E, Bamba T. (2017). "Development of a split-flow system for high precision variable sample introduction in supercritical fluid chromatography." *Journal of Chromatography A.* **1515**: p218-231. https://doi.org/10.1016/j.chroma.2017.07.077

S_1. SUPPLEMENTAL MATERIALS

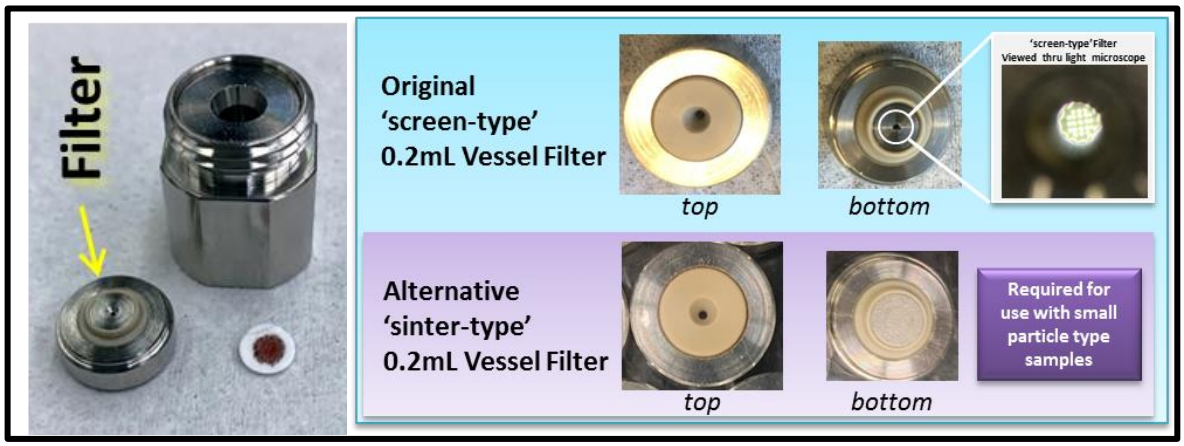

S_Figure 1. Vessel filter types for 0.2-mL Vessels: [Blue] 'Screen'-type filters, not compatible with small particle-type samples (Standard Original equipped, PN#: 228-59264-84)**; and [Purple] Alternative 'Sinter'-type filters**, for use with small-particle type samples (purchased separately, SSI PN#: 228-59264-81).

CHAPTER 2

MATERIALS AND METHODS

CHAPTER 2
MATERIALS AND METHODS

2.1. Materials

2.1.1. Solvents.

Methanol [MeOH], acetonitrile [ACN], isopropyl alcohol [IPA], formic acid [FA], trimethylamine [TEA] and ammonium formate [AmFo] were purchased from VWR International (Radnar, PA. USA). Analytical-grade carbon dioxide gas ([CO_2]; 60 lbs; with siphon), argon gas ([Ar]; 60 lbs tanks) and bulk liquid nitrogen [LN_2] were obtained from Airgas Corporation (Grand Prairie, TX, USA). Coolant for cryogenic grinding was refilled from the onsite bulk LN_2 supply via transportable liquid Dewar tanks. All solvents used for instrument mobile phases [MP], spiking solutions, and injection solutions for anti-doping were LCMS-grade; Pesticide-grade for microplastics and HPLC-grade and ACS-grade MeOH was utilized exclusively for cleaning extraction vessels.

Water [H_2O] used as exposure solvent during microplastics sample preparation, was either: 'fresh water' [qH_2O] which was Milli-Q grade and filtered on-site; -or- 'Salt water' [Sea-H_2O] which was collected from the field location where samples were deployed (**see Section 2.7.2. Marine-Exposed Microplastics; *Field collected control water***).

2.1.2. Analytical Standards.

Anabolic androgenic steroids (AAS). Twenty three anabolic agents were chosen from the 2021 WADA prohibited substances list: category S1.[19] All anabolic agents were purchased from Sigma Aldrich, Co. (St.Louis, MO, USA); purity, storage conditions and synonyms are provided in **Table 1** for each AAS analytical standard. Endogenous and exogenous androgenic steroids were targeted, including: 1-androsterone [1DHEA], androstenedione[STEN], androsterone [ADEN], androstanolone [ADON], epitestosterone [EPIT], etiocholanolone [ETIO], 7-keto-DHEA [KETO], mibolerone[MIBL], mestanolone [MSAL], mesterolone [MSEL], methyltestosterone

[MTHY], prasterone [PRST], trenbolone [TRNB], and testosterone [TSTO]. Other Anabolic Agents that were included in the study were either synthetic steroids (danazol [DNZL], gestrinone [GSTN], metandienone [METD], metribolone [MTRB], stanozolol [STNZ], and oxandrolone [OXAN]) or selective androgen receptor modulators [SARMS] (andarine [ADAR], and zeranol [ZRNL]) and clenbuterol [CLNB]. Deuterium labelled standard of testosterone- d_3 [T-d_3] was also obtained for use an internal standard.

Environmental pollutants. Polycyclic Aromatic Hydrocarbons (PAHs). Sixteen polycyclic aromatic hydrocarbons (PAHs) were chosen from EPA method 8310,[20] purity, storage conditions and synonyms are provided in **Table 2** for each PAH analytical standard. All PAH standards were obtained as powders from Sigma Aldrich, Co. (St.Louis, MO. USA); and included: acenaphthalene [ACEN], acenaphthylene [ANPY], anthracene [ANRN], benzo[*a*]anthracene [BARC], benzo[*a*]pyrene [BAPY], benzo[*b*]fluoranthene [BBFA], benzo[*g,h,i*]perylene [BGPY], benzo[*k*]fluoranthene [BKFA], chrysene [CHSY], dibenzo[*a,h*]anthracene [DBAR], fluoranthene [FLAT], fluorene [FLUR], indeno[1,2,3-*cd*]pyrene [IDPY], naphthalene [NAPL], phenanthrene [PHNR], and pyrene[PYRN]. Five deuterium labelled PAHs were also obtained for use an internal standards from C/D/N Isotopes, Inc. (Pointe-Claire, Quebec. Canada); and included: acenaphthene-d_{10} [A-d_{10}], benzo[*e*]pyrene-D_{12} [B-d_{12}], chrysene-D_{12} [C-d_{12}], fluoranthene-D_{10} [F-d_{10}], and naphthalene-d_8 [N-d_8].

Table 1. Androgenic Anabolic Agents (AAS) Analytical Standards: Analyte ID, CAS#, MW, LogP, Supplier, Purity, and synonyms.

ID	AAS	CAS #	MW	logP	Supplier	Purity	Purchased as	Synonym(s)
1DHEA	1-Androsterone	481-29-8	290.4	3.7	Sigma-Aldrich	Solid, not specified	powder	3α-hydroxy-5α-androst-1-ene-17-one, 1-Dehydroepiandrosterone
1STEN	Androstenedione	63-05-08	286.4	3.6	Sigma-Aldrich	Cerilliant® inACN	ampule (1.0 mg/mL)	Androst-4-ene-3,17-dione
ADAR	Andarine	401900-40-1	441.4	2.2	Sigma-Aldrich	analytical standard**	powder	-
ADEN	Androsterone	53-41-8	290.4	3.7	Sigma-Aldrich	VETRANAL™	powder	cis-Androsterone; Androstanon-3α-ol-17-one
ADON	Androstanolone	521-18-6	290.4	3.7	Sigma-Aldrich	Cerilliant® inMeOH	ampule (1.0 mg/mL)	5α-dihydrotestosterone, 17β-hydroxy-5α-androstan-3-one
CLNB	Clenbuterol	37148-27-9	277.2	2.2	Sigma-Aldrich	(USP) Standard	powder	Clenbuterol hydrochloride (CAS# :21898-19-1; MW =313.65)
DNZL	Danazol	17230-88-5	337.5	3.8	Sigma-Aldrich	(USP) Standard	powder	[1,2]oxazolo[4',5':2,3]pregna-4-en-20-yn-17α-ol
EPIT	Epitestosterone	481-30-1	288.4	3.3	Sigma-Aldrich	Cerilliant® inACN	ampule (1.0 mg/mL)	androst-4-en-17α-ol-3-one, cis-Testosterone
ETIO	Etiocholanolone	53-42-9	290.4	3.7	Sigma-Aldrich	regulated under CDSA	powder	5-isoandrosterone, 3α-Hydroxy-5β-androstan-17-one
GSTN	Gestrinone	16320-04-0	308.4	2.2	Sigma-Aldrich	≥97% (HPLC)	powder	17α-Ethynyl-18-methyl-δ9,11-19-nortestosterone
KETO	7-Keto-DHEA	1449-61-2	302.2	2.6	Sigma-Aldrich	98.5%; Chem Impex Int., Inc.	powder	7-Ketodehydroepiandrosterone, 7-keto-DHEA; 7-Oxo-dehydroepiandrosterone ace
METD	Metandienone	72-63-9	300.4	3.7	Sigma-Aldrich	Cerilliant® inDMOE	ampule (1.0 mg/mL)	17β-hydroxy-17α-methylandrosta-1,4-dien-3-one, 1-Dehydromethyltestosterone
MIBL	Mibolerone	3704-09-4	302.5	3.2	Sigma-Aldrich	(USP) Standard	powder	7α,17α-Dimethyl-19-nortestosterone
MSAL	Mestanolone	521-11-9	304.5	3.8	Sigma-Aldrich	analytical standard	powder	17α-Methylandrostan-17β-ol-3-one, Methylandrostanolone
MSEL	Mesterolone	1424-00-6	304.5	4.1	Sigma-Aldrich	analytical standard	powder	1α-Methylandrostan-17β-ol-3-one
MTHY	Methyltestosterone	58-18-4	302.5	3.6	Sigma-Aldrich	(USP) Standard	powder	17α-Methyl-4-androsten-17β-ol-3-one
MTRB	Metribolone	965-93-5	284.4	3.4	Sigma-Aldrich	≥98% (HPLC)	powder	methyltrienolone, 17β-hydroxy-17α-methylestra-4,9,11-trien-3-one
OXAN	Oxandrolone	43-39-4	306.4	3.7	Sigma-Aldrich	≥98% (HPLC)	powder	17β-Hydroxy-17α-methyl-2-oxa-5α-androstan-3-one
PRST	Prasterone (DHEA)	53-43-0	288.2	3.2	Sigma-Aldrich	≥99%	powder	Dehydroepiandrosterone, DHEA, 3β-Hydroxy-5-androsten-17-one
STNZ	Stanozolol	10418-03-8	328.5	4.5	Sigma-Aldrich	Cerilliant® inDMOE	ampule (1.0 mg/mL)	17α-Methylpyrazolo[4',3':2,3]-5α-androstan-17β-ol
TRNB	Trenbolone	10161-33-8	270.4	1.9	Sigma-Aldrich	Cerilliant® inACN	ampule (1.0 mg/mL)	17β-hydroxyestr-4,9,11-trien-3-one
TSTO	Testosterone	58-22-0	288.4	3.3	Sigma-Aldrich	Cerilliant® inACN	ampule (1.0 mg/mL)	17β-Hydroxyandrost-4-en-3-one
ZRNL	Zeranol	26538-44-3	322.4	4.3	Sigma-Aldrich	AnalStd inACN	ampule (10 µg/mL)	-
T-d3	Testosterone-d_3	77546-39-5	291.4	3.3	Sigma-Aldrich	98 atom %D	powder	17β-Hydroxyandrost-4-en-3-one-16,16,17-d3

Table 2. Polycyclic Aromatic Hydrocarbons (PAHs) Analytical Standards: Analyte ID, CAS#, MW, LogP, Log Kow, Supplier, Purity, Storage Conditions, and Synonyms.

ID	PAH	CAS#	MW	LogP	Log K_{ow}	Supplier	Purity	Storage	Synonym(s)
ACEN	acenaphthalene	83-32-9	154.2	3.9	3.9**	Sigma-Aldrich	99%	room temp	1,2-Dihydroacenaphthylene, 1,8-Ethylenenaphthalene
ANPY	acenaphthylene	208-96-8	152.2	3.9	4.0**	Sigma-Aldrich	analytical standard	room temp	Cyclopenta[d,e]naphthalene
ANRN	anthracene	120-12-7	178.2	4.4	4.6**	Sigma-Aldrich	TraceCERT®	under inert gas	Anthraxcene, Paranaphthalene
BARC	benzo[*a*]anthracene	56-55-3	222.3	5.8	5.8**	Sigma-Aldrich	99%	room temp	Benz[a]anthracene, 1,2-Benzanthracene, Tetraphene
BAPY	benzo[*a*]pyrene	50-32-8	252.3	6.0	6.1**	Sigma-Aldrich	≥96% (HPLC)	room temp	3,4-Benzopyrene, 3,4-Benzpyrene, Benzo[def]chrysene
BBFA	benzo[*b*]fluoranthene	205-99-2	252.3	6.4	5.9**	Sigma-Aldrich	98%	room temp	2,3-Benzfluoranthene, 3,4-Benzofluoranthene, Benzo[e]acephenanthrylene
BGPY	benzo[*g,h,i*]perylene	191-24-2	276.3	6.6	6.8***	Sigma-Aldrich	Analytical std	2 - 8 °C	1,12-Benzoperylene
BKFA	benzo[*k*]fluoranthene	207-08-9	252.3	6.4	5.9**	Sigma-Aldrich	>99%	room temp	11,12-Benzofluoranthene, 2,3,1′,8′-Binaphthylene, 8,9-Benzfluoranthene
CHSY	chrysene	218-01-9	228.3	5.7	5.7**	Sigma-Aldrich	<= 100 %	room temp	Benzo[a]phenanthrene, 1,2-Benzophenanthrene
DBAR	dibenzo[*a,h*]anthracene	53-70-3	278.3	6.5	6.9***	Sigma-Aldrich	analytical standard	room temp	1,2:5,6-Dibenzanthracene
FLAT	fluoranthene	206-44-0	202.3	5.2	5.0**	Sigma-Aldrich	98%	room temp	Benzo[j,k]fluorene
FLUR	fluorene	86-73-7	166.2	4.2	4.1**	Sigma-Aldrich	98%	room temp	Diphenylenemethane
IDPY	indeno[1,2,3-*cd*]pyrene	193-39-5	276.3	7.0	6.7***	Sigma-Aldrich	TraceCert	room temp	o-Phenylenepyrene, 1,10-(o-Phenylene)pyrene
NAPL	naphthalene	91-20-3	128.2	3.3	3.3****	Sigma-Aldrich	≥99.7% (GC)	room temp	Naphthalin
PHNR	phenanthrene	85-01-8	178.2	4.5	4.5**	Sigma-Aldrich	98%	under inert gas	Phenanthrin, [3]Helicene
PYRN	pyrene	129-00-0	202.3	4.9	5.0**	Sigma-Aldrich	≥99.0% (GC)	room temp	Benzo[d,e,f]phenanthrene
A-d10	acenaphthene-d_{10}	15067-26-2	164.3	3.9	-	CDN Isotopes	99 atom %D	room temp	1,8-Ethylenenaphthalene; 1,2-Dihydroacenaphthylene
B-d12	benzo[*e*]pyrene-d_{12}	205440-82-0	264.4	6.4	-	CDN Isotopes	98 atom %D	room temp	1,2-Benzopyrene; 1,2-Benzpyrene; 4,5-Benzopyrene
C-d12	chrysene-d_{12}	1719-03-5	240.4	5.7	-	CDN Isotopes	98 atom %D	room temp	Benzo[a]phenanthrene, 1,2-Benzophenanthrene
F-d10	fluoranthene-d_{10}	93951-69-0	212.3	5.2	-	CDN Isotopes	98 atom %D	room temp	Benzo[j,k]fluorene
N-d8	naphthalene-d_8	1146-65-2	136.2	3.3	-	CDN Isotopes	99 atom %D	room temp	Naphthalin

** K_{ow} from [21]; ***[22] K_{ow}'s from http://www.env.gov.bc.ca/wat/wq/BCguidelines/pahs/pahs-01.htm; ****K_{ow} from [23]

2.1.3. Dried Blood Spots (DBS) Materials.

Biological Fluids: Blood, Plasma and Red Blood Cells. All biofluids (**Table 3**) were obtained from Innovative Research (Novi, MI. USA) and stored at 4 °C until the time of use. Whole blood was obtained for both Bovine (US Origin-grade bovine whole blood [P#:IWB1K2E]) and Human (Single donor human whole blood [P#:IGBOWBK2E]) donors. Whole blood was utilized during extraction optimization, matrix evaluations, and extraction method validation. To demonstrate final method applicability, fortified samples were created using human plasma (Single donor, blood-derived, human plasma [P#:IPLASK2E]) and packed red blood cells (Single donor, human red blood cells, type O-negative [P#:IWB3CPDA]).

Blood Spot Collection Materials. Whatman™ 903 FTA classic collection/preservation cards (P#:WHAWB120205) were obtained from Sigma Aldrich, Co. (St.Louis, MO. USA). Standard, single-hole punch devices were obtained from local sources (Pen+Gear brand, Walmart, Arlington, TX. USA).

2.1.4. Microplastics Materials.

Virgin Plastic Pellets. Plastic pellets were obtained for nine types of common plastics: low-density polyethylene [LDPE], high-density polyethylene [HDPE], polypropylene [PPrp], thermoplastic polyurethane [TPUr], high-impact polystyrene [HIPS], polyethylene terephthalate [PETE], polyethylene terephthalate glycol [PETG], polycarbonate [PCrb], and acrylonitrile butadiene styrene [ABSt]. Supplier information, purity and color for each pellet type are provided in **Table 4**.

Microplastics Exposure/Sampling Materials. Premium rosin screen filter press bags (Mesh: 25µm, Nylon, 2 x 4 inch) were obtained from (Ryzenberg's Products storefront, Fort Collins, CO. USA.); Glass square bottles (120 mL, 42mm) were obtained from (Aozita storefront, Jiangsu, China.); generic braided rope (1mm, polyester cord) and cable ties (100 mm) were obtained via amazon.com, Inc. (Seattle, WA. USA). Polypropylene and glass beakers, petri dishes and amber glass storage vials were obtained from VWR International (Radnar, PA. USA).

Table 3. Biological Fluids Supplier and Donor information for Whole Blood, Plasma and Red Blood Cells.

		Biofluid			Donor Information				
Date Received	**ID**	**Type**	**Lot #**	**Anti-coagulant**	**Species**	**Gender**	**Age**	**Ethnicity**	**Data Contribution**
02/2020	**PB1**	WB	31296	K2 EDTA	Bovine	unknown	unknown	n/a	Large-DBS Initial Sample Prep Testing
06/2020	**PB2**	WB	32208	K2 EDTA	Bovine	unknown	unknown	n/a	Large and Micro-DBS initial sample prep testing
08/2020	**PB3A**	WB	34271	K2 EDTA	Bovine	unknown	unknown	n/a	**Chapter #7.** SFE-Optimization; **Chapter #8.** Sample matrix evaluation; **Chapter #8.** DBS Validation (Specificity [setA]).
02/2021	**PB4B**	WB	34271	K2 EDTA	Bovine	unknown	unknown	n/a	**Chapter #7.** Initial LOD evaluation; **Chapter #8.** DBS Validation (Specificity [setB]).
04/2021	**PB5C**	WB	34802	K2 EDTA	Bovine	unknown	unknown	n/a	**Chapter #8.** DBS Validation (Linearity, Accuracy&Precision, Stability, Matrix, Robustness, Recovery, LOD/LOQ, & Specificity [setC])
05/2021	**PB6D**	WB	35472	K2 EDTA	Bovine	unknown	unknown	n/a	**Chapter #8.** DBS Validation (Specificity [setD]).
n/a	**PF1**	WB	n/a	n/a	Human	Female	n/a	n/a	n/a
06/2020	**PF2**	WB	24 15491D (HF45)	K2 EDTA	Human	Female	45	hispanic	Large and Micro-DBS initial sample prep testing
08/2020	**PF3A**	WB	HMN457036	K2 EDTA	Human	Female	35	black	**Chapter #7.** SFE-Optimization; **Chapter #8.** Sample matrix evaluation; **Chapter #8.** DBS Validation (Specificity [setA]).
02/2021	**PF4B**	WB	HMN550021	K2 EDTA	Human	Female	18	black	**Chapter #8.** Initial LOD evaluation; **Chapter #8.** DBS Validation (Specificity [setB]).
04/2021	**PF5C**	WB	HMN582398	K2 EDTA	Human	Female	20	black	**Chapter #8.** DBS Validation (Linearity, Accuracy&Precision, Stability, Matrix, Robustness, Recovery, LOD/LOQ, & Specificity [setC]).
05/2021	**PF6D**	WB	HMN623417	K2 EDTA	Human	Female	50	caucasian	**Chapter #8.** DBS Validation (Specificity [setD]).
05/2021	**PF7E**	WB	HMN623418	K2 EDTA	Human	Female	55	hispanic	**Chapter #8.** DBS Validation (Specificity [setD]).
02/2020	**PM1**	WB	24 13978B	K2 EDTA	Human	Male	52	black	Large-DBS Initial Sample Prep Testing
06/2020	**PM2**	WB	24 15477C (HM29)	K2 EDTA	Human	Male	29	hispanic	Large and Micro-DBS initial sample prep testing
08/2020	**PM3A**	WB	HMN457035	K2 EDTA	Human	Male	37	hispanic	**Chapter #7.** SFE-Optimization; **Chapter #8.** Sample matrix evaluation; **Chapter #8.** DBS Validation (Specificity [setA]).
02/2021	**PM4B**	WB	HMN550022	K2 EDTA	Human	Male	65	black	**Chapter #8.** Initial LOD evaluation; **Chapter #8.** DBS Validation (Specificity [setB]).
04/2021	**PM5C**	WB	HMN581470	K2 EDTA	Human	Male	20	caucasian	**Chapter #8.** DBS Validation (Linearity, Accuracy&Precision, Stability, Matrix, Robustness, Recovery, LOD/LOQ, & Specificity [setC]).
05/2021	**PM6D**	WB	HMN623415	K2 EDTA	Human	Male	52	hispanic	**Chapter #8.** DBS Validation (Specificity [setD]).
05/2021	**PM7E**	WB	HMN623416	K2 EDTA	Human	Male	58	black	**Chapter #8.** DBS Validation (Specificity [setD]).
05/2021	**PLA1**	PLA	HMN616811	K2 EDTA	Human	Female	65	caucasian	**Chapter #8.** DBS Fortified Blood.
05/2021	**RBC1**	RBC	HMN620975	CPDA1	Human	Male	39	hispanic	**Chapter #8.** DBS Fortified Blood, Type O^-

WB: whole blood; PLA: Plasma; RBC: Red Blood Cells

Table 4. **Virgin Plastic Pellets Supplier and Polymer Information.**

									Single Pellet	
SMP ID	**PLASTIC**	**Common Acronym**	**Supplier**	**Supplier Location**	**TYPE**	**Purity**	**Color**	**RI**	**Average weight / Pellet (mg)**	**SD (mg)**
LDPE	Low-Density Polyethylene	LDPE	LNS technologies	Scotts Valley, Ca. USA	Pellet	Virgin	Natural	151	24.90	0.1528
HDPE	High-Density Polyethylene	HDPE	LNS technologies	Scotts Valley, Ca. USA	Pellet	Virgin	Natural	154	26.82	0.1732
PPrp	Polypropylene	PP	LNS technologies	Scotts Valley, Ca. USA	Pellet	Virgin	Clear	149	22.96	0.15
TPUr	Thermoplastic Polyurethane	TPU	LNS technologies	Scotts Valley, Ca. USA	Pellet	Virgin	White	152 - 157	18.67	0.2646
HIPS	High Impact Polystyrene	HIPS	LNS technologies	Scotts Valley, Ca. USA	Pellet	Virgin	Black	159 - 160	23.97	0.1155
PETE	Polyethylene terephthalate	PET	special spherical	Summerville, GA. USA	Pellet	Recycled	Gray	158 - 164	32.01	0.10
PETG	Polyethylene terephthalate glycol	PETG	3dXtech	Grand Rapids, MI. USA	Pellet	Virgin	Clear	16	18.98	0.0577
PCrb	Polycarbonate	PC	3dXtech	Grand Rapids, MI. USA	Pellet	Virgin	Clear	158	16.42	0.2646
ABSt	Acrylonitrile Butadiene Styrene	ABS	LNS technologies	Scotts Valley, Ca. USA	Pellet	Virgin	Natural	154	20.75	0.20

2.2. Instrumentation.

2.2.1. Nexera UC online SFE-SFC-MS

A Nexera UC® online supercritical fluid extraction/supercritical fluid chromatograph instrument was used and directly coupled to an LCMS-8050 triple quadrupole mass spectrometer (Shimadzu Scientific Instruments, Kyoto, Japan). The system was equipped with a liquid carbon dioxide delivery unit (Nexera UC [LC-30AD_{SF}] CO_2 pump) and quaternary modifier infusion pump (Nexera X2 [LC-30AD] Liquid chromatograph) with degasser (DGU-20A_{3R}); a binary modifier pump (Nexera XR (LC-20AD_{XR}) liquid chromatograph) with degasser (DGU-20A_{5R}) for make-up flow; two backpressure control units [Nexera UC (SFC-30A) backpressure regulators], one post-column (BPR_A) and the other pre-column (BPR_B); a thermostatted column oven (Prominance (CTO-20AC)]; an autosampler (Nexera X2 [SIL-30AC] liquid injector); a supercritical fluid extraction unit (Nexera UC [SFE-30A] auto extractor) with 48-vessel automated rack changer II; and communications bus (CBM-20A). The system was accessorized with 0.2-mL extraction vessels and racks, with the option of standard-type or sinter-type vessel filters.

Instrument control and data acquisition were achieved using RealtimeAnalysis, and data post-processing using DataAnalysis (LabSolutions® chromatography workstation software, v.5.98, Shimadzu Corporation, Japan). Further data evaluation was done using Excel (Office 2010, v.14.0.7268.5000; Microsoft Corp., Redmond, WA. USA).

2.2.2. Columns

Chromatographic columns of various phases and dimensions were used during method development for SFC-based separation optimizations. Vendor information, phase chemistry, particle size and column dimensions are provided in **Table 5**. The Shim-pack UC-Cyano, (5.0 µm, 4.6 x 150 mm) column from Shimadzu Corp. (Tokyo, Japan) was utilized for all subsequent analyses for AAS in DBS. The Cosmosil cholester (5.0 µm, 4.6 x 250 mm) column from Nacalai Tesque, Inc. (Kyoto, Japan) was used for all online extractions of PAHs from microplastics.

2.2.3. Other Equipment

Nitrogen Generator. A Genius 1051 PSA nitrogen gas generator provided a continuous flow (up to 25 L/min) of dry gas and high purity nitrogen gas (≥ 97%) for instrument operation (Peak Scientific®, Billerica, MA. USA).

Cryogenic Grinder. A Retsch® CryoMill™ laboratory ball mill; equipped with stainless steel [SS] grinding accessories, including: 50 mL screw-top jars and 23 mm grinding balls; were obtained from Retsch GmbH (Verder Scientific, Haan, Germany).

Particle Analyzer. Particle size distribution via laser defraction was achieved with a Shimadzu Powder and Particle Size Analyzer (SALD-7500) and data analysis achieved using WingSALD II Particle Size Analysis Software (Shimadzu Corp. Japan, v.3.3.0).

Light Microscope. An Eclipse E100, binocular Light microscope (Nikon Instruments, Inc., Melville, NY. USA) was used for visual evaluation of particles larger than 800 µm diameter. The microscope was equipped with a high luminescent white LED illuminator, and CFI BE Plan Achromat Series objectives (4X [0.1/30 mm], 10X [0.25/7.0 mm], 40X (0.65/0.6 mm), 100X [1.25/0.14 mm]) for magnification. A set of ocular eyepiece lens calibration slides with high precision ruler grids were purchased (MUHWA Scientific, Shanghai, China). Three grid sizes were obtained (each 19 mm diameter): [Grid 1] C6-type, 0.2 mm net eyepiece ruler (Grid scale: 5x5 mm^2, divisions: 25 equal parts [0.04mm^2]); [Grid 2] C7-type, 0.1 mm ocular eyepiece cross ruler (grid scale: crossed rulers [each. 10mm long], divisions: 100 cells, 0.1mm each [x: 0.1mm; y: 0.1mm]); [Grid 3] C5-type, 0.5 mm net eyepiece ruler (grid scale: 5x5 mm^2, divisions: 10 equal parts [0.25mm^2]). Photographs were captured via an iPhone X, 12-megapixel (f/1.8, 1.22-micron) rear-camera (Apple Corp., Cupertino, CA. USA). Further image evaluation was performed using PowerPoint (Office 2010, v.14.0.7268.5000; Microsoft Corp., Redmond, WA. USA).

Large-capacity Shaker Table. A MaxQ 5000 Incubated Floor shaker table (Thermo Fisher Scientific, Waltham, MA. USA) was used for the preparation of exposed-microplastics laboratory controls. The tables combines

incubated temperatures with an orbital shaker for large capacity applications and was equipped with a 30 x 18 inch platform, with clamps removed.

Analytical Balances. Three balances were utilized during the presented work:

[A] a TW423L Analytical Balance (0.001g) Precision Scale with sliding glass doors and internal calibration was obtained from Shimadzu Corp. (Columbia, MD, USA);

[B] Sartorius CP64 Analytical Balance, (60 g x 0.1 mg; ± 0.1mg), Precision Scale with sliding glass doors was obtained from DWS (Wood Dale, Il, USA);

[C] Citizen CX165 Analytical Balance, (160g x 0.00001g ± 0.025 mg), Precision Scale with sliding glass doors. was obtained from Aczet, Inc. (Piscataway, NJ, USA).

Balance A was utilized for weighing 1g portions of milled plastic for transfer to sampling bags for microplastics exposure test sets. Balance B was used for weighing 10 mg portions of exposed µPs-RMs during vessel prep for Analysis, and for average pellet masses. Balance C was utilized for weighing cryomill jar contents for milling plastic pellets.

Table 5. Stationary Phase Vendor Information and Column Dimensions.

ID	Phase	Vendor (location)		Brand	Phase Trade Name	Particle Size (µm)	Dimensions (mm)
[2EP]	**2-ethylpyridine**	**Princton Chrom.**	(Cranbury, NJ. USA)	PrincetonSFC	2-Ethylpyridine	3.0	3.0 x 100
[NH2]	**amino**	**Agilent Technologies**	(Santa Clara, CA. USA)	Zorbax®	NH_2	5.0	4.6 x 150
[DIOL]	**diol**	**Daiso Fine Chem USA**	(Torrance, CA. USA)	DAISO	SP-60-5-Diol-P	5.0	4.6 x 150
[HILIC]	**silica (hilic)**	**Restek Corp.**	(Belefonte, PA. USA)	Raptor	HILIC-Si	2.7	4.6 x 150
[RX-SIL]	**silica**	**Agilent Technologies**	(Santa Clara, CA. USA)	Zorbax®	RX-SIL	1.8	3.0 x 150
[Z-CN]	**cyano**	**Agilent Technologies**	(Santa Clara, CA. USA)	Zorbax®	Cyano	3.5	4.6 x 150
[UC-CN]	**cyano**	**Shimadzu Corp.**	(Tokyo, Japan)	Shim-pack	UC-Cyano	5.0	4.6 x 150
[C18]	**C18**	**Phenomenex, Inc.**	(Torrance, CA. USA)	Luna®	C18(2)	5.0	4.6 x 150
[Cos]	**cholesteryl**	**Nacalai Tesque, Inc.**	(Kyoto, Japan)	Cosmosil®	cholester	5.0	4.6 x 250
[Cho]	**cholesteryl**	**Shimadzu Corp.**	(Tokyo, Japan)	Shim-pack	UC-Choles	5.0	4.6 x 250
[HyP]	**hydroxyphenyl**	**Shimadzu Corp.**	(Tokyo, Japan)	Shim-pack	UC-HyP	5.0	4.6 x 250
[Tri]	**triazolyl**	**Shimadzu Corp.**	(Tokyo, Japan)	Shim-pack	UC-Triazole	5.0	4.6 x 250
[PBr]	**pentabromobenzyl**	**Shimadzu Corp.**	(Tokyo, Japan)	Shim-pack	UC-PBr	5.0	4.6 x 250
[Py]	**Pyridinyl**	**Shimadzu Corp.**	(Tokyo, Japan)	Shim-pack	UC-HyP	5.0	4.6 x 250
[Px]	***np***	**Restek Corp.**	(Belefonte, PA. USA)	Raptor	PolarX	2.7	4.6 x 250

**np* = not provided (proprietary)

2.3. Solutions Preparation.

2.3.1. Solutions for Anti-Doping

2.3.1.1. AAS Stock Solutions.

Stock solutions were prepared for each AAS analytical standard in methanol at two concentrations (**Table 6; *stock solutions***). Once prepared solutions were transferred to glass scintillation vials for storage at -18 °C until the time of use.

AAS standards obtained as powders. A high concentration (500 ppm) stock solution [AASp-HC-stock] was prepared by accurately weighing 5.0 mg of powder on weigh paper, which was then transferred to a 10-mL (class A) volumetric flask and dissolved with MeOH. Solutions were sonicated for 20 minutes before being transferred for storage. Later a second stock solution was prepared for each of the powdered AAS standards by transferring 1.0 mL of the original AASp-HC-stock to a second 10-mL volumetric flask and diluted with MeOH and homogenized for a final concentration of 50 ppm [AASp-LC-stock].

AAS standards obtained as solutions (1.0 mg/mL) in ampules. A High concentration (100 ppm) stock solution [AASa-HC-stock] was made for each ampule by quantitatively transferring the contents to a 10-mL volumetric flask and diluting with MeOH. A second stock solution was prepared by transferring 5.0 mL of the AASa-HC-stock to a second 10-mL volumetric flask, where it was diluted with MeOH and homogenized for a final concentration of 50 ppm [AASa-LowC-stock].

Zeranol standard obtained as a (10µg/mL) solution. A High concentration (1 ppm) stock solution [ZRNL-HC-stock] was made by quantitatively transferring the ampule contents to a 10-mL volumetric flask and diluting with MeOH. A second stock solution was prepared by transferring 1.0 mL of the ZRNL-HC-stock to a second 10-mL volumetric flask, where it was diluted with MeOH and homogenized for a final concentration of 0.1 ppm [ZRNL-LC-stock].

Testosterone-d_3 internal standard obtained as (100 µL/mL) solution. A High concentration (10 ppm) stock solution [Td_3-HighC-stock] was made by quantitatively transferring the ampule contents to a 10-mL volumetric flask and diluting with MeOH. A second stock solution was prepared by transferring 1.0 mL of the ZRNL-HighC-stock to a second 10-mL volumetric flask, where it was diluted with MeOH and homogenized for a final concentration of 1.0 ppm [Td_3-LowC-stock].

2.3.1.2. AAS MS-Optimization Solutions.

Test solutions were prepared at a range of concentrations for each AAS standard by diluting stock solutions to 10, 5, 1, and 0.1 ppm, in small aliquots using a volumetric pipet and used immediately. High (100 and 50 ppm) and Low (0.5 and 0.05 ppm) solutions were made as-needed for individual compounds (**Table 6**; ***MRM Solutions***).

2.3.1.3. AAS Injection and Spiking Solutions.

AAS Test mixture [AAS-mix]. A test mixture was created by combining 0.100 mL of each of the stock solutions as follows: using the HC-stock (AASp-HC-stock) for each powder, the LowC-stock (AASa-LC-stock) for each ampule and the HighC spike for ZRNL (ZRNL-HC-stock). The resulting mixture was diluted with an additional 0.300 mL of MeOH to a final volume of 2.6 mL (final concentrations for each AAS are listed in **Table 6**; ***AAS-mix***. Making a final concentration of 20 ppm for each steroid standard originating from a powder and 2 ppm for each steroid standard originating from an ampule; with the exception of ZRNL, where the final concentration was 0.04 ppm, due to initial low concentration and high cost of the initial standard.

AAS Initial Calibration Mixture [AASc1,000]. An initial calibration mixture was created by combining 0.200 mL of the 50 ppm stock solution [LowC-stock] for each AAS (except ZRNL) into a 10-mL volumetric flask. For ZRNL 5.0 mL of the 1 ppm stock solution [ZRNL-HighC-Stock] was added to the same flask. And finally the internal standard, T-d_3, 0.250 mL of the 10 ppm stock [Td_3-LowC-stock] was also added to the same flask before filling to volume with MeOH. Making the final concentration of each AAS 1,000 ng/mL, with the exception of ZRNL which was 500 ng/mL, and the internal standard, Td_3, which was 250 ng/mL (**Table 7***; **Initial Calibration Mix**)*.

AAS Calibration Solutions. Calibration solutions were prepared by serial dilution of the initial calibration mixture (*AASc1,000*). All subsequent dilutions were done in 10-mL volumetric flasks using MeOH, to produce a total of nine calibration solutions [c1,000] 1,000 ng/mL, [c750] 750 ng/mL, [c500] 500 ng/mL, [c375] 375 ng/mL, [c250] 250 ng/mL, [c125] 125 ng/mL, [c050] 50 ng/mL, [c010] 10 ng/mL and [c000] 0 ng/mL. Final concentrations each AAS standard is provided in **Table 6*; AAS Calibration Solutions*.** In each dilution step before being brought to volume, the solution was first fortified with the appropriate amount of T-d_3 stock solution to ensure a constant final concentration of 250 ng/mL of the internal standard.

Table 6. **Anabolic Agents Stock and MRM Solution concentrations**

		Stock Solutions (ppm)		MRM Solutions (ppm)								
ID	Compound Name	HighC-Stock	LowC-Stock	MRM [100]	MRM [50]	MRM [10]	MRM [5]	MRM [1]	MRM [0.1]	MRM [0.5]	MRM [0.05]	AAS-mix Concentration (ppm)
1-DHEA	1-Androsterone	500	50	100	50	10	5	1	0.1	0.5	-	20
STEN	Androstenedione	100	50	-	-	10	5	1	0.1	0.5	-	2
ADAR	Andarine	500	50	100	50	10	5	1	0.1	-	0.05	20
ADEN	Androsterone	500	50	100	50	10	5	1	0.1	-	0.05	20
ADON	Androstanolone	100	50	-	-	10	5	1	0.1	0.5	-	2
CLNB	Clenbuterol	500	50	100	50	10	5	1	0.1	-	0.05	20
DNZL	Danazol	500	50	100	50	10	5	1	0.1	-	0.05	20
EPIT	Epitestosterone	100	50	-	-	10	5	1	0.1	0.5	-	2
ETIO	Etiocholanolone	500	50	100	50	10	5	1	0.1	-	0.05	20
GSTN	Gestrinone	500	50	100	50	10	5	1	0.1	-	0.05	20
KETO	7-Keto-DHEA	500	50	100	50	10	5	1	0.1	-	0.05	20
METD	Metandienone	100	50	-	-	10	5	1	0.1	-	0.05	2
MIBL	Mibolerone	500	50	100	50	10	5	1	0.1	0.5	-	20
MSAL	Mestanolone	500	50	100	50	10	5	1	0.1	0.5	-	20
MSEL	Mesterolone	500	50	100	50	10	5	1	0.1	0.5	-	20
MTHY	Methyltestosterone	500	50	100	50	10	5	1	0.1	0.5	-	20
MTRB	Metribolone	500	50	100	50	10	5	1	0.1	0.5	-	20
OXAN	Oxandrolone	500	50	100	50	10	5	1	0.1	0.5	-	20
PRST	Prasterone (DHEA)	500	50	100	50	10	5	1	0.1	0.5	-	20
STNZ	Stanozolol	100	50	-	-	10	5	1	0.1	-	0.05	2
TRNB	Trenbolone	100	50	-	-	10	5	1	0.1	-	0.05	2
TSTO	Testosterone	100	50	-	-	10	5	1	0.1	-	0.05	2
ZRNL	Zeranol	1	0.1	-	-	-	-	1	0.1	-	0.05	0.04
T-d3	Testosterone-d_3	10	1	-	-	10	5	1	0.1	-	-	-

Table 7. **Anabolic Agents Calibration Solutions**

ID	Compound Name	Initial Calibration Mixture (ng/µL)	AAS Calibration Solutions (ng/µL)									AAS Calibration Spiked-DBS Concentrations (ng/mL)									Testosterone Spiking Solution [TSTOv500] (ng/mL)
			c1,000	c750	c500	c375	c250	c125	c50	c10	c0	v200	v150	v100	v75	v50	v25	v10	v2	v0	
1-DHEA	1-Androsterone	1,000	1,000	750	500	375	250	125	50	10	0	200	150	100	75	50	25	10	2	0	0
STEN	Androstenedione	1,000	1,000	750	500	375	250	125	50	10	0	200	150	100	75	50	25	10	2	0	0
ADAR	Andarine	1,000	1,000	750	500	375	250	125	50	10	0	200	150	100	75	50	25	10	2	0	0
ADEN	Androsterone	1,000	1,000	750	500	375	250	125	50	10	0	200	150	100	75	50	25	10	2	0	0
ADON	Androstanolone	1,000	1,000	750	500	375	250	125	50	10	0	200	150	100	75	50	25	10	2	0	0
CLNB	Clenbuterol	1,000	1,000	750	500	375	250	125	50	10	0	200	150	100	75	50	25	10	2	0	0
DNZL	Danazol	1,000	1,000	750	500	375	250	125	50	10	0	200	150	100	75	50	25	10	2	0	0
EPIT	Epitestosterone	1,000	1,000	750	500	375	250	125	50	10	0	200	150	100	75	50	25	10	2	0	0
ETIO	Etiocholanolone	1,000	1,000	750	500	375	250	125	50	10	0	200	150	100	75	50	25	10	2	0	0
GSTN	Gestrinone	1,000	1,000	750	500	375	250	125	50	10	0	200	150	100	75	50	25	10	2	0	0
KETO	7-Keto-DHEA	1,000	1,000	750	500	375	250	125	50	10	0	200	150	100	75	50	25	10	2	0	0
METD	Metandienone	1,000	1,000	750	500	375	250	125	50	10	0	200	150	100	75	50	25	10	2	0	0
MIBL	Mibolerone	1,000	1,000	750	500	375	250	125	50	10	0	200	150	100	75	50	25	10	2	0	0
MSAL	Mestanolone	1,000	1,000	750	500	375	250	125	50	10	0	200	150	100	75	50	25	10	2	0	0
MSEL	Mesterolone	1,000	1,000	750	500	375	250	125	50	10	0	200	150	100	75	50	25	10	2	0	0
MTHY	Methyltestosterone	1,000	1,000	750	500	375	250	125	50	10	0	200	150	100	75	50	25	10	2	0	0
MTRB	Metribolone	1,000	1,000	750	500	375	250	125	50	10	0	200	150	100	75	50	25	10	2	0	0
OXAN	Oxandrolone	1,000	1,000	750	500	375	250	125	50	10	0	200	150	100	75	50	25	10	2	0	0
PRST	Prasterone (DHEA)	1,000	1,000	750	500	375	250	125	50	10	0	200	150	100	75	50	25	10	2	0	0
STNZ	Stanozolol	1,000	1,000	750	500	375	250	125	50	10	0	200	150	100	75	50	25	10	2	0	0
TRNB	Trenbolone	1,000	1,000	750	500	375	250	125	50	10	0	200	150	100	75	50	25	10	2	0	0
TSTO	Testosterone	1,000	1,000	750	500	375	250	125	50	10	0	200	150	100	75	50	25	10	2	0	500
ZRNL	Zeranol	500	500	375	250	188	125	63	25	5	0	100	75	50	37.5	25	12.5	5	1	0	0
T-d3	Testosterone-d_3	250	250	250	250	250	250	250	250	250	250	50	50	50	50	50	50	50	50	50	250

2.3.2. Solutions for Microplastics work.

2.3.2.1. PAHs Stock Solutions (Table 8; *Stock concentrations*).

Stock solutions were made for individual PAH standards by weighing 20.00 mg with weigh paper. Weighed powder was transferred to 10-mL volumetric flasks and dissolved in MeOH to produce a final concentration of 2.00 mg/mL. ANRN, BAPY, IDPY, BBFA, and BKFA could not be dissolved at this concentration, and therefore were made with 5.00 mg of powder instead producing a 0.5 mg/mL final stock solution concentration. For DBAR and CHSY, 5.00 mg of powder were dissolved using 25.0 mL volumetric flasks to produce a final stock concentration of 0.20 mg/mL. And finally for BGPY, 5.00 mg of powder were dissolved using 100.0 mL volumetric flasks to produce a final stock concentration of 0.05 mg/mL.

2.3.2.2. PAHs Spiking Solutions for Microplastics Exposure solutions.

High concentration Spiking solution **([HC:PAHs]; 1,250 ng/g).** A high concentration spiking solution [HC:PAHs] was created by combining 0.100 mL of each of the 2.0 mg/mL stocks; 0.400 mL of each of the 0.5 mg/mL stocks; 1.00 mL of the 0.2 mg/mL stocks; and finally 4.00 mL of the 0.05 mg/mL stock solutions. The final volume was brought to 12.8 mL with MeOH to produce a final concentration where a spike volume of 80.0 µL would represent 1250 ng of each PAH standard.

Low concentration Spiking solution **([LC:PAHs]; 50 ng/g).** A low concentration spiking solution [LC:PAHs] was created by transferring 0.400 mL of the high concentration spiking solution (HC:PAHs) to a 10-mL volumetric flask and bringing to volume with methanol. The final concentration provides 50 ng of each PAH standard in a spike volume of 80.0 µL.

Table 8. Polycyclic Aromatic Hydrocarbons Solution Concentrations.

ID	PAH Standard	Stock Concentration (mg/mL)	High Concentration Spiking Solution **[HC:PAHs]** (ng /80µL spike)	Low Concentration Spiking Solution **[LC:PAHs]** (ng /80µL spike)
ACEN	acenaphthalene	2.00	1250	50
ANPY	acenaphthylene	2.00	1250	50
ANRN	anthracene	0.50	1250	50
BARC	benzo[*a*]anthracene	2.00	1250	50
BAPY	benzo[*a*]pyrene	0.50	1250	50
BBFA	benzo[*b*]fluoranthene	0.50	1250	50
BGPY	benzo[*g,h,i*]perylene	0.05	1250	50
BKFA	benzo[*k*]fluoranthene	0.50	1250	50
CHSY	chrysene	0.20	1250	50
DBAR	dibenzo[*a,h*]anthracene	0.20	1250	50
FLAT	fluoranthene	2.00	1250	50
FLUR	fluorene	2.00	1250	50
IDPY	indeno[1,2,3-*cd*]pyrene	0.50	1250	50
NAPL	naphthalene	2.00	1250	50
PHNR	phenanthrene	2.00	1250	50
PYRN	pyrene	2.00	1250	50
A-d10	acenaphthene-d_{10}	-	-	-
B-d12	benzo[*e*]pyrene-d_{12}	-	-	-
C-d12	chrysene-d_{12}	-	-	-
F-d10	fluoranthene-d_{10}	-	-	-
N-d8	naphthalene-d_8	-	-	-

2.4. Sample Preparation: Micro-Dried Blood Spot (Micro-DBS)

2.4.1. Micro-DBS Sampling Technique

For blood sampling, a micro-spotting technique was implemented. This was beneficial in overcoming the variability inherent to blood sampling due to differences in hematocrit between donors. As the entire sample (whole spot) was excised from the card for analysis. An added benefit of this technique is that samples and QCs can be applied and collected from a single card. As long as the diameter of the spot did not exceed the diameter of the hole puncher (6mm); volumes could later be calculated directly from the volumetric application.

Blood application pre-tests were performed using volumetric pipettes by applying 100, 80, 60, 40, 20, 10, and 5 µL whole blood to cellulose based sample collection cards. The volume that created a spot with diameter < 6mm was chosen. Both 10 µL and 5 µL of blank bovine blood did not exceed the 6mm punch size. But MeOH (applied at 30, 25, 20, 15, 10, 5, 3 and 1 µL) was observed to spread farther on the card than blood (methanol shown with red food dye added for visual assessment). Therefore a 5.0 µL blood spotting volume was chosen for further testing, enabling ample excess blank paper to surround each spot, so that when MeOH was added (for spiked and blank quality controls [Micro-QCs]), it would not exceed the punch size sampling area.

Final spot tests were performed using a 5.0 µL spotting volume for blank blood; 1.0 µL for MeOH-only blanks and QCs; and 6.0 µL for spots containing both blood and MeOH. Final spot tests were performed on bovine and human blood (male and female), and in all cases the spotting volume did not exceed the 6 mm punch size, and therefore these volumes were utilized for the remainder of the work.

All spots were collected using a single-hole punch producing a 6 mm paper core. The entire spot was excised in all cases. Three separate cards were prepared for each type of blood (bovine and human [male & female]). On each card four replicate spots were applied for each spot type. Cards were allowed to dry, elevated, for at least 3 hours, before spots were excised. Punchers were cleaned thoroughly by sonication in two consecutive methanol baths for 20 min and allowed to dry completely, between each spot type.

2.4.2. Quality Controls and Blanks.

Blood collection cards contain a preservative. Therefore, to evaluate potential matrix effects, a blank portion of each card (Paper blank [Pøøø]) was cored in triplicate and analyzed for comparison. Additional quality control spots [micro-QCs] were prepared in triplicate on each collection card; using 1.0 µL blank methanol with no blood (MeOH QC [PøMø]); and 1.0 µL of the AAS-mix spiking solution (Steroid standards [PøMA]). Blanks of each type of blood (blank blood: Bovine [PBøø]; Female [PFøø]; and male [PMøø]) and blank blood with blank methanol (blood:MeOH QCs: bovine [PBMø]; female [PFMø] and male [PMMø]) were also used to evaluate potential interferences.

2.4.3. Micro-DBS Spot Types.

(0) Blank Paper QC	6 mm paper core
(1) MeOH QC	1.0 µL Blank MeOH applied
(2) Steroid Standards	1.0 µL AAS-mix
(3) Blood	5.0 µL whole Blood
(4) Blood : MeOH QC	5.0 µL Blood + 1.0µL Blank MeOH*
(5) Spiked Blood	5.0 µL Blood + 1.0µL AAS-mix*

* Spiked spot volume = 6µL = Total volume applied to card of mixture

Mixture = [1:5 MeOH : blood]; 40µL methanolic AAS-mix in 200 µL blank blood, mixed and sonicated for 20 minutes.

2.4.4. Micro-QCs for SFE Extraction Optimization

The same steroid mixture (AAS-mix) was used in both the SFC and SFE method screenings. In the SFC screening 1.0 µL injections were used, and therefore for SFE method development, 1.0 µL spots of the same standard mix was quantitatively applied to the Whatman collection cards, allowed to dry for 3 hours, then cored using the single hole punch (PøMA).

2.4.5. Micro-DBS sets for Method Evaluations & Matrix-specific optimizations.

The three replicate cards created with bovine blood were used for initial matrix-specific method evaluation and optimizations.

2.4.6. Micro-DBS sets for Matrix Evaluations

The three cards prepared using human blood (male & female) were used to perform a comprehensive evaluation of the sampling matrix. For each card, three replicate spots of each spot-type were extracted online using SFE-SFC-MS for comparison.

2.5. DBS Validation

2.5.1. Micro-DBS sets for Validation

Calibration spiking solutions using a mixture of the target analytes, were created by 9-fold serial dilution (see **Section 2.3.1.3. AAS Injection and Spiking Solutions; *AAS Calibration Solutions*).** The target analytes were spiked into whole blood specimens to attain final concentrations between 0 and 100 ng/mL. The concentration of the internal standard (T-d3) was held constant at 50 ng/mL blood for all spots.

Calibration Spots for Linearity. Calibrations spots were created by spiking 100 µL of AAS calibration solution into 500 µL of blank bovine blood, the mixture mixed thoroughly by sonication for 20 minutes before 6.0 µL was spotted, allowed to dry for at least 3 hours, cored and stored for immediate use. A separate collection card was used for each calibration concentration and/or spot type to avoid cross contamination. Separate aliquots from the same stock of whole blood were prepared at the same time to make nine calibration concentrations (ng/mL blood): [v200] 100 ng/mL, [v150] 150 ng/mL, [v100] 100 ng/mL, [v075] 75 ng/mL, [v050] 50 ng/mL, [v025] 25 ng/mL, [v010] 10 ng/mL, [v002] 2 ng/mL, and [v000] 0 ng/mL. Final concentrations of each AAS standard is provided in **Table 8; *Spiked-DBS Concentrations***, and especially should be referenced in for interest in ZRNL, as the concentrations are half that of the other standards present due to the high cost and low concentration of the original standard.

Calibration spots for Precision and Accuracy. Replicate spots sets of spots of the v25, v50 and v100 type spots were created for use evaluation of accuracy and inter, and intra-day precision.

Stability Spots. Replicate sets of the v100 calibrations spots were made and stored at stored at 4° C for evaluation of stability.

Matrix Spots. A replicate set of the v100 calibrations spots were made for evaluation of matrix effects. Additionally spots were created using 1.0 µL of the c500 calibration solution with no blood present were applied to the same card for comparison.

Robustness Spots. Replicate sets of v100 were made for evaluation of robustness. Additionally spots were created using a 1.0 µL spotting volume of the c000 calibration solution with no blood present were applied to the same card for comparison.

Specificity Spots. Blank blood from 6 bovine and 12 human donors (6 male and 6 female) were used to make 5.0 µL spots for evaluation of specificity. Replicate sets of v100 spiked calibration spots were made for each type of blood evaluated for reference.

2.5.2. Micro-DBS Validation

Linearity. An external calibration curve was created for each AAS using spotted spiked-blood as described above. Concentrations are reported in ng/mL of blood. The calibration curve was established with at least five concentration points (with 3 spots [n = 3] extracted per concentration). The range was considered to be linear if the square of the regression coefficient (R^2) > 0.99 and the accuracy of all points was < ± 15% (< ± 20% for the lowest concentration).

Accuracy. Whole blood samples spiked at three concentrations of the target analytes: low (25 ng/mL); medium (50 ng/mL); and high (100 ng/mL). Accuracy was determined as the percent bias between the actual spiked concentration and the measured concentration calculated by the calibration curves.

Precision. Inter- and intra-day precision was determined using whole blood samples spiked at three concentrations of the target analytes: low (25 ng/mL); medium (50 ng/mL); and high (100 ng/mL). Precision was calculated as percent relative standard deviation (%RSD) from a three-fold determination (3 replicate vessels) at three concentration levels and on two consecutive days.

Level of Detection (LOD). In MRM-mode, essentially negligible noise, prevents accurately calculating the LOD by using the standard deviation of the signal. Therefore the LOD was instead estimated (multiplying the standard deviation by three and dividing by the slope of the calibration curve). A spiking mixture was created using the estimated LOD of each analyte [LOD-mix]. Whole blood samples were spiked with the LOD-mix, spotted and cored

and analyzed in triplicate. The lowest concentration that could be successfully detected (signal-to-noise ratio of 3) was reported as the LOD and verified by preparing spots with a spiking mixture at ½ that concentration [1/2LOD-mix], and confirmed that no signal was observed.

Level of Quantitation (LOQ). LOQs were determined by estimation using 3.5 times the LOD. A spiking mixture was created using the estimated LOQ of each analyte [LOQ-mix]. Whole blood samples were spiked with the LOQ-mix, spotted and cored and analyzed in triplicate. The concentrations that produced signals with a coefficient of variance of < 15% were determined to be the LOQ.

Stability. Whole blood samples spiked at a concentration of 100 ng/mL were spotted, cored and stored under two conditions (room temperature and 4° C), and later analyzed in triplicate, after 7 and 14 days of storage.

Specificity. Micro-DBS from three (n=6) healthy donors (3 female and 3 male) were analyzed in triplicate for the presence of interfering signals at the respective retention times of the analytes.

Matrix Effect. Matrix effects were investigated by comparing the peak areas of online extracts of spiked blood (PBMAv100; at 100 ng/mL) to the peak areas of online extracts of paper spiked with the same solvent matrix with no blood present (PoMAc500). Matrix effects are reported in % of the area observed with no blood present.

Robustness. The robustness regarding the difference between cards was evaluated by spotting aliquots of fortified blood samples of three separate cards and comparing them to blank cards to visually examine for interfering signals.

2.5.3. Micro-DBS fortified 'Doped' Blood.

Human plasma (PLA1) was diluted with red blood cells from type O^- donors (RBC1) at a ratio of 6:4 (PLA1:RBC1) to mimic the expected average hematocrit (40%) for the adult population. To make fortified samples, the plasma was first spiked with a solution containing testosterone and internal standard to produce a final concentration of 100

ng/mL and 50 ng/mL, respectively. The mixture was then incubated with mixing (at 37° C) for 1 hour. Micro-DBS were spotted onto a blank collection card, allowed to dry, cored, and stored at 4° C until use.

Blank Plasma QC **[oPoo]** **(Final spot represents = 3µL of Plasma).** Blank plasma (PLA1) were incubated and then 3.0 µL was directly spotted.

Spiked Plasma QC **[oPMTv100]** **(Final spot represents = 3µL of Plasma + 1µL TSTO).** Six hundred microliters of plasma (PLA1) was spiked with 200 µL spiking solution (TSTOc500) before incubation. Micro-DBS were created by spotting 4.0 µL ***oPMTv100*** onto a blank collection card.

Blank Plasma:Blood QC **[RPMTv000]** **(Final spot represents = 3µL of Plasma + 2µL RBC).** Six hundred microliters of plasma (PLA1) was diluted with 400 µL of RBC1, before incubation. Micro-DBS were created by spotting 5.0 µL ***RPMAv0*** onto a blank collection card.

"Doped' Plasma:Blood [RPMTv100] **(Final spot represents = 3µL of Plasma + 2µL RBC + 1µL TSTO).** Six hundred microliters of plasma (PLA1) was spiked with 200µL spiking solution and then diluted with 400µL of RBC1 [6:4:2], before being incubated. Micro-DBS were created by spotting 6.0 µL ***RPMTv100*** onto a blank collection cards.

2.6. Sample Preparation: Microplastics Reference Materials

2.6.1. Plastics Initial Pellet Evaluation.

Average weight per pellet. For each plastic, 3 aliquots of 20 pellets were separated, weighed, and the average and standard deviation (n=3) was calculated. An average weight (mg) and SD for a single pellet was then calculated by dividing the average of the three replicate measurements by 20.

Determination of Optimal Milling weight. To ensure homogenous particle size, optimal grinding volumes for each plastic type, was determined by an initial round of milling tests. The material produced during this initial test was stored separately from and not included in the final stocks of reference materials. Plastic pellets of each plastic type were cryomilled to a fine powder using an initial starting weight of 12.00 g of pellets for each type of plastic, the resulting powder was evaluated for particle consistency and that a smaller sized diameter was achieved. If too course (e.g., large chunks remained un-milled) the volume would be reduced by 1.00 g increments in succeeding milling rounds until an acceptable consistency was observed for three consecutive milling rounds, this milling weight was considered to be optimal for that particular plastic.

2.6.2. Milling of Microplastics Reference Materials (µPs:RMs)

Plastic Pellets of each plastic type were cryomilled to a fine powder using the optimal milling weight. Each plastic was milled in consecutive rounds until a total of 60 g had been processed. The material collected from each milling round for a single plastic was combined and homogenized before being transferred to several large storage drams for later use.

Grinding Method. CryoMilling was accomplished through cryogenic grinding (at -196° C) using LN_2 as cryogenic coolant. Weighed plastics were enclosed inside a grinding jar with a single 23 mm SS grinding ball, and placed inside CryoMill. The auto pre-cooling function was used. Three cryo cycles were used with intermediate cooling between each cycle. The shaking frequency was set to 30 Hz and a grind duration of 3 minutes for each cycle.

2.6.3. Size Analysis via light microscope (for Particles Larger than 800 µm Diameter).

Metal spatula was used to scoop a small portion of plastic powder directly from homogenized stock. Care was taken to make sure the distribution of particle sizes seemed to reasonably represent the stock as a whole [this was evaluated visually]. Water was added and a top slide cover, to ensure particles were spread evenly across the grid. In all situations, a photo was taken once an appropriate view was obtained that the user believed was representative for the whole sample. Photographs were captured directly thru the microscope eyepiece. Photos were then analyzed visually on a computer (in Microsoft PowerPoint) by zooming in on particles of interest. Approximation of maximum and minimum diameter was recorded by mark up on the picture.

Smallest diameter particle (mm) was approximated (as described above) using Grid 1, under 4X magnification.

Largest diameter particle (mm) was approximated (as described above), using Grid3, under 20X magnification.

Approx. average particle diameter (mm), was determined using Grid 2, under 10X magnification.

Visual modal, was approximated (on a scale 1-10) by the user, using the optimal Grid for each plastic type;

- where (1) would indicate that the majority of particles present were closest to the smallest diameter particle;
- and (10) would indicate that the majority of particles present were closest to the Largest diameter particle;
- A range may also be indicated (e.g., 5-7; would indicate that the majority of the particles were larger than the a median but smaller than the largest particles observed).

The visual modal is not meant to be a precise measurement, more to give an overall feeling to the distribution of the sample.

2.7. Sample Preparation: Exposed-Microplastics

2.7.1. Microplastics sample bags.

Sampling bags were made by weighing 1.00 g µPs-RMs and placing in a 25 µm mesh nylon bag. Bags were made from homogenized stock for five types of plastic: LDPE, HDPE, PETE, PP and ABSt. Bags were closed with a short portion of rope for suspension and a colored ziptie to mark the plastic type. Average weight per bag (and standard deviations) were calculated for each plastic type

2.7.2. Marine-Exposed Microplastics [µPs:Marine].

Sample sets were exposed to marine environments, in shallow inter-coastal mangrove protected shoreline. In late spring, early summer 2021, five replicate bags for each plastic were deployed in three separate locations, all within Lemon Bay on the west coast of central Florida, USA.

Study Area. Lemon Bay is located in Charlotte County, Florida and Sarasota County, Florida. It is a long, shallow intercoastal waterway, fed by one major outlet to the Gulf of Mexico (Stump pass), and seven tributaries. The Field location for Marine-exposed microplastic samples is shown in **Figure 20**. Three sampling sites were chosen in close proximity to the Gulf outlet to ensure maximum water circulation and boat traffic. Sample deployment locations in relation to boat traffic and water circulation from Stump Pass: (O) Outlet sample set; (C) Inter-Coastal sample set; (S) Sheltered sample set (**Table 9**).

Table 9. Marine-Exposed Microplastics Sample Deployment Sites

Site	ID	Short Description	General Water Circulation	Sample depth	Boat Traffic
Outlet	[O]	Major gulf outlet	Direct from Gulf	Submerged	High
Intercoastal	[C]	Intercoastal boat traffic	Tidal	Tidal	High
Sheltered	[S]	Sheltered Lagoon	Tidal	Submerged	Low

Sample Deployment. Exposure-sets were created, and collected after 1, 7, and 14 days of exposure. Each set contained 5 replicate bags for each plastic. Bags were suspended from wooden frames that were then secured and submerged, where care was taken to allow maximal submersion at each location. At the time of collection, each bag was rinsed individually using three consecutive fresh water baths. The content was then removed from the bag and spread over a petri dish for final drying (~12 hours in a fume hood), before being transferred to amber glass storage drams and stored (protected from light) at room temperature until the time of use. Samples were inspected for signs of marine-life interference, and when applicable, observations were noted for each sample at the time of drying.

Field collected control water. Surface water was collected one year prior to sample deployment (**Figure 20).** *SeaH_2O* collection site [*]) in Six 1.5L bottles and transported back to the laboratory for use in lab controlled exposure tests.

Ambient Conditions. Meteorological data was obtained from the National Oceanic and Atmospheric Administrations (NOAA) National Data Buoy Center from the closest meteorological buoy (Station 42013 - C10 - WFS Central Buoy, 25m Isobath: 27°10'23" N 82°55'26" W) historical database for the period of time of sample deployment. Air temperature (ATMP) and Sea surface water temperature (WTMP) and salinity (SAL) were obtained and averages calculated for the two week period samples were deployed. Average air temperature = 20.8 ± 2.0° C (n = 668); average water temperature = 21.1° C (n=668); Average salinity = 35.9 ± 3.5 psu (n = 670).

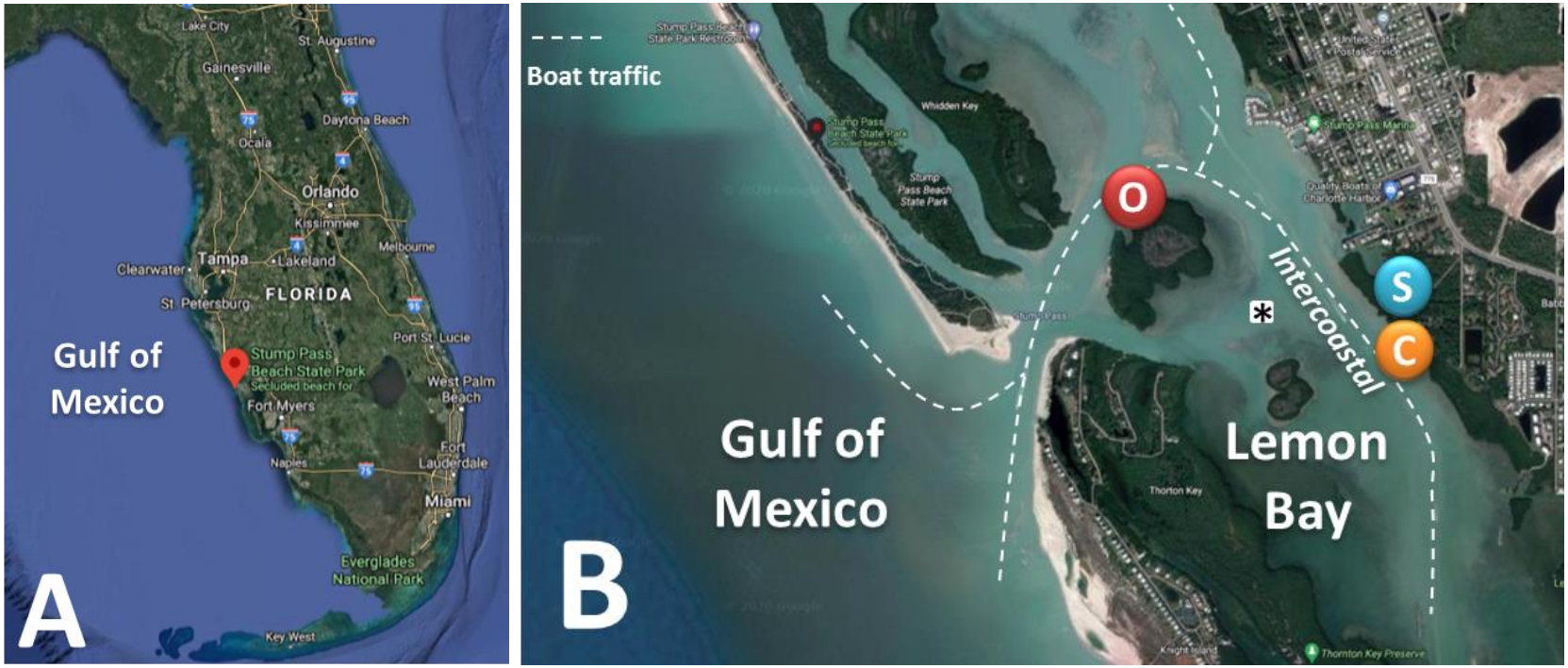

Figure 20. Field Location for Marine-exposed Microplastic Samples showing [A] Lemon Bay, location on the western central Gulf Coast of Florida, USA.; and [B] Sample deployment locations in relation to boat traffic and water circulation influx thru Stump Pass, a major outlet to the Gulf. *(O) Outlet sample set; (C) Inter-Coastal sample set; (S) Sheltered sample set; (*) Collection Site for Field Control Exposure solution [SeaH_2O].*

2.7.3. µPs:PAHs Laboratory-exposed Blanks and QCs.

Individual sampling bags were suspended in 125 mL clear glass bottles, where 50 mL exposure solution was added. Bottles were closed and placed inside a box to protect them from light. The box was then placed inside a thermostatted, large capacity, shake table, and shaken (at 50 rpm, ~32° C) for a duration of time. Exposure test-sets were created, and collected after 1, 7, and 14 days of exposure. At the time of collection, the water was immediately removed and each bag rinsed individually using three consecutive fresh water baths. The content was then removed from the bag and spread over a petri dish for final drying (~12 hours in a fume hood), before being transferred to amber glass storage drams and stored (protected from light) at room temperature until the time of use.

The location of bottles from each test set were randomized to ensure minimal effects of temperature or motion differences between bottle location within the shake table chamber.

2.7.4. Laboratory control Exposure Solutions.

Laboratory control exposure solutions were aqueous based, and were either: 'fresh water' -or- 'salt water'

Laboratory Control Water **[qH_2O].** 'fresh water' was Milli-Q grade and filtered on-site;

Field Control Water **[Sea-H_2O].** 'salt water' was marine water, which was collected from the field location where samples were deployed (**Figure 20**).

2.7.5. Lab Control Test-Sets.

For each plastic, 3 control test-sets were created; One for each collection day: 1, 7 and 14 days of exposure. Each test-set included: a null, having no water at all; a blank of each water type; and triplicate high and low spiked samples for each plastic (for example on day 1, forty-five bottles would be collected; 15 for each microplastic):

Lab Null (1x/test-set). To control for the possibility of inherent contamination of the sampling materials and/or degradation of the target compounds due to light or temperature; a null was made for each plastic by

suspending a sample bag in an empty bottle with no water added. The bottle was then exposed to the same test conditions, and once collected, the contents treated as any other sample (i.e., washed and spread to dry).

Lab Blank **([qH$_2$O:Blank]; 1x/test-set).** To control for the possibility of PAH contamination in the on-site Milli-Q filtering system, a milli-Q water blank was created [Q-H$_2$O:Blank] for each plastic by suspending sample bags in bottles with 50 mL blank milli-Q water. The bottle was then exposed to the same test conditions, and once collected, the contents treated as any other sample.

Field Blank **([SeaH$_2$O:Blank]; 1x/test-set).** To control for the possibility of PAH contamination during transport of field-collected control water, a blank was created for each plastic by suspending sample bags in bottles with 50 mL blank Sea-Water [Sea-H$_2$O:Blank]. The bottle was then exposed to the same test conditions, and once collected, the contents treated as any other sample (i.e., washed and spread to dry).

High Concentration Laboratory Control samples **([qH$_2$O:HC], 3x/test-set).** High concentration lab controls were created in triplicate for each plastic by suspending sampling bags in bottles with 50 mL of Milli-Q water spiked with 80 µL of the high concentration spiking solution (HC:PAHs), ultimately exposing the bag (1.0 g of µPs-RMs) to 1,250 ng of each PAH standard.

High Concentration Field Control samples **([SeaH$_2$O:HC], 3x/test-set).** Low concentration field controls were created in triplicate for each plastic by suspending sampling bags in bottles with 50 mL of Sea-water spiked with 80 µL of the high concentration spiking solution (HC:PAHs).

Low Concentration Laboratory Control samples **([qH$_2$O:LC], 3x/test-set).** Low concentration lab controls were created in triplicate for each plastic by suspending sampling bags in bottles with 50 mL of Milli-Q water spiked with 80 µL of the low concentration spiking solution (LC:PAHs).

Low Concentration Field Control samples **([SeaH$_2$O:LC], 3x/test-set).** Low concentration field controls were created in triplicate for each plastic by suspending sampling bags in bottles with 50 mL of Sea-water spiked with 80 µL of the low concentration spiking solution (LC:PAHs).

Bag QC Check (1x/plastic). Acknowledging that the presence of the nylon bag during exposure, also being made of plastic, may have an effect, to evaluate this a 10.0 mg portion of bag (before and after 14-days exposure) was excised and placed directly into a vessel for online extraction to evaluate for any positive or negative effect.

2.8. General Workflow for Online Extractions.

Online extractions were performed using 0.2-mL vessels, with no desiccant added. All samples were placed directly into empty, clean, dry, extraction chambers. The automated rack changer was programmed (and calibrated) for the use with 0.2-mL vessels and equipped with 0.2-mL vessel racks. Pragramming of the rack changer was accomplished on the front panel of the module. Calibration for the extractor needle position was additionally necessary, and was accomplished by a Shimadzu service representative. The special torque wrench (**1.5 N-m)** for 0.2-mL vessels was used at all times to close and open the vessels.

2.8.1. Vessel filters

Vessel filters used for all extractions from the Whatman paper (e.g., Anabolic Agents, DBS, and Anti-doping analysis) were performed using the standard 0.2-mL vessel filters (Screen-type filter, SSI Part #: 228-59264-84). Although either type of filter could be used for extraction from the paper, the screen-type filters are adequate to retain the paper within the extraction vessel during analysis, are less expensive and less specialized, and therefore are preferred for this type of analyisis. For extractions of microplastics, the special sinter-type 0.2-mL vessel filters were required at all times (SSI Part #: 228-59264-81). Failure to use the appropriate filter-type during the analysis of fine particles will result in damage to the instrument.

2.8.2. Vessel cleaning

Vessels were prepared for use in online extractions by being washed in two consecutive fresh MeOH baths. Vessel filters were separated from the main body parts (lids, body, and spacer) in a separate large beaker. The parts submerged, and sonicated for 20 minutes. The methanol removed and re-submerged with fresh methanol and sonicated a second time. A final rinse with LCMS-grade methanol completes the washing cycle. Individual parts were then spread in a single layer over paper towel to dry under ambient conditions.

2.8.3. Vessel assembly

The smaller 0.2-mL vessels are not as rugged as the 5.0-mL vessels. Mis-alignment of parts will very quickly result in damage to the cap threads (e.g., through burring of the metal). Care must be taken to not damage the body, thru mis-alignment or over-tightening. Vessels were carefully matched previous to use for best fit-alignment of all parts. Vessels were only fully closed if the screw cap would slide freely without force (approximately 3 full turns). Once assembled, final closure was accomplished with the appropriate torque wrench and subject to a 'rattle/shake' test. A rattle test was used where each vessel was lightly shaken after assembly to check for moving parts (which would indicate mis-alignment of the internal parts and would result in a leak during analysis). Vessels in which failed the shake test would be taken apart and re-assembled if possible to not contaminate or loose sample.

2.9. General Data Processing Approaches.

Three replicate vessels (i.e., three replicate samples [ex. Cores]) were used for each sample/condition, and were referred to with lower-case letters: the first replicate vessel **[a];** the second replicate vessel **[b];** and third replicate **[c]**. Each vessel was extracted three consecutive times: the first extraction **[EXT1]**; the second extraction **[EXT2]**; and third extraction **[EXT3]**. All other sample IDs referring to replicate conditions (for example, collection cards, sampling locations, etc.) used numbers or capital letters as reference for clarity. Area refers to the integrated area under the peak for an individual compound. Example bar plots are given.

2.9.1. Total Area Extracted.

Total Area Extracted per vessel **[T_{Area}/vessel].** The total area extracted per vessel [T_{Area}/vessel] was calculated by summing the area from all three consecutive extractions [EXT1 + EXT2 + EXT3] for a single vessel (**Figure 21; top**).

Total Area Extracted **[T_{area}].** The total area extracted [T_{area}] was calculated by summing the total area extracted per vessel (T_{Area}/vessel) for all replicate vessels (a + b + c) of a sample-type (**Figure 21; middle**).

2.9.2. Average Total Area.

Average Total Area Extracted **[Av_{total}].** The average total area extracted [Av_{total}] was calculated by taking the average and standard deviation of the total area extracted per vessel (T_{area}/vessel) using all replicate vessels [a : b : c (n = 3)] of a sample-type (**Figure 21; bottom**).

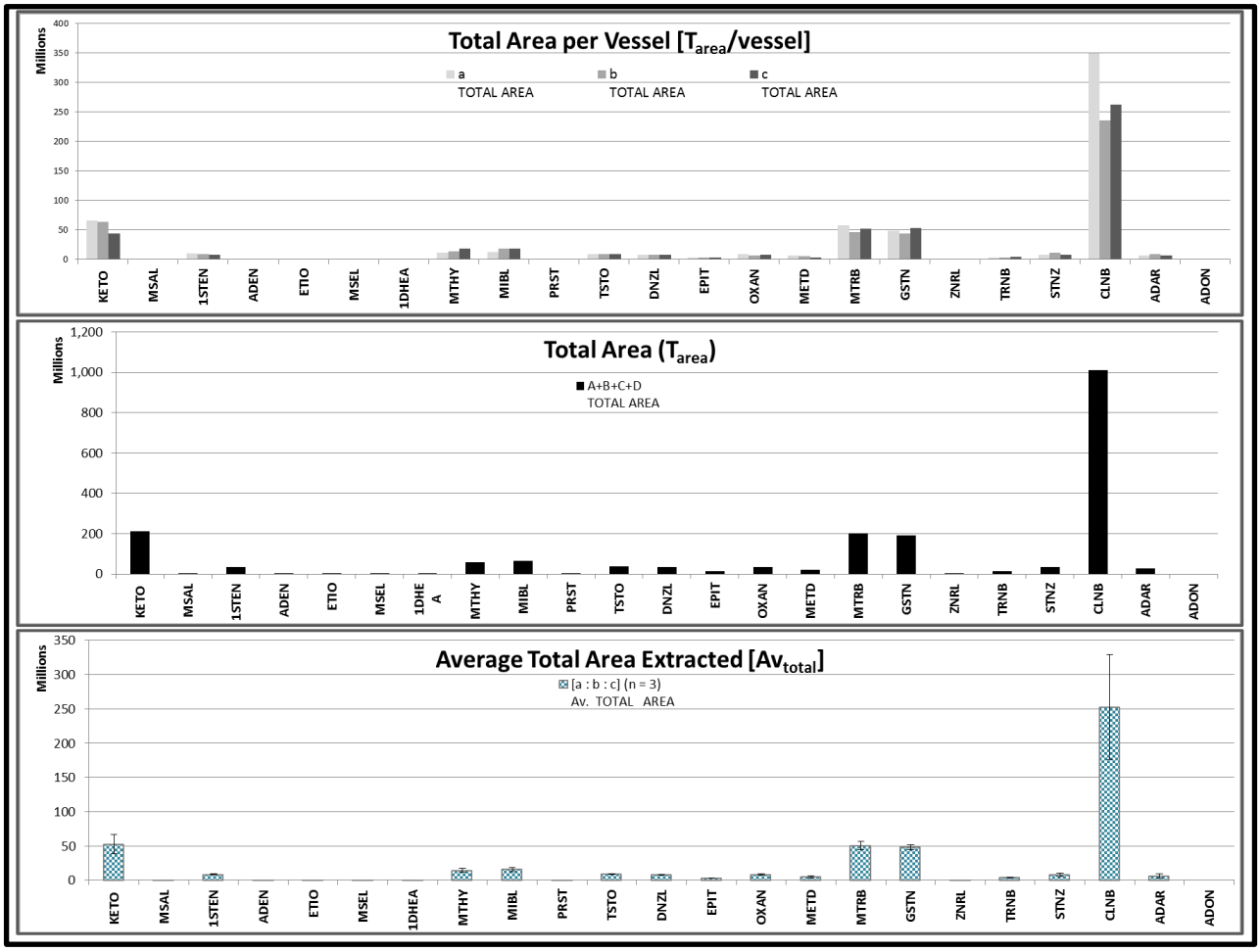

Figure 21. Example Bar Graphs for Total Area Extracted: [top] per vessel (T_{Area}/vessel), first replicate vessel [a, light gray], second replicate vessel [b, gray], and third replicate vessel [c, dark gray]; and **[middle]** for all replicate vessels (T_{area}). **[bottom] Example Bar Graph for Average Total Area Extracted (Av_{total}).** Error bars = standard deviation (n = # of vessels).

2.9.3. Area per Extraction Round.

Total Area Extracted in the first Extraction per Vessel **[T_{EXT1}/vessel].** The total area extracted in the first extraction per vessel [T_{EXT1}/vessel] is the area from the first extraction (EXT1) for a single vessel replicate (**Figure 22; top**).

Total Area Extracted in the Second Extraction per Vessel **[T_{EXT2}/vessel].** The total area extracted in the second extraction per vessel [T_{EXT2}/vessel] is the area from the second extraction (EXT2) for a single vessel replicate [a, b, -or- c] (**Figure 22; middle**).

Total Area Extracted in the Third Extraction per Vessel **[T_{EXT3}/vessel].** The total area extracted in the third extraction per vessel [T_{EXT3}/vessel] is the area produced from the third extraction (EXT3) for a single vessel replicate [a, b, -or- c] (**Figure 22; bottom**).

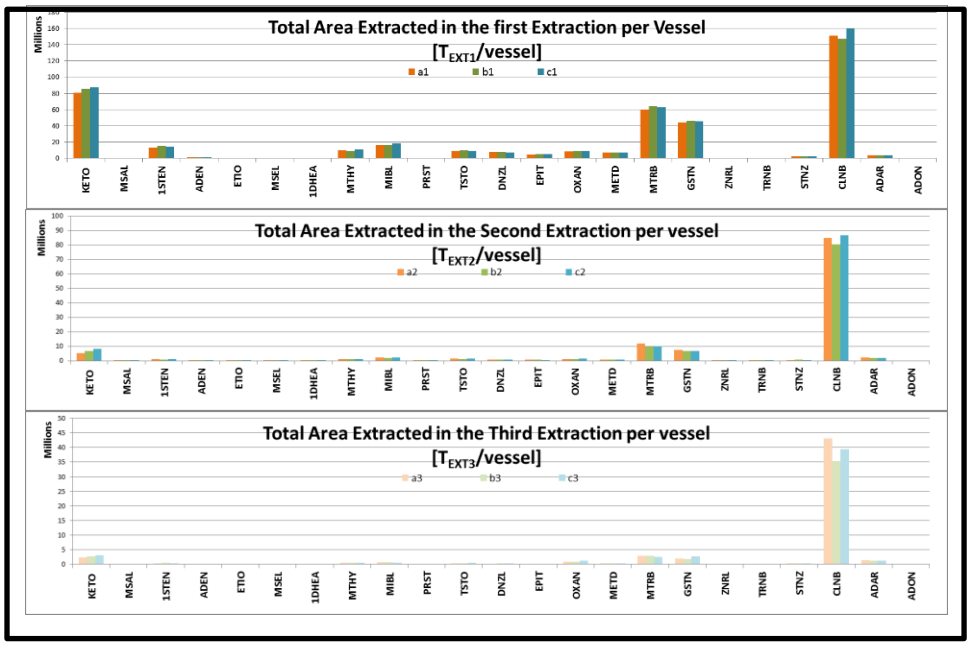

Figure 22. Example Bar Graphs for Total Area (T_{area}) per Extraction Round, showing [top] total area extracted in the first extraction round (T_{EXT1}/vessel), [middle] total area extracted in the second extraction round (T_{EXT2}/vessel), and [bottom] total area extracted in the third extraction round (T_{EXT3}/vessel), for Individual Vessels: first replicate vessel [a, orange], second replicate vessel [b, green], and third replicate vessel [c, blue].

2.9.4. Total Area per Extraction Round (Figure 23).

Total Area in the First Extraction **[T_{EXT1}].** The total area in the first extraction [T_{EXT1}] was calculated by summing the area produced by the first extraction (EXT1) for all replicate vessels [a + b + c] of a sample-type (**Figure 23; orange**).

Total Area in the Second Extraction **[T_{EXT2}].** The total area in the second extraction [T_{EXT2}] was calculated by summing the area produced by the second extraction (EXT2), for all replicates vessels [a + b + c] of a sample-type (**Figure 23; green**).

Total Area in the Third Extraction **[T_{EXT3}].** The total area in the third extraction [T_{EXT3}] was calculated by summing the area produced by the third extraction (EXT3), for all replicates vessels [a + b + c] of a sample-type (**Figure 23; blue**).

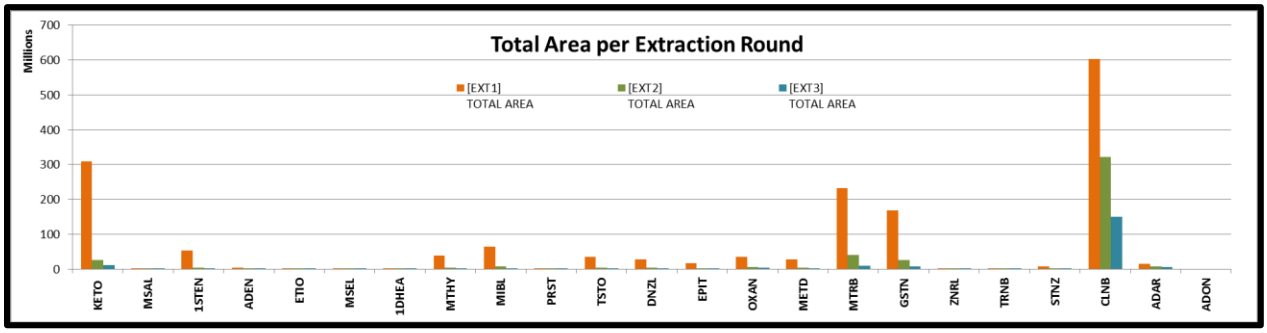

Figure 23. Example Bar Graph for Total Area per Extraction Round: extraction 1 (orange); extraction 2 (green); extraction 3 (blue), showing summed area for three replicate vessels [a + b + c].

2.9.5. Area in the 1st-Two Extractions.

Total Area in the First-Two Extractions per Vessel **[T_{1+2}/vessel].** The total area in the first two extractions per vessel [T_{1+2}/vessel] was calculated by summing the area from the first and second extraction (EXT1 + EXT2) for a single vessel [a, b, -or- c]. Bar graphs for T_{1+2}/vessel are useful for identifying outliers between replicate vessels (**Figure 24**).

Total Area in the First Two Extractions **[T_{1+2}].** The total area in the first two extractions [T_{1+2}] was calculated by summing the total area from the first and second extraction per vessel (T_{1+2}/vessel) for all replicates vessels [a + b + c] (**Figure 25**).

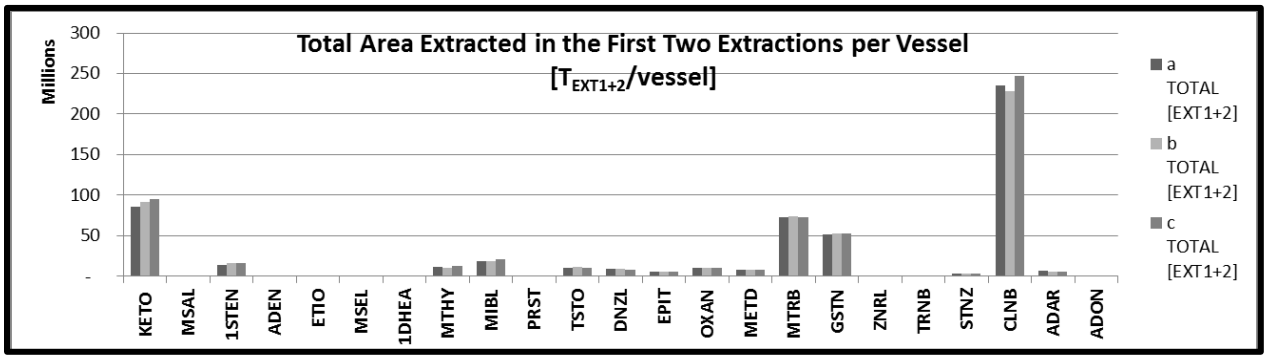

Figure 24. Example Bar Graph for Total Area in the First Two Extraction Rounds for each vessel [T_{1+2}/vessel]: replicate vessel 1 (a, dark gray); replicate vessel 2 (b, light gray); and replicate vessel 3 (c, gray).

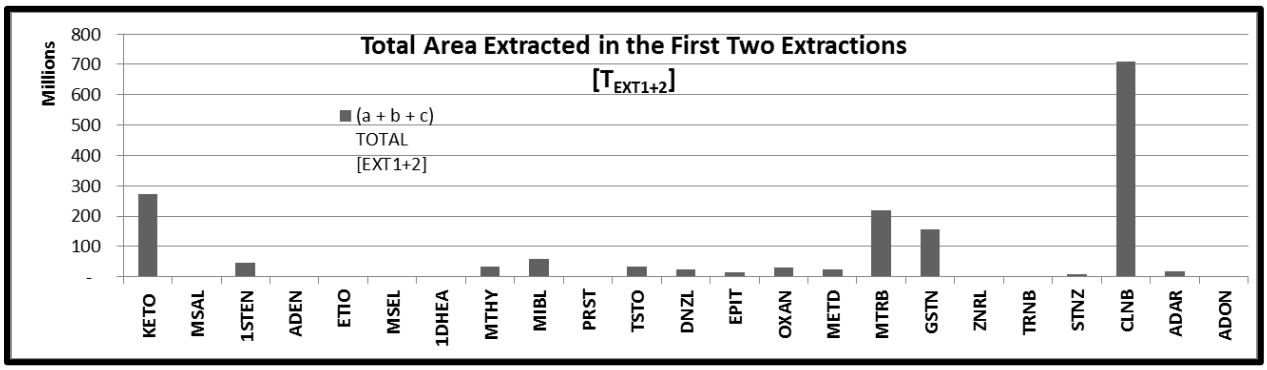

Figure 25. Example Bar Graph for Total Area in the First Two Extraction Rounds for all replicate vessels [T_{EXT1+2}].

2.9.6. Average Area per Extraction Round (Figure 26).

Average Area for the first Extraction **[Av_{EXT1}].** The average area for the first extraction [Av_{EXT1}] was calculated by taking the average and standard deviation for the area from the first extraction (EXT1) for all replicate vessels [a : b : c (n = 3)] for a sample-type (**Figure 26; dark gray**).

Average Area for the Second Extraction **[Av_{EXT2}].** The average area for the second extraction [Av_{EXT2}] was calculated by taking the average and standard deviation for the area from the second extraction (EXT2) for all replicate vessels [a : b : c (n = 3)] for a sample-type (**Figure 26; gray**).

Average Area for the Third Extraction **[Av_{EXT3}].** The average area for the third extraction [Av_{EXT3}] was calculated by taking the average and standard deviation for the area from the third extraction (EXT3) for all replicate vessels [a : b : c (n = 3)] for a sample-type (**Figure 26; light gray**).

Average Total Area in the 1st-Two Extractions **[Av_{1+2}].** The average total area in the first-two extractions [Av_{1+2}] was calculated by taking the average and standard deviation for the total area from the first-two extractions per vessel (T_{1+2}/vessel) for all replicates vessels [a : b : c (n=3)] for a sample-type (**Figure 26; white striped**).

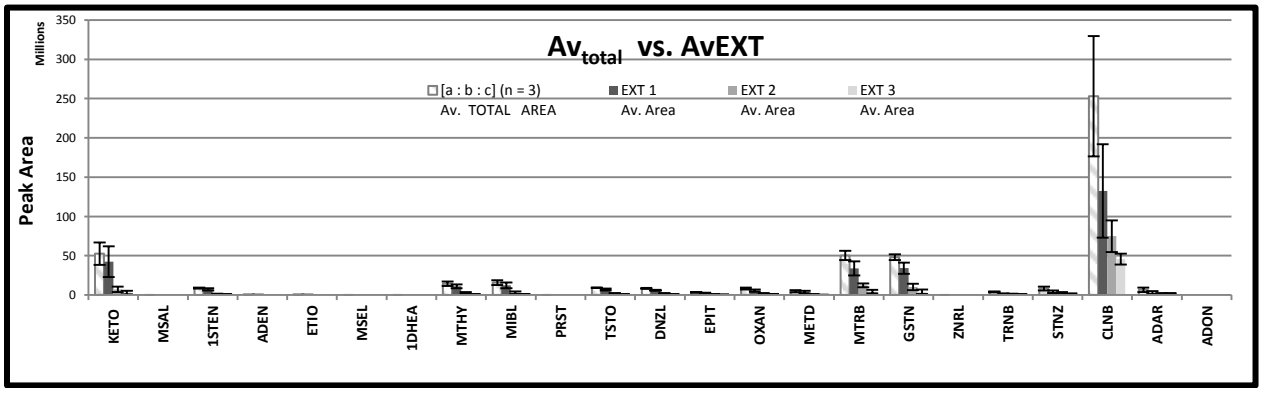

Figure 26. Example Bar Graph for Average Total Area (Av_{total}) per Extraction Round: the first extraction (**[Av_{EXT1}]**, dark gray); the second extraction (**[Av_{EXT2}]**, gray); the third extraction (**[Av_{EXT3}]**, light gray); and the first two extractions (**[AV_{EXT1+2}]**, gray stripes). Error bars = standard deviation (n = # of vessels).

2.9.7. Percent Total Area per Extraction Round (Figure 27).

Percent of the Total Area in the First Extraction per Vessel **[%EXT$_1$].** The percent of the total area in the first extraction per vessel [%EXT$_1$] was calculated by taking the area from the first extraction (EXT1) for a single vessel and dividing it by the total area extracted (T_{area}/vessel) for the same vessel (**Figure 27; blue**).

Percent of the Total Area in the Second Extraction per vessel **[%EXT$_2$].** The percent of the total area in the second extraction per vessel [%EXT$_2$] was calculated by taking the area from the second extraction (EXT2) for a single vessel and dividing it by the total area extracted (T_{area}/vessel) for the same vessel (**Figure 27; red**).

Percent of the Total Area in the Third Extraction per vessel **[%EXT$_3$].** The percent of the total area in the third extraction per vessel [%EXT$_3$] was calculated by taking the area from the third extraction (EXT3) for a single vessel and dividing it by the total area extracted (T_{area}/vessel) for the same vessel (**Figure 27; green)**.

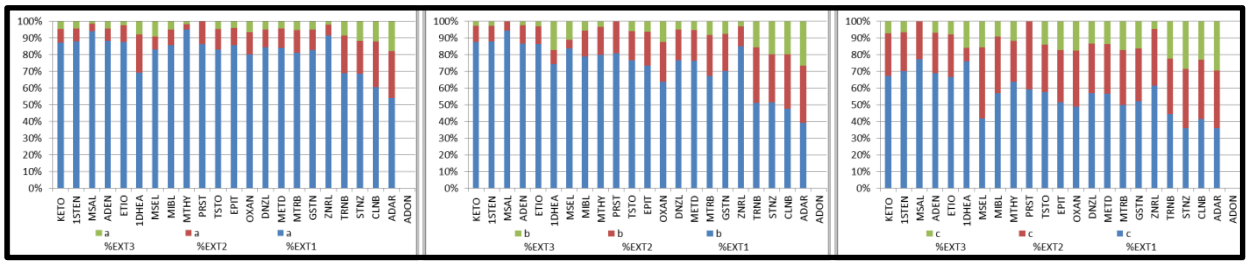

Figure 27. Example Bar graphs for Extraction Performance for a single vessels. Showing percent (%) of the total area extracted for each compound in three consecutive extraction rounds**.** **Red = %EXT$_1$; blue = %EXT$_2$; green = %EXT$_3$. (left = vessel a; middle = vessel b; right = vessel c), **Used to observe trends in extractability across several parameters while screening methods.**

2.9.8. Average Percent Total Area per Round (Figure 28)

Average Percent Total Area Extracted in the first Extraction **[Av%EXT$_1$].** The average percent total area extracted in the first extraction [Av%EXT$_1$] was calculated by taking the average and standard deviation of the area from the first extraction (EXT1) and dividing it by the average total area extracted [Av$_{total}$] for all replicates vessels [a : b : c (n = 3)] of a sample-type (**Figure 28; blue**).

Average Percent Total Area Extracted in the Second Extraction **[Av%EXT$_2$].** The average percent total area extracted in the second extraction [Av%EXT$_2$] was calculated by taking the average and standard deviation of the area from the second extraction (EXT2) and dividing it by the average total area extracted [Av$_{total}$] for all replicates vessels [a : b : c (n = 3)] of a sample-type (**Figure 28; red**).

Average Percent Total Area Extracted in the Third Extraction **[Av%EXT$_3$].** The average percent total area extracted in the third extraction [Av%EXT$_3$] was calculated by taking the average and standard deviation of the area from the third extraction (EXT3) and dividing it by the average total area extracted [Av$_{total}$] for all replicates vessels [a : b : c (n = 3)] of a sample-type (**Figure 28; green**).

Figure 28. Example Bar Graph for Average Percent of the Total Area per Extraction Round. Showing average percent of average total area (%AVtotal) in three consecutive extractions: Round 1 (**[%AvEXT$_1$]**, blue); Round 2 (**[%AvEXT$_2$]**, red); and Round 3 (**[%AvEXT$_3$]**, green). Error bars = standard deviation (n = # of vessels).

Literature Cited:

[19] World Anti-Doping Agency. International Standard Prohibited List, 2021. Resources. https://www.wada-ama.org/sites/default/files/resources/files/2021list_en.pdf. (Accessed January 03 2021).

[20] U.S. Environmental Protection Agency, Office of Research and Development, National Center for Environmental Assessment. *Method 8310: Polycyclic aromatic hydrocarbons in ground water.* Washington, DC, 1986.

[21] Lohmann R. (2012). "Critical review of low-density polyethylene's partitioning and diffusion coefficients for trace organic contaminants and implications for its use as a passive sampler." *Environmental Science & Technology.* **46**(2): p606-618. https://doi.org/10.1021/es202702y

[22] Ministry of Environment, Lands and Parks Province of British Columbia. **"***Ambient Water Quality Criteria For Polycyclic Aromatic Hydrocarbons (PAHs). February 1993*." Approved Water Quality Guidelines, Technical Reports, Polycyclic Aromatic Hydrocarbons (PAHs), Technical Appendix. K_{OW}'s from https://www2.gov.bc.ca/assets/gov/environment/air-land-water/water/waterquality/water-quality-guidelines/approved-wqgs/pahs/pahs-tech.pdf (accessed August 25 2021).

[23] Hansch C, Leo A, Hoekman D. (1995). "Exploring QSAR - Hydrophobic, Electronic, and Steric Constants." In: S.R. Heller (ed.). ACS professional reference books, vol 2. American Chemical Society: Washington, DC. ISBN 0-8412-2993-7

CHAPTER 3

MS OPTIMIZATION FOR DETECTION OF AAS: Q3 SCANS IDENTIFICATION OF OPTIMAL PRECURSORS

CHAPTER 3
MS OPTIMIZATION FOR DETECTION OF AAS:
Q3 SCANS FOR PRECURSORS
RESULTS & DISCUSSION

3.1. Steroids in Anti-Doping Testing.

3.1.1. Androgenic Anabolic Steroids (AAS).

Androgenic Steroids are derived from the male hormone, testosterone. These steroids stimulate anabolic activity, promoting muscle growth, and therefore are commonly misused by professional and amateur athletes. Often synthetic analogs are wanted that have more anabolic and less androgenic activity than does testosterone.

The World Anti-doping Agency (WADA) is charged with the responsibility of regulating potential drug abuse in elite athletes. Due to continuous introduction of designer drugs, synthesized specifically to circumvent doping controls, there is a constant need to update lists of restricted compounds. Additionally, endogenous compounds, as in naturally occurring steroids and metabolites, pose unique challenges, making determination between 'natural' versus 'doped' levels hard to establish.[24]

Drug doping remains a prevalent and potent form of drug cheating among elite athletes.[25] The world anti-doping association (WADA) publishes a list of prohibited substances,[19] which includes a wide range of xenobiotics. Anabolic agents (category S1), prohibited in sports since 1974 provide a special challenge to anti-doping controllers, as they include endogenously produced hormones, such as testosterone, as well as synthetic analogs.[26] Although most of separation methods are based on either HPLC or GC, SFC has been shown to be a highly sensitive and selective tool in the analysis of androgenic steroids.[27],[28]

3.1.2. Analyte Selection

Anabolic androgenic steroids (AAS) continue to be the most frequently abused substances among elite athletes according to the "adverse analytical findings" (AAFs) listed by WADA annual anti-doping testing figures.[29],[30] The

ever expanding market for new artificial derivatives synthesized specifically to attempt to circumvent doping controls requires continuing improvement in analytical methodologies.[31]

The AAS, largely composed of highly similar compounds, are a good targets for SFC which is excellent at separating similarly shaped compounds, including isomers. Commercial availability restricted the list of targeted analytes for this work. From those available, a list of 23 substances were selected and are listed in **Table 10** with their structures shown in **Figure 29.** This group includes 21 compounds that share either molecular weight and/or LogP, making their separation a challenge.

3.2. Mass Spectrometry (MS) in Anti-Doping Testing.

3.2.1. Analysis of AAS using MS.

The unequivocal identification and quantification of performance enhancing drugs and other banned substances including their metabolites is critical to the integrity of sports. The task is made all the more difficult by the continuing development of new synthetic compounds specifically designed to avoid detection. The analytical methods used must be robust, rapid, and versatile.[32] Mass spectrometry, coupled with chromatography, has become the method of choice in modern drug testing for sports due to its sensitive, selective, and versatile nature.[33] Using MS detection requires detailed studies of the ionization process of the analytes in the chromatographic mobile phase, including electron ionization (EI), electrospray ionization (ESI), and subsequent collision-induced dissociation (CID).

3.2.2. MP Compositions and Adduct Formation Approach.

Most anabolic steroids lack acidic or basic groups making it difficult to ionize them to $[M+H]^+$ or $[M-H]^-$ using positive or negative electrospray ionization (ESI). Consequently, the development of LC-MS/MS methods for the detection and quantitation of steroids has lagged,[34] due to lack of sensitivity.

One approach to circumvent the problem is to form adducts with one or more of the components in the mobile phase. Either co-solvents, such as methanol (MeOH) or acetonitrile (ACN), or components capable of forming ions,

such as NH_4^+, Na^+, or $HCOO^-$, have been used to generate adducts. The chemical structure of each steroid can be used to predict the chromatographic conditions needed for adduct formation. Complex adduct such as $[M+NH_4]^+$, $[M+CH_3COO]^-$, $[M+H+MeOH]^+$, $[M+Na+MeOH]^+$, or $[M+H+CH_3N\text{-}H_2O]^+$ may be required in order to ionize and detect these compounds at the sensitivity required (lower than 10 ng/mL).[35],[34] The ionization of most anabolic steroids can now be accomplished using the adduct formation approach.[36] However, some mobile phase components, such as acetonitrile and ammonium acetate, can lower the sensitivity to some steroids.

SFC-MS has also been used to analyze doping agents, and was found to be more sensitive with less matrix effects when directly compared to LC methods.[37],[38],[39],[40] There is minimal information on the effect added CO_2 would have on the fragmentation patterns of specific steroids investigated using GC-MS and LC-MS ionization techniques.[41],[42]

Table 10. Anabolic Agents Structural Classification and General Description.

Structure Classification		Full Name	ID	General Description
I	Nitrogen Containing Steroids	**Danazol**	**DNZL**	AAS (exogenous[≠]) [synthetic]
I	Nitrogen Containing Steroids	**Stanozolol**	**STNZ**	AAS (exogenous[≠]) [synthetic]
II-(a)	C3-Keto, Conjugated - (3-keto-4-ene)	**Epitestosterone**	**EPIT**	AAS (endogenous [stereoisomer])
II-(a)	C3-Keto, Conjugated - (3-keto-4-ene)	**Testosterone**	**TSTO**	AAS (endogenous [major])
II-(a)	C3-Keto, Conjugated - (3-keto-4-ene)	**Mibolerone**	**MIBL**	AAS (exogenous[≠]) [synthetic]
II-(a)	C3-Keto, Conjugated - (3-keto-4-ene)	**Methyltestosterone**	**MTHY**	AAS (exogenous[≠]) [synthetic]
II-(b)	C3-Keto, Conjugated - (3-keto-1-ene)	**1-Androstenedione**	**1STEN**	AAS (endogenous [precursor]) AAS (exogenous[≠]) [major & metabolite]
II-(c)	C3-Keto, Conjugated - (4-9-11-triene)	**Gestrinone**	**GSTN**	AAS (exogenous[≠]) [synthetic]
II-(c)	C3-Keto, Conjugated - (4-9-11-triene)	**Metribolone**	**MTRB**	AAS (exogenous[≠]) [synthetic]
II-(c)	C3-Keto, Conjugated - (4-9-11-triene)	**Trenbolone**	**TRNB**	AAS (exogenous[≠]) [metabolite of synthetic]
II-(d)	C3-Keto, Conjugated - (1,4-diene)	**Methandienone**	**METD**	AAS (exogenous[≠]) [synthetic]
III-(a)	C3-Hydroxyl, Non-conjugated - (7-keto)	**7-Keto-DHEA**	**KETO**	AAS (endogenous [precursor])
III-(b)	C3-Hydroxyl, Non-conjugated	**Androsterone**	**ADEN**	AAS (endogenous [major, precursor & metabolite])
III-(b)	C3-Hydroxyl, Non-conjugated	**Etiocholanolone**	**ETIO**	AAS (endogenous [metabolite])
IV	C3-Hydroxyl, Conjugated	**1-Androsterone**	**1DHEA**	AAS (endogenous [major, precursor & metabolite]) AAS (exogenous[≠]) [precursor]
IV	C3-Hydroxyl, Conjugated	**Prasterone**	**PRST**	AAS (endogenous [major & precursor])
V	C3-Keto, Non-conjugated	**Androstanolone**	**ADON**	AAS (endogenous [metabolite])
V	C3-Keto, Non-conjugated	**Mestanolone**	**MSAL**	AAS (exogenous[≠]) [synthetic]
V	C3-Keto, Non-conjugated	**Mesterolone**	**MSEL**	AAS (exogenous[≠]) [synthetic]
V	C3-Keto, Non-conjugated	**Oxandrolone**	**OXAN**	AAS (exogenous[≠]) [synthetic]
OTHER ANABOLIC AGENTS [selective androgen receptor modulators (SARMs)]				
VI	Non-specified Structure	**Clenbuterol**	**CLNB**	non-steroidal (other)
VI	Non-specified Structure	**Andarine**	**ADAR**	non-steroidal (SARM)
VI	Non-specified Structure	**Zeranol**	**ZRNL**	non-steroidal (SARM)

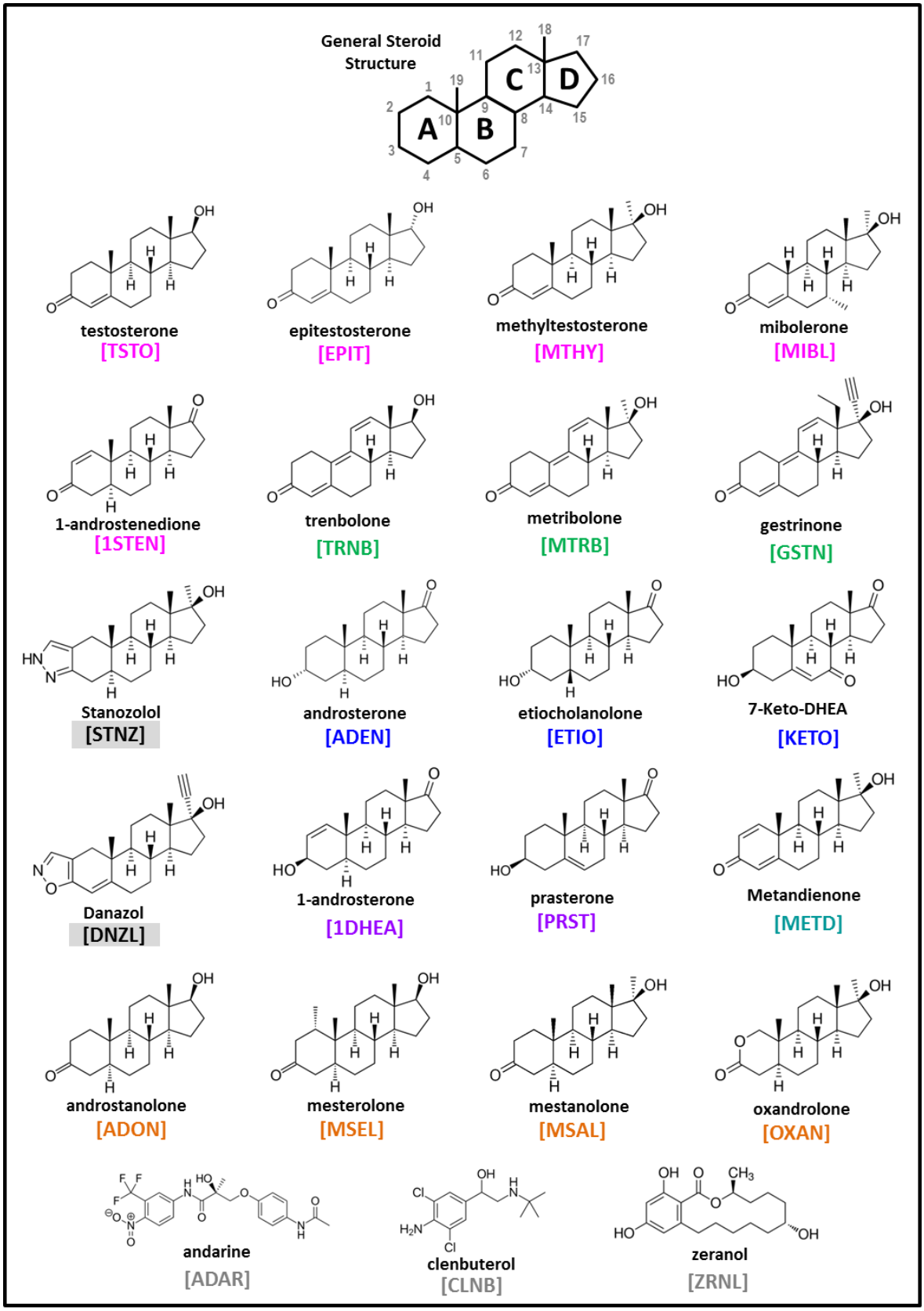

Figure 29. Structure of Targeted Anabolic Anabolic Steroids and Bio-Mimics (AAS).

3.2.3. Expected Precursors from the Literature.

Strong relationships between the ionization profile, sensitivity, and structures of steroids has now been well established. Even small differences in stereoisomeric structure can have a large effect on ion formation and the resulting possible fragmentation pathways.[43] The stability of protonated steroid ions can be dependent on steroid structure, which has been suggested to be explained by the gas phase proton affinity (PA) of the resulting protonated ions stability in the gas phase. Proton affinities in the gas phase generally are amines > ketones > alcohols. Steroids are expected to have relatively low proton affinities, since their structures naturally, only contain ketones and alcohols, which limits the choices of mobile phase composition (including types of additives). The characteristic structure of the specific steroid, leads to stable $[M+H]^+$, or alternatively $[M+H-nH_2O]^+$ ions as dominant precursors.[44]

The formation of $[M+H-H_2O]^+$, or $[M+H-2H_2O]^+$ as the most abundant ion, corresponds to losses of neutral H_2O. The keto-functional group at C3 plays an important role in protonation and neutral loss of water molecules, regardless of the substitution at C17. Additionally, functional group conjugation (via a double bond) tends to increase proton affinity. Steroids that are not conjugated at C3, can easily produce fragment ions by in-source dissociation, resulting from the poor stability of protonated molecular ions. This tends to form a loss of water from the A ring, as depicted in **Figure 30,** which is adapted from **Thevis et. al., 2005.**[45]

Anabolic agents can be classified generally into groups, based on the substitutions at C3:

I. Amine containing synthetic steroids

II. Steroids with a conjugated, keto-functional group at the C3 position;

III. Steroids with an unconjugated, C3-hydroxyl group

IV. Steroids with a conjugated, C3-hydroxyl group

V. Steroids with an unconjugated, C3-keto functional group

VI. Un-specified, non-steroidal structure.

3.2.4. Expected Ionization by Group:

Group I. Steroids containing a nitrogen.

The primary ionization center for nitrogen containing steroids is expected in the nitrogen containing ring. Therefore, this group is expected to have high proton affinity. Stable $[M+H]^+$ precursor ions are expected for Group I steroids, meaning high sensitivity is expected for this group.

Group II. Conjugated; C-3 Ketosteroids

For ketosteroids, protonation predominantly occurs on the ketone group. Steroids with the keto-functional group at C3, have good proton affinity and conjugation significantly stabilizes the protonated molecule, which results in the generation of stable, abundant $[M+H]^+$ ions. Conjugated ketosteroids are quite stable, can produce large amounts of the $[M+H]^+$ ion, and tend to have low LODs.[34] Low levels of detection have many benefits, especially for small sample sizes. Since less sample often means lower concentrations of targeted analytes will be present for detection. If an analyte can be detected easily at low levels (i.e., low concentrations), less sample would be required for analysis. Conjugated ketosteroids, as a group, contain several sub-categories, each having structural significance that can effect the ionization and fragmentation:

Group II-(a). **3-keto-4-ene steroids.** Steroids with a single conjugation in ring A, located at C4, adjacent to the keto functional group at C3 (**Figure 31**; **A**). The C3 Keto-function favors protonation, and the resulting ion is stabilized by the conjugation.

Group II-(b). **3-keto-1-ene steroids**. Steroids with a single conjugation in the A ring, located at C1 (also adjacent to the keto functional group at C3 (**Figure 31**; **B**). Protonation and stabilization is the similar to 4-ene above, but becomes more important for fragmentation patterns.[46]

Group II-(c). **4,9,11-triene steroids**. Steroids containing three double bonds across the backbone of the structure, provides a large 8-π electron system (**Figure 31**; **C**). Protonation and stabilization is similar to 4-ene above, but becomes more important for fragmentation patterns.[47]

Group II-(d). **1,4-diene steroids**. Steroids with a cross-conjugated π-electron system across the A ring (**Figure 31**; **D**). The presence of the diene within ring A, promotes a single neutral water loss, which results in a highly stable aromatic structure (**Figure 30**).[48]

Group III. Non-Conjugated; C3-Hydroxyl Steroids.

Steroids containing a hydroxyl-functional group at C3 produce protonated molecular ions, which due to instability, dissociate to $[M+H-H_2O]^+$ or $[M+H-2H_2O]^+$ ions. Steroids with unconjugated hydroxyl groups, that contain a keto substitution at C17, will follow alternative protonation and dissociation pathways, and always form the $[M+H-H_2O]^+$ (**Figure 31**; **E**). With saturated steroids, the formation of multiple ions, due to water loss, and low proton affinities result in relatively high LODs when using ESI,[44] which can make detection at lower concentrations more difficult for these types of steroids.

Group IV. Conjugated; C3-Hydroxyl Steroids.

Compounds containing an unconjugated, hydroxyl-functional group at position C3 (**Figure 31**; **F**), gave rise to the protonated molecular ion, which then readily dissociates to $[M+H-H_2O]^+$ or $[M+H-2H_2O]^+$ ions, due to instability of the protonated molecules. Protonation can only occur at the hydroxyl group which results in a neutral loss of H_2O.[49]

Group V. Non-Conjugated; C3-Keto Steroids

The expected loss of water is not limited to steroids with the hydroxyl-functional group. Steroids containing an unconjugated keto-functional group (**Figure 31**; **G**), can generate the $[M+H-2H_2O]^+$, although the ions generated tend to be minor, which can lower sensitivity due to multiple ion generation, but tends to not be as pronounced as in unconjugated hydroxylated steroids.[45],[49]

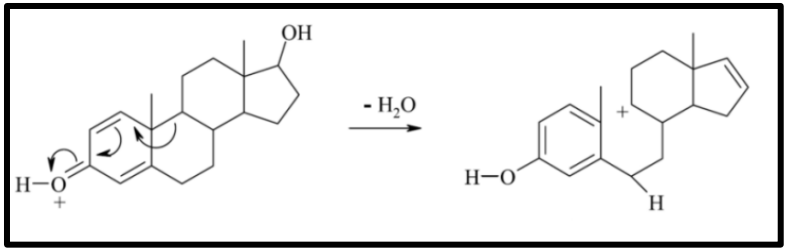

Figure 30. Example Ionization Pattern through Neutral Water Loss for Anabolic Steroids (Mechanism Proposed by and Figure Adapted from **Thevis et. al., 2005**[45]).

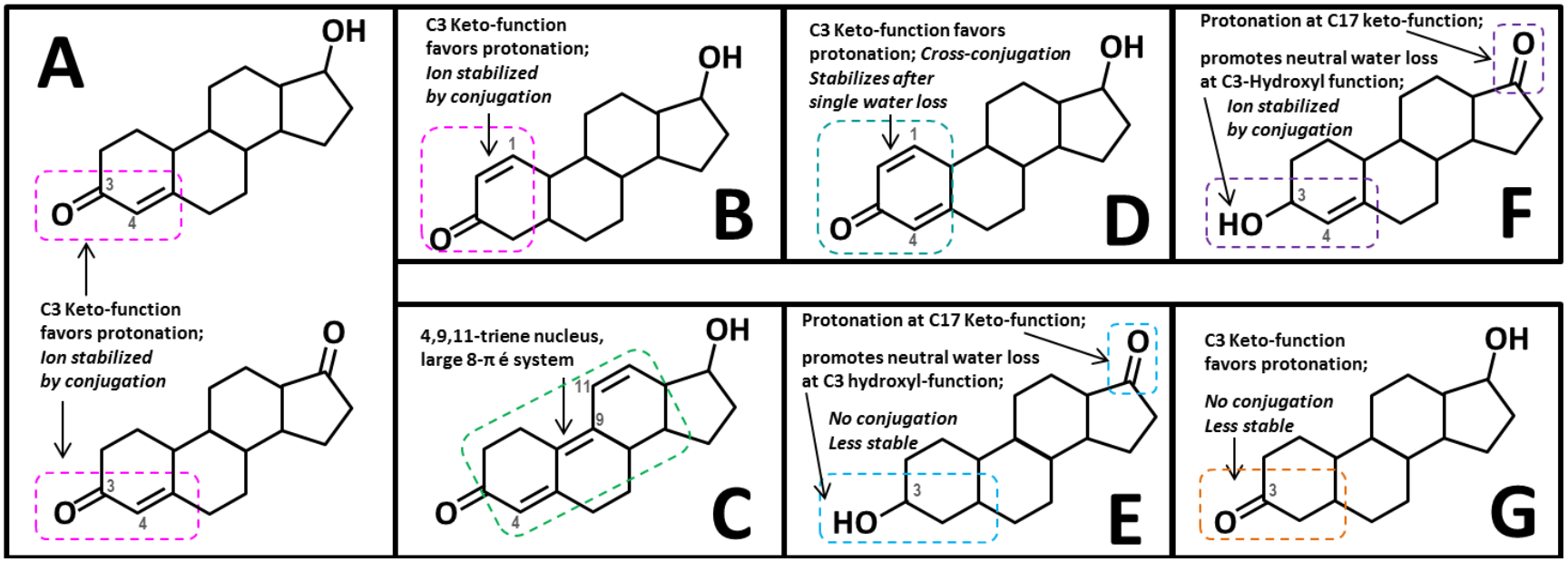

Figure 31. Generic Steroid structures showing significant Sites for Protonation.
[A] 3-keto-4-ene steroids (Group II-[a]); **[B] 3-keto-1-ene steroids** (Group II-[b]); **[C] 4,9,11-triene steroids** (Group II-[c]); **[D] 1,4-diene steroids** (Group II-[d]); **[E] Non-Conjugated, C3-Hydroxyl Steroids** (Group III); **[F] Conjugated, C3-Hydroxyl Steroids** (Group IV); **[G] Non-Conjugated, C3-Keto Steroids** (Group V).

3.3. Approach for MS-Optimizations.

3.3.1. Initial MS-Optimization using Flow Injection Analysis.

For initial detection optimization the instrument was set up for direct flow injection. Solutes were dissolved in methanol. Pure methanol was pumped through the system as the mobile phase, the solutes injected into the flowing stream, without a column installed, then into the MS, as described in **Chapter #1. Hyphenated Instrumentation; Section. 1.4.1. Instrument Configurations; *FIA-MS Optimization Configuration***;. MS optimization for detection in SFE-SFC-MS analysis is the first step in method development for online methods, and is broken down into three main steps:

1. **Q3 Scans** are performed to determine optimal precursors from characteristic Ionization patterns for each compound. Optimal solutions concentrations for further MS-optimization is are also chosen in this step.

2. **MRM-Optimization.** Multiple reaction monitoring (MRM) optimizations are performed for each of the target compounds to choose optimal product ions, and associated optimal MS parameters.

3. **Identification of Critical Pair Groups.** The MRM-transitions from step 2, plus the Q3 scans from step 1, are used to identify critical pair groups, (i.e., compounds cannot be separated by MS-alone).

The current chapter focuses on step 1 of MS-Detection optimizations: the determination of optimal precursor ions using Q3 Scans (**Figure 32**).

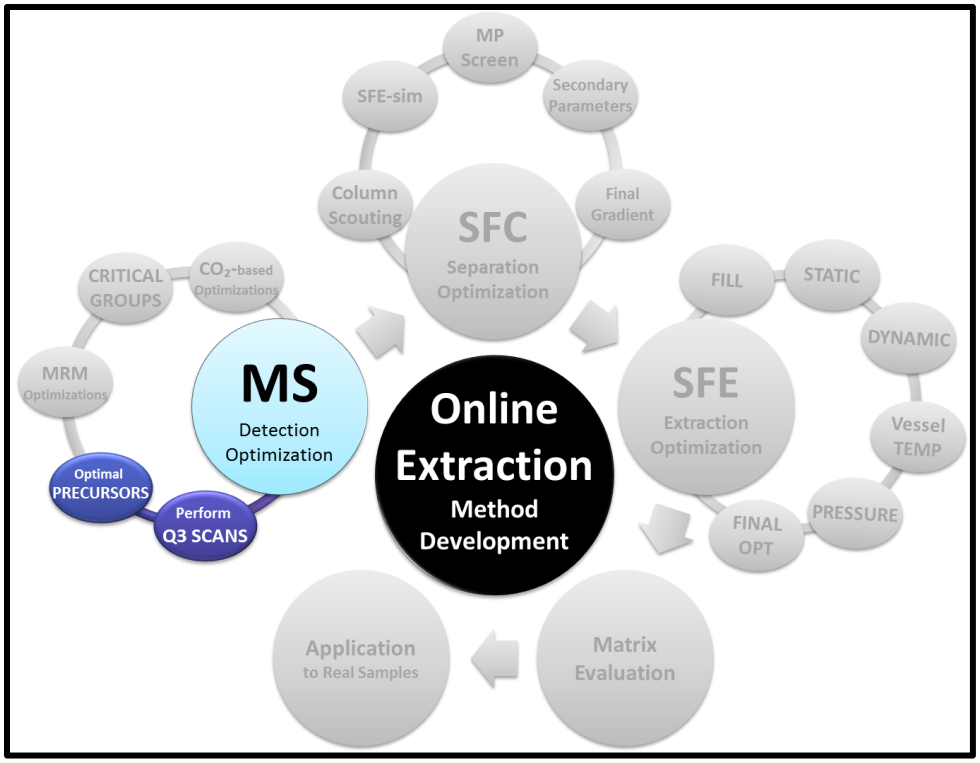

Figure 32. **Online Extraction Method Development Focus for Chapter #3 Q3 Scans in MS Detection Optimization**.

3.3.2. Acquisition of Q3 Scans

Flow injection analysis (FIA) was used to create Q3 scans (120 – 1,200 m/z) in ESI-positive and negative mode for each compound. Individual stock solutions were injected at four concentrations (10, 5, 1 and 0.1 ppm in methanol), detailed conditions are described at the end of this chapter in **Section 3.i. SFE-SFC-MS Instrument Methods for Q3 Scans; 3.i.2. MS Parameters – Q3 Scans**. Scans were performed under normal LC-based conditions, and then compared to SFC-based MPs containing CO_2.

MS-based optimization involved three mobile phase compositions. For LC-based mobile phases, flow injection analysis (FIA) was utilized with no column in the flow path. LC MPs included: methanol with no additive (**FIA - MeOH**), methanol with 0.1% formic acid (**FIA-FA**), and methanol + 5mM ammonium formate (**FIA-AmFo**).

The same solvent compositions were then used as modifiers for SFC-based MPs at three concentrations: High (40%, [**SFC-40%**]), moderate (20%, [**SFC-20%**]) and low (10%, [**SFC-10%**]) modifier in CO_2. Although the 'low' modifier is by no means representative of the lowest range of modifier for SFC, anything lower would have produced excessively long runs for a full scan acquisition, especially for later eluting compounds, so 10% was chosen as the low concentration. Since SFC operation requires a pressure drop between the pumps and the outlet of the system, to maintain a dense MP throughout the entire flowpath, SFC Q3 scans were run with a column in-line between the injector and BPR_A. At this early stage makeup flow to the MS was not utilized.

Obtained spectra were compared to known precursors from the literature. Optimal precursor and solution concentrations were chosen for each standard and used for further MRM optimization (covered in **Chapter #4: MRM Optimization**), using the LabSolutions 'optimize MRM event from product ion search' function.

Methanol was chosen for multiple reasons: It is the most polar common solvent completely miscible with CO_2; It is the most widely studied modifier and steroids have been shown to be more easily ionized with methanol, when compared to alternative solvents, such as acetonitrile (where many difficult AAS would not generate ions);[35] and lastly, there is little in the LC literature describing and characterizing the ionization of steroids with alternative modifiers such as ethanol or IPA.

3.4. Discussion of Optimal Precursors in Q3 Scans.

3.4.1. Dominant Ion Profiles from Q3 Scans with Flow Injection Analysis (FIA).

For all 23 targeted anabolic agents, $[M+H]^+$, $[M+H-H_2O]^+$, $[M+H-2H_2O]^+$, and $[M+Na]^+$ ions were detected as the most abundant ions in scan mode (**Table 11**). Ionization profiles differed between steroid classes. Nitrogen containing steroids (Group I), having the highest proton affinity, as expected gave $[M+H]^+$ as the most dominant ion (**Figure 33; A**). Conjugated, keto-steroids (Group II) gave both the $[M+H]^+$ protonated molecular ion and a sodium adduct ion $[M+Na]^+$ as the most dominant ions (**Figure 33; B**).

The $[M+H-H_2O]^+$ and $[M+H-2H_2O]^+$ ions were only observed for AAS containing the characteristic steroid backbone of groups III, IV, and V. Both groups III and IV contain a hydroxyl-functional group at C3, and therefore as expected produced the dominant ions of $[M+H-H_2O]^+$ and $[M+H-2H_2O]^+$, due to the neutral loss of water (**Figure 33; C**). Group V steroids, having an unconjugated keto-functional group at C3, produced, as expected, both protonated molecular ions $[M+H]^+$ as the most dominant ions, and much less abundant, alternative adduct and/or fragment ions due to successive water losses and/or adducts with the mobile phase solvents (**Figure 33; D**).

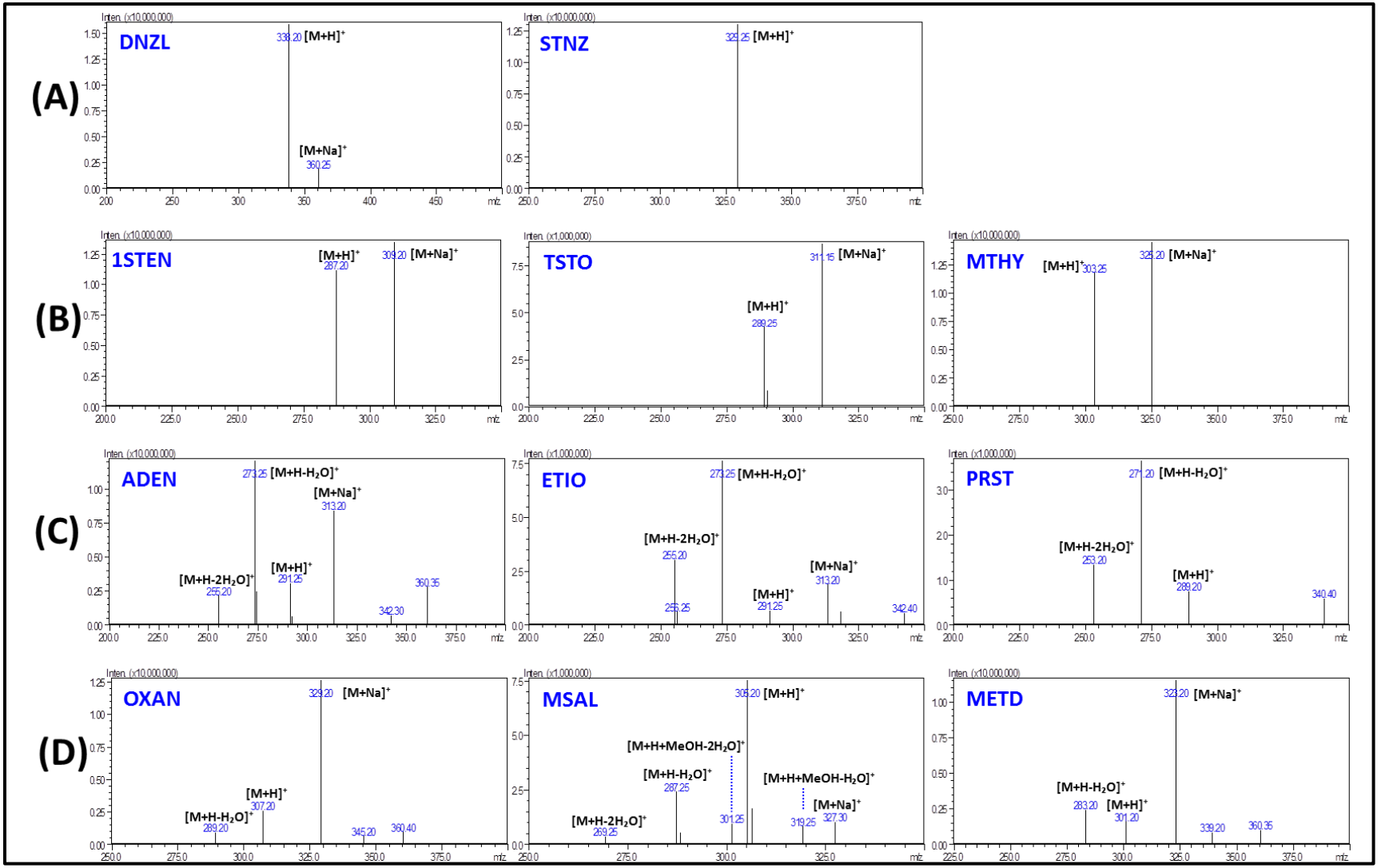

Figure 33. Representative ESI- Q3 Scan Spectra of Steroids Groups using Flow Injection Analysis (FIA) with Methanol (MeOH), for (A) Group I steroids: danazol (DNZL, left), and stanazolol (STNZ, middle); **(B) Group II steroids**: 1-Androstenedione (1STEN, left), testosterone (TSTO, middle), and Methyltestosterone (MTHY, right); **(C) Group III & IV steroids**: androsterone (ADEN, left), etiocholanolone (ETIO, middle) and Prasterone (DHEA, left); **and (D) Group V steroids**: oxandrolone (OXAN, left), mestanolone (MSAL, middle), and metandienone (METD, left). ***Conditions****: 100% Methanol, with no column installed, Flow rate 0.25 mL/min, 1.0µL injections of MRM-solutions of each steroid in MeOH, Detection: ESI-positive mode.*

Table 11. Q3 Scan Summary of Dominant Ion and Optimal Solution Concentrations for Anabolic Agents using Flow Injection Analysis (FIA).

				FIA (MeOH) Q3 Scan Base Peak			FIA (5mM AmFo) Q3 Scan Base Peak			FIA (0.1 % FA) Q3 Scan Base Peak				
Class	Steroid	MW	ID	m/z	Ion	Conc.	m/z	Ion	Conc.	m/z	Ion	Conc.	material	AAS mix
GROUP I. Nitrogen Containing steroids														
I	Danazol	337.46	DNZL	338	$[M+H]^+$	0.1 ppm	338	$[M+H]^+$	0.1 ppm	338	$[M+H]^+$	0.1 ppm	powder	20ppm
I	Stanozolol	328.49	STNZ	329	$[M+H]^+$	0.1 ppm	329	$[M+H]^+$	1 ppm	329	$[M+H]^+$	1 ppm	ampule	2ppm
GROUP II. Conjugated, C3 Keto function														
II-(a). 3-keto-4-ene steroids														
II-(a)	Epitestosterone	288.42	EPIT	311	$[M+Na]^+$	0.1 ppm	289	$[M+H]^+$	1 ppm	289	$[M+H]^+$	1 ppm	ampule	2ppm
II-(a)	Methyltestosterone	302.45	MTHY	325	$[M+Na]^+$	0.1 ppm	303	$[M+H]^+$	0.1 ppm	303	$[M+H]^+$	1 ppm	powder	20ppm
II-(a)	Mibolerone	302.50	MIBL	325	$[M+Na]^+$	0.1 ppm	303	$[M+H]^+$	0.1 ppm	303	$[M+H]^+$	1 ppm	powder	20ppm
II-(a)	Testosterone	288.42	TSTO	311	$[M+Na]^+$	0.1 ppm	289	$[M+H]^+$	0.1 ppm	289	$[M+H]^+$	1 ppm	ampule	2ppm
II-(b). 3-keto-1-ene nucleus														
II-(b)	1-Androstenedione	286.41	1STEN	309	$[M+Na]^+$	0.1 ppm	287	$[M+H]^+$	1 ppm	287	$[M+H]^+$	0.1 ppm	ampule	2ppm
II-(c). 4,9,11-triene nucleaus														
II-(c)	Gestrinone	308.41	GSTN	331	$[M+Na]^+$	0.1 ppm	309	$[M+H]^+$	0.1 ppm	309	$[M+H]^+$	1 ppm	powder	20ppm
II-(c)	Metribolone	284.39	MTRB	307	$[M+Na]^+$	0.1 ppm	285	$[M+H]^+$	0.1 ppm	285	$[M+H]^+$	1 ppm	powder	20ppm
II-(c)	Trenbolone	270.37	TRNB	293	$[M+Na]^+$	0.1 ppm	271	$[M+H]^+$	1 ppm	271	$[M+H]^+$	1 ppm	ampule	2ppm
II-(d). 1,4-diene-3-keto														
II-(d)	Methandienone	300.44	METD	323	$[M+Na]^+$	0.1 ppm	283	$[M+H-H_2O]^+$	1 ppm	283	$[M+H-H_2O]^+$	1 ppm	ampule	2ppm
GROUP III. Non-conjugated, C3 Hydroxyl function														
III-(a). 7-keto steroids														
III-(a)	7-Keto-DHEA	302.20	KETO	285	$[M+H-H_2O]^+$	0.1 ppm	285	$[M+H-H_2O]^+$	0.1 ppm	285	$[M+H-H_2O]^+$	0.1 ppm	powder	20ppm
III-(b). Hydroxy-androstenes														
III-(b)	Androsterone	290.44	ADEN	273	$[M+H-H_2O]^+$	10 ppm	273	$[M+H-H_2O]^+$	1 ppm	273	$[M+H-H_2O]^+$	1 ppm	powder	20ppm
III-(b)	Etiocholanolone	290.44	ETIO	273	$[M+H-H_2O]^+$	5 ppm	273	$[M+H-H_2O]^+$	5 ppm	273	$[M+H-H_2O]^+$	5 ppm	powder	20ppm
GROUP IV. Conjugated, C3 Hydroxyl function														
IV	1-Androsterone	290.44	1DHEA	273	$[M+H-H_2O]^+$	10 ppm	273	$[M+H-H_2O]^+$	10 ppm	273	$[M+H-H_2O]^+$	5 ppm	powder	20ppm
IV	Prasterone	288.21	PRST	271	$[M+H-H_2O]^+$	10 ppm	271	$[M+H-H_2O]^+$	5 ppm	271	$[M+H-H_2O]^+$	5 ppm	powder	20ppm
GROUP V. Non-conjugated, C3 Hydroxyl function														
V	Oxandrolone	306.44	OXAN	329	$[M+Na]^+$	0.1 ppm	307	$[M+H]^+$	1 ppm	307	$[M+H]^+$	1 ppm	powder	20ppm
V	Mesterolone	304.47	MSEL	305	$[M+H]^+$	5 ppm	305	$[M+H]^+$	5 ppm	305	$[M+H]^+$	5 ppm	powder	20ppm
V	Mestanolone	304.47	MSAL	305	$[M+H]^+$	5 ppm	305	$[M+H]^+$	5 ppm	305	$[M+H]^+$	1 ppm	powder	20ppm
V	Androstanolone	290.44	ADON	291	$[M+H]^+$	5ppm	305	$[M+MeOH-H_2O]^+$	10 ppm	291	$[M+H]^+$	5 ppm	ampule	2ppm
GROUP VI. Un-specified Structure														
VI	Andarine	441.36	ADAR	464	$[M+Na]^+$	0.1 ppm	442	$[M+H]^+$	0.1 ppm	442	$[M+H]^+$	0.1 ppm	powder	20ppm
VI	Clenbuterol	277.19	CLNB	277	$[M+H]^+$	0.1 ppm	277	$[M+H]^+$	0.1 ppm	277	$[M+H]^+$	0.1 ppm	powder	20ppm
VI	Zeranol	322.40	ZRNL	321	$[M-H]^-$	1ppm	321	$[M-H]^-$	1 ppm	321	$[M-H]^-$	1ppm	10ug/ml	0.04ppm

3.5. GROUP I. Nitrogen containing steroids: DNZL, STNZ

3.5.1. Group I; Q3 Scans with Flow Injection Analysis

DNZL and STNZ are both synthetic steroid mimics, where a pyrazol (in the case of STNZ) or a oxazole (in the case of DNZL) ring was added to the structure, which greatly slows the rate of metabolic transformation, increasing effectiveness during oral administration.[49] Amines have high proton affinity, the nitrogen favors ionization, and therefore this group of steroids are expected to easily ionize with protonated molecular ions $[M+H]^+$ as the most intense ion.

During FIA analysis, both DNZL and STNZ produced the protonated molecular ion $[M+H]^+$ as the most dominant ion (**S_Figure 2; A & B**), with and without additive, and required only the lowest concentration MRM-solutions, regardless of the MP (**Table 11; Group I**). Few other peaks were observed for either compounds with the exception of a minor sodium adduct ion (<15%) produced by DNZL, but only while using methanol with no additive. DNZL may be more likely to form adducts with sodium since its structure contains an oxygen atom positioned close to the nitrogen, where protonation is thought to occur. Oxygen atoms near the protonation center of steroids have been reported to promote sodium coordination.[36] Addition of an additive to the mobile phase while using FIA, had little effect on the characteristic spectra for nitrogen containing steroids, and therefore there was no change in dominant ion. STNZ required slightly higher concentration with the use of an additive (**S_Table 1; [Group I]**).

3.5.2. Group I; Q3 Scans with CO_2-based MPs.

Nitrogen containing steroids were also easily ionized with $[M+H]^+$ as the most intense ion in CO_2-based MPs (**Table 12**). Adduct formation was observed for DNZL-only, and these adducts were only seen under LC-FIA conditions (**Section 3.5.1 above**) using methanol with no additive. The sodium adduct was not observed under any of the conditions used with CO_2 as the majority of the MP (**S_Table 2**). This suggests, $[M+H]^+$ could easily be selected as precursor ion respective of the MP composition, and furthermore there may be a slight increase in sensitivity for DNZL using SFC-MPs.

Table 12. Q3 Scan Summary of Dominant Ion and Optimal Solution Concentration of Groups I, II, and VI Anabolic Agents for Carbon Dioxide (CO_2)-based Mobile Phases.

				SFC (40% MeOH) (CO_2 + 40% MeOH) Q3 Scan Base Peak			SFC (20% MeOH) (CO_2 + 20% MeOH) Q3 Scan Base Peak			SFC (10% MeOH) (CO_2 + 10% MeOH) Q3 Scan Base Peak		
Class	Steroid	MW	ID	m/z	Ion	Conc.	m/z	Ion	Conc.	m/z	Ion	Conc.
I	Danazol	337.46	DNZL	338	$[M+H]^+$	< 1 ppm	338	$[M+H]^+$	< 1 ppm	338	$[M+H]^+$	< 1 ppm
I	Stanozolol	328.49	STNZ	329	$[M+H]^+$	< 5 ppm	329	$[M+H]^+$	< 5 ppm	329	$[M+H]^+$	< 5 ppm
II-(a)	1-Androstenedione	286.41	1STEN	287	$[M+H]^+$	< 1 ppm	287	$[M+H]^+$	< 1 ppm	287	$[M+H]^+$	< 1 ppm
II-(a)	Epitestosterone	288.42	EPIT	289	$[M+H]^+$	< 5 ppm	289	$[M+H]^+$	< 5 ppm	289	$[M+H]^+$	< 5 ppm
II-(a)	Mibolerone	302.50	MIBL	303	$[M+H]^+$	< 1 ppm	303	$[M+H]^+$	< 1 ppm	303	$[M+H]^+$	< 1 ppm
II-(a)	Methyltestosterone	302.45	MTHY	303	$[M+H]^+$	< 1 ppm	303	$[M+H]^+$	< 1 ppm	303	$[M+H]^+$	< 1 ppm
II-(b)	Testosterone	288.42	TSTO	289	$[M+H]^+$	< 1 ppm	289	$[M+H]^+$	< 1 ppm	289	$[M+H]^+$	< 1 ppm
II-(c)	Gestrinone	308.41	GSTN	309	$[M+H]^+$	< 1 ppm	309	$[M+H]^+$	< 5 ppm	309	$[M+H]^+$	< 5 ppm
II-(c)	Metribolone	284.39	MTRB	285	$[M+H]^+$	< 1 ppm	285	$[M+H]^+$	< 1 ppm	285	$[M+H]^+$	< 1 ppm
II-(c)	Trenbolone	270.37	TRNB	271	$[M+H]^+$	< 1 ppm	271	$[M+H]^+$	< 1 ppm	271	$[M+H]^+$	< 1 ppm
VI	Andarine	441.36	ADAR	442	$[M+H]^+$	< 1 ppm	442	$[M+H]^+$	< 1 ppm	464	$[M+H]^+$	< 1 ppm
VI	Clenbuterol	277.19	CLNB	277	$[M+H]^+$	< 0.1 ppm	-	-	-	-	-	-
VI	Zeranol	322.40	ZRNL	321	$[M-H]^-$	< 1 ppm	321	$[M-H]^-$	< 1 ppm	323	$[M-H]^-$	< 1 ppm

				SFC (40% AmFo) (CO_2 + 40% MeOH + 5mM AmFo) Q3 Scan Base Peak			SFC (20% AmFo) (CO_2 + 20% MeOH + 5mM AmFo) Q3 Scan Base Peak			SFC (10% AmFo) (CO_2 + 10% MeOH + 5mM AmFo) Q3 Scan Base Peak		
Class	Steroid	MW	ID	m/z	Ion	Conc.	m/z	Ion	Conc.	m/z	Ion	Conc.
I	Danazol	337.46	DNZL	338	$[M+H]^+$	< 1 ppm	338	$[M+H]^+$	< 1 ppm	338	$[M+H]^+$	< 1 ppm
I	Stanozolol	328.49	STNZ	329	$[M+H]^+$	< 5 ppm	329	$[M+H]^+$	< 5 ppm	329	$[M+H]^+$	< 5 ppm
II-(a)	1-Androstenedione	286.41	1STEN	287	$[M+H]^+$	> 1 ppm	287	$[M+H]^+$	> 1 ppm	287	$[M+H]^+$	< 1 ppm
II-(a)	Epitestosterone	288.42	EPIT	289	$[M+H]^+$	< 5 ppm	289	$[M+H]^+$	< 5 ppm	289	$[M+H]^+$	< 5 ppm
II-(a)	Mibolerone	302.50	MIBL	303	$[M+H]^+$	< 1 ppm	303	$[M+H]^+$	< 1 ppm	303	$[M+H]^+$	< 1 ppm
II-(a)	Methyltestosterone	302.45	MTHY	303	$[M+H]^+$	< 1 ppm	303	$[M+H]^+$	< 1 ppm	303	$[M+H]^+$	< 1 ppm
II-(b)	Testosterone	288.42	TSTO	289	$[M+H]^+$	< 1 ppm	289	$[M+H]^+$	< 1 ppm	289	$[M+H]^+$	< 1 ppm
II-(c)	Gestrinone	308.41	GSTN	309	$[M+H]^+$	< 1 ppm	309	$[M+H]^+$	< 1 ppm	309	$[M+H]^+$	< 1 ppm
II-(c)	Metribolone	284.39	MTRB	285	$[M+H]^+$	< 1 ppm	285	$[M+H]^+$	< 1 ppm	285	$[M+H]^+$	< 1 ppm
II-(c)	Trenbolone	270.37	TRNB	271	$[M+H]^+$	< 1 ppm	271	$[M+H]^+$	< 1 ppm	271	$[M+H]^+$	< 1 ppm
VI	Andarine	441.36	ADAR	442	$[M+Na]^+$	< 1 ppm	442	$[M+H]^+$	< 1 ppm	442	$[M+H]^+$	< 1 ppm
VI	Clenbuterol	277.19	CLNB	277	$[M+H]^+$	< 1 ppm	277	$[M+H]^+$	< 1 ppm	277	$[M+H]^+$	< 1 ppm
VI	Zeranol	322.40	ZRNL	321	$[M-H]^-$	< 1 ppm	321	$[M-H]^-$	< 1 ppm	321	$[M-H]^-$	< 1 ppm

				SFC (40% FA) (CO_2 + 40% MeOH + 0.1% FA) Q3 Scan Base Peak			SFC (20% FA) (CO_2 + 20% MeOH + 0.1% FA) Q3 Scan Base Peak			SFC (10% FA) (CO_2 + 10% MeOH + 0.1% FA) Q3 Scan Base Peak		
Class	Steroid	MW	ID	m/z	Ion	Conc.	m/z	Ion	Conc.	m/z	Ion	Conc.
I	Stanozolol	328.49	STNZ	329	$[M+H]^+$	< 5 ppm	329	$[M+H]^+$	< 5 ppm	329	$[M+H]^+$	< 5 ppm
I	Danazol	337.46	DNZL	338	$[M+H]^+$	< 1 ppm	338	$[M+H]^+$	< 1 ppm	338	$[M+H]^+$	< 1 ppm
II-(a)	Epitestosterone	288.42	EPIT	289	$[M+H]^+$	< 5 ppm	289	$[M+H]^+$	< 5 ppm	289	$[M+H]^+$	< 5 ppm
II-(a)	Testosterone	288.42	TSTO	289	$[M+H]^+$	< 1 ppm	289	$[M+H]^+$	< 1 ppm	289	$[M+H]^+$	< 1 ppm
II-(a)	Mibolerone	302.50	MIBL	303	$[M+H]^+$	< 1 ppm	303	$[M+H]^+$	< 1 ppm	303	$[M+H]^+$	< 1 ppm
II-(a)	Methyltestosterone	302.45	MTHY	303	$[M+H]^+$	< 1 ppm	303	$[M+H]^+$	< 1 ppm	303	$[M+H]^+$	< 1 ppm
II-(b)	1-Androstenedione	286.41	1STEN	287	$[M+H]^+$	< 1 ppm	287	$[M+H]^+$	< 1 ppm	287	$[M+H]^+$	< 1 ppm
II-(c)	Trenbolone	270.37	TRNB	271	$[M+H]^+$	< 1 ppm	271	$[M+H]^+$	< 1 ppm	271	$[M+H]^+$	< 1 ppm
II-(c)	Gestrinone	308.41	GSTN	301	$[M+H]^+$	< 1 ppm	309	$[M+H]^+$	< 1 ppm	309	$[M+H]^+$	< 1 ppm
II-(c)	Metribolone	284.39	MTRB	285	$[M+H]^+$	< 1 ppm	285	$[M+H]^+$	< 1 ppm	285	$[M+H]^+$	< 1 ppm
VI	Andarine	441.36	ADAR	442	$[M+H]^+$	< 1 ppm	442	$[M+H]^+$	< 1 ppm	442	$[M+H]^+$	< 1 ppm
VI	Clenbuterol	277.19	CLNB	277	$[M+H]^+$	< 0.1 ppm	-	-	-	-	-	-
VI	Zeranol	322.40	ZRNL	323	$[M-H]^-$	> 1 ppm	323	$[M-H]^-$	< 1 ppm	323	$[M-H]^-$	< 1 ppm

3.6. GROUP II. Conjugated; C3-Keto-steroids.

3.6.1. Group II; Q3 Scans with Flow Injection Analysis.

Group II steroids are characterized by a conjugated, keto-functional group at position C-3; where ionization is expected to occur and are stabilized by the conjugation. This combination produces abundant, stable, protonated molecular ions $[M+H]^+$ due to good proton affinity and stability, which additionally means they are expected to give lower LODs compared to steroids that form alternative ions.

In the current work, all 3-keto-steroids with a single conjugation in the A- ring (Groups II-(a), II-(b) and II-(c)), produced both the protonated molecular ion $[M+H]^+$ as well as a sodium adduct ion $[M+Na]^+$ under FIA conditions (S_Figure 3 and S_Figure 4). When MeOH-only was used, the dominant ion was always $[M+Na]^+$, but alternatively, when an additive was utilized the protonated molecular ion $[M+H]^+$ was always dominant. Ammonium formate was more successful in suppression of adduct formation and produced the lowest % abundance of the adduct (S_Table 1; **Groups II-a, II-b** and **II-c**). This group also tended to only require the lowest concentration solutions while using methanol with and without ammonium formate, but required slightly higher concentrations when using formic acid as additive. 1STEN, EPIT & TRNB required an increase in concentration with AmFo (**Table 11; Groups II-a, II-b** and **II-c**).

When pure MeOH was used, $[M+Na]^+$ was the base peak for group II steroids as expected.[44] HPLC solvents are stored in borosilicate glass containers, which generally tends to be a sodium source for cationization. The presence of sodium appears to result in competition between the sodium adduct formation and protonation during the electrospray process. Apparently this effect was easily corrected by adding an additive to the methanol (increasing the available proton source), which in both the cases (formic acid and ammonium formate) resulted in the dominant ion as $[M+H]^+$. The addition of ammonium formate resulted in increased protonation, and therefore reduced the abundance of $[M+Na]^+$ ions.

3.6.2. Group II: Q3 Scans with CO_2-based MPs.

The presence of CO_2 in the mobile phase had a significant effect on sodium adduct formation for conjugated keto-steroids. In all circumstances the sodium adduct formation was reduced in the presence of CO_2, and the protonated molecular ion was the dominant ion (**Table 12**)**.** The weakest effect was observed with AmFo as additive. However, with 0.1% FA the sodium adduct was not observed no matter the modifier concentration for many of the group 1 steroids (**S_Table 2**). For the compounds where the sodium adduct was observed, abundance was nearly half that observed in FIA. Most remarkably, even using methanol with no additive sodium adduct formation was greatly reduced, as shown in **Figure 34** for Group II-(a) steroids, and **S_Figure 4** for Group II-(c) steroids.

The fact that CO_2-based MPs suppress sodium adduct formation could simply be due to the lower concentration of MeOH, compared to using FIA, but this explanation seems insufficient. Even 10% MeOH + additive is strong enough to promote $[M+H]^+$ as the dominant ion, and suppress sodium adduct formation. Regardless, $[M+H]^+$ can be chosen as precursor for Group II: 4-ene, 1-ene, and triene C3-keto steroids, using CO_2 based MP's.

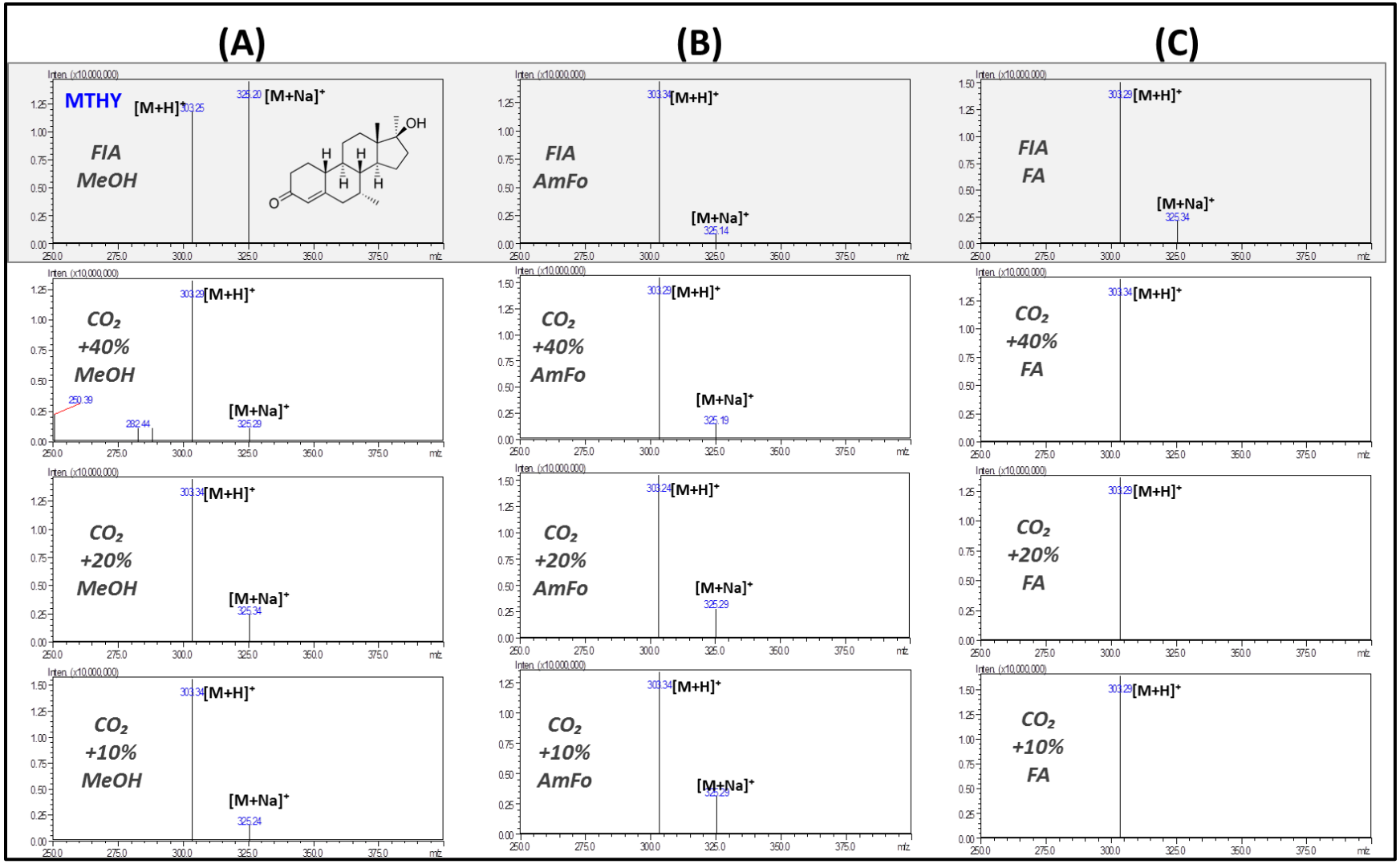

Figure 34. Representative ESI- Q3 Scan Spectra Showing Characteristic Effect of Carbon Dioxide (CO_2) Based Mobile Phases on Ionization Profile for Group II-(b) Steroids (containing a conjugated; keto-function; using Methytestosterone [MTHY] as example); showing comparison between flow injection analysis [FIA, top] versus three modifier concentrations (40%, 20% and 10%) in CO_2 of: (A) methanol [MeOH], (B) MeOH + 5mM ammonium formate [AmFo], and (C) MeOH + 0.1% formic acid [FA] as modifier.

3.7. GROUP II-(d). 1,4-Diene Steroids.

3.7.1. Group II-(d): Q3 Scans with Flow Injection Analysis.

Similar to the other group II steroids, METD also gave the dominant ion of $[M+Na]^+$ for Q3 scans performed using FIA with MeOH alone. But unlike any other Group II steroid, METD, also gave fragment $[M+H-H_2O]^+$ ions, which no other conjugated, C3-keto-steroid produced (**Table 11; Group II-d**). Although this fragment ion was minor when using methanol with no additive, the $[M+H-H_2O]^+$ ion was more abundant than the $[M+H]^+$ ion (**S_Figure 2; C, Top**), but both were much lower abundance than the $[M+Na]^+$ dominant ion. So METD did not follow the same pattern as all the other conjugated keto-steroids, where only the protonated molecular ion or adduct ion were observed.

When using additive (**S_Figure 2; C, middle & bottom**), the $[M+H-H_2O]^+$ was the dominant ion for METD. Using AmFo and FA as additives, the second most abundant ion was now $[M+H]^+$, and the abundance of the sodium adduct was reduced (**S_Table 1; Group II-d**). METD is structurally different from the rest of Group II steroids, where it is cross-conjugated in the A ring (1,4-diene-3-keto form), this has been reported to lead to alternative fragmentation patterns (even to alternative diene steroids such as 4,9-diene-3-keto forms), which can promote the loss of water during gas phase formation.[45]

3.7.2. Group II-(d): Q3 Scans with CO_2-based MPs.

Using FIA, METD did not follow the same pattern as the other conjugated keto steroids, having significant fragmentation, producing the dominant ion of $[M+H-H_2O]^+$, with additive in the mobile phase. With CO_2, under all conditions using SFC MPs, $[M+H]^+$ was the dominant ion for METD (**Table 13**).

Using CO_2 based mobile phases, the sodium adduct $[M+Na]^+$ of METD was more prominent than what was observed using FIA with 100% modifier (with no additive and with AmFo), but alternatively with formic acid, the sodium adduct $[M+Na]^+$ was decreased when compared to FIA (**Figure 35**). Furthermore, with SFC-based MPs, a change in relative abundance was observed based on concentration; as the percent modifier was increased, the proportion of $[M+H-H_2O]^+$ increased with all modifiers in CO_2 (**S_Table 3**). Although a decrease in sensitivity may

be observed with methanol alone or with AmFo, regardless of the increased abundance of $[M+Na]^+$, either $[M+H]^+$ or $[M+H-H_2O]^+$ could easily be used as precursor while using SFC-MPs.

Table 13. Q3 Scan Summary of Dominant Ion for Groups III, IV and V Steroids for Carbon Dioxide (CO_2)-based Mobile Phases.

				SFC (40% MeOH) (CO_2 + 40% MeOH) Q3 Scan Base Peak			SFC (20% MeOH) (CO_2 + 20% MeOH) Q3 Scan Base Peak			SFC (10% MeOH) (CO_2 + 10% MeOH) Q3 Scan Base Peak		
Class	Steroid	MW	ID	m/z	Ion	Conc.	m/z	Ion	Conc.	m/z	Ion	Conc.
II-(d)	Methandienone	300.44	METD	301	$[M+H]^+$	< 5 ppm	301	$[M+H]^+$	< 5 ppm	301	$[M+H]^+$	< 5 ppm
III-(a)	7-Keto-DHEA	302.20	KETO	285	$[M+H-H_2O]^+$	< 1 ppm	285	$[M+H-H_2O]^+$	< 1 ppm	285	$[M+H-H_2O]^+$	< 1 ppm
III-(b)	Androsterone	290.44	ADEN	273	$[M+H-H_2O]^+$	< 10 ppm	273	$[M+H-H_2O]^+$	< 10 ppm	273	$[M+H-H_2O]^+$	< 10 ppm
III-(b)	Etiocholanolone	290.44	ETIO	273	$[M+H-H_2O]^+$	> 10 ppm	273	$[M+H-H_2O]^+$	> 10 ppm	273	$[M+H-H_2O]^+$	> 10 ppm
IV	1-Androsterone	290.44	1DHEA	255	$[M+H-2H_2O]^+$	> 10 ppm	273	$[M+H-H_2O]^+$	> 10 ppm	273	$[M+H-H_2O]^+$	> 10 ppm
IV	Prasterone	288.21	PRST	271	$[M+H-H_2O]^+$	> 10 ppm	271	$[M+H-H_2O]^+$	> 10 ppm	271	$[M+H-H_2O]^+$	> 10 ppm
V	Oxandrolone	306.44	OXAN	329	$[M+Na]^+$	> 10 ppm	329	$[M+Na]^+$	> 10 ppm	307	$[M+H]^+$	> 10 ppm
V	Mesterolone	304.47	MSEL	305	$[M+H]^+$	< 10 ppm	305	$[M+H]^+$	< 10 ppm	305	$[M+H]^+$	< 10 ppm
V	Mestanolone	304.47	MSAL	305	$[M+H]^+$	< 1 ppm	305	$[M+H]^+$	< 1 ppm	305	$[M+H]^+$	< 1 ppm
V	Androstanolone	290.44	ADON	305	$[M+H+MeOH-H_2O]^+$	< 5 ppm	305	$[M+H+MeOH-H_2O]^+$	< 5 ppm	305	$[M+H+MeOH-H_2O]^+$	< 5 ppm

				SFC (40% AmFo) (CO_2 + 40% MeOH + 5mM AmFo) Q3 Scan Base Peak			SFC (20% AmFo) (CO_2 + 20% MeOH + 5mM AmFo) Q3 Scan Base Peak			SFC (10% AmFo) (CO_2 + 10% MeOH + 5mM AmFo) Q3 Scan Base Peak		
Class	Steroid	MW	ID	m/z	Ion	Conc.	m/z	Ion	Conc.	m/z	Ion	Conc.
II-(d)	Methandienone	300.44	METD	301	$[M+H]^+$	< 5 ppm	301	$[M+H]^+$	< 5 ppm	301	$[M+H]^+$	< 5 ppm
III-(a)	7-Keto-DHEA	302.20	KETO	285	$[M+H-H_2O]^+$	> 1 ppm	285	$[M+H-H_2O]^+$	> 1 ppm	285	$[M+H-H_2O]^+$	< 1 ppm
III-(b)	Androsterone	290.44	ADEN	273	$[M+H-2H_2O]^+$	> 10 ppm	273	$[M+H-2H_2O]^+$	< 10 ppm	273	$[M+H-2H_2O]^+$	< 10 ppm
III-(b)	Etiocholanolone	290.44	ETIO	273	$[M+H-2H_2O]^+$	> 10 ppm	273	$[M+H-2H_2O]^+$	< 10 ppm	273	$[M+H-2H_2O]^+$	< 10 ppm
IV	1-Androsterone	290.44	1DHEA	273	$[M+H-2H_2O]^+$	> 10 ppm	273	$[M+H-2H_2O]^+$	> 10 ppm	273	$[M+H-2H_2O]^+$	> 10 ppm
IV	Prasterone	288.21	PRST	271	$[M+H-H_2O]^+$	> 10 ppm	271	$[M+H-H_2O]^+$	< 10 ppm	271	$[M+H-H_2O]^+$	< 10 ppm
V	Oxandrolone	306.44	OXAN	307	$[M+Na]^+$	> 10 ppm	307	$[M+H]^+$	> 10 ppm	307	$[M+H]^+$	> 10 ppm
V	Mesterolone	304.47	MSEL	305	$[M+H]^+$	< 10 ppm	305	$[M+H]^+$	< 10 ppm	305	$[M+H]^+$	< 10 ppm
V	Mestanolone	304.47	MSAL	304	$*[M]^+$	< 1 ppm	304	$*[M]^+$	< 1 ppm	304	$*[M]^+$	< 1 ppm
V	Androstanolone	290.44	ADON	305	$[M+H+MeOH-H_2O]^+$	< 5 ppm	305	$[M+H+MeOH-H_2O]^+$	< 5 ppm	305	$[M+H+MeOH-H_2O]^+$	< 5 ppm

				SFC (40% FA) (CO_2 + 40% MeOH + 0.1% FA) Q3 Scan Base Peak			SFC (20% FA) (CO_2 + 20% MeOH + 0.1% FA) Q3 Scan Base Peak			SFC (10% FA) (CO_2 + 10% MeOH + 0.1% FA) Q3 Scan Base Peak		
Class	Steroid	MW	ID	m/z	Ion	Conc.	m/z	Ion	Conc.	m/z	Ion	Conc.
II-(d)	Methandienone	300.44	METD	301	$[M+H]^+$	< 5 ppm	301	$[M+H]^+$	< 5 ppm	301	$[M+H]^+$	< 5 ppm
III-(a)	7-Keto-DHEA	302.20	KETO	285	$[M+H-H_2O]^+$	< 1 ppm	285	$[M+H-H_2O]^+$	< 1 ppm	285	$[M+H-H_2O]^+$	< 1 ppm
III-(b)	Androsterone	290.44	ADEN	273	$[M+H-2H_2O]^+$	< 10 ppm	273	$[M+H-2H_2O]^+$	< 10 ppm	273	$[M+H-2H_2O]^+$	< 10 ppm
III-(b)	Etiocholanolone	290.44	ETIO	273	$[M+H-H_2O]^+$	< 10 ppm	273	$[M+H-H_2O]^+$	< 10 ppm	273	$[M+H-H_2O]^+$	< 10 ppm
IV	1-Androsterone	290.44	1DHEA	291	$[M+H]^+$	> 10 ppm	291	$[M+H]^+$	> 10 ppm	273	$[M+H-2H_2O]^+$	> 10 ppm
IV	Prasterone	288.21	PRST	288	$[M]^+$	> 10 ppm	271	$[M+H-H_2O]^+$	> 10 ppm	271	$[M+H-H_2O]^+$	< 10 ppm
V	Oxandrolone	306.44	OXAN	307	$[M+H]^+$	> 10 ppm	307	$[M+H]^+$	> 10 ppm	307	$[M+H]^+$	> 10 ppm
V	Mesterolone	304.47	MSEL	305	$[M+H]^+$	< 10 ppm	305	$[M+H]^+$	< 10 ppm	305	$[M+H]^+$	< 10 ppm
V	Mestanolone	304.47	MSAL	288	$[M+H-H_2O]^+$	< 1 ppm	305	$[M+H]^+$	< 1 ppm	305	$[M+H]^+$	< 1 ppm
V	Androstanolone	290.44	ADON	305	$[M+H+MeOH-H_2O]^+$	< 5 ppm	305	$[M+H+MeOH-H_2O]^+$	< 5 ppm	305	$[M+H+MeOH-H_2O]^+$	< 5 ppm

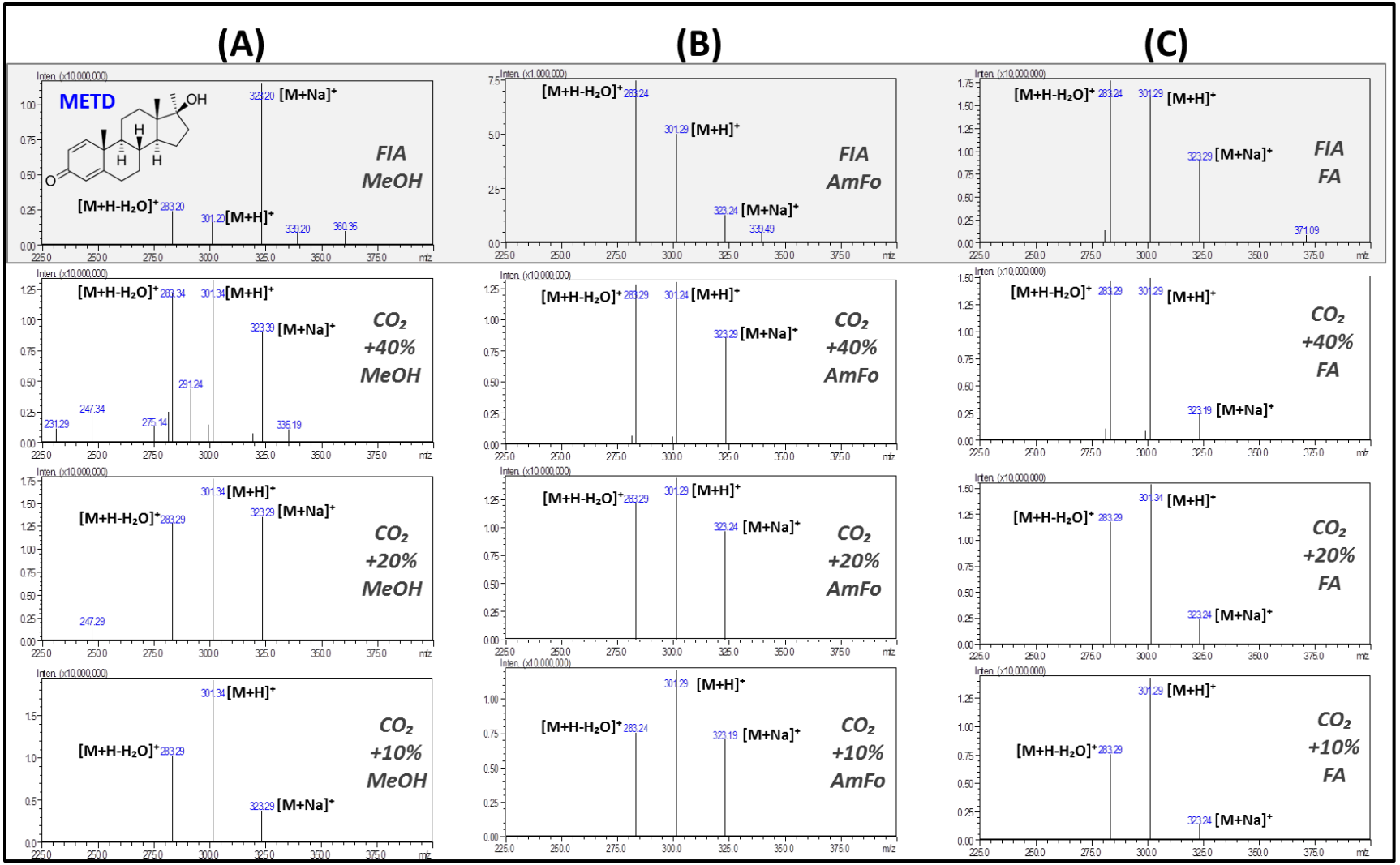

Figure 35. ESI- Q3 Scan Spectra Showing Characteristic Effect of Carbon Dioxide (CO_2) Based Mobile Phases on Ionization Profile of Group II-(d) steroid: Methandienone [METD] (containing 1-4-diene-3-keto nucleus); showing comparison between flow injection analysis [FIA, gray, top] versus three modifier concentrations (40%, 20% and 10%) using: (A) methanol [MeOH, left], (B) MeOH + 5mM ammonium formate [AmFo, middle], and (C) MeOH + 0.1% formic acid [FA, right] as modifier.

3.8. Group III & IV. C3-Hydroxyl Steroids.

Compounds containing a hydroxyl-functional group at position C3, gave rise to not only protonated molecular ions and adducts, but also to fragment ions $[M+H-H_2O]^+$ or $[M+H-2H_2O]^+$, due to instability of the protonated molecules. This was to be expected, as protonation can only occur at the C17 ketone group, which often results in a neutral loss of H_2O. For groups III and IV the base peak was always $[M+H-H_2O]^+$, regardless of if an additive was or was not used under FIA conditions (S_Figure 5).

3.8.1. GROUP III-(a). Non-conjugated; C-3 Hydroxyl, 7-Keto.

3.8.1.1. Group III-(a): Q-3 Scans with Flow Injection Analysis.

KETO also did not follow the pattern observed for other steroids in its class. Having an unconjugated hydroxyl group at C3, KETO is expected to form multiple fragment ions due to the loss of water. Therefore KETO should be expected to have high LODs, requiring higher concentrations of the analyte for detection due to signal loss from multiple ion formation. But this was not what was observed for KETO. Instead, no matter the mobile phase used (S_Figure 2; **D**), KETO produced the $[M+H-H_2O]^+$ ion, but no other ions were observed under any FIA conditions (S_Table 1; **Group III-a**). KETO would also be expected to have a high LOD, but KETO only required the lowest concentration MRM-solutions (**Table 11; Group III-a)**. These observations can be explained by the conjugated keto group at C7, this would be expected to be the favored position for protonation, where the conjugation at C6-C7 would stabilize the ion. This is supported by observations from literature where $[M+Na+MeOH]^+$ was used for precursor ion using methanol with and without additive, but they also observed $[M+H-H_2O]^+$ but only while using acetonitrile as modifier.[36]

3.8.1.2. Group III-(a): Q-3 Scans with CO_2-based MPs.

Using FIA, KETO gave the fragment $[M+H-H_2O]^+$ as the dominant ion, and only with methanol with no additive were any other fragments observed, which corresponded to a fragment with 3 waters lost $[M+H-3H_2O]^+$. With CO_2, $[M+H-H_2O]^+$ was also always the dominant ion (**Table 13).**

Although the characteristic ions $[M+H]^+$, $[M+Na]^+$, and $[M+H-2H_2O]^+$ were not produced (S_Table 3) other ions were detected, and the presence of alternative ions was dependent on the additive used (**Figure 36**). With both methanol with no additive and with AmFo, additional adducts were observed with the presence of CO_2, especially when modified with high concentrations of the modifier (> 20%). The $[M+H-3H_2O]^+$ ion was observed, but also sodium and/or modifier adducts; all alternative ions observed for KETO are presented in **Table 14**. All additional ions were < 30% relative abundance to the dominant ion, which was always the $[M+H-H_2O]^+$ fragment ion, suggesting that this ion could easily be chosen as precursor for KETO, regardless of the MP additive for SFC-based MPs modified with MeOH.

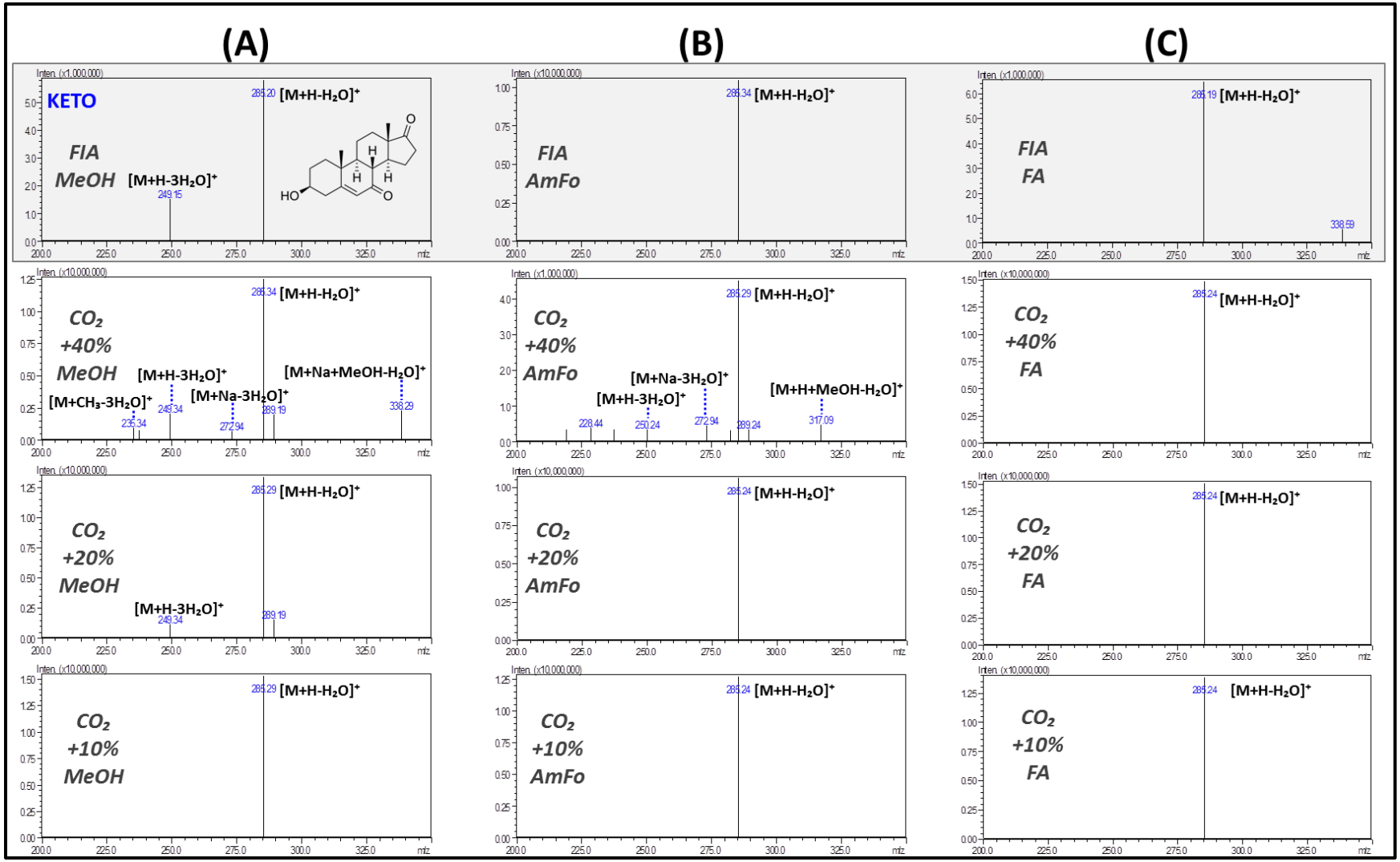

Figure 36. ESI- Q3 Scan Spectra Showing Characteristic Effect of Carbon Dioxide (CO_2) Based Mobile Phases on Ionization Profile of Group III-(a) steroid: 7-keto-DHEA [KETO] (containing non-conjugated, hydroxyl function at C3 and conjugated keto at C7); showing comparison between flow injection analysis [FIA, gray, top] versus three modifier concentrations (40%, 20% and 10%) using: (A) methanol [MeOH, left], (B) MeOH + 5mM ammonium formate [AmFo, middle], and (C) MeOH + 0.1% formic acid [FA, right] as modifier.

Table 14. **Q3 Scan Summary of Alternative Ions for 7-Keto-DHEA [KETO] using Carbon Dioxide (CO_2)-based Mobile Phases.**

	ID:	KETO											
	Steroid:	7-keto-DHEA											
	Molecular Weight:	302.20											
	Mobile Phase:	Methanol (MeOH)				Methanol + 5mM Ammonium Formate				Methanol + 0.1% Formic Acid (FA)			
		FIA	SFC			FIA	SFC			FIA	SFC		
		100%	40%	20%	10%	100%	40%	20%	10%	100%	40%	20%	10%
		Relative abundance of characteristic ions (%)				Relative abundance of characteristic ions (%)				Relative abundance of characteristic ions (%)			
NOI	$[M+H]^+$	-	-	-	-	-	-	-	-	-	-	-	-
	$[M+Na]^+$	-	-	-	-	-	-	-	-	-	-	-	-
	$[M+H-H_2O]^+$	285 (100%)	285 (100%)	285 (100%)	285 (100%)	285 (100%)	285 (100%)	285 (100%)	285 (100%)	285 (100%)	285 (100%)	285 (100%)	285 (100%)
	$[M+H-2H_2O]^+$	-	-	-	-	-	-	-	-	-	-	-	-
	$[M+H-3H_2O]^+$	249 (27%)	249 (18%)	249 (15%)	-	-	250 (7%)	-	-	-	-	-	-
	$[M+Na-3H_2O]^+$	-	272 (5%)	-	-	-	272 (10%)	-	-	-	-	-	-
	$[M+H+MeOH-H_2O]^+$	-	-	-	-	-	317 (11%)	-	-	-	-	-	-
	$[M+Na+MeOH-H_2O]^+$	-	338 (36%)	-	-	-	-	-	-	-	-	-	-

3.8.2. GROUP III. Non-conjugated; C3-Hydroxy Steroids.

3.8.2.1. Group III-(b): Q3 Scans with Flow Injection Analysis.

All steroids with an unconjugated hydroxyl–function at C3 gave the dominant ion of $[M+H-H_2O]^+$ under FIA conditions as expected (**Table 11; Group III-b**). Although both ETIO and ADEN always gave $[M+H-H_2O]^+$ as the most abundant ion (**S_Figure 5; A & B**), other ions were also produced (although at much lower abundance) fragments from an additional water loss $[M+H-2H_2O]^+$, which was always over twice the abundance of the molecular ion $[M+H]^+$ (~40% and ~10% respectively) for ETIO (not shown). Group III-(b) steroids also produced the sodium adduct ions, but they were only significant (> 60% abundance) when MeOH with no additive was used under FIA conditions (**S_Table 1; Group III-b**).

Although KETO did not produce additional fragments, due to conjugation at C-6, allowing for other protonation pathways for more stable protonated fragment ion formation, and so did not require higher concentrations, even though the dominant ion was not the protonated molecular ion, and instead produced the stable abundant fragment from the neutral loss of water (**Table 11; Group III-a**).

3.8.2.2. Group III-(b): Q3 Scans with CO_2-based MPs.

While using CO_2 as the majority of the mobile phase, $[M+H-H_2O]^+$ was still always the most abundant ion (**Table 13**). The sodium adduct $[M+Na]^+$ was observed in CO_2 + MeOH with no additive (**Figure 37; panel A**), but was greatly reduced when CO_2 was present in the mobile phase (< 16% relative abundance [**S_Table 3**]) versus what was observed using flow injection analysis with 100% modifier, where the sodium adduct was much more pronounced for these steroids being nearly as abundant as the base peak (< 70% relative abundance). This suggests reduced competition for ionization in SFC-based mobile phases, even when no additive is used, for these steroids.

Non-conjugated steroids are thought to be less stable, readily fragmenting in source to form multiple ions. Using CO_2, the greatest variety of ions was observed for group II-(b) steroids using MeOH + 0.1% FA, where the most additional solvent adducts were observed (**Figure 37; panel C**); these were especially noticeable at higher modifier concentrations. The least amount of alternative ions were observed with AmFo (**Figure 37; panel B**), and just as in FIA, the sodium adduct, is not observed.

****Under closer inspection, several additional peaks were found that co-elute with the main ADEN peak at high modifier concentration, but are fully resolved at lower modifier concentration (see Section: S_3.4.1. ADDITIONAL PEAKS observed for ADEN). ****

****Under closer inspection, several additional peaks were found that co-elute with the main ETIO peak at high modifier concentration, but are fully resolved at lower modifier concentration (see Section: S_3.4.2. ADDITIONAL PEAKS observed for ETIO). ****

Generally, no matter the composition of the modifier used, $[M+H-H_2O]^+$ should be chosen as precursor for Group III-(b) steroids.

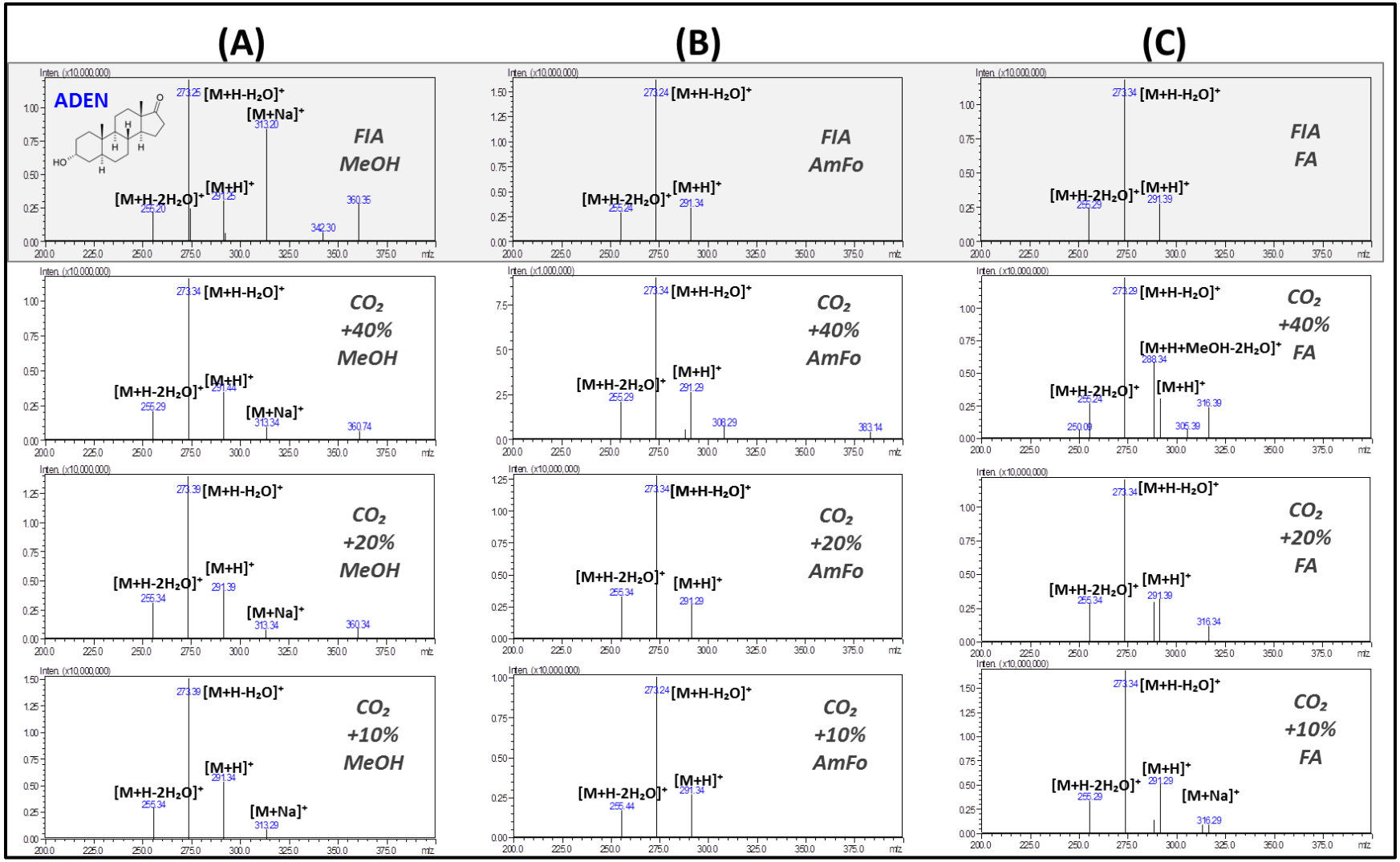

Figure 37. Representative ESI- Q3 Scan Spectra Showing Characteristic Effect of Carbon Dioxide (CO_2) Based Mobile Phases on Ionization Profile of Group III-(b) steroids (containing non-conjugated,hydroxyl function at C3, using Androsterone [ADEN] for example); showing comparison between flow injection analysis [FIA, top] versus three modifier concentrations (40%, 20% and 10%) in CO_2 of: (A) methanol [MeOH], (B) MeOH + 5mM ammonium formate [AmFo], and (C) MeOH + 0.1% formic acid [FA] as modifier.

3.8.3. GROUP IV. Conjugated; C3-Hydroxyl Steroids

3.8.3.1. Group IV: Q3 Scans with Flow Injection Analysis.

1DHEA is the only steroid in this work having a conjugation adjacent to the hydroxyl function at C3. PRST also has a conjugation, but in the adjacent ring at C5. Most ions associated with this group are related to water loss. After the loss of water, the double bond can stabilize the positive charge generated.[36]

Using FIA, both 1DHEA and PRST produced the same 3 dominant ions with relative abundance following the order: $[M+H-H_2O]^+$ > $[M+H-2H_2O]^+$ > $[M+H]^+$. With 1DHEA the relative abundance of the 3 ions were fairly similar, whereas with PRST, the $[M+H-H_2O]^+$ ion was much larger than the others. Additives had little effect. The highest concentrations of the standards were required to obtain a stable signal (**Table 11**). The presence of multiple significant ions point to lower sensitivity compared to Group III.

3.8.3.2. Group IV: Q3 Scans with CO_2-based MPs.

1DHEA. With CO_2 present, the dominant ion for 1DHEA was dependent on the composition of the mobile phase (**Table 13**). At low and medium methanol concentrations, fragmentation was similar to the FIA result except $[M+H]^+$ abundance was slightly higher than $[M+H-2H_2O]^+$, with several small additional adducts appearing. At the high methanol concentration, several additional adducts, incorporating MeOH and others formed (**Figure 38**). With FA as additive, the $[M+H+MeOH-2H_2O]^+$ ion was dominant. The highest modifier concentration (40%) produced the least similar result to that observed using 100% modifier. No matter the dominant ion, higher solution concentrations were always needed compared to FIA. It is difficult to choose an optimal precursor, as any of the three most intense ions for 1DHEA: $[M+H]^+$, $[M+H-H_2O]^+$, or $[M+H-2H_2O]^+$ could perform nearly the same.

****Under closer inspection, several additional peaks were found that co-elute with the main 1DHEA peak at high modifier concentration, but are fully resolved at lower modifier concentration (see Section: S_3.4.3. ADDITIONAL PEAKS observed for 1DHEA). ****

PRST. With CO_2 present, the dominant ion was almost always $[M+H-H_2O]^+$. With lower methanol concentrations, fragmentation was again most similar to the FIA result. At high methanol concentration a number of lower abundance ions formed, along with several large and unusual ions: $[M]^+$ and $[M+Na+MeOH-H_2O]^+$ were present.

The most dominant ion for PRST was also variable while using CO_2 in the MP (**Table 13**). Ion formation was the most stable (e.g., least amount of alternative ions observed) while using methanol with no additive (**Figure 39**; **Panel A**). Although minor solvent adduct ions were observed (mainly $[M+H+MeOH-H_2O]^+$, a significant unidentified ion (*m/z* 316), and its corresponding sodium adduct (*m/z* 336), the dominant ion was always $[M+H-H_2O]^+$. This was not the case when an additive was used.

Using AmFo (**Figure 39; Panel B**), the solvent adduct $[M+Na+MeOH-H_2O]^+$ was observed, and at high modifier concentration this adduct was the dominant ion. Furthermore, using formic acid as additive (**Figure 39; Panel C**) produced the most variable result. Where a significant unidentified ion (*m/z* 316) was consistently formed at high modifier concentration (≥ 20%), but even more striking the molecular ion $[M]^+$ was the dominant ion. At lower methanol concentration the protonated molecular ion $[M+H]^+$ was observed and the $[M+H-H_2O]^+$ fragment was the dominant ion. Adequate signal strength was obtained with lower sample concentrations compared to FIA (S_Table 3).

Using methanol with no additive should produce the best sensitivity for this compound and the most reliable result, since at all modifier concentrations $[M+H-H_2O]^+$ should be expected to be the optimal precursor for PRST at all modifier concentrations without additive.

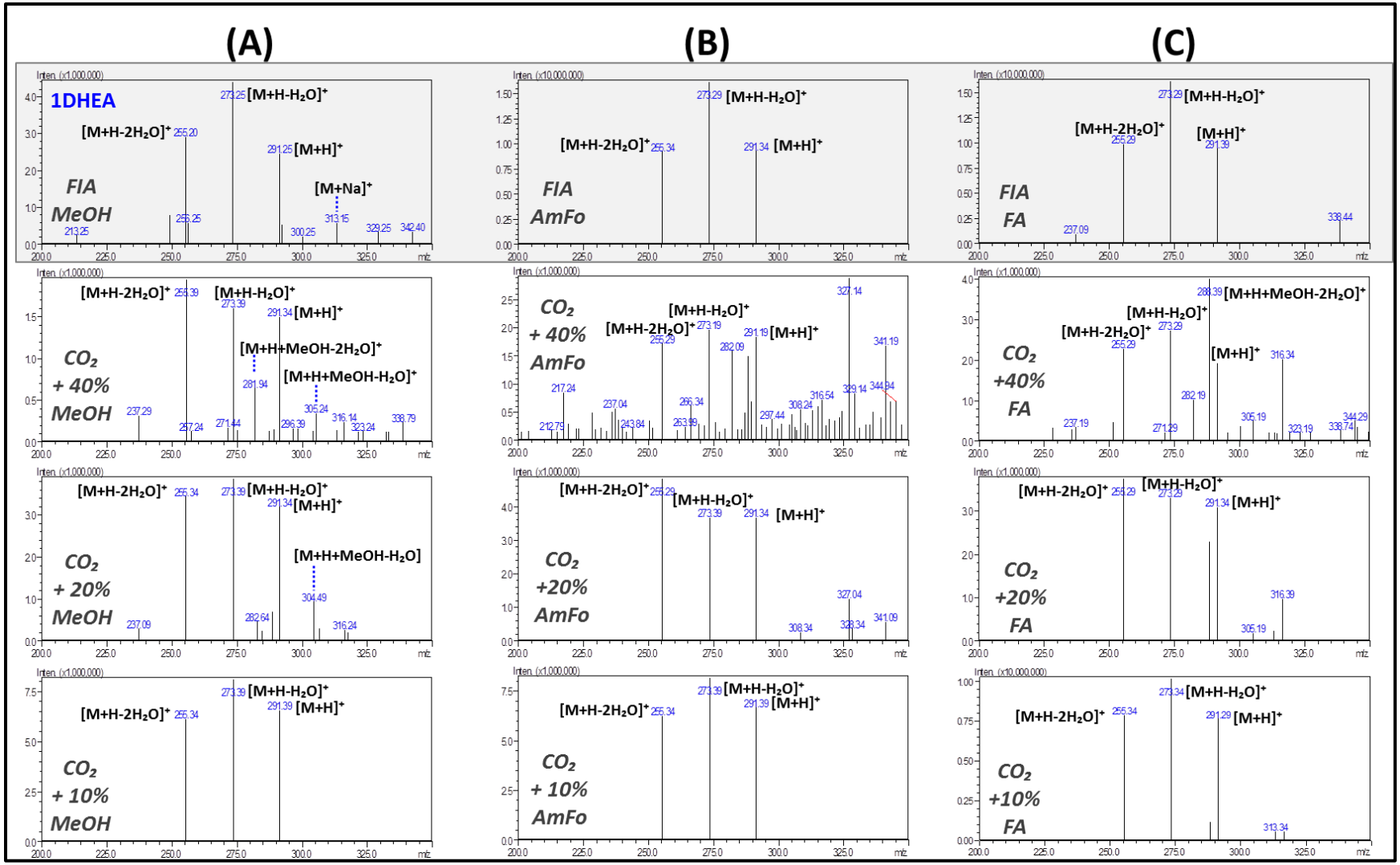

Figure 38. Representative ESI-Q3 Scan Spectra Showing Characteristic Effect of Carbon Dioxide (CO_2) Based Mobile Phases on Ionization Profile of Group IV steroids (containing conjugated, hydroxyl function at C3, using 1-androsterone [1DHEA] for example); showing comparison between flow injection analysis [FIA, top] versus three modifier concentrations (40%, 20% and 10%) in CO_2 of: (A) methanol [MeOH], (B) MeOH + 5mM ammonium formate [AmFo], and (C) MeOH + 0.1% formic acid [FA] as modifier.

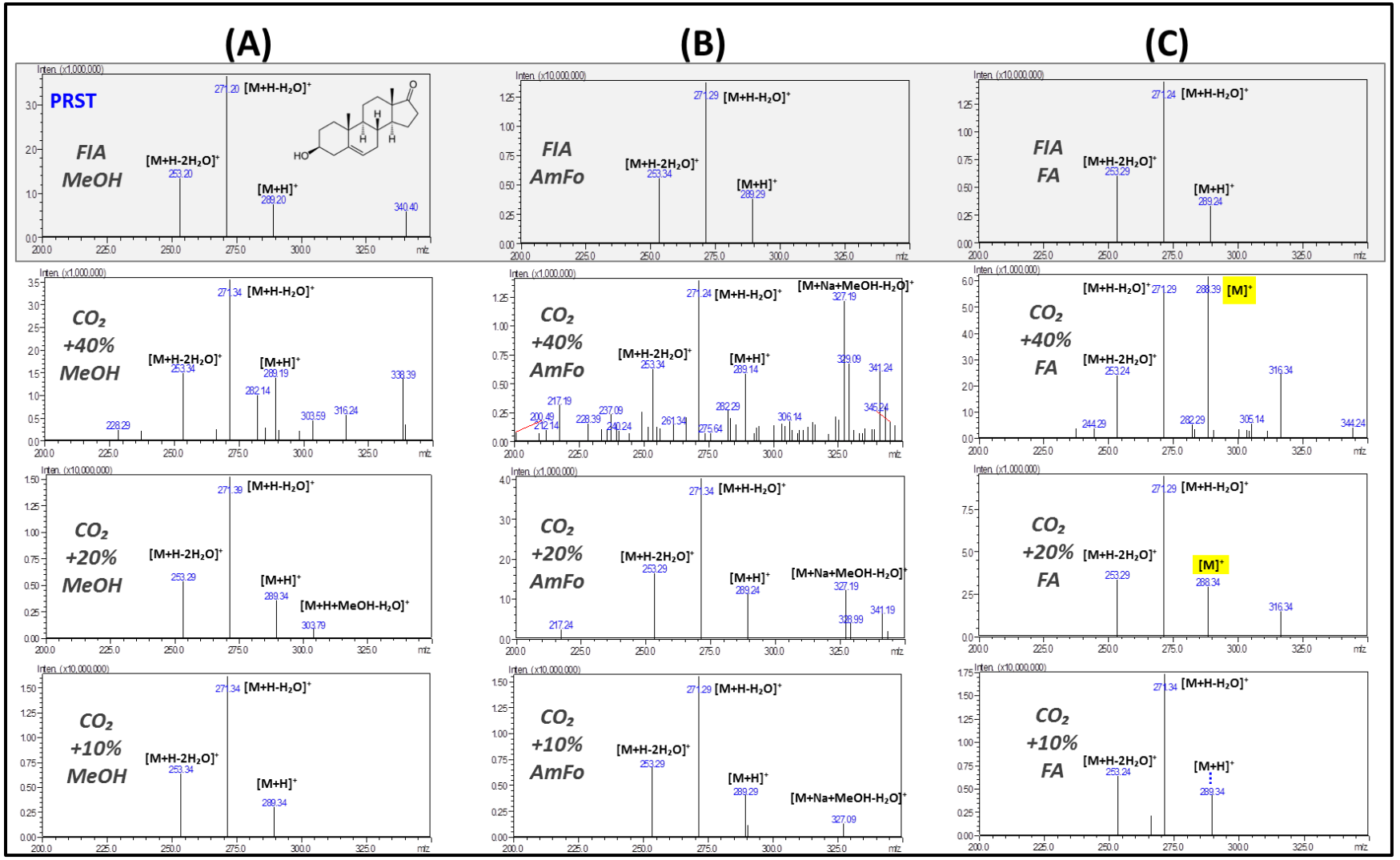

Figure 39. Representative ESI-Q3 Scan Spectra Showing Characteristic Effect of Carbon Dioxide (CO_2) Based Mobile Phases on Ionization Profile of Group IV steroids (containing conjugated, hydroxyl function at C3, using **prasterone [PRST]** for example); showing comparison between flow injection analysis [FIA, top] versus three modifier concentrations (40%, 20% and 10%) in CO_2 of: (A) methanol [MeOH], (B) MeOH + 5mM ammonium formate [AmFo], and (C) MeOH + 0.1% formic acid [FA] as modifier.

3.9. GROUP V. Non-conjugated; Keto-steroids.

Steroids containing an unconjugated keto-functional group at C3, are expected to produce either $[M+H]^+$ or $[M+H-H_2O]^+$. The protonation site is expected to occur on the keto group but no conjugation is present to stabilize the ion, therefore both $[M+H]^+$ or $[M+H-H_2O]^+$ can be expected.

In the current work, group V steroids, had a few factors in common. $[M+H]^+$ was the dominant ion produced, no matter the mobile phase used under FIA conditions and nearly always required higher concentration MRM-solutions (**Table 11; Group V**). This group produced the most variety and range of characteristic ions across the spectrum for each compound (**S_Figure 6**).

Group V steroids, containing a non-conjugated keto-functional group at C3, did not follow any observable pattern using FIA analysis, and this was also true for when CO2 based MPs were used. Each compound produced a unique set of ions and therefore will be discussed separately.

3.9.1. Q3 Scans for Oxandrolone [OXAN]

OXAN: Flow Injection Analysis. Of the group V steroids OXAN produced the most consistent spectrum across all mobile phases used during FIA operation. The protonated molecular ion $[M+H]^+$ or sodium adduct ion $[M+Na]^+$ was always the dominant ion for OXAN (**Table 11**). The sodium adduct being dominant when no additive was used, but was also significant (>70% abundance) while using formic acid as additive.

Significant presence of the fragment ion $[M+H-H_2O]^+$ was also observed for OXAN, from the neutral loss of water regardless of the MP used for FIA (**S_Figure 6; A**). The addition of formic acid also resulted in higher fragmentation due to water loss (greater than 40%). AmFo had the same effect by increasing the fragmentation, but was more efficient than FA, in suppressing the sodium adduct formation (< 30%) (**S_Table 1; Group V**).

OXAN: CO_2-based MPs. The addition of CO_2 to the mobile phase, had little effect on the dominant ion for OXAN, as the adduct $[M+Na]^+$ or $[M+H]^+$ remained the most intense ion **(Table 13)**. Higher concentration solution

was needed with higher modifier concentration, which was accompanied by an increase in observed alternative ions. Sodium adducts were significant in both MeOH without additive and with ammonium formate (**Figure 40**). In methanol with no additive, the $[M+H]^+$ ion was much higher than that observed in FIA (100% modifier). Other ions were also observed, including the solvent adducts $[M+H+MeOH]^+$ and $[M+Na+MeOH]^+$ and when using AmFo the ammonium adduct $[M+NH_4]^+$ and $[M+H-2H_2O]^+$ were also observed. The protonated molecular ion $[M+H]^+$ was always the dominant ion for OXAN while FA was used as additive in CO_2-based MPs. This suggests the optimal precursor for OXAN may be highly dependent on the additive used (**S_Table 3**). Optimal precursor for OXAN, most likely would be $[M+H]^+$ for MeOH + FA as additive, but the sodium adduct $[M+Na]^+$ may be more effective as precursor if using AmFo as MP additive.

****Under closer inspection, several additional peaks were found that co-elute with the main OXAN peak at high modifier concentration, but are fully resolved at lower modifier concentration (*data not shown*). ****

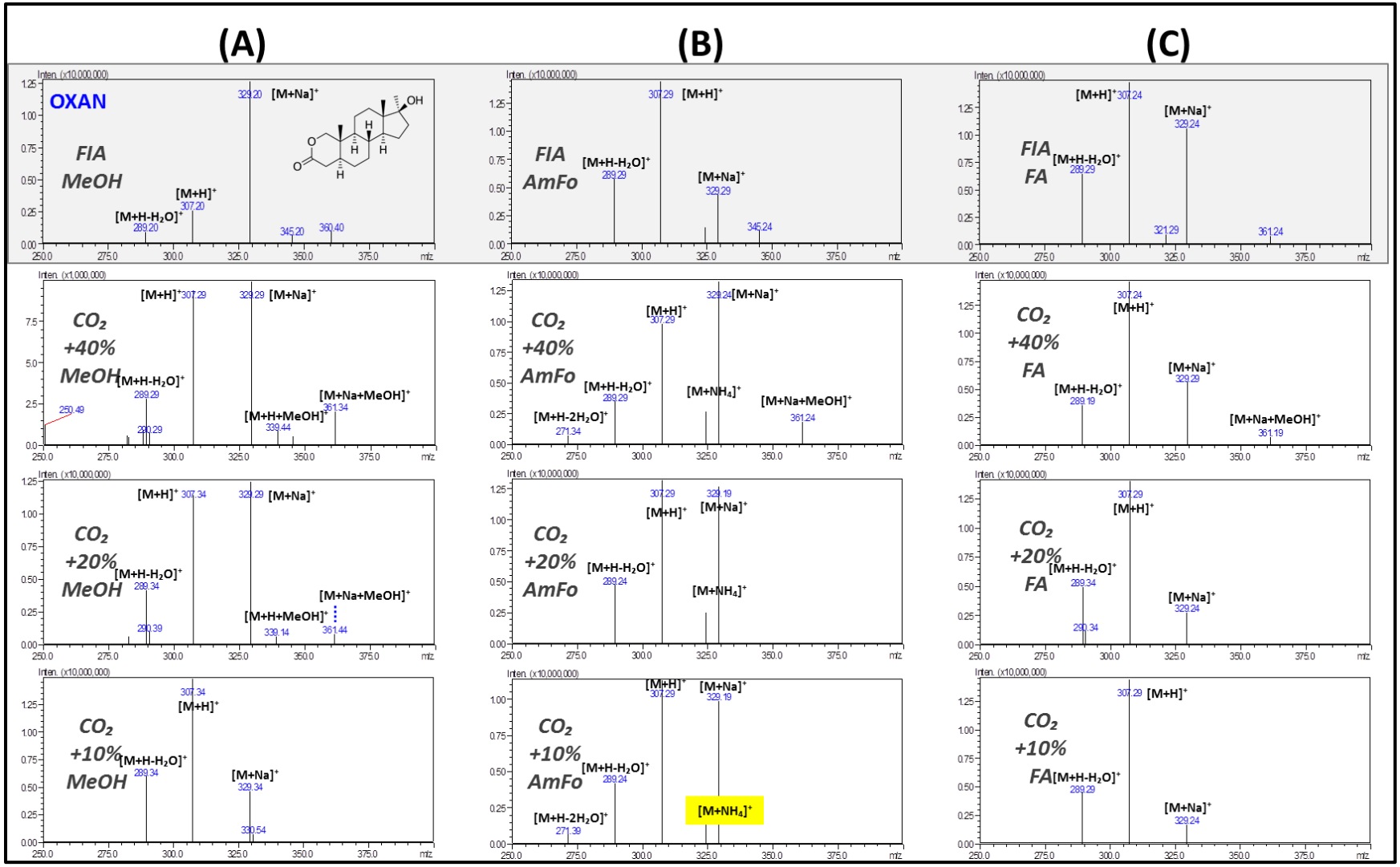

Figure 40. ESI-MS, Q3 Scan Spectra for oxandrolone [OXAN], a Group V steroid; (containing a non-conjugated, keto-function at C3), Showing Effect of Carbon Dioxide (CO_2) Based Mobile Phases on Ionization Profile using three modifier concentrations (40%, 20% and 10% [white; top-to-bottom]); with comparison to flow injection analysis [FIA, Gray top]. (A) methanol [MeOH], (B) MeOH + 5mM ammonium formate [AmFo], and (C) MeOH + 0.1% formic acid [FA] as modifier.

3.9.2. Saturated C3-Keto Steroids.

MSAL and MSEL share the same base structure with ADON, having no conjugation throughout the entire ring system. MSAL & MSEL both have an additional methyl group incorporated into their structure and therefore have a different MW (304 g/mol) than ADON (290 g/mol). The abundant differences between the spectra of the three compounds are remarkable. Each compound produced its own set of characteristic ions using flow injection analysis, with some changes due to additive (**Table 15)**.

3.9.3. Q3 Scans for Mesterolone (MSEL)

MSEL: Q3 Scans with Flow Injection Analysis. MSEL having an additional methyl group on C1 (ring A, adjacent to the hydroxyl group at C3), seems to provide some level of stability for the resulting ions, which were of much lower relative abundance compared to MSAL and ADON. $[M+H]^+$ was the dominant ion under all FIA conditions for MSEL (**Table 11**). Other ions were observed, including a minor sodium adduct while using MeOH with no additive (S_Table 1). Most notably a solvent adduct ion $[M+H+MeOH]^+$ was present when using both additives. Also a minor $[M-CH_3]$ ion was present when using FIA with AmFo (S_Figure 6**; B**).

MSEL: Q3 Scans with CO_2-based MPs. When CO_2 was used as the majority of the MP, the dominant ion was still always $[M+H]^+$ for MSEL (**Table 13**). The fragment due to water loss, $[M+H-H_2O]^+$, was also observed for MSEL, but only at higher modifier concentration while using methanol with no additive, and with FA as additive (S_Table 3).

Additional ions, to those observed using FIA, were produced for MSEL, using CO_2 in the MP (**Figure 41**). For MeOH with no additive, $[M+Na]^+$ was present in flow injection analysis, but not observed when using methanol without additive as modifier in CO_2. The sodium/solvent ion, and solvent ions $[M+H+MeOH]^+$, and $[M+Na+MeOH]^+$ were also observed. Oddly, no sodium adduct had been observed using AmFo as additive during flow injection analysis, but when CO_2 was added to the MP, a significant sodium adduct was present, where at higher modifier (> 20%), the abundance nearly rivaled that of the protonated molecular ion. For MeOH + FA as additive, minor

[M+H+MeOH]$^+$adducts were present, but more notably, the [M+H-H_2O]$^+$ fragment ion (which was notably absent in FIA analysis with FA) was quite significant when CO_2 was present.

****Under closer inspection, several additional peaks were found that co-elute with the main MSEL peak at high modifier concentration, but are fully resolved at lower modifier concentration (see Section: S_3.4.5. ADDITIONAL PEAKS observed for MSEL). ****

Optimal precursor for MSEL, will most likely depend on whether an additive is used, and also will possibly change depending on the concentration of the modifier present in the MP. Low modifier would give the best result as at low concentration (<10%) all MP compositions gave [M+H]$^+$ as the dominant precursor.

Table 15. **Q3 Scan Summary of Alternative Ions for Group V Steroids using Flow Injection Analysis (FIA).**

	ID:	MSEL			MSAL			ADON		
	Steroid:	Mesterolone			Mestanolone			Androstanolone		
	Molecular Weight:	304.00			304.00			290.00		
		Relative abundance of characteristic ions (%)			Relative abundance of characteristic ions (%)			Relative abundance of characteristic ions (%)		
	Mobile Phase:	FIA (MeOH)	FIA (AmFo)	FIA (FA)	FIA (MeOH)	FIA (AmFo)	FIA (FA)	FIA (MeOH)	FIA (AmFo)	FIA (FA)
ION	$[M+H]^+$	305 (100%)	305 (100%)	305 (100%)	305 (100%)	305 (100%)	305 (100%)	291 (100%)	291 (56%)	291 (100%)
	$[M+Na]^+$	325 (15%)	-	-	327 (14%)	-	-	-	-	-
	$[M+H+MeOH]^+$	-	338 (22%)	337 (8%)	-	337 (3%)	337 (5%)	-	-	-
	$[M+H-H_2O]^+$	-	-	-	287 (32%)	287 (80%)	287 (24%)	273 (8%)	273 (8%)	273 (5%)
	$[M+H-2H_2O]^+$	-	-	-	269 (5%)	269 (17%)	-	-	-	-
	$[M+H-3H_2O]^+$				-	-	-	237 (8%)	237 (20%)	237 (18%)
	$[M+H+MeOH-H_2O]^+$	-	-	-	319 (11%)	319 (95%)	319 (6%)	305 (32%)	305 (100%)	305 (17%)
	$[M+H+MeOH-2H_2O]^+$	-	-	-	301 (12%)	301 (78%)	301 (5%)	287 (14%)	287 (42%)	287 (6%)
	$[M+H+MeOH-3H_2O]^+$	-	-	-	-	-	-	-	-	-

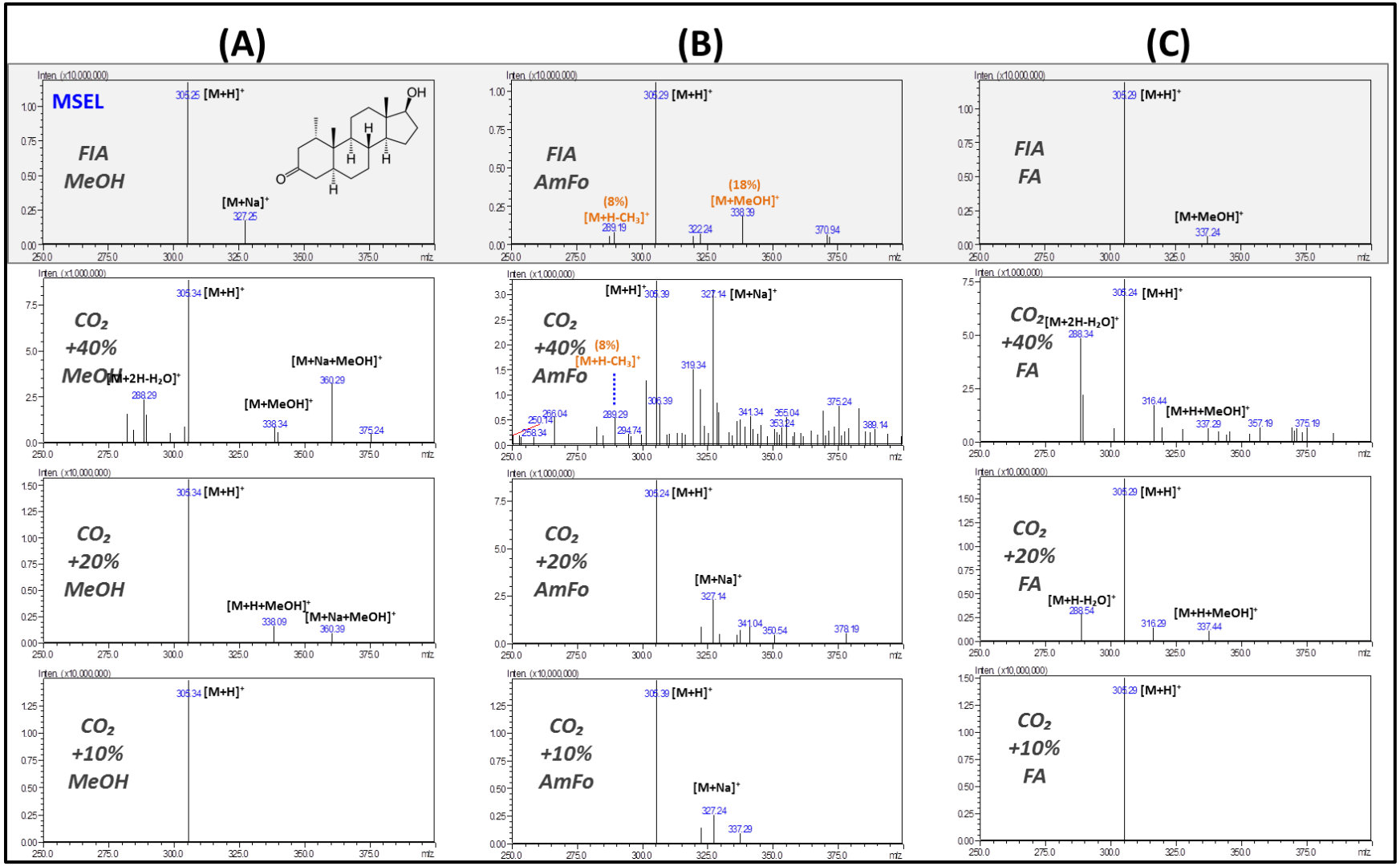

Figure 41. Representative ESI- Q3 Scan Spectra Showing Characteristic Effect of Carbon Dioxide (CO_2) Based Mobile Phases on Ionization Profile of Group V steroids (containing a non-conjugated, keto-function; showing mesterolone [MSEL] for example); showing comparison between flow injection analysis [FIA, top] versus three modifier concentrations (40%, 20% and 10%) in CO_2 of: (A) methanol [MeOH], (B) MeOH + 5mM ammonium formate [AmFo], and (C) MeOH + 0.1% formic acid [FA] as modifier.

3.9.4. ADON Q3 Scans

ADON: Flow Injection Analysis. With FIA, the dominant ion for ADON was the protonated molecular ion $[M+H]^+$, except when AmFo was used as additive, which alternatively produced a dehydrated solvent adduct ion $[M+H+MeOH-H_2O]^+$ as the most dominant ion (**Table 11**). Although $[M+H]^+$ and $[M+H-H_2O]^+$ were observed, significant abundance of other ions were also present. This was especially important, as stated above, when AmFo was used, where the dominant ion was a solvent adduct ion (S_Table 1). Various other fragment and adduct ions were observed with and without additive under FIA conditions for ADON (S_Figure 6**; D**), mainly involving sequential fragment ions from neutral water losses ($[M+H-H_2O]^+$ and $[M+H-2H_2O]^+$) and the associated solvent adducts with methanol ($[M+H+MeOH-H_2O]^+$, and $[M+H+MeOH-2H_2O]^+$). Relative abundances of observed ions are presented in **Table 15** for ADON under FIA conditions.

ADON: CO_2-based MPs. Alternative to what was observed while using flow injection analysis with 100% modifier (where the dominant ion for ADON was dependent on the additive used), with SFC MPs, the dominant ion was always $[M+H+MeOH-H_2O]^+$, which provides more opportunity in MP choices (**Table 13**). Although no additive dependent change was observed for the dominant ion using CO_2-based MPs, there were more subtle changes in the ion profile seen based on concentration when AmFo was used as additive, where at high modifier the $[M+H]^+$ ion was negligible (**Figure 42**). Alternatively, at low modifier concentration the protonated molecular ion $[M+H]^+$ was minor (< 15% abundance). Notably only with CO_2+AmFo had a significant single neutral water loss fragment ion (S_Table 3), where the fragments for two water losses were much more significant across all modifiers. The minor ions observed generally followed the same pattern, where the same types of ions were seen when the same modifier was used as in FIA (**Table 16**).

****Under closer inspection, several additional peaks were found that co-elute with the main 1DHEA peak at high modifier concentration, but are fully resolved at lower modifier concentration (see Section: S_3.4.4. ADDITIONAL PEAKS observed for ADON). ****

For ADON, $[M+H+MeOH-H_2O]^+$ will likely be the best performing precursor for CO_2-based MPs modified with methanol.

Table 16. **Q3 Scan Summary of Alternative Ions for Androstanolone [ADON] using Carbon Dioxide (CO_2)-based Mobile Phases.**

	ID:	ADON											
	Steroid:	androstanolone											
	Molecular Weight:	290.44											
	Mobile Phase:	Methanol (MeOH)				Methanol + 5mM Ammonium Formate				Methanol + 0.1% Formic Acid (FA)			
		FIA	SFC			FIA	SFC			FIA	SFC		
		100%	40%	20%	10%	100%	40%	20%	10%	100%	40%	20%	10%
		Relative abundance of characteristic ions (%)				Relative abundance of characteristic ions (%)				Relative abundance of characteristic ions (%)			
NOI	$[M+H]^+$	291 (100%)	291 (10%)	291 (10%)	291 (21%)	291 (56%)	-	291 (5%)	291 (14%)	291 (100%)	291 (8%)	291 (8%)	291 (14%)
	$[M+Na]^+$	-	-	-	-	-	-	-	-	-	-	-	-
	$[M+H-H_2O]^+$	273 (8%)	273 (6%)	-	-	273 (8%)	273 (41%)	273 (6%)	273 (6%)	273 (5%)	-	-	-
	$[M+H-2H_2O]^+$	-	255 (8%)	255 (7%)	255 (7%)	-	255 (28%)	255 (7%)	255 (6%)	-	255 (6%)	255 (6%)	255 (6%)
	$[M+H-3H_2O]^+$	237 (8%)	237 (7%)	-	-	237 (20%)	237 (25%)	-	-	237 (18%)	237 (6%)	-	-
	$[M+H+MeOH]^+$	-	-	-	-	-	-	-	-	-	-	-	-
	$[M+H+MeOH-H_2O]^+$	305 (32%)	305 (100%)	305 (100%)	305 (100%)	305 (100%)	305 (100%)	305 (100%)	305 (100%)	305 (17%)	305 (100%)	305 (100%)	305 (100%)
	$[M+H+MeOH-2H_2O]^+$	287 (14%)	287 (41%)	287 (52%)	287 (62%)	287 (42%)	287 (45%)	287 (52%)	287 (44%)	287 (6%)	287 (37%)	287 (54%)	287 (50%)

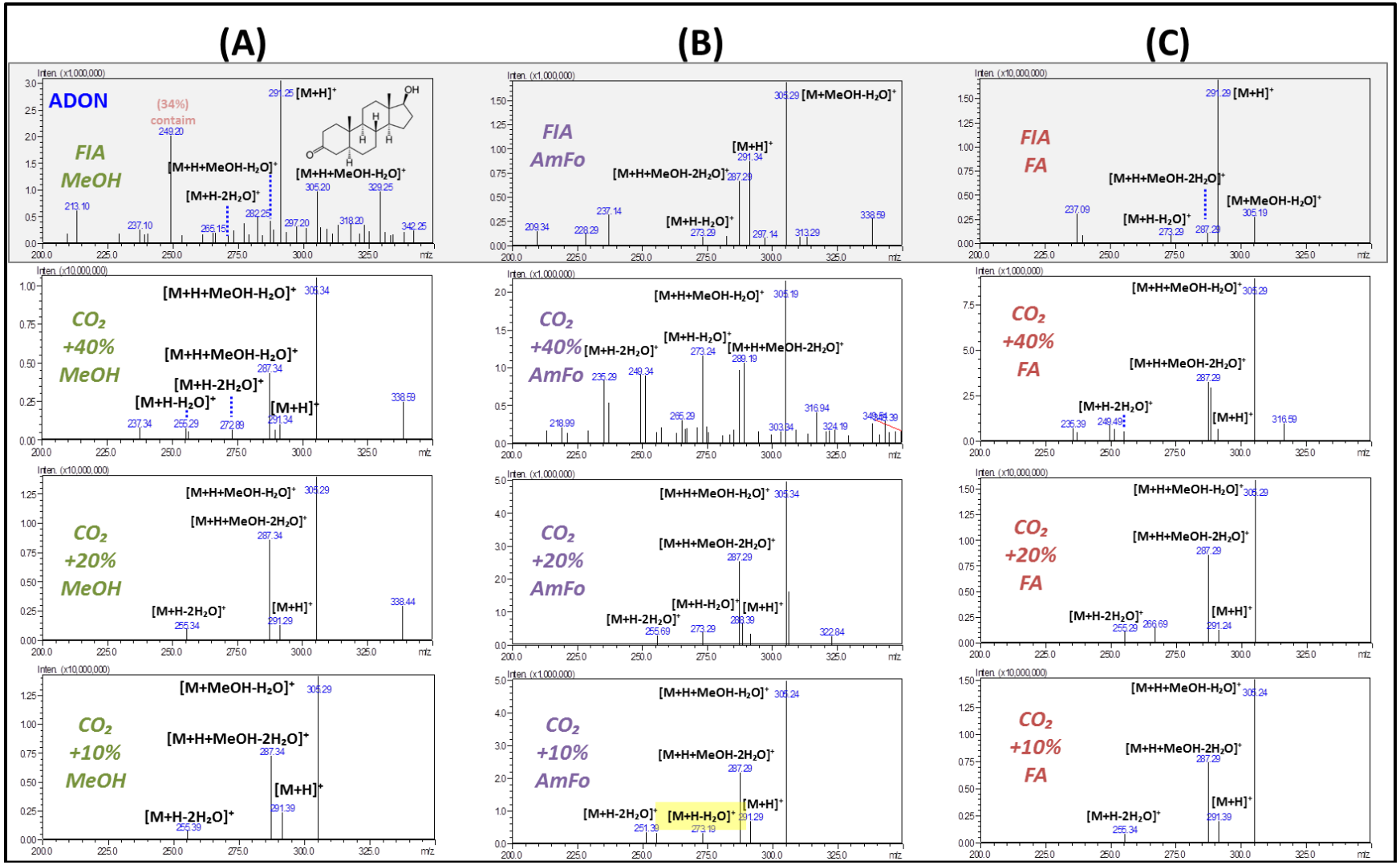

Figure 42. Representative ESI- Q3 Scan Spectra Showing Characteristic Effect of Carbon Dioxide (CO_2) Based Mobile Phases on Ionization Profile of Group V steroids (containing a non-conjugated, keto-function; showing androstanolone [ADON] for example); showing comparison between flow injection analysis [FIA, top] versus three modifier concentrations (40%, 20% and 10%) in CO_2 of: (A) methanol [MeOH], (B) MeOH + 5mM ammonium formate [AmFo], and (C) MeOH + 0.1% formic acid [FA] as modifier.

3.10. GROUP VI. Non-Specified Structure.

3.10.1. Group VI: Q3 Scans with Flow Injection Analysis

ADAR, CLNB and ZRNL are all structurally very different from the other compounds studied since their structures do not contain the characteristic steroid backbone. Both ADAR and CLNB produced $[M+H]^+$ as the dominant ion, and ZRNL produced the $[M-H]^-$ as the dominant ion, as expected (**Table 11; Group VI**). ADAR also produced the sodium adduct $[M+Na]^+$ as the major ion using methanol with no additive, but when an additive was added, this adduct was much lower in abundance, as shown in **S_Figure 7** and **S_Table 1; Group VI.**

3.10.2. Group VI: Q3 Scans with CO_2-based MPs

Addition of CO_2 to the MP had little effect on the dominant ion for CLNB and ZRNL(**Table 12**), but did have an effect on ADAR, where the formation of the sodium adduct was promoted when CO_2 was present in the MP (a **Figure 43; B**). This effect was so strong using AmFo that the sodium adduct was the dominant ion, while using high modifier concentration (>20% AmFo in CO_2), as well as with methanol with no additive. CLNB sensitivity was reduced using formic acid (**S_Table 2**).

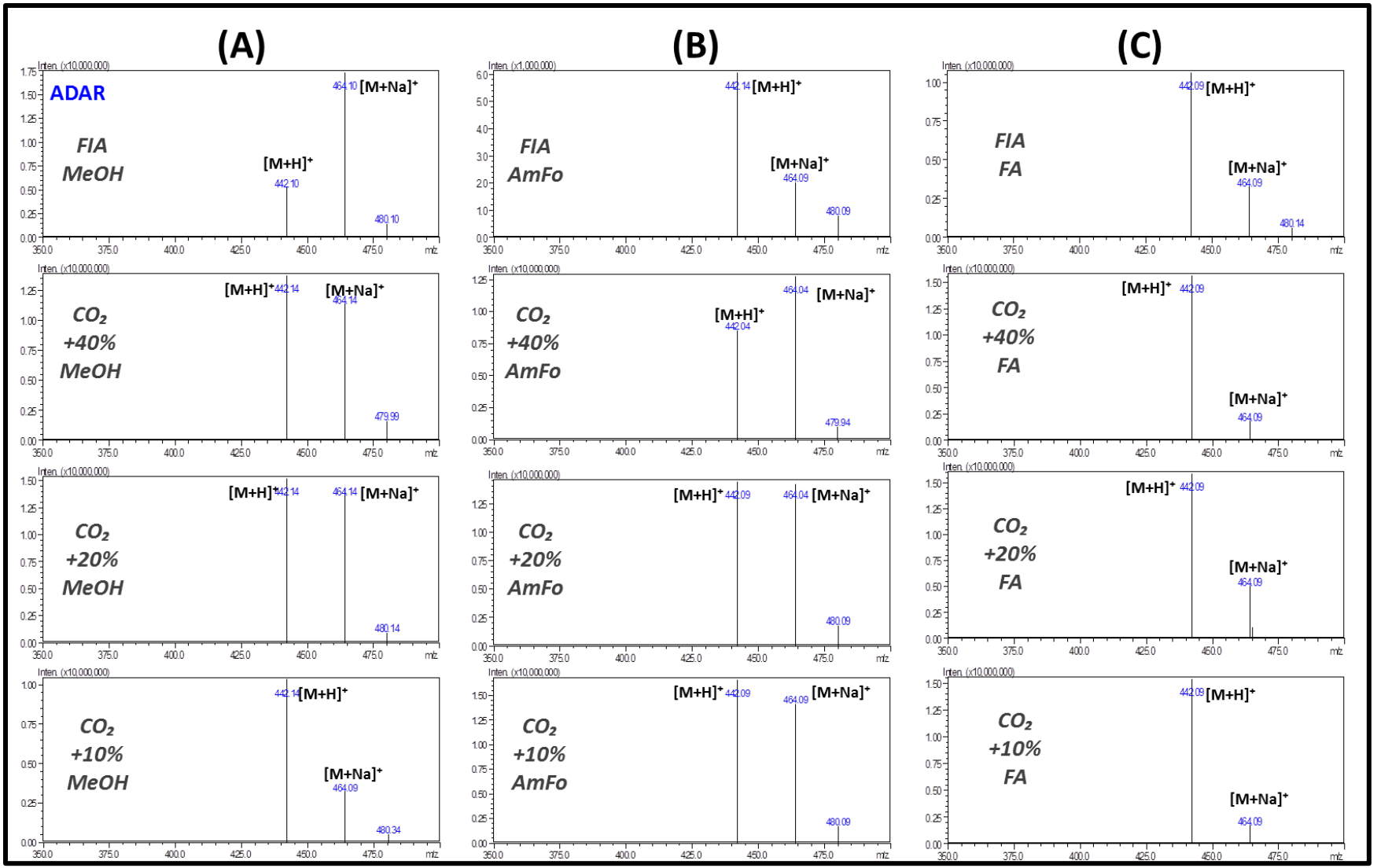

Figure 43. Representative ESI- Q3 Scan Spectra Showing Characteristic Effect of Carbon Dioxide (CO_2) Based Mobile Phases on Ionization Profile of Group VI Anabolic Agents (non-steroidal structure; using andarine for example [ADAR]); showing comparison between flow injection analysis [FIA, top] versus three modifier concentrations (40%, 20% and 10%) in CO_2 of: (A) methanol [MeOH], (B) MeOH + 5mM ammonium formate [AmFo], and (C) MeOH + 0.1% formic acid [FA] as modifier.

3.11. Summary and Conclusions.

Twenty-three anabolic agents from WADA's yearly list of restricted compounds were chosen as target analytes. Q3 scans were obtained for each analyte and compared to those expected from the literature. Methanol was used as modifier in carbon dioxide and compared to scans obtained using flow injection analysis (FIA), using 100% Modifier. The effect of a mobile phase additives was investigated using 5 mM Ammonium Formate (AmFo) and 0.1% formic acid (FA) in methanol. Optimal precursors were determined for each analyte for use in further method optimizations:

Group I: Nitrogen containing steroids were easily ionizable as $[M+H]^+$, regardless of the MP composition used. A slight increase in sensitivity should be expected for DNZL using CO_2-based MPs.

Group II: Conjugated, C3-Keto functional group: $[M+H]^+$ could easily be chosen as precursor for **group II**; **-(a)** 4-ene, **-(b)** 1-ene, and **–(c)** triene steroids, especially while using CO_2-based MPs (which were shown to suppress sodium adduct formation even when no additive was present).

***Group II*-(d)**: For the diene containing steroid, METD, either $[M+H]^+$ or $[M+H-H_2O]^+$ could easily be used as precursor while using SFC-MPs.

***Group III*-(a):** 7 keto-DHEA, $[M+H-H_2O]^+$ fragment ion, could easily be chosen as precursor for KETO, regardless of the MP additive for SFC-based MPs modified with MeOH.

Group III-(b)*: For the non-conjugated, C3-hydroxyl steroids (ADEN and ETIO): Generally no matter the composition of the modifier used, $[M+H-H_2O]^+$ should be chosen as precursor.

Group IV*: Conjugated; C3-hydroxyl steroids (1DHEA and PRST), did not follow a common ionization pattern. For 1DHEA, multiple precursors may be optimal: $[M+H]^+$, $[M+H-H_2O]^+$, or $[M+H-2H_2O]^+$ could be used, especially when using SFC-MPs the optimal precursor may change depending on if and what type of additive may be needed.

For PRST, depending on the additive used, the optimal precursor should be expected to change for PRST while using CO_2-based mobile phases. When an acidic mobile phase is used, $[M+H-H_2O]^+$ or $[M]^+$, may perform the best as precursor, but alternatively while using AmFo $[M+H-H_2O]^+$or $[M+Na+MeOH-H_2O]^+$ may be optimal as precursor. Using methanol with no additive should produce the best sensitivity for this compound and the most reliable result, since at all modifier concentrations $[M+H-H_2O]^+$ should be expected to be the optimal precursor for PRST at all modifier concentrations without additive.

Group V*: Non-Conjugated; C3-keto Steroids (OXAN, MSEL, MSAL & ADON) also did not follow a common ionization pattern:

Optimal precursor for OXAN, most likely would be $[M+H]^+$ for MeOH + FA as additive, but the sodium adduct $[M+Na]^+$ may be more effective as precursor if using AmFo as MP additive. Optimal precursor for MSEL, will most likely depend on whether an additive is used, and also will possibly change depending on the concentration of the modifier present in the MP. Low modifier would give the best result as at low concentration (< 10%) all MP compositions gave $[M+H]^+$ as the dominant precursor. For ADON, alternative to what was observed while using flow injection analysis with 100% modifier (where the dominant ion for ADON was dependent on the additive used), instead with CO_2-based MPs always produced the dominant ion of $[M+H+MeOH-H_2O]^+$, which will likely be the best performing precursor.

Group VI. Other anabolic agents produced the protonated molecular ion $[M+H]^+$ for both ADAR and CLNB, and the deprotonated ion $[M-H]^-$ for ZRNL under most MP compositions. Care should be taken with ADAR with using no additive and/or AmFo as these compositions promoted sodium adduct formation for ADAR.

Overall, it is likely that one set of conditions will not be optimal for all analytes. Depending on MP compositions required for chromatographic separation and analyte peak shape, compromises may be necessary with respect to sensitivity of individual analytes.

3.i. Instrument Methods: MS-Optimization for Q3 Scans.

3.i.1. General Method Information.

Detailed information on materials and equipment used for Q3 scans performed in this study can be found in the following sections of **Chapter #2. Materials and Methods**:

3.i.1.1. Materials.

- Solvents used for mobile phases and dilution solutions can be found in **Section 2.1.1. Solvents**.
- Analytical standards information for targeted anabolic agents can be found in **Section 2.1.2. Analytical Standards; *Anabolic androgenic steroids (AAS)*** **and in Table 1.**

3.i.1.2. Instrumentation.

- The Instrumentation used is detailed in **Section 2.2.1. Instrumentation; *Nexera UC online SFE-SFC-MS***.
- Other equipment used is detailed in **Section 2.2.3. Other Equipment.**
    - ***Nitrogen Generator***
    - ***Analytical balances***

3.i.1.3. Solutions Preparation.

- Stock Solutions prep and storage detailed in **Section 2.3.1.1. AAS Stock Solutions** and **Table 6; Stock Solutions.**
- Injection solutions prep and concentrations are described in **Section 2.3.1.2. AAS MS-Optimization Solutions** and **Table 6; *MRM Solutions*.**

3.i.2. MS Parameters – Q3 Scans

Detection was achieved using an LCMS-8050 triple quadrupole mass spectrometer, equipped with an DUIS-source, and operated in Electrospray Ionization (ESI-), positive (+) and negative (-) ionization mode. Interface voltages were set to 4.0 kV (for positive Q3 scan mode) and -3.0 kV (for negative Q3 scan mode) and temperature set to 300 °C. Nitrogen gas was used for both drying and nebulizing gas; with flow rate of 2.0 L/min for nebulizing gas and 10.0 L/min for drying gas. Desolvation and DL temperatures were 526 °C and 250 °C respectively. Heat Block temperature was set to 400 °C, and heating gas used was dry air. Gas used for collision induced dissociation (CID) was argon at 270 kPa. DL bias/Q-array bias were set in tuning file as 0 V, and Q3 pre-rod bias at -15 V (for positive scan mode) and 15 V (for negative scan mode). Scan range was 120 to 1,200 m/z with scan speed 15,000 u/sec, with 0.100 sec Event time with Q3 resolution set to unit.

3.i.3. Mobile Phases (MP).

Three modifiers were used: [MeOH] LCMS-grade methanol; FA] LCMS-grade methanol + 0.1% formic acid (LCMS-grade); [AmFo] LCMS-grade methanol + 5 mM ammonium formate (LCMS-grade). All modifier solutions were sonicated for 20 minutes prior to use.

In the case of FIA-analysis, 100% modifier was used as MP. In the case of SFC/CO_2-based MPs, up to 40% modifier was mixed with liquid Carbon Dioxide ([CO_2] – Instrument grade) via the instrument solvent delivery pumps. See below for specific details for each case.

Typically if CO_2 was used, injections were performed using multiple modifier concentrations (e.g., 40, 20 & 10% modifier). Runtimes would be changed accordingly if and when a column was installed. All injections were automated via Batch Table.

3.i.4. Instrument Parameters for Q3 Scan: Flow Injection Analysis (FIA).

3.i.4.1. Instrument Setup: FIA-MS Optimization Mode.

Detailed instrument configuration details can be found in **Chapter #1: Hyphenated Instrumentation; Section 1.4.1: Instrument Configurations: *FIA-MS Optimization Configuration***). In short the solvent modifier pump (Pump B), was connected directly to the injector switching valve, MRM solution were introduced into the flow stream via a 5.0 µL external loop using partial loop injections of 1.0 µL injections. A short piece of restrictive tubing was placed between the injector outlet and connected to the MS interface inlet.

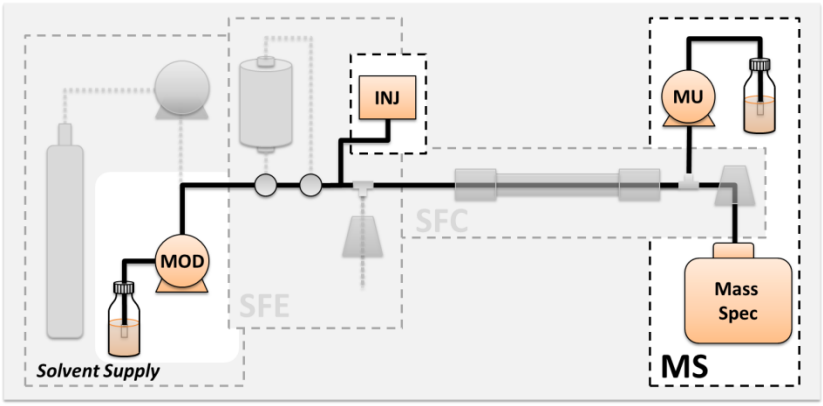

See Figure 12 in Chapter #1

3.i.4.2. Instrument Parameters: used for FIA-mode Q3 Scans.

Total Flow of 0.25 mL/min, of 100% Pump B, were delivered. All CO_2 delivery units were switched off, and CO_2 shutoff valve set to closed. BPRs and column oven switched to Off. One microliter injections were made via a 5.0 µL external loop, with 0.1 µL air gaps, 5.0 µL/sec sampling speed, and 1.0 µL/sec discharge speed. Needle rinse mode set to before and after aspiration, with rinsing speed of 35 µL/sec and rinsing volume of 500 µL using methanol.

3.i.5. Instrument Parameters for Q3 Scans: Carbon Dioxide-based MPs (CO_2).

3.i.5.1. Instrument Setup: CO_2-MS Optimization Mode

Detailed instrument configuration details can be found in **Chapter #1: Hyphenated Instrumentation; Section 1.4.2: Instrument Configurations: *CO_2-MS Optimization Mode***). In short, the solvent modifier pump (Pump B), was connected directly to the injector switching valve, MRM solution were introduced into the flow stream via a 5.0 µL external loop using partial loop injections of 1.0 µL injections. A short piece of restrictive tubing was placed between the injector outlet and connected to the MS interface inlet.

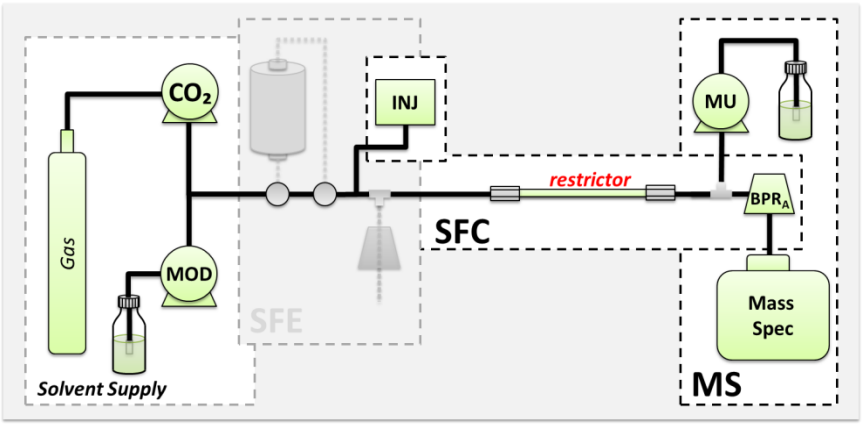

See Figure 13 in Chapter #1

3.i.5.2. Instrument Parameters: used for CO_2-mode Q3 Scans.

Operation with CO_2-based MPs requires not only the operation of the CO_2-delivery pump and outlet pressure regulation, but additionally, in order to maintain pressure equilibrium across the system, a restrictor or column must be installed, to provide a stable delta pressure between the pumps and back pressure regulator (BPR). Therefore, a mixer (post-pumps & pre-injector), and a BPR (post-column & pre-MS inlet) is plumbed into the flow path. The column used was an Agilent Zorbax Cyano (3.5 µm d_p, 4.6 x 150 mm) (Agilent Technologies, Santa-Clara, CA. USA). Modifier concentrations of 40, 20 and 10% in CO_2 were delivered at 3.0 mL/min, using a BPR [A] outlet pressure of 15 MPa and column oven temperature of 50 °C.

Literature Cited:

FIRST CITED IN PREVIOUS CHAPTERS

[19] World Anti-Doping Agency. International Standard Prohibited List 2021, 2021. Resources. https://www.wada ama.org/sites/default/files/resources/files/2021list_en.pdf. (Accessed January 03 2021).

NEW TO THIS CHAPTER

[24] van Eenoo P, Delbeke FT. (2006). "Metabolism and excretion of anabolic steroids in doping control—New steroids and new insights." *The Journal of Steroid Biochemistry and Molecular Biology*. **101**(4-5): p161–178. https://doi.org/10.1016/j.jsbmb.2006.06.024

[25] Handelsman DJ,Bermon S. (2019). "Detection of testosterone doping in female athletes." *Drug Testing and Analysis.* **11**(10): p1566–1571. https://doi.org/10.1002/dta.2689

[26] Fragkaki AG, Angelis YS, Koupparis M, Tsantili-kakoulidou A, Kokotos G, Georgakopoulos C. (2009). "Structural characteristics of anabolic androgenic steroids contributing to binding to the androgen receptor and to their anabolic and androgenic activities applied modifications in the steroidal structure." *Steroids*. **74**(2): p172–197. https://doi.org/10.1016/j.steroids.2008.10.016

[27] de Kock N, Acharya, SR, Ubhayasekera SJKA, Bergquist J. (2018). "A Novel Targeted Analysis of Peripheral Steroids by Ultra-Performance Supercritical Fluid Chromatography Hyphenated to Tandem Mass Spectrometry." *Nature Scientific Reports*. **8**: e16993. https://doi.org/10.1038/s41598-018-35007-0

[28] Teubel J, Wüst B, Schipke CG, Peters O, Parr MK. (2017). "Methods in endogenous steroid profiling – A comparison of gas chromatography mass spectrometry (GC–MS) with supercritical fluid chromatography tandem mass spectrometry (SFC-MS/MS)." *Journal of Chromatography A.* **1554**: p101-116. https://doi.org/10.1016/j.chroma.2018.04.035

[29] Thevis M, Kuuranne T, Geyer H. (2020). "Annual banned-substance review: Analytical approaches in human sports drug testing 2019/2020." *Drug Testing and Analysis.* **13**(1): p8–35. https://doi.org/10.1002/dta.2969

[30] World Anti-Doping Agency. 2018 anti-doping testing figures; 2019. https://www.wada-ama.org/sites/default/files/resources/files/2018_testing_figures_report.pdf (accessed on 06 July 2021).

[31] Thevis M, Kuuranne T, Geyer H. (2019). "Annual banned-substance review – Analytical approaches in human sports drug testing." *Drug Testing and Analysis.* **12**(1): p7–26. https://doi.org/10.1002/dta.2735

[32] Thevis M, Schanzer W. (2006). "Mass spectrometry in sports drug testing: structure characterization and analytical assays." *Mass Spectrometry Reviews*. **26**(1): p79-107. https://doi.org/10.1002/mas.20107

[33] Schanzer W, Thevis M. (2015). "human sports drug testing by mass spectrometry." *Mass Spectrometry Reviews.* **36**(1): p16–46. https://doi.org/10.1002/mas.21479

[34] Cha E, Kim S, Kim HJ, Lee KM, Kim KH, Kwon O-S, Lee J. (2015). "Relationships between structure, ionization profile and sensitivity of exogenous anabolic steroids under electrospray ionization and analysis in human urine using liquid chromatography–tandem mass spectrometry." Biomedical Chromatography. **30**(4): p555-65. https://doi.org/10.1002/bmc.3583

[35] Pozo OJ, Van Eenoo P, Deventer K, Delbeke FT. (2017). "Development and validation of a qualitative screening method for the detection of exogenous anabolic steroids in urine by liquid chromatography-tandem mass spectrometry." *Analytical and Bioanalytical Chemistry.* **389**: p1209–1224. https://doi.org/10.1007/s00216-007-1530-6

[36] Pozo OJ, Van Eenoo P, Deventer K, Delbeke FT. (2007). "Ionization of anabolic steroids by adduct formation in liquid chromatography electrospray mass spectrometry." *Journal of Mass Spectrometry.* **42**(4): p497-516. https://doi.org/10.1002/jms.1182

[37] Berger T. (1997). "Review: Separation of polar solutes by packed column supercritical fluid chromatography." *Journal of Chromatography A.* **785**: p3-33. https://doi.org/10.1016/S0021-9673(97)00849-2

[38] Desfontaine V, Guillarme D, Francotte E, Novakova L. (2015). "Review: Supercritical fluid chromatography in pharmaceutical analysis." *Journal of Pharmaceutical and Biomedical Analysis.* **113**: p56–71. http://dx.doi.org/10.1016/j.jpba.2015.03.007

[39] Quanson JL, Stander MA, Pretorius E, Jenkinson C, Taylor AE, Storbeck KH. (2016). "High-throughput analysis of 19 endogenous androgenic steroids by ultra-performance convergence chromatography tandem mass spectrometry." *Journal of Chromatography B.* **1031**: p131-138. https://doi.org/10.1016/j.jchromb.2016.07.024

[40] Teubel J, Wust B, Schipke CG, Peters O, Parr MK. (2018). "Methods in endogenous steroid profiling – A comparison of gas chromatography mass spectrometry (GC–MS) with supercritical fluid chromatography tandem mass spectrometry (SFC-MS/MS)." *Journal of Chromatography A.* **1554**: p101-116. https://doi.org/10.1016/j.chroma.2018.04.035

[41] Joseph JF, Parr MK. (2020). "I.5. Techniques for identifying and quantifying drugs and metabolites: Application of SFC for bioanalysis." In S. Ma & S.K. Chowdhury (Eds.). Identification and Quantification of Drugs, Metabolites, Drug Metabolizing Enzymes, and Transporters (Second Edition) (pp.354-392). Amsterdam, Netherlands: Elsevier.

[42] Akbal L, Hopfgartner G. (2020). "Hyphenation of packed column supercritical fluid chromatography with mass spectrometry: where are we and what are the remaining challenges?" *Analytical and Bioanalytical Chemistry*. **412**: p6667–6677. https://doi.org/10.1007/s00216-020-02715-4

[43] Gurst JE, Djerassi C. (1964). "Mass Spectrometry in Structural and Stereochemical Problems. LIX. Mechanism of the formal loss of acetone from 2-oxo-5α-steroids." *Journal of the American Chemical Society.* **86**(24): p5542 – 5547. https://doi.org/10.1021/ja01078a029

[44] Ma Y-C, Kim H-Y. (1997). "Determination of Steroids by Liquid Chromatography/Mass Spectrometry." *Journal of the American Society for Mass Spectrometry.* **8**(9): p1010-1020. https://doi.org/10.1016/S1044-0305(97)00122-0

[45] Thevis M, Schanzer W. (2005). "Mass Spectrometric Analysis of Androstan-17ß-ol-3-one and Androstadiene-17ß-ol-3-one Isomers." *Journal of the American Society for Mass Spectrometry.* **16**(10): p1660–1669. https://doi.org/10.1016/j.jasms.2005.06.007

[46] Verheyden K, Bizec BL, Coutheyn D, Mortier V, Vandewiele M, Gillis W, Vanthemsche P, De Brabander HF, Noppe H. (2006). "Mass spectrometric detection of and similarities between 1-androgens." *Analytica Chimica Acta.* **586**(1-2): p57–72. https://doi.org/10.1016/j.aca.2006.10.058

[47] Thevis M, Guddat S, Schanzer W. (2009). "Doping control analysis of trenbolone and related compounds using liquid chromatography–tandem mass spectrometry." Steroids. **74**(3): p315-321. https://doi.org/10.1016/j.steroids.2008.10.004

[48] Guan F, Soma LR, Luo Y, Uboh CE, Peterman S. (2006). "Collision-Induced Dissociation Pathways of Anabolic Steroids by Electrospray Ionization Tandem Mass Spectrometry." *Journal of the American Society for Mass Spectrometry.* **17**(4): p477–489. https://doi.org/10.1016/j.jasms.2005.11.021

[49] Schanzer W. (1996). "Metabolism of anabolic androgenic steroids." *Clinical Chemistry.* **42**(7): p1001-1020. https://doi.org/10.1093/CLINCHEM/42.7.1001

S_3. SUPPLEMENTARY MATERIALS

S_3.1. Supplemental: FIA-Q3 Scans.

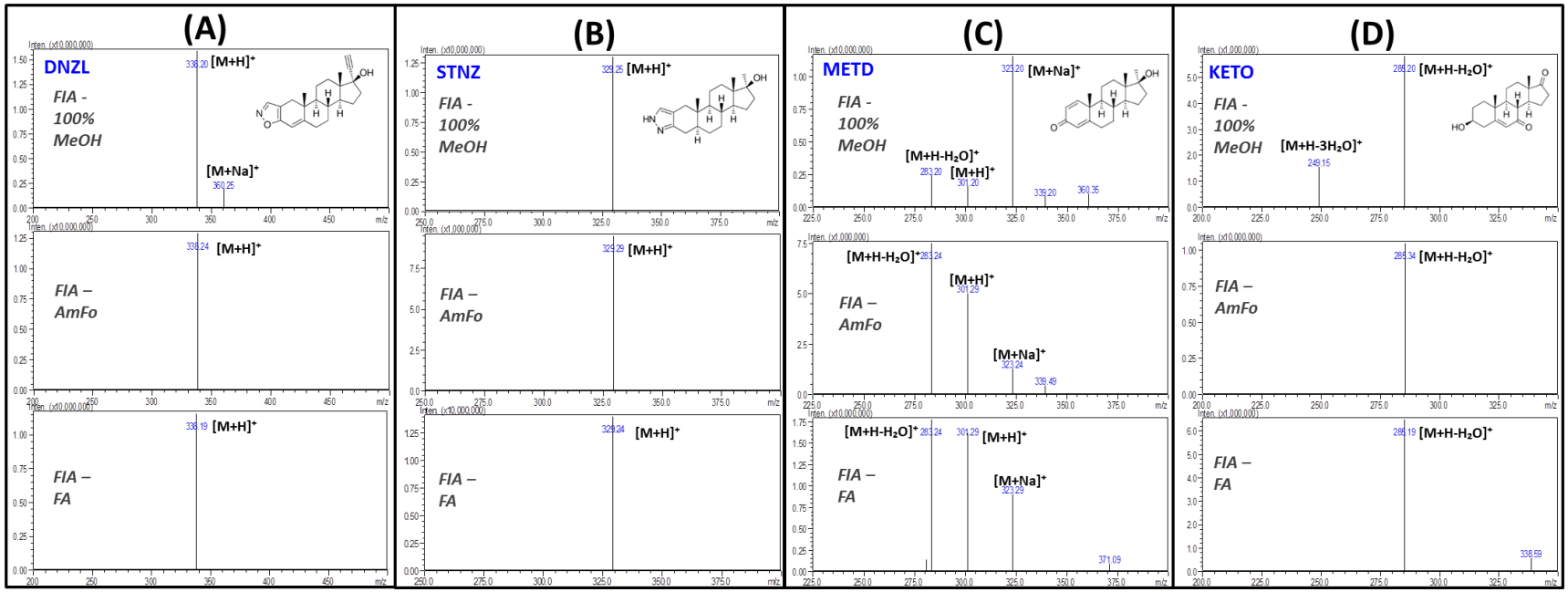

S_Figure 2. ESI-MS Q3-Scan Spectra for Group I, Group II-(d) and Group III-(a) Steroids using Flow Injection Analysis (FIA) with Methanol (MeOH, [top]), MeOH + 5mM Ammonium Formate (AmFo, [middle]) and MeOH + 0.1% Formic Acid (FIA – FA, [bottom]) for (A) danazol [DNZL], (B) stanazolol [STNZ], (C) 7-keto-DHEA [KETO], and (D) methandienone [METD]. ***Conditions****: 100% Modifier, with no column installed, Flow rate 0.25 mL/min, 1.0µL injections of MRM-solutions of each steroid in MeOH, Detection: ESI-positive mode.*

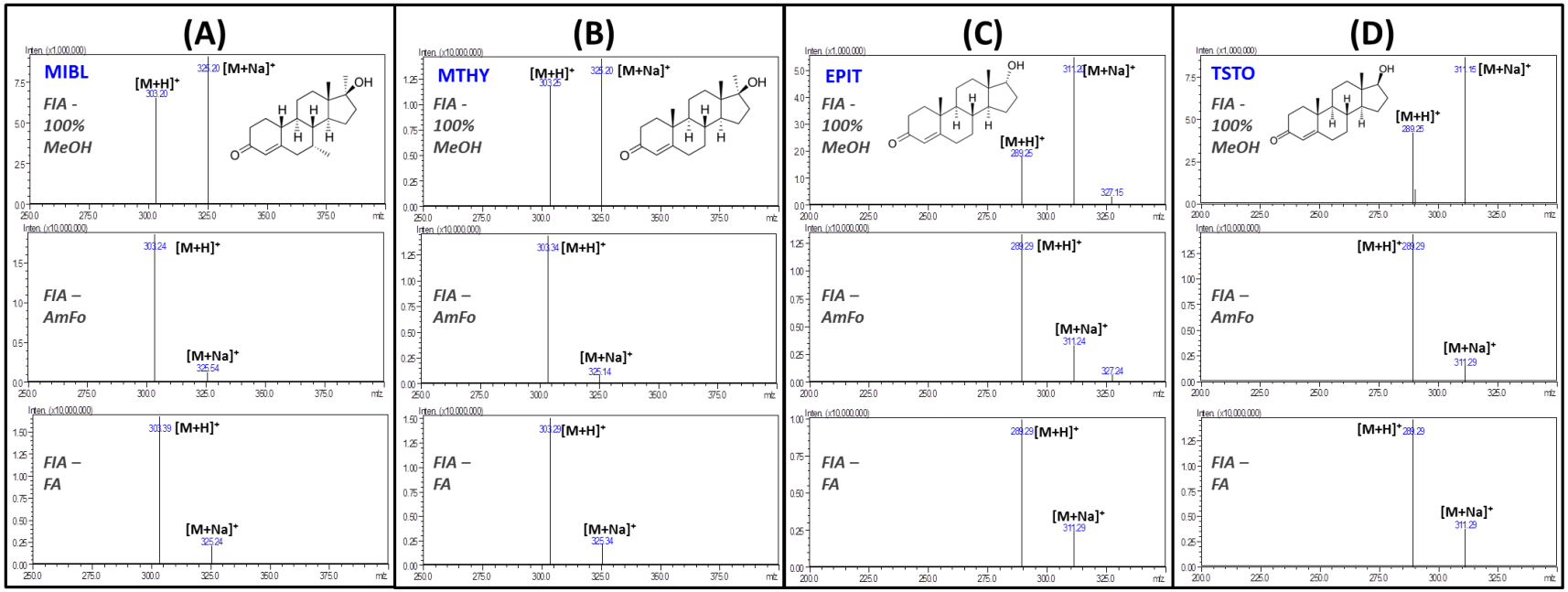

S_Figure 3. ESI-MS Q3-Scan Spectra for Group II-(a) Steroids using Flow Injection Analysis (FIA) with Methanol (MeOH, [top]), MeOH + 5mM Ammonium Formate (AmFo, [middle]) and MeOH + 0.1% Formic Acid (FA, [bottom]); showing Ionization profile and most abundant ions for (A) mibolerone [MIBL], (B) methyltestosterone [MTHY], (C) epitestosterone [EPIT] and (D) testosterone [TSTO]. ***Conditions****: 100% Modifier, with no column installed, Flow rate 0.25 mL/min, 1.0µL injections of MRM-solutions of each steroid in MeOH, Detection: ESI-positive mode.*

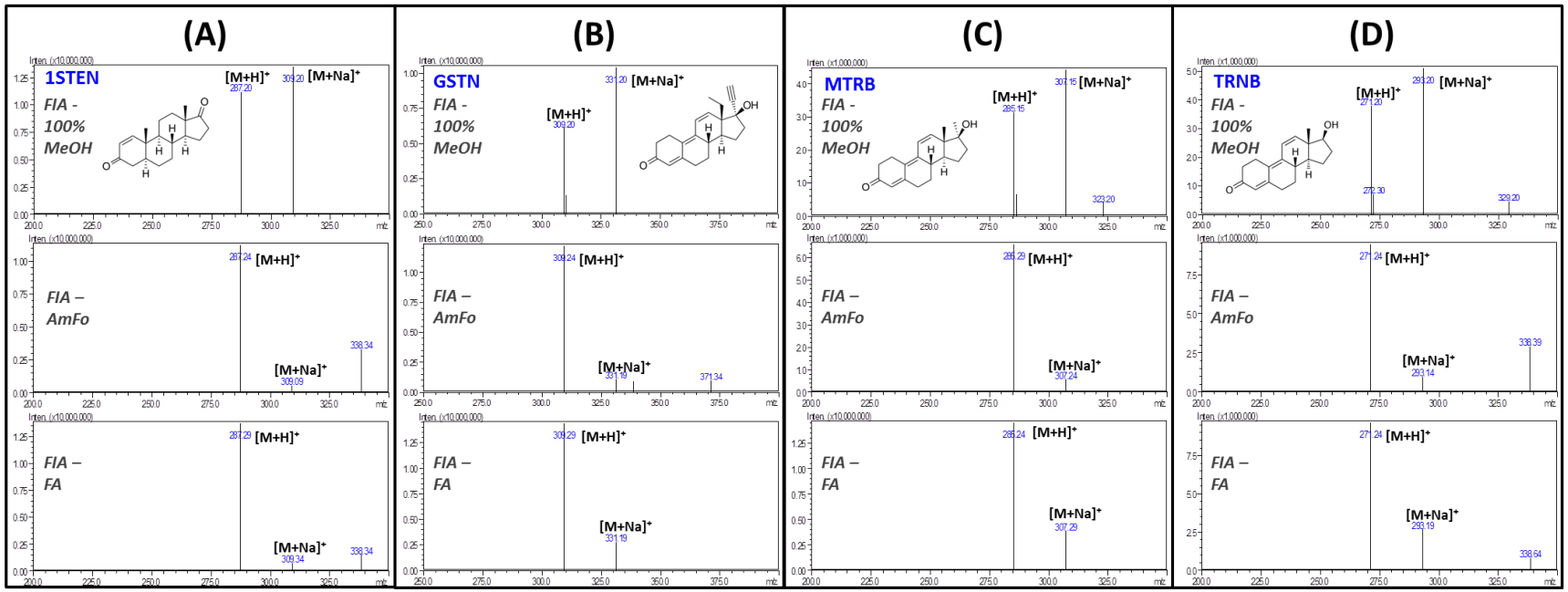

S_Figure 4. ESI-MS Q3-Scan Spectra for Group II-(b) and II-(c) Steroids from Flow Injection Analysis (FIA) with Methanol (MeOH, [top]), MeOH + 5mM Ammonium Formate (AmFo, [middle]) and MeOH + 0.1% Formic Acid (FA, [bottom]); showing Ionization profile and most abundant ions for (A) 1-androstenedione [1STEN], (B) gestrinone [GSTN], (C) metribolone [MTRB] and (D) trenbolone [TRNB]. ***Conditions****: 100% Modifier, with no column installed, Flow rate 0.25 mL/min, 1.0µL injections of MRM-solutions of each steroid in MeOH, Detection: ESI-positive mode.*

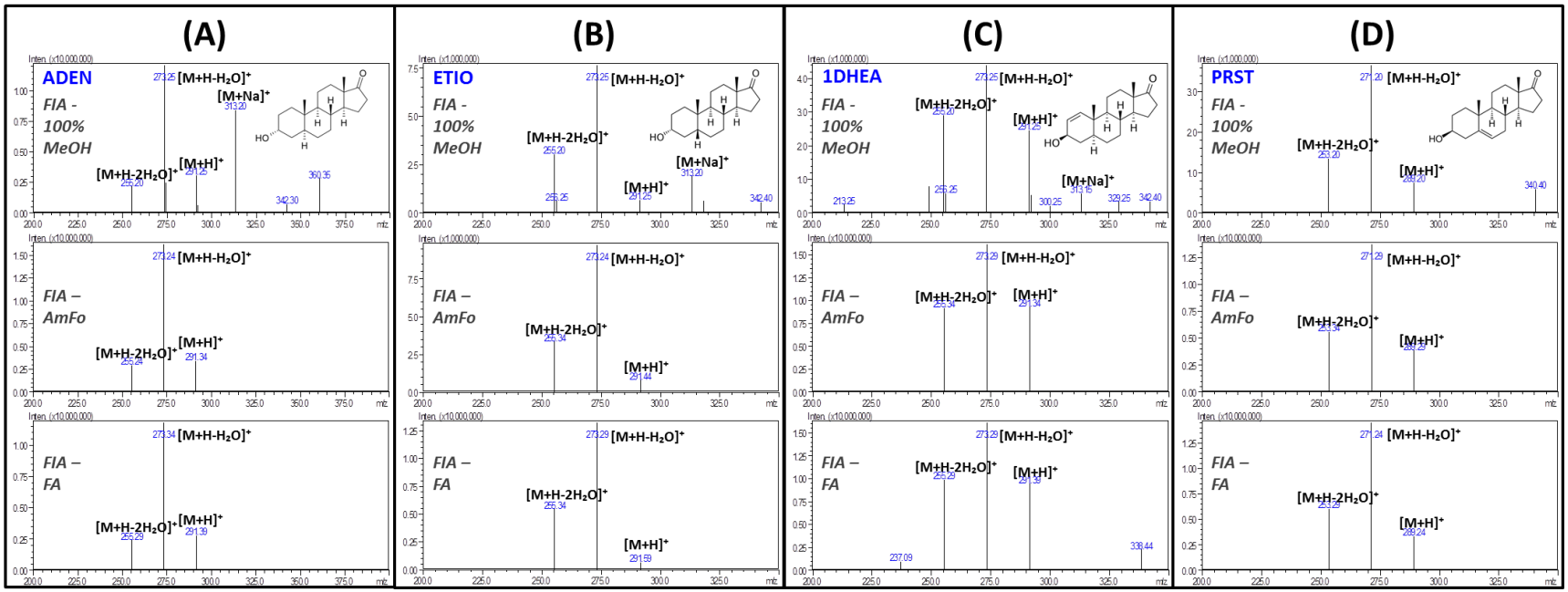

S_Fig ure 5. ESI-MS Q3-Scan Spectra for Group III-(b) and Group IV Steroids from Flow Injection Analysis (FIA) with Methanol (MeOH, [top]), MeOH + 5mM Ammonium Formate (AmFo, [middle]) and MeOH + 0.1% Formic Acid (FA, [bottom]); showing Ionization profile and most abundant ions for (A) androsterone [ADEN], (B) etiocholanolone [ETIO], (C) 1-androsterone [1DHEA], and prasterone [PRST]. ***Conditions****: 100% Modifier, with no column installed, Flow rate 0.25 mL/min, 1.0µL injections of MRM-solutions of each steroid in MeOH, Detection: ESI-positive mode.*

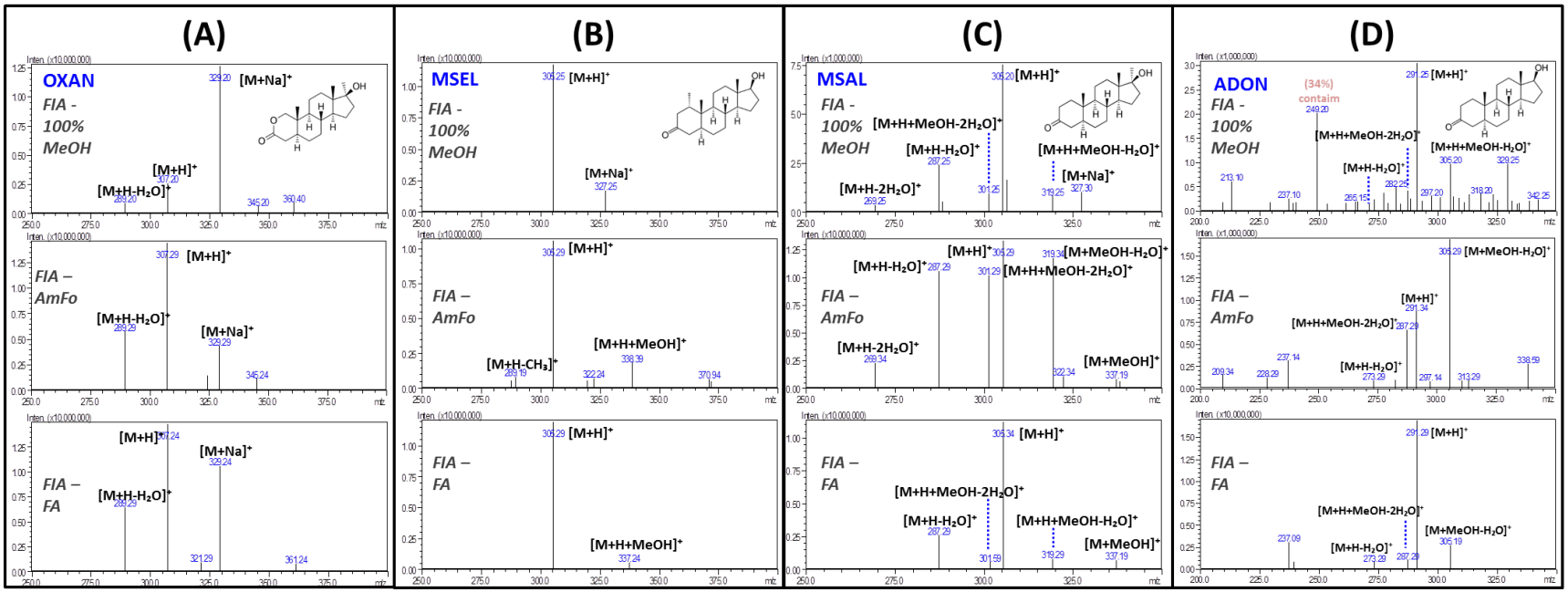

S_Figure 6. ESI-MS Q3-Scan Spectra for Group V Steroids from Flow Injection Analysis (FIA) with Methanol (MeOH, [top]), MeOH + 5mM Ammonium Formate (AmFo, [middle]) and MeOH + 0.1% Formic Acid (FA, [bottom]); showing Ionization profile and most abundant ions for (A) oxandrolone [OXAN], (B) mesterolone [MSEL], (C) mestanolone [MSAL], and (D) androstanolone [ADON]. ***Conditions****: 100% Modifier, with no column installed, Flow rate 0.25 mL/min, 1.0µL injections of MRM-solutions of each steroid in MeOH, Detection: ESI-positive mode.*

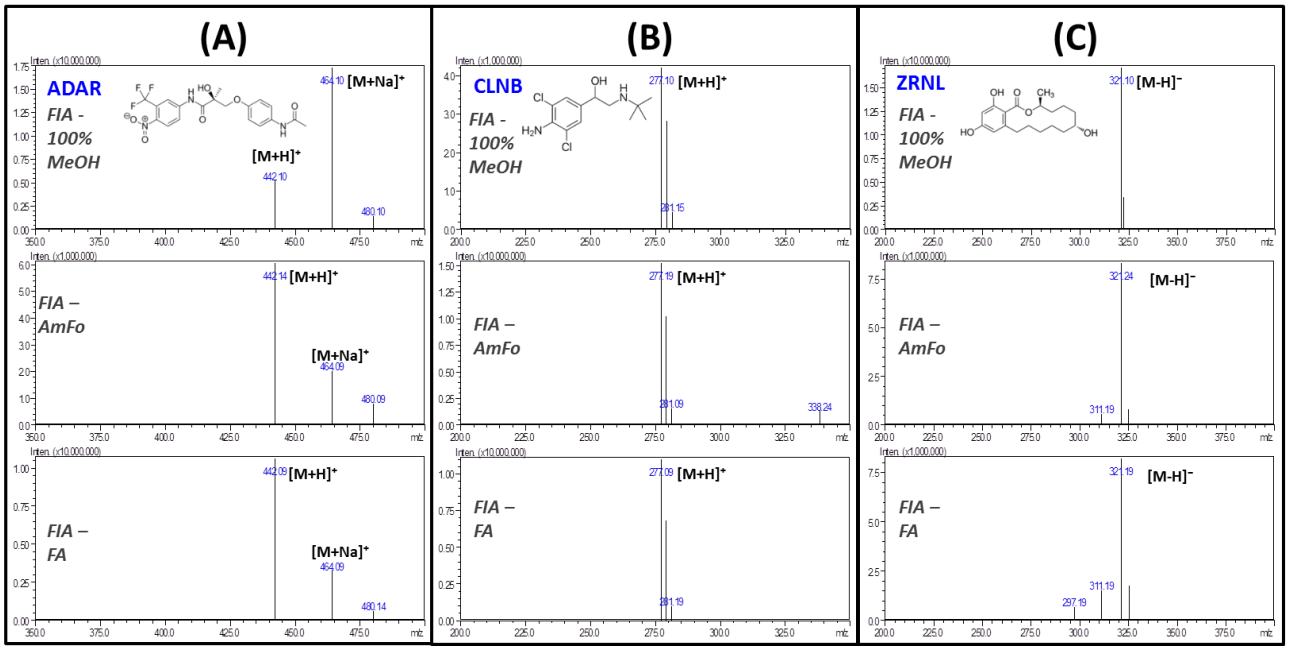

S_Figure 7. ESI-MS Q3-Scan Spectra for Group VI Non-Steroidal Anabolic Agents from Flow Injection Analysis (FIA) with Methanol (MeOH, [top]), MeOH + 5mM Ammonium Formate (AmFo, [middle]) and MeOH + 0.1% Formic Acid (FA, [bottom]); showing Ionization profile and most abundant ions for (A) andarine [ADAR], (B) clenbuterol [CLNB], and (C) zeranol [ZRNL]. ***Conditions****: 100% Modifier, with no column installed, Flow rate 0.25 mL/min, 1.0µL injections of MRM-solutions of each steroid in MeOH, Detection: ESI-positive mode.*

S_Table 1. Relative Abundance of Characteristic Ions for Anabolic Agents using Flow Injection Analysis (FIA).

				FIA (MeOH) Relative abundance of characteristic ions (%)				FIA (5mM AmFo) Relative abundance of characteristic ions (%)				FIA (0.1 % FA) Relative abundance of characteristic ions (%)			
Class	Steroid	MW	ID	$[M+H]^+$	$[M+H-H_2O]^+$	$[M+H-2H_2O]^+$	$[M+Na]^+$	$[M+H]^+$	$[M+H-H_2O]^+$	$[M+H-2H_2O]^+$	$[M+Na]^+$	$[M+H]^+$	$[M+H-H_2O]^+$	$[M+H-2H_2O]^+$	$[M+Na]^+$
GROUP I. Nitrogen Containing steroids															
I	Stanozolol	328.49	STNZ	329 (100%)	-	-	-	329 (100%)	-	-	-	329 (100%)	-	-	-
I	Danazol	337.46	DNZL	338 (100%)	-	-	360 (12%)	338 (100%)	-	-	-	338 (100%)	-	-	-
GROUP II. Conjugated, C3 Keto function															
II-(a). 3-keto-4-ene steroids															
II-(a)	Epitestosterone	288.42	EPIT	289 (32%)	-	-	311 (100%)	289 (100%)	-	-	311 (25%)	289 (100%)	-	-	311 (24%)
II-(a)	Mibolerone	302.50	MIBL	303 (88%)	-	-	325 (100%)	303 (100%)	-	-	325 (5%)	303 (100%)	-	-	325 (10%)
II-(a)	Methyltestosterone	302.45	MTHY	303 (81%)	-	-	325 (100%)	303 (100%)	-	-	325 (6%)	303 (100%)	-	-	325 (14%)
II-(a)	Testosterone	288.42	TSTO	289 (49%)	-	-	311 (100%)	289 (100%)	-	-	311 (11%)	289 (100%)	-	-	311 (26%)
II-(b). 3-keto-1-ene nucleus															
II-(b)	1-Androstenedione	286.41	1STEN	287 (81%)	-	-	309 (100%)	287 (100%)	-	-	309 (5%)	287 (100%)	-	-	309 (6%)
II-(c). 4,9,11-triene nucleaus															
II-(c)	Gestrinone	308.41	GSTN	309 (59%)	-	-	331 (100%)	309 (100%)	-	-	331 (9%)	309 (100%)	-	-	331 (19%)
II-(c)	Metribolone	284.39	MTRB	285 (57%)	-	-	307 (100%)	285 (100%)	-	-	307 (9%)	285 (100%)	-	-	307 (27%)
II-(c)	Trenbolone	270.37	TRNB	271 (74%)	-	-	293 (100%)	271 (100%)	-	-	293 (10%)	271 (100%)	-	-	293 (27%)
II-(d). 1,4-diene-3-keto															
II-(d)	Methandienone	300.44	METD	301 (13%)	283 (21%)	-	323 (100%)	301 (67%)	283 (100%)	-	323 (17%)	301 (91%)	283 (100%)	-	323 (51%)
GROUP III. Non-conjugated, C3 Hydroxyl function															
III-(a). 7-keto steroids															
III-(a)	7-Keto-DHEA	302.20	KETO	-	285 (100%)	-	-	-	285 (100%)	-	-	-	285 (100%)	-	-
III-(b). Hydroxy-androstenes															
III-(b)	Androsterone	290.44	ADEN	291 (26%)	273 (100%)	255 (18%)	313 (70%)	291 (21%)	273 (100%)	255 (19%)	-	291 (24%)	273 (100%)	255 (21%)	-
III-(b)	Etiocholanolone	290.44	ETIO	291 (9%)	273 (100%)	255 (40%)	313 (24%)	291 (8%)	273 (100%)	255 (34%)	-	291 (5%)	273 (100%)	255 (41%)	-
GROUP IV. Conjugated, C3 Hydroxyl function															
IV	1-Androsterone	290.44	1DHEA	291 (56%)	273 (100%)	255 (65%)	-	291 (57%)	273 (100%)	255 (58%)	-	291 (59%)	273 (100%)	255 (61%)	-
IV	Prasterone	288.21	PRST	289 (20%)	271 (100%)	253 (37%)	-	289 (40%)	271 (100%)	253 (28%)	-	289 (23%)	271 (100%)	253 (42%)	-
GROUP V. Non-conjugated, C3 Hydroxyl function															
V	Oxandrolone	306.44	OXAN	307 (100%)	289 (8%)	-	329 (100%)	307 (100%)	289 (40%)	-	329 (30%)	307 (100%)	289 (44%)	-	329 (72%)
V	Mesterolone	304.47	MSEL	305 (100%)	-	-	325 (15%)	305 (100%)	-	-	-	305 (100%)	-	-	-
V	Mestanolone	304.47	MSAL	305 (100%)	287 (32%)	269 (5%)	327 (14%)	305 (100%)	287 (80%)	269 (17%)	-	305 (100%)	287 (24%)	-	-
V	Androstanolone	290.44	ADON	291 (100%)	273 (8%)	-	-	291 (56%)	273 (8%)	-	-	291 (100%)	273 (5%)	-	-
GROUP VI. Un-specified Structure															
VI	Andarine	441.36	ADAR	442 (34%)	-	-	464 (100%)	442 (100%)	-	-	464 (33%)	442 (100%)	-	-	464 (31%)
VI	Clenbuterol	277.19	CLNB	277 (100%)	-	-	-	277 (100%)	-	-	-	277 (100%)	-	-	-
VI	Zeranol	322.40	ZRNL	321 (100%)*	-	-	-	321 (100%)*	-	-	-	321 (100%)*	-	-	-

*Negative mode $[M-H]^-$

S_3.2. Supplemental: CO_2- Based Q3 Scans - Group I, II & VI.

S_Table 2. Relative Abundance for Characteristic Ions for Groups I, II and V Anabolic Agents using Carbon Dioxide (CO_2)-based Mobile Phases.

				SFC (40% MeOH) (CO_2 + 40% MeOH) Relative abundance of characteristic ions (%)				SFC (20% MeOH) (CO_2 + 20% MeOH) Relative abundance of characteristic ions (%)				SFC (10% MeOH) (CO_2 + 10% MeOH) Relative abundance of characteristic ions (%)			
Class	Steroid	MW	ID	$[M+H]^+$	$[M+H-H_2O]^+$	$[M+H-2H_2O]^+$	$[M+Na]^+$	$[M+H]^+$	$[M+H-H_2O]^+$	$[M+H-2H_2O]^+$	$[M+Na]^+$	$[M+H]^+$	$[M+H-H_2O]^+$	$[M+H-2H_2O]^+$	$[M+Na]^+$
I	Danazol	337.46	DNZL	338 (100%)	-	-	360 (19%)	338 (100%)	-	-	-	338 (100%)	-	-	-
I	Stanozolol	328.49	STNZ	329 (100%)	-	-	-	329 (100%)	-	-	-	329 (100%)	-	-	-
II-(a)	1-Androstenedione	286.41	1STEN	287 (100%)	-	-	309 (10%)	287 (100%)	-	-	309 (10%)	287 (100%)	-	-	309 (8%)
II-(a)	Epitestosterone	288.42	EPIT	289 (100%)	-	-	311 (28%)	289 (100%)	-	-	311 (19%)	289 (100%)	-	-	311 (27%)
II-(a)	Mibolerone	302.50	MIBL	303 (100%)	-	-	325 (60%)	303 (100%)	-	-	325 (18%)	303 (100%)	-	-	325 (7%)
II-(a)	Methyltestosterone	302.45	MTHY	303 (100%)	-	-	325 (9%)	303 (100%)	-	-	325 (17%)	303 (100%)	-	-	325 (10%)
II-(b)	Testosterone	288.42	TSTO	289 (100%)	-	-	311 (20%)	289 (100%)	-	-	311 (47%)	289 (100%)	-	-	311 (47%)
II-(c)	Gestrinone	308.41	GSTN	309 (100%)	-	-	331 (13%)	309 (100%)	-	-	331 (35%)	309 (100%)	-	-	331 (10%)
II-(c)	Metribolone	284.39	MTRB	285 (100%)	-	-	307 (19%)	285 (100%)	-	-	307 (30%)	285 (100%)	-	-	307 (8%)
II-(c)	Trenbolone	270.37	TRNB	271 (100%)	-	-	293 (20%)	271 (100%)	-	-	293 (25%)	271 (100%)	-	-	293 (23%)
VI	Andarine	441.36	ADAR	442 (100%)	-	-	464 (83%)	442 (100%)	-	-	464 (93%)	442 (100%)	-	-	464 (31%)
VI	Clenbuterol	277.19	CLNB	277 (100%)	-	-	-	-	-	-	-	-	-	-	-
VI	Zeranol	322.40	ZRNL	321 (100%)*	-	-	-	321 (100%)*	-	-	-	321 (100%)*	-	-	-

*Negative mode $[M-H]^-$

				SFC (40% AmFo) (CO_2 + 40% MeOH + 5mM AmFo) Relative abundance of characteristic ions (%)				SFC (20% AmFo) (CO_2 + 20% MeOH + 5mM AmFo) Relative abundance of characteristic ions (%)				SFC (10% FA) (CO_2 + 10% MeOH + 5mM AmFo) Relative abundance of characteristic ions (%)			
Class	Steroid	MW	ID	$[M+H]^+$	$[M+H-H_2O]^+$	$[M+H-2H_2O]^+$	$[M+Na]^+$	$[M+H]^+$	$[M+H-H_2O]^+$	$[M+H-2H_2O]^+$	$[M+Na]^+$	$[M+H]^+$	$[M+H-H_2O]^+$	$[M+H-2H_2O]^+$	$[M+Na]^+$
I	Danazol	337.46	DNZL	338 (100%)	-	-	-	338 (100%)	-	-	-	338 (100%)	-	-	-
I	Stanozolol	328.49	STNZ	329 (100%)	-	-	-	329 (100%)	-	-	-	329 (100%)	-	-	-
II-(a)	1-Androstenedione	286.41	1STEN	287 (100%)	-	-	-	287 (100%)	-	-	-	287 (100%)	-	-	309 (10%)
II-(a)	Epitestosterone	288.42	EPIT	289 (100%)	-	-	311 (12%)	289 (100%)	-	-	311 (21%)	289 (100%)	-	-	311 (38%)
II-(a)	Mibolerone	302.50	MIBL	303 (100%)	-	-	325 (10%)	303 (100%)	-	-	325 (13%)	303 (100%)	-	-	325 (19%)
II-(a)	Methyltestosterone	302.45	MTHY	303 (100%)	-	-	325 (9%)	303 (100%)	-	-	325 (18%)	303 (100%)	-	-	325 (25%)
II-(b)	Testosterone	288.42	TSTO	289 (100%)	-	-	311 (9%)	289 (100%)	-	-	311 (16%)	289 (100%)	-	-	311 (26%)
II-(c)	Gestrinone	308.41	GSTN	309 (100%)	-	-	331 (19%)	309 (100%)	-	-	331 (29%)	309 (100%)	-	-	331 (34%)
II-(c)	Metribolone	284.39	MTRB	285 (100%)	-	-	307 (19%)	285 (100%)	-	-	307 (30%)	285 (100%)	-	-	307 (25%)
II-(c)	Trenbolone	270.37	TRNB	271 (100%)	-	-	293 (24%)	271 (100%)	-	-	293 (28%)	271 (100%)	-	-	293 (26%)
VI	Andarine	441.36	ADAR	442 (67%)	-	-	464 (100%)	442 (100%)	-	-	464 (98%)	442 (100%)	-	-	464 (85%)
VI	Clenbuterol	277.19	CLNB	277 (100%)	-	-	-	277 (100%)	-	-	-	277 (100%)	-	-	-
VI	Zeranol	322.40	ZRNL	321 (100%)*	-	-	-	321 (100%)*	-	-	-	321 (100%)*	-	-	-

*Negative mode $[M-H]^-$

				SFC (40% FA) (CO_2 + 40% MeOH + 0.1% FA) Relative abundance of characteristic ions (%)				SFC (20% FA) (CO_2 + 20% MeOH + 0.1% FA) Relative abundance of characteristic ions (%)				SFC (10% FA) (CO_2 + 10% MeOH + 0.1% FA) Relative abundance of characteristic ions (%)			
Class	Steroid	MW	ID	$[M+H]^+$	$[M+H-H_2O]^+$	$[M+H-2H_2O]^+$	$[M+Na]^+$	$[M+H]^+$	$[M+H-H_2O]^+$	$[M+H-2H_2O]^+$	$[M+Na]^+$	$[M+H]^+$	$[M+H-H_2O]^+$	$[M+H-2H_2O]^+$	$[M+Na]^+$
I	Stanozolol	328.49	STNZ	329 (100%)	-	-	-	329 (100%)	-	-	-	329 (100%)	-	-	-
I	Danazol	337.46	DNZL	338 (100%)	-	-	-	338 (100%)	-	-	-	338 (100%)	-	-	-
II-(a)	Epitestosterone	288.42	EPIT	289 (100%)	-	-	311 (13%)	289 (100%)	-	-	311 (24%)	289 (100%)	-	-	311 (25%)
II-(a)	Testosterone	288.42	TSTO	289 (100%)	-	-	-	289 (100%)			-	289 (100%)			311 (7%)
II-(a)	Mibolerone	302.50	MIBL	303 (100%)	-	-	-	303 (100%)	-	-	325 (7%)	303 (100%)	-	-	-
II-(a)	Methyltestosterone	302.45	MTHY	303 (100%)	-	-	-	303 (100%)	-	-	-	303 (100%)	-	-	-
II-(b)	1-Androstenedione	286.41	1STEN	287 (100%)	-	-	305 (8%)	287 (100%)	-	-	305 (5%)	287 (100%)	-	-	309 (7%)
II-(c)	Trenbolone	270.37	TRNB	271 (100%)	-	-	-	271 (100%)	-	-	-	271 (100%)	-	-	-
II-(c)	Gestrinone	308.41	GSTN	309 (100%)	-	-	-	309 (100%)	-	-	-	309 (100%)	-	-	-
II-(c)	Metribolone	284.39	MTRB	285 (100%)	-	-	-	285 (100%)	-	-	307 (6%)	285 (100%)	-	-	-
VI	Andarine	441.36	ADAR	442 (100%)	-	-	464 (12%)	442 (100%)	-	-	464 (32%)	442 (100%)	-	-	464 (11%)
VI	Clenbuterol	277.19	CLNB	277 (100%)	-	-	-	-	-	-	-	-	-	-	-
VI	Zeranol	322.40	ZRNL	321 (100%)*	-	-	-	321 (100%)*	-	-	-	321 (100%)*	-	-	-

*Negative mode $[M-H]^-$

S_3.3. Supplemental: CO_2-Based Q3 Scans - Groups III, IV and V.

S_Table 3. Relative Abundance for Characteristic Ions for Groups III and IV Steroids using Carbon Dioxide (CO_2)-based Mobile Phases.

				SFC (40% MeOH) (CO_2 + 40% MeOH) Relative abundance of characteristic ions (%)				SFC (20% MeOH) (CO_2 + 20% MeOH) Relative abundance of characteristic ions (%)				SFC (10% MeOH) (CO_2 + 10% MeOH) Relative abundance of characteristic ions (%)			
Class	Steroid	MW	ID	$[M+H]^+$	$[M+H-H_2O]^+$	$[M+H-2H_2O]^+$	$[M+Na]^+$	$[M+H]^+$	$[M+H-H_2O]^+$	$[M+H-2H_2O]^+$	$[M+Na]^+$	$[M+H]^+$	$[M+H-H_2O]^+$	$[M+H-2H_2O]^+$	$[M+Na]^+$
II-(d)	Methandienone	300.44	METD	301 (100%)	283 (91%)	-	323 (68%)	301 (100%)	283 (72%)	-	323 (76%)	301 (100%)	283 (53%)	-	323 (20%)
III-(a)	7-Keto-DHEA	302.20	KETO	-	285 (100%)	-	-	-	285 (100%)	-	-	-	285 (100%)	-	-
III-(b)	Androsterone	290.44	ADEN	291 (30%)	273 (100%)	255 (18%)	313 (9%)	291(30%)	273(100%)	255 (23%)	313 (16%)	291 (35%)	273 (100%)	255 (19%)	313 (6%)
III-(b)	Etiocholanolone	290.44	ETIO	291 (12%)	273 (100%)	255 (28%)	313 (15%)	291 (17%)	273 (100%)	255 (36%)	313 (6%)	291 (12%)	273 (100%)	255 (34%)	313 (5%)
IV	1-Androsterone	290.44	1DHEA	291 (75%)	273 (89%)	255 (100%)	313 (8%)	291 (84%)	273 (100%)	255 (85%)	-	291 (81%)	273 (100%)	255 (75%)	-
IV	Prasterone	288.21	PRST	289 (43%)	271 (100%)	253 (38%)	-	289 (24%)	271 (100%)	253 (35%)	-	289 (19%)	271 (100%)	253 (40%)	-
V	Oxandrolone	306.44	OXAN	307 (94%)	289 (82%)	-	329 (100%)	307 (92%)	289 (34%)	-	329 (100%)	307 (100%)	289 (42%)	-	329 (29%)
V	Mesterolone	304.47	MSEL	305 (100%)	288 (27%)	-	-	305 (100%)	-	-	-	305 (100%)	-	-	-
V	Mestanolone	304.47	MSAL	305 (100%)	287 (59%)	269 (8%)	-	305 (100%)	287 (77%)	269 (8%)	-	305 (100%)	287 (53%)	269(5%)	-
V	Androstanolone	290.44	ADON	291 (10%)	273 (8%)	255 (6%)	-	291(10%)	-	255 (7%)	-	291 (21%)	-	255 (7%)	-

				SFC (40% AmFo) (CO_2 + 40% MeOH + 5mM AmFo) Relative abundance of characteristic ions (%)				SFC (20% AmFo) (CO_2 + 20% MeOH + 5mM AmFo) Relative abundance of characteristic ions (%)				SFC (10% FA) (CO_2 + 10% MeOH + 5mM AmFo) Relative abundance of characteristic ions (%)			
Class	Steroid	MW	ID	$[M+H]^+$	$[M+H-H_2O]^+$	$[M+H-2H_2O]^+$	$[M+Na]^+$	$[M+H]^+$	$[M+H-H_2O]^+$	$[M+H-2H_2O]^+$	$[M+Na]^+$	$[M+H]^+$	$[M+H-H_2O]^+$	$[M+H-2H_2O]^+$	$[M+Na]^+$
II-(d)	Methandienone	300.44	METD	301 (100%)	283 (98%)	-	323 (65%)	301 (100%)	283 (84%)	-	323 (67%)	301 (100%)	283 (63%)	-	323 (58%)
III-(a)	7-Keto-DHEA	302.20	KETO	-	285 (100%)	-	-	-	285 (100%)	-	-	-	285 (100%)	-	-
III-(b)	Androsterone	290.44	ADEN	291 (30%)	273 (100%)	255 (26%)	-	291 (21%)	273 (100%)	255 (26%)	-	291 (29%)	273 (100%)	255 (19%)	-
III-(b)	Etiocholanolone	290.44	ETIO	291 (14%)	273 (100%)	255 (35%)	-	291 (12%)	273 (100%)	255 (45%)	-	291 (11%)	273 (100%)	255 (39%)	-
IV	1-Androsterone	290.44	1DHEA	291 (82%)	273 (100%)	255 (76%)	-	291 (88%)	273 (100%)	255 (93%)	-	291 (82%)	273 (100%)	255 (76%)	-
IV	Prasterone	288.21	PRST	289 (33%)	271 (100%)	253 (44%)	-	289 (31%)	271 (100%)	253 (42%)	-	289 (27%)	271 (100%)	253 (43%)	-
V	Oxandrolone	306.44	OXAN	307 (74%)	289 (26%)	271 (5%)	329 (100%)	307 (100%)	289 (36%)	271 (2%)	329 (96%)	307 (100%)	289 (37%)	271 (6%)	329 (88%)
V	Mesterolone	304.47	MSEL	305 (100%)	-	-	327 (95%)	305 (100%)	-	-	327 (27%)	305 (100%)	-	-	327 (18%)
V	Mestanolone	304.47	MSAL	*304 (100%)	-	-	-	*304 (100%)	-	-	-	*304 (100%)	-	-	-
V	Androstanolone	290.44	ADON	-	273 (41%)	249 (28%)	-	291 (5%)	273 (5%)	255 (7%)	-	291 (14%)	273 (6%)	255 (6%)	-

				SFC (40% FA) (CO_2 + 40% MeOH + 0.1% FA) Relative abundance of characteristic ions (%)				SFC (20% FA) (CO_2 + 20% MeOH + 0.1% FA) Relative abundance of characteristic ions (%)				SFC (10% FA) (CO_2 + 10% MeOH + 0.1% FA) Relative abundance of characteristic ions (%)			
Class	Steroid	MW	ID	$[M+H]^+$	$[M+H-H_2O]^+$	$[M+H-2H_2O]^+$	$[M+Na]^+$	$[M+H]^+$	$[M+H-H_2O]^+$	$[M+H-2H_2O]^+$	$[M+Na]^+$	$[M+H]^+$	$[M+H-H_2O]^+$	$[M+H-2H_2O]^+$	$[M+Na]^+$
II-(d)	Methandienone	300.44	METD	301 (100%)	283 (98%)	-	323 (16%)	301 (100%)	283 (77%)	-	323 (16%)	301 (100%)	283 (53%)	-	323 (10%)
III-(a)	7-Keto-DHEA	302.20	KETO	-	285 (100%)	-	-	-	285 (100%)	-	-	-	285 (100%)	-	-
III-(b)	Androsterone	290.44	ADEN	291 (25%)	273 (100%)	255 (23%)	-	291 (26%)	273 (100%)	255 (24%)	-	291 (30%)	273 (100%)	255 (21%)	-
III-(b)	Etiocholanolone	290.44	ETIO	291 (11%)	273 (100%)	255 (37%)	-	291 (12%)	273 (100%)	255 (37%)	-	291 (17%)	273 (100%)	255 (42%)	-
IV	1-Androsterone	290.44	1DHEA	291 (100%)	273 (75%)	255 (70%)	-	291 (100%)	273 (89%)	255 (81%)	-	291 (81%)	273 (100%)	255 (82%)	-
IV	Prasterone	288.21	PRST	-	271 (95%)	253 (45%)	-	289 (28%)	271 (100%)	253 (36%)	-	289 (25%)	271 (100%)	253 (37%)	-
V	Oxandrolone	306.44	OXAN	307 (100%)	289 (25%)	-	329 (38%)	307 (100%)	289 (36%)	-	329 (20%)	307 (100%)	289 (31%)	-	329 (12%)
V	Mesterolone	304.47	MSEL	305 (100%)	288 (64%)	-	-	305 (100%)	288 (17%)	-	-	305 (100%)	-	-	-
V	Mestanolone	304.47	MSAL	305 (66%)	288 (100%)	269 (8%)	-	305 (100%)	287 (65%)	269 (10%)	327 (6%)	305 (100%)	287 (57%)	-	-
V	Androstanolone	290.44	ADON	291 (8%)	-	255 (6%)	-	291 (8%)	-	255 (7%)	-	291 (14%)	-	255 (6%)	-

S_3.4. Supplemental:

Additional Peaks Observed for Hydroxy- & Saturated Steroids

When additional peaks were observed for a standard solution, Q3 scans were re-evaluated by taking extracted ion chromatograms for relevant ions for that compound. Peaks were verified across each modifier concentration for changing elution (e.g., Monitoring separation of each peak as modifier concentration was reduced). The ion spectrum extracted for each peak, and then those spectrums compared between different mobile phases which is presented in this section. The largest peak was always indicated by the number 1, and corresponds to the data presented in all figures in the preceding sections (important note: the peak numbers do not indicate elution order).

S_3.4.1. ADEN Additional Peaks.

Three additional peaks were separated for ADEN at low modifier concentrations (S_Figure 8). Peaks 1 and 2 were present in all three MPs. Peak 3 was only observed while using no additive and while using formic acid.

The main characteristic ions for each peak were as follows:

- **Peak 1.** *(largest area; latest eluting)*; dominant ion was $[M+H-H_2O]^+$; significant $[M+H]^+$ and $[M+H-H_2O]^+$ ions present, but no MeOH adducts were present in this peak.
- **Peak 2.** *(second largest)*; spectra contained no $[M+H]^+$, and instead contained two water fragments $[M+H-H_2O]^+$ & $[M+H-2H_2O]^+$, and the corresponding solvent adducts $[M+H+MeOH-H_2O]^+$ and $[M+H+MeOH-2H_2O]^+$. The dominant ion was $[M+H -H_2O]^+$ but nearly equal abundance $[M+H+MeOH-H_2O]^+$ adduct also present. This peak was observed using methanol with no additive and with formic acid, but was notably absent in AmFo.
- **Peak 3.** *(smallest Area; earliest eluting)*; dominant ion was $[M+H]^+$; unidentified *m/z* 237 (would match $[M+H-3H_2O]^+$, but structure only contains 2 Oxygens, so should not be an option), and other minor adducts were difficult to identify.

Using AmFo, the least amount of secondary adducts were observed (even at low modifier, the additional peaks were negligible), e.g., only additional peak 2 was present.

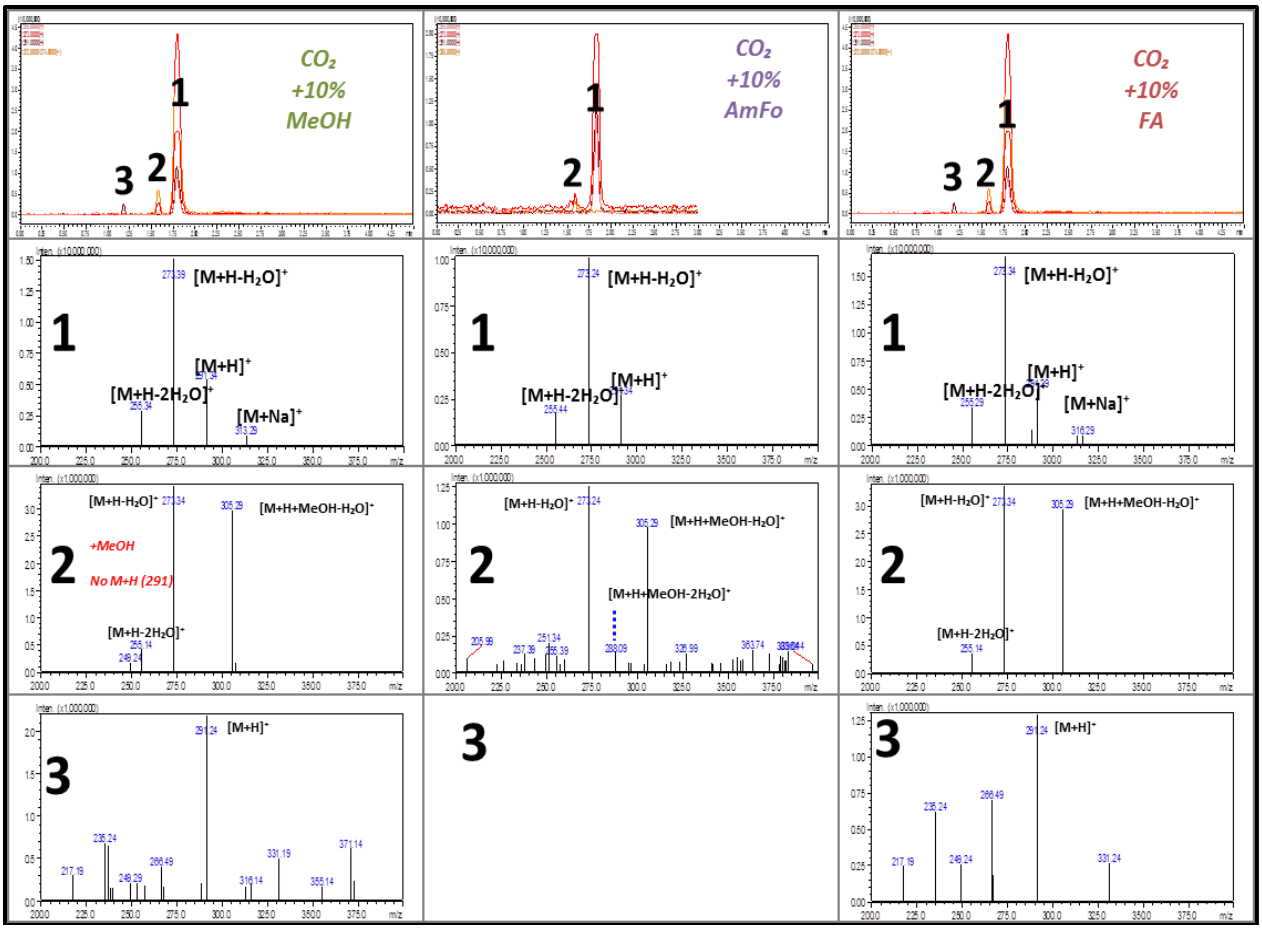

S_Figure 8. Additional peaks for ADEN separated at 10% modifier in CO_2. Comparing three modifiers: **(left)** methanol with no additive; **(middle)** methanol + 5 mM ammonium formate; **(right)** methanol + 0.1% formic acid**.** Showing **[Top]** Extracted Ion Chromatograms (EIC) for 255 *m/z* ($[M+H-2H_2O]^+$; pink); 273 *m/z* ($[M+H-H_2O]^+$; red); 291 *m/z* ($[M+H]^+$; maroon); 305 *m/z* ($[M+H+MeOH-H_2O]^+$; orange); and **[Bottom]** Ion spectra for each peak [1-3] Extracted Ion Spectrum (200-400 m/z) for the corresponding retention time for each peak.

S_3.4.2. ETIO Additional Peaks.

Four additional peaks were separated for ETIO at low modifier concentrations (S_Figure 9). All four peaks were observed using MeOH without additive (MeOH) and with formic acid as additive (FA). Only peaks 1 and 2 were observed while using ammonium formate as additive (AmFo).

The characteristic ions for each peak were as follows:

- **Peak 1.** (same as ADEN above);
- **Peak 2.** (same as ADEN above, except); $[M+H-2H_2O]^+$ at much higher abundance.
- **Peak 3.** (same as ADEN above).
- **Peak 4.** (smallest area; elutes between 2 and 3); unidentified m/z 251 ion, and $[M+H-H_2O]^+$, also notably absent with AmFo.

Comparing ADEN and ETIO, it is interesting to note that peak 2, having a higher relative abundance of $[M+H-2H_2O]^+$ to the $[M+H-H_2O]^+$ ion. This would be in line with literature where α-/ß- isomerisms of C5 has been distinguished using MS alone, α- isomers favor ion formation due to water loss due to positional advantage after ring cleavage.[68]

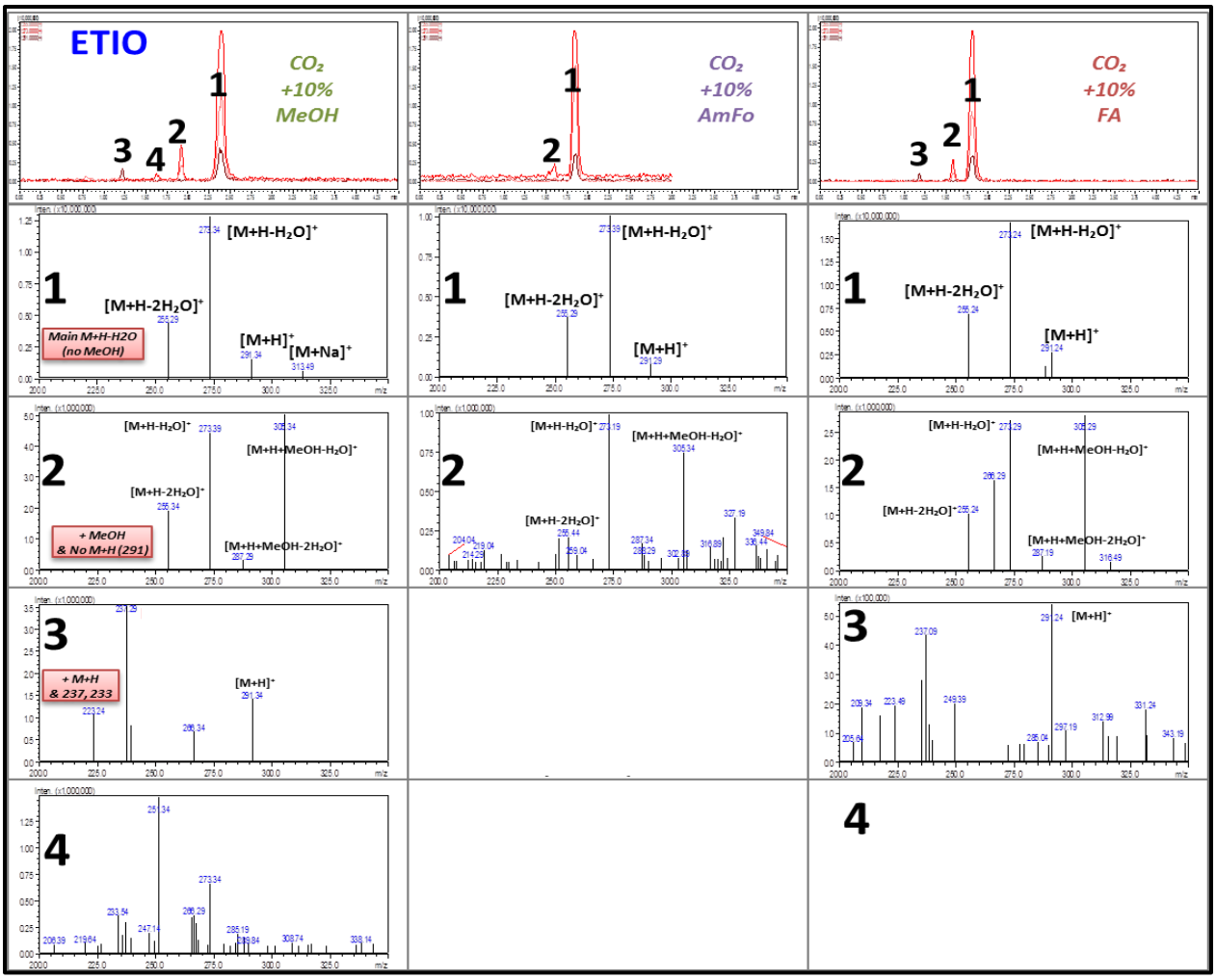

S_Figure 9. ETIO extra peaks separated at 10% modifier in CO_2: Comparing Ion Spectrum for each peak. [Top] Extracted Ion Chromatograms (EIC) for 255 m/z ($[M+H-2H_2O]^+$; pink); 273 m/z ($[M+H-H_2O]^+$; red); 291 m/z ($[M+H]^+$; maroon). **[1-4]** Extracted Ion Spectrum (200-400 m/z) corresponding retention time for each peak.

S_3.4.3. 1DHEA Additional Peaks.

Four additional peaks were separated for 1DHEA at low modifier concentrations (S_Figure 10). All four peaks were observed using MeOH and FA. Only peaks 1 and 2 were observed using AmFo.

The characteristic ions for each peak were as follows:

- **Peak 1.** (same as ADEN above);
- **Peak 2.** (same as ADEN above, except); $[M+H+MeOH-2H_2O]^+$ was dominant ion.
- **Peak 3.** (same as ADEN above);
- **Peak 4.** (same as ETIO above).

1DHEA is the 1-ene isomer of PRST. Notably PRST followed a completely different pattern, as discussed later.

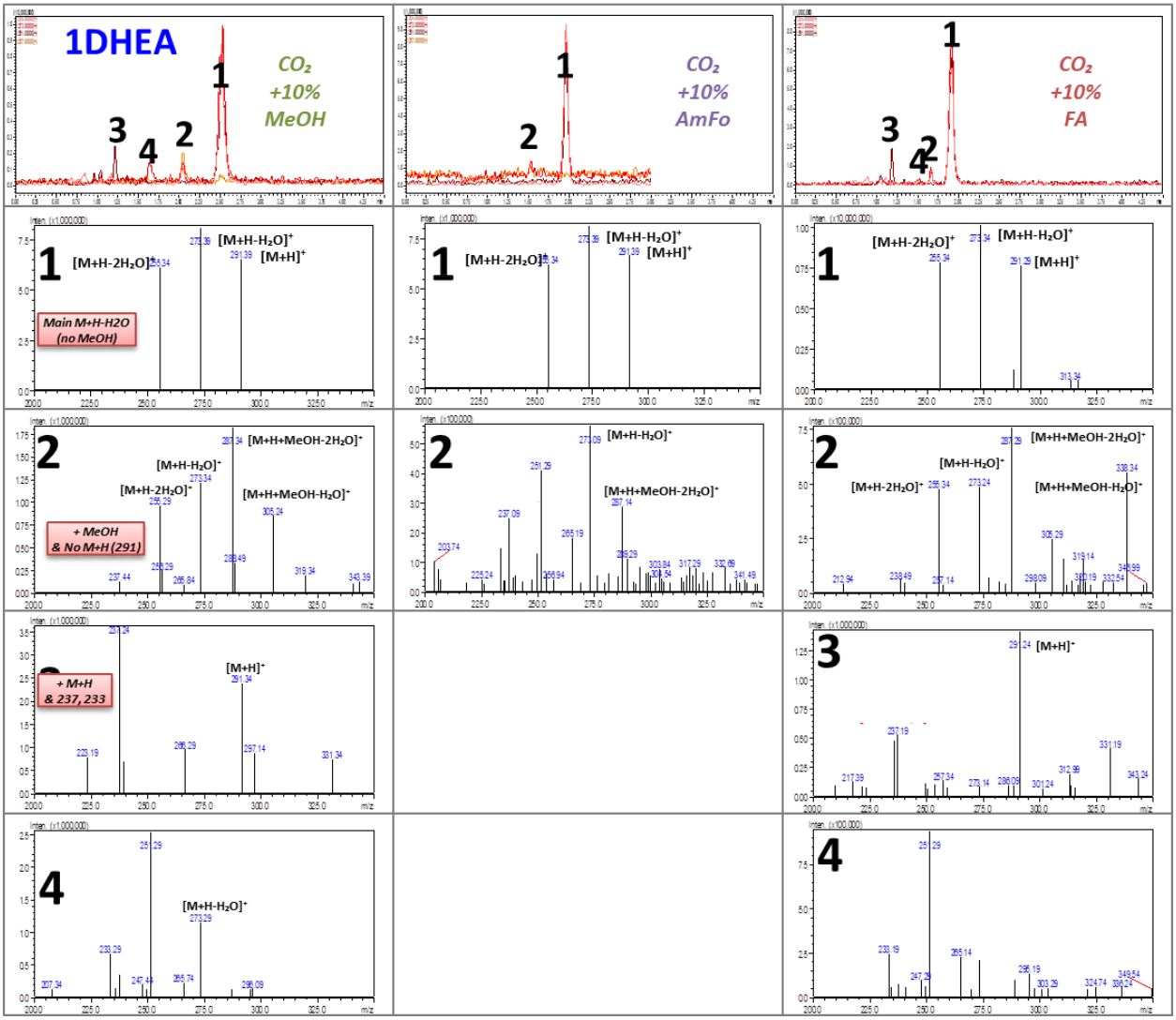

S_Figure 10. 1DHEA extra peaks separated at 10% modifier in CO_2: Comparing Ion Spectrum for each peak. [Top] Extracted Ion Chromatograms (EIC) for 255 m/z ($[M+H-2H_2O]^+$; pink); 273 m/z ($[M+H-H_2O]^+$; red); 291 m/z ($[M+H]^+$; maroon). **[1-4]** Extracted Ion Spectrum (200-400 m/z) corresponding retention time for each peak.

S_3.4.4. ADON Additional Peaks.

Four additional peaks were separated for ADON at low modifier concentrations (S_Figure 11). Peaks 1, 2, 3 & 4 were observed in all three mobile phases (although peak 2 is nearly insignificant in AmFo). Peak 5 was only observed in AmFo.

The characteristic ions for each peak were as follows:

- **Peak 1.** Spectrum was dominated by methanol adducts $[M+H+MeOH-H_2O]^+$ & $[M+H+MeOH-2H_2O]^+$; with $[M+H+MeOH-2H_2O]^+$ being the dominant ion. $[M+H-2H_2O]^+$ & $[M+H]^+$ were also present for this peak.
- **Peak 2.** Dominant peak was $[M+H]^+$. This peak was notably absent while using AmFo. Both $[M+H+MeOH-H_2O]^+$ & $[M+H+MeOH-2H_2O]^+$ were also present.
- **Peak 3.** Dominant ion was the unidentified peak m/z 237 (would match $[M+H-3H_2O]^+$, but structure only contains 2x Oxygens, so should not an option).
- **Peak 4.** Dominant peak was $[M+H]^+$. unidentified peak m/z 237 also present.
- **Peak 5.** Only observed using AmFo. Matches closely peak 4, except the peak at 291 [M+H] in pk4 > now 290 [M].

For ADON, $[M+H+MeOH-H_2O]^+$ was always the dominant ion while using SFC, except that depends on which peak. As stated above, the same profile (i.e., same types of ions were seen in both FIA & SFC, when the same modifier was used), but it was observed that the FIA profiles matched more closely to the SFC profiles using 40% modifier, although this could be expected if the ions are dependent on the presence of the modifier (e.g., to promote coordination of methanol for adduct formation), but under closer inspection, applying extracted ion chromatograms (EIC) using the most dominant ions in FIA on the lowest concentration runs in SFC, it appears the same ions are still present, but have been separated chromatographically, (S_Figure 11**; top**). As each peak contains multiple peaks that match adducts present in the 100% modifier Q3 scans using flow injection analysis with no column installed (S_Table 4**).**

Peak 1 was chosen as the analyte due to the most similarities across all mobile phases to the FIA counterparts. Although it could be argued that peak 2 which was characterized by a protonated molecular ion, and the $[M+H+MeOH]^+$ solvent adduct, and dehydrated solvent adduct $[M+H+MeOH-H_2O]^+$, but if this peak was followed thru to higher modifier concentration the presence of the protonated molecule was reduced and the molecular ion $[M]^+$ increased. If this was due to the solvent then this would be expected to be the dominant ion observed in the 100% modifier FIA runs.

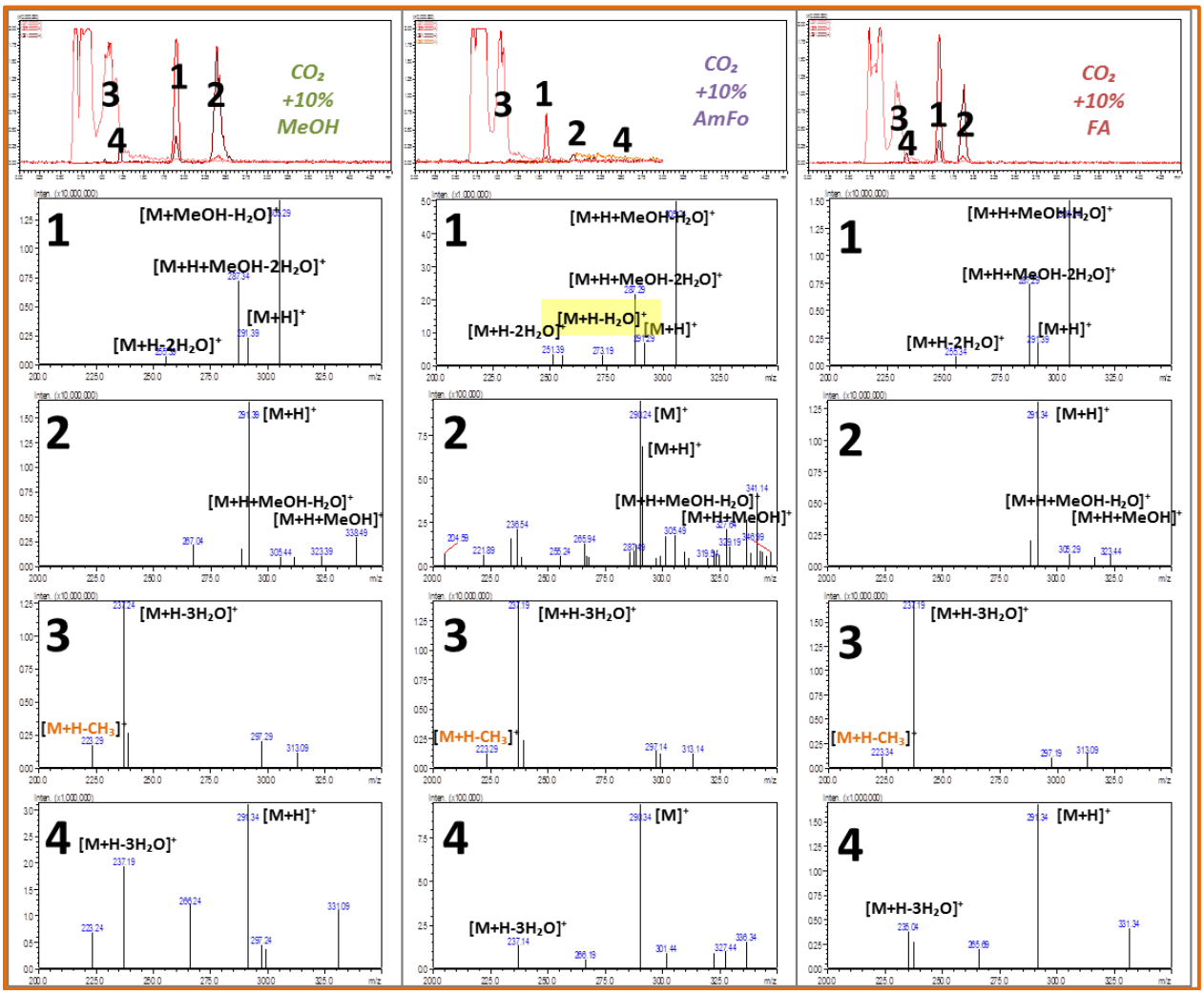

S_Figure 11. ADON extra peaks separated at 10% modifier in CO_2: Comparing Ion Spectrum for each peak. [Top] Extracted Ion Chromatograms (EIC) for 305 m/z ($[M+H+MeOH-H_2O]^+$; red); 291 m/z ($[M+H]^+$; maroon); 290 m/z ($[M]^+$; orange); and 237 m/z (unidentified, pink). **[1-4]** Extracted Ion Spectrum (200-350 m/z) corresponding retention time for each peak.

S_Table 4. Relative Abundance for Characteristic Ions for Alternative Peaks Separated at low modifier concentration for ADON.

	ID:	ADON											
	Steroid:	androstanolone											
	Molecular Weight:	290.44											
		Relative abundance of characteristic ions (%)				Relative abundance of characteristic ions (%)				Relative abundance of characteristic ions (%)			
	Mobile Phase:	Peak 1 (Rt = 1.78 min)	Peak 2 (Rt = 2.48 min)	Peak 3 (Rt = 1.11 min)	Peak 4 (Rt = 1.24 min)	Peak 1 (Rt = 1.62 min)	Peak 2 (Rt = 1.91 min)	Peak 3 (Rt = 1.11 min)	Peak 5 (Rt = 2.00 min)	Peak 1 (Rt = 1.62 min)	Peak 2 (Rt = 1.91 min)	Peak 3 (Rt = 1.11 min)	Peak 4 (Rt = 1.20 min)
ION	$[M+H]^+$	291 (21%)	291 (100%)	-	291 (100%)	291 (14%)	291 (77%)	-	-	291 (100%)	291 (100%)	-	291 (100%)
	$[M]^+$	-	-	-	-	-	290 (100%)	-	290 (100%)	-	-	-	-
	$[M+Na]^+$	-	-	-	-	-	-	-	-	-	-	313 (9%)	-
	$[M+H-CH3]^+$	-	-	223 (7%)	223 (14%)	-	-	223 (8%)	223 (14%)	-	-	223 (7%)	223 (27%)
	$[M+H-H_2O]^+$	-	-	-	-	273 (6%)	-	-	-	273 (5%)	-	-	-
	$[M+H-2H_2O]^+$	255 (7%)	-	-	-	255 (6%)	-	-	-	-	-	-	-
	$[M+H-3H_2O]^+$	-	-	237 (100%)	237 (54%)	-	-	237 (100%)	237 (16%)	237 (18%)	-	237 (100%)	237 (27%)
	$[M+H+MeOH]^+$	-	323 (7%)	-	-	-	323 (5%)	-	-	-	323 (9%)	-	-
	$[M+H+MeOH-H_2O]^+$	305 (100%)	305 (6%)	-	-	305 (100%)	305 (20%)	-	-	305 (17%)	305 (9%)	-	-
	$[M+H+MeOH-2H_2O]^+$	287 (62%)	-	-	-	287 (44%)	-	-	-	287 (6%)	-	-	-
	$[M+H+MeOH-3H_2O]^+$	-	-	-	-	-	-	-	-	-	-	-	-

S_3.4.5. MSEL Additional Peaks.

Four additional peaks were separated for MSEL at low modifier concentrations (S_Figure 12). Peaks 1-4 were present in all three MPs. Peak 5 was only observed while using no additive and while using formic acid.

The main characteristic ions for each peak were as follows:

- **Peak 1.** $[M+H]^+$ (minor $[M+Na]^+$ in AmFo)
- **Peak 2.** Methanol adducts of both water fragments $[M+H+MeOH-H_2O]^+$ and $[M+H+MeOH-2H_2O]^+$
- **Peak 3.** Dominant ion = $[M+H-CH_3]^+$; minor $[M+H]^+$ in all MPs except AmFo = $[M]^+$ instead
- **Peak 4.** (Same as pk3, plus); minor $[M+Na-CH_3]^+$ in all MPs.
- **Peak 5**. $[M+Na-H_2O]^+$ and m/z 266 (unidentified)

Using AmFo, least amount ions could be found (as in even the main peak was very low sensitivity). FA seemed to give the best result but still multiple peaks.

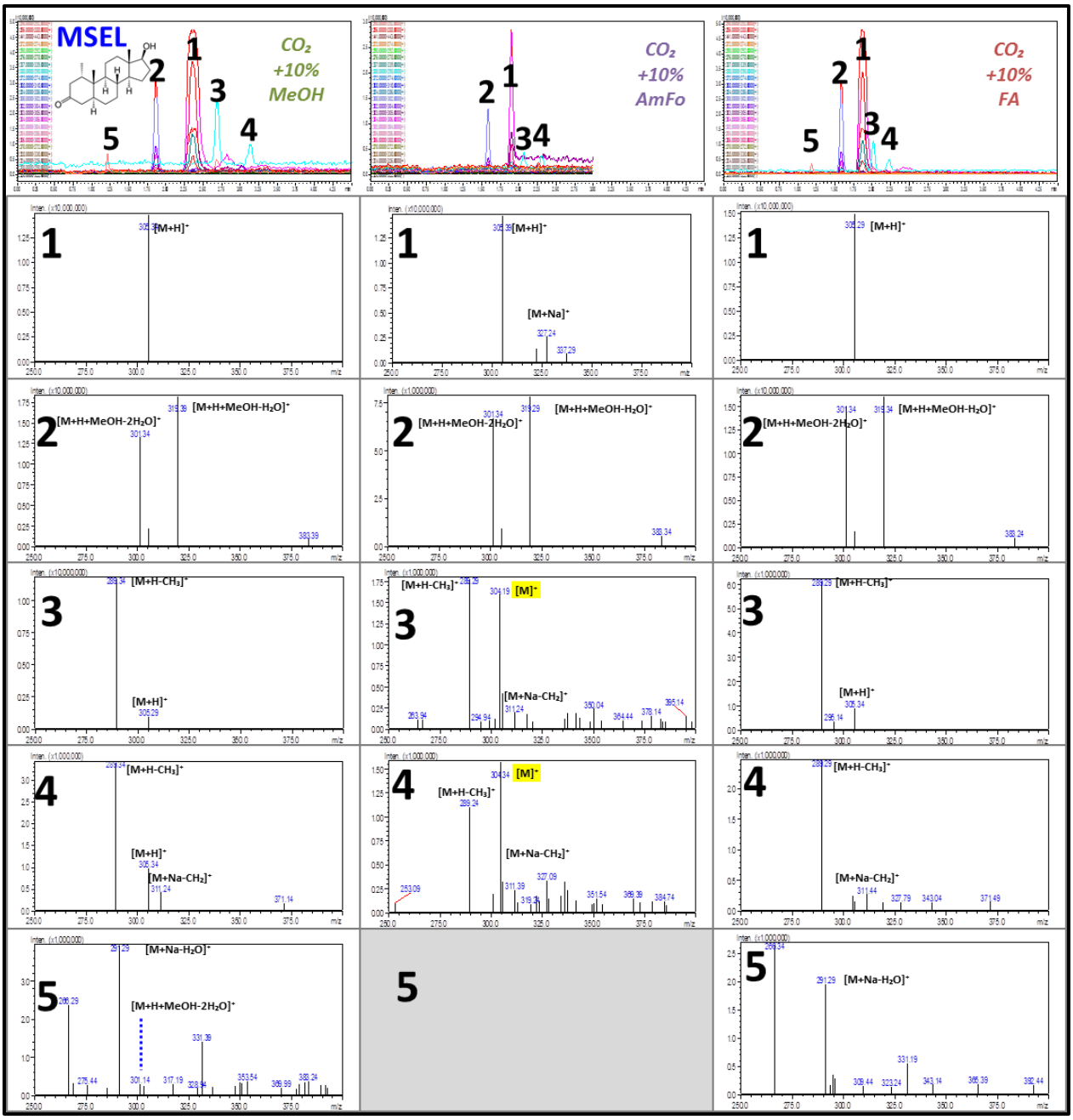

S_Figure 12. MSEL extra peaks separated at 10% modifier in CO_2: Comparing Ion Spectrum for each peak. [Top] Extracted Ion Chromatograms (EIC) for 305 m/z ($[M+H+MeOH-H_2O]^+$; red); 291 m/z ($[M+H]^+$; maroon); 290 m/z ($[M]^+$; orange); and 237 m/z (unidentified, pink). **[1-4]** Extracted Ion Spectrum (200-350 m/z) corresponding retention time for each peak.

CHAPTER 4

MS OPTIMIZATION FOR DETECTION OF AAS: MRM OPTIMIZATIONS USING CARBON DIOXIDE-BASED MOBILE PHASES

CHAPTER 4
MS OPTIMIZATION FOR DETECTION OF AAS:
MRM OPTIMIZATIONS
USING CARBON DIOXIDE-BASED MOBILE PHASES

4.1. Multiple Reaction Monitoring (MRM).

Multiple reaction monitoring (MRM) provides highly selective and sensitive mass spectrometric detection. MRMs utilize a triple quadrupole mass spectrometer. Increased sensitivity stems from only the selected ions (precursors) are allowed to pass thru the first stage of the mass analyzer. These ions correspond to the analyte of interest and are related to the structure (e.g., molecular weight or fragments thereof) of targeted compounds. All other ions are filtered out (i.e., ejected or lost thru collisional trajectories), in the first stages of ion sorting. This reduces unwanted background signals and increases signal to noise ratios. MRM detection also provides high selectivity, as the ions that make it thru to detection have been sorted twice (one specific precursor [Q1] → fragmented → product [Q3]). Both the precursor and product are optimized specifically to the targeted analyte, and all other ions are ignored.

Each of the selected ions used for detection represents a single 'transition' (i.e., a specific ion produced from the fragmentation of a single specific precursor). MRM quickly scans over multiple mass windows to enable monitoring of multiple fragment ion masses in parallel. Therefore, one (or more) fragments can be selected for a single precursor and allows for both qualitative and quantitative analysis. A qualitative comparison can be made by comparing peak intensities for all selected fragments (helpful in identification). MRMs also allow for quantitative analysis, by selecting a single fragment, the amount of analyte present can be determined (via calibration) of the integrated peak area under the curve. Further details of the triple-quad setup and MRM-transitions were discussed in a previous chapter (**Chapter #1. Section 1.2.4. *Triple-Quad: Multiple Reaction Monitoring***).

4.2. Steroid Fragmentation

4.2.1. Characterization Fragmentation and Expected Product Ions.

The classification and characterization of the ionization and fragmentation pathways of steroids has been extensively studied. The mass spectral fragmentation patterns and their relationship to the structure of testosterone and related substances was established for Electron Ionization (EI) in the early 1960's.[50] GC-MS is the standard method for the detection of AAS, but requires a trimethylsilyl (TMS) derivatization to make the compounds more volatile. However, the derivatization step does not always produce satisfactory derivatives.[36],[51]

LC-MS/MS methods have been developed as a complementary technique to the standard GC-MS procedures, since the derivatization step is not needed, and sensitivity is often better. However, efficiency in LC is significantly lower than in capillary GC, producing lower resolution for compounds with similar structures. The detection of steroids by LC-MS, using electrospray ionization (ESI), is hindered by the absence of acidic or basic functional groups which help generate $[M+H]^+$.[52] Consequently, adduct ions such as $[M+NH_4]^+$, $[M+H+MeOH]^+$, $[M+Na+MeOH]^+$, and $[M+H+CH_3CN-H_2O]^+$ have been used to detect anabolic steroids.[35]

While the classification and characterization of the ionization and fragmentation pathways of steroids has been extensively studied. There is minimal information on the effect of the addition of carbon dioxide (CO_2) would have on the fragmentation patterns of specific steroids normally investigated using GC-MS and LC-MS ionization techniques.[42]

4.2.2. General Fragmentation themes for all anabolic steroids

Although ionization and fragmentation patterns can differ greatly between steroid groups, some general rules have been outlined by **Schanzer et. al., 2008.**[53]

Water losses are directly related to the number of oxygen atoms present in the molecule. The formation of $[M+H-H_2O]^+$ or $[M+H-2H_2O]^+$ ions corresponds to losses of neutral H_2O. Fragments generated thru

the neutral loss of water, are limited to the number of oxygens present in the structure (i.e., if there is only one oxygen atom present in a compounds structure, then it is only possible for that analyte to produce the $[M+H-H_2O]^+$). Water losses can also be inhibited by the number of conjugations and/or the relative location of conjugations versus keto-functional groups.

Isomers (α- & ß-) have the same CID spectra but each is expected to produce different intensity ratios of some characteristic ions for the steroid group.[54]

Number of rings containing double bonds can influence steroid fragmentation patterns. At medium collision energies (e.g., 30 eV) the number of rings containing double bonds guides fragmentation. For example, a compound containing double bonds only in the A-ring of its structure, will tend to produce fragments containing one ring.

Common Ions for all Steroids. At high collision energies (e.g., 50 eV) all steroids will produce the common ions of *m/z* 77, 91 and 105. Therefore these ions would not provide any structural information specific to any steroid, or furthermore, of these ions are also generally common to any aromatic compound.

Steroid fragmentation patterns can be highly dependent on the specific steroid structure. Even small differences in isomeric structure can result in large deviations in dissociation pathways.

4.3. MS-Optimizations in SFE-SFC-MS Method Development.

For initial detection optimization the instrument was set up for direct flow injection. Solutes were dissolved in methanol. Pure methanol was pumped through the system as the mobile phase, the solutes injected into the flowing stream, without a column installed, then into the MS, as described in **Chapter #1. SFE-SFC-MS Hyphenated Instrumentation: Section. 1.4.1. Instrument Configurations. FIA-MS Optimization Configuration and 1.4.2. CO_2-MS Optimization Mode**. MS-optimization for detection in SFE-SFC-MS analysis is the first step in method development for online methods, and is broken down into three main steps:

1. **Q3 Scans** are used to determine optimal precursors from characteristic Ionization patterns and optimal solutions concentrations for further MS-optimization for each compound.

2. **MRM-Optimization.** Multiple reaction monitoring (MRM) optimization is performed for each of the targeted compounds to choose optimal product ions, collision energies (CE) and associated voltages. The resulting MRM-transitions as well as Q3 scans are used to identify critical pair groups.

3. **Identification of Critical Pair Groups.** The MRM-transitions from step 2, plus the Q3 scans from step 1, are used to identify critical pair groups, by re-injecting each analyte. Compounds which give signal for 2 or more MRMs are grouped and evaluated for structural similarities. If further optimization is unsuccessful in increasing selectivity, the compounds cannot be separated by MS-alone. They are flagged as high priority groups for future chromatographic separation. The final MRM-method is utilized for further MD; while utilizing the identified critical groups to evaluate method performance.

In the previous chapter twenty-three anabolic agents from WADA's yearly list of restricted compounds were chosen as target analytes. Analytes were grouped based on structural similarities known to influence the ionization patterns of steroids. Q3 scans were obtained and compared to those expected from the literature. The effect of mobile phase composition on the characteristic ionization profiles of each group was investigated. Q3 scans obtained with flow injection analysis (FIA), using 100% Modifier were compared to scans taken with carbon

dioxide-(CO_2) based mobile phases. The effect of a mobile phase additives was also investigated using 5 mM Ammonium Formate (AmFo) and 0.1% formic acid (FA) in methanol. Ultimately optimal precursors were determined for each analyte for use in further method optimizations.

4.3.1. MRM-Optimization Approach.

This chapter focuses on the second and third steps of MS-Detection optimization. First MRM-optimizations are performed guided by the information obtained from Q3 scans. The layout of this chapter is similar to that of the previous chapter for Q3 scans and the targeted analytes are grouped into the same categories based on common ionization profiles. Each section of this chapter will cover one of the groups. But the focus is shifted from precursor ion to instead determining the optimal product ions for each analyte. In consideration of the wide range of structures included in this study, each section of this chapter will cover:

- ***A short introduction of the expected fragmentation patterns*** from the literature, specific to the structure of the targeted group.
- ***MRM optimization results*** (e.g., monitoring of CE select product ion overlays) and comparison of product ion scans to relevant literature.
- ***Results of an MRM-method selectivity test***. Individual analytes are re-injected using the optimized MRM method to look for analytes that produce signal for more than their own MRM. If further optimization is unsuccessful in increasing selectivity, the analytes are grouped and flagged as critical pairs, which will be high priority for future chromatographic separation.

The final goal of the current chapter is to determine optimal product ions, collision energies, and voltages for each of the targeted analytes, in the form of a final optimized MRM detection method. This method will be hyphenated with SFE-SFC in further method optimization steps. A list of critical compounds (which cannot be differentiated by MS-alone) will be compiled to be used for method evaluations in further method development steps for chromatographic separation.

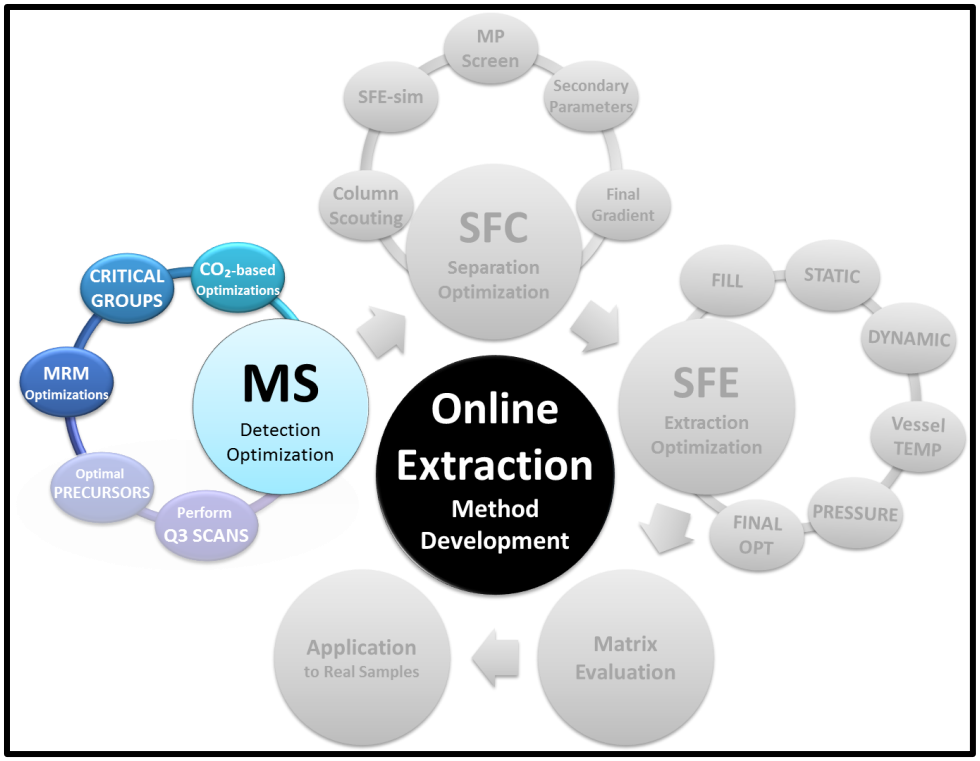

Figure 44. Online Extraction Method Development Focus for Chapter #4 MRM-optimizations and Critical Group Identification in MS Detection Optimization.

4.3.2. MRM-Optimization using FIA - MeOH

Optimal precursor and solution concentrations were chosen from Q3 scans (for details refer to the previous **Chapter #3: Determination of Optimal Precursor via Q3 Scans**) and used in further development of the MS method, using multiple reaction monitoring (MRM) optimization, using the LabSolutions 'optimize MRM event from product ion search' function. Detailed instrument methods are provided at the end of this chapter in **Section 4.i. Instrument Methods for MRM-Optimizations.** Resulting MRM-transition details are detailed in **Table 17**.

4.3.3. Monitoring Product Ions thru CE Select - Ion Overlays.

The CE-select step of the automatic MRM optimization program (LabSolutions software), automatically chooses optimal product ions, from a user specified precursor. This is accomplished by repetitive injections of a single analyte, each time using a different collision energy (CE). The resulting fragments, from each injection (i.e., each CE) are scanned, and the program automatically selects the most frequently produced fragment ions with the highest abundance, which are chosen as 'MRM-transitions' for a given precursor.

CE select ion spectra can be overlaid to monitor the results of this process. If overlaid using absolute intensity, the effect of CE on ion intensity can be viewed. Best performing ions are considered to be those that give high intensity over a range of collision energies. These best performing ions will give the best sensitivity, but at times, the best performing ions may not be optimal for the application. In steroid analysis, for example, often their identification requires the use of characteristic ions based on fragmentation pathways specific to the analytes structure. These characteristic ions are not always the best performing ions, and therefore could be overlooked by the automatic selection process in software. Comparing automatically chosen ions to literature values, is helpful to reveal if automatically selected MRM methods could be further optimized to provide higher selectivity for specific steroids.

4.3.4. MRM-Method Selectivity Tests

Up to Four transitions (precursor ion → product ion) were chosen optimized for each compound (if possible, depending on the production of product ions of adequate intensity). Standard solutions were then reinjected for each analyte, using the MRM method with all 23 events (e.g., MRM-TICs), to evaluate method selectivity for each compound. An MRM-TIC is similar to a total Ion chromatogram (TIC) for a single MS event, when multiple reaction monitoring (MRM) transitions are combined to make a total Ion chromatogram (MRM-TIC) representing all the transitions for a single compound (MRM-TIC).

MRM-TICs for all 23 events were overlaid for each injection. Injections were made to test the effect of modifier composition of both flow injection analysis (FIA) and SFC-based MPs. Modifiers utilized were methanol with and without additive. Two additives were used for method tests: 5 mM ammonium formate ([AmFo]; Panel [B] in all presented method tests) and 0.1% formic acid ([FA]; data not shown). Methanol without additive is presented in all method test figures in panel [A]). For SFC-MPs, three modifier concentrations were tested (40, 20, and 10%).

4.3.5. Further Optimization *(when applicable)*

If initial MRM-optimization with FIA-MeOH was unsuccessful (e.g., gave no signal for its own MRM upon injection of the standard solution), further optimization was performed. Specific conditions were situation specific. Generally, tactics employed one, or more, of the following:

A. increase/decrease in solution concentration.

B. Optimize MRM event voltages, after manual product ion input.

C. Change of precursor ion (via re-evaluation of Q3 scans data).

D. Change of MP composition for use during MRM optimization (e.g., addition of an additive or CO_2 to the MP).

Table 17. **Multiple reaction monitoring Optimal Transitions, Collision energies (CE) and Q1/Q3 Bias Voltages for Targeted Anabolic Agents.**

				Precursor			Product Ion							
							(m/z)	[V/V, eV]	(m/z)	[V/V, eV]	(m/z)	[V/V, eV]	(m/z)	[V/V, eV]
Class	Steroid	ID	MW	+/-	(m/z)	Ion	Transition 1	(Q1/Q3 Bias, CE)	Transition 2	(Q1/Q3 Bias, CE)	Transition 3	(Q1/Q3 Bias, CE)	Transition 4	(Q1/Q3 Bias, CE)
I	Danazol	DNZL	337.5	+	338	$[M+H]^+$	148	(-24/-30, -25)	91	(-26/-32,-55)	120	(-24/-22,-28)	310	(-24/-32,-20)
I	Stanozolol	STNZ	328.5	+	329	$[M+H]^+$	81	(-24/-30, -51)	95	(-24/-20,-42)	121	(-24/-22,-37)	107	(-24/-20,-41)
II-(a)	Epitestosterone	EPIT	288.4	+	289	$[M+H]^+$	109	(-20/-20, -24)	97	(-22/-38,-25)	79	(-22/-30,-44)	253	(-22/-26,-18)
II-(a)	Mibolerone	MIBL	302.5	+	303	$[M+H]^+$	271	(-22/-30, -12)	285	(-22/-20,-17)	121	(-22/-24,-25)	-	-
II-(a)	Methyltestosterone	MTHY	302.5	+	303	$[M+H]^+$	109	(-22/-20, -28)	97	(-20/-20,-26)	97	(-22/-20,-27)	285	(-22/-30,-16)
II-(a)	Testosterone	TSTO	288.4	+	289	$[M+H]^+$	109	(-22/-20, -25)	97	(-22/-36,-22)	253	(-22/-28,-17)	79	(-22/-28,-46)
II-(b)	1-Androstenedione	1-STEN	286.4	+	287	$[M+H]^+$	97	(-20/-20, -22)	109	(-22/-22,-24)	79	(-20/-30,-46)	109	(-20/-40,-35)
II-(c)	Gestrinone	GSTN	308.4	+	309	$[M+H]^+$	241	(-22/-26, -23)	199	(-24/-40,-32)	291	(-24/-20,-16)	262	(-22/-28,-21)
II-(c)	Metribolone	MTRB	284.4	+	285	$[M+H]^+$	227	(-22/-24, -23)	267	(-20/-28,-17)	198	(-22/-20,-30)	159	(-20/-30,-23)
II-(c)	Trenbolone	TRNB	270.4	+	271	$[M+H]^+$	253	(-20/-26, -19)	199	(-20/-20,-22)	165	(-20/-36,-56)	128	(-20/-26,-57)
II-(d)	Methandienone	METD	300.4	+	301	$[M+H]^+$	121	(-22/-46, -28)	149	(-22/-26,-15)	283	(-22/-30,-11)	121	(-22/-22,-24)
III-(a)	7-Keto-DHEA	KETO	302.2	+	285	$[M+H-H_2O]^+$	81	(-22/-32, -27)	79	(-20/-30,-44)	107	(-20/-20,-27)	149	(-20/-26,-21)
III-(b)	Androsterone	ADEN	290.4	+	273	$[M+H-H_2O]^+$	255	(-20/-26, -14)	147	(-22/-32,-21)	199	(-22/-20,-21)	161	(-20/-36,-20)
III-(b)	Etiocholanolone	ETIO	290.4	+	273	$[M+H-H_2O]^+$	255	(-20/-28, -12)	215	(-20/-42,-17)	105	(-20/-20,-35)	91	(-20/-38,-43)
IV	1-Androsterone	1-DHEA	290.4	+	291	$[M+H]^+$	273	(-20/-30, -10)	255	(-15/-26, -15)	135	(-20/-28,-20)	91	(-22/-36, -10)
IV	Prasterone	PRST	288.2	+	271	$[M+H-H_2O]^+$	253	(-20/-26, -12)	213	(-22/-46,-15)	213	(-20/-40,-17)	157	(-20/-32,-22)
V	Androstanolone	ADON	290.4	+	291	$[M+H]^+$	255	(-11/-12, -16)	173	(-10/-18,-21)	227	(-10/-23,-10)	-	-
V	Mestanolone	MSAL	304.4	+	305	$[M+H]^+$	269	(-20/-28, -16)	229	(-20/-24,-20)	159	(-20/-34,-23)	187	(-20/-36,-22)
V	Mesterolone	MSEL	304.4	+	305	$[M+H]^+$	269	(-22/-28, -17)	173	(-20/-40,-24)	287	(-22/-30,-16)	133	(-24/-22,-28)
V	Oxandrolone	OXAN	306.4	+	307	$[M+H]^+$	289	(-22/-30, -12)	271	(-22/-30,-14)	121	(-22/-22,-24)	229	(-24/-24,-18)
VI	Andarine	ADAR	441.4	+	442	$[M+H]^+$	108	(-32/-20, -37)	208	(-32/-20,-21)	190	(-32/-20,-25)	148	(-32/-32,-31)
VI	Clenbuterol	CLNB	277.2	+	227	$[M+H]^+$	203	(-32/-36, -16)	259	(-20/-26,-10)	132	(-20/-24,-28)	168	(-20/-32,-28)
VI	Zeranol	ZRNL	322.4	-	321	$[M-H]^+$	277	(34/28, 23)	303	(36.0/20,22)	259	(36.0/26,24)	235	(36.0/28,24)

4.4 Group I. Nitrogen containing steroids.

4.4.1. Expected Fragmentation Patterns for Group 1 Steroids from Literature.

Expected Fragmentation for Stanazolol [STNZ]. The product ions 81 and 95 *m/z*, have been identified as characteristic ions for STNZ, and the fragmentation pathways detailed in literature.[35],[55],[57]

m/z 81. The origin of ion with *m/z* 81 is from cleavage of the steroidal A-ring (C-1 to C-2 and C-4 to C-5 bonds), leaving the pyrazole ring (including C-2 to C-4). Charge-driven rearrangement and dissociation mechanisms stem from the protonation of N-2, and the relocation of the charge (presumably to C-2) triggers the formation of a six-membered ring structure (**Figure 45**; ***Ion c***). Cleavage of C-4 - C-5 liberates the fragment at *m/z* 81. This fragment has a stable heterocyclic structure with a conjugated pi-electron system (**Figure 45**; ***Ion d***).

m/z 95. The fragment ion at *m/z* 95, also originates from protonation at N-2. Via a rearrangement of bonds at C-10 and C-1 along with C-4 to C-5, produces the fragment (**Figure 45**; ***Ion e***). Other fragments from literature, 91, 119, and 135 are specific to STNZ as well.[55]

Expected Fragmentation for Danazol [DNZL]. Fragmentation patterns are not well discussed in the literature specifically for DNZL, due to that most of the patterns can be explained by those observed in metabolites of STNZ. Danazol differs in structure with an oxygen in the N-ring, and has a conjugation at C4.

148 *m/z.* A fragment ion with *m/z* 148 has been reported for DNZL. This ion is common for nitrogen containing steroids with a conjugated N-ring, due to bond fragmentation at C6-C7 and C9-C10. The resulting fragment contains both the N- and A- rings.

120 *m/z* and 91 *m/z.* The loss of the N-/A- ring is common among nitrogen containing steroids.[56] The fragment ion at 120 *m/z* is associated with the elimination of methane and 91 *m/z* with elimination of the N-ring.[55]

310 *m/z*. Involves the 3-ene, conjugated double bond facilitates the transfer of the positive charge to the carbon skeleton, and promotes the loss of water, -CO.[56]

4.4.3. MRM-Optimizations for Group I Steroids.

As discussed in the previous chapter, nitrogen containing steroids are easily ionized as the protonated molecular ion $[M+H]^+$, due to high proton affinity. This was in agreement with Q3 scans performed with both FIA and using CO_2-based MPs. Therefore, for further MRM-optimizations, $[M+H]^+$ was used as precursor, for both STNZ and DNZL. In both cases, the resulting MRM-transitions produced product ions (**Table 17**) corroborated by known fragmentation pathways for these compounds.

The 328 *m/z* precursor was used for STNZ (Q1 bias of -24V). The 91, 119 and 135 *m/z* product ions were not observed (**Figure 46**). But the characteristic Fragment ions 81, 95, and 121 were chosen along with an unidentifiable product at 107 *m/z*. For DNZL precursor 338 *m/z* (Q1 = -24V), produced 148, 91, 120, and 310 *m/z* product ions (**Figure 47**), all supported in literature for DNZL.

4.4.4. MRM-method Tests for Group I Steroids.

The MRM-method selectivity test results showed both STNZ and DNZL produced signal for only their own MRMs regardless of the MP used (**S_Figure 13**; **A & B**).

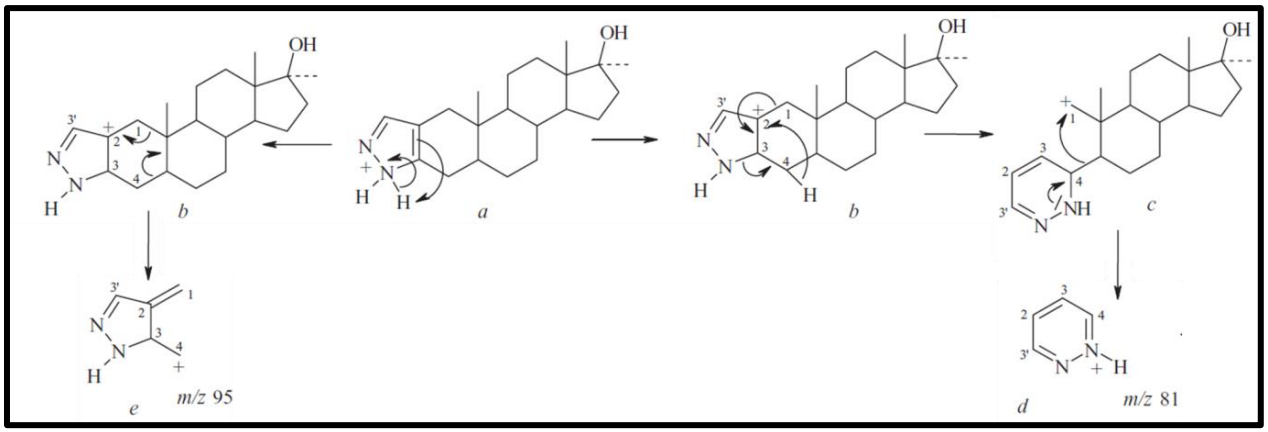

Figure 45. Fragmentation Pattern for Stanozolol, showing characteristic fragment ions at *m/z* 81 and *m/z* 91 (Mechanism Proposed by and Figure Adapted from **Thevis et. al., 2005**[55]).

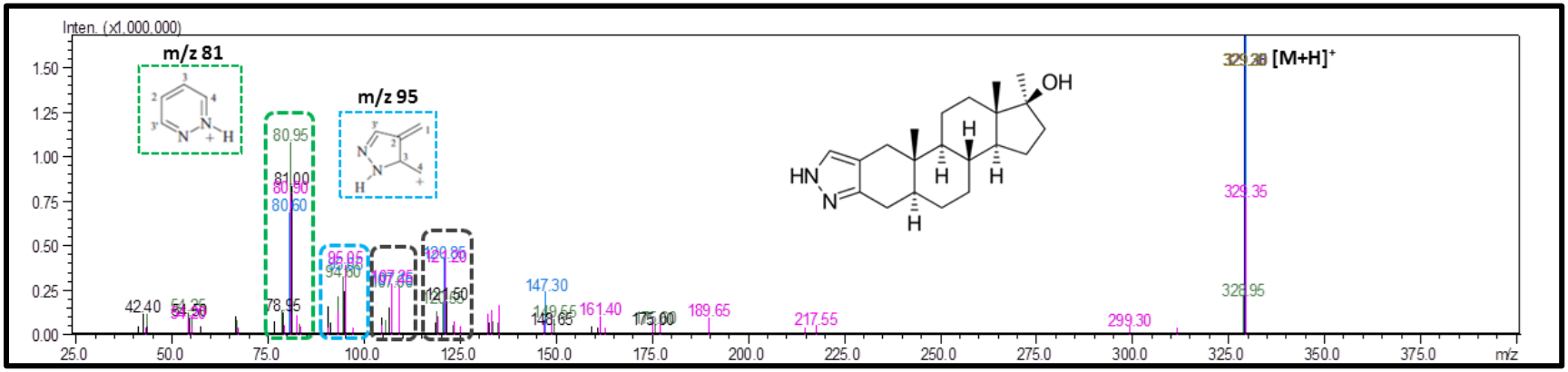

Figure 46. **Overlaid ESI product Ion Spectra of the protonated molecule $[M+H]^+$ at m/z 329 of Stanozolol [STNZ] During the Collision Energy (CE) Selection Step of MRM-Optimization**; showing resulting product ions at 81 *m/z* (CE range = -55 : -35 eV), 95 *m/z* (CE range = -50 : -30 eV) and 121 *m/z* (CE range = -45 : -25 eV) ions expected from literature produced during the 'CE Select' step of MRM-optimization. **CE select scan range = 1V steps; Centroid-spectrums overlaid and displayed in absolute intensity**.

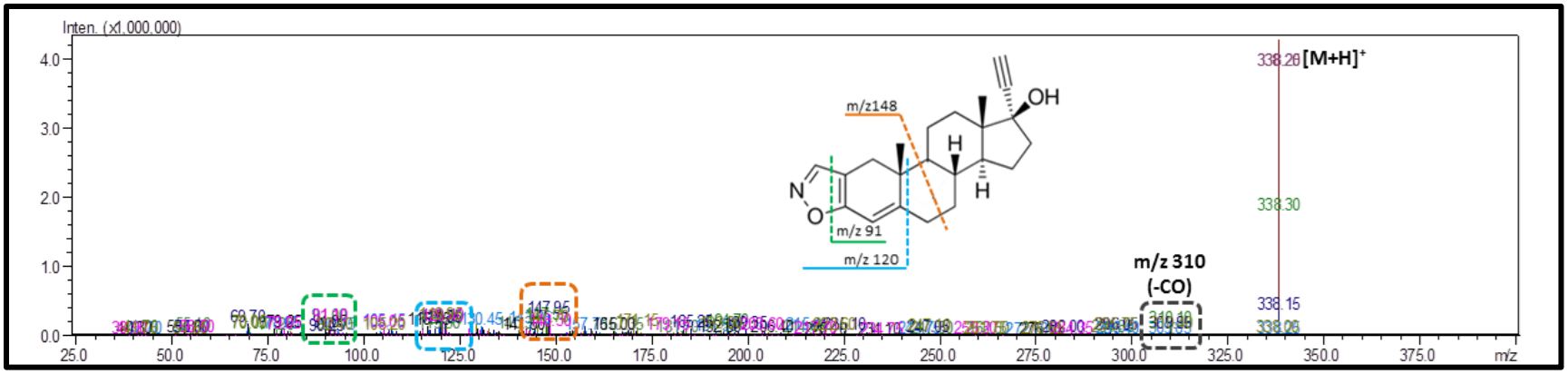

Figure 47. **Overlaid ESI product Ion Spectra of the protonated molecule $[M+H]^+$ at *m/z* 338 of Danazol [DNZL] During the Collision Energy (CE) Selection Step of MRM-Optimization**; showing resulting product ions at 148 *m/z* (CE range = -35 : -15 eV), 91 *m/z* (CE range = -55 : -35 eV) and 120 *m/z* (CE range = -35 : -14 eV) and 310 *m/z* (CE range = -29 : -18 eV) expected from literature produced during the 'CE Select' step of MRM-optimization. **CE select scan ranges = 1V steps; Centroid-spectrums overlaid and displayed in absolute intensity**.

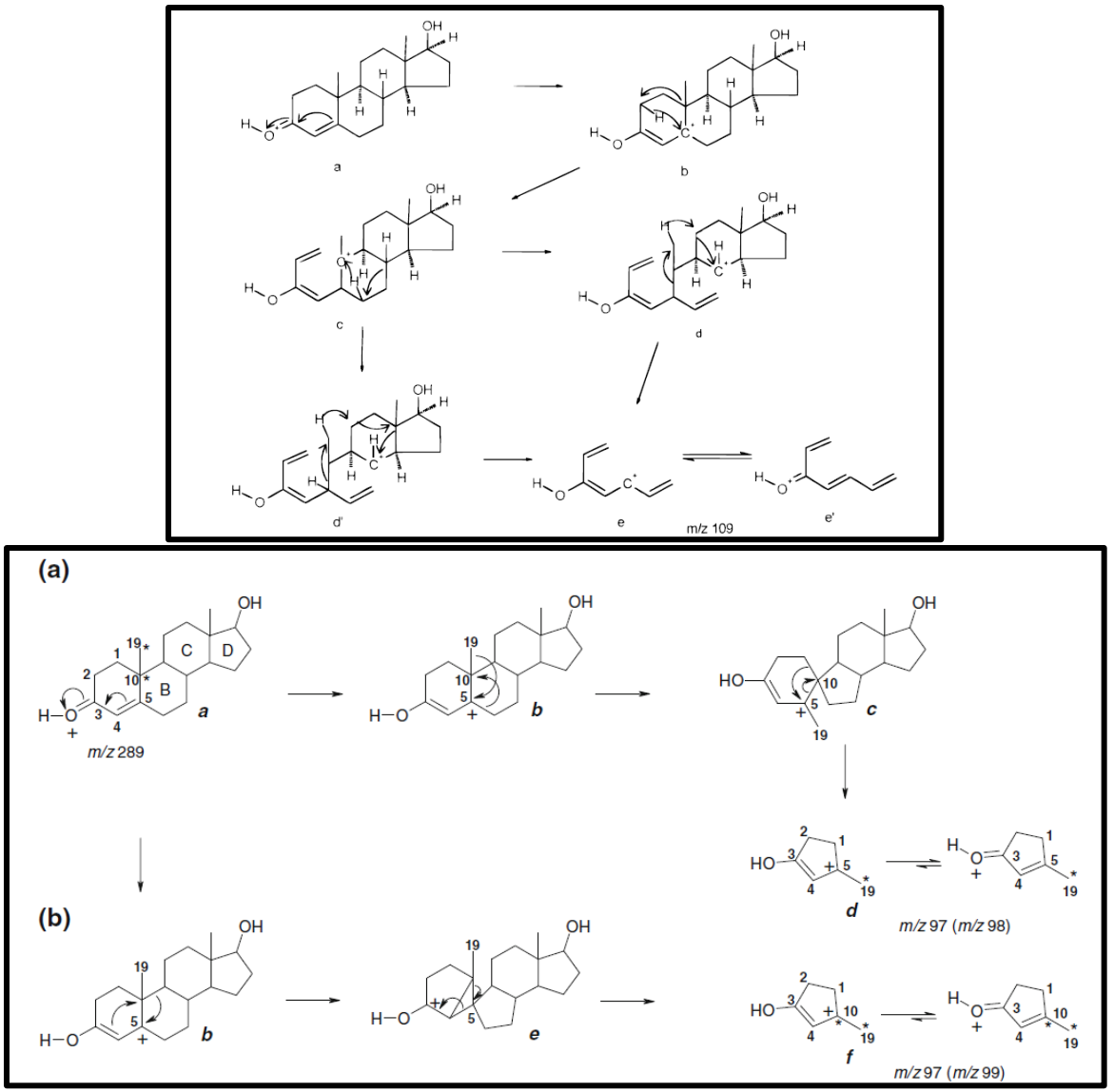

Figure 48. Fragmentation Mechanisms for Common Product Ions of Testosterone: showing [Top] Fragment Ion of *m/z* 109 (mechanism proposed by and figure adapted from **Williams et. al., 1999**[50]); and [bottom] Fragment Ions of *m/z* 97 (mechanism proposed by and figure adapted from **Thevis et. al. 2012**[58]).

4.5. Group II-(a). 3-keto-4-ene Steroids

4.5.1. Expected Fragmentation for Group II-(a) from Literature.

Several fragment ions for Group II-(a) steroids are expected that coincide with the neutral loss of water, where the losses of water are expected to equal the number of oxygens in the structure.[56] Therefore, fragment ions could be expected at 271 *m/z* $[M+H-H_2O]^+$ and 253 *m/z* $[M+H-2H_2O]^+$ for both TSTO and for EPIT, and at 285 *m/z* $[M+H-H_2O]^+$ and 267 *m/z* $[M+H-2H_2O]^+$ for MIBL and MTHY.

Characteristic Ions for Testosterone (all androst-4-ene-3-one) analogs. Abundant ions of 109 and 97 *m/z* are highly relevant ions for TSTO and hydroxyl-TSTO analogs. Both ions stem directly from the $[M+H]^+$ precursor ion, but each following a different dissociation path. The fragmentation pathway for 109 *m/z* (**Figure 48; top [e]**), proposed by **Williams et. al., 1999**, is the result of three hydrogen transfers; It starts with a charge site migration from the C-3 oxygen → C-5 (**Figure 48; top [b]**). Followed by the first hydrogen transfer from C-2 → C-5, and cleavage of C-1 – C-10, migrates the positive charge to C-10 (**Figure 48; top [c]**). Then hydrogen transfer from C-6 → C-10, with cleavage of C7-C8, migrates the positive charge to C-8 (**Figure 48; top [d]**), and finally cleavage between C5 – C10, gives the final structure (**Figure 48; top [e]**). The final fragment is composed of C1, C2, C4, C7 (including all their associated hydrogens), plus C6 (and one of its hydrogens), as well as C3 with its associated oxygen (giving 109 *m/z*).[50] The composition of the fragment of 97 *m/z* was also first detailed by **Williams et. al., 1999**. The fragmentation pathway was partially proposed by **Pozo et. al., 2008**, and a similar but complete proposed mechanism by **Thevis et. al., 2012.** This fragment is composed of the A-ring hydrogens and carbons (excluding C-5), plus C19 (and its three hydrogens), and the 3-one oxygen, and either the C-5 or the C-10 carbon, which gives at least two dissociation routes, confirmed by stable isotope labeling and high accuracy MS. This composition is quite unusual but establishes a highly conjugated π-electron system (**Figure 48; bottom, *Ion a* & *Ion b***).[50],[56],[58]

Fragment from the loss of Acetone. 17-methyl, 3-keto steroids, produce a characteristic ion due to the neutral loss of acetone.[56] This fragmentation involves the D ring of the steroid backbone resulting in a loss of 58 Da, and additionally can be in association with losses of one or two waters.

MIBL. 95 m/z, 107 m/z and 121 m/z. MIBL cannot produce the *m/z* 109 ion (due to lack of a 10-methyl group in the its structure). However, MIBL's structure contains an electron-donating 7-methyl group, which leads to characteristic fragment ions of 95, 107 and 121 *m/z* for MIBL.[48]

4.5.3. *MRM Optimizations for Group II-(a)*.

For Group II-(a) steroids, ionization is expected to occur at the keto functional group at C3, which is stabilized by the conjugation at C4; Therefore, they are expected to form stable $[M+H]^+$ or $[M+Na]^+$ precursor ions. As discussed in the previous chapter, for all group-II-(a) steroids, the optimal precursor ion is expected to be $[M+H]^+$ in all CO_2 based MPs. Therefore, $[M+H]^+$ was used as precursor for MRM-optimizations (**Table 17**).

TSTO and EPIT. Sharing the same molecular weight, in the case of TSTO (**Figure 49**) and EPIT (**Figure 50**), the 289 *m/z* precursor gave rise to three most abundant product ions: 253 *m/z* $[M+H-2H_2O]^+$, and characteristic fragments of 109 and 97 *m/z* characteristic of all testosterone analogs (as expected from the literature). The ion Ratio was the same for both analytes.

MIBL and MTHY. Sharing the same molecular weight, using the $[M+H]^+$ precursor of 303 *m/z*, Both MIBL (**Figure 51**) and MTHY (**Figure 52**), gave rise to abundant ions of 285 *m/z* $[M+H-H_2O]^+$ and 267 *m/z* $[M+H-2H_2O]^+$ product ions. Additionally MTHY produced the characteristic fragments of all testosterone analogs of 109 and 97 *m/z* (as expected from the literature). Alternatively MIBL being unable to produce the *m/z* 109 ion (due to lack of a 10-methyl group in the its structure), instead gave rise to the expected diagnostic ions for MIBL at 95, 121, and 109 *m/z*. Both the *m/z* 121 and 109 ions were abundant enough to be chosen by the automatic selection program of the software, but 95 *m/z* was not automatically chosen. Ultimately the transitions for MIBL were manually entered choosing 285, 121, and 109 *m/z* for MIBL.

4.5.4. *MRM-Method Specificity Tests for Group II-(a).*

Methods tests via injections of Group II-(a) steroids were performed using the original MRM transitions optimized using MeOH with no additive, and were tested under FIA and SFC conditions (**S_Figure 14**). TSTO and EPIT gave signal for their own MRMs as well as for each other's MRMs under all conditions.

(for detailed discussion of critical group implications see **Section 4.14.3: Critical Group 3; *Pair 3-D*** at the end of this chapter).

Injections of MIBL and MTHY also gave signal for their own MRMs, as well as for each other's. But the Ion ratios produced were not the same for both analytes. The addition of CO_2 had little effect on the response of Group II-(a) steroids, with the exception that CO_2 did have an effect on the ratio of ions for MIBL.

(for detailed discussion of critical group implications see **Section 4.14.2: Critical Group 2; *Pair 2-B*** at the end of this chapter).

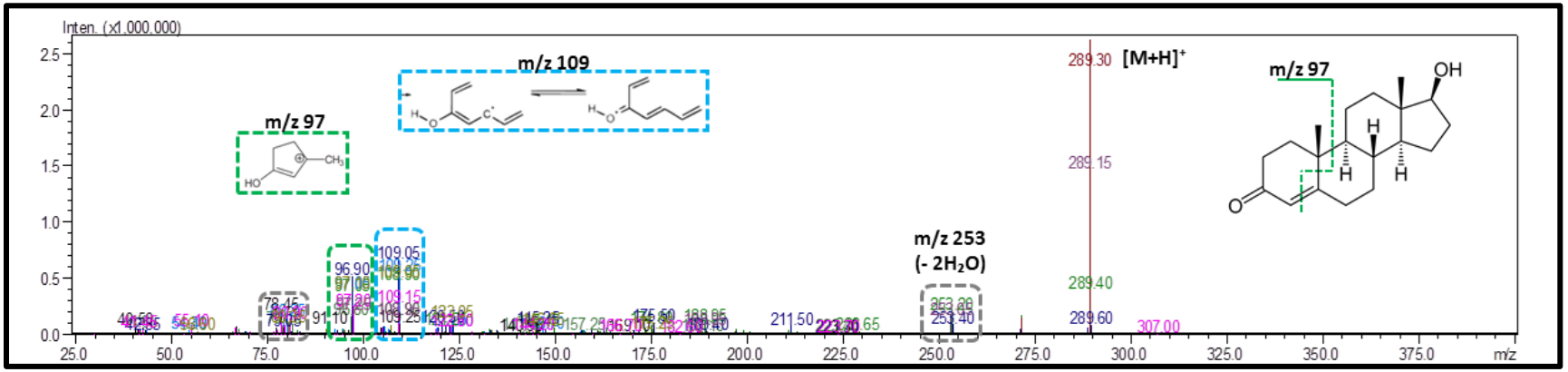

Figure 49. **Overlaid ESI product Ion Spectra of the protonated molecule [M+H]⁺ at *m/z* 289 of Testosterone [TSTO] During the Collision Energy (CE) Selection Step of MRM-Optimation**; showing resulting product ions at 109 *m/z* (CE range = -35 : -15 eV), 97 *m/z* (CE range = -30 : -10 eV) and 253 *m/z* (CE range = -25 : -10 eV) expected from literature produced during the 'CE Select' step of MRM-optimization. **CE select scan range = 1V steps; Centroid-spectrums overlaid and displayed in absolute intensity**.

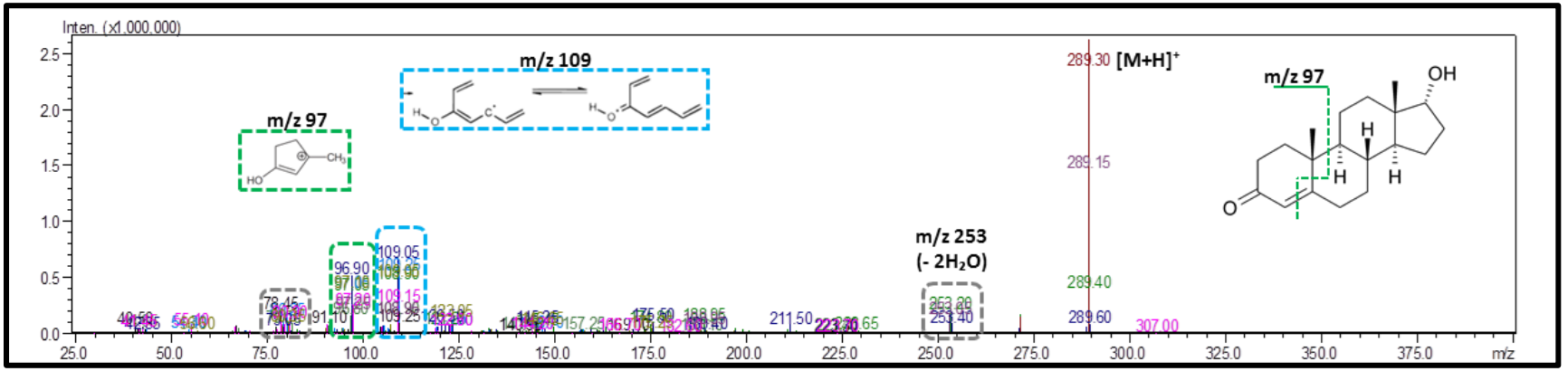

Figure 50. **Overlaid ESI product Ion Spectra of the protonated molecule [M+H]⁺ at *m/z* 289 of Epitestosterone [EPIT] During the Collision Energy (CE) Selection Step of MRM-Optimization**; showing resulting product ions at 109 *m/z* (CE range = -35 : -15 eV), 97 *m/z* (CE range = -35 : -15 eV) and 253 *m/z* (CE range = -29 : -18 eV) expected from literature produced during the 'CE Select' step of MRM-optimization. **CE select scan range = 1V steps; Centroid-spectrums overlaid and displayed in absolute intensity**.

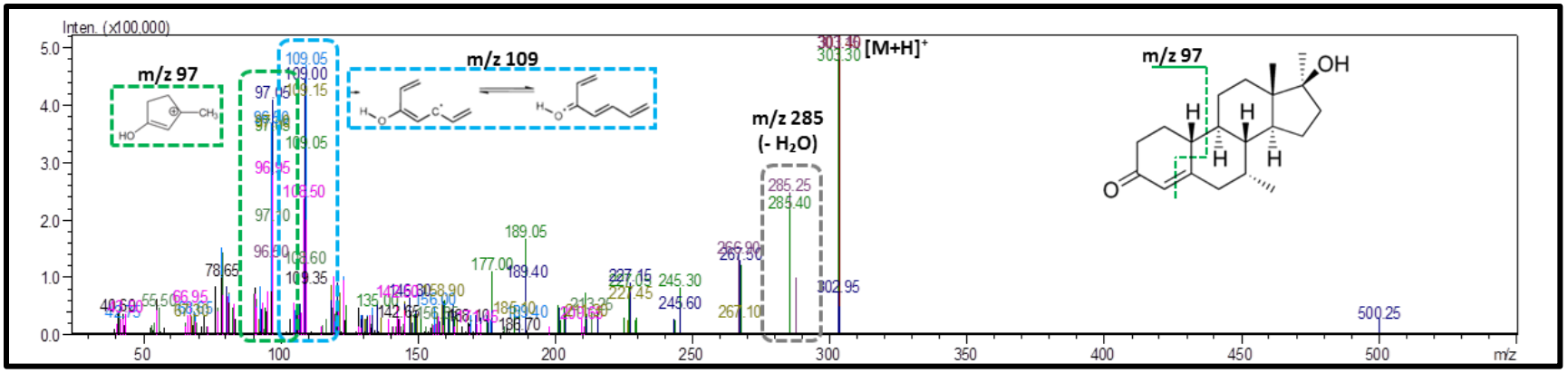

Figure 51. **Overlaid ESI product Ion Spectra of the protonated molecule [M+H]⁺ at *m/z* 303 of Methyltestosterone [MTHY] During the Collision Energy (CE) Selection Step of MRM-Optimization**; showing resulting product ions at 109 *m/z* (CE range = -45 : -25 eV), 97 *m/z* (CE range = -35 : -15 eV) and 285 *m/z* (CE range = -25 : -13 eV) expected from literature produced during the 'CE Select' step of MRM-optimization. **CE select scan range = 1V steps; Centroid-spectrums overlaid and displayed in absolute intensity**.

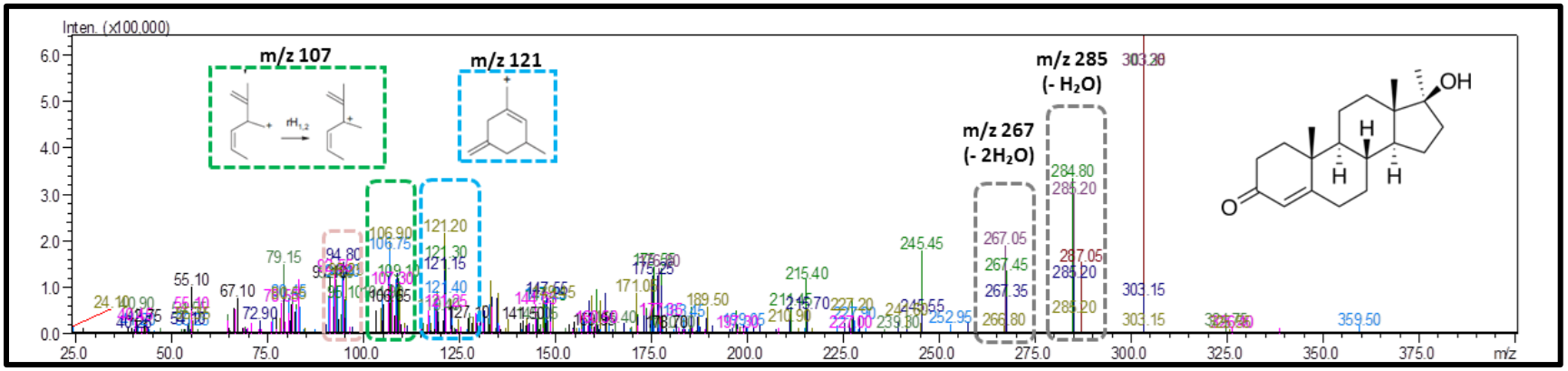

Figure 52. **Overlaid ESI product Ion Spectra of the protonated molecule [M+H]⁺ at *m/z* 303 of Mibolerone [MIBL] During the Collision Energy (CE) Selection Step of MRM-Optimization**; showing resulting product ions at 109 *m/z* (CE range = -40 : -20 eV), 121 *m/z* (CE range = -40 : -20 eV), 267 *m/z* (CE range = -25 : -13 eV) and 285 *m/z* (CE range = -30 : -10 eV) expected from literature produced during the 'CE Select' step of MRM-optimization. **CE select scan range = 1V steps; Centroid-spectrums overlaid and displayed in absolute intensity**.

4.6. Group II-(b). 3-keto-1-ene Steroids.

The optimal precursor for 1STEN identified in Q3 scans was the protonated molecular ion $[M+H]^+$ at 287 *m/z*, as was corroborated in the literature.[59],[60]

4.6.1. *Expected Fragmentation for Group II-(b) from Literature.*

Steroids with a conjugation at position C1 (the 1-ene steroids) are expected to produce intense fragment ions at *m/z* 185 (**Figure 53**) when using a higher CE (e.g., > 30 eV). The formation of this ion involves the fragmentation of the protonated molecular ion, $[M+H]^+$ 287 *m/z,* to *m/z* 203 (-ring A, including migration of C19 from C10 to C1 of the leaving group). Subsequent water loss (-18 u), produces the fragment at *m/z* 185.[59],[60],[61],[62]

One fragment, specific to 1-STEN that is not present for other 1-ene steroids, is a fragment at 128 *m/z*. The production of this ion involves a fragment including the B-/C- rings, which after the loss of water (-18 u) creates a second double bond in the B-/C- ring system resulting in a fragment at 143 *m/z*. This promotes the further loss of the methyl radical (-15 u) to produce a final fragment 128 *m/z*, absent in other 1-ene steroid product ion spectra.[56]

4.6.2. *MRM Optimizations for Group II-(b)*.

Steroids with a conjugation at position C1 are expected to produce fragments at *m/z* 185 and 203, and specific to 1STEN a fragment is expected at 128 *m/z*. But expected fragment ions were not observed for 1STEN (**Figure 54**), the 203 and 128 *m/z* fragment were not observed at all, and 185 *m/z*, although present, was generated at very low abundance. Neither expected product ions were generated at sufficient intensities within the range of voltages used in MRM-optimization. Instead fragments at 108, 97, and 79 (which are reported as non-diagnostic fragments which all steroids share),[63] but were chosen as products as they produced the strongest response for 1STEN (**Table 17**).

4.6.3. *MRM-Method Specificity Tests for Group II-(b).* Reinjections of 1STEN using the MRM method produced a strong signal for its own TIC-only (1STEN-MRM), with no change or difference when additives or CO_2 were added to the MP (**S_Figure 15; A**). However other AAS did produce signal for 1STEN making it a watch member of critical group #2 (see **Section 4.14.2. Critical Group 2** for detailed discussion of critical group implications).

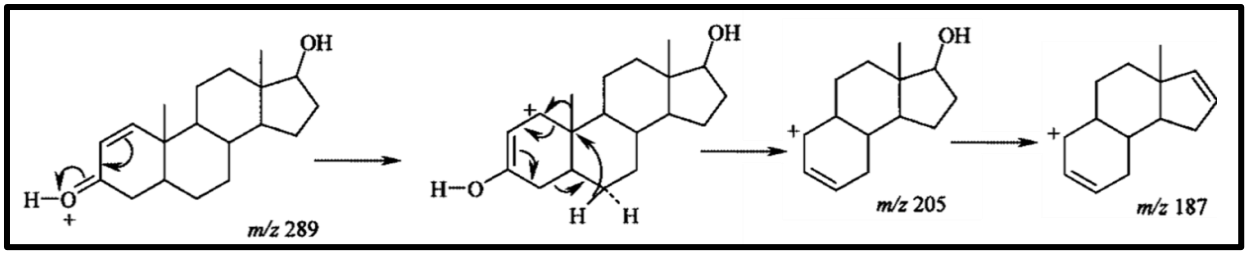

Figure 53. Fragmentation Pattern for 3-keto-1-ene Steroids, Showing Characteristic Fragments of *m/z* 205 and *m/z* 187 (Mechanism Proposed by and Figure Adapted from **Thevis et. al., 2005**[59]).

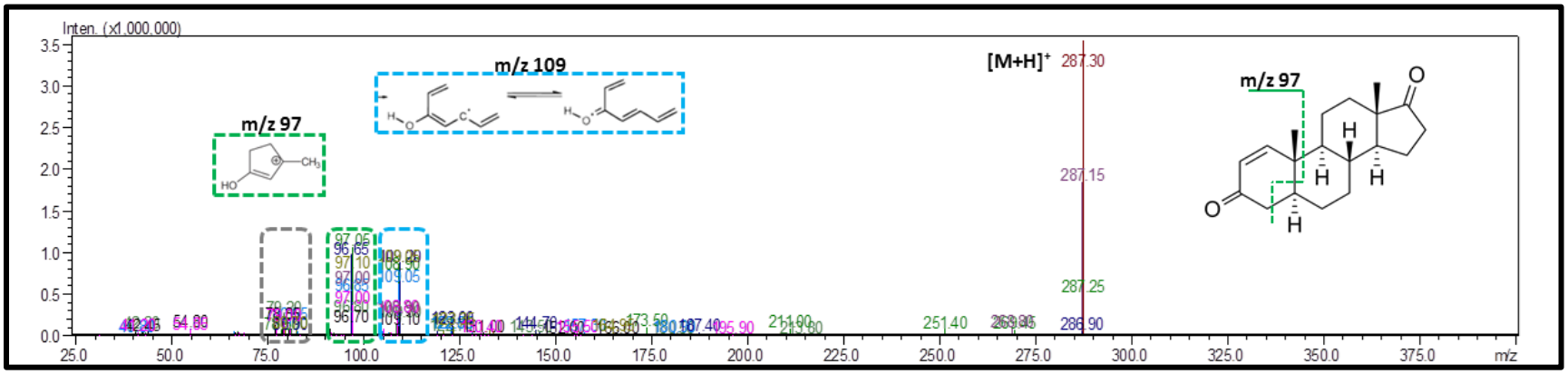

Figure 54. Overlaid ESI product Ion Spectra of the protonated molecule $[M+H]^+$ at *m/z* 287 of 1-Androstenedione [1STEN] During the Collision Energy (CE) Selection Step of MRM-Optimization; showing resulting product ions at 79 *m/z* (CE range = -55 : -30 eV), 97 *m/z* (CE range = -30 : -10 eV) and 109 *m/z* (CE range = -35 : -15 eV) produced during the 'CE Select' step of MRM-optimization. **CE select scan range = 1V steps; Centroid-spectrums overlaid and displayed in absolute intensity**.

4.7. *Group II-(c). Triene steroids.*

In the previous chapter, via Q3 scans, the optimal precursor for triene steroids was determined to be the protonated molecular ion $[M+H]^+$. Although group II-(c) steroids were shown to form significant adducts with sodium using FIA, with CO_2 in the mobile phase, sodium adduct formation was effectively suppressed. Even without the use of an additive, the dominant ion was the protonated molecular ion $[M+H]^+$ under all SFC-based MPs. This was corroborated in literature (GSTN = 309 *m/z*[35]; MTRB = 285 *m/z*; and TRNB = 271 *m/z*[47]).

4.7.1. Expected Fragmentation for Group II-(c) from the Literature.

$[M+H-H_2O]^+$. All Triene steroids are expected to produce an abundant fragment ion from the $[M+H]^+$ precursor, due to the loss of water (-18 u) from C-17 position. This produces the $[M+H-H_2O]^+$ ion for each triene steroid (GSTN = 291 *m/z*[59]; MTRB = 267 *m/z;* and TRNB = 253 *m/z*[47]), but since this is a characteristic ion of many steroids, it is not sufficient to characterize the group.

An additional point is that, although each contains two oxygens, these steroids are not expected to produce $[M+H-2H_2O]^+$ ions, due to the highly stable nature of the large conjugated system.[56]

-ethyl/-methyl. The next two fragments are diagnostic to families within this group of steroids. The release of the substituent, allylic to the large 8-π-conjugated system, at C-13, describes the formation of these diagnostic ions. For gestrinone analogs, this involves the loss of an ethyl radical (-29 u) to give rise to an ion at 262 *m/z*. For trenbolone analogs ([MTRB and TRNB], instead of an ethyl group, this involves instead the loss of a methyl radical (-15 u) from the same location, giving rise to ions at *m/z* 252 for MTRB and *m/z* 238 for TRNB.[59]

***m/z* 241 and *m/z* 227 Ions**. Result from the dissociation of the protonated molecular ion, and involves the elimination of propene (C-16 and C-17) from the D-ring including all substituents at C-17, and the subsequent migration of the a hydrogen from C-14 to C13, resulting in an ion at *m/z* 241[59] in the case of GSTN (**Figure 55**; **A**) and *m/z* 227[47] in the case of MTRB and TRNB (**Figure 55**; **B**).

m/z 199 Ion. The subsequent elimination of ethylene (-28 u) from the 241 or 227 *m/z* ion, results in an ion characteristic of all 4,9,11-triene steroids, at 199 *m/z.* [35],[47], [59],[64]

4.7.2. MRM-Optimizations for Group II-(c).

GSTN. In the case of GSTN, the $[M+H]^+$ precursor (309 *m/z*) gave rise to four most abundant product ions: 291, 262, 241, and 199 *m/z*, as expected from literature (**Figure 56**).

MTRB. In the case of MTRB, the $[M+H]^+$ 285 *m/z* precursor gave rise to four most abundant product ions at 267, 227, and 199 *m/z*, as expected from literature. But *m/z* 252 was not generated at sufficient intensity, and therefore 159 *m/z* was chosen (**Figure 57**).

TRNB. In the case of TRNB, the $[M+H]^+$ 271 *m/z* precursor gave rise to four most abundant product ions at 253 and 199 *m/z* (**Figure 58**) as expected from literature. But *m/z* 227 and *m/z* 238 were lower abundance than m/a 165 and 128, which were automatically chosen by the MRM-optimization software.

4.7.3. MRM-Method Specificity Tests for Group II-(c)

GSTN. Injections of GSTN using the automatically generated MRM-transitions yielded signal only for its own MRMs (**S_Figure 15; B**).

MTRB. Injections of MTRB using the automatically generated MRM-transitions (**S_Figure 15; C**), gave a strong signal for its own MRM-TIC chromatogram but additionally gave a minor response for the KETO-MRM.

TRNB. Injections of TRNB using the automatically generated MRM-transitions produced a strong signal for MIBL (a group II-(a) steroid), and very little response for its own MRM. Final transitions used for TRNB, resulted in production of signal for its own MRM but also produced significant signal for the PRST signal (see **Section 4.14.3. Critical Group 3; P*air 3-E***), for detailed discussion of critical group implications), the ratio (PRST:TRNB) of which was effected by the concentration of modifier while using CO_2-based mobile phases as shown in **S_Figure 15; C,**

where while using CO_2 in the mobile phase the MRM transition for TRNB was greatly reduced at higher modifier when compared to FIA analysis. Further optimization would be necessary.

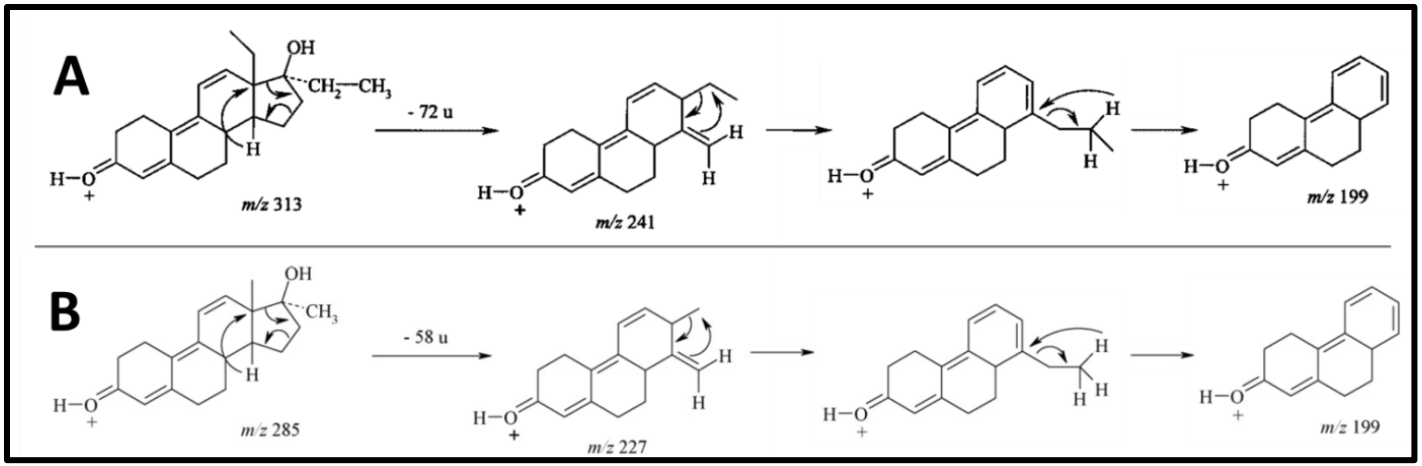

Figure 55. Fragmentation Patterns for 3-Keto Steroids Containing a 4,9,11-Triene Nucleus; for [A] Gestrinone analogs containing a C-13 ethyl group; and [B] Trenbolone analogs containing a C-13 methyl group; showing diagnostic fragments of *m/z* 241 for C-13 ethyl analogs [e.g., GSTN] and *m/z* 227 for C-13 methyl analogs [e.g., TRNB and MTRB] and characteristic fragment of *m/z* 199 for all triene containing steroids. Figure [A] mechanism proposed by and figure adapted from **Thevis et. al., 2005**[59] and [B] mechanism proposed by and adapted from **Thevis et. al., 2008**[47]); ***Showing model compounds; tetrahydrogestrinone in [A] and metribolone [MTRB] in [B]).***

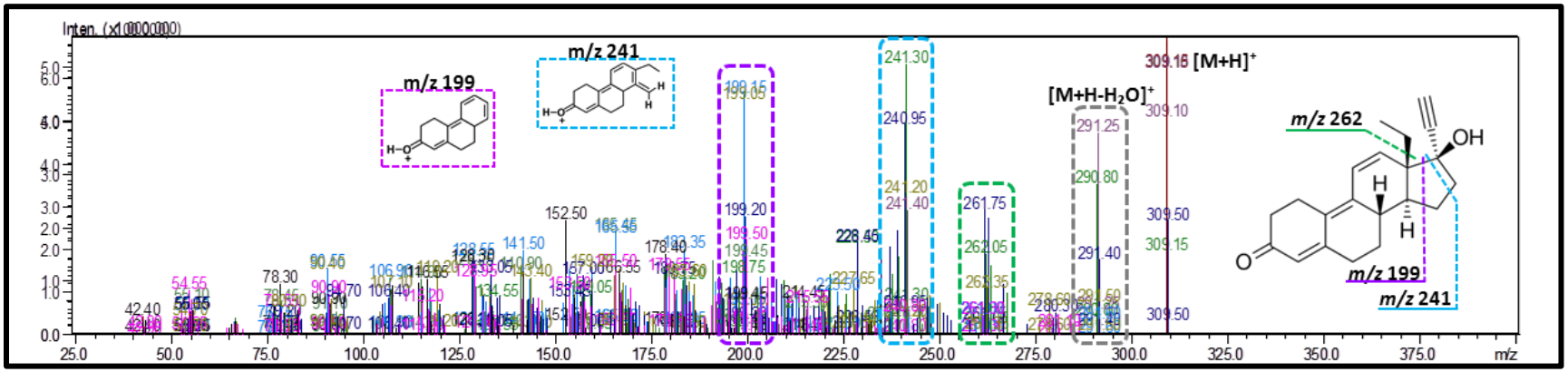

Figure 56. Zoomed Overlaid ESI product Ion Spectra of the protonated molecule $[M+H]^+$ at m/z 309 of Gestrinone [GSTN] During the Collision Energy (CE) Selection Step of MRM-Optimization; showing resulting product ions at 199 *m/z* (CE range = -40 : -20 eV), 241 *m/z* (CE range = -30 : -10 eV), 291 *m/z* (CE range = -25 : -4 eV) and 262 *m/z* (CE range = -34 : -23 eV) produced during the 'CE Select' step of MRM-optimization. **CE select scan range = 1V steps; Centroid-spectrums overlaid and displayed in absolute intensity**.

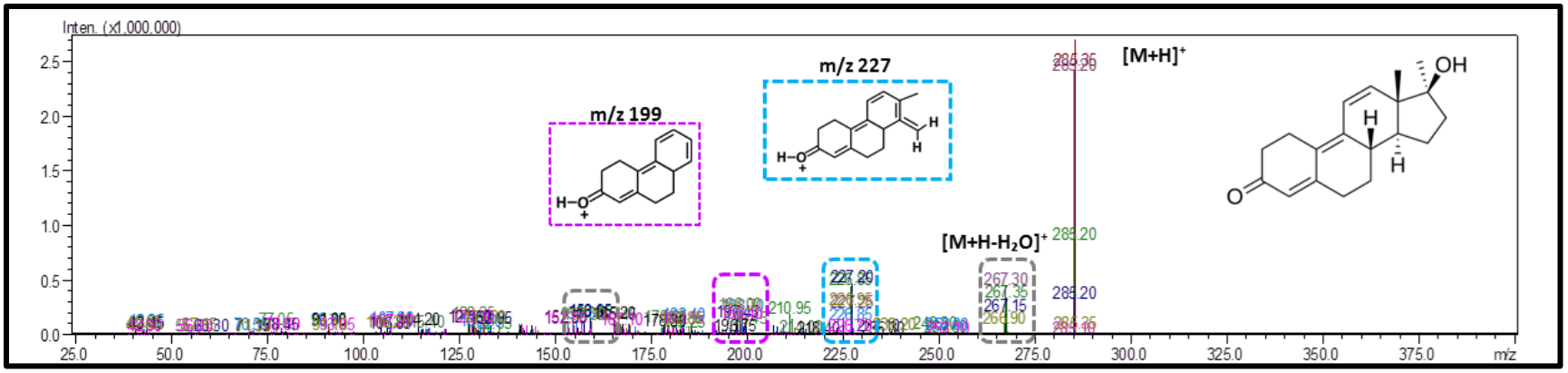

Figure 57. **Overlaid ESI product Ion Spectra of the protonated molecule [M+H]⁺ at m/z 285 of Metribolone [MTRB] During the Collision Energy (CE) Selection Step of MRM-Optimization**; showing resulting product ions at 159 *m/z* (CE range = -34 : -23 eV), 199 *m/z* (CE range = -45 : -20 eV), 227 *m/z* (CE range = -35 : -15 eV), and 267 *m/z* (CE range = -25 : -5 eV) produced during the 'CE Select' step of MRM-optimization. **CE select scan range = 1V steps; Centroid-spectrums overlaid and displayed in absolute intensity**.

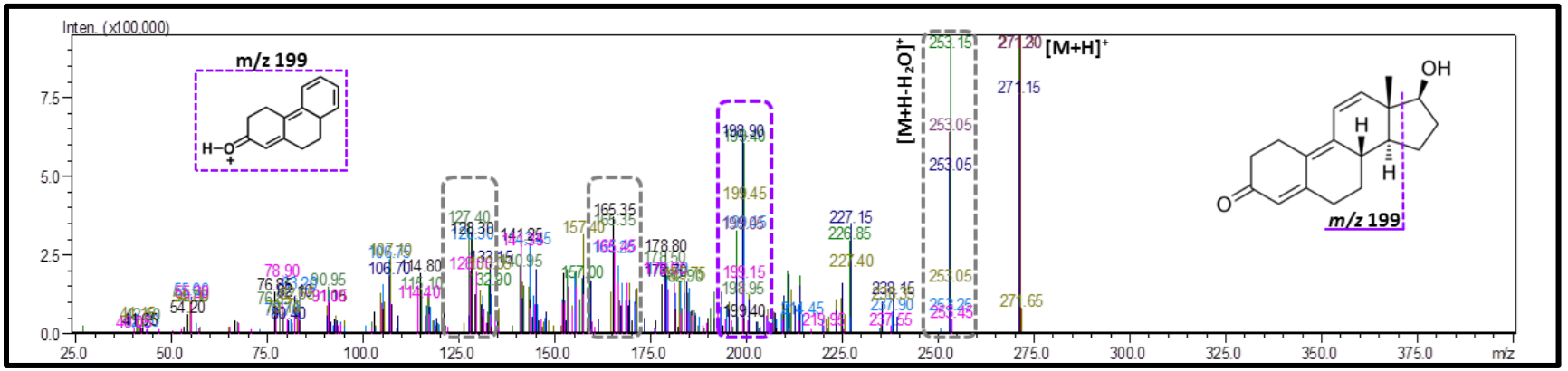

Figure 58. **Overlaid ESI product Ion Spectra of the protonated molecule [M+H]⁺ at m/z 271 of Trenbolone [TRNB] During the Collision Energy (CE) Selection Step of MRM-Optimization**; showing resulting product ions at 253 *m/z* (CE range = -30 : -10 eV), 199 *m/z* (CE range = -30 : -10 eV), 165 *m/z* (CE range = -59 : -39 eV) and 128 *m/z* (CE range = -59 : -48 eV) produced during the 'CE Select' step of MRM-optimization. **CE select scan range = 1V steps; Centroid-spectrums overlaid and displayed in absolute intensity**.

4.8. Group II-(d). 1,4-diene Steroid.

1, 4-diene steroids have a cross-conjugated π-electron system across the A ring.[65],[66] The aromatic ring after a single water loss hampers the loss of the second oxygen.[56]

4.8.1. Expected Fragmentation for Group II-(d) from the Literature.

m/z 121. The keto oxygen (participating in the cross conjugation) is protonated (**Figure 59; A [Ion *a*]**) → hydrogen migration from C-8, and cleavage of C-9 to C-10 bond (**Figure 59; A [Ion *b*]**). → charge transfer to C-8 → cleavage between C-5 to C-6 (**Figure 59; A [Ion *c*]**), and finally charge delocation (**Figure 59; A [Ion *d*]**) stabilizes the resulting ion with *m/z* 121.

m/z 149. protonated molecule (**Figure 59; B [Ion *a*]**)→ neutral water loss → charge driven dissociation pathway results in the cleavage between C-6 to C-7 and C9 to C10, with migration of two hydrogens produces an ion of 149 *m/z* (**Figure 59; B [Ion *e*]**).[45]

4.8.2. MRM Optimizations for Group II-(d). The protonated molecular ion $[M+H]^+$ was chosen as precursor ion for MRM optimization, and three major ions were selected as products (**Figure 60**). The most abundant product ion for METD was *m/z* 121, which coincides with a fragment containing the A-ring. The second most abundant ion was the $[M+H-H_2O]^+$ fragment ion. And lastly the Ion at 149 *m/z*, which includes the C- and D-rings. **Thevis et. al., 2005**[45] reported METD (includes a methyl group at C17) since the corresponding product increased to 166 *m/z* (+14, methyl). The 163 ion intensity was quite low, not unreasonable in that the additional loss of the methyl group resulted in the much more abundant ion at 149 *m/z* (**Table 17**).

4.8.3. MRM-Method Specificity Tests for Group II-(d). Methods tests via injections of METD using the optimized MRM method, gave signal only for its own MRM transitions (**S_Figure 13; D**).

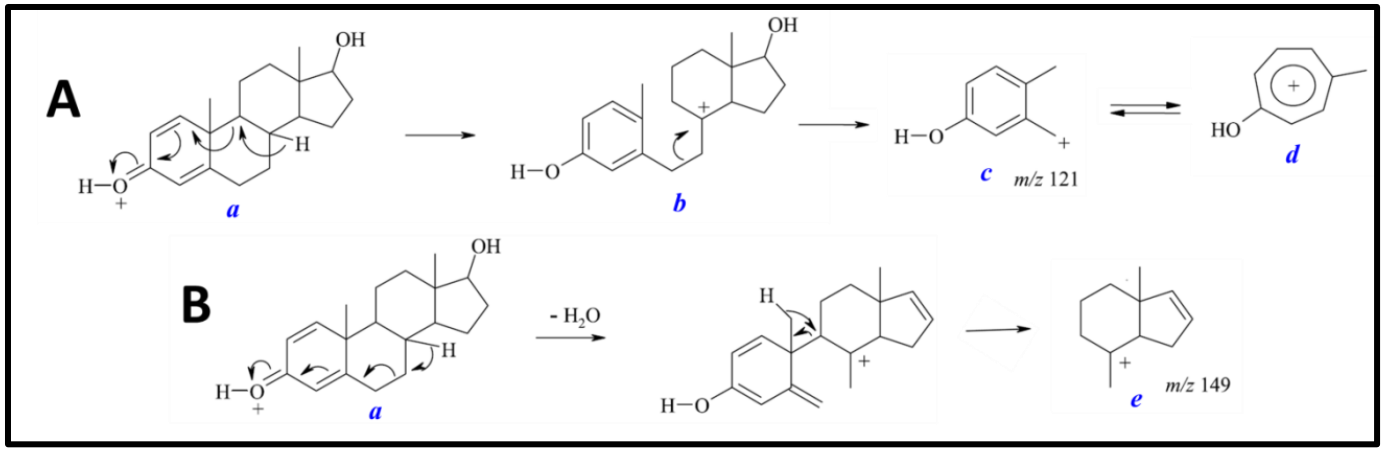

Figure 59. **Fragmentation Pattern for C3-Keto Steroids Containing a 1,4-Diene Function**; showing characteristic fragment Ions of **[A]** 121 *m/z* **(Ion [*c*])** and **[B]** 149 *m/z* **(Ion [*e*])** (Mechanisms Proposed by and figure Adapted from **Thevis et. al., 2005**[45]; ***Showing 5α-androst-1-en-17β-ol-3-one.)***

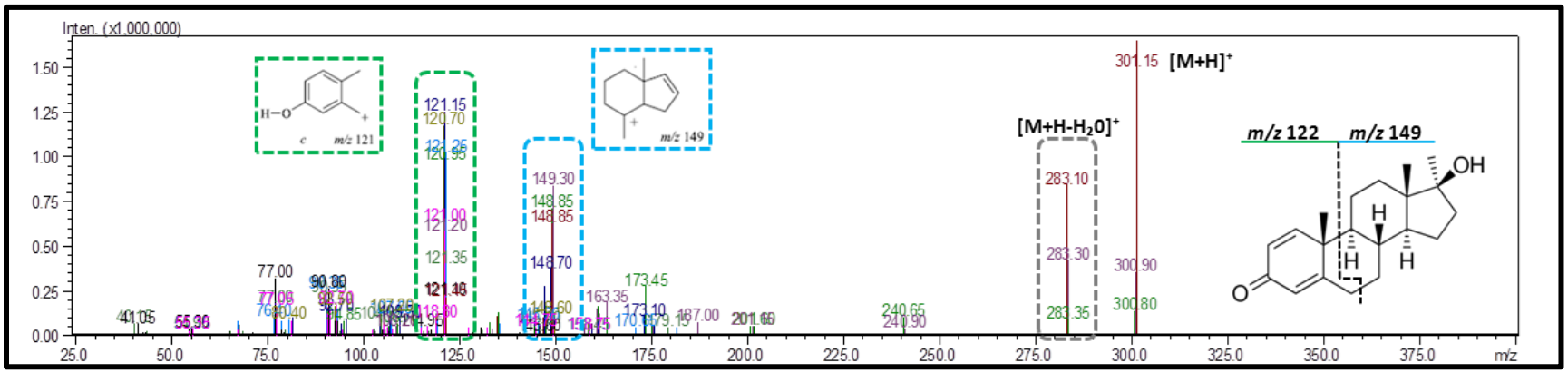

Figure 60. **Overlaid ESI product Ion Spectra of the protonated molecule [M+H]⁺ at m/z 301 of Metandienone [METD] During the Collision Energy (CE) Selection Step of MRM-Optimization**; showing resulting product ions at 121 *m/z* (CE range = -35 : -15 eV), 149 *m/z* (CE range = -25 : -5 eV) and 283 *m/z* (CE range = -20 : -1 eV) produced during the 'CE Select' step of MRM-optimization. **CE select scan range = 1V steps; Centroid-spectrums overlaid and displayed in absolute intensity**.

4.9. Group III-(a). 7-Keto Steroid.

4.9.1. Expected Fragmentation for Group III-(a) from Literature.

Although there is a multitude of analyses of derivatized KETO with GC-MS,[67] there appears to be no literature on dissociation of KETO with ESI-MS without a derivatizing agent. **Thevis et. al.**, stated that KETO is expected to have a non-specific dissociation, where all resulting ions can be explained by small partial ring fragments that are non-diagnostic.[58] Early investigations using EI in GC gives some insight.[68]

4.9.2. MRM Optimizations for Group III-(a).

The ion, $[M+H-H_2O]^+$ was determined to be the optimal precursor for 7-keto-DHEA. The $[M+H-H_2O]^+$ precursor at 285 *m/z* gave rise to four most abundant product ions at 79, 81, 107, and 149 *m/z* (**Figure 61**), although no examples could be found in literature to corroborate specific expected products for KETO, for ESI-based LC dissociation, therefore the automatically generated ions were used without modification (**Table 17**).

4.9.3. MRM-Method Specificity Tests for Group III-(a).

Although the expected fragmentation pattern for KETO from literature was expected to be non-specific to KETO, specificity tests for the automatically optimized MRM-transitions revealed little cross-over for the other steroids in this study. Although MTRB gave a minor signal for KETO, no other steroid generated signal for the KETO MRM. Furthermore with the exception of a very minor response for MTRB-MRM, Injections of KETO produced signal for only its own MRM (**S_Figure 13; C**)

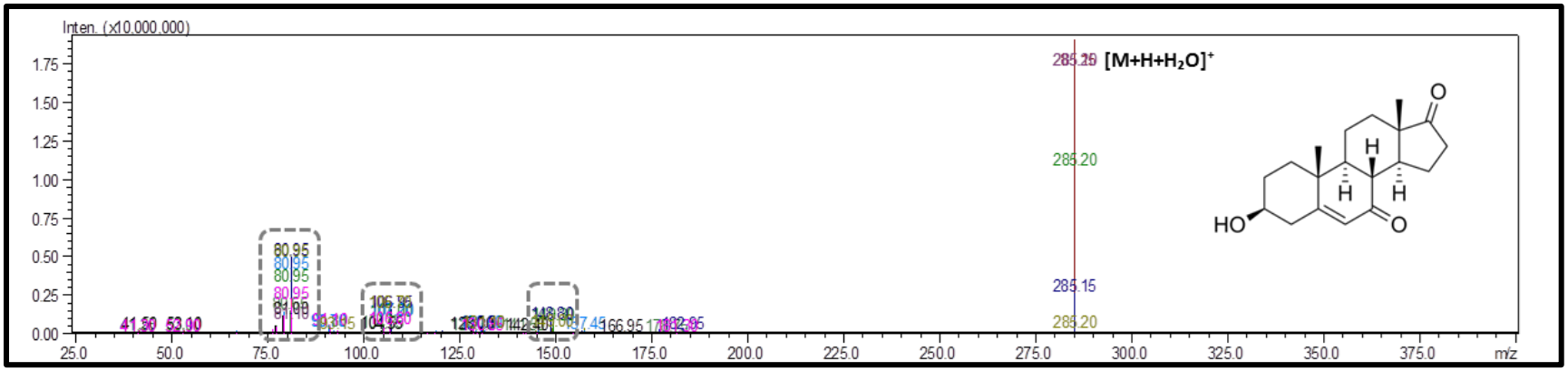

Figure 61. **Overlaid ESI product Ion Spectra of the protonated molecule $[M+H+H_2O]^+$ at m/z 285 of 7-Keto-DHEA [KETO] During the Collision Energy (CE) Selection Step of MRM-Optimization**; showing resulting product ions at 81 *m/z* (CE range = -40 : -20 eV), 79 *m/z* (CE range = -55 : -35 eV), 107 *m/z* (CE range = -40 : -20 eV) and 149 *m/z* (CE range = -35 : -23 eV) produced during the 'CE Select' step of MRM-optimization. **CE select scan range = 1V steps; Centroid-spectrums overlaid and displayed in absolute intensity**.

4.10. C3-Hydroxyl; C17-Keto Steroids

4.10.1. Group III-(b). Saturated; C3-Hydroxyl Steroids.

Expected Fragmentation for Group III-(b) from Literature. Steroids containing a non-conjugated C-3 Hydroxyl function readily lose both oxygens from the protonated molecular ion $[M+H]^+$ at 291 *m/z* (**Figure 62; Ion *a***) via neutral water loss. This results in the much more reliable precursor, at 273 *m/z* from the loss of the first water molecule from C-3 produces the $[M+H-H_2O]^+$ ion, (**Figure 62; Ion *b***). The second water molecule is also readily lost from C-17 producing the fragment ion of 255 *m/z* = $[M+H-2H_2O]^+$. Other common fragments to pertain to fragments of either the 273 or 255 *m/z* fragments. Elimination of acetone (-58Da; C_3H_6O) from the 273 *m/z* $[M+H-H_2O]^+$ ion results in a fragment with *m/z* 215 (**Figure 62; Ion *c***). Alternatively, loss of 56 amu from the 255 *m/z* $[M+H-2H_2O]^+$ ion results in a fragment with *m/z* 199 $[M+H-2H_20-(C_3H_4O)]$ (-56Da). Other expected fragments for this group are generically associated with the steroid skeleton and include ions of 107, 121, 145, 147, 159, and 161 *m/z.*[68],[69],[70]

MRM Optimizations for Group III-(b). Using the optimal precursor from Q3 scans for both ADEN and ETIO was chosen as the protonated fragment ion $[M+H-H_2O]^+$ at 273 *m/z*. Product ions were produced at 255, 199, 161, and 147 *m/z* for ADEN (**Figure 63**) and 90, 105, 215 and 255 *m/z* for ETIO (**Figure 64**). Final MRM transitions for ADEN and ETIO are provided in **Table 17**.

MRM-Method Specificity Tests for Group III-(b). Methods tests via injections of ADEN (**S_Figure 16; A**) and ETIO (**S_Figure 16; B**), produced signal for each analytes own MRM as well as signal for each other's MRM, and additionally gave significant signal for 1DHEA and ADON, regardless of the MP-composition used (see **Section 4.14.1. Critical Group 1**, for detailed discussion of critical group implications). The addition of CO_2 does not seem to have an effect, although additional peaks (resolved at lower modifier percent) were observed for all four compounds **(for detailed discussion see Chapter #3. MS Optimizations - Q3 Scans, Section S_3.4. Supplemental: Additional Peaks Observed for Hydroxy- & Saturated Steroids: S_3.4.1. ADEN, S_3.4.2. ETIO, S_3.4.3. 1DHEA, and S_3.4.4. ADON).**

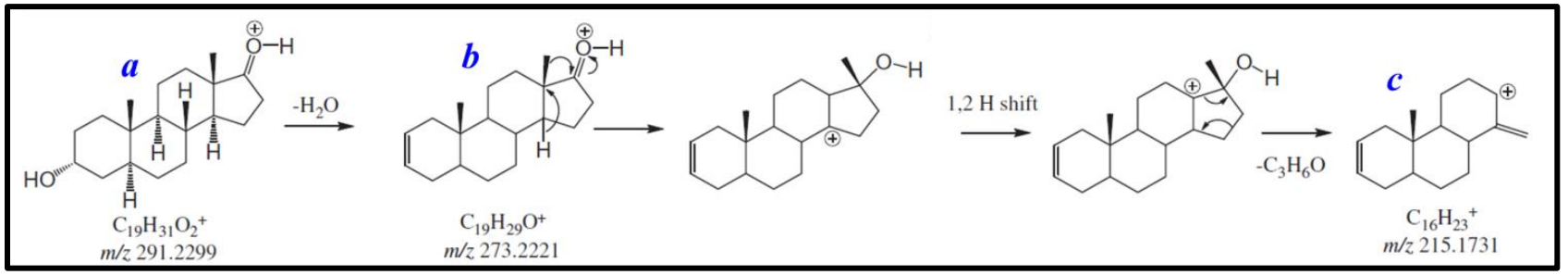

Figure 62. Fragmentation Pattern for Non-conjugated; C3-Hydroxy Steroids, showing characteristic fragments of *m/z* 273 **[Ion *b*]** and *m/z* 215 **[Ion *c*]**; *Showing cis-Androsterone* (Mechanism Proposed by and Figure Adapted from **Musharraf et. al., 2013**[69]).

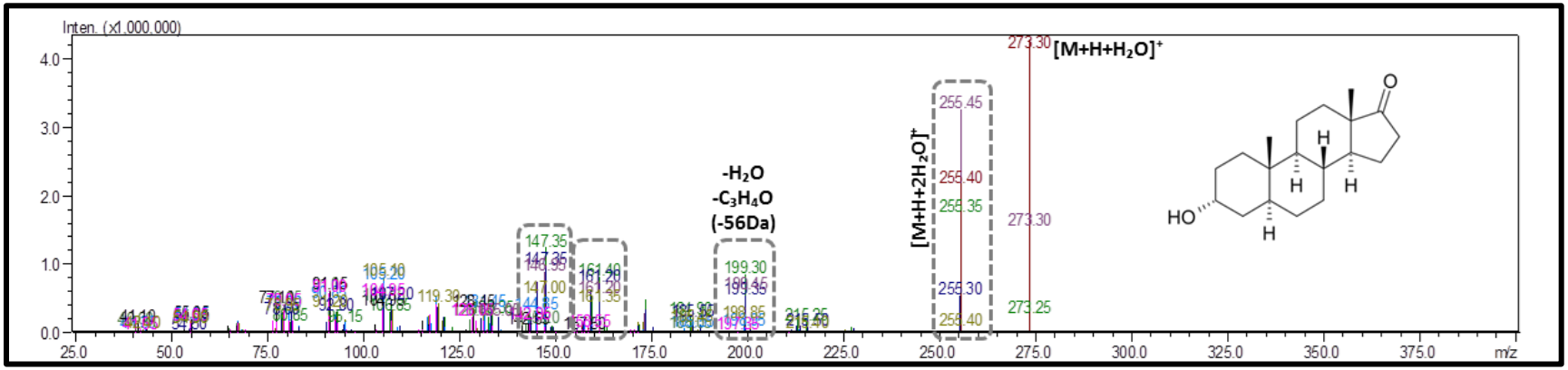

Figure 63. **Overlaid ESI product Ion Spectra of the protonated molecule $[M+H+H_2O]^+$ at *m/z* 273 of Androsterone [ADEN] During the Collision Energy (CE) Selection Step of MRM-Optimization**; showing resulting product ions at 255 *m/z* (CE range = -25 : -5 eV), 147 *m/z* (CE range = -30 : -10 eV), 199 *m/z* (CE range = -30 : -10 eV) and 161 *m/z* (CE range = -30 : -18 eV) produced during the 'CE Select' step of MRM-optimization. **CE select scan range = 1V steps; Centroid-spectrums overlaid and displayed in absolute intensity**.

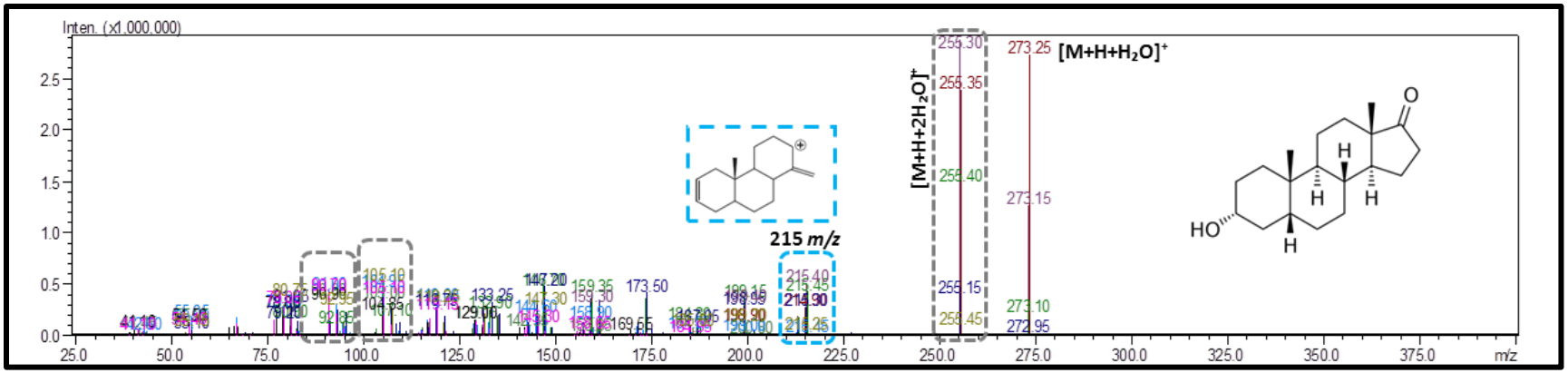

Figure 64. **Overlaid ESI product Ion Spectra of the protonated molecule $[M+H+H_2O]^+$ at *m/z* 273 of Etiocholanolone [ETIO] During the Collision Energy (CE) Selection Step of MRM-Optimization**; showing resulting product ions at 255 *m/z* (CE range = -25 : -5 eV), 215 *m/z* (CE range = -25 : -5 eV), 105 *m/z* (CE range = -40 : -20 eV) and 91 *m/z* (CE range = -50 : -38 eV) produced during the 'CE Select' step of MRM-optimization. **CE select scan range = 1V steps; Centroid-spectrums overlaid and displayed in absolute intensity**.

4.10.2. Group IV. Conjugated; C3-Hydroxyl Steroid.

Expected Fragmentation for Group IV from Literature. Little information is available on the expected fragmentation patterns for conjugated C3-hydroxyl steroids with C17-keto functional group. Although little information could be found specifically outlining expected fragments for conjugated; C3-hydroxyl steroids in literature using LC-based ESI-MS detection, the product ion scans of 1DHEA and PRST were quite similar to those of ADEN and ETIO above. Although the fragmentation patterns likely would be different due to the conjugations in the structures of this group, the resulting ions would most certainly be quite similar, for fragments with the same *m/z*, especially for the smallest ions related directly to the steroid skeleton (e.g., 107, 121, 145, 147, 159 and 161 *m/z).*

MRM Optimizations for Group IV. The protonated fragment ion $[M+H-H_2O]^+$ was chosen as precursor from Q3 scans for PRST at 271 *m/z*. During MRM-optimization (**Table 17**), sufficient product ions were produced for PRST using 157, 213, and 253 *m/z* (**Figure 65**). Since at this stage it is unclear whether an additive will be required in the MP for further optimization, and Q3 scans revealed that the optimal precursor for 1DHEA may change depending on the use of additives, the protonated molecular ion $[M+H]^+$ using 291 *m/z* was initially chosen as precursor for 1DHEA. The resulting product ions were 91, 135, 255, and 273 *m/z* (**Figure 66**). Again, little information could be found specifically outlining expected fragments for conjugated C3-hydroxyl steroids in literature using LC-based ESI-MS detection. The product ion scans of 1DHEA and PRST were similar to those of ADEN and ETIO above. Although the fragmentation patterns likely would be different due to the conjugations in the structures of this group, the resulting ions would most certainly be quite similar, for fragments with the same *m/z*, especially for the smallest ions related directly to the steroid skeleton.

MRM-Method Specificity Tests for Group IV. Methods tests via injections of 1DHEA (**S_Figure 16; C**) produced signal for its own MRM as well as signal for ADEN, ETIO, and ADON, regardless of the MP-composition used (see **Section 4.14.1. Critical Group 1**, for detailed discussion of critical group implications). The addition of CO_2 does not seem to have an effect, although additional peaks (resolved at lower modifier percent) were

observed for all four compounds **(for detailed discussion see Chapter #3. MS Optimizations - Q3 Scans, Section: S_3.4. Supplemental: Additional Peaks Observed for Hydroxy- & Saturated Steroids: S_3.4.1. ADEN , S_3.4.2. ETIO, S_3.4.3. 1DHEA, and S_3.4.4. ADON).** Further MRM-optimization was performed, using FIA with AmFo and SFC-20% AmFo to evaluate if sensitivity could be improved.

Methods tests via injections of PRST (S_Figure 16**; D**) produced signal for its own MRM as well as signal for EPIT, regardless of the MP-composition used (see **Section 4.14.3. Critical Group 3; *Pair 3-E***, for detailed discussion of critical group implications). Further MRM-optimization was performed, using FIA with AmFo and SFC-20% AmFo, using alternative precursor ions from Q3 scans, to evaluate if sensitivity could be improved. Using the protonated molecular ion $[M+H]^+$ at 288 *m/z* was unsuccessful in producing adequate response for fragmentation. Using the protonated fragment ion $[M+H-H_2O]^+$ and performing MRM-optimizations using CO_2 + 20% AmFo showed an marked increase in sensitivity *(data not shown)*.

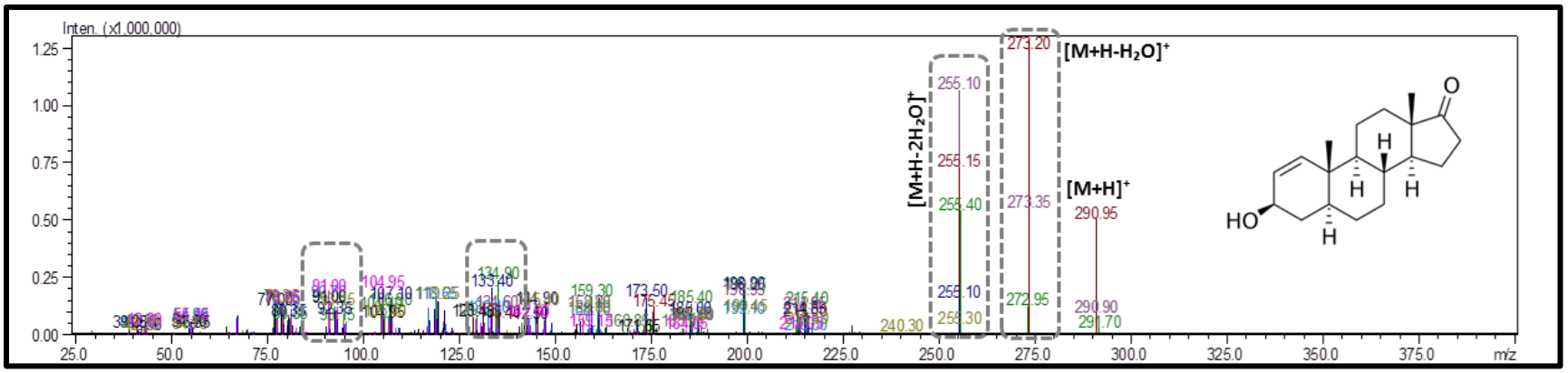

Figure 65. **Overlaid ESI product Ion Spectra of the protonated molecule [M+H]⁺ at m/z 291 of 1-Androsterone [1DHEA] During the Collision Energy (CE) Selection Step of MRM-Optimization**; showing resulting product ions at 273 *m/z* (CE range = -20 : -1 eV), 255 *m/z* (CE range = -25 : -5 eV), 135 *m/z* (CE range = -30 : -10 eV) and 91 *m/z* (CE range = -50 : -34 eV) produced during the 'CE Select' step of MRM-optimization. **CE select scan range = 1V steps; Centroid-spectrums overlaid and displayed in absolute intensity**.

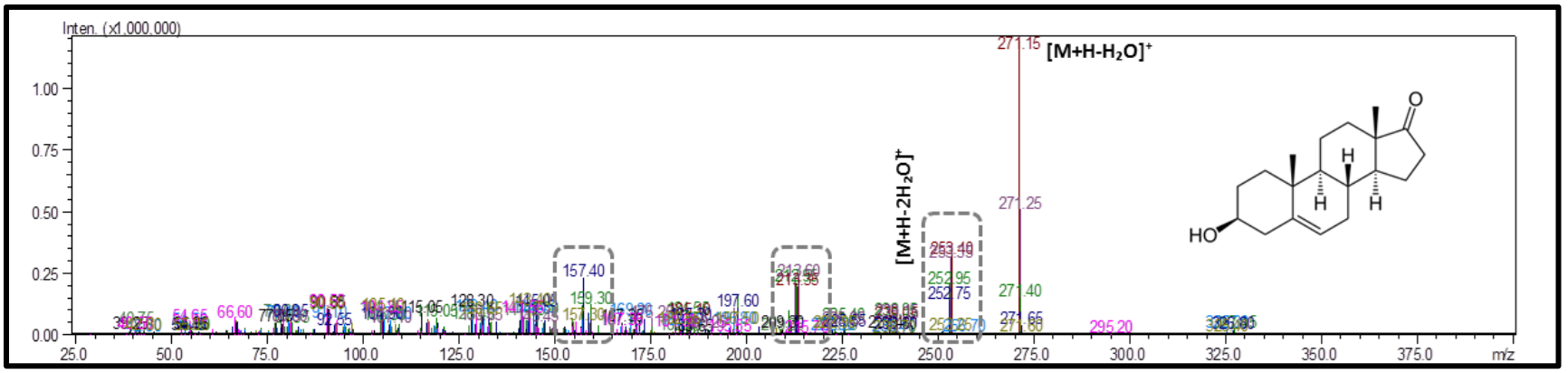

Figure 66. **Overlaid ESI product Ion Spectra of the protonated molecule [M+H+H₂O]⁺ at m/z 271 of Prasterone [PRST] During the Collision Energy (CE) Selection Step of MRM-Optimization**; showing resulting product ions at 253 *m/z* (CE range = -25 : -5 eV), 214 *m/z* (CE range = -25 : -5 eV), 213 *m/z* (CE range = -30 : -10 eV) and 157 *m/z* (CE range = -35 : -23 eV) produced during the 'CE Select' step of MRM-optimization. **CE select scan range = 1V steps; Centroid-spectrums overlaid and displayed in absolute intensity**.

4.11. Group V. Non-Conjugated; C3-Keto Steroid.

4.11.1. Oxandrolone [OXAN].

Expected Fragmentation for OXAN from Literature. Fragments expected for OXAN include ions corresponding to three neutral water losses, which is expected due to the presence of three oxygen molecules in its structure, these ions are 289 *m/z* $[M+H-H_2O]^+$, 271 *m/z* $[M+H-2H_2O]^+$[56] and 253 *m/z* $[M+H-3H_2O]^+$. [35],[56],[71] Additional ions expected for OXAN include a fragment involving the B- and C- rings giving an ion at 121 *m/z* and a fragment produced from the single dehydrated fragment 289 *m/z* $[M+H-H_2O]^+$ involving the loss of acetic acid (-60 Da) from the A-ring producing an ion of 229 *m/z*.[56]

MRM Optimizations for OXAN. Initial MRM-optimizations for OXAN were performed using the protonated molecular ion $[M+H]^+$ at 307 *m/z* as precursor. During MRM-optimization sufficient product ions were produced for OXAN using 121, 229, 271 and 289 *m/z* (**Figure 67**). All product ions were corroborated in literature as discussed above. Final MRM-transitions for OXAN are given in **Table 17**.

MRM-Method Specificity Tests for OXAN. Methods tests via injections of OXAN (**S_Figure 16; C**) produced signal for its own MRM, and additionally while using flow injection analysis also gave signal for EPIT and TSTO and the addition of CO_2 to the MP increased this effect, especially when an additive was used in the MP, Therefore OXAN was flagged as a watch member of critical group #3 (see **Section 4.14.3. Critical Group 3**, for detailed discussion of critical group implications).

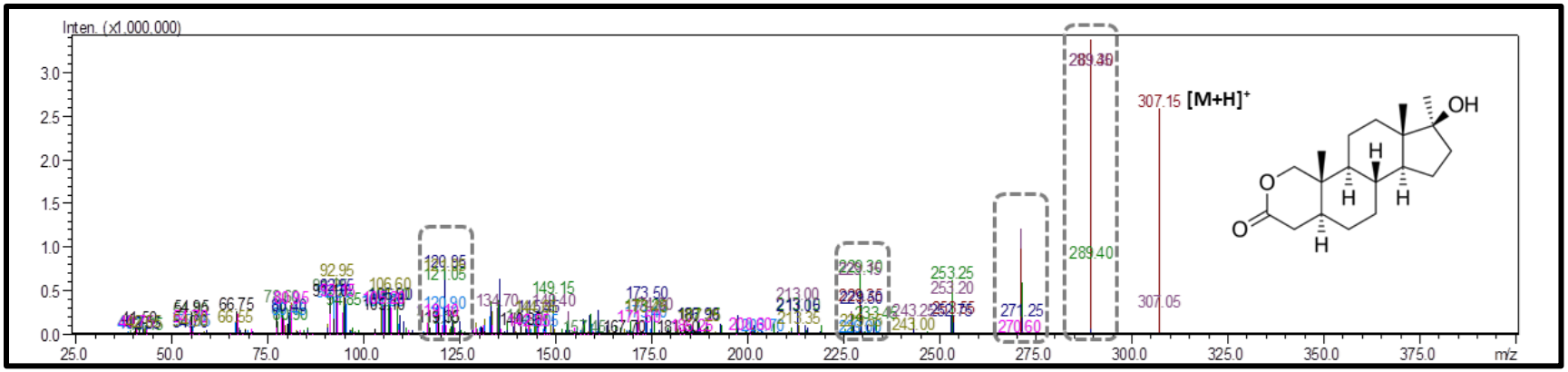

Figure 67. **Overlaid ESI product Ion Spectra of the protonated molecule [M+H]⁺ at m/z 307 of Oxandrolone [OXAN] During the Collision Energy (CE) Selection Step of MRM-Optimization**; showing resulting product ions at 289 *m/z* (CE range = -20 : -1 eV), 271 *m/z* (CE range = -25 : -5 eV), 121 *m/z* (CE range = -35 : -15 eV) and 229 *m/z* (CE range = -30 : -18 eV) produced during the 'CE Select' step of MRM-optimization. **CE select scan range = 1V steps; Centroid-spectrums overlaid and displayed in absolute intensity**.

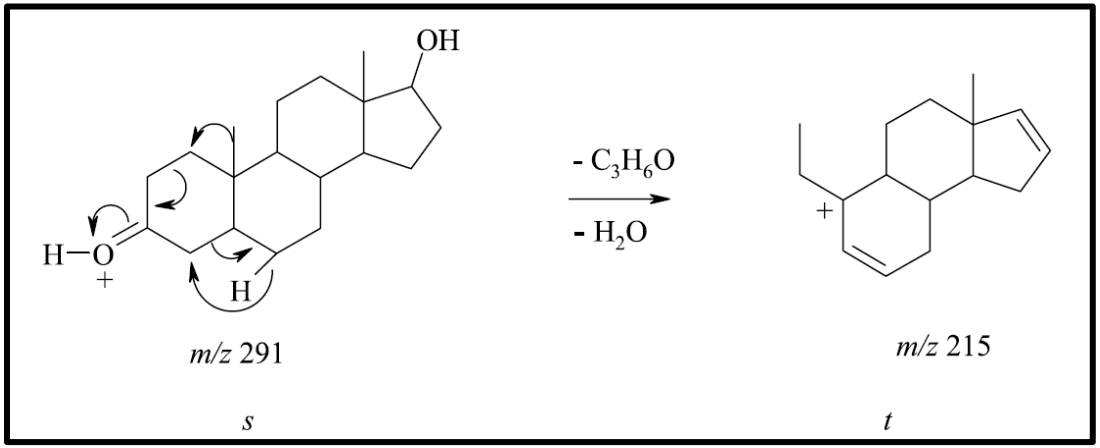

Figure 68. Fragmentation Pattern for Non-conjugated; C3-Keto Steroids, showing characteristic fragment of 215 *m/z*; ***Showing androstan-17ß-ol-3-one [ADON]*** (Mechanism Proposed by and Figure Adapted from **Thevis et. al., 2005**[45]).

4.11.2. Expected Fragmentation for α-/ß- Saturated C3-Keto Steroids

Expected Fragmentation for ADON from Literature. The protonated molecular ion $[M+H]^+$ for ADON at 291 *m/z*[56],[45] is expected to produce a variety of fragments, including those associated with water losses, 273 *m/z* for $[M+H-H_2O]^+$[32],[56] and 255 *m/z* for $[M+H-2H_2O]^+$.[45],[56],[72] A fragment associated with the elimination of acetone (-58) from the A- ring, then subsequent loss of water (-18) produces a fragment with *m/z* 215 for ADON; the proposed fragmentation pattern by **Thevis et. al., 2005** is shown in **Figure 68**.[45] This fragment can also be found in the product ion spectra of MSAL and MSEL (shifted to *m/z* 229, due to the additional methyl group at C17 or C1 respectively). This loss of acetone has been related to and allows for stereoisomeric determination, where the 5α-isomer favors this fragment in ESI-MS.[43],[56],[45] Other product ions have also been described at *m/z* 81, 161, 173, and 189, all formed from A-ring fragments.[69] Ions with 145 and 119 *m/z* (B-/C-ring fragments),[56] have all been observed for ADON. Other ions reported for ADON using EI include: a fragment of (-15 u) giving 276 *m/z* from elimination of a radical methyl;[32] and (-58 u) giving 233 *m/z* due to the elimination of the steroidal D-ring;[70],[32],[69] and a fragment of (-70 u) giving *m/z* 221,[68],[32] are common to 5ß-analogs.

Expected Fragmentation for MSEL from Literature. The fragment associated with the elimination of acetone (-58) from the A- ring then subsequent loss of water (-18) produces a fragment with *m/z* 229 for MSEL (shifted from 215 *m/z*, due to the additional methyl group at C1); described above, the proposed fragmentation pattern by **Thevis et. al., 2005** is shown for ADON (lacking the additional methyl group) in **Figure 68**.[35],[45],[59] Also 305 *m/z* $[M+H]^+$ and 269 *m/z* $[M+H-2H_2O]^+$ reported in[35],[56]. 287m/z $[M+H-H_2O]^+$[56], 133 *m/z,*[35],[56] 119 *m/z*, 109 *m/z*, and 105 *m/z* (B-/C- ring fragments) have also been reported for MSEL.[35],[56]

Expected Fragmentation for MSAL from Literature. The fragment associated with the elimination of acetone (-58) from the A- ring then subsequent loss of water (-18) produces a fragment with *m/z* 229 for MSAL (shifted from 215 *m/z*, due to the additional methyl group at C17); described above, the proposed fragmentation pattern by **Thevis et. al., 2005** is shown for ADON (lacking the additional methyl group) in **Figure 68**.[45] Ions of *m/z* 305 $[M+H]^+$ and *m/z* 269 $[M+H-2H_2O]^+$ have also been reported for MSAL.[35],[56]

4.12.3. Discussion over the Expected Fragmentation for α-/ß-Saturated C3-Keto Steroids.

As outlined quite beautifully in **Schanzer et. al., 2015**[73] there was an historical trend towards advancing doping control screening protocols with technology-driven methodologies which included the replacement of GC-MS with derivatization, to liquid chromatography/(tandem) mass spectrometry (LC-MS/MS). During the transition a wave of papers aimed at the identification and characterization of diagnostic approaches to untargeted doping screening for the multitude of metabolites associated with the new and upcoming, ever evolving black market of illicit substances synthesized specifically to circumvent doping controls. Metabolic studies clearly documented the extreme complexity of the biosynthetic pathways involved and the huge number of highly similar (in most cases differing by a single α-/ß- hydrogen configuration) compounds. These metabolites tend to be the reduced or hydroxylated analogs which were well known to be the most difficult targets to establish diagnostic detection methods based in MS alone. They have highly efficient dissociation pathways once exposed to collision induced dissociation energies, and easily thermally degrade and/or are hydroxylated

There seems to be a distinct gap, a 2-4 year period, where innovation ceased. The one thing that is clear is that the next wave of literature (post-blackout), GC-MS via TFA trimethylsilylated derivatization was not only the preferred method, but had been effectively locked in via regulations, with the apparent reasoning for the switch claiming the same benefits that were originally described for the switch to LC-MS! One is left to insinuate the circumstances, since it is clear this gap also coincides with the historical moment in time when the synthetic market began to explode. The complexity and multitude of metabolites that are necessary to monitor at any given time to determine within all certainty a 'doped' versus ' natural' level has necessitated a multi-level metabolite ratio determination to be implemented for doping assay to sufficiently monitor potential doping. It's not that I see a problem with a need for a change (even if it was a reversal back to 'what we know works') but I would like to read about it. The distinct lack of documentation seems an unfortunate circumstance of the times, where when things didn't work perfectly, its considered a failure and therefore unpublishable. Unfortunately, this makes it so that many do not get the benefit of the lessons learned.

4.12.3. Mesterolone [MSEL]

MRM Optimizations for MSEL. Using the optimal precursor from Q3 scans for MSAL of $[M+H]^+$ at 305 *m/z*, product ions were generated at 287, 269, 173 and 133 *m/z* (**Figure 69**). Final MRM transitions for MSEL are provided in **Table 17**. Both the 287 *m/z* and 269 *m/z* ions correspond to expected fragments due to water losses ($[M+H-H_2O]^+$ and $[M+H-2H_2O]^+$, respectively). The 133 m/z ion has also previously been reported for MSEL, but the expected 229 m/z (ion due to acetone loss) was also produced for MSEL, but was not chosen by the automatic selection program.

MRM-Method Specificity Tests for MSEL. Method tests via injections of MSAL (**S_Figure 17; B**) produced signal for its own MRM as well as nearly equal signal for the MSAL-MRM. Additionally MSEL also produced signal at much lower intensity for the DNZL-MRM, and the METD-MRM while using flow injection analysis (with and without additive). (See **Section 4.14.2. Critical Group 2; *Pair 2-C***, for detailed discussion of critical group implications). The addition of CO_2 had a significant effect, where further investigation of the implications are necessary. Additional peaks (resolved at lower modifier percent) were observed for MSEL, which may provide insight into the observed behavior, as the presence of adulterants may be affecting the result. (for detailed discussion see **Chapter #3. MS Optimizations - Q3 Scans, Section S_3.4. Supplemental: Additional Peaks Observed for Hydroxy- & Saturated Steroids: S_3.4.5. MSEL**).

4.12.4. Mestanolone [MSAL]

MRM Optimizations for MSAL. Using the optimal precursor from Q3 scans for MSAL of $[M+H]^+$ at 305 *m/z*, product ions were generated at 269, 229, 187, and 159 *m/z* (**Figure 70**). Final MRM transitions for MSAL are provided in **Table 17**.

MRM-Method Specificity Tests for MSAL. Methods tests via injections of MSAL (**S_Figure 17; C**) produced signal for its own MRM as well as signal for MSEL and DNZL while using flow injection analysis (with and without additive). (See **Section 4.14.2. Critical Group 2; *Pair 2-C***, for detailed discussion of critical group

implications). The addition of CO_2 had a significant effect, where further investigation of the implications is necessary. Additional peaks (resolved at lower modifier percent) for MSAL were observed, which may provide insight into the observed behavior, as the presence of adulterants may be affecting the result. **(for detailed discussion see Chapter #3. MS Optimizations - Q3 Scans, Section S_3.4. Supplemental: Additional Peaks Observed for Hydroxy- & Saturated Steroids: S_3.4.5. MSEL).**

4.12.5. Androstanolone [ADON]

MRM Optimizations for ADON. Initial attempts at MRM optimization for ADON using methanol with no additive were difficult and ultimately were unsuccessful. The first conditions which produced an adequate response was when AmFo was utilized as additive under FIA condition, using the protonated solvent adduct ion $[M+H+MeOH-H_2O]^+$ of *m/z* 305, which produces product ions at 79, 91 and 255 *m/z* (**Figure 71**). Final MRM transitions and associated CEs and voltages are presented in **Table 17**.

MRM-Method Specificity Tests for ADON. Methods tests via injections of ADON using the original MRM transitions optimized using MeOH with no additive, were tested under FIA and SFC conditions (**S_Figure 17; D**), Injections of ADON produced signal for its own MRM as well as signal for many other compounds (see **Section 4.14.1. Critical Group 1**, for detailed discussion of critical group implications). ADON was the most difficult compound to obtain a sufficient signal and optimal conditions are still currently being investigated.

Additional peaks (resolved at lower modifier percent) for ADON were observed, which may provide insight into the observed behavior, as the presence of adulterants may be affecting the result (**for detailed discussion see Chapter #3. MS Optimizations - Q3 Scans, Section: S_3.4. Supplemental: Additional Peaks Observed for Hydroxy- & Saturated Steroids: S_3.4.4. ADON).**

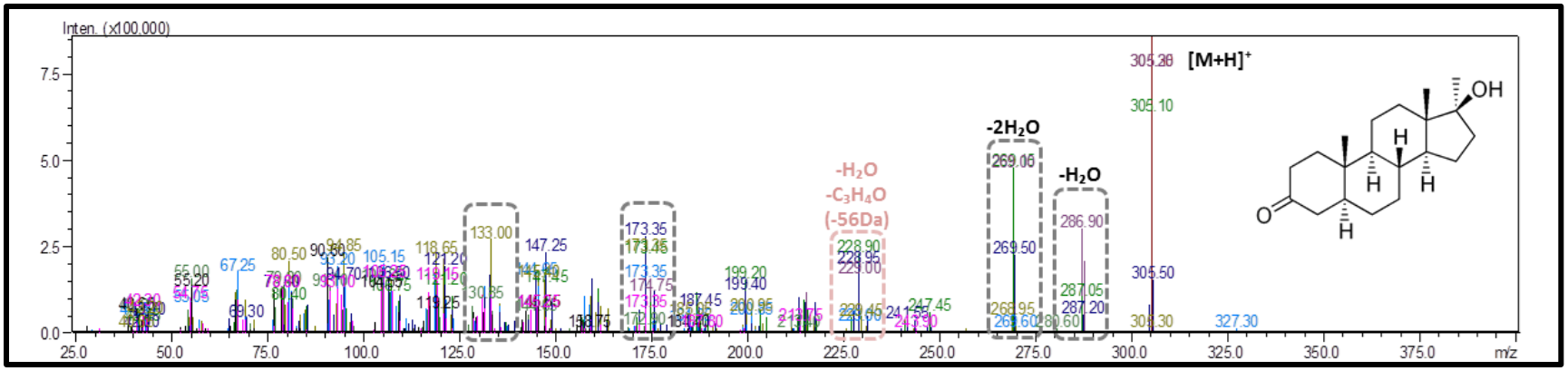

Figure 69. **Overlaid ESI product Ion Spectra of the protonated molecule [M+H]⁺ at m/z 305 of Mesterolone [MSEL] During the Collision Energy (CE) Selection Step of MRM-Optimization**; showing resulting product ions at 269 *m/z* (CE range = -25 : -5 eV), 173 *m/z* (CE range = -30 : -10 eV), 287 *m/z* (CE range = -25 : -5 eV) and 133 *m/z* (CE range = -40 : -28 eV) produced during the 'CE Select' step of MRM-optimization. **CE select scan range = 1V steps; Centroid-spectrums overlaid and displayed in absolute intensity**.

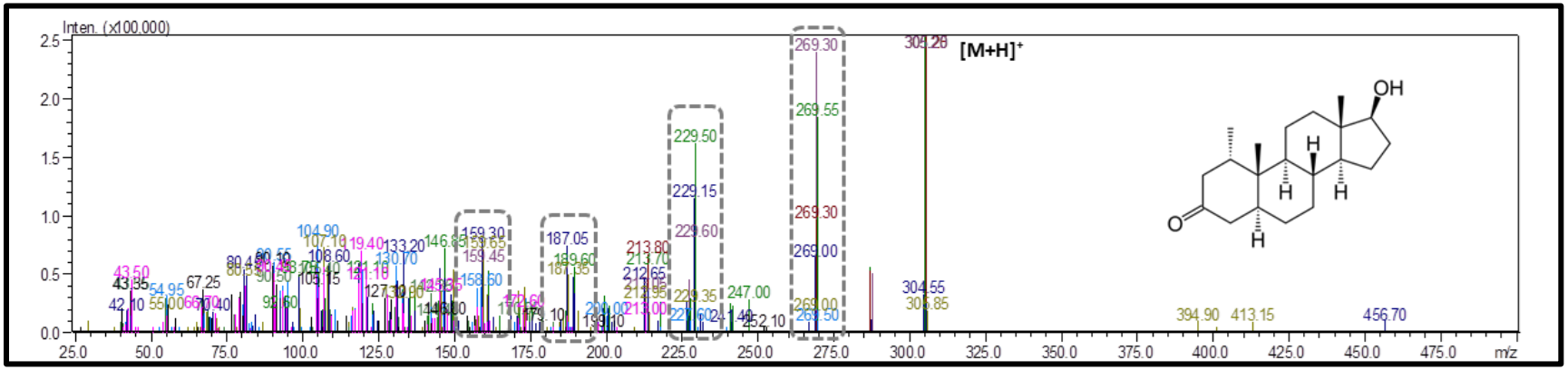

Figure 70. **Overlaid ESI product Ion Spectra of the protonated molecule [M+H]⁺ at m/z 305 of Mestanolone [MSAL] During the Collision Energy (CE) Selection Step of MRM-Optimization**; showing resulting product ions at 269 *m/z* (CE range = -25 : -5 eV), 229 *m/z* (CE range = -30 : -10 eV), 159 *m/z* (CE range = -35 : -15 eV) and 187 *m/z* (CE range = -35 : -23 eV) produced during the 'CE Select' step of MRM-optimization. **CE select scan range = 1V steps; Centroid-spectrums overlaid and displayed in absolute intensity**.

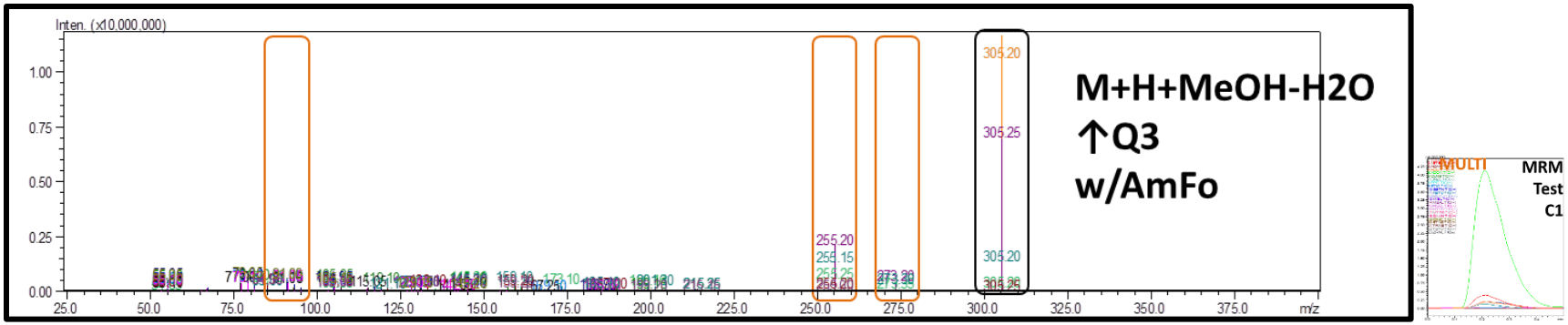

Figure 71. **Overlaid ESI product Ion Spectra of the protonated solvent adduct ion [M+H+MeOH-H_2O]$^+$ at *m/z* 305 of Androstanolone [ADON] During the Collision Energy (CE) Selection Step of MRM-Optimization *USING FIA-AmFo as MP****; showing resulting product ions at 79 *m/z* (CE range = - : - eV), 91 *m/z* (**CE range = - : - eV**), and 255 *m/z* (CE range = - : - eV) produced during the 'CE Select' step of MRM-optimization. **CE select scan range = 1V steps; Centroid-spectrums overlaid and displayed in absolute intensity**.

4.13. Group VI. Other Anabolic Agents

4.13.1. Clenbuterol [CLNB]

Expected Fragmentation for CLNB from Literature. Protonation is expected to occur at the nitrogen (on ethanolamine side-chain), and further fragmentation occurs thru both charge-driven and charge-remote fragmentation. Protonated molecule for CLNB at 277 *m/z* is expected to produce characteristic fragment ions for ß$_2$-agonists at 259, 203, 168/167 and 132 *m/z*.[74],[75],[76] A common fragmentation pattern for CLNB is shown in (**Figure 72**), adapted from **Cai et. al.,**[77] At high collision energies (20V CE), product ion scans are expected to produce a fragment at *m/z* 259 due to the neutral loss of water (-18 u). Further fragmentation is expected to produce a fragment at *m/z* 203 via isobutene elimination (-56 u), along with a hydrogen migration to the leaving group. Further fragments from the elimination of chlorine (or HCl) give product ions at *m/z* 168/167 (-Cl), and *m/z* 132.

MRM Optimizations for CLNB. The precursor $[M+H]^+$ at *m/z* 277 was chosen for CLNB, and produced intense product ions of 203, 259, 132 and 168 *m/z* (**Figure 73**), all of which were corroborated in literature, as described above.

MRM-Method Specificity Tests for CLNB. Method tests via injections of CLNB, produced signal for its own MRM-only, regardless of the MP-composition used (**S_Figure 18; B**).

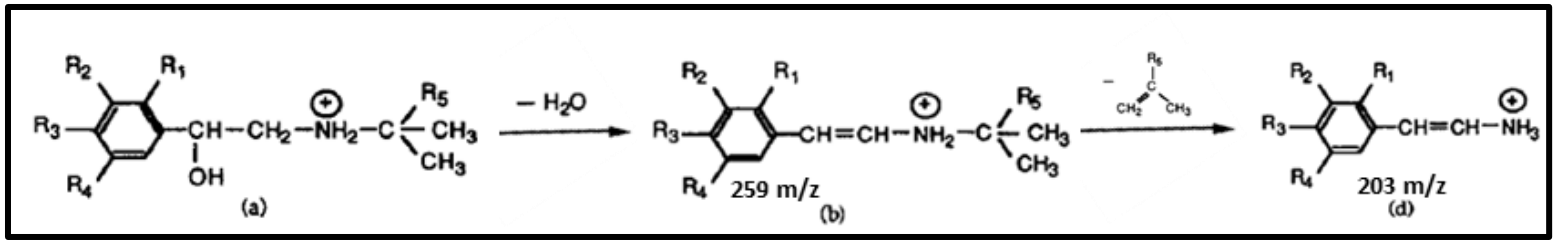

Figure 72. Fragmentation Pattern for ß-Agonists, showing characteristic fragment ions of *m/z* 259 **[Ion *b*]**, and *m/z* 203 **[Ion *d*]** (Mechanism Proposed by and Figure Adapted from **Cai et. al., 1997**[77]).

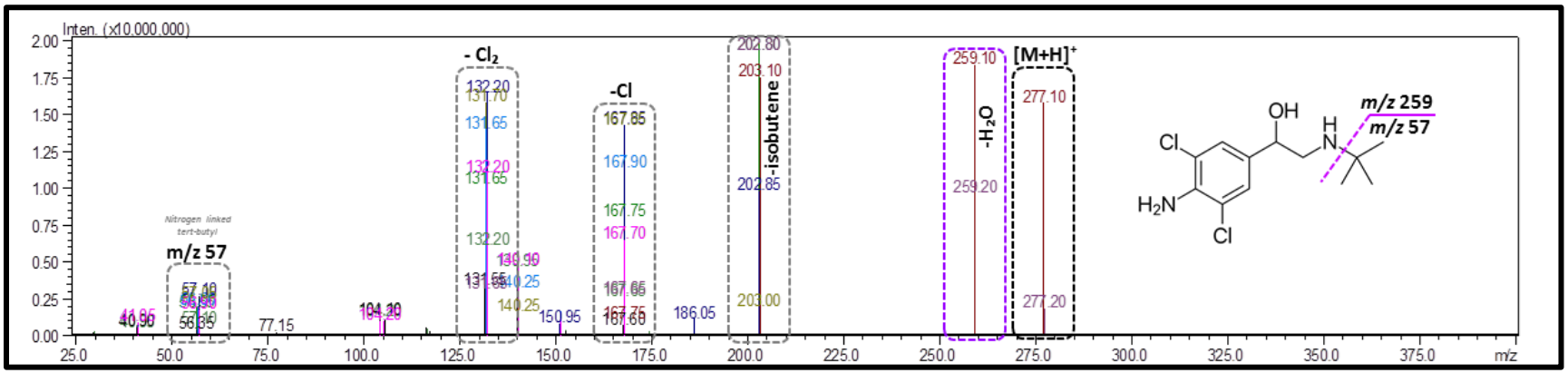

Figure 73. **Overlaid ESI product Ion Spectra of the protonated molecule $[M+H]^+$ at m/z 259 of Clenbuteral [CLNB] During the Collision Energy (CE) Selection Step of MRM-Optimization**; showing resulting product ions at 203 *m/z* (CE range = -25 : -5 eV), 259 *m/z* (CE range = -20 : -1 eV), 132 *m/z* (CE range = -35 : -14 eV) and 168 *m/z* (CE range = -39 : -28 eV) produced during the 'CE Select' step of MRM-optimization. **CE select scan range = 1V steps; Centroid-spectrums overlaid and displayed in absolute intensity**.

4.13.2. *Andarine* [ADAR]

Expected Fragmentation for ADAR from Literature. Detection of arylpropionamide-derived SARMs have been extensively studied via GC-EI-MS(/MS) and negative and positive ionization modes for LC-MS/MS analysis.[78],[79],[80],[81] The analysis of most SARMs are preferably accomplished via LCMS.[33] Expected fragments for protonated molecules after collisional activation are expected to include *m/z* 422, 400, 396, 354, 206 and 109, as shown in the adapted figure from **Thevis et. al., 2009**[78] in **Figure 74**.

MRM Optimizations for ADAR. The protonated molecule $[M+H]^+$ at *m/z* 442 of Andarine [ADAR] produced intense product ions at 400, 109, and 208, as expected from literature. Additional intense product ions were produced at 190 and 148 *m/z* (**Figure 75**). The automatic MRM-optimization program chose 108, 148, 190 and 208 *m/z* as transitions for ADAR.

MRM-Method Specificity Tests for ADAR. Methods tests via injections of ADAR produced signal for its own MRM-only, regardless of the MP-composition used (**S_Figure 18; A**).

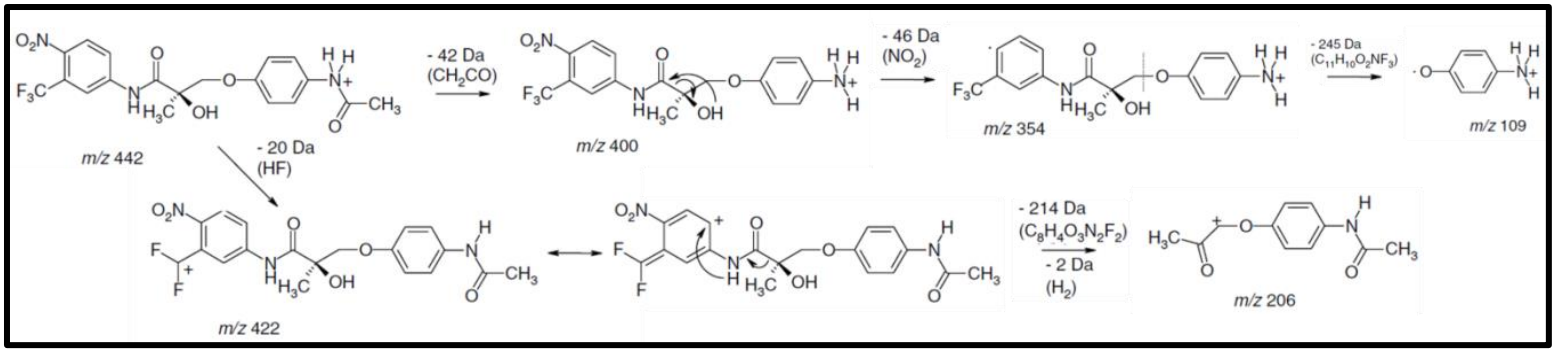

Figure 74. Fragmentation Pattern for Andarine [ADAR] a Selective Androgen Receptor Modulator (SARM), showing characteristic fragments of 400, 206 and 109 *m/z* (Mechanism Proposed by and Figure Adapted from **Thevis et. al., 2009**[78]).

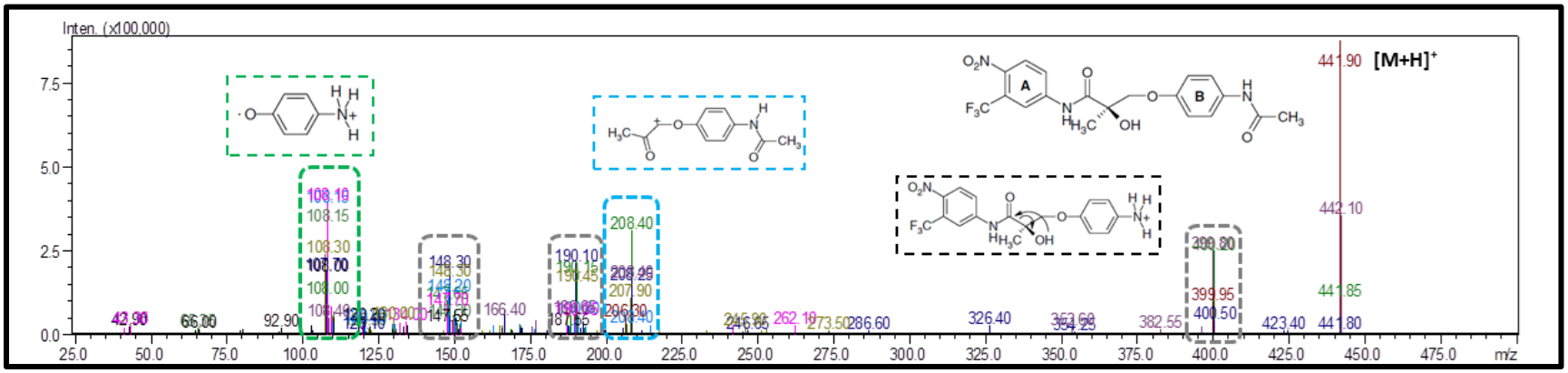

Figure 75. **Overlaid ESI product Ion Spectra of the protonated molecule [M+H]⁺ at m/z 442 of Andarine [ADAR] During the Collision Energy (CE) Selection Step of MRM-Optimization**; showing resulting product ions at 108 *m/z* (CE range = -50 : -30 eV), 208 *m/z* (CE range = -30 : -10 eV), 190 *m/z* (CE range = -35 : -15 eV) and 148 *m/z* (CE range = -40 : -28 eV) produced during the 'CE Select' step of MRM-optimization. **CE select scan range = 1V steps; Centroid-spectrums overlaid and displayed in absolute intensity**.

4.13.3. Zeranol [ZRNL]

Expected Fragmentation for Zeranol from Literature. Fragmentation behavior of ZRNL and its associated metabolites is nearly identical, yielding non-characteristic fragmentation pathways. Due to nearly identical structures and molecular masses this cannot be avoided. Expected fragments that provide the highest sensitivity for these analytes have been described, and include for ZRNL derivatives: 303 *m/z* due to the loss of water and 277 *m/z* formed via cleavage of carbon dioxide.[82],[83],[84]

MRM Optimizations for Zeranol. The deprotonated molecular ion $[M-H]^-$ at *m/z* 321 of Zeranol [ZRNL] produced intense product ions at 235, 259, 277, and 303 *m/z* (**Figure 76**).

MRM-Method Specificity Tests for Zeranol. Methods tests via injections of ZRNL, produced signal for its own MRM-only, while using FIA with no additive as well as with AmFo. The addition of CO_2 to the mobile phase had an effect on the response for ZRNL (**S_Figure 18; C**), where when using methanol as a modifier with no additive ZRNL also gave response for additional MRMs than its own.

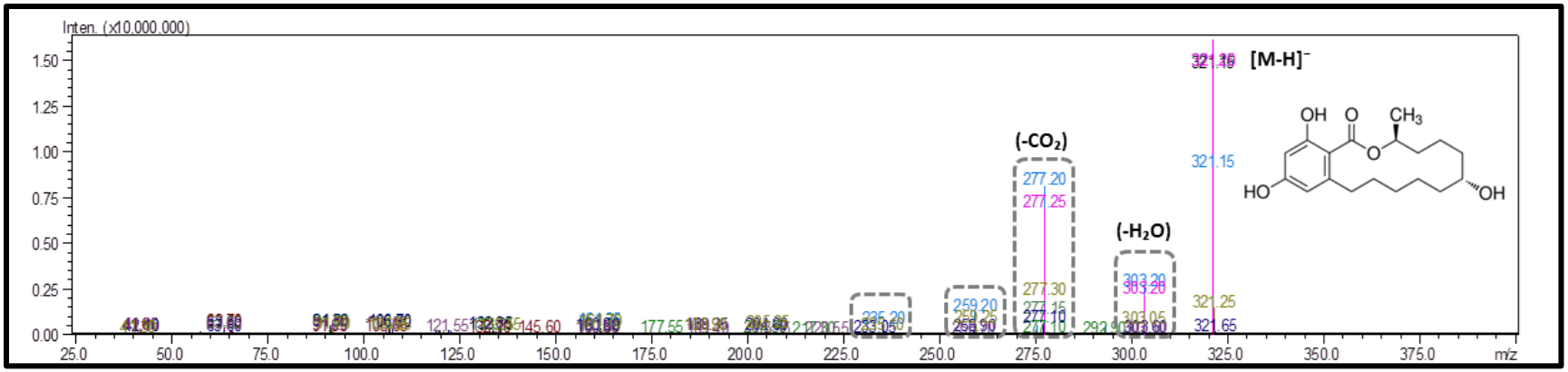

Figure 76. **Overlaid ESI product Ion Spectra of the protonated molecule [M-H]⁻ at m/z 321 of Zeranol [ZRNL] During the Collision Energy (CE) Selection Step of MRM-Optimization**; showing resulting product ions at 277 *m/z* (CE range = +15 : +35 eV), 303 *m/z* (CE range = +15 : +35 eV),259 *m/z* (CE range = +15 : +35 eV) and 235 *m/z* (CE range = +15 : +27 eV) produced during the 'CE Select' step of MRM-optimization. **CE select scan range = 1V steps; Centroid-spectrums overlaid and displayed in absolute intensity**.

4.14. MRM method tests & Critical Groups

The resulting MRM-transitions from optimization with MeOH as MP, as well as Q3 scans are used to ID critical pair groups, by re-injecting each one of our analytes. For example, showing Testosterone and EPIT (**Figure 77)** having the same chemical composition, differing only in the configuration of a single hydroxyl group, give the same mass transitions, and so we will need to rely on our chromatography to separate them. In the case of these steroids, after re-optimizations for mobile phase changes, this process identified three critical groups of compounds we will need to pay special attention to during further development steps.

The 23 anabolic agents were then individually reinjected using the newly optimized MRM method (**Table 17**). Steroids that produced signal for two or more MRMs were investigated further for structural similarities and their Q3 scans compared. This identified five groups of compounds as 'critical pairs', where due to fundamental similarities in structure and/or molecular weight, make differentiation with MS-alone impractical/impossible, and therefore would require chromatographic separation for definitive identification (Final critical groups and relevant transitions are depicted in (**Figure 78**).

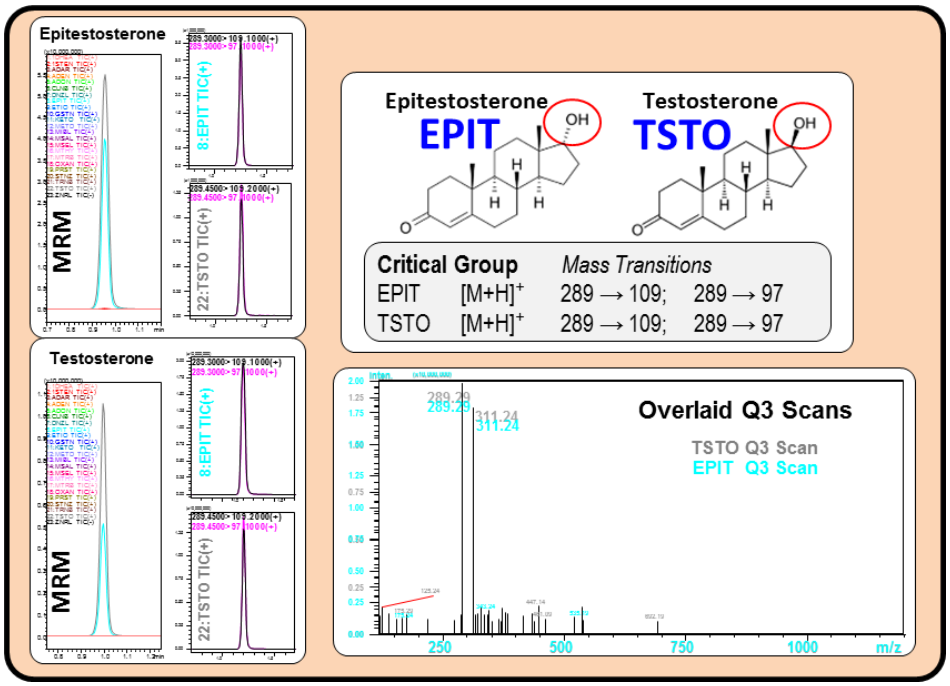

Figure 77. Example Comparison for Critical Group Determination showing EPIT & TSTO.

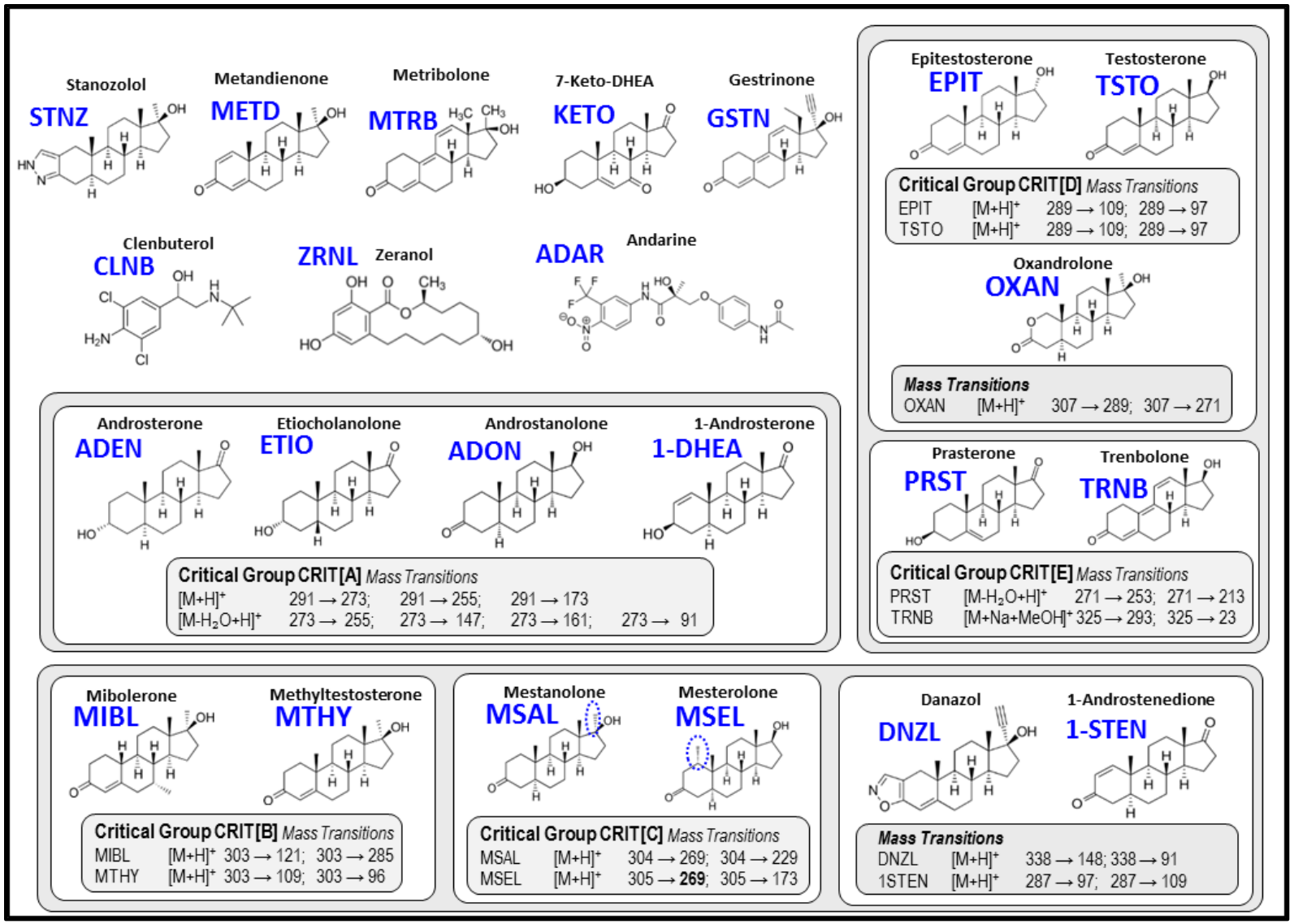

Figure 78. **Structures of Targeted Anabolic agents showing Critical Groups for Chromatographic separation.**

4.14.1. Critical Pair Group #1: *1DHEA, ADEN, ADON & ETIO* (Figure 79).

Individual injections of 1DHEA, ADEN, ADON and ETIO, produced signal for all four MRMs (1DHEA-MRM, ADEN-MRM, ADON-MRM and ETIO-MRM). But each analyte produces a different ion ratio for each MRM depending on the isomer injected. Although all four members of this critical pair' group gave signal for the ADON-MRM, ADON gives signal for only the 1DHEA-MRM and low for its own ADON-MRM, when a signal could be produced. 1DHEA gave the strongest signal for its own 1DHEA-MRM, but also gave signal for both the ETIO-MRM and ADEN-MRM at lower intensity. ADEN and ETIO both give the strongest signal for the ETIO-MRM, followed by the ADEN-MRM, then 1DHEA-MRM and finally the ADON-MRM. But ADEN gives a much stronger signal for its own ADEN-MRM in ratio to the ETIO-MRM intensity. ETIO, on the other hand, gives a much higher signal for its own ETIO-MRM.

ADEN, ETIO and 1DHEA, all C3 hydroxyl steroids, readily lose 2 waters. All start with the $[M+H-H_2O]^+$ precursor ion, and no matter the MP, all produce signal on all three MRMs, although at differing ratios. Each gives the strongest signal for its own MRM when using CO_2 as the majority of the mobile phase, which will need to be relied upon during chromatographic method development, for monitoring initial stages for chromatographic separation.

Summary of Critical Group 1 Implications for Further MD

Critical group 1 contains four analytes: androsterone (ADEN), etiocholanolone (ETIO), 1-androsterone (1DHEA), and androstanolone (ADON). All four members of group 1 are critical to one-another as they all give signal for their own as well as each other's MRMs. ADON was ruled out for use in the current work, as a reliable MRM method could not be determined at this time. The remaining three members of critical group 1 can be distinguished via ion ratios, but only if they are chromatographically separated.

Group 1 Guidelines for Future chromatographic Separation:

- All members must be separated.

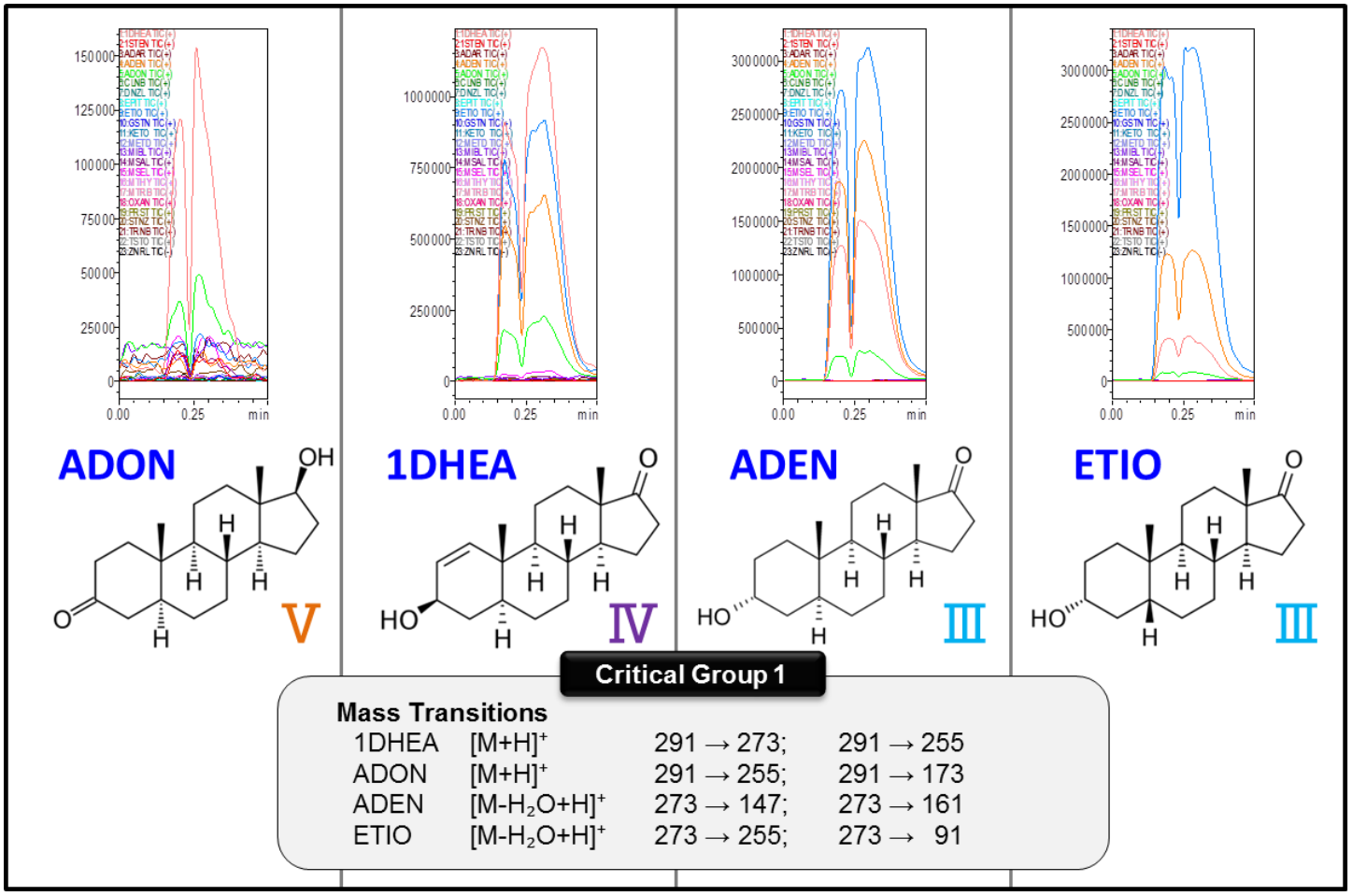

Figure 79. **'Critical Pair' Group #1: 1DHEA, ADEN, ADON & ETIO**

4.14.2. Critical Group #2.

'Critical Pair' 2-B: *MIBL & MTHY* (**Figure 80; Pair 2-B**). Individual Injections of MIBL and MTHY produced signal for both the MIBL-MRM & MTHY-MRM, no matter the mobile phase used. Although always producing signal for eachother's MRMs this is at different ion ratios, depending on which compound is present; When only MIBL is present, both MRMs give equal intensity, but when only MTHY is present, a much lower response is observed for the MIBL-MRM compared to the MTHY-MRM. Although, the most abundant ion for both compounds remains the $[M+H-H_2O]^+$ fragment that both MRMs share. This difference is due to the characteristic fragment ions of 95, 107 and 121 *m/z* chosen to be specific to the MIBL-MRM, making it easy to distinguish between these two compounds if physical separation can be achieved. Chromatographic separation will be required between MIBL and MTHY in quantitative analyses.

'Critical Pair' 2-C: *MSAL & MSEL* (**Figure 80; group 2-C**). Individual injections of both MSAL and MSEL gave relatively equal signal for both the MSAL-MRM and the MSEL-MRM. Additionally both compounds also produce a low signal for the DNZL-MRM. To distinguish between MSAL and MSEL; of the two only MSAL produces a low response to the 1STEN-MRM,

Additional Overlap forming Critical Group 2 (**Figure 80; gray**). Using MeOH with no additive this group is two separate pairs, groups 2-B and 2-C. However, when a buffer is used, additional overlap between MSAL and MSEL with MIBL/MTHY and DNZL and 1STEN, forms "critical Group #2" consisting of all six compounds.

Watch Members of Group 2. DNZL and Pair 2-C. Both MSAL and MSEL (Pair 2-C) also produce a low signal for the DNZL-MRM. Alternatively when DNZL is injected, no response is seen on either the MSAL-MRM, nor on the MSEL-MRM. This points to formation of the $[M+H+MeOH]^+$ adducts of MSAL & MSEL being responsible for producing the signal on the DNZL-MRM, which would match the mass of the DNZL parent ion $[M+H]^+$. Additionally it makes sense that DNZL does not produce signal for the MSAL and MSEL MRMs since there are no possible

fragments of DNZL that would match the mass of the $[M+H]^+$ precursor ions utilized for MSAL or MSEL. Therefore DNZL was not included in this 'critical pair' (group 2-C) and instead included as a watch member of critical group 2 as a whole.

Watch Members of Group 2. 1STEN and Pair 2-C. MSAL (member of pair 2-C) also produces a low response to the 1STEN-MRM, due to the $[M+H-2H_20]^+$ ion producing the same mass as the $[M+H]^+$ ion of 1STEN, but is not observed when only MSEL is present, and furthermore when only 1-STEN is present no response is seen for the MSAL, MSEL &/or the DNZL-MRMs. Therefore, 1STEN was also not included in this 'critical pair' group.

Summary of Critical Group 2 Implications for Further MD

Critical group #2 involves six analytes: 1-androstenedione (1STEN), mestanolone (MSAL), mesterolone (MSEL), methyltestosterone (MTHY), mibolerone (MIBL), and danazol (DNZL). Using MeOH with no additive this group is two separate pairs, groups 2-B and 2-C. However, when a buffer is used, results in additional overlap ultimately including all six compounds collectively representing "critical Group #2". MSAL and MSEL are high priority, critical pair 2-B, as they give equal signal for each other's MRMs and cannot be distinguished via ion ratios. MTHY and MIBL are critical pair 2-C, giving significant signal for each other's MRMs. Unlike pair 2-B, MTHY & MIBL, can be distinguished via ion ratios, if they are chromatographically separated. The separation between these two pairs is also high priority for chromatographic separation, as MIBL and MTHY also give signal for both the MSAL and the MSEL-MRM's when CO_2 is present in the MP. 1STEN and DNZL are watch members of group 2, mainly for Group 2-B, as MSAL and MSEL both give signal for the DNZL-MRM, and MSAL gives signal for the 1STEN-MRM.

Group 2 Guidelines for Future chromatographic Separation:

- MTHY must be separated from MIBL (highest priority), MSAL and MSEL.
- MIBL must be separated from MTHY (highest priority), MSAL and MSEL.
- MSAL must be separated from all members of Group 2.
- MSEL must be separated from MSAL (highest priority), DNZL, and lower priority (MTHY, MIBL).
- DNZL must be separated from MSAL and MSEL.
- 1STEN must be separated from MSAL.

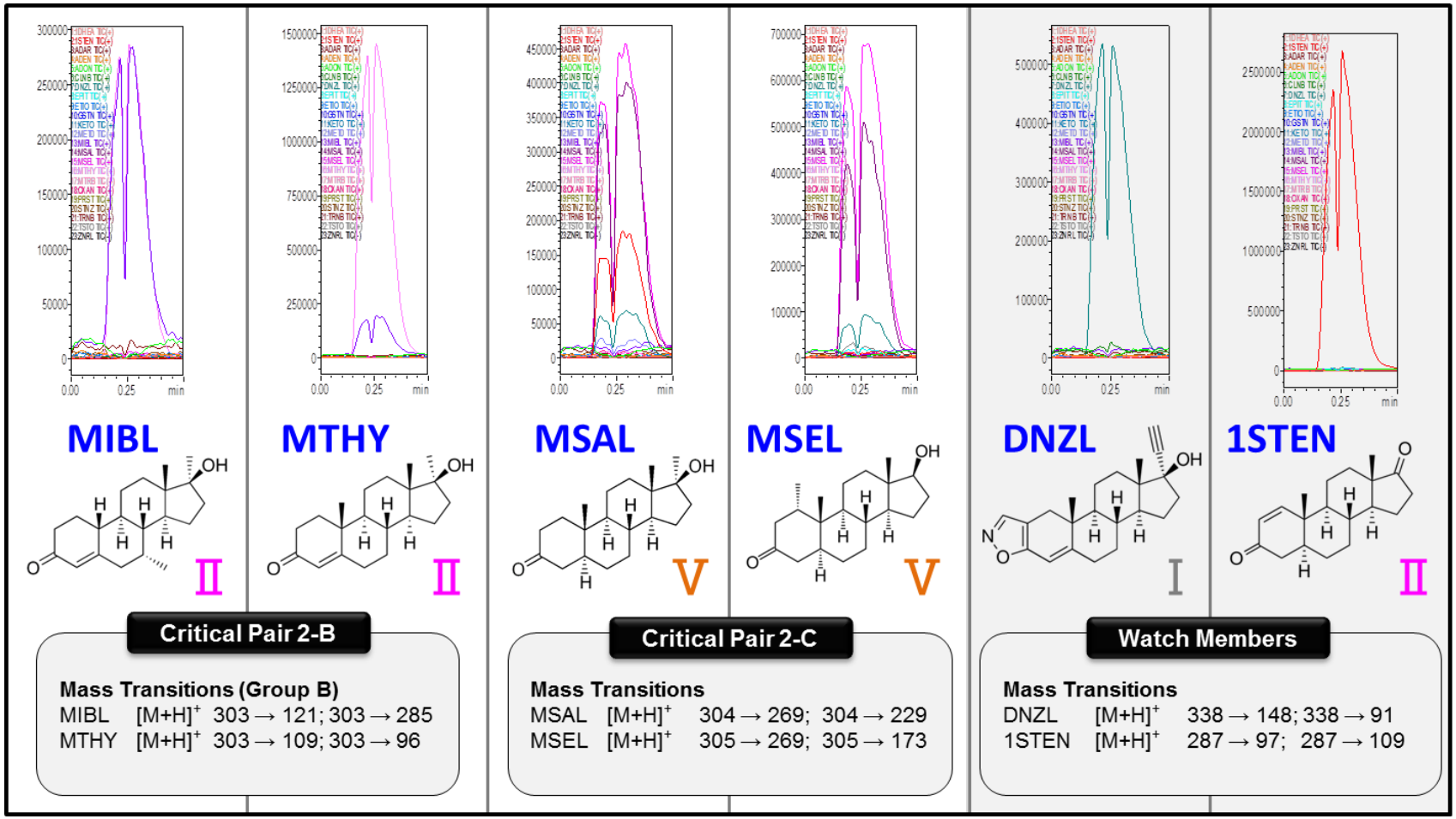

Figure 80. **Critical Group 2: showing similar mass transitions for [Group B] critical pair 2-B (MIBL & MTHY), [Group C] critical pair 2-C (MSAL & MSEL), and [gray] Watch members of critical group 2 (DNZL and 1STEN).**

4.14.3. Critical Group #3.

'Critical Pair' 3-D: *EPIT & TSTO* (**Figure 81; group D**). Injections of both the EPIT and TSTO gave equal intensity response for both the EPIT-MRM and TSTO-MRM. The difference between the two analytes structurally, is simply the position of the C-17 hydroxyl, making them epimers. Being α-/ß- epimers on the position of a single hydroxyl group at C17, the molecular weights and fragmentation patterns are identical. Since the D ring does not influence the fragmentation, this positional isomerization is not helpful to differentiate between the two using MS alone. *(note that if the α-/ß- isomerism was located at C5, ion ratio could have possibly been helpful via isomeric differences in ion production ratios due to differing fragmentation patterns)*. Maybe the most critical of the critical pairs identified in this work, differentiation between EPIT and TSTO will require individual injections after chromatographic separation, and differentiation will depend on retention time verification.

'Critical Pair' 3-E: ***PRST & TRNB*** (**Figure 81; group E**).

Although injections of TRNB produces signal for both its own MRM and for the PRST-MRM (transitions #1; 271 *m/z* → 253 *m/z*, and transition #2 [271 → 213 *m/z*]), this must be expected as the precursor ion for TRNB (271 *m/z;* $[M+H]^+$) is the same *m/z* as the precursor for PRST (*m/z* 271; $[M+H-H_2O]^+$). Additionally transition #1 for TRNB corresponds with the major fragment ion for TRNB (*m/z* 253; $[M+H-H_2O]^+$) which coincides with the major fragment ion due to two water losses for PRST (*m/z* 253; $[M+H-2H_2O]^+$). Alternatively, injections of PRST does not produce a signal for the TRNB-MRM, as should be expected as PRST would not produce the precursor ion for TRNB that is much higher than its own MW. This difference in selectivity makes this critical pair the easiest to distinguish between the two isomers, but chromatographic separation will be required to avoid bias for quantitative applications.

Additional Overlap forming Critical Group 3 (Figure 81)

PRST and Pair 3-D. Injections of PRST also produced low signals for other MRMs, including both the EPIT-MRM & TSTO-MRM (Critical pair 3-D, described above). Although, neither EPIT nor TSTO gave signal for the PRST-MRM. Chromatographic separation of PRST from critical pair 3-D will be important in further method optimizations.

Watch Members of Group 3. OXAN. Additionally Injections of OXAN also gave signal for both the EPIT-MRM and TSTO-MRMs, pointing towards the formation of the OXAN $[M+H-H_20]^+$ ion (289 *m/z*; $[M+H]^+$) which matches the precursor ions of both EPIT and TSTO. Alternatively, neither injections of EPIT-alone, nor TSTO-alone gave signal for the OXAN-MRM, and therefore OXAN was not included in 'critical pair 3-D'; but instead the addition of OXAN as a 'watch member' completes critical group 3.

Summary of Critical Group 3 Implications for Further MD

Critical group #3 involves five analytes: testosterone (TSTO), epitestosterone (EPIT), oxandrolone (OXAN), prasterone (PRST), and trenbolone (TRNB). EPIT and TSTO are high priority, critical pair 3-D, giving nearly equal signal for each other's MRMs and cannot be distinguished via ion ratios. PRST and TRNB are critical pair 3-E, as TRNB gives strong signal for the PRST-MRM. The separation of PRST from group 3-D is also important as PRST gives signal for both the TSTO and EPIT-MRMs, especially with CO_2-based MPs. Additionally, the separation of OXAN from 3-D is also important, as it also gives signal for both the TSTO and EPIT-MRMs.

Group 3 Guidelines for Future chromatographic Separation:

- PRST must be separated from all members of group 3, except OXAN.
- OXAN must be separated from EPIT and TSTO.
- TSTO & EPIT must be separated from eachother and OXAN.
- TRNB must be separated from PRST only.

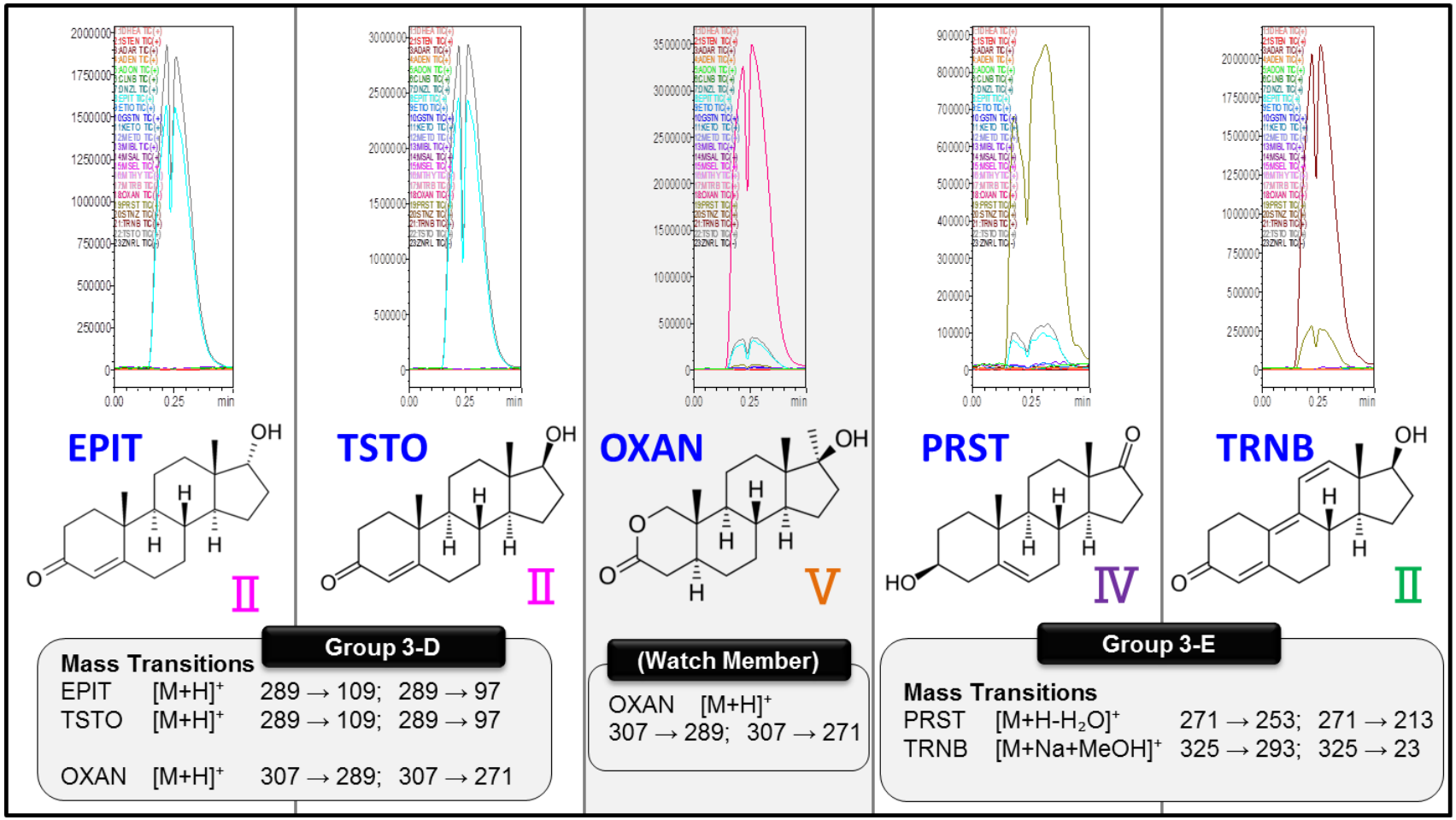

Figure 81. **Critical Group 3 : showing similar mass transitions for critical pair 3-D (TSTO & EPIT) and critical pair 3-E (TRNB & PRST), and Watch member of critical group 3 (OXAN).**

4.15. Final Comments

Original optimization was performed using the molecular weight for each compounds and the resulting MRMs were tested by reinjecting each compound (still using FIA with MeOH). For the majority of the compounds, using the molecular weight obtained from literature was successfully used as the precursor ion for during MRM optimization (using FIA with MeOH) which included: 1DHEA, 1STEN, ADAR, CLNB, DNZL, EPIT, GSTN, METD, MIBL, MTRB, OXAN, STNZ, TSTO, and ZRNL. For the remaining compounds, the most intense ion from the Q3 scans using MeOH, were successfully used as the precursor ion for ADEN, ETIO, KETO, and PRST. This was corroborated from literature where it is reported that the androgen steroids commonly ionize thru the neutral loss of water producing a reliable fragment precursor ion $[M+H-H_2O]^+$. ADON, MSAL, and MSEL all required additional optimization which is ongoing. Three major 'critical groups' were identified which due to MRM overlap will require chromatographic separation in further method development steps.

Final Recommendations: For ADON, no reliable MRM-method could be established at this time. Further optimization is necessary, and therefore ADON will not be included in the current work. Similar issues were seen between MSAL and MSEL, where under some conditions produce very unreliable signals, presumably due to changes either in precursor ion and/or excessive multiple ion formation reducing the sensitivity to below detection. MSAL and MSEL do produce a reliable signal most of the time, so could be monitored qualitatively for resolution purposes in the meantime, but they are not recommended for quantitative analysis under the current conditions. Furthermore, PRST and all of critical group 1 will need to be closely watched for any changes in response.

4.i. Instrument Methods: MS-Optimization for MRMs.

4.i.1. General Method Information.

Detailed information on materials and equipment used for MRM-optimizations performed in this study can be found in the following sections of **Chapter #2. Materials and Methods**:

4.i.1.1. Materials.

- Solvents used for mobile phases and dilution solutions can be found in **Section 2.1.1. Solvents**.
- Analytical standards information for targeted anabolic agents can be found in **Section 2.1.2. Analytical Standards; *Anabolic androgenic steroids (AAS)*** **and** **Table 1.**

4.i.1.2. Instrumentation.

- The Instrumentation used is detailed in **Section 2.2.1. Instrumentation; *Nexera UC online SFE-SFC-MS***.
- Other equipment used is detailed in **Section 2.2.3. Other Equipment:**
    - ***Nitrogen Generator***
    - ***Analytical balances***

4.i.1.3. Solutions Preparation.

- Stock Solutions prep and storage detailed in **Section 2.3.1.1. AAS Stock Solutions** and **Table 6; Stock Solutions.**
- Injection solutions prep and concentrations are described in **Section 2.3.1.2. AAS MS-Optimization Solutions** and **Table 6; *MRM Solutions*.**

4.i.2. MS Parameters – MRM Optimizations

Detection was achieved using an LCMS-8050 triple quadrupole mass spectrometer, equipped with an DUIS-source, and operated in Electrospray Ionization (ESI-), positive (+) and negative (-) ionization mode. Interface voltages were set to 4.0 kV (for positive Q3 scan mode) and -3.0 kV (for negative Q3 scan mode) and temperature set to 300 °C. Nitrogen gas was used for both drying and nebulizing gas; with flow rate of 2.0 L/min for nebulizing gas and 10.0 L/min for drying gas. Desolvation and DL temperatures were 526 °C and 250 °C respectively. Heat Block temperature was set to 400 °C, and heating gas used was dry air. Gas used for collision induced dissociation (CID) was argon at 270 kPa. DL Bias/Q-array Bias were set in tuning file as 0 V, and Q3 Pre-rod Bias at -15 V (for positive scan mode) and 15 V (for negative scan mode).

4.i.3. Mobile Phases (MP).

Three modifiers were used: [MeOH] LCMS-grade methanol; [FA] LCMS-grade methanol + 0.1% formic acid (LCMS-grade); [AmFo] LCMS-grade methanol + 5 mM ammonium formate (LCMS-grade). All modifier solutions were sonicated for 20 minutes prior to use.

In the case of FIA-analysis, 100% modifier was used as MP. In the case of SFC/CO_2-based MPs, up to 40% modifier was mixed with liquid Carbon Dioxide ([CO_2] – Instrument grade) via the instrument solvent delivery pumps. See below for specific details for each case.

Typically if CO_2 was used, injections were performed using multiple modifier concentrations (e.g., 40, 20 & 10% modifier). Runtimes would be changed accordingly if and when a column was installed. All injections were automated via Batch Table.

4.i.4. Instrument Parameters for MRM-optimizations using FIA.

4.i.4.1. Instrument Setup: FIA-MS Optimization Mode

Detailed instrument configuration details can be found in **Chapter #1: Hyphenated Instrumentation: SFE-SFC-MS** (**Section 1.3.1: Instrument Configurations: *FIA-MS Optimization Mode***). In short, the solvent modifier pump (Pump B), was connected directly to the injector switching valve, MRM solutions were introduced into the flow stream via a 5.0-µL external loop using partial loop injections of 1.0 µL. A short piece of restrictive tubing was placed between the injector outlet and connected to the MS interface inlet.

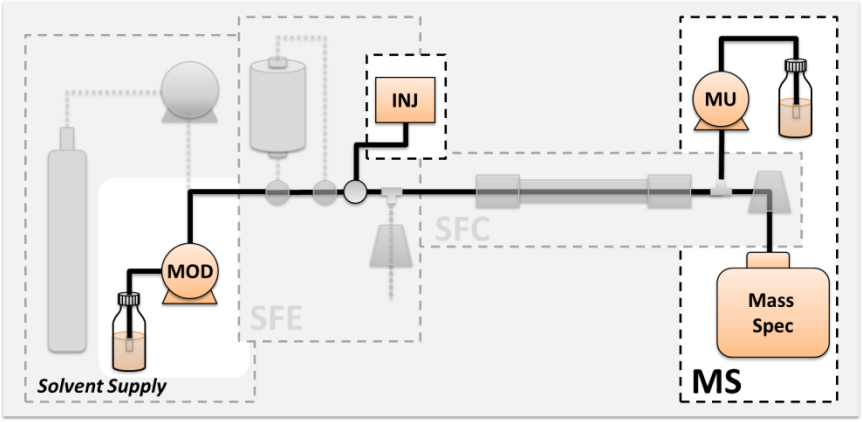

See Figure 12 in Chapter #1

4.i.4.2. Instrument Parameters: used for FIA-mode MRM Optimizations.

Total Flow of 0.25 mL/min, of 100% Pump B, were delivered. All CO_2 delivery units were switched off, and CO_2 shutoff valve set to closed. BPRs and column oven switched to Off. One microliter injections were made via a 5.0-µL external loop, with 0.1 µL air gaps, 5.0 µL/sec sampling speed, and 1.0 µL/sec discharge speed. Needle rinse mode set to before and after aspiration, with rinsing speed of 35 µL/sec and rinsing volume of 500 µL using methanol.

4.i.5. Instrument Parameters for MRM-optimizations using CO_2-based MPs.

4.i.5.1. Instrument Setup: CO_2-MS Optimization Mode

Detailed instrument configuration details can be found in **Chapter #1: Hyphenated Instrumentation: SFE-SFC-MS** (**Section 1.3.2: Instrument Configurations: *CO_2-MS Optimization Mode***). In short, operation with CO_2-based MPs requires not only the operation of the CO_2-delivery pump and outlet pressure regulation, but additionally in order to maintain pressure equilibrium across the system, a restrictor or column must be installed, to provide a stable delta pressure between the pumps and back pressure regulator (BPR). Therefore, a mixer (post-pumps & pre-injector), and a BPR (post-column & pre-MS inlet) is plumbed into the flow path.

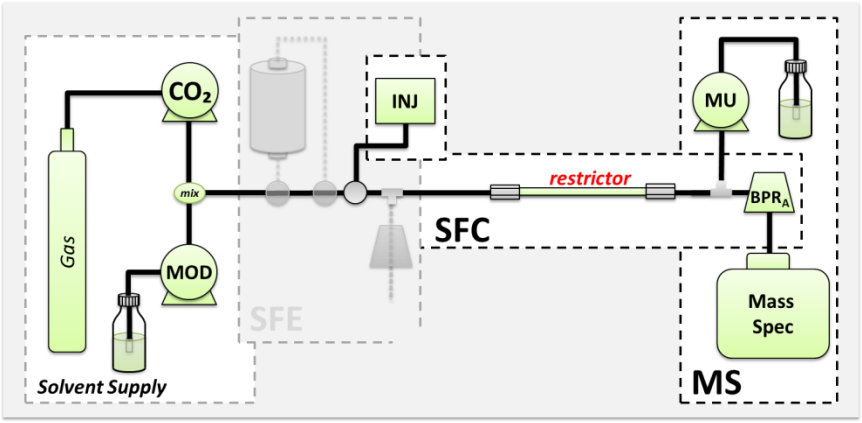

See Figure 13 in Chapter #1

4.i.5.2. Instrument Parameters: used for CO_2-mode MRM Optimizations.

A column used, and was an Agilent Zorbax Cyano (3.5 µm d_p, 4.6 x 150 mm) column (Agilent Technologies, Santa-Clara, CA. USA). Modifier concentrations of 40, 20 and 10% in CO_2 were delivered at 3.0 mL/min, using a BPR [A] outlet pressure of 15 MPa and column oven temperature of 50 °C. One microliter injections were made via a 5.0-µL external loop, with 0.1 µL air gaps, 5.0 µL/sec sampling speed, and 1.0 µL/sec discharge speed. Needle rinse mode set to before and after aspiration, with rinsing speed of 35 µL/sec and rinsing volume of 500 µL using methanol.

Literature Cited:

FIRST CITED IN PREVIOUS CHAPTERS

[32] Thevis M, Schanzer W. (2006). "Mass spectrometry in sports drug testing: structure characterization and analytical assays." *Mass Spectrometry Reviews*. **26**(1): p79-107. https://doi.org/10.1002/mas.20107

[33] Schanzer W, Thevis M. (2015). "human sports drug testing by mass spectrometry." *Mass Spectrometry Reviews.* **36**(1): p16–46. https://doi.org/10.1002/mas.21479

[35] Pozo OJ, Van Eenoo P, Deventer K, Delbeke FT. (2017). "Development and validation of a qualitative screening method for the detection of exogenous anabolic steroids in urine by liquid chromatography-tandem mass spectrometry." *Analytical and Bioanalytical Chemistry.* **389**: p1209–1224. https://doi.org/10.1007/s00216-007-1530-6

[36] Pozo OJ, Van Eenoo P, Deventer K, Delbeke FT. (2007). "Ionization of anabolic steroids by adduct formation in liquid chromatography electrospray mass spectrometry." *Journal of Mass Spectrometry.* **42**(4): p497-516. https://doi.org/10.1002/jms.1182

[43] Gurst JE, Djerassi C. (1964). "Mass Spectrometry in Structural and Stereochemical Problems. LIX. Mechanism of the formal loss of acetone from 2-oxo-5α-steroids." *Journal of the American Chemical Society.* **86**(24): p5542 – 5547. https://doi.org/10.1021/ja01078a029

[45] Thevis M, Schanzer W. (2005). "Mass Spectrometric Analysis of Androstan-17ß-ol-3-one and Androstadiene-17ß-ol-3-one Isomers." *Journal of the American Society for Mass Spectrometry.* **16**(10): p1660–1669. https://doi.org/10.1016/j.jasms.2005.06.007 **[42]** Akbal L, Hopfgartner G. (2020). "Hyphenation of packed column supercritical fluid chromatography with mass spectrometry: where are we and what are the remaining challenges?" *Analytical and Bioanalytical Chemistry*. **412**: p6667–6677. https://doi.org/10.1007/s00216-020-02715-4

[47] Thevis M, Guddat S, Schanzer W. (2009). "Doping control analysis of trenbolone and related compounds using liquid chromatography–tandem mass spectrometry." Steroids. **74**(3): p315-321. https://doi.org/10.1016/j.steroids.2008.10.004

[48] Guan F, Soma LR, Luo Y, Uboh CE, Peterman S. (2006). "Collision-Induced Dissociation Pathways of Anabolic Steroids by Electrospray Ionization Tandem Mass Spectrometry." *Journal of the American Society for Mass Spectrometry.* **17**(4): p477–489. https://doi.org/10.1016/j.jasms.2005.11.021

NEW TO THIS CHAPTER

[50] Williams TM, Kind AJ, Houghton E, Hill DW. (1999). "Electrospray Collision-induced Dissociation of Testosterone and Testosterone Hydroxy Analogs." *Journal of Mass Spectrometry.* **34**(3): p206-216. https://doi.org/10.1002/(SICI)1096-9888(199903)34:3<206::AID-JMS785>3.0.CO;2-1

[51] Schanzer W, Thevis M. (2017). "human sports drug testing by mass spectrometry." *Mass Spectrometry Reviews.* **36**(1): p16–46. https://doi.org/10.1002/mas.21479

[52] Cha E, Kim S, Kim HJ, Lee KM, Kim KH, Kwon O-S, Lee J. (2015). "Sensitivity of GC-EI/MS, GC-EI/MS/MS, LC-ESI/MS/MS, LC-Ag+CIS/MS/MS, and GC-ESI/MS/MS for analysis of anabolic steroids in doping control." *Drug Testing and Analysis.* **7**(11-12): p1040–1049. https://doi.org/10.1002/dta.1906

[53] Pozo OJ, van Eenoo, Deventer K, Lootens L, Grimalt S, Sancho JV, Hernandez F, Delbeke FT. (2008). "General guidelines for the CID fragmentation of 3-keto-anabolic steroids." In: W Schänzer, H Geyer, A Gotzmann, U Mareck (eds.) Recent Advances In Doping Analysis (16). Sport und Buch Strauß - Köln 2008. pp. 131. https://www.dshs-koeln.de/fileadmin/redaktion/Institute/Biochemie/PDF/Proceedings/Proceedings_16/16_pp_131-140.pdf

[54] Karliner J, Budzikiewicz H, Djerassi C. (1966). " Mass Spectrometry in Structural and Sterochemical Problems. XCI. The electron Impact induced Elimination of Water from 3-Hydroxy Steroids." *The Journal of Organic Chemistry.* **31**(3): p710–713. https://doi.org/10.1021/jo01341a015

[55] Thevis M, Makarov AA, Horning S, Schanzer W. (2005). "Mass spectrometry of stanozolol and its analogues using electrospray ionization and collision-induced dissociation with quadrupole-linear ion trap and linear ion trap-orbitrap hybrid mass analyzers." *Rapid Communications in Mass Spectrometry.* **19**(22): p3369–3378. https://doi.org/10.1002/rcm.2204

[56] Pozo OJ, van Eenoo P, Deventer K, Grimalt S, Sancho JV, Hernandez F, Delbeke FT. (2008). "Collision-induced dissociation of 3-keto anabolic steroids and related compounds after electrospray ionization. Considerations for structural elucidation." *Rapid Communications in Mass Spectrometry.* **22**(24): p4009–4024. https://doi.org/10.1002/rcm.3823

[57] Thevis M, Fubholler G, Geyer H, Rodchenkov G, Mareck U, Sigmund G, Koch A, Thomas A, Schanzer W. (2006). "Detection of Stanozolol and Its Major Metabolites in Human Urine by Liquid Chromatography-Tandem Mass Spectrometry." *Chromatographia*. **64**: p441-446. https://doi.org/10.1365/s10337-006-0043-3

[58] Thevis M, Beuck S, Hoppner S, Thomas A, Held J, Schafer M, Oomens J, Schanzer W. (2012). "Structure Elucidation of the Diagnostic Product Ion at *m/z* 97 Derived from Androst-4-en-3-One-Based Steroids by ESI-CID and IRMPD Spectroscopy." *Journal of the American Society for Mass Spectrometry.* **23**(3): p537-546. https://doi.org/10.1007/s13361-011-0308-4

[59] Thevis M, Bommerich U, Opfermann G, Schanzer W. (2005). "Characterization of chemically modified steroids for doping control purposes by electrospray ionization tandem mass spectrometry." *Journal of Mass Spectrometry.* **40**(4): p494–502. https://doi.org/10.1002/jms.820

[60] Verhayden K, Le Bizec B, Courtheyn D, Mortier V, Vandewiele M, Gillis W, Vanthemsche P, De Brabander HF, Noppe H. (2007). "Mass spectrometric detection of and similarities between 1-androgens." *Analytica Chimica Acta.* **586**(1-2): p57–72. https://doi.org/10.1016/j.aca.2006.10.058

[61] Shapiro RH, Williams DH, Budzikiewicz H, Djerassi C. (1964). " Mass Spectrometry in Structural and stereochemical problems. LIII. Fragmentation and Hydrogen Transfer Reactions of a Typical 3-Keto Steroid, 5α-Androstan-3-one." *Journal of the American Chemical Society.* **86**(14): 2837-2845. https://doi.org/10.1021/ja01068a016

[62] Shapiro RH, Djerassi C. (1964). "Mass Spectrometry in Structural and stereochemical problems. L. Fragmentation and hydrogen migration Reactions of α,ß-Unsaturated 3-Keto Steroids." *Journal of the American Chemical Society.* **86**(14): p2825–2832. https://doi.org/10.1021/ja01068a014

[63] Kochnova E, Sobolevsky T, Sizoi V, Rodchenkov G. (2009). "Calibration issue for the quantitative determination of endogenous steroids: the comparison of 6 matrices." In: Schanzer W, Geyer H, Gotzmann A, Mareck U (eds.). Recent Advances in Doping Analysis (17), Köln, pp. 47-62. https://www.dshs-koeln.de/fileadmin/redaktion/Institute/Biochemie/PDF/Proceedings/Proceedings_17/17_pp_253-256.pdf

[64] Putz M, Piper T, Thevis M. (2020). "Identification of Trenbolone Metabolites Using Hydrogen isotope Ratio Mass Spectrometry and Liquid Chromatography/High Accuracy/High Resolution Mass Spectrometry for Doping Control Analysis." *Frontiers in Chemistry.* **8**: p435. https://doi.org/10.3389/fchem.2020.00435

[65] Schanzer W, Geyer H, Donike M. (1999). "Metabolism of Metandienone in man: Identification and Synthesis of conjugated excreted urinary metabolites, determination of excretion rates and gas chromatographic-mass spectrometric identification of bis-hydroxylated metabolites." *The Journal of Steroid Biochemistry and Molecular Biology.* **38**(4): p441-464. https://doi.org/10.1016/0960-0760(91)90332-Y

[66] Thevis M, Piper T, Horning S, Juchelka D, Schanzer W. (2013). "Hydrogen isotope ratio mass spectrometry and high-resolution/high-accuracy mass spectrometry in metabolite identification studies: Detecting target compounds for sports drug testing." *Rapid Communications in Mass Spectrometry.* **27**(17): p1904–1912. https://doi.org/10.1002/rcm.6648

[67] Martinez-Brito D, de la Torre X, Colamonici C, Curcio D, Botre F. (2019). "7-ketoDHEA metabolism in humans. Pitfalls in interpreting the analytical results in the antidoping field." *Drug Testing and Analysis.* **11**(11-12): p1629-1643. https://doi.org/10.1002/dta.2734

[68] Budzikiewicz H, Djerassi C. (1962). "Mass Spectrometry in Structural and Stereochemical Problems. I. Steroid Ketones." *Journal of the American Chemical Society.* **84**(8): p1430–1439. https://doi.org/10.1021/ja00867a019

[69] Musharraf SG, Ali A, Khan NT, Yousuf M, Chaudhary MI, Rahman A. (2013). "Tandem mass spectrometry approach for the investigation of the steroidal metabolism: Structure–fragmentation relationship (SFR) in anabolic steroids and their metabolites by ESI-MS/MS analysis." *Steroids*. **78**(2): p171-181. https://doi.org/10.1016/j.steroids.2012.10.017

[70] Egger H, Spiteller G. (1966). "Massenspektren und stereochemie von hydroxyverbindungen, 1. Mitt.: Hydroxysteroide." *Mh Chem* **97**: p579–601. https://doi.org/10.1007/BF00905276

[71] Leinonen A, Kuuranne T, Kotiaho T, Kostianinen R. (2004). "Screening of free 17-alkyl-substituted anabolic steroids in human urine by liquid chromatography-electrospray ionization tandem mass spectrometry." *Steroids*. **69**(2): p101-109. https://doi.org/10.1016/j.steroids.2003.10.007

[72] Gorityala S, Yang S, Montano MM, Xu Y. (2018). "Simultaneous determination of dihydrotestosterone and its metabolites in mouse sera by LC-MS/MS with chemical derivatization." *Journal of Chromatography B.* **1090**: p22–35. https://doi.org/10.1016/j.jchromb.2018.05.008

[73] Schanzer W, Thevis M. (2015). "human sports drug testing by mass spectrometry." *Mass Spectrometry Reviews*. **36**(1): p16–46. https://doi.org/10.1002/mas.21479

[74] Yan Z, Wu M, He G, Dong Y, Ouyang G, Wu Y, Lu J, Yang S, Xu Y, Wang X. (2013). "An Improved LC-MS-MS method for the determination of Clenbuterol in Human Urine." *LCGC North America*. **31**(3): p240-247.

[75] Thevis M, Opfermann G, Schanzer W. (2003). "Liquid chromatography/electrospray ionization tandem mass spectrometric screening and confirmation methods for ß2-agonists in human or equine urine." *Journal of Mass Spectrometry.* **38**(11): p1197–1206. https://doi.org/10.1002/jms.542

[76] Biancotto G, Angeletti R, Piro RDM, Favretto D, Traldi P. (1997). "Ion Trap High-performance Liquid Chromatography/Multiple Mass Spectrometry in the Determination of $ß_2$-Agonists in Bovine Urines." *Journal of mass spectrometry*. **32**(7): p781-784. https://doi.org/10.1002/(SICI)1096-9888(199707)32:7<781::AID-JMS532>3.0.CO;2-5

[77] Cai J, Henion J. (1997). "Quantitative multi-residue determination of ß-agonists in bovine urine using on-line immunoaffinity extraction-coupled column packed capillary liquid chromatography-tandem mass spectrometry." *Journal of Chromatography B*. **691**(2): p357-370. https://doi.org/10.1016/S0378-4347(96)00433-1

[78] Thevis M. (2009). "Detection of the arylpropionamide-derived selective androgen receptor modulator (SARM) S-4 (Andarine) in a black-market product." *Drug Testing and Analysis.* **1**(8): p387–392. https://doi.org/10.1002/dta.91

[79] Thevis M, Schanzer W. (2008). "Mass Spectrometry of selective androgen receptor modulators." *Journal of Mass Spectrometry.* **43**(7): p865-876. https://doi.org/10.1002/jms.143

[80] Thevis M, Volmer DA. (2018). "Mass spectrometric studies on selective androgen receptor modulators (SARMs) using electron ionization and electrospray ionization/collision-induced dissociation." European Journal of Mass Spectrometry. **24**(1): p145–156. https://doi.org/10.1177/1469066717731228

[81] Thevis M, Thomas A, Fubholler G, Beuck S, Geyer H, Schanzer W. (2010). "Mass spectrometric characterization of urinary metabolites of the selective androgen receptor modulator andarine (S-4) for routine doping control purposes." *Rapid Communications in Mass Spectrometry.* **24**(15): p2245–2254. https://doi.org/10.1002/rcm.4637

[82] Launay FM, Young PB, Sterk SS, Blokland MH, Kennedy DG. (2004). "Confirmatory assay for zeranol, taleranol and the Fusarium spp. toxins in bovine urine using liquid chromatography-tandem mass spectrometry." *Food Additives and Contaminants*. **21**(1): p52–62. https://doi.org/10.1080/02652030310001636930

[83] Jodlbauer J, Zollner P, Lindner W. (2000). "Determination of Zeranol, Taleranol, Zearalenone, α- and ß-Zearalenol in Urine and Tissue by High-Performance Liquid Chromatography-Tandem Mass Spectrometry." *Chromatographia*. **51**: p681-687. https://doi.org/10.1007/BF0250540

[84] Thevis M, Fubholler G, Schanzer W. (2011). "Zeranol: doping offence or mycotoxin? A case-related study." *Drug Testing and Analysis.* **3**(11/12): p777–783. https://doi.org/10.1002/dta.352

S_4. SUPPLEMENTARY MATERIALS

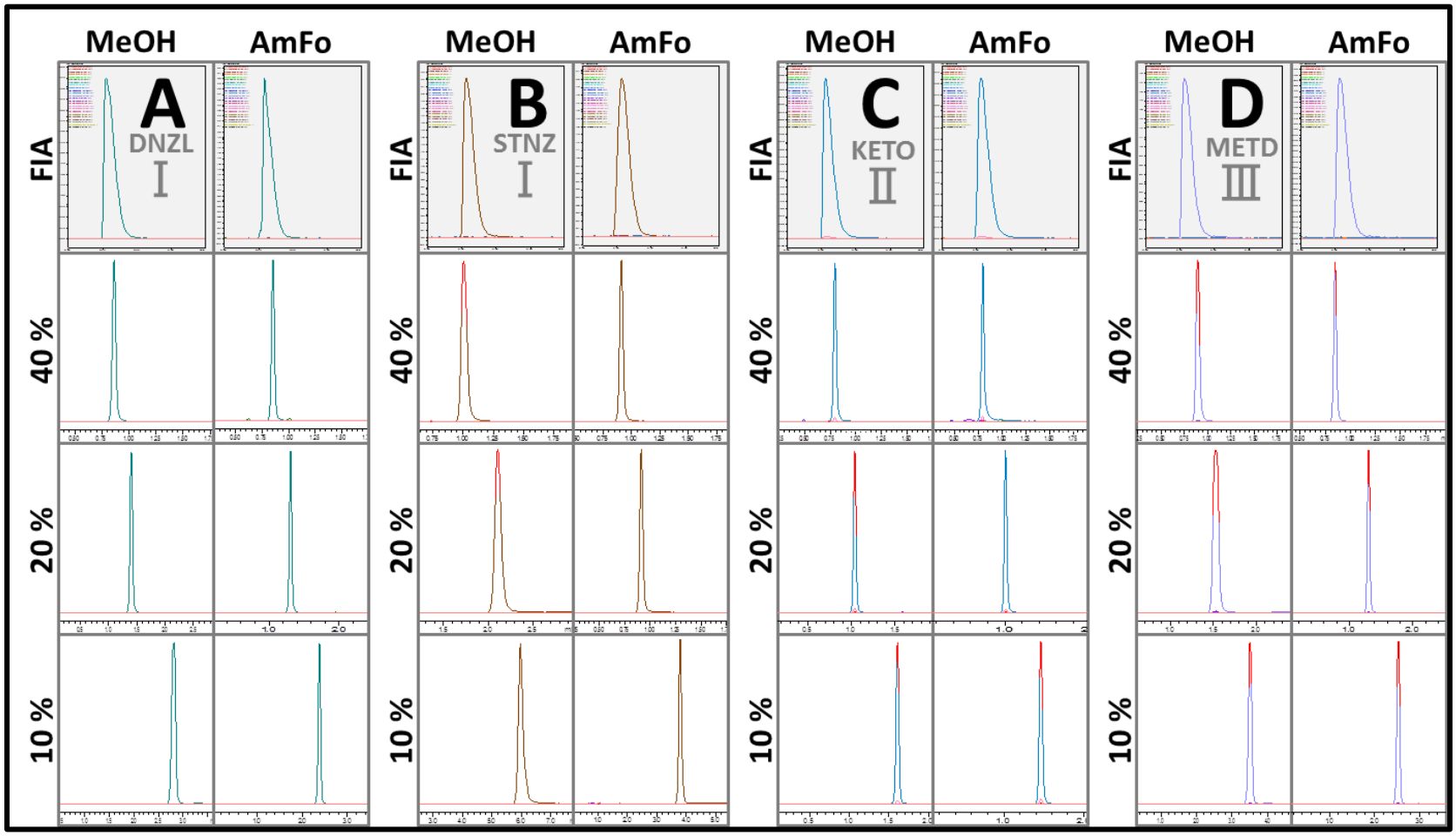

S_Figure 13. **SFC-MS Chromatograms MRM-Specificity Test for Injections of (A) danazol [DNZL]; (B) stanozolol [STNZ]; (C) 7-Keto-DHEA [KETO] and (D) metandienone [METD] showing Effect of Mobile Phase Composition.** Comparing Flow Injection Analysis [(FIA); Top Gray Panel] to Carbon Dioxide modified with methanol; without additive (MeOH) and with additive (MeOH +5mM ammonium formate [AmFo]) at three concentrations (40%, 20% and 10%).

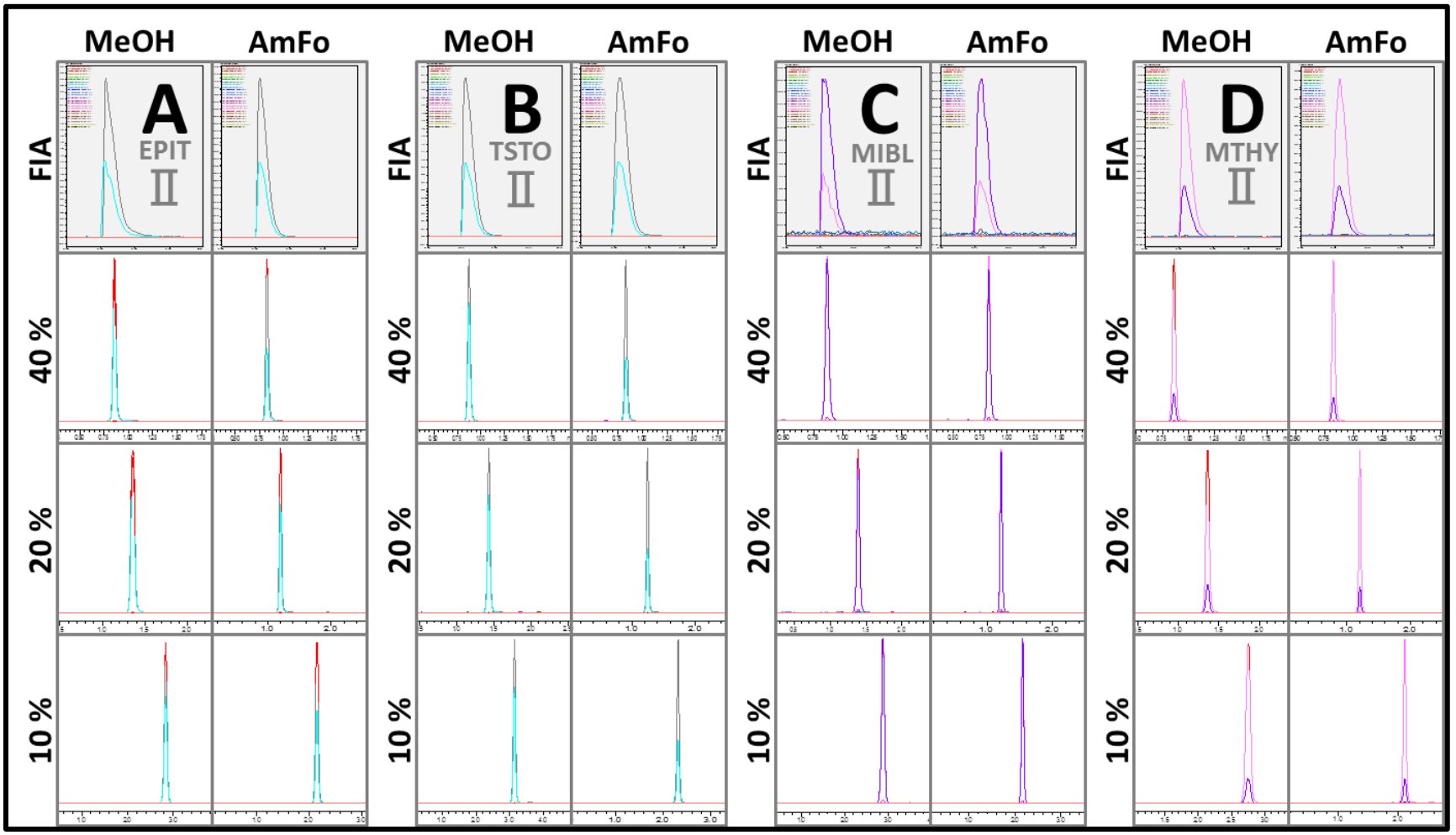

S_Figure 14. **SFC-MS Chromatograms MRM-Specificity Test for Injections of (A) epitestosterone [EPIT], (B) testosterone [TSTO], (C) mibolerone [MIBL] and (D) methyltestosterone [MTHY] showing Effect of Mobile Phase Composition.** Comparing Flow Injection Analysis [(FIA); Top Gray Panel] to Carbon Dioxide modified with methanol; without additive [MeOH] and with additive (MeOH +5mM ammonium formate [AmFo]) at three concentrations (40%, 20% and 10%).

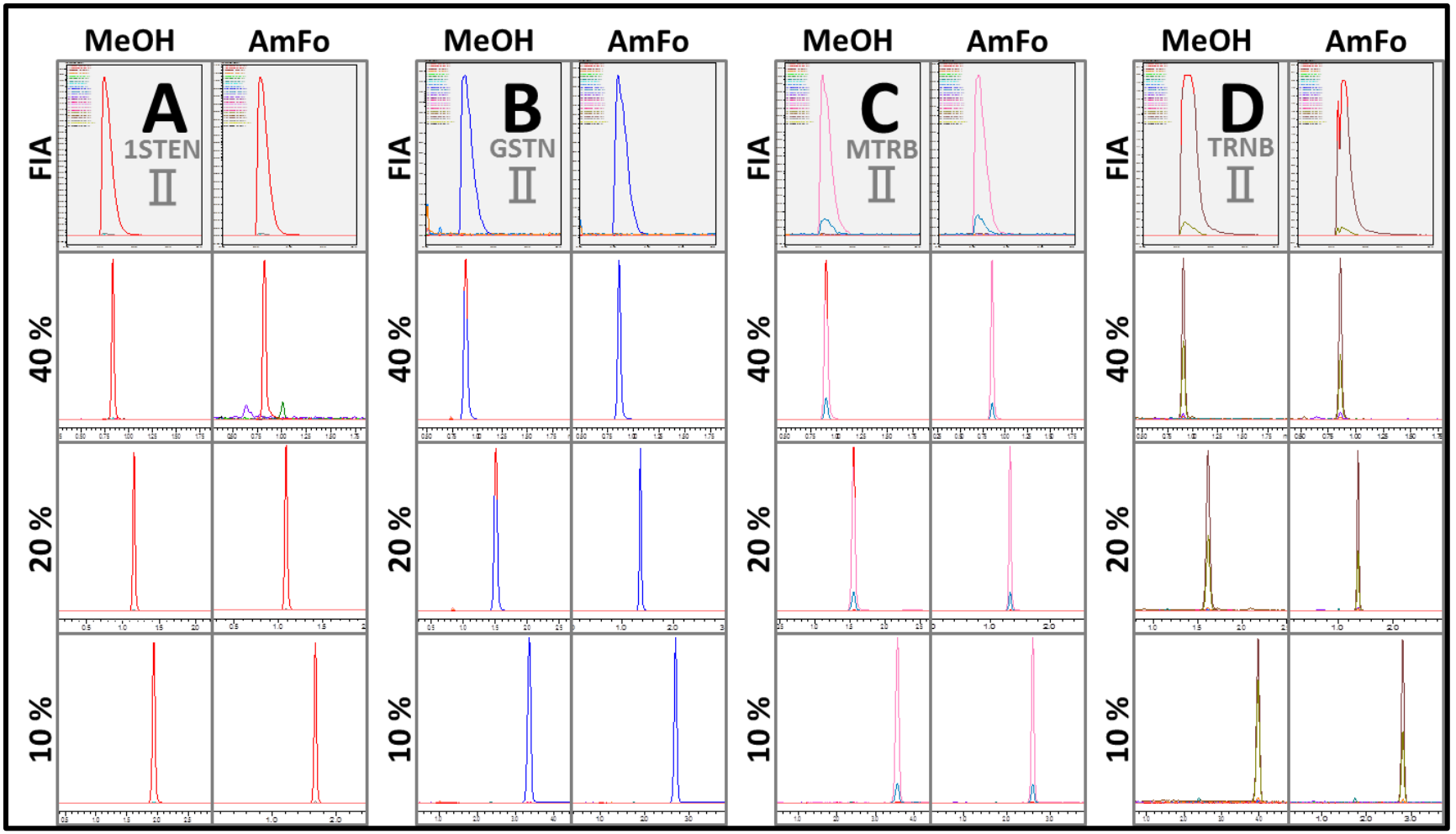

S_Figure 15 SFC-MS Chromatograms MRM-Specificity Test for Injections of (A) 1-androstenedione [STEN], (B) gestrinone [GSTN], (C) metribolone [MTRB], and (D) trenbolone [TRNB] showing Effect of Mobile Phase Composition. Comparing Flow Injection Analysis [(FIA); Top Gray Panel] to Carbon Dioxide modified with methanol; without additive [MeOH] and with additive (MeOH +5mM ammonium formate [AmFo]) at three concentrations (40%, 20% and 10%).

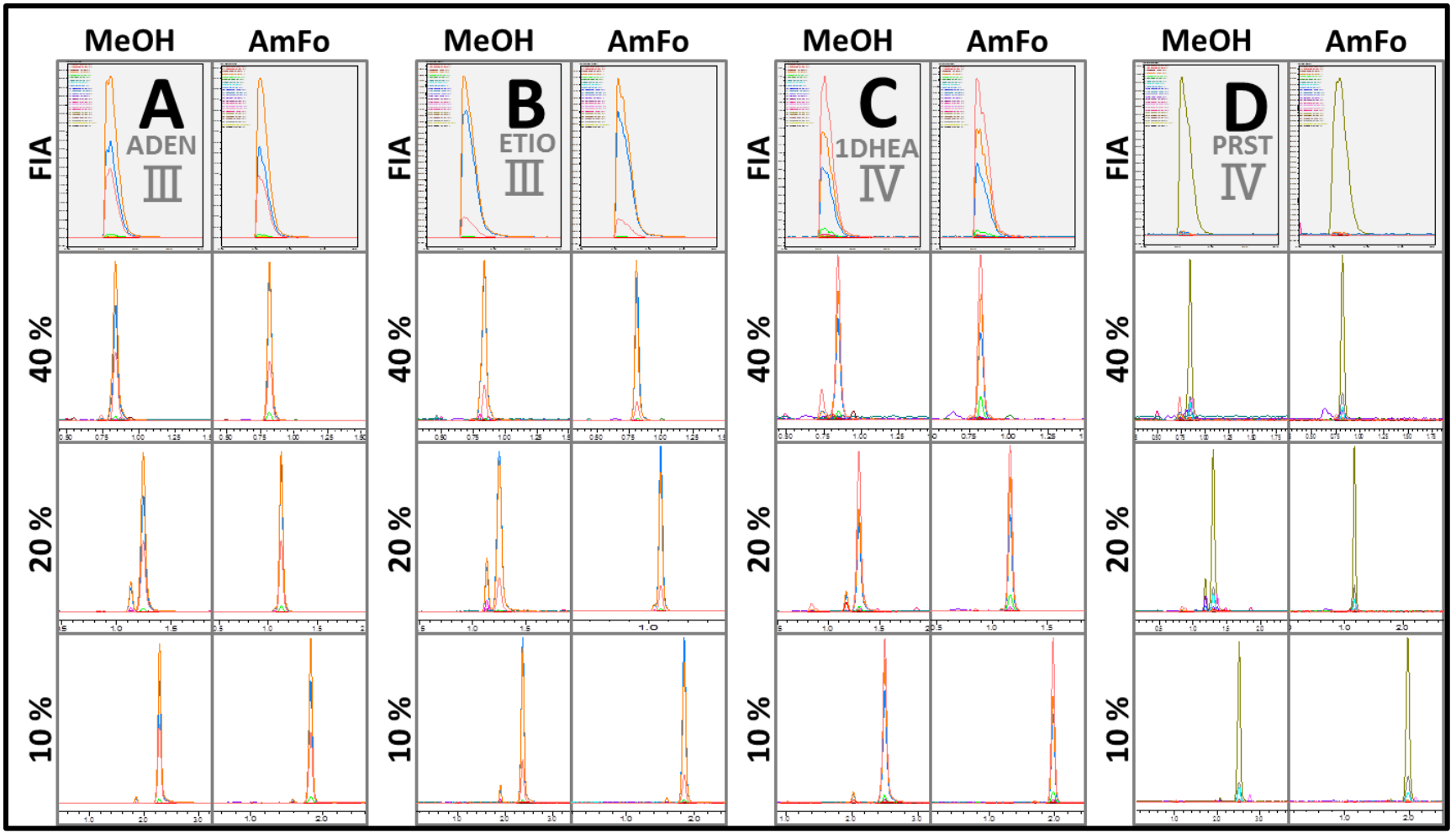

S_Figure 16. SFC-MS Chromatograms MRM-Specificity Test for Injections of (A) Androdrosterone [ADEN], (B) Etiocholanolone [ETIO], (C) 1-androsterone [1DHEA] and (D) Prasterone [PRST] showing Effect of Mobile Phase Composition. Comparing Flow Injection Analysis [(FIA); Top Gray Panel] to Carbon Dioxide modified with methanol; without additive [MeOH] and with additive (MeOH +5mM ammonium formate [AmFo]) at three concentrations (40%, 20% and 10%).

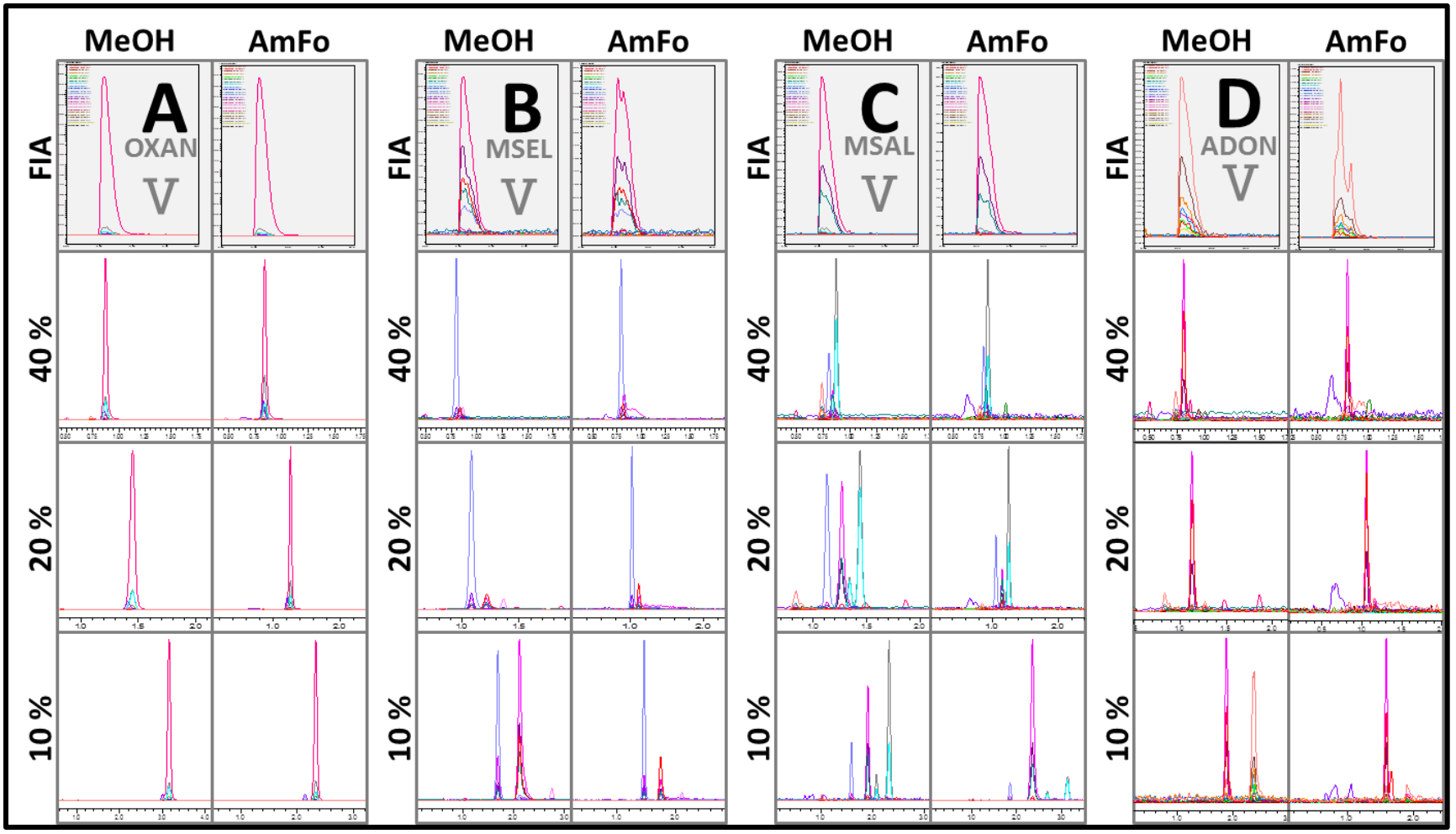

S_Figure 17. SFC-MS Chromatograms MRM-Specificity Test for Injections of (A) Oxandrolone [OXAN], (B) Mesterolone [MSEL], (C) Mestanolone [MSAL], and (D) Androstanolone [ADON] showing Effect of Mobile Phase Composition. Comparing Flow Injection Analysis [(FIA); Top Gray Panel] to Carbon Dioxide modified with methanol; without additive [MeOH] and with additive (MeOH + 5mM ammonium formate [AmFo]) at three concentrations (40%, 20% and 10%)

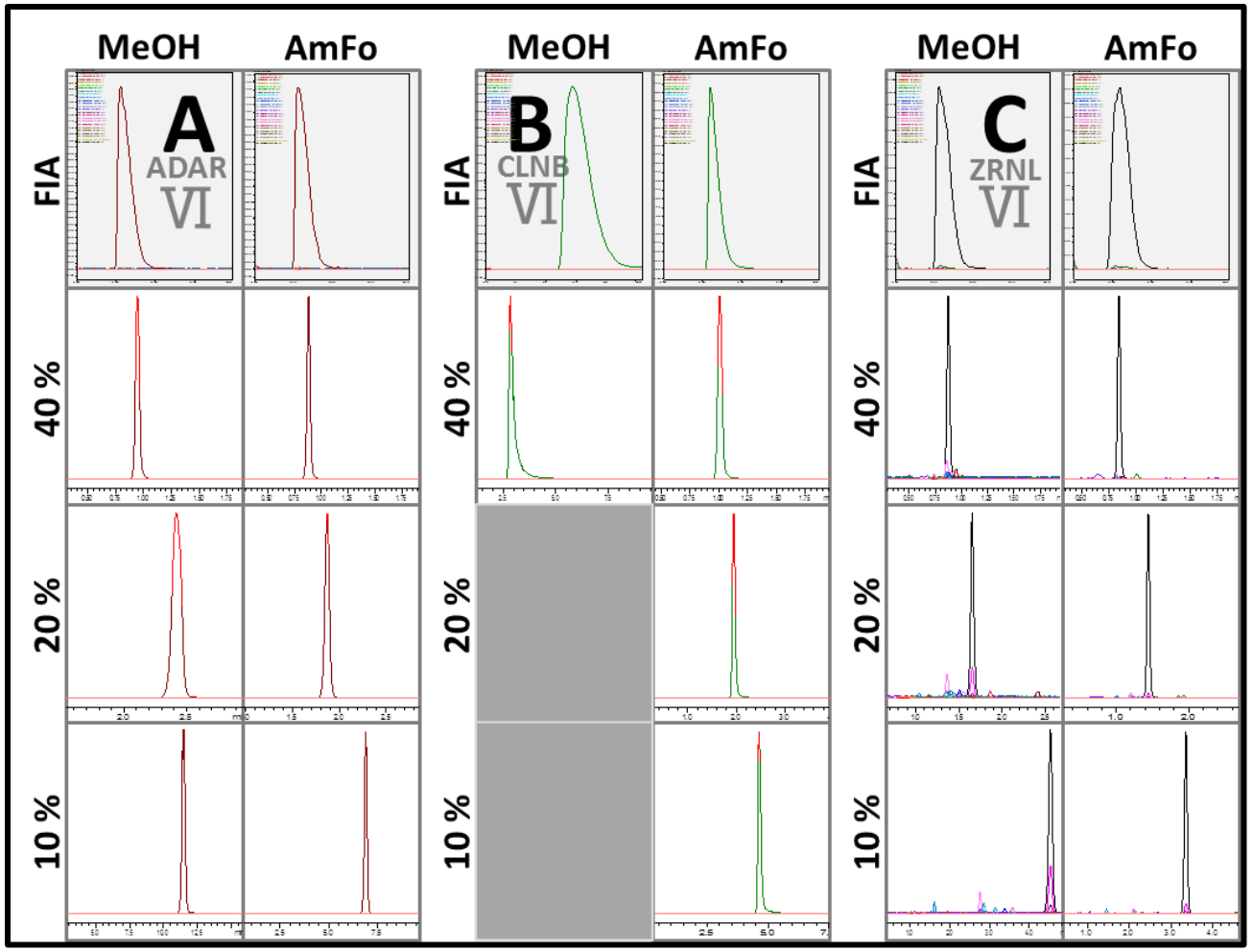

S_Figure 18. SFC-MS Chromatograms MRM-Specificity Test for Injections of (A) Andarine [ADAR], (B) Clenbuteral [CLNB] and (C) Zeranol [ZRNL] showing Effect of Mobile Phase Composition. Comparing Flow Injection Analysis [(FIA); Top Gray Panel] to Carbon Dioxide modified with methanol; without additive (MeOH) and with additive (MeOH + 5mM ammonium formate [AmFo]) at three concentrations (40%, 20% and 10%).

CHAPTER 5

SFC-SEPARATION OPTIMIZATION FOR AAS: COLUMN SCOUTING AND EXTRACTION PLUG SIMULATION

CHAPTER 5
SFC-SEPARATION OPTIMIZATION FOR AAS:
COLUMN SCOUTING
STATIONARY PHASE SCREENING AND EXTRACTION PLUG SIMULATION

5.1. SFC Separation Optimizations.

5.1.1. Common SFC MPs & SPs.

SFC is usually a normal phase technique, when the mobile phase composition is programmed from low to high polarity. Common mobile phases (MPs) and stationary phases (SPs) are discussed in more detail in **Chapter #1. Hyphenated Instrumentation: SFE-SFC-MS; Section 1.1.1. What is SFC?**. Generally, more polar solutes will require more polar MPs and SPs. SFC method development often starts by simply using a silica column and methanol as a modifier to obtain an initial evaluation of the separation of targeted analytes. This is an over simplification but is a general starting point where if the analytes are not retained or alternatively, excessively retained, the user has options to move to higher or lower polarity ranges to compensate. Changing the column is not normally a first tool used to try to improve a separation.[1] But in online SFE-SFC-MS methods, more emphasis is placed on column selection, as even if the targeted analytes are similar, sample matrix will add to the complexity of the separation and will likely put greater demand on the separations capabilities of the column used. Therefore, more often in online method development, you will see screening of a wide range of columns.

5.1.2. Overall MD Process for Online Extractions.

Method development (MD) for online extractions is a multistep process, involving four main steps:

1. **MS-based detection optimizations**
2. **SFC-based separation optimizations**
3. **SFE-based extraction optimizations**
4. **Matrix-specific optimizations**

The methods used for detection in the current work, were optimized in previous development steps of the online MD process (via MS-Optimizations: Step 1, detailed in **Chapter #3 Q3 Scans** and **Chapter #4 MRM Optimizations**). The work presented in the current chapter, focuses on the SFC-based separation optimizations (mainly step 2) in the development of a hyphenated methods for the online extraction of anabolic agents from dried blood spots for anti-doping analysis.

5.1.3. SFC Separation Optimizations in SFE-SFC-MS Method Development

SFC-based separation optimizations for SFE-SFC-MS analysis is the second step in method development for online methods, and can be broken down into three main steps:

1. **Column Selection**. An appropriate stationary phase is chosen for further development. Column screening is normally performed with a generic method for rapid comparison between phases. Comparing the resolution of critical MS-groups identified in previous method steps (mainly MS-optimizations) can be helpful in narrowing down potential phases.

2. **Separation Optimization**. Best performing columns are chosen during screening for further separation optimizations, where mobile phase compositions are evaluated,

3. **SFC-MS Method Evaluations**. Final methods are evaluated for reproducibility.

The current Chapter focuses on the column selection which involved a rapid screening of traditional and non-traditional phases used in SFC using a generic screening gradient and an SFE-simulation for retention of an extraction plug (**Figure 82**).

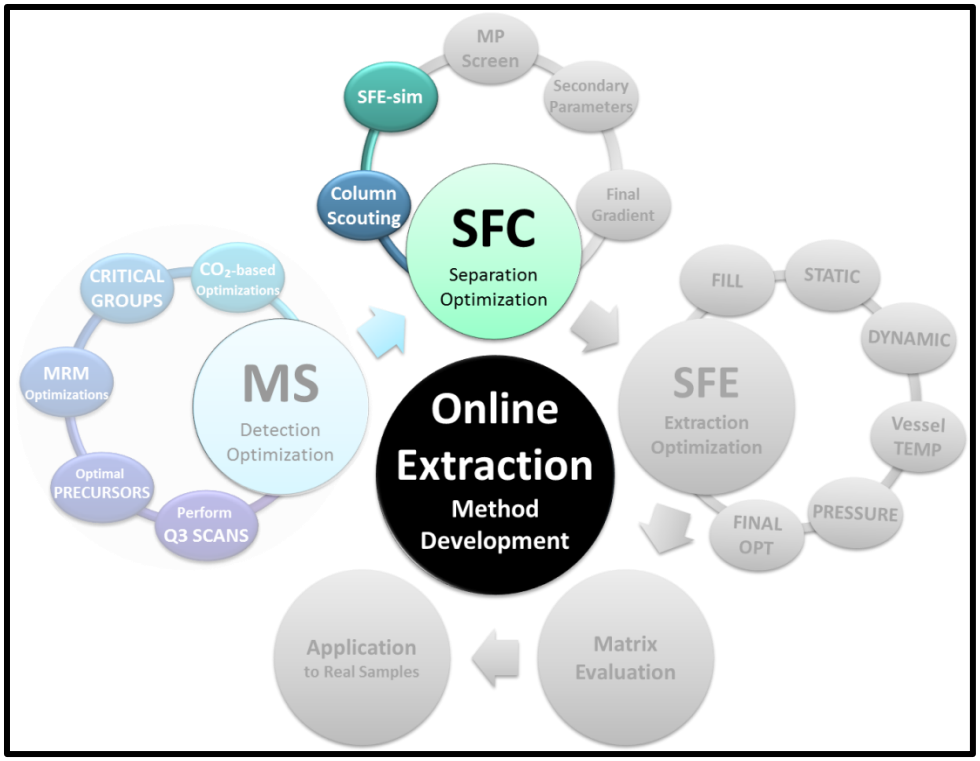

Figure 82. Online Extraction Method Development Focus for Chapter #5 SFC-Separation Optimizations: Column Screening facilitated by an SFE-Simulation for Extraction Plug Retention.

5.1.4. Column Screening for SFE-SFC-MS Method Development

SFE-SFC-MS method development flow charts are shown in **Figure 83;** the **left panel** depicts the traditional approach to developing online methods and highlights the steps most relevant to column selection. This traditional approach involves SFC-only column screening focused on the optimization of the separation of targeted analytes. But ultimately, the phase chosen must be capable to not only give adequate resolution, but it must also adequately retain an 'extraction plug' that would be loaded onto the column during an online extraction process, which can take several minutes. Therefore, in the traditional approach, it is not uncommon, when coupling SFC methods to online SFE in later development steps, to need to re-start column screening (**Figure 83; red dotted line**) in the event the phase chosen is not capable of sufficiently retaining the 'extraction plug'.

The aim of the current work was to provide an alternative approach to column screening to include an evaluation of the 'plug retention' capabilities for each phase. The proposed method development flow involves using a an SFE simulation during the early steps of SFC column screening (**Figure 83; right panel**). This allows a pre-emptive evaluation of plug retentivity at an early MD step. Enabling more informed column selection should circumvent the need to re-start MD at later stages and allow for a more straightforward flow of the development process; it should also save large amounts of time normally spent on re-optimizations. Performing a rapid screening on potential columns, should allow better decision-making in choosing best performing columns for further development, not only for potential for chromatographic separation of critical groups, but also good potential for plug retention.[17]

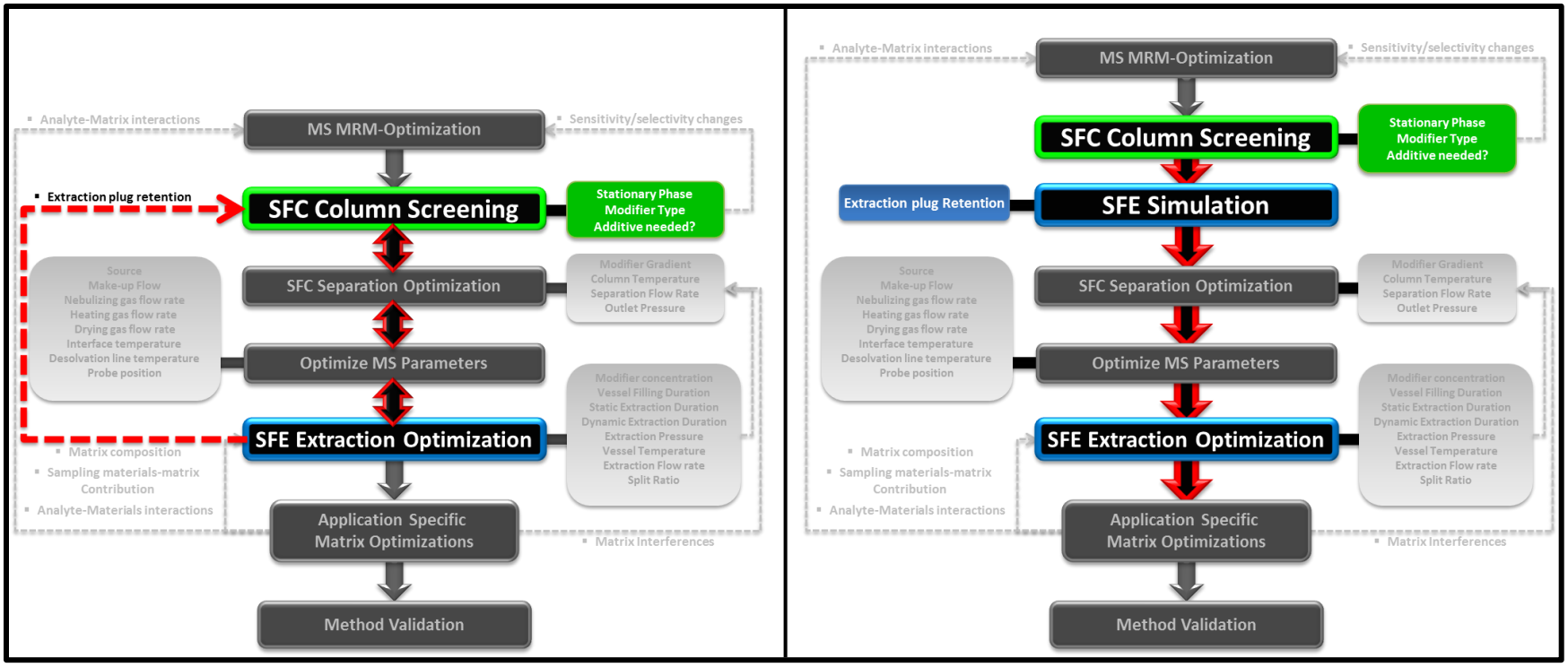

Figure 83. SFE-SFC-MS Method Development Flow Charts: (left) traditional method development flow for coupling SFC methods to online SFE may require re-starting SFC column screening in the event the phase chosen is not capable of sufficiently retaining the 'extraction plug'; (right) Proposed method development flow using a an SFE simulation during SFC column screening to evaluate plug retentivity at an early MD step. Figure adapted from **Wicker et. al., 2020.**[17]

5.2. SFE-SFC-MS Column Screening Instrument Methods.

5.2.1. MS-Critical Groups

Detection of compounds were made via ESI-MS analysis on a triple quadrupole mass spectrometer in positive and negative mode by MRM. In previous development steps, MRM-optimizations were performed using the LabSolutions software to determine optimal precursors, products, voltages and collision energies for the target analytes in this work (discussed in **Chapter 4. MS-Detection: MRM Optimizations**). The 23 androgenic anabolic steroids were then individually reinjected using the newly optimized MRM method (**Table 18**). Structures for each analyte are given in **Figure 84**. Steroids that produced signal for two or more MRMs were investigated further for structural similarities and their Q3 scans compared. This identified five groups of compounds as 'critical pairs', where due to fundamental similarities in structure and/or molecular weight, differentiation with MS-alone was impractical/impossible; these were flagged as critical groups that would require chromatographic separation. Comparison of the resolution within MS critical groups is a helpful tool to select best performing columns for further development of online methods.

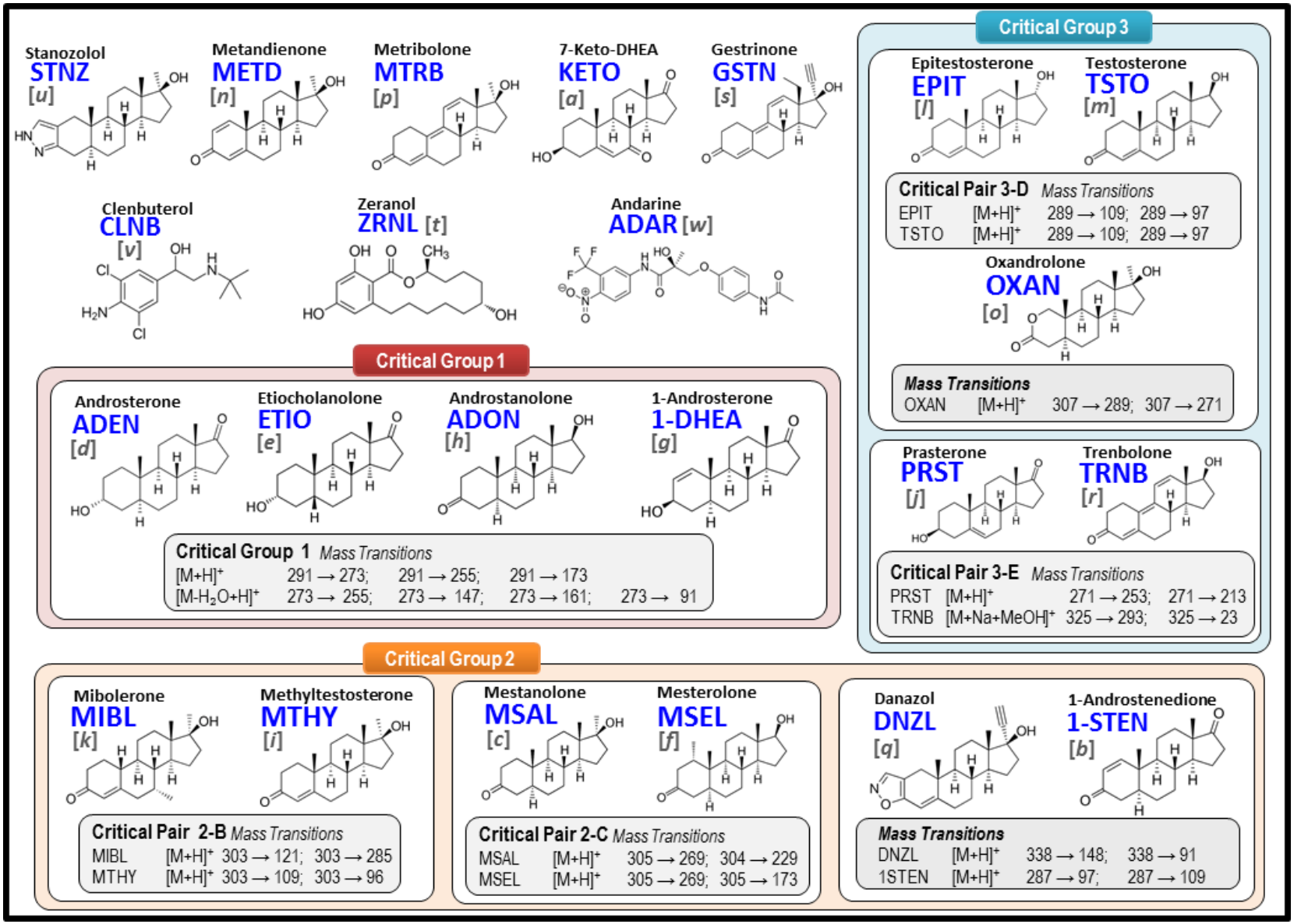

Figure 84. Structure of targeted anabolic androgenic steroids and bio mimics, showing critical pair groups and (similar) MRM transitions highlighting Critical groups for Chromatographic separation.

Table 18. MRM Details for Targeted Anabolic Agents (AAS): Highlighting Critical Groups for Chromatographic Separation and Peak IDs.

				Precursor			Product Ion							
				MW	+/-	(m/z)	Transition 1	(Q1/Q3 Bias, CE)	Transition 2	(Q1/Q3 Bias, CE)	Transition 3	(Q1/Q3 Bias, CE)	Transition 4	(Q1/Q3 Bias, CE)
Peak	Steroid	ID	Critical Group				(m/z)	([V]/[V], [eV])	(m/z)	([V]/[V], [eV])	(m/z)	([V]/[V], [eV])	(m/z)	([V]/[V], [eV])
[*a*]	7-Keto-DHEA	KETO	n/a	302.2	+	285	81	(-22/-32, -27)	79	(-20/-30,-44)	107	(-20/-20,-27)	149	(-20/-26,-21)
[*b*]	1-Androstenedione	1-STEN	2	286.4	+	287	97	(-20/-20, -22)	109	(-22/-22,-24)	79	(-20/-30,-46)	109	(-20/-40,-35)
[*c*]	Mestanolone	MSAL	2-C	304.4	+	305	269	(-20/-28, -16)	229	(-20/-24,-20)	159	(-20/-34,-23)	187	(-20/-36,-22)
[*d*]	Androsterone	ADEN	1	290.4	+	273	255	(-20/-26, -14)	147	(-22/-32,-21)	199	(-22/-20,-21)	161	(-20/-36,-20)
[*e*]	Etiocholanolone	ETIO	1	290.4	+	273	255	(-20/-28, -12)	215	(-20/-42,-17)	105	(-20/-20,-35)	91	(-20/-38,-43)
[*f*]	Mesterolone	MSEL	2-C	304.4	+	305	269	(-22/-28, -17)	173	(-20/-40,-24)	287	(-22/-30,-16)	133	(-24/-22,-28)
[*g*]	1-Androsterone	1-DHEA	1	290.4	+	291	273	(-20/-30, -10)	255	(-15/-26, -15)	135	(-20/-28,-20)	91	(-22/-36, -10)
[*h*]	Androstanolone	ADON	1	290.4	+	291	255	(-11/-12, -16)	173	(-10/-18,-21)	227	(-10/-23,-10)	-	-
[*i*]	Methyltestosterone	MTHY	2-B	302.5	+	303	109	(-22/-20, -28)	97	(-20/-20,-26)	97	(-22/-20,-27)	285	(-22/-30,-16)
[*j*]	Prasterone	PRST	3-E	288.2	+	271	253	(-20/-26, -12)	213	(-22/-46,-15)	213	(-20/-40,-17)	157	(-20/-32,-22)
[*k*]	Mibolerone	MIBL	2-B	302.5	+	303	271	(-22/-30, -12)	285	(-22/-20,-17)	121	(-22/-24,-25)	-	-
[*l*]	Epitestosterone	EPIT	3-D	288.4	+	289	109	(-20/-20, -24)	97	(-22/-38,-25)	79	(-22/-30,-44)	253	(-22/-26,-18)
[*m*]	Testosterone	TSTO	3-D	288.4	+	289	109	(-22/-20, -25)	97	(-22/-36,-22)	253	(-22/-28,-17)	79	(-22/-28,-46)
[*n*]	Methandienone	METD	NON (mid)	300.4	+	301	121	(-22/-46, -28)	149	(-22/-26,-15)	283	(-22/-30,-11)	121	(-22/-22,-24)
[*o*]	Oxandrolone	OXAN	3	306.4	+	307	289	(-22/-30, -12)	271	(-22/-30,-14)	121	(-22/-22,-24)	229	(-24/-24,-18)
[*p*]	Metribolone	MTRB	NON (mid)	284.4	+	285	227	(-22/-24, -23)	267	(-20/-28,-17)	198	(-22/-20,-30)	159	(-20/-30,-23)
[*q*]	Danazol	DNZL	2	337.5	+	338	148	(-24/-30, -25)	91	(-26/-32,-55)	120	(-24/-22,-28)	310	(-24/-32,-20)
[*r*]	Trenbolone	TRNB	3-E	270.4	+	271	253	(-20/-26, -19)	199	(-20/-20,-22)	165	(-20/-36,-56)	128	(-20/-26,-57)
[*s*]	Gestrinone	GSTN	NON (mid)	308.4	+	309	241	(-22/-26, -23)	199	(-24/-40,-32)	291	(-24/-20,-16)	262	(-22/-28,-21)
[*t*]	Zeranol	ZRNL	n/a	322.4	-	321	277	(34/28, 23)	303	(36.0/20,22)	259	(36.0/26,24)	235	(36.0/28,24)
[*u*]	Stanozolol	STNZ	n/a	328.5	+	329	81	(-24/-30, -51)	95	(-24/-20,-42)	121	(-24/-22,-37)	107	(-24/-20,-41)
[*v*]	Clenbuterol	CLNB	NON (late)	277.2	+	227	203	(-32/-36, -16)	259	(-20/-26,-10)	132	(-20/-24,-28)	168	(-20/-32,-28)
[*w*]	Andarine	ADAR	NON (late)	441.4	+	442	108	(-32/-20, -37)	208	(-32/-20,-21)	190	(-32/-20,-25)	148	(-32/-32,-31)

5.2.2. SFC-Column Screening Methods.

Instrument methods for column screening are described in detail at the end of the chapter in **Section 5.i. Instrument Methods: SFC SP Screening**. In total thirteen stationary phases were screened to evaluate chromatographic resolution, separation time, and sample plug retentivity. Each column was run isocratically at 40, 20 and 10% modifier and then with a 'generic screening Gradient' and lastly with an SFE-Simulation method.

Scouting Traditional SFC Stationary Phases . Eight stationary phases (SP), traditionally used in SFC, were screened in order to evaluate effect of SP polarity on the separation of the steroid mixture. Traditional SPs ranged in polarity (from C18 [non-polar] to more polar phases such as Amino and Ethyl-pyridine. The traditional phases screened in the current work are shown in **Table 19**. Each column was run isocratically at 40, 20 and 10% modifier and then with a 'generic screening Gradient'. All screening runs were performed using a column temperature of 50 °C and outlet pressure of 15 MPa, which were arbitrarily chosen.

Scouting Non-Traditional Phases. Five non-traditional stationary phases were screened using the generic screening gradient. The phases and dimensions are given in **Table 20**.

Generic Screening Gradient. Chromatographic resolution was first evaluated using a generic 'screening gradient' (**Figure 85**), at 15.0 MPa back pressure and a 50 °C column temperature.

Table 19. Screened Traditional SFC Columns.

ID	Phase	Vendor	Brand	Phase Trade Name	Particle Size (µm)	Dimensions (mm)
[2EP]	2-ethylpyridine	Princton Chrom.	PrincetonSFC	2-Ethylpyridine	3.0	3.0 x 100
[NH2]	amino	Agilent Technologies, Inc.	Zorbax®	NH_2	5.0	4.6 x 150
[DIOL]	diol	Daiso Fine Chem USA, Inc.	DAISO	SP-60-5-Diol-P	5.0	4.6 x 150
[HILIC]	silica (hilic)	Restek Corp.	Raptor	HILIC-Si	2.7	4.6 x 150
[RX-SIL]	silica	Agilent Technologies, Inc.	Zorbax®	RX-SIL	1.8	3.0 x 150
[Z-CN]	cyano	Agilent Technologies, Inc.	Zorbax®	Cyano	3.5	4.6 x 150
[UC-CN]	cyano	Shimadzu Corp.	Shim-pack	UC-Cyano	5.0	4.6 x 150
[C18]	C18	Phenomenex, Inc.	Luna®	C18(2)	5.0	4.6 x 150

Table 20. Screened Non-Traditional SFC Columns.

ID	Phase	Vendor	Brand	Phase Trade Name	Particle Size (µm)	Dimensions (mm)
[Cho]	cholesteryl	Shimadzu Corp.	Shim-pack	UC-Choles	5.0	4.6 x 250
[HyP]	hydroxyphenyl	Shimadzu Corp.	Shim-pack	UC-HyP	5.0	4.6 x 250
[Tri]	triazolyl	Shimadzu Corp.	Shim-pack	UC-Triazole	5.0	4.6 x 250
[PBr]	pentabromobenzyl	Shimadzu Corp.	Shim-pack	UC-PBr	5.0	4.6 x 250
[Py]	Pyridinyl	Shimadzu Corp.	Shim-pack	UC-HyP	5.0	4.6 x 250
[Px]	*np*	Restek Corp.	Raptor	PolarX	2.7	4.6 x 250

*np = not provided (proprietary)

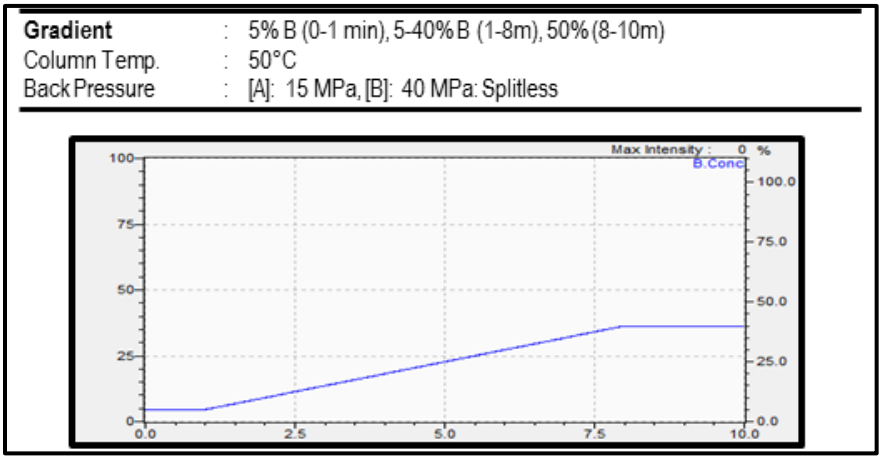

Figure 85. Generic Screening Gradient for Column Scouting.

5.3. SFE-Simulation Description.

5.3.1. Simulation Purpose.

During online extraction, an 'extraction plug' is loaded onto the head of the column during the dynamic extraction step. One significant challenge of method development for online extraction techniques is predicting a column's capability of adequately retaining an 'extraction plug'. With that in mind a simulation was performed, using SFC injections, where the system pressures were adjusted to simulate system conditions during online extraction (e.g. split flow and extraction plug loading).

5.3.2. Simulation Instrument Setup.

Detailed instrument configuration details can be found in **Chapter #1. Hyphenated Instrumentation; Section 1.6. SFE Simulation Configurations**). In short, the **s**ystem setup is almost identical to that used during SFC-only operation (**Figure 86**). The liquid injector is the source of sample introduction. BPR_A functions as the system outlet pressure, and BPR_B is plumbed in for use in split-mode simulations. The biggest difference is in the system operation, where the method utilized for the simulation more resembles a time program that would be used during online extractions, but the time program is setup around the injection to mimic as many of the conditions as possible of a n online extraction, including changes in flow rates, MP compositions and active trapping of the analytes at the head of the column.

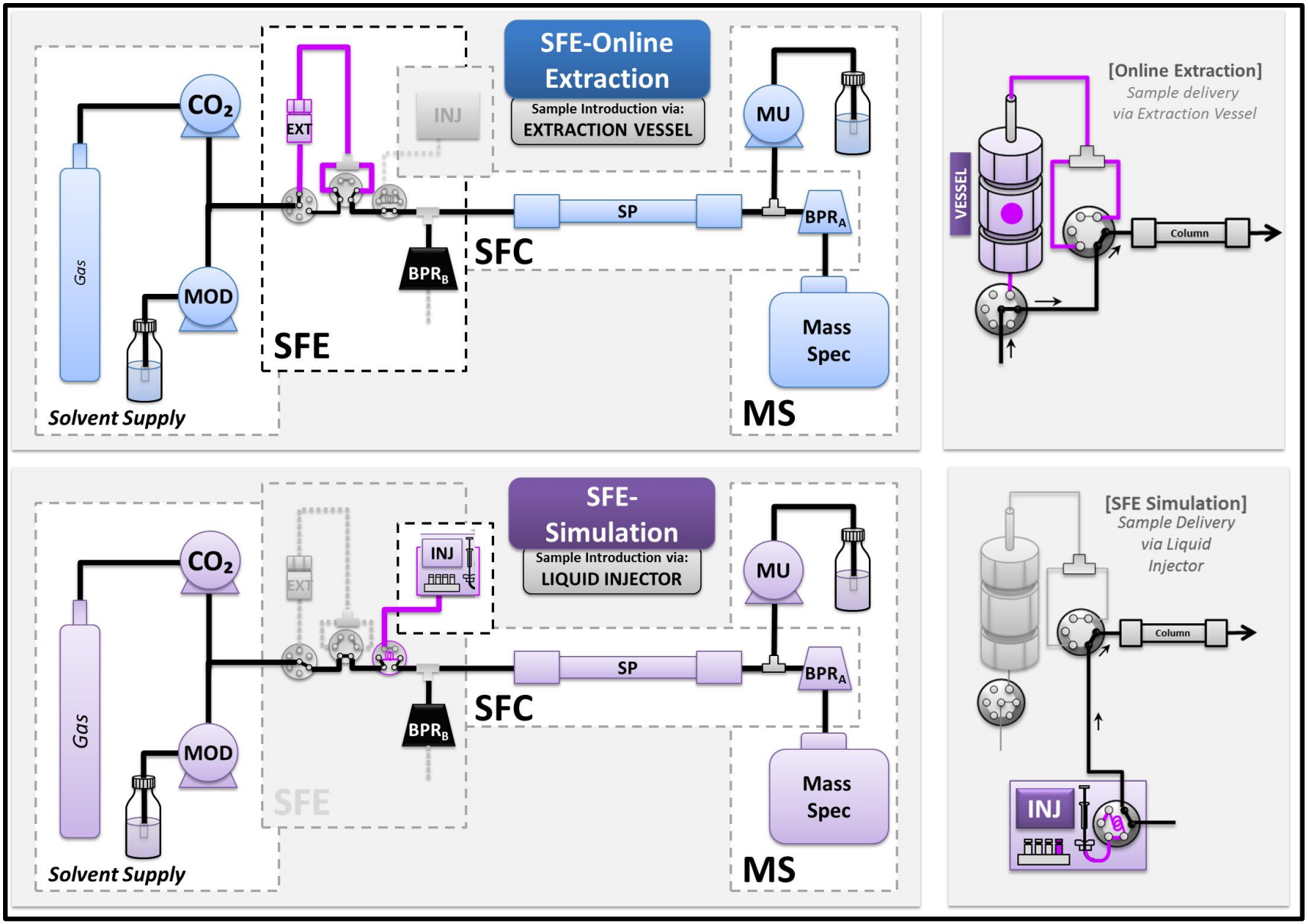

Figure 86. Comparison of Instrument Setup for Online Extractions and for SFE Simulation

5.3.3. Simulation Methods.

The online extraction simulation was also performed on all fifteen columns, to evaluate the retentivity of each phase for the potential online loading of an 'extraction plug", using a 'SFE simulation' method (**Figure 87**). This involved multiple steps, each simulating a different "extraction step", before ultimately starting the same generic gradient used in the original column screening. Hypothetically, if the plug is successfully retained, the only effect that should be seen in the chromatograms is a time delay equal to that of the simulation.

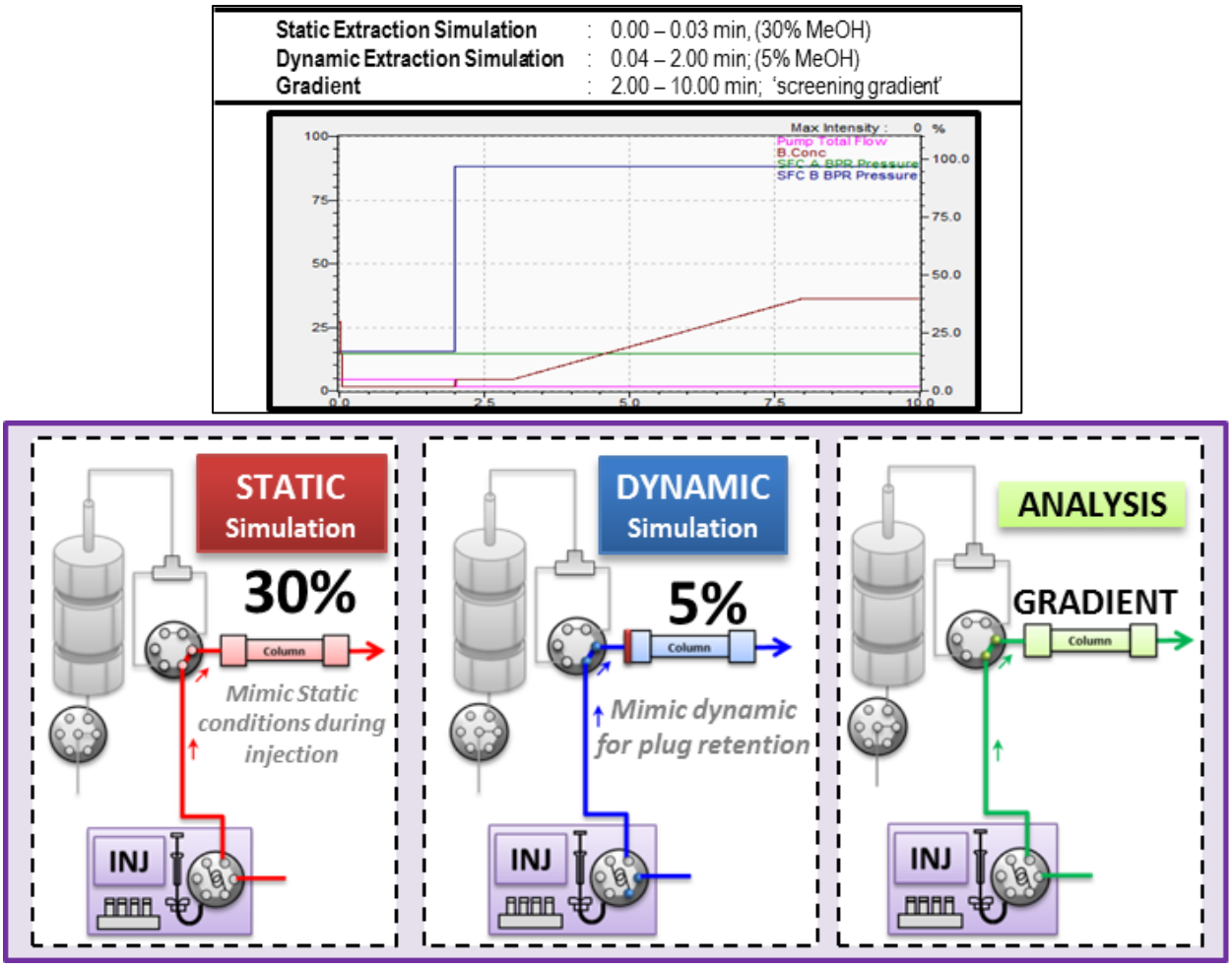

Figure 87. SFE Simulation method

5.3.4. Extraction Factors Simulated.

Fill-Factors simulated (Figure 88; Filling Simulation, orange). Initial vessel filling is normally performed at high modifier concentration. In this simulation, the injection plug (being a 1.0 µL slug of 100% modifier), simulates the initial filling of the extraction vessel.

Static-Factors simulated (Figure 88; Static Simulation, red). Although Static Extraction is performed previous to the 'extract plug' transport to and loading on the column, static conditions can also affect the integrity of the retention of the plug. During this passive extraction step, the contents of the extraction vessel should be mostly isolated from the main flowpath, but MP continues to flow over the column. This could be thought of as a pre-conditioning step, where if a high modifier concentration is utilized, the phase is effectively being equilibrated with a high percentage of modifier just prior to loading of the plug. Since at the end of static extraction, the valves switch to dynamic (directing flow thru the vessel and out to over the column) this would make it harder to retain analytes (especially less polar compounds) at the head of the column, therefore static conditions tend to also have a significant effect on the integrity of the trapping of the plug.

To simulate static extraction, the column is equilibrated at a higher percent modifier, previous to and for a brief time during the injection. By using a high modifier concentration for a short duration during injection, we mimic static conditions.

Dynamic-Factors simulated (Figure 88; Dynamic Simulation, blue). During normal online extraction, the 'extract plug' is carried to the column during the dynamic extraction step, but it is also important that for the entire duration of this 'active extraction', the mobile phase continues to flow thru the vessel and ultimately on-column. This means that during online extraction, even after the plug has been delivered to the column, MP flows for some time thru the column. Therefore, the plug must be retained at the head of the column. In order to effectively trap analytes at the head of the column, the modifier concentration must be low enough and/or the column must be retentive enough to allow retention of all the analytes present. For these reasons the dynamic extraction has the largest effect on the integrity of the trapping of the plug.

In the SFE-simulation, in order to simulate the delivery of the sample plug, immediately after injection, the composition of the mobile phase is changed to a much lower modifier concentration and held for a duration of 2 minutes. Simulating the delivery of the 'extract plug' and the proceeding active flow over the column, before ultimately starting the gradient for analysis.

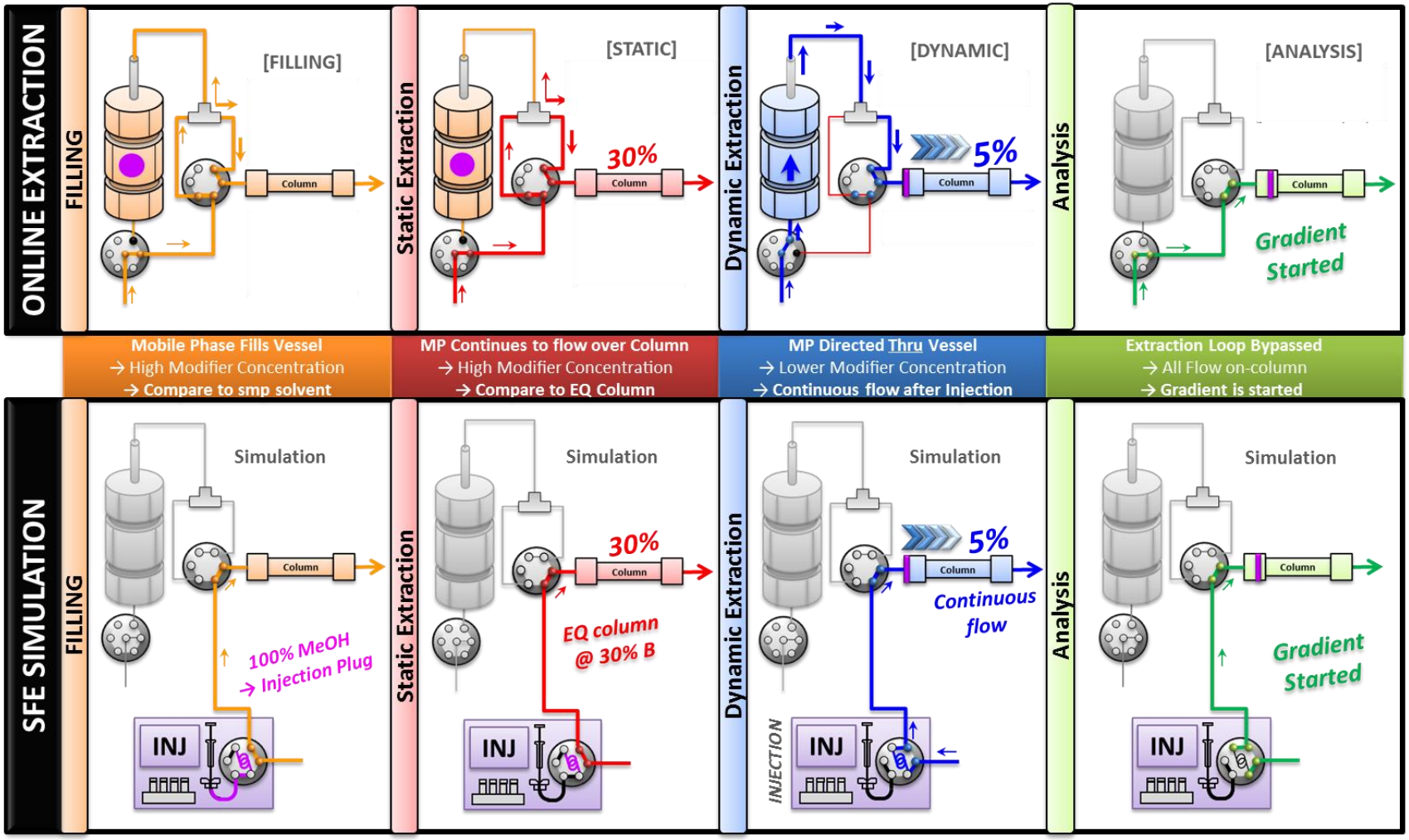

Figure 88. Instrument Flow diagrams showing system configurations and conditions for SFE-simulations of Extraction Plug Trapping using SFC-injections.

5.4. Generic Screening Gradient Results.

5.4.1. Rapid Screening of Traditional Phases

Eight stationary phases (SP), traditionally used in SFC, were screened in order to evaluate effect of SP polarity on the separation of the steroid mixture . Resulting chromatograms were compared (**Figure 89**) paying close attention to resolution between critical pairs (**Table 21**). Note that ideally the set of traditional columns would have the same dimension (e.g., length, diameter, and particle size), but due to availability, the set of traditional SFC columns used in this work were not of the same column dimensions. Although the normal comparison between phase polarities was hard to make, some trends could clearly be identified based on differences in polarity.

5.4.2. Traditional Phases: Overall Performance for Generic Gradient.

The Full runtime is compared in panel **A** of **Figure 89.** Improved retention was observed for all compounds on the higher polarity phases. The majority of the compounds were virtually un-retained on the non-polar C18 phase, with most of the target analytes (especially those having the characteristic steroid backbone) eluting in the first 1.5 minutes of the run and producing very low resolution between all critical groups. Alternatively, using the more polar cyano column and the same generic gradient, the majority of the target analytes were much more retained. Spreading the earliest eluters out across the first five minutes of runtime resulted in much improved resolution within each critical group; baseline resolution was achieved for many critical compounds, even with the generic gradient. The Silica column was even more retentive, where the latest eluting compounds (e.g. mainly the non-steroid, androgen mimics, CLNB and ADAR), were retained beyond the runtime of the generic gradient. The silica columns had similar selectivity to the cyano column, but as the phase polarity increases, a notable gap in elution forms between the first two steroids (earliest eluters) and the bulk of the remaining steroid analytes (mid-eluters). Another interesting note is that the latest eluters (CLNB and ADAR), became less retained on the most polar

columns. This is a result of a peak reversal between CLNB & ADAR. CLNB elutes later on C-18, co-elutes on Silica, and elutes earlier than ADAR on the most polar phases.

5.4.3. Traditional Phases: Resolution within Critical Pair Groups.

Traditional Phases. MS-Critical Group 1 Resolution. Generally, members of critical group 1 appeared to be the most difficult to separate (**Figure 89; B [Group 1, red]**). Regardless of stationary phase, androsterone (ADEN [***d***]) always eluted first and 1-androsterone (1DHEA [***a***]) last. Although, little resolution was seen using the non-polar, C18 phase, the higher polarity columns gave varying results with apparently etiocholanolone (ETIO [***i***]) and 1DHEA being the most difficult to separate. The source of the varying result could not be determined at this stage, but seemed to be attributable to selectivity changes mainly for ETIO; most likely due to differences in modifier concentration during the gradient elution. The highest resolution for 1DHEA from the other members of group 1 was observed on the 2-EP column ($Rs_{[d/i:a]}$ = 1.1), but ADEN and ETIO co-elute (**Table 21; [Group 1]**). Cyano and Diol were the only two columns where three distinct peak apex were observed. Therefore, these were considered to be the most promising phases for the potential separation of group 1.

Traditional Phases. MS-Critical Group 3 Resolution (**Figure 89; B [Group 3, blue]**). Prasterone (PRST [***j***]) and trenbolone (TRNB [***r***]) are high priority members of critical group 3, with TRNB giving nearly equal response for both its own and for PRST's MRM-transition (discussed in **Chapter 4. MRM Optimization: Section 4.14.3. critical group 3: *Pair 3-E***). Apparently, the separation of this pair will be easily achieved chromatographically in SFC, as the minimum resolution observed was on the C18 column and was above 8 on any of the other, more polar, columns. TRNB elutes later than PRST and adequate resolution between the pair was observed on all stationary phases regardless of polarity. Resolution increased with polarity, giving the lowest resolution ($Rs_{[j:r]}$ = 2.7) on the C18 column which increased ($Rs_{[j:r]}$ > 5) with higher polarity SPs.

The epimers, testosterone (TSTO [***l***]) and epitestosterone (EPIT [***m***]), are also high priority members of critical group 2 giving equal response for each-others MRM-transitions (discussed in **Chapter 4. MRM Optimization: Section 4.14.3. critical group 3: *Pair 3-D***). This pair, although not resolved on the non-polar C18 column, showed

increasing resolution with increasing SP polarity. The hilic silica column provided the highest observed resolution ($Rs_{[l:m]}$ = 2.3). Amino gave surprisingly low resolution between this pair, possibly due to a peak reversal with modifier concentration.

Being a high priority watch member for this group, Oxandrolone (OXAN [***o***]) elutes very close to both EPIT and TSTO across all phase polarities. UC-CN was the only phase where OXAN eluted later than TSTO, and also gave the best (albiet poor) Rs between the two compounds ($Rs_{[o:m]}$ = 0.6), using the generic screening gradient.

Traditional Phases. MS-Critical Group 2 Resolution (Figure 89; **B [Group 2, orange]**). Mibolerone (MIBL [***i***]) and methyltestosterone (MTHY [***k***]) are high priority members of critical group 2, giving low response for each-others MRM-transitions (discussed in **Chapter 4. MRM Optimization: Section 4.14.2. critical group 2: *Pair 2-B***). Separation of MTHY and MIBL may be difficult, as these two compounds co-eluted on all phases except for the RX-SIL and Amino columns, the later giving the greatest resolution, which was just barely baseline resolved ($Rs_{[i:k]}$ = 1.5).

Mesterolone (MSEL [***f***]) and Mestanolone (MSAL [***c***]) are also high priority members of critical group 2, giving nearly equal response for each-others MRM-transitions (discussed in **Chapter 4. MRM Optimization: Section 4.14.2. critical group 2: *Pair 2-C***). Baseline resolution was achieved for MSAL and MSEL ($Rs_{[c:f]}$ > 2.0) on every column except for the C18 and the Amino columns ($Rs_{[c:f]}$ < 0.1). Both MSAL and MSEL also produce low signal for 1-androstenedione (1STEN [***b***]) and Danazol (DNZL [***q***]). 1STEN, was the earliest eluter of group 2 and was well resolved from critical pair C (Rs > 1.5) on all columns except for the Agilent Cyano column, where a peak reversal occurs and 1STEN nearly co-elutes ($Rs_{[b:f]}$ = 0.5) with MSEL. DNZL is much better resolved from group 2 on the more polar columns. Overall, for critical group 2, the RX-SIL column produced the best overall group separation, where all six compounds were nearly baseline resolved (Rs > 1.3).

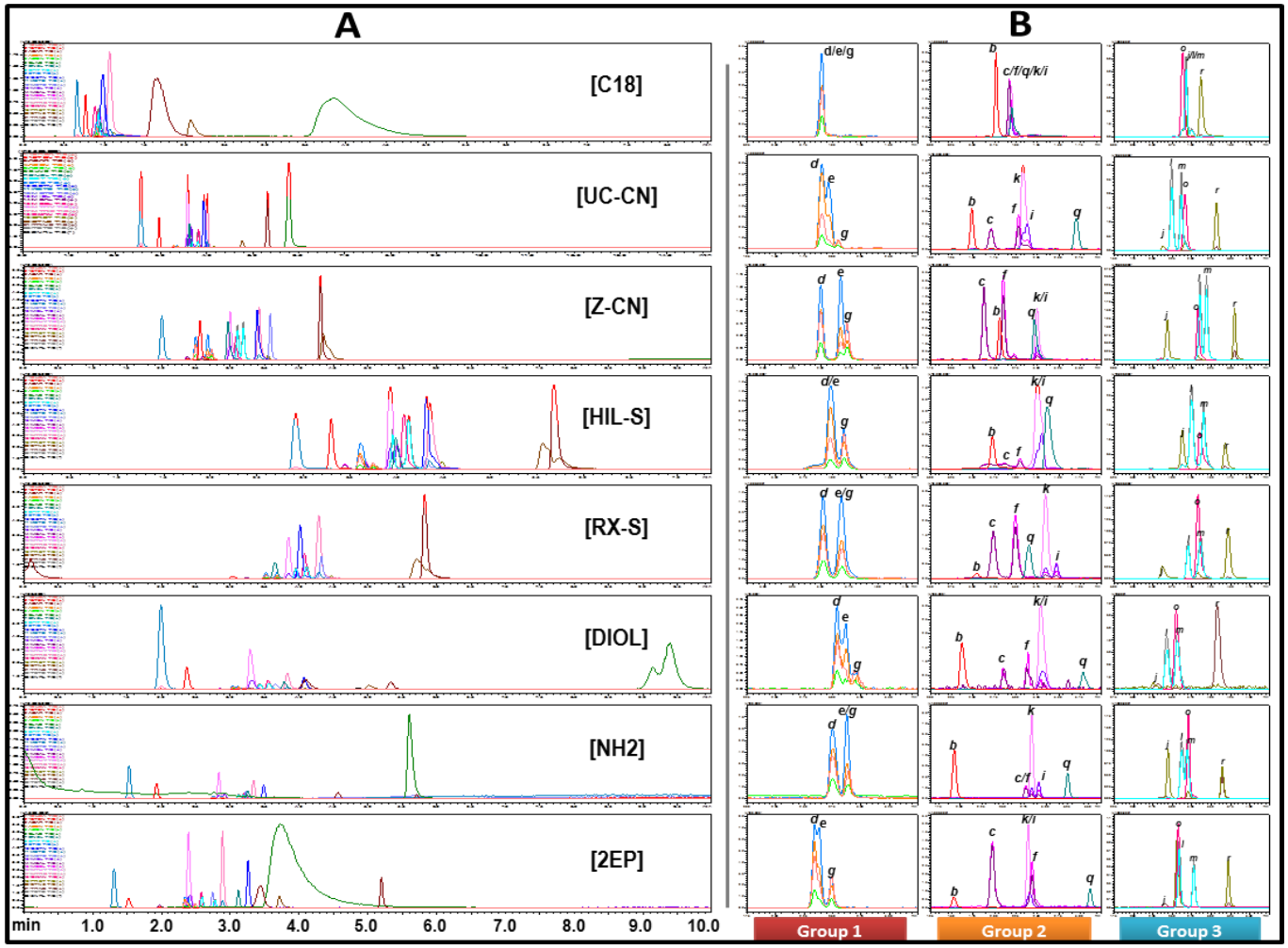

Figure 89. Column Scouting on Traditional Stationary Phases using SFC-MS injections of androgenic steroid mix [AAS-mix]. [Panel A] Full runtime; **[Panel B]** Overlays of critical Groups: **[Group 1, left]** androsterone (ADEN-MRM [orange; ***d***]), etiocholanolone (ETIO-MRM [blue; ***e***]), 1-androsterone (1-DHEA [pink; ***g***]); **[Group 2, middle]** epitestosterone (EPIT-MRM [cyan; ***m***]), testosterone (TSTO-MRM [gray; ***l***]), oxandrolone (OXAN-MRM [hot pink; ***o***]), prasterone (PRST-MRM [gold; ***j***]), trenbolone (TRNB-MRM [brown; ***r***]); **[Group 3, right]** 1-androstenedione (1STEN-MRM [red; ***b***]); mestanolone (MSAL-MRM [magenta; ***c***]); mesterolone (MSEL-MRM [rose; ***f***]); mibolerone (MIBL-MRM [purple; ***k***]); methyltestosterone (MTHY-MRM [light pink; ***l***]); and danazol (DNZL-MRM [turquoise; ***q***]). **Conditions: generic screening gradient (5 - 40% MeOH over 8 minutes), with column temperature of 50 °C and outlet pressure of 15 MPa.**

Table 21. Resolution of Critical Pair Groups during Screening of Traditional SFC Stationary Phases.

Critical Group	Critical Group Resolution								Column	
	C18	UC-CN	Z-CN	HILIC	RX-SIL	DIOL	Amino	2EP		
1	d/e/g	d, e, g	d, e, g	d/e, g	d, e/g	d, e, g	d, e/g	d, e, g	ADEN (d)	Group 1 Key
	< 0.1	0.5	2.2	< 0.1	1.5	0.6	1.2	0.3	ETIO (e)	
	< 0.1	0.8	0.7	0.9	0.1	0.2	0.2	1.1	1DHEA (g)	
2	b, c/f/i/k/q	b, c, f, k, i, q	b, c, f, q, k/i	b, c, f, k/l, q	b, c, f, q, k, i	b, c, f, k/l, q	b, c/f, k, l, q	b, c, k/l, f, q	1STEN (b)	Group 2 Key
	4.4	2.5	2.3	1.5	1.6	6.1	9.7	4.6	MSAL (c)	
	< 0.1	3.5	0.5	2.5	2.3	3.7	< 0.1	4.6	MSEL (f)	
	< 0.1	0.5	4.5	2.7	1.3	1.4	0.6	0.1	MTHY (i)	
	< 0.1	0.4	0.4	0.6	1.7	0.1	1.5	0.2	MIBL (k)	
	< 0.1	5.0	< 0.1	0.2	1.3	2.6	4.3	4.5	DNZL (q)	
2-B	< 0.1	3.5	2.7	2.5	2.3	3.7	< 0.1	5.1	MSAL : MSEL	
2-C	< 0.1	0.4	< 0.1	0.8	1.3	0.1	1.5	0.1	MIBL : MTHY	
3	o, j/l/m, r	j, l, m, o, r	j, o, l, m, r	j, l, o, m, r	j, l, o, m, r	j, l, o, m, r	j, l, o, m, r	j, o, l, m, r	PRST (j)	Group 3 Key
	1.1	1.3	5.2	2.4	3.5	2.2	2.1	0.3	EPIT (l)	
	0.1	1.6	0.4	1.4	1.4	1.0	0.7	0.1	TSTO (m)	
	< 0.1	0.6	1.2	0.6	0.3	0.2	0.2	2.5	OXAN (o)	
	5.3	5.0	5.4	4.6	4.1	4.7	6.0	5.9	TRNB (r)	
3-D	5.2	8.4	12.4	8.9	8.4	8.7	9.5	8.4	PRST:TRNB	
3-E	< 0.1	1.6	1.2	2.3	1.7	1.3	0.7	2.5	EPIT:TSTO	

Elution Order

5.5. Non-Traditional SFC Stationary Phases.

5.5.1. Non-Traditional Phases: Overall Performance for Generic Gradient.

Five non-traditional stationary phases were screened using the generic screening gradient. Resulting chromatograms are compared in **Figure 90** and resolution between critical group compounds are given in **Table 22**. Of the non-traditional phases, the UC-Choles column gave little overall retention for the majority of the compounds. Alternatively, UC-PBr was excessively retentive with nearly half the compounds requiring high modifier concentration (> 40%) for elution. The PolarX and the UC-triazole columns showed good potential for overall resolution between all 22 compounds. Tailing was observed for many of the later eluting compounds on PolarX and it was less retentive than UC-triazole.

5.5.2. Non-Traditional Phases: Resolution within Critical Pair Groups

Non-traditional Phases. MS-Critical Group 1 Resolution (**Figure 90; B [Group 1, red]**). Generally resolution for critical group 1 was much better on the non-traditional phases (**Table 22; [Group 1]**). Elution order was different on both UC-Choles and UC-PBr (reversal of ETIO and ADEN) from most of the other columns screened. The largest resolution between ETIO and ADEN ($Rs_{[d:e]}$ = 4.3) was on the UC-Choles column, but 1DHEA now co-eluted with ADEN instead of ETIO. UC-HyP and UC-PBr gave the best overall resolution for critical group 1, but out of all the screened columns, only UC-PBr gave extended baseline separation ($Rs_{[d:e:g]}$ > 3) for all compounds of this group.

Non-traditional Phases. MS-Critical Group 2 Resolution (**Figure 90; B [Group 2, orange]**). Elution order was very different on some of the non-traditional phases for the critical group 2 compounds (**Table 22; [Group 2]**). The UC-Choles column was one of the few to resolve MTHY and MIBL, but did not give significant improvement over the resolution observed on the traditional RX-SIL phase. The best overall resolution for group 2

was on the PolarX column, except that MSAL and MSEL showed significant tailing. Generally, none of the non-traditional phases out performed the traditional phases for the resolution of critical group 2.

Non-traditional Phases. MS-Critical Group 3 Resolution (**Figure 90; B [Group 3, blue]**)**.** Of all the phases screened, the baseline separation of OXAN (*o*) from TSTO (*m*) and EPIT (*l*) was only accomplished on two phases, the UC-Choles and the UC-PBr columns (**Table 22; [Group 3]**). TSTO and EPIT were also separated on UC-HyP, but co-eluted on both UC-triazole and the PolarX column.

Non-traditional Phases. Summary. Triazole had the least resolution for the main pairs using the generic screening gradient (all having Rs < 1). Although the best Rs for most of the critical compounds was observed (Rs > 3) on UC-PBr, elution for CLNB and ADAR required > 60% modifier concentration, and peak shape of STNZ and DNZL deteriorated at lower % modifier.

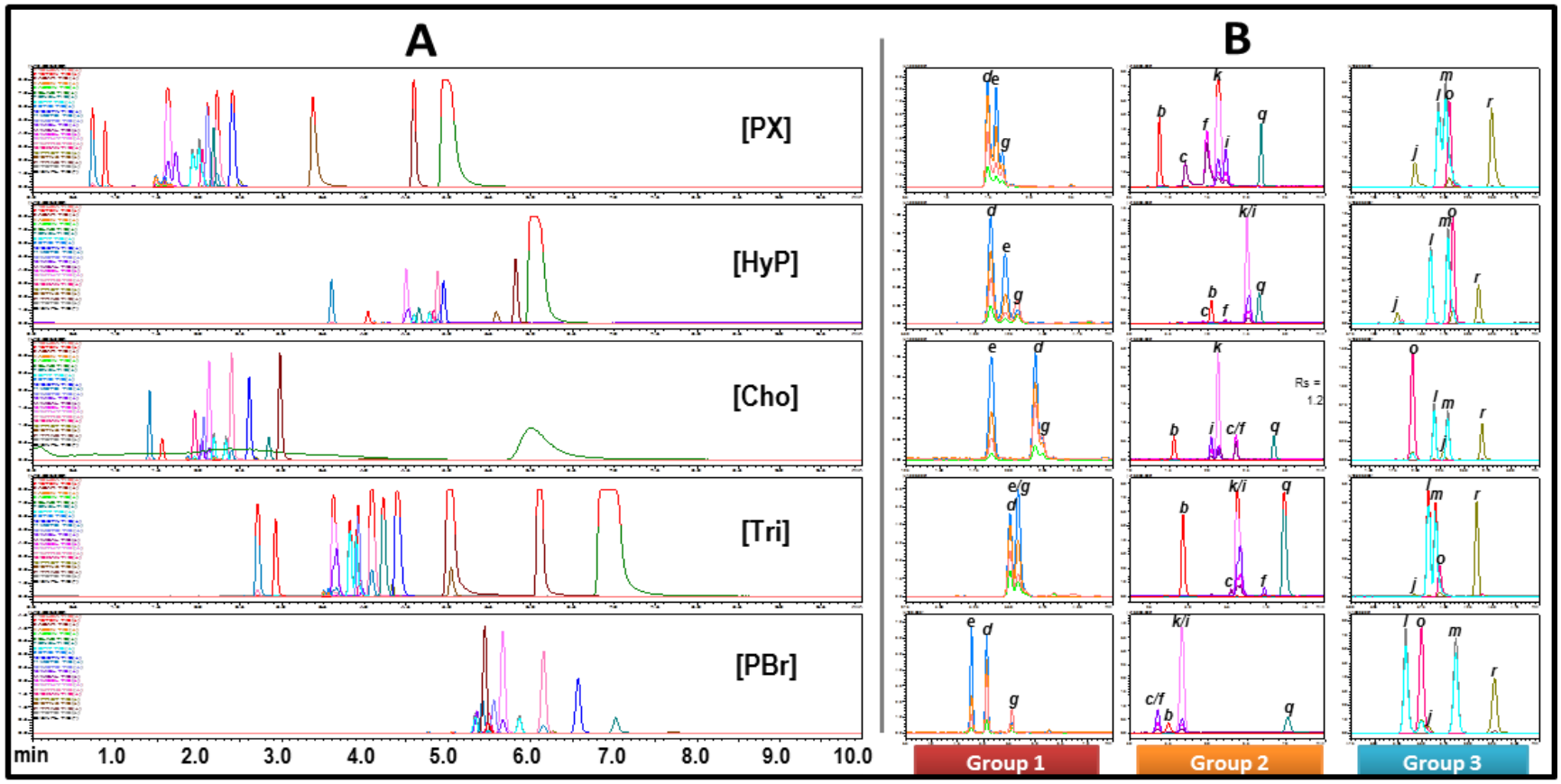

Figure 90. Column Scouting on Non-Traditional Stationary Phases using SFC-MS injections of androgenic steroid mix [AAS-mix]. [Panel A] Full runtime; **[Panel B]** Overlays of critical Groups: **[Group 1, left]** androsterone (ADEN-MRM [orange; ***d***]), etiocholanolone (ETIO-MRM [blue; ***e***]), 1-androsterone (1-DHEA [pink; ***g***]); **[Group 2, middle]** epitestosterone (EPIT-MRM [cyan; ***m***]), testosterone (TSTO-MRM [gray; ***l***]), oxandrolone (OXAN-MRM [hot pink; ***o***]), prasterone (PRST-MRM [gold; ***j***]), trenbolone (TRNB-MRM [brown; ***r***]); **[Group 3, right]** 1-androstenedione (1STEN-MRM [red; ***b***]); mestanolone (MSAL-MRM [magenta; ***c***]); mesterolone (MSEL-MRM [rose; ***f***]); mibolerone (MIBL-MRM [purple; ***k***]); methyltestosterone (MTHY-MRM [light pink; ***i***]); and danazol (DNZL-MRM [turquoise; ***q***]). **Conditions: generic screening gradient (5 - 40% MeOH over 8 minutes), with column temperature of 50 °C and outlet pressure of 15 MPa.**

Table 22. Resolution of Critical Pair Groups during Screening of Non-Traditional SFC Stationary Phases.

Critical Group	Critical Group Resolution					Column		Elution Order
	PolarX	HyP	UC-CHOLES	UC-Triazole	UC-Pbr			
1	d, e, g	d, e, g	e, d, g	d, e/g	e, d, g	ADEN (d)	Group 1 Key	
	1.10	1.4	4.3	0.0	3.3	ETIO (e)		
	0.6	1.2	0.4	0.2	5.1	1DHEA (g)		
2	b, c, f, k, i, q	c, b, f, k/i, q	b, i, k, c/f, q	b, c, k/i, f, q	c/f, b, k/i, q	1STEN (b)	Group 2 Key	
	4.3	1.4	6.6	8.7	0.0	MSAL (c)		
	3.02	2.3	1.2	0.3	0.0	MSEL (f)		
	1.37	3.5	3.4	0.1	1.4	MTHY (i)		
	0.94	0.2	0.0	3.0	1.7	MIBL (k)		
	5.5	1.1	6.8	3.2	12.0	DNZL (q)		
2-B	3.0	3.7	0.0	8.1	0.0			
2-C	0.9	0.2	1.2	0.1	3.2			
3	j, l, m, o, r	j, l, m, o, r	o, l, j, m, r	j, l, m, o, r	l, o, j, m, r	PRST (j)	Group 3 Key	
	2.8	4.6	3.2	1.9	1.8	EPIT (l)		
	0.8	2.4	1.4	1.0	0.0	TSTO (m)		
	0.4	0.7	0.7	0.5	3.9	OXAN (o)		
	5.5	3.4	5.0	5.2	4.3	TRNB (r)		
3-D	10.1	10.9	5.8	8.2	8.0			
3-E	0.8	2.4	2.1	1.0	5.7			

5.6. SFE-simulation Results.

A comparison between the SFE-Simulation and the generic column screening gradient is presented in **Figure 91**; with the resulting chromatograms overlaid over the gradients for two different columns. Where an example of a column exhibiting high sample plug retentivity is shown in the left panel (**Figure 91; [A]**) and on the right shows a column exhibiting poor plug retention (**Figure 91; [B]**). For both columns, the top chromatogram was produced using the generic screening gradient (showing the ramp in modifier concentration in blue). The bottom chromatogram for each column was produced using the SFE-simulation gradient (modifier ramp shown overlaid on the chromatogram in red). Note that in the SFE simulation that the gradient does not start until 2 minutes into the run. This 2 minute period is the duration where the SFE-simulation is performed, to mimic the delivery of the 'plug' to the column. Once the simulation is complete, the same generic gradient ramp (as in the top chromatogram) is started. If the SFE-simulation has no effect, the only difference between the top and bottom chromatograms should be a delay (of approximately 2 minutes).

The column showing good plug retention was the UC-cyano column. The chromatogram from the simulation (bottom) looks similar to the separation using the generic screening gradient (top). A longer delay before the start of elution is also notable, but generally peak shapes have not degraded. On, the 2-ethylpyridine column, shown in [B], peak shapes were good (except for CLNB in dark green), when using the generic gradient (top). However, the online simulation, in the bottom chromatogram, shows a distinct deterioration in the quality of the chromatography. Some of the analytes have migrated down the column before analysis could begin. The high baseline noise in multiple MRMs, indicate the compounds have been smeared across the entire chromatogram. This migration (e.g., non-retention of the plug) clearly degrades the chromatography and some of the peaks have disappeared completely, and others result in high noise across the entire chromatogram.

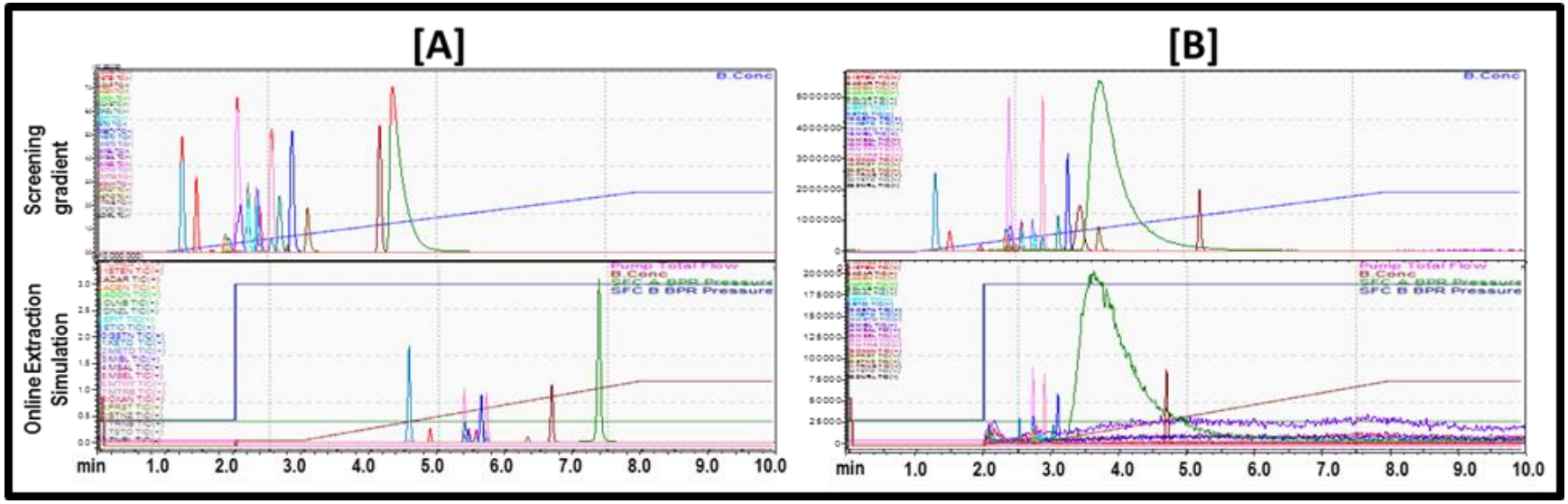

Figure 91. Example Chromatograms comparing separations produced by the generic gradient to separations produced using the SFE-simulation. SFC-MS MRM-TIC chromatograms, comparing separations on two different columns: **[A]** UC-Cyano column and **[B]** 2-ethylpyridine column; using [top] the generic screening gradient and [bottom] SFE-simulation gradient.

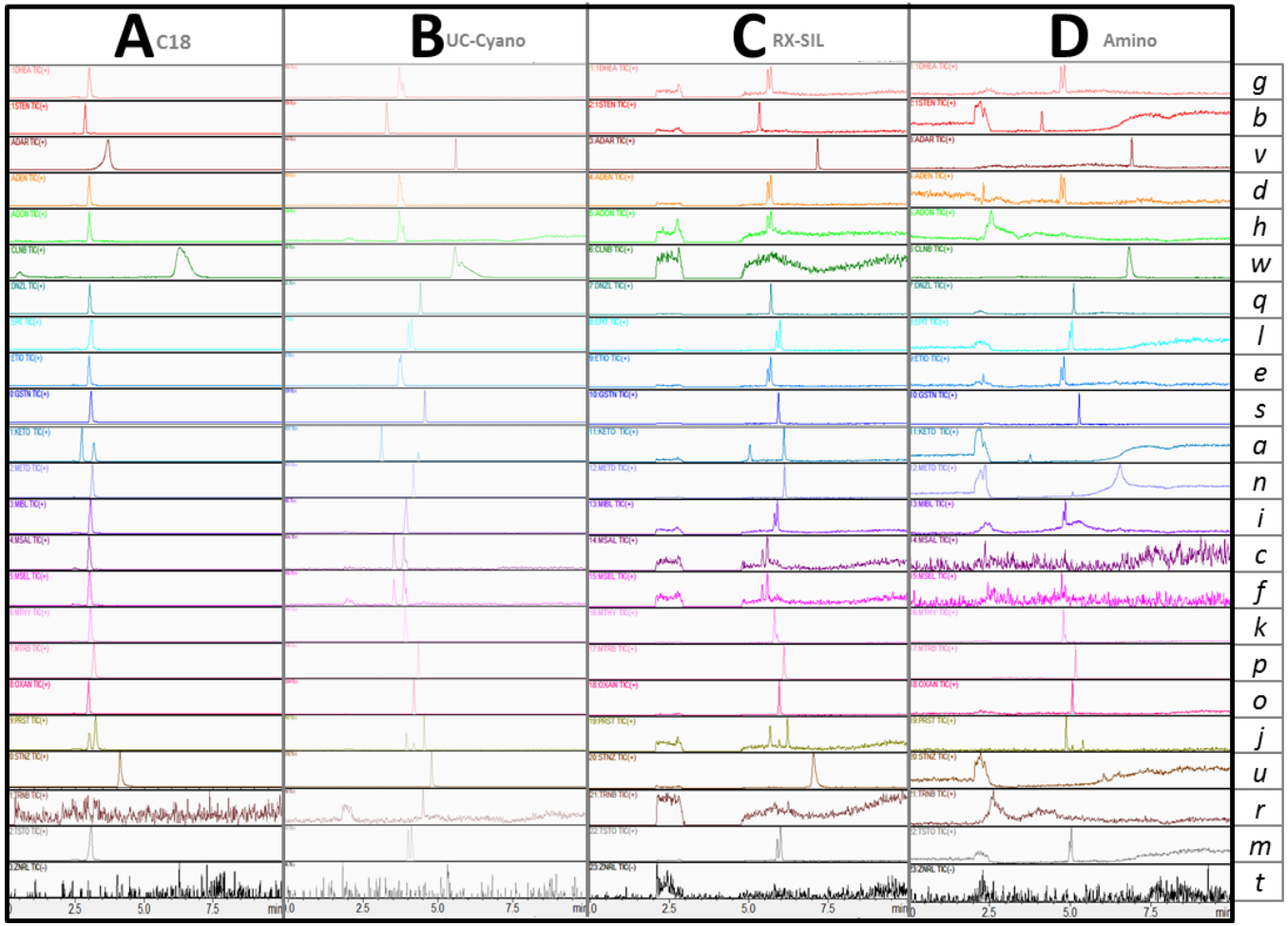

Figure 92. Stacked MRM-TIC Chromatograms Produced by the Extraction Simulation Across a Polarity Range of Traditional SFC Stationary Phases; Shown in order of increasing polarity from left to right: [A] C18 column; [B] UC-Cyano column; [C] RS-SIL Silica Column; and [D] Amino column. Stacked MRM-TIC chromatograms for Targeted Anabolic Agents: for targeted anabolic agents: 7-keto-DHEA ([a], KETO-MRM, [teal]); 1-androstenedione ([b], 1STEN-MRM, [red]); mestanolone ([c], MSAL-MRM, [magenta]); androsterone ([d], ADEN-MRM, [orange]); etiocholanolone ([e], ETIO-MRM, [blue]); mesterolone ([f], MSEL-MRM, [rose]); 1-androsterone ([g], 1DHEA-MRM, [pink]); mibolerone ([i], MIBL-MRM, [purple]); prasterone ([j], PRST-MRM, [gold]); methyltestosterone ([k], MTHY-MRM, [light pink]); epitestosterone ([l], EPIT-MRM, [cyan]); testosterone ([m], TSTO-MRM, [gray]); methandienone ([n], METD-MRM, [lilac]); oxandrolone ([o], OXAN-MRM, [hot pink]), metribolone ([p], MTRB-MRM, [coral]); danazol ([q], DNZL-MRM, [turquoise]); trenbolone ([r], TRNB-MRM, [brown]); gestrinone ([s], GSTN-MRM, [cobalt]); zeranol ([t], ZRNL-MRM, [black]); stanozolol ([u], STNZ-MRM, [mocha]); andarine ([v], ADAR-MRM, [maroon]); and clenbuteral ([w], CLNB-MRM, [dark green]).

5.6.1. SFE-simulation Results: Traditional SFC Phases.

Stacked MRM-chromatograms for each of the targeted analytes are shown in **Figure 92** for 4 columns ranging from a non-polar, C18 phase (Left), to a more polar, Amino phase (right). Stacking the MRMs, allows an overview of the compound specific effect of the simulation. The high signal noise shows the deterioration in plug retention of later eluting (more polar) compounds, especially on the more polar SPs. This is to be expected as a general trend, but since it is compound specific, a manner to rapidly screen this important factor for online extraction method development, adds to the ability to choose a legitimate column candidate for further online SFE-method development.

5.6.2. SFE-simulation Results: Non-Traditional SFC Phases.

The usefulness of the simulation is especially well exemplified with the screening of the non-traditional phases, as especially if a phase is proprietary as in the PolarX column, predicting where column performance may lay within a range of column polarities would be difficult. For example many of the non-traditional phases screened produced much better resolution between critical pair groups and normally would have been taken to further development steps and much time could have been spent on development. Both the PolarX and the UC-HyP columns are good examples of this, where both produced very promising resolution with the generic screening gradient, but with the simulation, showed very poor plug retention during the simulation.

5.6.3. SFE-simulation: Discussion/Summary of all

Figures **S_Figure 19** and **S_Figure 20**, show the results of the extraction simulation for all 15 screened columns. Some columns that gave the best resolution between critical pairs were ruled out as candidates for further development due to low potential for retention of online extraction plug loading. For example, phases that showed little capability for retaining an online extraction plug, such as Diol, Amino, and 2-EP (**S_Figure 19; [F], [G] & [H]**), as well as UC-HyP and UC-PBr (**S_Figure 20; [B] & [E]**), all had high migration of all compounds down the column before analysis was started, resulting in the loss of most peaks. UC-HyP and UC-PBr did not successfully

retain the sample plug, so most compounds have migrated thru the columns before analysis was started. Both Silica columns (S_Figure 19**; [C], [D] & [E]**), UC-Choles and UC-Triazole (S_Figure 20**; [C] & [D]**) all showed better potential for extraction plug loading with improved peak shapes on the earlier eluting compounds, but were still inadequate, having decreasing peak areas, especially for the early eluting compounds, therefore these phases were also ruled out for further development.

5.6.4. Best Performing phases.

Best overall potential for extraction plug loading was seen using both Cyano phases, C18 (S_Figure 19**; [A], [B] & [C]**), and PolarX (S_Figure 20**; [A]**). Out of this group, ultimately UC-Cyano, which exhibited the best peak shapes for late eluting compounds, was chosen for further development.

5.7. Online-Extraction for Proof of Concept.

Three online extractions were performed on the UC-Cyano column using a minimally optimized (non-fully developed method), to show a proof of concept for the validity of the column selected via the simulation. Retention time and peak area reproducibility's were compared to that obtained via SFC injections and are presented in **Table 23**.

The three extractions are shown in **Figure 93**, peak shapes and resolution are similar throughout all three first extractions. Retention times were reproducible (SD ≤ ± 0.02 min) for all compounds, except ZRNL (Rt = 11.1 ± 0.38 min). The signal for ZRNL was much lower than the other targeted compounds due to lower initial concentrations of the standard. Peak areas were all within reason for online extraction, ranging from 4 - 20% (av. peak area RSD = 7%), especially if considered that this is a fully un-optimized method. The exception was the latest eluting compounds CLNB and ADAR, both having > 45% RSD. Considering again that the method has not been optimized, poor performance especially for later eluting compounds would be expected.

Finally, these proof of concept extractions were performed in the splitless extraction mode. Since the system configuration is splitless, all effluent from the extraction is directed on-column during dynamic extraction. This

allows for direct comparison of average extracted peak areas to those obtained from SFC injections. SFC injections using (1.0 µL) of the same steroid mix was spotted (1.0 µL/spot) onto the Whatman collection cards for use in the online extractions. Percent of the SFC area (%$Area_{SFC}$) was calculated and are shown in **Figure 94** for each AAS. The %$Area_{SFC}$ area was compound specific and ranged from 5 - 102% (av. = 52%). All compounds were above 25%, except CLNB (13%) & ADAR (5%). Lower extractability was expected, both being late eluting (more polar) compounds, using the un-optimized extraction method. Alternatively, KETO, gave %$Area_{SFC}$ > 100% of the SFC injections. This could be an effect of pressure differences during extraction plug loading onto the column changing peak shape/broadening of peaks, and or decreasing resolution between neighboring compounds, contributing co-eluting area which was not present in the SFC-only injections, but is most likely an effect of background matrix from the sampling materials (e.g., the cellulose-based collection card). Both background matrix and optimization of the extraction will be evaluated in later development steps.

Table 23. Proof-of-Concept Online Extraction, Average Area and Retention times for Anabolic Agents.

Elution Order	AAS	Av. Rt	SD (Rt)	Av. Area	Area %RSD	% SFC inj. Area
1	KETO	7.730	0.01	20,229,634	13%	102 ± 7%
2	1STEN	8.076	0.01	4,163,800	13%	42 ± 3%
3	MSAL	8.304	0.02	123,388	7%	99 ± 4%
4	ADEN	8.735	0.02	214,025	3%	78 ± 1%
5	ETIO	8.900	0.03	686,942	12%	38 ± 2%
6	MSEL	8.990	0.01	352,996	12%	81 ± 5%
7	1DHEA	9.027	0.01	73,242	15%	23 ± 2%
8	ADON	-	-	-	-	-
9	MTHY	9.126	0.01	11,619,077	19%	52 ± 5%
10	PRST	9.168	0.02	62,130	8%	67 ± 3%
11	MIBL	9.215	0.01	6,105,414	16%	44 ± 4%
12	EPIT	9.805	0.01	1,828,895	10%	43 ± 2%
13	TSTO	9.801	0.01	2,223,698	9%	46 ± 2%
14	METD	9.876	0.01	759,311	4%	35 ± 1%
15	OXAN	9.945	0.01	2,039,467	7%	35 ± 1%
16	MTRB	10.324	0.02	4,892,309	5%	63 ± 2%
17	DNZL	10.529	0.01	240,431	2%	26 ± 1%
18	TRNB	11.229	0.01	42,751	10%	8 ± 1%
19	GSTN	11.119	0.02	3,386,141	5%	58 ± 1%
20	ZNRL	11.120	0.38	1,708	10%	29 ± 1%
21	STNZ	11.854	0.01	1,155,362	16%	26 ± 2%
22	CLNB	13.762	0.01	13,102,459	45%	10 ± 2%
23	ADAR	14.029	0.01	3,136,093	62%	4 ± 1%

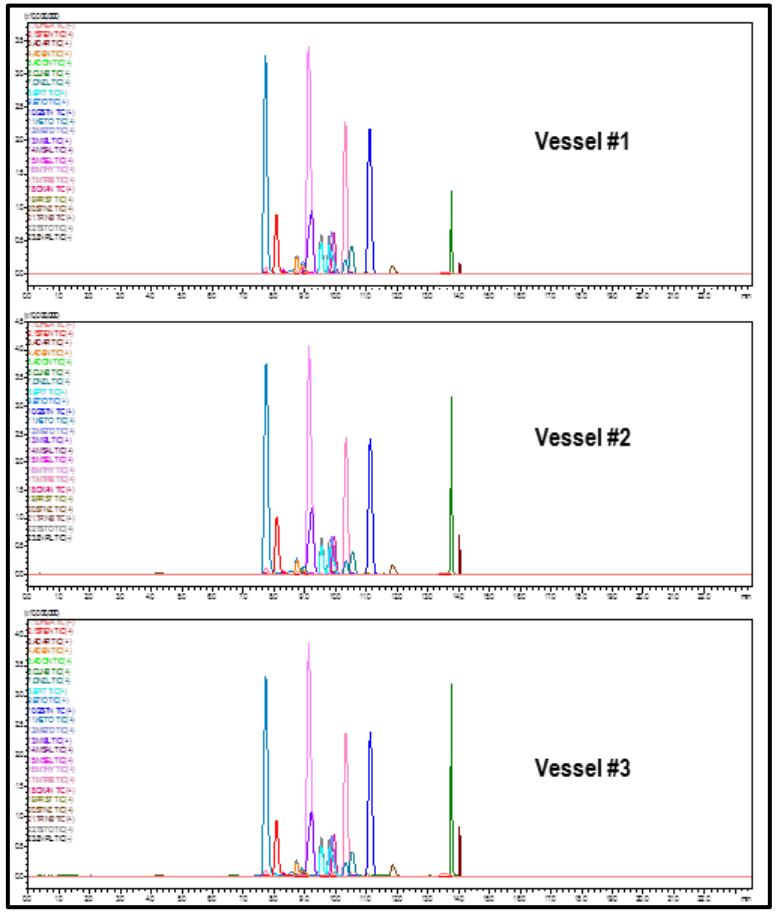

Figure 93. Three Online Extractions of AAS from Cellulose Collection Cards from 1.0 µL spots of AAS-mix using a preliminary Un-optimized SFE-SFC-MS Method on UC-Cyano

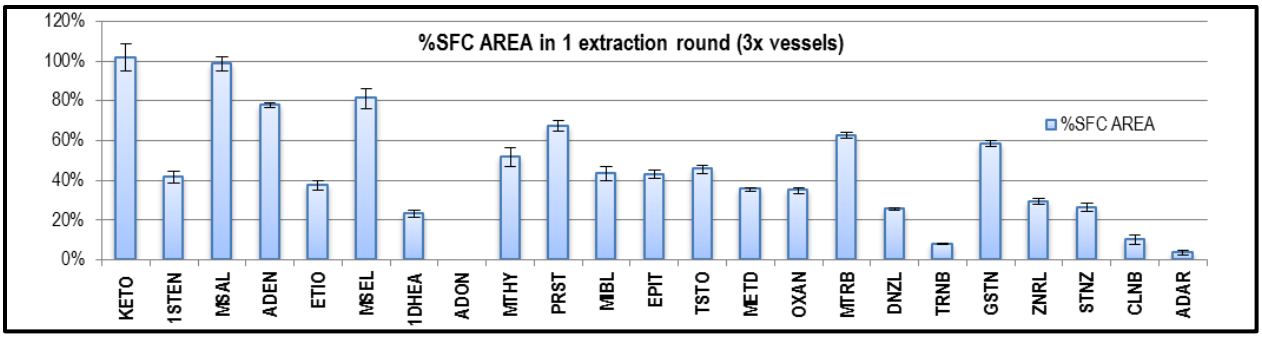

Figure 94. Bar Graph showing Percent (%) Average Area of SFC injection Area, for three separate extraction vessels (1 extraction each [n=3]) using optimized Online SFE-SFC-MS Extraction method on UC-Cyano.

5.8. Conclusions.

Thirteen phases were screened including eight traditional SFC phases ranging from (non-polar to polar) and five non-traditional phases. Columns were compared using a generic screening gradient with special attention to resolution of critical groups for chromatographic separation identified in earlier work during MS-optimization steps. Columns were then also evaluated via an SFE-simulation which mimicked online loading of a sample plug, using SFC injections.

The best performing column was determined to be the UC-cyano column for not only for potential for chromatographic separation of critical groups, but also good potential for plug retention during the SFE-simulation. Proof of concept extractions were performed online using the selected column with a generic extraction method. Most importantly the SFE-simulation allowed the successful selection of a phase clearly capable of retaining a plug on the first round of column selection.

5.i. Instrument Methods: SFC SP Screening

5.i.1. General Method Information.

Detailed information on materials and equipment used for Column Screening in this study can be found in the following sections of **Chapter #2. Materials and Methods**:

5.i.1.1. Materials.

- Solvents used for mobile phases and dilution solutions can be found in **Section 2.1.1. Solvents**.
- Analytical standards information for targeted anabolic agents can be found in **Section 2.1.2. Analytical Standards; *Anabolic androgenic steroids (AAS)*** **and** **Table 1.**

5.i.1.2. Instrumentation.

- The Instrumentation used is detailed in **Section 2.2.1. Instrumentation; *Nexera UC online SFE-SFC-MS***.
- Column details are given in **Section 2.2.2. Columns** and **Table 5.**
- Other equipment used is detailed in **Section 2.2.3. Other Equipment**:
    - ***Nitrogen Generator***
    - ***Analytical balances***

5.i.1.3. Solutions Preparation.

- Stock Solutions prep and storage detailed in **Section 2.3.1.1. AAS Stock Solutions** and **Table 6; Stock Solutions.**
- Injection solutions prep and concentrations are described in **Section 2.3.1.3. AAS Injection Solutions; *AAS Test Mixture [AAS-mix]*** and **Table 6; *AAS-mix*.**
    - ***AAS Test Mixture [AAS-mix]***

5.i.2. MS Detection Parameters – MRM method

Detection was achieved using an LCMS-8050 triple quadrupole mass spectrometer, equipped with an DUIS-source, and operated in Electrospray Ionization (ESI-), positive (+) and negative (-) ionization mode. Interface voltages were set to 4.0 kV (for positive Q3 scan mode) and -3.0 kV (for negative Q3 scan mode) and temperature set to 300 °C. Nitrogen gas was used for both drying and nebulizing gas; with flow rate of 2.0 L/min for nebulizing gas and 10.0 L/min for drying gas. Desolvation and DL temperatures were 526 °C and 250 °C, respectively. Heat Block temperature was set to 400 °C, and heating gas used was dry air. Gas used for collision induced dissociation (CID) was argon at 270 kPa. DL Bias/Q-array Bias were set in tuning file as 0 V, and Q3 Pre-rod Bias at -15 V (for positive scan mode) and 15 V (for negative scan mode). Scan range was 120 to 1,200 m/z with scan speed 15,000 u/sec, with 0.100 sec Event time with Q3 resolution set to unit.

5.i.3. Mobile Phases (MP) and Stationary Phases (SP).

MPs. All work in this chapter utilized SFC/CO_2-based MPs, where up to 40% modifier was mixed with liquid Carbon Dioxide ([CO_2] – Instrument grade) via the instrument solvent delivery pumps using isocratic or gradient elution. Four modifiers were used: [MeOH] LCMS-grade methanol; [FA] methanol + 0.1% formic acid (LCMS-grade); [TEA] methanol + 0.1% trimethylamine (LCMS-grade); and [AmFo] methanol + 5 mM ammonium formate (LCMS-grade). All modifier solutions were sonicated for 20 minutes prior to use.

Columns. Thirteen stationary phases were screened. Traditional phases are summarized in **Table 19** and Non-traditional columns in **Table 20.**

5.i.5. Parameters held constant.

The following settings were held constant as default parameters unless otherwise specified. A methanolic mixture of 23 anabolic agents [AAS-mix] was injected onto a 5-µL external loop, using partial-loop (1.0 µL) injections with 0.10 µL air gaps. Mobile Phase [A] was carbon dioxide (CO_2) and mobile phase [B] was methanol (unless specified otherwise). The column temperature was 50 °C and the system outlet pressure was 15 MPa (BPR_A).

5.i.5. Methods for Stationary Phase Screening

5.i.5.1. Approach to Column Screening.

A rapid screening approach was utilized. Separations were performed on each column, first using isocratic runs at 40, 20, and 10% modifier, and then using a generic screening gradient described below. Equilibration runs were performed between each injection. Retention times were recorded for each analyte. Resolution was calculated and elution order compared between columns for: A. the overall separation (for all 23 analytes), B. between critical group members (e.g., between all five analytes in critical group 2), and C. between critical pairs (e.g., between EPIT and TSTO [critical pair 3-D])

5.i.5.1. Generic Screening Gradient.

A generic gradient (**Figure 85**) was used as a screening gradient and was as follows: initial concentration of 5% B was held constant for 1.0 minutes (0-1 min), before ramping from 5% to 40% B over 7 minutes (1-8m), and finally holding at 50%B for two minutes (8-10m).

5.i.5.2. Instrument Setup: SFC-Separation Optimization Configuration.

Detailed instrument configuration details can be found in **Chapter #1: Hyphenated Instrumentation: SFE-SFC-MS** (**Section 1.4.2: Instrument Configurations used for SFC Optimizations: *SFC-Separation Optimization***).

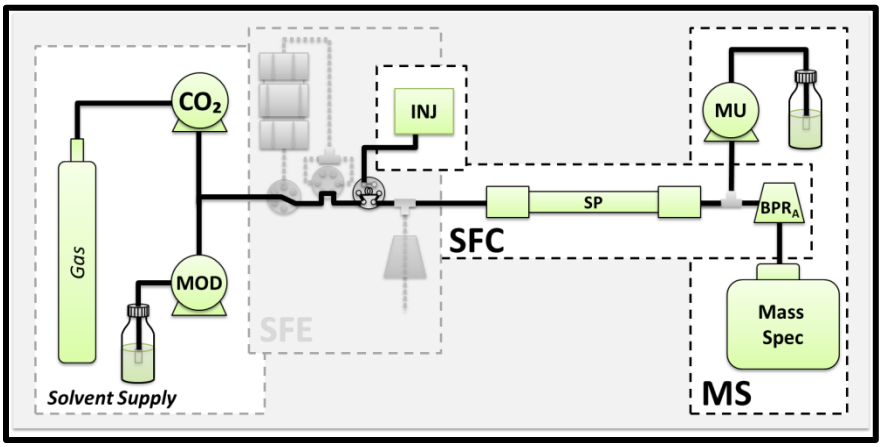

See Figure 13 in Chapter #1

5.i.6. Extraction Plug Simulation Screening.

5.i.6.1. Instrument Method: SFE-Simulation Gradient.

The extraction plug (SFE-) simulation method used a time program similar to that for an online extraction (**Figure 90**): static extraction was simulated by two method points: first the column was equilibrated at high modifier concentration (50%[B]) for 1 minute before the start of the run; and second, this high concentration was held for a short duration (an additional 0.03 minutes after the start of the run [i.e., after the injection]) (0.00 – 0.03 minutes 50% methanol was used at 5.0 mL/min). Dynamic extraction was simulated from 0.04 – 2.00 minutes at 5% methanol also at 5.0 mL/min. At 2.00 minutes the system flow rate changed to the gradient flow rate (column specific) and the screening gradient began and was as follows: initial concentration of 5% B was held constant for 1.0 minutes (2-3 min), before ramping from 5% to 40% B over 7 minutes (3-10m), and finally holding at 50%B for two minutes (10-12m). System outlet pressure (BPR_A) was held at 15 MPa throughout all steps. Extraction mode simulated was Split-mode, where for the first 2.0 minutes, BPR_B was held at 15.2 MPa (0.0 – 2.0 minutes) and then closed (BPR_B = 40 MPa) for the duration of the analysis (2.1 – 12 min).

5.i.6.2. Instrument Setup: SFE-Simulation Configuration.

Detailed instrument configuration details can be found in **Chapter #1: Hyphenated Instrumentation: SFE-SFC-MS** (**Section 1.6. SFE Simulation Configurations**).

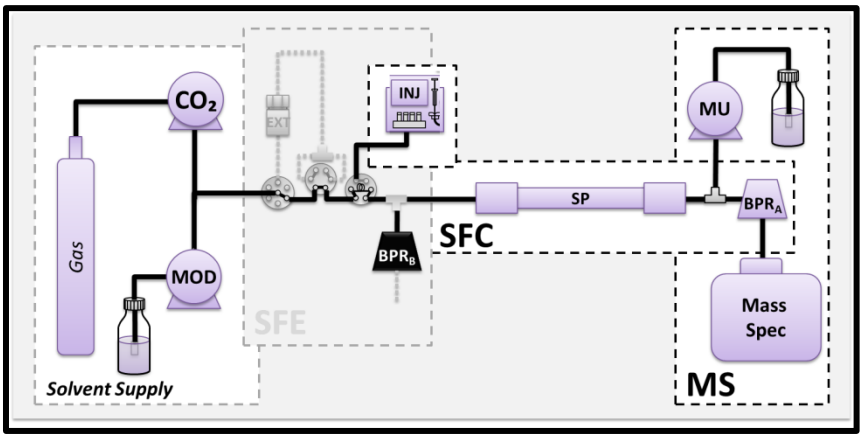

See Figure 18 in Chapter #1

5.i.7. Generic Extraction Method.

5.i.7.3.1 Instrument Method: Proof-of-Concept Online Extraction.

The method parameters used for the proof of concept extractions are given in **Table 24.** For extraction, 1.0 µL of the same AAS-mix was applied to Whatman® FTA®, classic, cellulose based, sample collection/preservation cards, allowed to dry for more than 3 hours and cored using a standard (6 mm) single hole punch [PøMA]. Punched spots were enclosed into 0.2-mL extraction vessel and set to the SFE automated rack changer to enable rapid method screening.

5.i.7.3.1 Instrument Setup: Online Extraction (Splitless-mode) Configuration.

Detailed instrument configuration details can be found in **Chapter #1: Hyphenated Instrumentation: SFE-SFC-MS** (**Section 1.5.4. 'Splitless' Extraction Mode**).

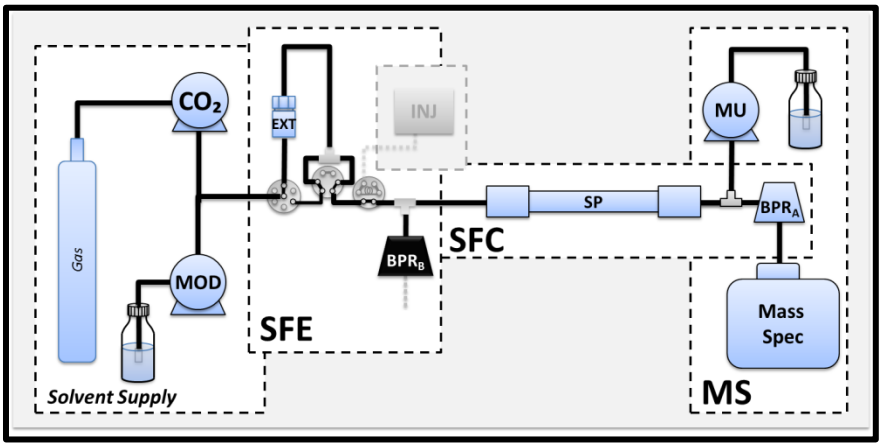

See Figure 17 in Chapter #1

Table 24. Generic Extraction Method Parameters used for proof-of-concept for SFE-Simulation Online Extractions for Online SFE-SFC-MS Extraction of AAS from Whatman Cellulose Paper.

Online SFE-SFC-MS Conditions:				
Mobile Phase	:	[A]: CO_2; [B]: Methanol + 5mM ammonium formate		
SFE				
Vessel Size	:	0.2 mL		
Vessel Temp.	:	35 °C		
Extraction Pressure	:	[BPR(A)]: 12.5 MPa; [BPR(B)]: 40 MPa		
Mode	:	Splitless		
Filling	:	2ml/min;	2% [B];	1.0 min; (0.00 – 1.00m).
Static Extraction	:	3ml/min;	0% [B];	6.0 min; (1.01 – 7.00m).
Dynamic Extraction	:	3ml/min;	0% [B];	1.0 min; (7.00 – 8.00m).
Wash	:	3ml/min;		3.0 min; (23.01 – 26.00m).
SFC-MS				
Column	:	Shimadzu, Shim-pack, UC-CN (4.6 x 150mm, 5 µm)		
Flowrate	:	3mL/min		
Gradient	:	2 - 12.5% [B];	8.0 min;	(8.01 - 16.00m),
		12.5 - 30% [B];	2.0 min;	(16.00 - 18.00m),
		30% [B];	5.0 min;	(18.00 - 23.00m).
Column Temp.	:	60 °C		
Back Pressure	:	[BPR(A)]: 15 MPa; [BPR(B)]: 40 MPa		
Detector	:	LCMS-8050 (ESI, MRM mode, Positive [+] & Negative [-])		

Literature Cited:

FIRST CITED IN PREVIOUS CHAPTERS

[1] Berger TA. (2015). "Supercritical fluid chromatography" Primer series; publication number 5991-5509EN; Agilent Technologies, USA. https://www.agilent.com/cs/library/applications/5991-8554EN_SFC_appcompendium_LR.pdf

[17] Wicker AP, Tanaka K, Nishimura M, Chen V, Ogura T, Hedgepeth W, Schug KA. (2020). "Multivariate approach to on-line supercritical fluid extraction - supercritical fluid chromatography - mass spectrometry method development." *Analytica Chimica Acta*. **1127**: p282-294. https://doi.org/10.1016/j.aca.2020.04.068

S_5. SUPPLEMENTARY MATERIALS

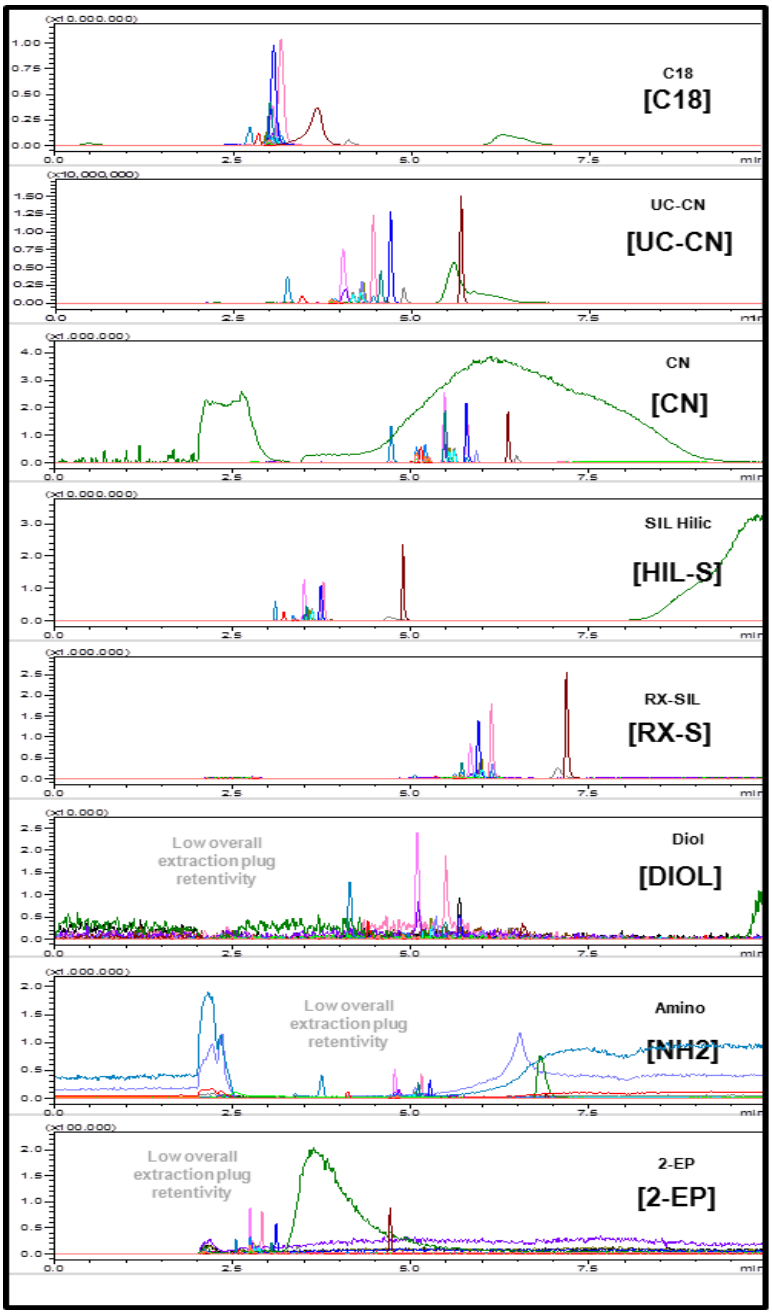

S_Figure 19. Extraction Simulation on 8 Traditional SFC SPs Shown in order of increasing polarity from top to bottom.

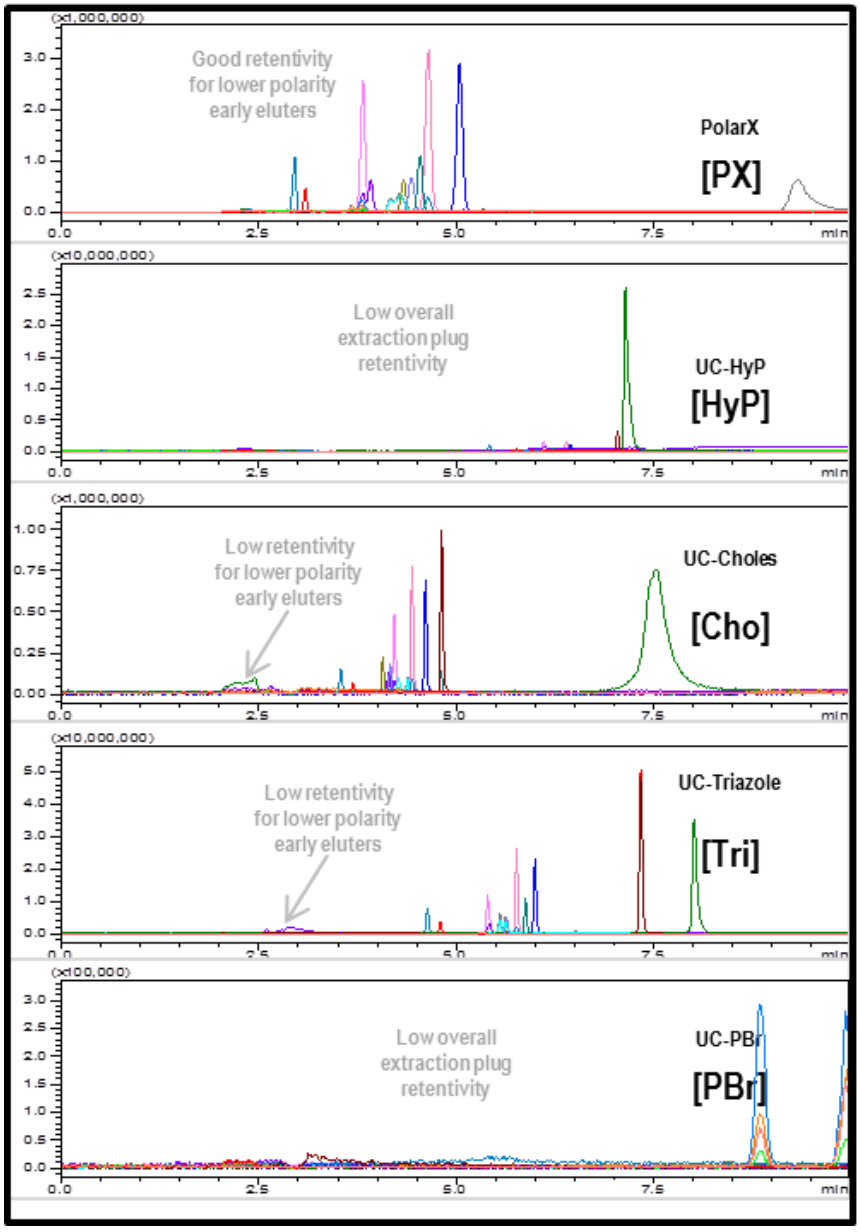

S_Figure 20. **Extraction Simulation on 5 non-Traditional SFC SPs.**

CHAPTER 6

SFC-OPTIMIZATIONS FOR SEPARATION OF AAS: CHROMATOGRAPHIC SEPARATION

CHAPTER 6
SFC-SEPARATION OPTIMIZATION FOR AAS:
CHROMATOGRAPHIC SEPARATION
MOBILE PHASE OPTIMIZATIONS & SECONDARY PARAMETERS

6.1. SFC Separation Optimizations.

6.1.1. Retention Controls in SFC.

Retention controls are discussed in more detail in **Chapter #1. Hyphenated Instrumentation; Section 1.1.6. *Retention Controls in SFC.*** In short, both flow rate and modifier concentration are considered primary control variables. Flow rate has a near linear effect on retention, where a modest effect on resolution favors a super-optimum flow rate (μ_{opt}). Modifier concentration is the most powerful tool in changing retention, having a non-linear effect, where even the first small additions of modifier can have large impacts on retention, and the effect is expected to follow the general rule: when modifier concentration is halved, the retention is expected to nearly double. Column temperature and outlet pressure are considered secondary control variables. Outlet pressure tends to mimic flow rate (with higher pressures mimicking higher flow rates) and usually has little effect on retention and resolution. Column temperature on the other hand, can have significant effect on the relative retention of compounds (e.g., selectivity changes). The effect of secondary parameters can be very useful to improve difficult separations.

6.1.2. SFC Separation Optimizations

SFC-based separation optimizations for SFE-SFC-MS analysis are the second step in method development for online methods, and can be broken down into three main steps:

1. **Column Selection**. An appropriate stationary phase is chosen for further development. Column screening is normally performed with a generic method for rapid comparison between phases. Comparing the resolution of critical MS-groups identified in previous method steps (mainly MS-optimizations) can be helpful in narrowing down potential phases.
2. **Separation Optimization**. Further separation optimizations are performed on the best performing column: where mobile phase compositions and the effect of instrument parameters are evaluated.
3. **SFC-MS method evaluations**. Final methods are evaluated for reproducibility.

This chapter focuses on Steps 2 and 3 for SFC Optimizations, around the creation of a final SFC method to be used, later, (hyphenated) with online SFE-based extractions. In the previous chapter, thirteen columns were screened to evaluate chromatographic resolution, speed, and sample plug retentivity. The UC-Cyano column was determined to be the best overall performing phase and was chosen for further method development. This chapter focuses on the optimization of retention of the targeted analytes using the UC-Cyano column (**Figure 95**).

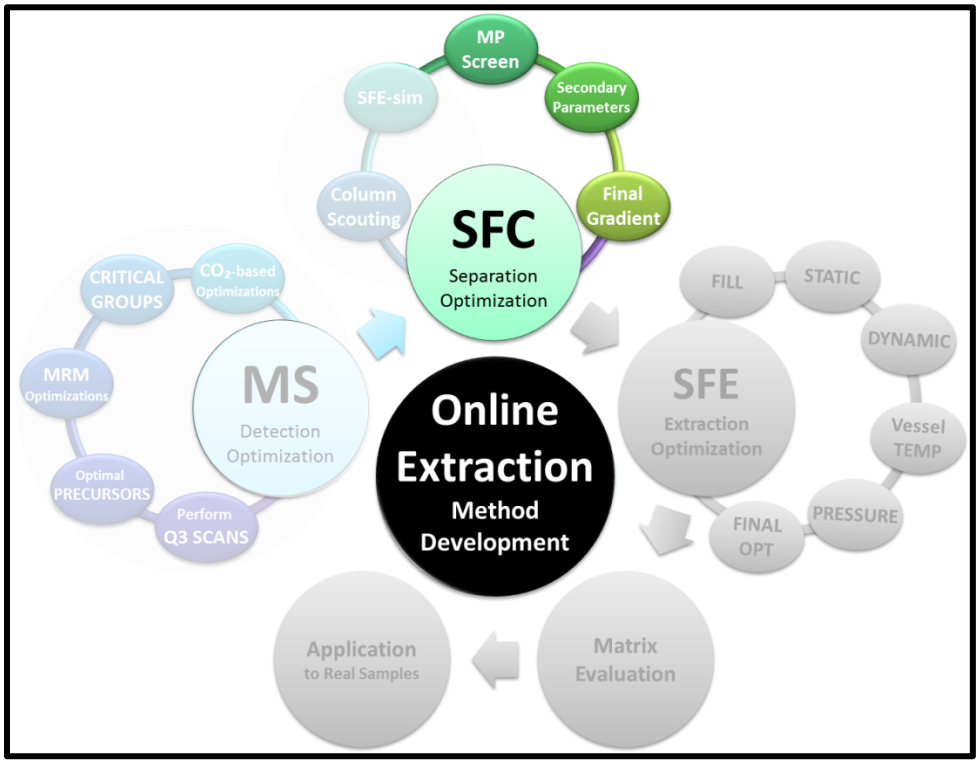

Figure 95. Online Extraction Method Development Focus for Chapter #6 SFC-Separation Optimizations: Effect of Modifier Composition and Secondary Parameters on Retention, Resolution and Selectivity.

6.1.3. Screening SFC-Parameters with UC-Cyano Column

Screened parameters in the work presented in this chapter include:

- Mobile phase additive (effect on peak shapes).
- Modifier concentration (effect on retention and resolution).
- Secondary parameters (effect on retention and resolution).
- Final gradient optimizations.

The final method is then evaluated for reproducibility of retention times and peak areas.

6.2. Watch Groups Used to Evaluate SFC-Separation Optimization.

6.2.1. MS-Critical Groups

In previous development steps, MRM-optimizations were performed for 23 anabolic agents. Structures for each analyte are shown in **Figure 96**. Using the LabSolutions software optimal precursors, products, voltages and collision energies were determined (discussed in **Chapter 4: MS-Detection: *MRM Optimizations***). Standards were individually reinjected to evaluate the MRM method (**Table 25**). Steroids that produced signal for two or more MRMs were grouped. This identified five groups of compounds as 'critical pairs'. Where fundamental similarities in structure and/or molecular weight, make differentiation with MS-alone impractical, and therefore flagged as critical groups requiring chromatographic separation. Comparison of the resolution within critical groups is a helpful tool to evaluate the effectiveness of the chromatographic method under each set of conditions.

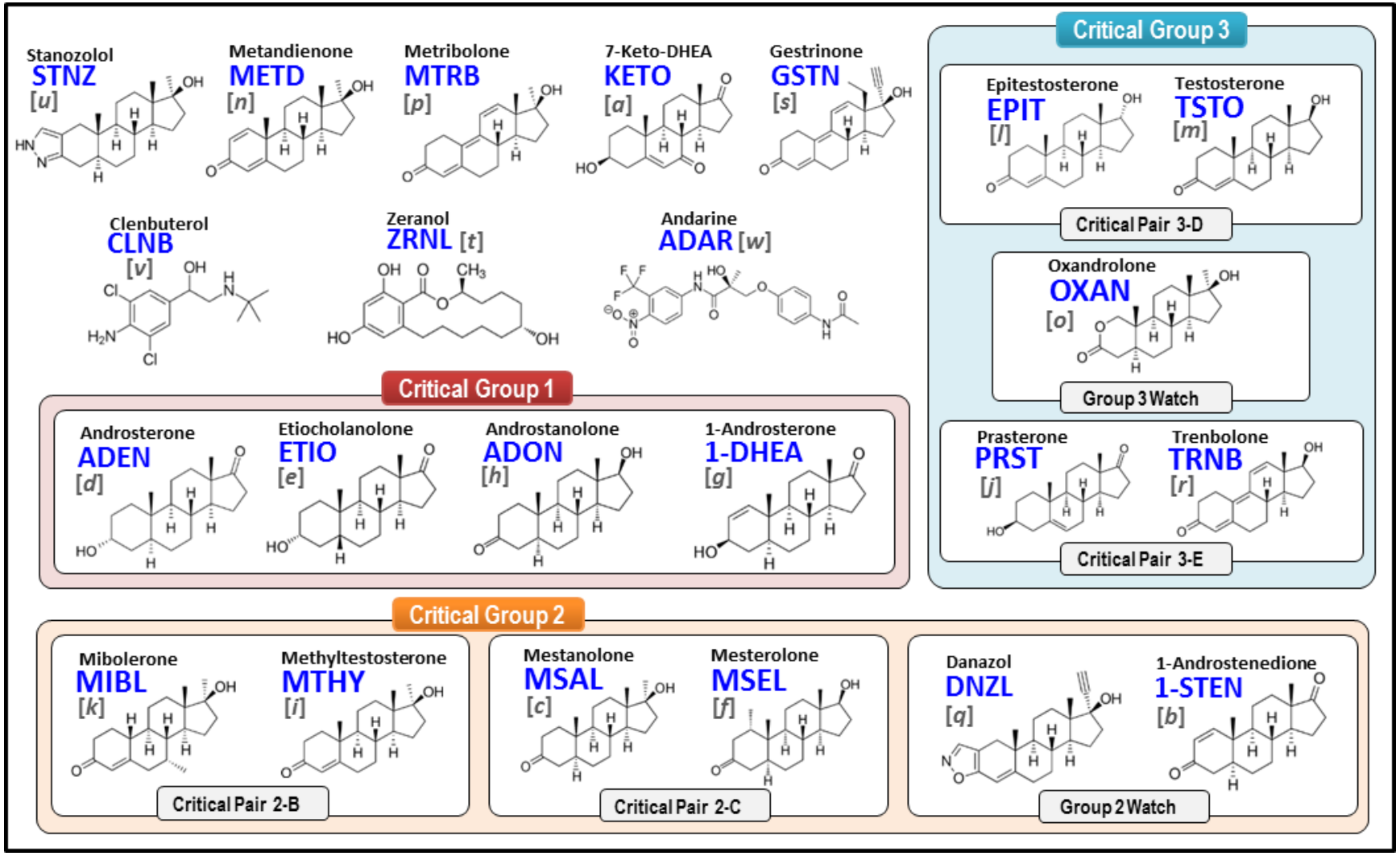

Figure 96. Structure of targeted anabolic androgenic steroids and bio mimics, showing critical pair groups and (similar) MRM transitions.

Table 25. MRM Details for Targeted Anabolic Agents (AAS).

				Precursor			Product Ion							
				MW	+/-	(m/z)	Transition 1	(Q1/Q3 Bias, CE)	Transition 2	(Q1/Q3 Bias, CE)	Transition 3	(Q1/Q3 Bias, CE)	Transition 4	(Q1/Q3 Bias, CE)
Peak	Steroid	ID	Critical Group				(m/z)	([V]/[V], [eV])	(m/z)	([V]/[V], [eV])	(m/z)	([V]/[V], [eV])	(m/z)	([V]/[V], [eV])
[*a*]	7-Keto-DHEA	KETO	n/a	302.2	+	285	**81**	(-22/-32, -27)	**79**	(-20/-30,-44)	**107**	(-20/-20,-27)	**149**	(-20/-26,-21)
[*b*]	1-Androstenedione	1-STEN	2	286.4	+	287	**97**	(-20/-20, -22)	**109**	(-22/-22,-24)	**79**	(-20/-30,-46)	**109**	(-20/-40,-35)
[*c*]	Mestanolone	MSAL	2-C	304.4	+	305	**269**	(-20/-28, -16)	**229**	(-20/-24,-20)	**159**	(-20/-34,-23)	**187**	(-20/-36,-22)
[*d*]	Androsterone	ADEN	1	290.4	+	273	**255**	(-20/-26, -14)	**147**	(-22/-32,-21)	**199**	(-22/-20,-21)	**161**	(-20/-36,-20)
[*e*]	Etiocholanolone	ETIO	1	290.4	+	273	**255**	(-20/-28, -12)	**215**	(-20/-42,-17)	**105**	(-20/-20,-35)	**91**	(-20/-38,-43)
[*f*]	Mesterolone	MSEL	2-C	304.4	+	305	**269**	(-22/-28, -17)	**173**	(-20/-40,-24)	**287**	(-22/-30,-16)	**133**	(-24/-22,-28)
[*g*]	1-Androsterone	1-DHEA	1	290.4	+	291	**273**	(-20/-30, -10)	**255**	(-15/-26, -15)	**135**	(-20/-28,-20)	**91**	(-22/-36, -10)
[*h*]	Androstanolone	ADON	1	290.4	+	291	**255**	(-11/-12, -16)	**173**	(-10/-18,-21)	**227**	(-10/-23,-10)	-	-
[*i*]	Methyltestosterone	MTHY	2-B	302.5	+	303	**109**	(-22/-20, -28)	**97**	(-20/-20,-26)	**97**	(-22/-20,-27)	**285**	(-22/-30,-16)
[*j*]	Prasterone	PRST	3-E	288.2	+	271	**253**	(-20/-26, -12)	**213**	(-22/-46,-15)	**213**	(-20/-40,-17)	**157**	(-20/-32,-22)
[*k*]	Mibolerone	MIBL	2-B	302.5	+	303	**271**	(-22/-30, -12)	**285**	(-22/-20,-17)	**121**	(-22/-24,-25)	-	-
[*l*]	Epitestosterone	EPIT	3-D	288.4	+	289	**109**	(-20/-20, -24)	**97**	(-22/-38,-25)	**79**	(-22/-30,-44)	**253**	(-22/-26,-18)
[*m*]	Testosterone	TSTO	3-D	288.4	+	289	**109**	(-22/-20, -25)	**97**	(-22/-36,-22)	**253**	(-22/-28,-17)	**79**	(-22/-28,-46)
[*n*]	Methandienone	METD	NON (mid)	300.4	+	301	**121**	(-22/-46, -28)	**149**	(-22/-26,-15)	**283**	(-22/-30,-11)	**121**	(-22/-22,-24)
[*o*]	Oxandrolone	OXAN	3	306.4	+	307	**289**	(-22/-30, -12)	**271**	(-22/-30,-14)	**121**	(-22/-22,-24)	**229**	(-24/-24,-18)
[*p*]	Metribolone	MTRB	NON (mid)	284.4	+	285	**227**	(-22/-24, -23)	**267**	(-20/-28,-17)	**198**	(-22/-20,-30)	**159**	(-20/-30,-23)
[*q*]	Danazol	DNZL	2	337.5	+	338	**148**	(-24/-30, -25)	**91**	(-26/-32,-55)	**120**	(-24/-22,-28)	**310**	(-24/-32,-20)
[*r*]	Trenbolone	TRNB	3-E	270.4	+	271	**253**	(-20/-26, -19)	**199**	(-20/-20,-22)	**165**	(-20/-36,-56)	**128**	(-20/-26,-57)
[*s*]	Gestrinone	GSTN	NON (mid)	308.4	+	309	**241**	(-22/-26, -23)	**199**	(-24/-40,-32)	**291**	(-24/-20,-16)	**262**	(-22/-28,-21)
[*t*]	Zeranol	ZRNL	n/a	322.4	-	321	**277**	(34/28, 23)	**303**	(36.0/20,22)	**259**	(36.0/26,24)	**235**	(36.0/28,24)
[*u*]	Stanozolol	STNZ	n/a	328.5	+	329	**81**	(-24/-30, -51)	**95**	(-24/-20,-42)	**121**	(-24/-22,-37)	**107**	(-24/-20,-41)
[*v*]	Clenbuterol	CLNB	NON (late)	277.2	+	227	**203**	(-32/-36, -16)	**259**	(-20/-26,-10)	**132**	(-20/-24,-28)	**168**	(-20/-32,-28)
[*w*]	Andarine	ADAR	NON (late)	441.4	+	442	**108**	(-32/-20, -37)	**208**	(-32/-20,-21)	**190**	(-32/-20,-25)	**148**	(-32/-32,-31)

6.2.2. Groups used for Evaluation of Method Optimizations:

In the current work, special attention was paid to the resolution of a total of 5 groups of analytes:

A) critical group 1
B) critical group 2
C) critical group 3
D) non-critical, late eluters
E) non-critical, mid-eluters

Critical group 1 contains four analytes: androsterone ([***d***], ADEN-MRM, orange), etiocholanolone ([***e***], ETIO-MRM, blue), 1-androsterone ([***g***], 1DHEA-MRM, pink), and androstanolone ([***h***], ADON-MRM, green). All four members of group 1 are critical to one-another as they all give signal for their own as well as each other's MRMs. ADON was ruled out for use in the current work, as a reliable MRM method could not be determined at this time. The remaining three members of critical group 1 can be distinguished via ion ratios, but only if they are chromatographically separated.

Critical group 2. Separation of critical group 2 is also based on MRM overlap and contains six analytes: 1-androstenedione ([***b***], 1STEN-MRM, red), mestanolone ([***c***], MSAL-MRM, magenta), mesterolone ([***f***], MSEL-MRM, rose), methyltestosterone ([***k***], MTHY-MRM, light pink), mibolerone ([***i***], MIBL-MRM, purple), and danazol ([***q***], DNZL-MRM, turquoise). MSAL and MSEL are high priority, critical pair 2-B, as they give equal signal for each others MRMs and cannot be distinguished via ion ratios. MTHY and MIBL are critical pair 2-C, giving significant signal for each other's MRMs. Unlike pair 2-B, MTHY & MIBL, can be distinguished via ion ratios, if they are chromatographically separated. The separation between these two pairs is also high priority for chromatographic separation, as MIBL and MTHY also give signal for both the MSAL and the MSEL-MRM's. 1STEN and DNZL are watch members of group 2, mainly for Group 2-B, as MSAL and MSEL both give signal for the DNZL-MRM, and MSAL gives signal for the 1STEN-MRM.

Critical group 3. Also based on MRM overlap, critical group 3 involves five analytes: testosterone ([***m***], TSTO-MRM, gray), epitestosterone ([***l***], EPIT-MRM, cyan), oxandrolone ([***o***], OXAN-MRM, hot pink), prasterone ([***j***], PRST-MRM, gold), and trenbolone ([***r***], TRNB-MRM, brown). EPIT and TSTO are high priority, critical pair 3-D, as they give nearly equal signal for each other's MRMs and cannot be distinguished via ion ratios. Possibly the most critical of the critical pairs identified, differentiation between EPIT and TSTO will require individual injections after chromatographic separation, and will rely on retention time verification for identification. PRST and TRNB are critical pair 3-E, because TRNB gives strong signal for the PRST-MRM. The separation of PRST from group 3-D is also high priority as PRST gives signal for both the TSTO and EPIT-MRMs. Additionally, the separation of OXAN from 3-D is also important, as it also gives signal for both the TSTO and EPIT-MRMs.

Non-critical, Late-eluters. Although these two compounds are easily distinguishable via MS-alone, being the latest eluting compounds, their relative retention have an effect on overall runtime. This non-critical group includes two compounds: clenbuterol ([***v***], CLNB-MRM, dark green) and andarine ([***w***], ADAR-MRM, maroon). This group was formed since effects on retention determine the overall runtime.

Non-critical, Mid-eluters. A group of mid-eluting, non-critical, compounds were also watched during this work. This group included gestrinone ([***s***], GSTN-MRM, cobalt), metandienone ([***n***], METD-MRM, lilac), and metribolone ([***p***], MTRB-MRM, coral). Several changes in selectivity were seen within this group throughout the work and co-elution's tended to have a significant effect on the overall separation. Therefore, these three compounds were also watched during the separation optimization.

6.3. Methods for Separation Optimizations.

6.3.1. Approach for Additive Screening.

At times, polar analytes can have too strong an interaction with the stationary phase resulting in poor peak shape. To correct for this, a mobile phase additive can be used. In the current work, additives were screened. The

additives included a base, an acid, and a buffer. Injections were performed using the same screening gradient used for column selection, each time with a different additive and the resulting chromatograms were compared. All further optimizations were performed using ammonium formate (AmFo) as additive in methanol as modifier.

6.3.2. Approach for Screening Secondary Parameters.

To screen secondary parameters a total of 16 injections were repeated for each of two modifier concentrations. Each injection utilized a different combination of column temperature (30, 40, 50 or 60 °C) and system outlet pressure (11, 15, 20 or 25 MPa) (**Table 26**).

Table 26. Chart showing combination of Secondary Instrument parameters utilized for Screening Effect of Column Temperature and Outlet Pressure on Retention of Targeted Analytes.

		Column Temperature (°C)			
		30	40	50	60
Outlet Pressure (MPa)	11	30 °C, 11 MPa	40 °C, 11 MPa	50 °C, 11 MPa	60 °C, 11 MPa
	15	30 °C, 15 MPa	40 °C, 15 MPa	50 °C, 15 MPa	60 °C, 15 MPa
	20	30 °C, 20 MPa	40 °C, 20 MPa	50 °C, 20 MPa	60 °C, 20 MPa
	25	30 °C, 25 MPa	40 °C, 25 MPa	50 °C, 25 MPa	60 °C, 25 MPa

For example, the first of the sixteen injections utilized 30 °C column temperature and 11 MPa outlet pressure. The system outlet pressure was then increased to 15 MPa, and allowed to equilibrate (EQ) for 5 minutes before the second injection was performed. The instrument was then set to 20 MPa, with 5 min EQ, before injection, then to 25 MPa, with 5 min EQ, before the final injection. This sequence would be repeated using 10% modifier before changing to a higher (+10 °C) column temperature and repeating the entire sequence (11 MPa → EQ → 15 MPa → EQ → 20 MPa, etc.) at the new column temperature. When the temperature was changed extra time was allowed to reach the new temperature since the stirred bath oven was slow.

Secondary parameters screening was performed via batch table automation to ensure proper equilibration between analyses and allows a rapid, systematic evaluation of the effects of secondary parameters. Resulting chromatograms are then processed and retention times were then plotted versus change in temperature or change in pressure to evaluate effects on retention, resolution, and selectivity between targeted analytes.

6.4. Additive Screening.

6.4.1. Methods for Additive Screening.

Although most of the targeted analytes had relatively good peak shapes using methanol-alone as modifier **Figure 97; [B]**, excessive tailing on the latest eluting peak, clenbuterol (CLNB, **[dark green]**) prompted the need for the addition of an additive to the mobile phase. Additives were screened to evaluate effect on peak shapes, and included; a base (0.1% trimethylamine [TEA]), an acid (0.1% formic acid [FA]), and a buffer (5mM ammonium formate [AmFo]).

6.4.2. Additive Screening Results

Example SFC-MS chromatograms for each additive are presented in **Figure 97**. CLNB **[dark green]**, being an amine, as expected, using a basic additive **(Figure 97; [C])** greatly improved peak shape, but unfortunately had a strong secondary effect on the detection of all other analytes, possibly suppressing their ionization. Lowering the concentration of TEA to 0.01% (not shown), did not sufficiently improve the peak shape for CLNB and had minimal improvement of the signal for the other compounds. Although using a basic additive appeared to suppress signal for all compounds except CLNB, re-evaluation of MRMs showed a change in parent ion was responsible for the loss of signal using the MRMs optimized using methanol alone. Using an acid (FA) as MP additive **(Figure 97; [A]**) improved the MS signal for all other target analytes, but did not provide sufficient improvement to peak shape for CLNB. Alternatively, the use of a buffer as additive (**Figure 97; [D]**) had little negative effect on the ionization of the other analytes and provided significant improvement to the peak shape of CLNB.

An additional note, a change in selectivity was seen based on the addition of an additive in the MP. This was observed for the non-critical, late-eluting group, which includes CLNB **[dark green]** and ADAR **[maroon]** (two steroid mimics, not containing the characteristic steroid backbone). The improved peak shape for CLNB lead to a peak reversal between the two compounds. CLNB was less retained with both acidic and basic additives when compared to methanol alone, and ADAR was more retained with base as additive (Rt = 4.15m) when compared to acid as additive (Rt = 4.32m). Little effect was observed on peak shape or elution order for early- and mid-eluting

compounds (steroids with the characteristic backbone), which all showed little change in retention or selectivity with either an acidic or basic additive. Ultimately, the use of a buffer as MP additive gave the best result, giving improved peak shape on CLNB, simultaneously with little effect on MS sensitivity, and therefore was ultimately chosen as MP additive for further method development.

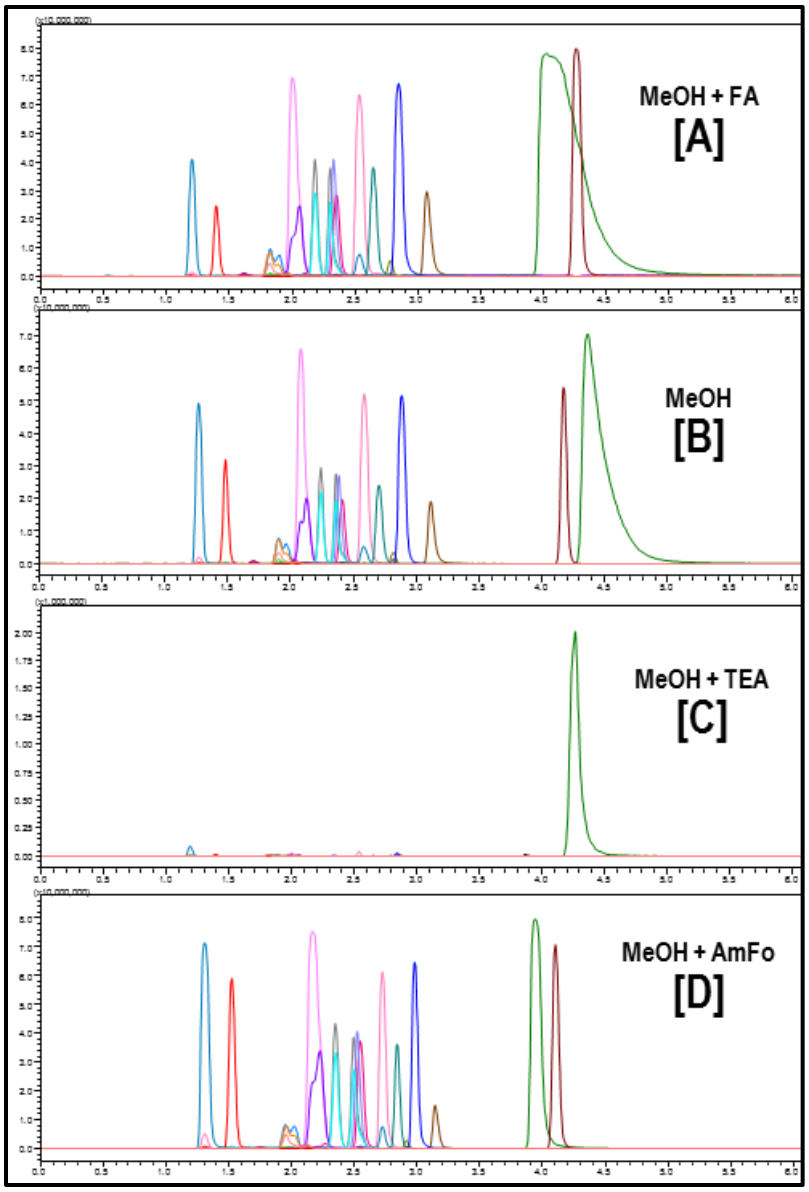

Figure 97. Mobile Phase Additive Scouting using SFC-MS Injections of Steroid Mixture (AAS-mix) on UC-Cyano Column: using methanol (MeOH) as modifier in carbon dioxide with various Additives: **[A]** 0.1% formic acid (FA), **[B]** no additive, **[C]** 0.1% trimethylamine (TEA), and **[D]** 5 mM ammonium formate (AmFo) . Overlaid MRM-TIC chromatograms (at full scale) for 23 anabolic agents: 7-keto-DHEA (KETO-MRM, [teal]), 1-androstenedione (1STEN-MRM, [red]), mestanolone (MSAL-MRM, [magenta]), androsterone (ADEN-MRM, [orange]); etiocholanolone (ETIO-MRM, [blue]), mesterolone (MSEL-MRM, [rose]), 1-androsterone (1DHEA-MRM, [pink]); methyltestosterone (MTHY-MRM, [light pink]), prasterone (PRST-MRM, [gold]), mibolerone (MIBL-MRM, [purple]), testosterone (TSTO-MRM, [gray]), epitestosterone (EPIT-MRM, [cyan]), methandienone [METD-MRM, [lilac]), oxandrolone (OXAN-MRM, [hot pink]), metribolone (MTRB-MRM, [coral]), danazol (DNZL-MRM, [torquoise]), trenbolone (TRNB-MRM, [brown]), gestrinone (GSTN-MRM, [cobalt]), zeranol (ZRNL-MRM, [black]), stanozolol (STNZ-MRM, [mocha]), clenbuteral (CLNB-MRM, [dark green]), and andarine (ADAR-MRM, [maroon]). **Conditions: 1.0 µL injection were made (via the autosampler) and separation was achieved using a Shimadzu Corp., UC-Cyano (4.6 x 150 mm, 5.0 µm) column. A generic screening gradient was used (5% modifier held for 1 minute, followed by a ramp to 40% modifier over 7 minutes, and held at 40% for two minutes). A flow rate of 3.0 mL/min was used with 50 °C column temperature and 15 MPa outlet pressure.**

6.5. Effect of Modifier Concentration on Retention

Modifier concentration is known to have a non-linear effect on retention in SFC, giving the general rule that halving the percent modifier will approximately double the retention time. Modifier concentration can occasionally also have an effect on selectivity. Especially with closely related compounds, the effect of modifier concentration may be stronger on one isomer versus the other. Initial adjustments to the generic gradient indicated peak reversals at lower modifier concentration; therefore the effect of modifier concentration on selectivity was investigated by comparing isocratic separations below 10% modifier while holding all other conditions (e.g. flow rate, column temperature and outlet pressure) constant. The effect of modifier concentration on retention was then evaluated and resolution between critical groups were compared (**S_Table 5).**

6.5.1. Critical Group 1 : Effect of Modifier Concentration.

Two peaks reversals were observed, for critical group 1, due to change in modifier concentration (**Figure 98; [A]**). Above 5% modifier, androsterone [ADEN, [***d***], orange) elutes first, followed by etiocholanolone (ETIO, [***e***], blue) and then 1-androsterone (1DHEA, [***g***], pink) elutes last. The first peak reversal for this group occurs between 1DHEA and ETIO at ~5% modifier; where below 5%, 1DHEA [***g***] elutes before ETIO [***e***]. The second peak reversal for the group occurs between 1DHEA and ADEN, where below 2% modifier 1DHEA [***g***] becomes the earliest eluting of the group, and co-elutes with ADEN [***d***] at 1.5% modifier.

6.5.2. Critical Group 2 : Effect of Modifier Concentration.

Figure **#MOD; [B] & [C**], both show the effect of change in modifier concentration on critical group 2, but **[B]** shows this group at higher concentration (15, 10, 7.5 and 5% modifier) and **[C]** shows the same compounds at low modifier concentrations (7.5, 5, 2.5 and 1.5%). The majority of the group 2 compounds produce adequate resolution at even moderate modifier concentrations. Critical pair 2-B (MSAL and MSEL) being baseline resolved starting at 15% modifier ($Rs_{[c:f]}$ > 1.6) and critical pair 2-C (MIBL and MTHY) baseline resolution ($Rs_{[k:i]}$ > 1.5) is achieved at ~8% modifier. Three peak reversals were observed for critical group 2, due to change in modifier concentration, and involve selectivity changes for the two group 2 watch compounds (1STEN and DNZL). MRM overlap and implications were discussed in detail in **Chapter #4. MRM-Optimizations; Section 4.14.2. Critical**

Group 2 discussion. In short, both MSAL and MSEL give low signal for DNZL and additionally, MSAL gives signal for 1STEN. Therefore, the separation of 1STEN and DNZL is mainly important for group 2-B compounds.

The first two reversals involves a change in retention of danazol (DNZL, [***q***], turquoise) versus methyltestosterone (MTHY, [***k***], light pink) and mibolerone (MIBL, [***i***], purple). Above 10% modifier (**Figure 98; [B], top**) DNZL [***q***] elutes last, but under 10%, MIBL [***i***] elutes last. As modifier concentration is decreased **[top-to-bottom]**, relative retention of DNZL decreases, until under ~ 7% modifier, DNZL elutes before MTHY [***k***]. Although, the separation of DNZL from MTHY and MIBL are not critical, any co-elution affects the overall resolution of critical group 2. Furthermore, the relative retention of DNZL continues to decrease at lower modifier concentrations (**Figure 98; [C], bottom two chromatograms**) and below 2% modifier DNZL nearly co-elutes with mesterolone (MSEL, [***f***], rose]. The third reversal was the result of the effect of modifier concentration on the retention of 1-androstenedione (1STEN, [***b***], red) versus the earliest eluting member of critical group 2; mestanolone (MSAL, [***c***],magenta). Above 5% modifier, 1STEN ([***b***], red) elutes first (**Figure 98; [C], 5%**). As the concentration is decreased, the relative retention of 1STEN increases versus MSAL [***c***], and a peak reversal occurs at ~2.5% modifier. At lower concentration MSAL elutes first (**Figure 98; [C], 1.5%**). This is a critical MS-pair and so is a critical watch item for final method optimizations, as co-elution should be avoided.

An additional observation for group 2, the predicted effect of modifier concentration on the ionization of MSAL [***c***] and MSEL [***f***], that was discussed in **Chapter #4. MRM-Optimizations, Section 4.15. Final Comments**, can be seen **Figure 98; [C]**. Note the stronger relative signals for MSAL & MSEL at 1.5% (**Figure 98; [C], bottom**) modifier versus 7.5% modifier (**Figure 98; [C], top**). This is likely due to a change in precursor ion intensity and further supports the recommendation that this pair should only be monitored qualitatively at this time.

Although overall chromatographic resolution is important, if in final method optimizations 1STEN and DNZL cannot be separated from the rest of group 3, they can be distinguished via ion ratios which makes their chromatographic separation less critical than for example, the critical pair 2-B (MSAL & MSEL), which cannot be differentiated via ion ratios. If compromises, in regards to the chromatographic separation are needed, 1STEN and DNZL would be less critical.

6.5.3. Critical Group 3 : Effect of Modifier Concentration.

Figure 98; [D] shows the effect of modifier concentration on the retention of critical group 3 compounds. Two important effects of modifier concentration were observed for this group, mainly involving critical pair 3-D (testosterone and epitestosterone) and oxandrolone.

First, modifier concentration had little effect on oxandrolone (OXAN, [***o***], hot pink), which co-elutes with testosterone (TSTO, [***m***], gray) regardless of modifier concentration. This is unfortunate, as the separation of OXAN is very important (since OXAN gives signal for both 3-D compounds). Since modifier concentration had little effect, it is unlikely that a set of conditions will be found where this pair will be separated.

The second out of the ordinary effect worth noting was that higher modifier concentration, produced higher resolution between TSTO and epitestosterone (EPIT, [***l***], cyan), and as the concentration is decreased **[top-to-bottom]**, the resolution between the pair decreases, resulting in a co-elution of the pair at lower modifier. As a result, at very low modifier (below 2%), all three critical compounds (TSTO, EPIT & OXAN) co-elute. This is opposite to expected behavior.

This suggests that the lowering modifier concentration to improve the resolution between this group will not have the desired effect, and instead would decrease the resolution. This will be an important watch item during final gradient optimizations, as EPIT and TSTO cannot be distinguished via ion ratios, and their separation will be of utmost importance for the final method.

6.5.4. 'Non-critical' Analytes: Effect of Modifier Concentration.

Two changes in selectivity were observed among the 'watched' non-critical targeted analytes; one for the late-eluters and one for the mid-eluters. For the late-eluters, clenbuterol (CLNB, [***v***], dark green) and andarine (ADAR, [***w***],maroon), modifier concentration had an effect on their relative retention. Although at higher concentration ADAR was less retained than CLNB (**Figure 98; [E], 15%**), a peak reversal was observed at ~ 10% modifier, which results in ADAR being more retained at lower concentration (**7.5%**). Although these two compounds are easily distinguishable via MS-alone, being the latest eluting compounds, their relative retention will have an effect on overall runtime.

For the mid-eluters, gestrinone (GSTN, [***s***], cobalt), metandienone (METD, [***n***], lilac), and metribolone (MTRB, [***p***], coral), modifier concentration also had an effect on relative retention (**Figure 98; [F]**). Although, GSTN always eluted first, a peak reversal between METD and MTRB was observed, where at high modifier concentration (**7.5%**) METD elutes before MTRB, and at low concentration (**2.5%**) METD elutes last.

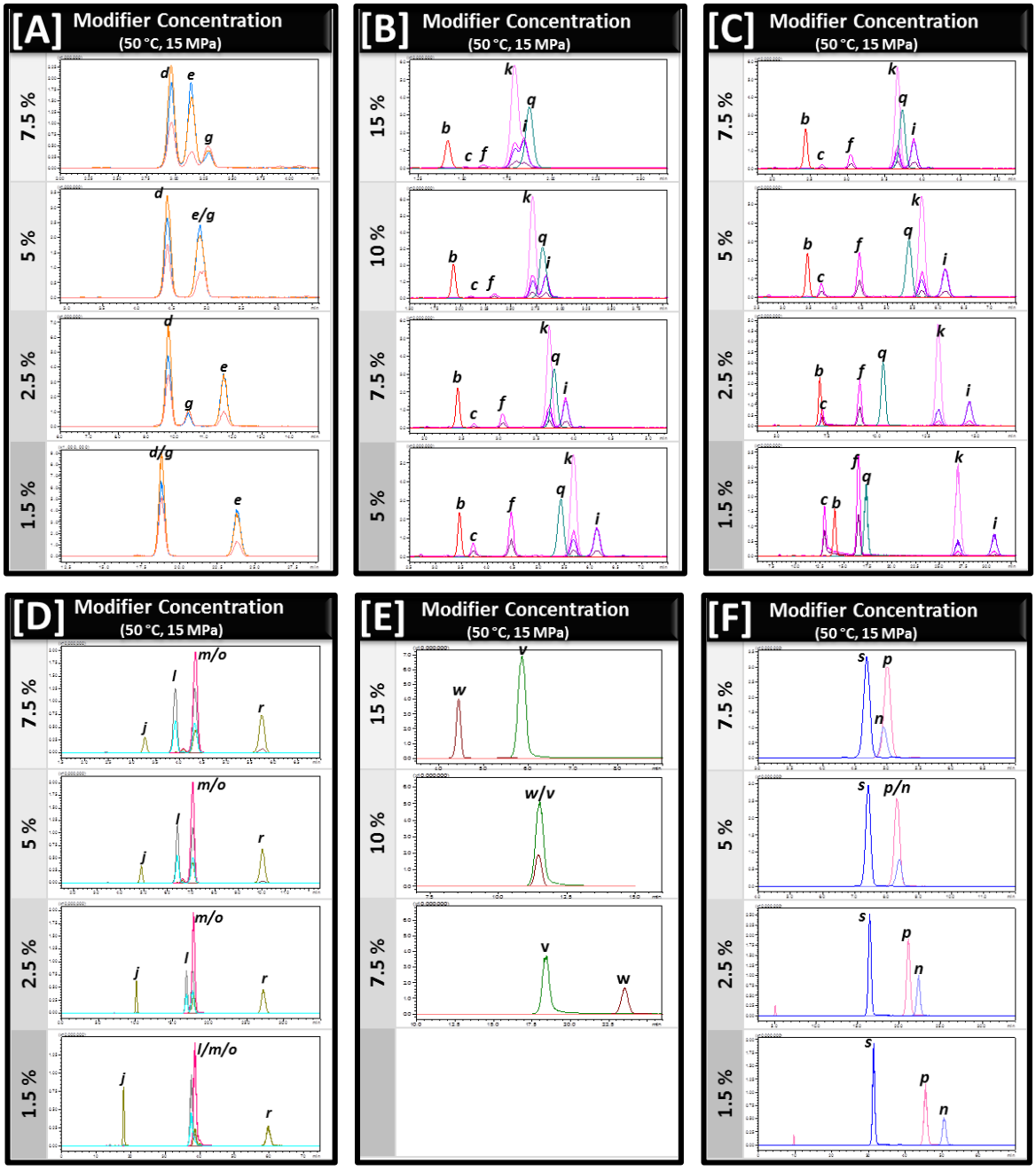

Figure 98. Effect of Change in Modifier Concentration on Retention for Critical Groups. [A] Critical Group 1 Compounds, [B]&[C] Critical Group 2 compounds, [D] Critical Group 3 Compounds, [E] Non-critical, Late-eluting Compounds and [F] Non-critical, Mid-eluting Compounds. Showing the Effect of Change in Modifier Concentration (%) *using isocratic runs at 15, 10, 7.5, 5, 2.5 and 1.5% modifier (specific concentration range stated in each pane*). Each panel displays on the [bottom] Scatter plots of retention time (minutes) versus modifier concentration; and on [top] Overlaid SFC-MS chromatograms for targeted anabolic agents: 1-androsterone (1DHEA, [**d**], pink); androsterone (ADEN, [**e**], orange); and etiocholanolone (ETIO,[**g**], blue); mestanolone (MSAL, [**c**], magenta); mesterolone (MSEL, [**f**], rose), mibolerone (MIBL, [**i**], purple), methyltestosterone (MTHY, [**k**], light pink), danazol (DNZL, [**q**], torquoise); 1-androstenedione (1STEN, [**b**], red); testosterone (TSTO, [***m***], gray); epitestosterone (EPIT, [***l***], cyan); oxandrolone (OXAN, [***o***], hot pink); prasterone (PRST, [***j***], gold); and trenbolone (TRNB, [***r***], brown); clenbuterol (CLNB, [***v***], dark green); and andarine (ADAR, [***w***], maroon), gestrinone (GSTN, [***s***], cobalt), Metandienone (METD, [***n***], lilac), and metribolone (MTRB, [***p***], coral). **Conditions: 1.0 µL injections were made (via the autosampler); separation was achieved using a Shimadzu Corp. UC-Cyano (4.6 x 150 mm, 5.0 µm d_p) column; Isocratic runs were used with a flow rate of 3.0 mL/min, 50 °C column temperature and 15 MPa outlet pressure.**

6.6. Effect of Secondary Parameters on Retention and Selectivity:

Two concentrations (5 and 10% modifier) were common to co-elution's due to selectivity changes observed among critical groups of analytes. The effect of secondary parameters on selectivity were evaluated and resolution between critical groups were compared using these two concentrations (5% modifier S_Table 6 and 10% modifier S_Table 7).

6.6.1. Secondary Parameters Effect on Resolution for Critical Group 1.

Critical Group 1: Effects of Column Temperature. Figure 99 shows the effect of temperature (30 , 40 , 50 and 60 °C) on the retention of critical group 1 compounds, under two sets of conditions: **[A]** 10% modifier at 15 MPa; and **[B]** 5% modifier at 25 MPa.

With 10% modifier and 15 MPa (**Figure 99; [A])** ADEN [**orange**] co-eluted with 1DHEA [**pink**] at 30°C and was progressively partially resolved with increasing temperature to 60°, becoming a shoulder at 50° with a distinct separate apex at 60°. The scatter plot at the bottom shows the gradual emergence of ADEN from the 1DHEA peak. At all temperatures, ETIO [**blue**] was nearly baseline resolved from the others.

With 5% modifier at 25 MPa (**Figure 99; [B])** one broad peak containing all three analytes at 30° resolved into 2 baseline resolved peaks, the first containing 1DHEA and the second the co-elution of ADEN and ETIO. Under both sets of conditions, ADEN moved relative to the others. –Note that at 40 °C, even at 5% modifier, the three compounds are better separated than at higher or lower temperatures.

Critical Group 1: Effects of Outlet Pressure. The effect outlet pressure on retention is characterized in **Figure 99; [C]**. At 11 MPa three distinct apexes are seen, with the order 1DHEA, ADEN, ETIO with ETIO nearly baseline resolved. With increasing pressure the peaks slowly merged into a single broad peak at 25MPa.

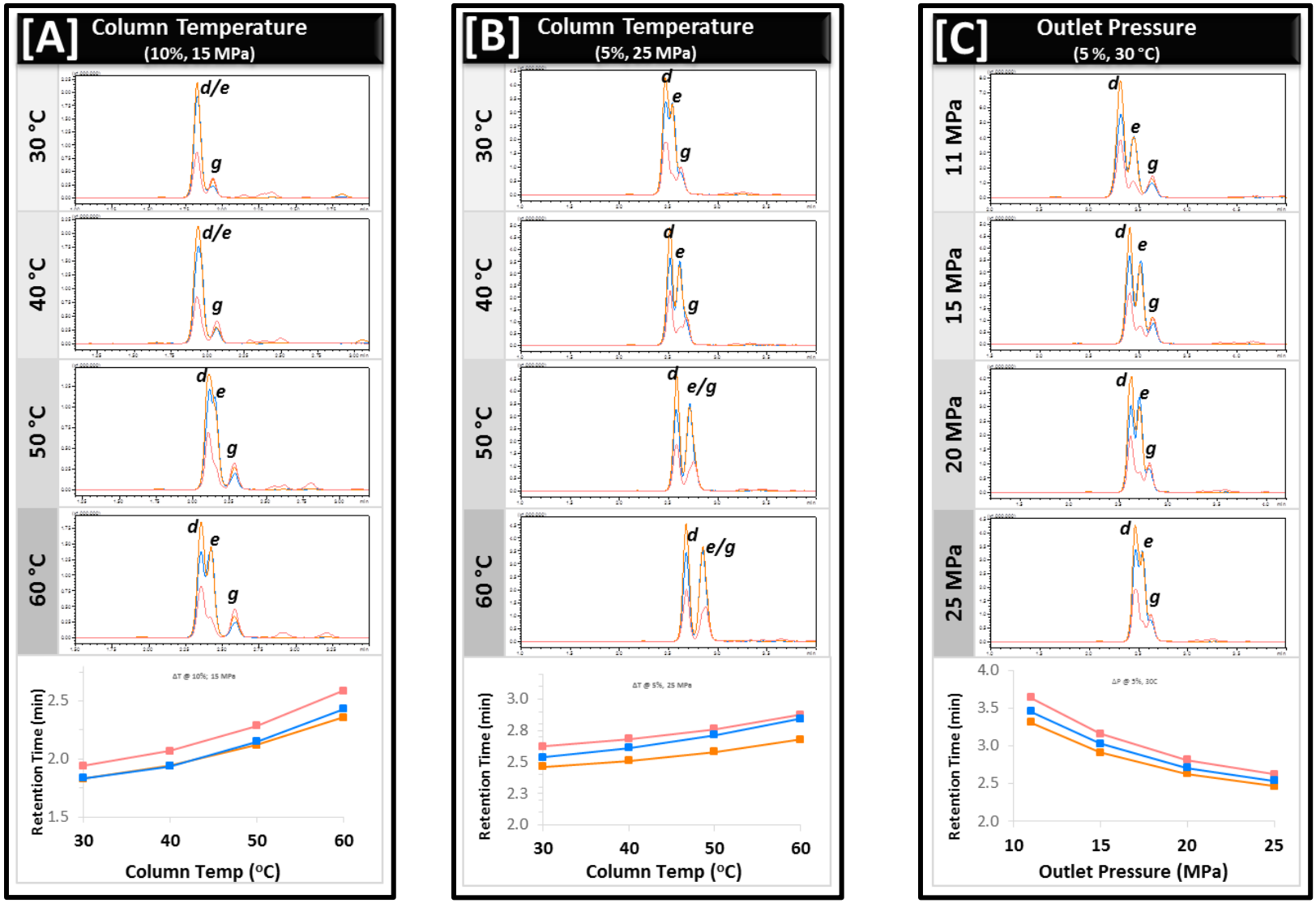

Figure 99. Effect of Secondary Parameters on Retention for MS-Critical Group 1 Compounds: Showing the Effect of Change in Column Temperature *(30, 40, 50 and 60 °C) using **[A]** 10% Modifier with 15 MPa outlet pressure and **[B]** 5% modifier with 25 MPa outlet pressure; and **[C]** Effect of Outlet Pressure (11, 15, 20 and 25 MPa) using 5% modifier with 30 °C column temperature.* *[bottom]Scatter plots of retention time (minutes) versus temperture or pressure and [top] SFC-MS chromatograms overlays of MRM-TICs for Critical Group 1 compounds: 1-androsterone [1DHEA-MRM, [d], pink]; Androsterone [ADEN-MRM, [e], orange]; and Etiocholanolone [ETIO-MRM,[g], blue].*

6.6.2. Secondary Parameters Effect on Resolution for Critical Group 2.

Critical Group 2: Column Temperature. **Figure 100; [A]** shows the effect of change in temperature (30, 40, 50, and 60 °C) on the retention in critical group 2. Column temperature had little effect on the majority of the compounds, having little to no change on the retention or resolution between critical pair 2-B, mestanolone (MSAL, [***c***]) and mesterolone (MSEL, [***f***]) and critical pair 2-C, mibolerone (MIBL, [***i***]), and methyltestosterone (MTHY, [***k***]). Alternatively, temperature had an effect on the retention of 1-androstenedione (1STEN, [***b***], red) and danazol (DNZL, [***q***], torquoise). This effect was only slight on DNZL, where higher temperature (**60 °C**) gave slightly lower retention for DNZL-only and resulted in slightly increased resolution ($Rs_{[q:i]}$ = 0.4) from MIBL. Instead, most notably for temperature, a change in selectivity was observed for 1STEN. Where at high temperature (**60 °C**), 1STEN **[red]** nearly co-elutes with MSAL ($Rs_{[b:c]}$ = 0.6), but lower temperature, produces significantly lower retention for 1STEN and at low temperature (**30 °C**) results in full baseline resolution of 1STEN from MSAL ($Rs_{[b:c]}$ = 3.3).

Critical Group 2: Outlet Pressure. **Figure 100; [B]** shows the effect of change in outlet pressure (11, 15, 20, and 25 MPa) on the retention for MS-critical group 2. Change in pressure had little effect on 1STEN, but had a greater effect on DNZL. Note in the relative retention for 1STEN and MSAL now changes very little when outlet pressure is changed. Generally, the relative retention of each member of critical group 2 changes very little with change in pressure, with the exception of DNZL where a change in selectivity due to change in outlet pressure results in a double peak reversal. At low pressure (**11MPa**) DNZL (**turquoise**) elutes last after MIBL (***i)*** and MTHY (***k***). As the outlet pressure is increased (top-to-bottom), a peak reversal occurs around 15 MPa with MTHY [***i***], and then above 20 MPa, DNZL elutes before MIBL. Consequently, this results in diminished resolution at moderate pressures between the last three members of group 3. Therefore, the best resolution would be obtained (for MIBL, MTHY and DNZL) at high or low pressure.

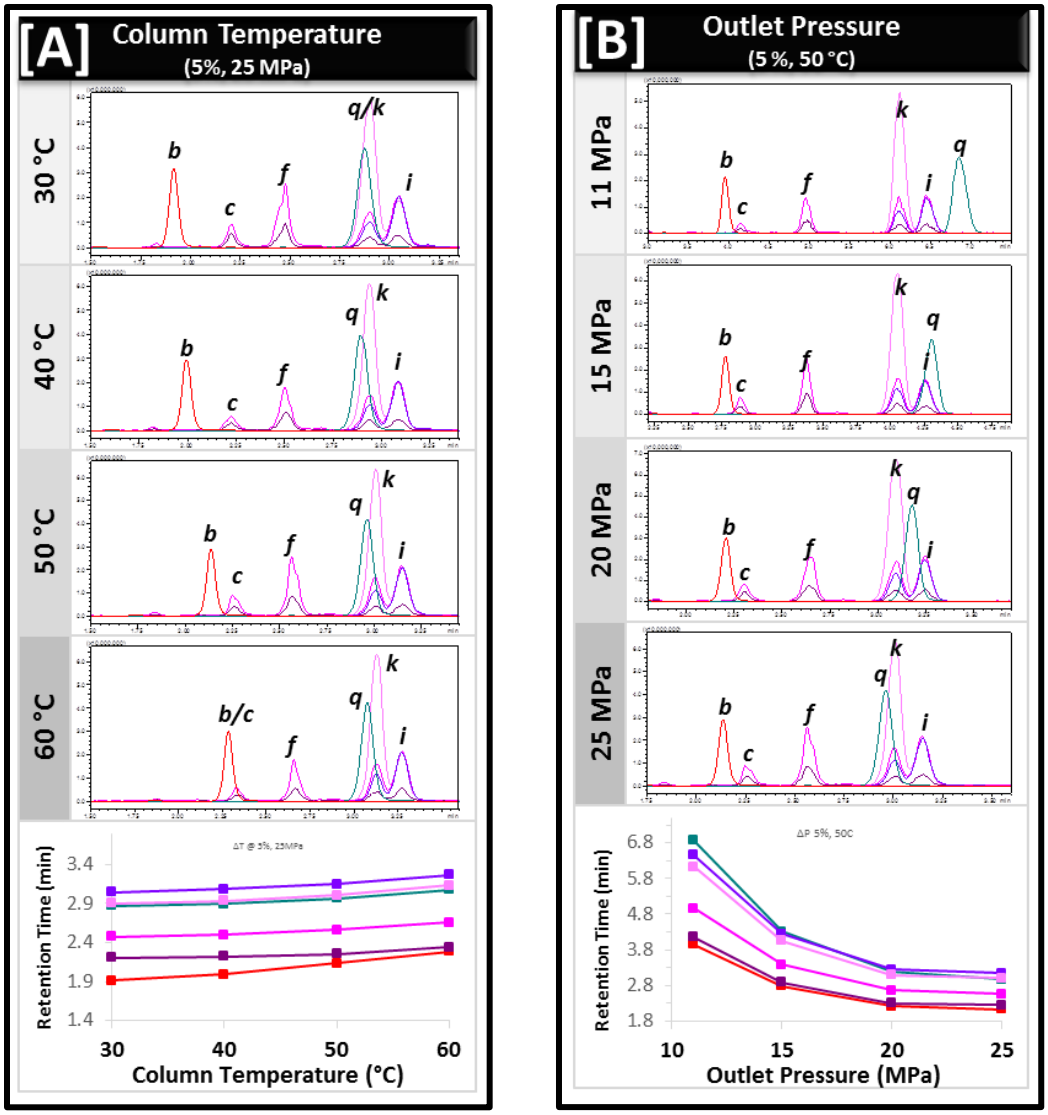

Figure 100. Effect of Secondary Parameters on Retention for MS-Critical Group 2: Showing the **[A]** Effect of Change in Column Temperature *(30, 40, 50 and 60 °C) using 5% Modifier with 25 MPa outlet pressure; and **[B]** Effect of Outlet Pressure (11, 15, 20 and 25 MPa) using 5% modifier with 50 °C column temperature. [bottom]Scatter plots of retention time (minutes) versus temperture or pressure and [top] SFC-MS chromatograms overlays of MRM-TICs for Critical Group 2 compounds: mestanolone (MSAL, [**c**], magenta) and mesterolone (MSEL, [**f**], rose) and critical pair 2-C, mibolerone (MIBL, [**i**], purple) and methyltestosterone (MTHY, [**k**], light pink), danazol (DNZL, [**q**], torquoise) and 1-androstenedione (1STEN, [**b**], red).*

6.6.3. Secondary Parameters: Effect on Resolution of Critical Group 3.

Neither column temperature or outlet pressure had little effect on the retention or resolution of critical group 3 compounds, with the exception of oxandrolone (OXAN,[***o***], hot pink). Although OXAN still always co-elutes with TSTO, a very slight effect for OXAN was seen. Where OXAN elutes just before TSTO, using the combination of high temperature and low pressure (**Figure 101; [A] & [B]**). But OXAN elutes just after TSTO using the opposite combination of parameters (e.g., low temperature and high pressure). Regardless, the effect was slight producing resolution less than 0.5 ($Rs_{[m:o]} < 0.5$) in both circumstances, giving no large benefit over the range of conditions screened.

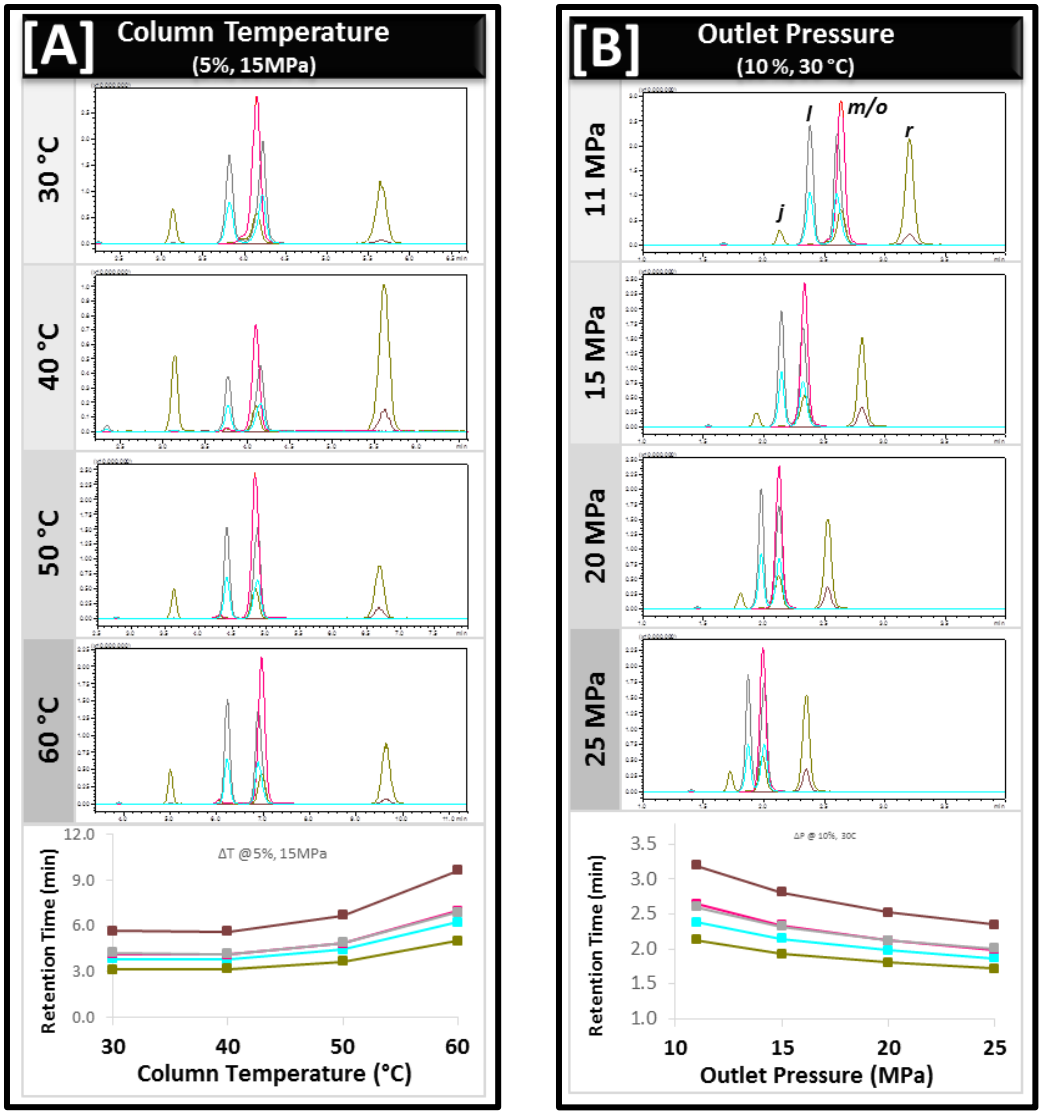

Figure 101. Effect of Secondary Parameters on Retention for MS-Critical Group 3: Showing the **[A]** Effect of Change in Column Temperature *(30, 40, 50 and 60 °C) using 10% Modifier with 20 MPa outlet pressure; and **[B]** Effect of Outlet Pressure (11, 15, 20 and 25 MPa) using 10% modifier with 30 °C column temperature.* *[bottom]Scatter plots of retention time (minutes) versus temperture or pressure and [top] SFC-MS chromatograms overlays of MRM-TICs for Critical Group 3 compounds: testosterone (TSTO-MRM, [**m**], gray), epitestosterone (EPIT-MRM, [**l**], cyan), oxandrolone (OXAN-MRM, [**o**], hot pink), prasterone (PRST-MRM, [**j**], gold), and trenbolone (TRNB-MRM, [**r**], brown)*

6.6.4. Secondary Parameters: Effect on Resolution of Non-critical Compounds.

Non-critical, Late-eluting Compounds. For non-critical, late-eluting compounds, the effect of column temperature for is shown in **Figure 102; [A]**, and the effect of outlet pressure is shown in **[B].** Outlet pressure had little effect, with all compounds having a lower retention at higher pressure (note how the effect looks very similar to what one would expect by increasing the flow rate). But alternatively, column temperature did have an effect on the relative retention of CLNB and ADAR. For CLNB ([***v***], dark green) the effect of temperature produced shorter retention times at higher temperature (**Figure 102; [A], 60 °C**) and longer retention at lower temperature (**30 °C**). The effect of column temperature was opposite for ADAR ([***w***], maroon), where low temperature produced shorter retention. This resulted in a peak reversal between, ADAR and CLNB, at ~40 °C.

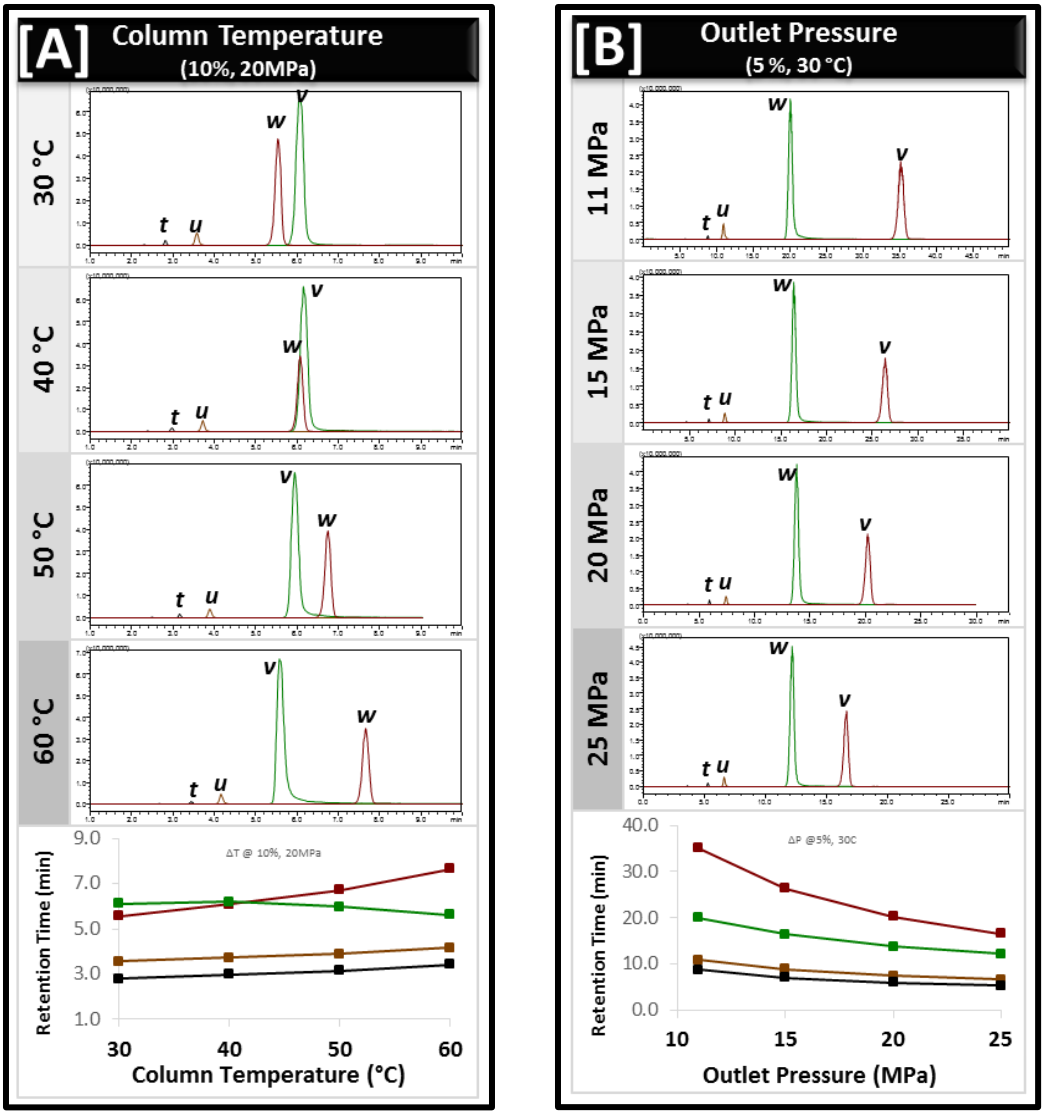

Figure 102. Effect of Secondary Parameters on Retention for Non-critical, Late-eluting Compounds: Showing the **[A]** Effect of Change in Column Temperature *(30, 40, 50 and 60 °C) using 10% Modifier with 20 MPa outlet pressure; and **[B]** Effect of Outlet Pressure (11, 15, 20 and 25 MPa) using 5% modifier with 30 °C column temperature.* *[bottom]Scatter plots of retention time (minutes) versus temperture or pressure and [top] SFC-MS chromatograms overlays of MRM-TICs for Non-Critical, Late-eluting compounds:: clenbuterol (CLNB-MRM, [**v**], dark green), andarine (ADAR-MRM, [**w**], maroon), Stanazolol (STNZ-MRM, [**u**], mocha), and zeranol (ZRNL-MRM, [**t**], black).*

Non-critical, mid-eluting compounds. Outlet pressure also had little effect on non-critical, mid-eluting compounds, again just producing shorter retention at higher pressure for all compounds (**Figure 103; [B], 25 MPa**). Temperature had a slight effect on selectivity, METD elutes first and GSTN elutes last at low pressure and high temperature (**Figure 103; [A], 60 °C)**. The retention of GSTN becomes shorter as temperature is decreased, and elutes first at low temperature (**30 °C)**. The effect is opposite for METD, and although the retention of METD becomes longer as temperature is decreased, the effect is not as strong.

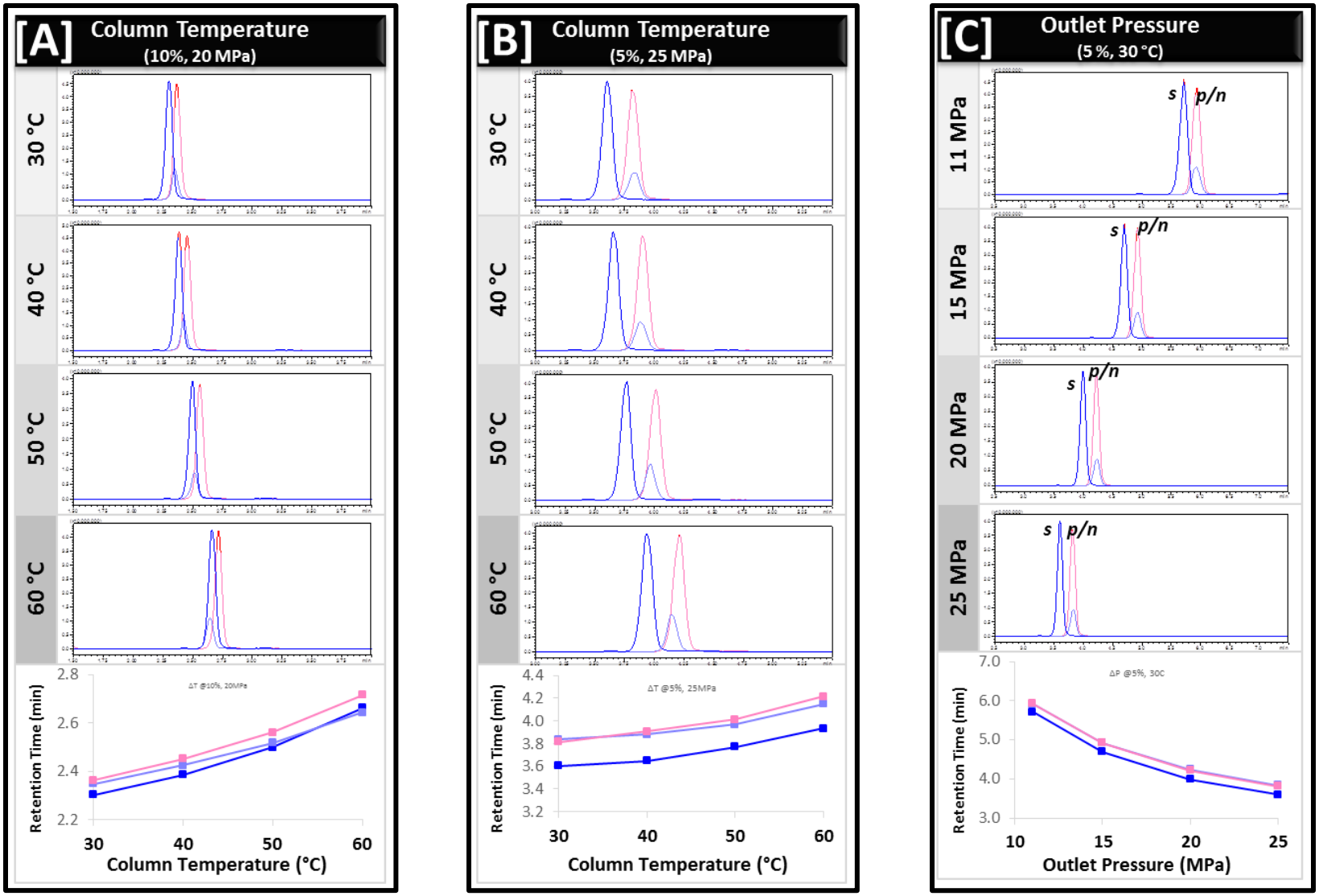

Figure 103. Effect of Secondary Parameters on Retention for Non-critical, Mid-eluting Compounds: Showing the Effect of Change in Column Temperature *(30, 40, 50 and 60 °C) using* **[A]** *10% Modifier with 20 MPa outlet pressure;* **[B]** *5% Modifier with 25 MPa outlet pressure; and* ***[C]*** *Effect of Outlet Pressure (11, 15, 20 and 25 MPa) using 5% modifier with 30 °C column temperature.* *[bottom]Scatter plots of retention time (minutes) versus temperture or pressure and [top] SFC-MS chromatograms overlays of MRM-TICs for Non-critical, mid-eluting compounds: gestrinone (GSTN-MRM, [**s**], cobalt), Metandienone (METD-MRM, [**n**], lilac), and metribolone (MTRB-MRM, [**p**], coral).*

6.6.5. Effect of Instrument Parameters Discussion/Summary

Group 1 Summary. Two peaks reversals were observed, for critical group 1, due to change in modifier concentration. Above 5% modifier, the three compounds should be resolved. Below 5% modifier, co-elution of 1DHEA should be expected with either ETIO (between 3-5% modifier) or with ADEN (below 3% modifier). Changes in selectivity were also observed based on changes in column temperature for critical group 1; but, a change in pressure had little to no effect on the relative retention. Since the three compounds are best separated at 40 °C and at lower pressure, this combination of parameters could be utilized to improve the separation of group 1.

Group 2 Summary. Two peak reversals were observed for critical group 2 due to changes in modifier concentration: the selectivity of DNZL changes dramatically compared to the other group 2 compounds, resulting in lower relative retention at lower modifier concentrations for DNZL. This results in multiple peak reversals: first with MIBL at ~10%, then MTHY at ~7%, and at eventually at very low modifier (<2%) would be expected to cross MSEL. Changes in selectivity based on modifier concentration (although less dramatic) were also seen for 1STEN, where relative retention increases with lower modifier concentrations and results in a peak reversal between 1STEN and MSAL at approximately 2.5% modifier. Column temperature also had an effect on the selectivity of 1STEN producing shorter relative retention at lower temperatures. And column pressure had an effect on the selectivity of DNZL producing longer relative retention at lower pressures.

Group 3 Summary. Both column temperature and outlet pressure had little effect on critical group 3 compounds, both having only a very slight effect on OXAN (with lower pressure and temperature providing a small boost in resolution between OXAN and TSTO).

Non-Critical Compounds Summary. Modifier concentration had an effect on selectivity for both late- and mid-eluting non-critical compounds. For the longest retained compounds, ADAR elutes last below 10% but above, CLNB elutes last. For mid-eluting non-critical compounds, a peak reversal for MTRB and METD is expected at ~5%

modifier. Although outlet pressure had little effect on late eluting compounds, column temperature did have an effect, where higher temperatures result in longer retention for ADAR but shorter retention for CLNB.

6.6. Final Gradient Optimization.

Using the information obtained above (based on modifier concentration, temperature, and pressure effects), eight generic gradients were devised for screening. Later, three additional more targeted gradients were added.

6.6.1. Screening gradients.

Half of the screening gradients had a starting modifier concentration of 2% (Gradients: **G[n], G[o], G[p] & G[q])** and the other half started at 5% (Gradients: **G[r], G[s], G[t],** and **G[u]**). Each gradient held the starting concentration for 2 minutes, before ramping to 10% (for **G[n]** and **G[r]**), 12% (for **G[o]** and **G[s]**), 15% (for **G[p]** and **G[t]**), or 20% (for **G[q]** and **G[u]**) over 6 minutes (2 - 8 min ramp for all). Initially, a less systematic (and ultimately unsuccessful) approach was used. This approach (using systematic screening gradients) was devised specifically due to the high number of peak reversals observed due to modifier concentration, which made non-systematic attempts difficult to interpret.

All eight gradients were run using two different column temperatures: high (60 °C) and low (30 °C). The system outlet pressure was held constant (15 MPa) throughout all gradient testing. Resulting chromatograms were compared for overall separation performance and resolution between critical compounds compared (S_Table 8 and S_Table 9).

6.6.2. Best Performing Gradients.

Gradient G[u] with 60 °C column temperature produced the best resolution for critical groups 1 and 3. Any gradient used with a starting concentration above 5% in combination with a 60 °C column temperature resulted in the best resolution between the members of critical group 1. Gradient **G[u]** in particular

produced the highest resolution for this group (**Figure 104; [A], Group 1**), with ADEN [***d***] and ETIO [***e***] being baseline resolved ($Rs_{[d:e]}$ = 1.8) and near baseline separation of 1DHEA [***g***] ($Rs_{[e:g]}$ = 0.94). Group 3 also had improved resolution using a 60 °C column temperature (**Figure 104; [A], Group 3**); since OXAN [***o***] co-elutes/elutes just after TSTO [***m***], and so does not interfere with the resolution between TSTO and EPIT [***l***] ($Rs_{[l:m:o]}$ = 2.4, 0.23).

Alternatively, the resolution between members of group 2 are the worst observed, using a 60 °C column temperature (**Figure 104; [A], Group 2**), due to three simultaneous issues: 1.) the co-elution of 1STEN [***b***] with MSAL [***c***]; 2.) reduced resolution between MIBL [***i***] and MTHY [***k***] at the higher temperature; and 3.) the near co-elution of DNZL [***q***] with both MIBL and MTHY, eluting just between the two, reducing resolution between all three compounds ($Rs_{[q:k:i]}$ = 0.8, 0.4). In an attempt to improve group 2 resolution ***[data not shown]***, outlet pressure was utilized (to take advantage of the selectivity change for DNZL due change in pressure; where lower pressure should push DNZL to a later retention time). Lower pressure did not help, as change in pressure does not produce a selectivity change for 1STEN, and more importantly, push TSTO and EPIT together, and OXAN then moved between them.

The overall separation using gradient **G[u]** was not ideal, with seven compounds having quite low resolution (Rs ≤ 0.5) and four additional compounds (0.6 > Rs ≤ 1.1). This means that ultimately less than half of the targeted analytes were baseline resolved (Rs > 2.0), using these conditions.

Gradient G[n] with 30 °C column temperature produced the best resolution for critical group 2 and the best overall separation. Any gradient with a 2% start concentration was the best for group 2, as long as a 30 °C column temperature was used. Particularly, gradient **G[n]** produced the highest resolution for group 2 (**Figure 104; [B], Group 2**), resulting in baseline resolution between all compounds ($Rs_{[b:c:f:q:k:i]}$ = 3.9, 4.0, 3.1, 2.5, 1.7). This gradient also resulted in the best overall separation for all targeted analytes, with only six of the compounds having low resolution (Rs ≤ 0.5) and only two additional compounds being less than baseline resolved (Rs ≤ 1.5). Out of the 8 unresolved analytes, only two are critical compounds. These conditions also produced the worst resolution for group 1 ($Rs_{[d:e:g]}$ = 2.0, 0.4) and group 3 ($Rs_{[j:l:o:m:r]}$ = 7.5, 1.6, 0.4, 6.7) compounds.

Two factors were important for group 3 (**Figure 104; [B], Group 3**). The use a 2% initial concentration reduces resolution between TSTO [***m***] and EPIT [***l***] (as expected, since lower modifier concentration was shown to reduce resolution between these isomers). In addition, a 30 °C column temperature, was shown to always result in OXAN [***o, hot pink***] eluting between TSTO and EPIT. Consequently, the resolution between the most critical members of group 3 ($Rs_{[l:o:m]}$ = 1.6, 0.4) was degraded.

For group 1, any gradient using the lower initial concentration of 2% produced improved resolution between ADEN [***d***] and ETIO [***e***] (baseline resolution ≥ 1.5). However, combined with the 30 °C column temperature (**Figure 104; [B], Group 1**) resolution was reduced between ETIO and 1DHEA [***g***], which co-elute due to the peak reversal at approx. 5% modifier.

6.6.3. Final Targeted Gradients for Group 1.

Critical group 1 was the most difficult critical group to resolve. The group elutes early in the gradient, which unfortunately coincided with the concentration range (between 4 - 8% modifier), where two peak reversals were observed for this group. Even slight shifts in retention, due to minor changes to the gradient would move the group into a different region of modifier concentration (that coincided with the region of one of the peak reversals). Therefore, three additional gradients were added later to attempt to improve resolution between this group. Attempts to utilize a lower starting concentration (< 5 %) resulted in pushing EPIT and TSTO together and attempts at utilizing a higher starting concentration (> 5%) reduced retention dramatically for all later eluting compounds. Therefore, unfortunately these gradients were unsuccessful in maintaining the overall separation, improving the resolution in group 1. In the end, it became clear that a gradient **G(m)** using a ramp from 2% to 12.5% with no initial hold (0-8 min) with a column temperature 60 °C produced the best overall separation, and would be used in the final SFC-MS method.

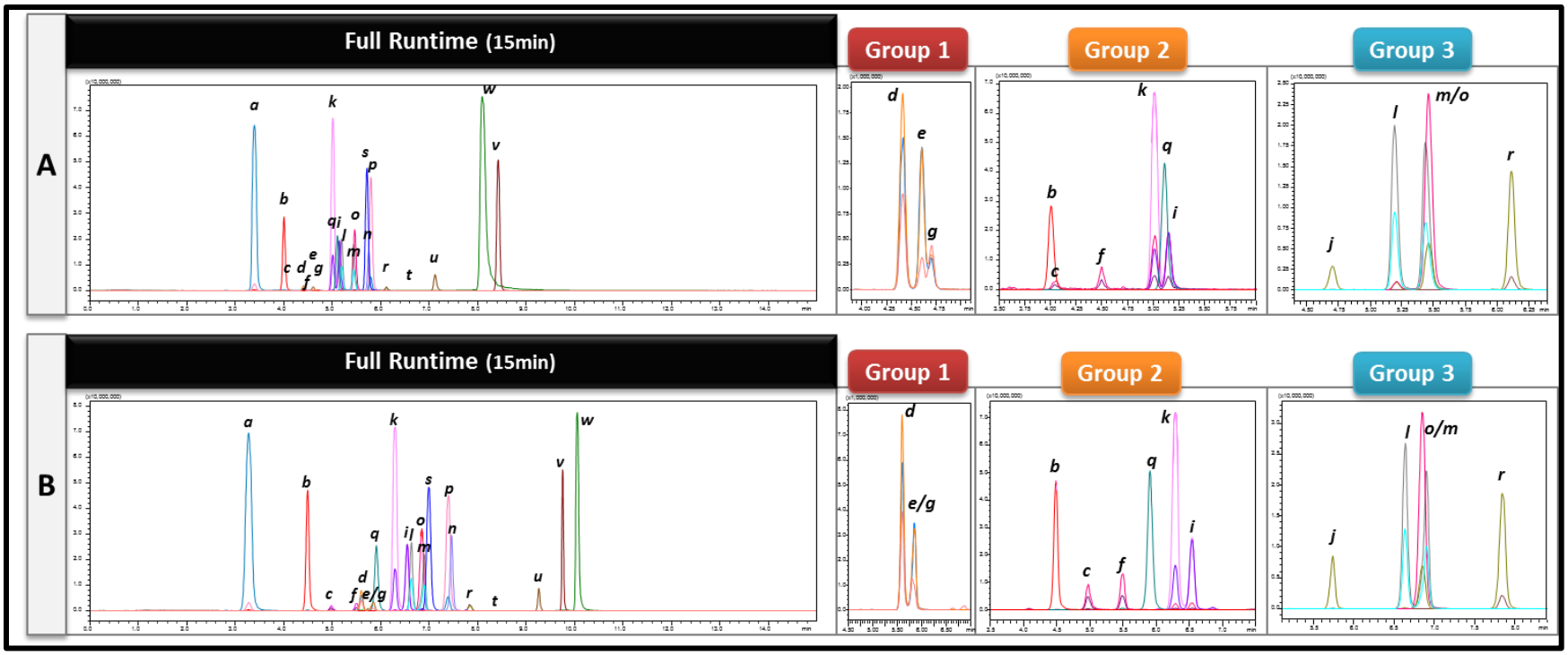

Figure 104. Gradient Optimizations for Separation of Anabolic agents on UC-Cyano Column, showing the [A] screening gradient, G[u], producing the best resolution for critical groups 1 and 2, and [B] screening gradient, G[n], producing the best resolution for critical group 3 and best overall separation. SFC-MS injections (1.0 µL via the autosampler) of steroid mixture (AAS-mix) separated on a Shimadzu Corp., UC-Cyano (4.6 x 150 mm, 5.0 µm) column: using methanol (MeOH) + 5 mM ammonium formate as modifier in carbon dioxide. Overlaid MRM-TIC chromatograms (at full scale) for targeted anabolic agents: 7-keto-DHEA ([***a***], KETO-MRM, [teal]); 1-androstenedione ([***b***], 1STEN-MRM, [red]); mestanolone ([***c***], MSAL-MRM, [magenta]); androsterone ([***d***], ADEN-MRM, [orange]); etiocholanolone ([***e***], ETIO-MRM, [blue]); mesterolone ([***f***], MSEL-MRM, [rose]); 1-androsterone ([***g***], 1DHEA-MRM, [pink]); mibolerone ([***i***], MIBL-MRM, [purple]); prasterone ([***j***], PRST-MRM, [gold]); methyltestosterone ([***k***], MTHY-MRM, [light pink]); epitestosterone ([***l***], EPIT-MRM, [cyan]); testosterone ([***m***], TSTO-MRM, [gray]); methandienone ([***n***], METD-MRM, [lilac]); oxandrolone ([***o***], OXAN-MRM, [hot pink]), metribolone ([***p***], MTRB-MRM, [coral]); danazol ([***q***], DNZL-MRM, [turquoise]); trenbolone ([***r***], TRNB-MRM, [brown]); gestrinone ([**s**], GSTN-MRM, [cobalt]); zeranol ([***t***], ZRNL-MRM, [black]); stanozolol ([***u***], STNZ-MRM, [mocha]); andarine ([***v***], ADAR-MRM, [maroon]); and clenbuteral ([***w***], CLNB-MRM, [dark green]). **Conditions: Gradients G(u): 5% held for 2 minutes, followed by a ramp to 10% over 6 minutes, using 60 °C column temperature; Gradient G(n): 2% held for 2 minutes, followed by a ramp to 10% over 6 minutes, using 30 °C column temperature. A flow rate of 3.0 mL/min was used with 15 MPa outlet pressure for both gradients.**

6.7. Final SFC-MS Method

6.7.1. Final Optimized SFC-MS Method on UC-Cyano (Figure 105).

Ultimately, a compromise was needed, where the resolution in groups 1 and 2 (particularly critical pair 2-B (MIBL and MTHY) were sacrificed for improved resolution in group 3, as well as improved overall resolution for all other targeted analytes. The final method utilized methanol with 5 mM ammonium formate as additive to improve peak shape for the late eluting non-steroidal anabolic agent, clenbuteral. The optimized gradient made a compromise between resolution within late versus early eluting critical pair groups. A column temperature of 60 °C was utilized to improve resolution of the early eluting critical group 1 compounds, and high priority critical pair 3-D (testosterone and epitestosterone), which sacrificed resolution for critical pair 2-C (methyltestosterone and mibolerone). The final optimized separation of the androgenic steroid mix is shown in **Figure 105; [A]**. Total runtime was 15 minutes for the separation of 22 anabolic agents.

6.7.2. Resolution within Critical Pair Groups

Critical Group 1 (Figure 105; [B]). Due to the peak reversal between 1DHEA and ETIO at ~ 4% modifier concentration, this group was not fully resolved ($Rs_{[d:e:g]}$ = 1.2, 1.1). A compromise favoring resolution on the remaining critical pair groups was made (mainly for the high priority critical pairs 2-B [MIBL and MTHY] and 3-D [EPIT and TSTO]), which required the initial concentration of the gradient to be lower than optimal for the resolution of group 1 analytes.

Critical Group 2 (Figure 105; [C]). The lowest resolution observed for this group involved the critical pair 2-B (MIBL and MTHY, $Rs_{[k:j]}$ = 0.5). Alternatively group 2-C (MSAL and MSEL) were well resolved (Rs >5). The watch members of critical group 2 (1STEN and DNZL) were also well resolved from any of the members in the group (Rs > 2).

Critical Group 3 (Figure 105; [D]). Both critical pairs within this group were well resolved. Critical pair 3-E was characterized by the best resolution of the group (Rs > 8). Critical pair 3-D, TSTO and EPIT, were also well resolved ($Rs_{[l:m]}$= 2.2) from one-another, but the watch member OXAN was not fully resolved from TSTO ($Rs_{[m:o]}$ = 1.0). This unfortunately was the best resolution seen in this work between the two compounds, as modifier concentration, pressure and temperature had little effect on the relative retention between the two compounds.

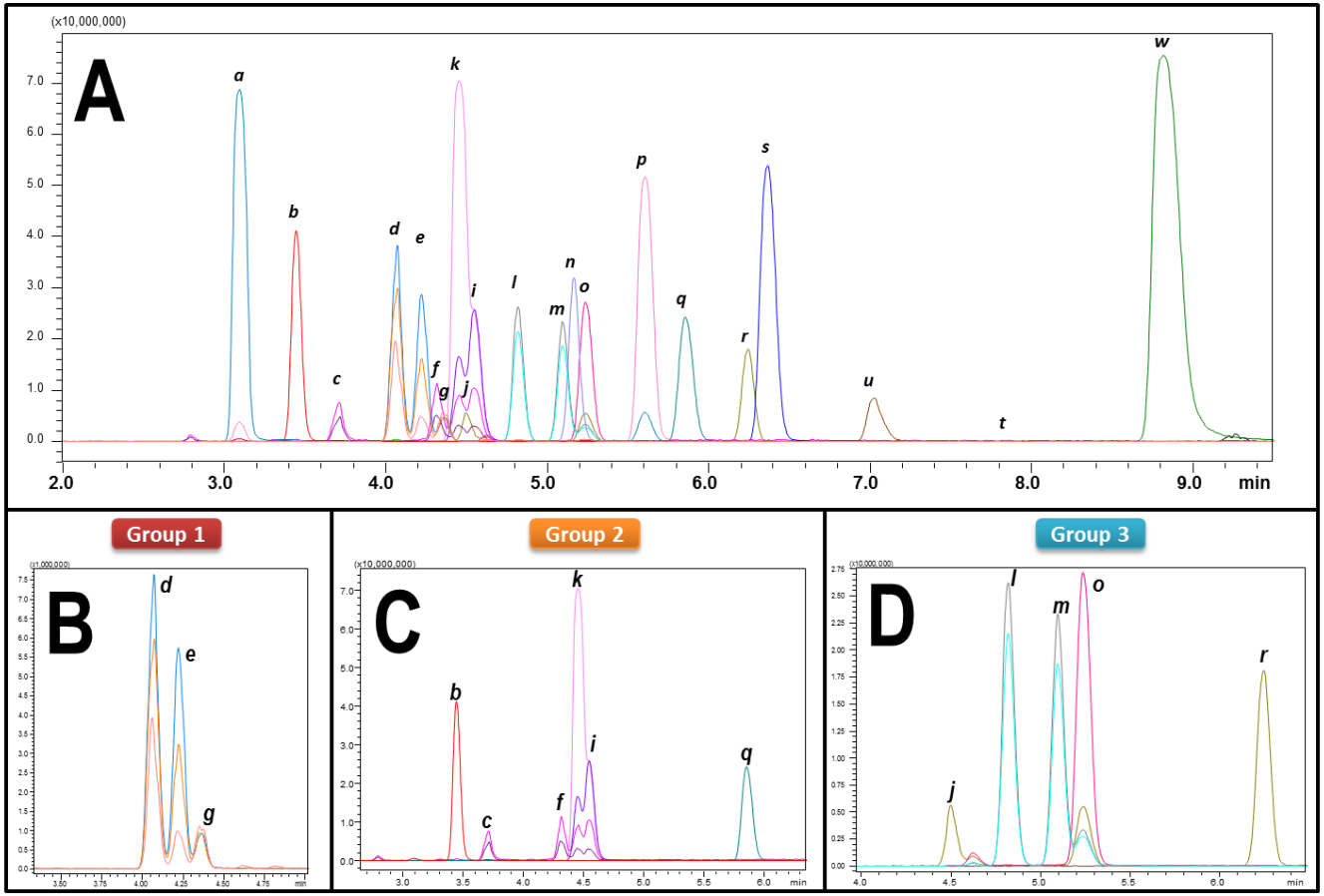

Figure 105. **SFC-MS Chromatograms using Final SFC Method for Optimized for the Separation of 22 Anabolic Agents on UC-Cyano Column. [A] MRM-overlays for all 22 anabolic agents, zoomed on elution timeframe for targeted analytes; [B] Critical Group 1 Analytes; [C] Critical Group 2 Analytes; [D] Critical Group 3 Analytes.** SFC-MS injections (1.0 µL via the autosampler) of a methanolic steroid mixture [AAS-mix] separated on a Shimadzu Corp., UC-Cyano (4.6 x 150 mm, 5.0 µm) column: using methanol + 5 mM ammonium formate as modifier in carbon dioxide. Overlaid MRM-TIC chromatograms (at full scale) for targeted anabolic agents: 7-keto-DHEA ([***a***], KETO-MRM, [teal]); 1-androstenedione ([***b***], 1STEN-MRM, [red]); mestanolone ([***c***], MSAL-MRM, [magenta]); androsterone ([***d***], ADEN-MRM, [orange]); etiocholanolone ([***e***], ETIO-MRM, [blue]); mesterolone ([***f***], MSEL-MRM, [rose]); 1-androsterone ([***g***], 1DHEA-MRM, [pink]); mibolerone ([***i***], MIBL-MRM, [purple]); prasterone ([***j***], PRST-MRM, [gold]); methyltestosterone ([***k***], MTHY-MRM, [light pink]); epitestosterone ([***l***], EPIT-MRM, [cyan]); testosterone ([***m***], TSTO-MRM, [gray]); methandienone ([***n***], METD-MRM, [lilac]); oxandrolone ([***o***], OXAN-MRM, [hot pink]), metribolone ([***p***], MTRB-MRM, [coral]); danazol ([***q***], DNZL-MRM, [turquoise]); trenbolone ([***r***], TRNB-MRM, [brown]); gestrinone ([**s**], GSTN-MRM, [cobalt]); zeranol ([***t***], ZRNL-MRM, [black]); stanozolol ([***u***], STNZ-MRM, [mocha]); andarine ([***v***], ADAR-MRM, [maroon]); and clenbuteral ([***w***], CLNB-MRM, [dark green]). **Conditions: Gradient elution using 2 -12.5 % [B] (0-8 minutes); 3.0 mL/min flow rate, with 30 °C column temperature and 15 MPa outlet pressure.**

6.7.3. Method Evaluation: Reproducibility

Six consecutive injections were performed using the optimized method to evaluate reproducibility of peak areas and retention times. Peak area reproducibility was below 5% RSD for all targeted analytes, except ADON, which was not evaluated in the current work. Retention times were also reproducible being ± 0.02 minutes for all compounds. Final elution order is listed in **S_Table 10.** Final resolution between critical groups was above 1.0 for all critical compounds except for critical pair 2B (MIBL and MTHY).

6.8. Conclusions.

The separation of 22 anabolic agents was optimized for SFC-MS analysis, as part of the second development step of a hyphenated SFE-SFC-MS method for online extractions. The method uses a stationary phase chosen in an earlier development step, the Shimadzu, Corp., UC-Cyano column. Tailing on late eluting compounds required an additive to be utilized. The optimal mobile phase was determined as methanol + 5 mM ammonium formate as modifier in carbon dioxide. Gradient elution was utilized and optimized to take advantage of concentration windows for difficult to resolve analytes. Column temperature and outlet pressure proved useful for final method optimizations improving resolution for some critical compounds. The final SFC-MS method produced an overall runtime of 15 minutes with reproducible retention times and peak areas for 22 anabolic agents.

6.i. Instrument Methods: SFC Separation Optimizations

6.i.1. General Method Information.

Detailed information on materials and equipment used for SFC-based separation optimizations performed in this study can be found in the following sections of **Chapter #2. Materials and Methods**:

6.i.1.1. Materials.

- Solvents used for mobile phases and dilution solutions can be found in **Section 2.1.1. Solvents**.
- Analytical standards information for targeted anabolic agents can be found in **Section 2.1.2. Analytical Standards; *Anabolic androgenic steroids (AAS)*** **and** **Table 1.**

6.i.1.2. Instrumentation.

- The Instrumentation used is detailed in **Section 2.2.1. Instrumentation; *Nexera UC online SFE-SFC-MS***.
- Column details are given in **Section 2.2.2. Columns** and **Table 5.**
- Other equipment used is detailed in **Section 2.2.3. Other Equipment**:
    - ***Nitrogen Generator***
    - ***Analytical balances***

6.i.1.3. Solutions Preparation.

- Stock Solutions prep and storage detailed in **Section 2.3.1.1. AAS Stock Solutions** and **Table 6; Stock Solutions.**
- Injection solutions prep and concentrations are described in **Section 2.3.1.3. AAS Injection Solutions**; ***AAS Test Mixture [AAS-mix]*** and **Table 6; *AAS-mix*.**
    - ***AAS Test Mixture [AAS-mix]***

6.i.2. MS Detection Parameters – MRM method

Detection was achieved using an LCMS-8050 triple quadrupole mass spectrometer, equipped with an DUIS-source, and operated in Electrospray Ionization (ESI-), positive (+) and negative (-) ionization mode. Interface voltages were set to 4.0 kV (for positive Q3 scan mode) and -3.0 kV (for negative Q3 scan mode) and temperature set to 300 °C. Nitrogen gas was used for both drying and nebulizing gas; with flow rate of 2.0 L/min for nebulizing gas and 10.0 L/min for drying gas. Desolvation and DL temperatures were 526 °C and 250 °C respectively. Heat Block temperature was set to 400 °C, and heating gas used was dry air. Gas used for collision induced dissociation (CID) was argon at 270 kPa. DL Bias/Qarray Bias were set in tuning file as 0 V, and Q3 Pre-rod Bias at -15 V (for positive scan mode) and 15 V (for negative scan mode). Scan range was 120 to 1,200 m/z with scan speed 15,000 u/sec, with 0.100 sec Event time with Q3 resolution set to unit.

6.i.3. Instrument setup

6.i.3.1. Mobile Phases (MP).

All work in this chapter utilized SFC/CO_2-based MPs, where up to 40% modifier was mixed with liquid Carbon Dioxide ([CO_2] – Instrument grade) via the instrument solvent delivery pumps using isocratic or gradient elution. Four modifiers were used: [MeOH] LCMS-grade methanol; [FA] methanol + 0.1% formic acid (LCMS-grade); [TEA] methanol + 0.1% trimethylamine (LCMS-grade); and [AmFo] methanol + 5 mM ammonium formate (LCMS-grade). All modifier solutions were sonicated for 20 minutes prior to use.

6.i.3.2. Stationary Phase (SP).

All separations performed in the current work utilized a Shimadzu Corp., UC-Cyano 4.6 mm x 150 mm 5.0 µm column.

6.i.3.3. Instrument Setup: SFC-Separation Optimization Configuration.

The instrument setup utilized in the work presented here was the 'SFC-Separation Optimization Configuration' detailed in **Chapter #1: Hyphenated Instrumentation: SFE-SFC-MS** (**Section 1.4.2: Instrument Configurations used for SFC Optimizations: *SFC-Separation Optimization***)..

Sample Introduction. Injections were made via the instrument autosampler of a methanolic mixture of 23 anabolic agents [AAS-mix], using partial loop injections on a 5.0 µL external loop.

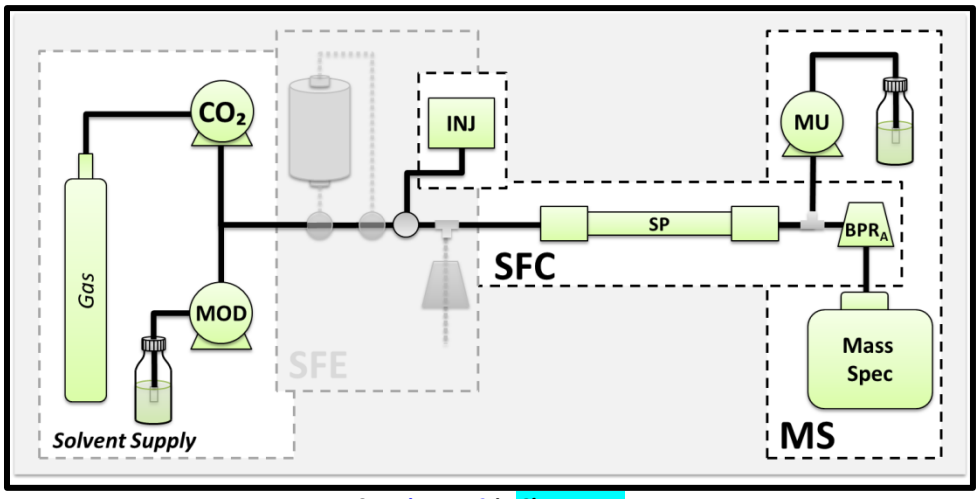

See Figure 13 in Chapter #1

6.i.4. Instrument Methods.

6.i.4.1. Additive Screening Methods.

Mobile phase (MP) additive screening was performed using four modifier compositions: [a] MeOH + 0.1% formic acid (FA); [b] MeOH + 0.1% trimethylamine (TEA); and [c] MeOH + 5 mM ammonium formate (AmFo). Each modifier was degassed and then metered and pumped via a different channel of the liquid solvent delivery pump (modifier pump **[B]**) and mixed with carbon dioxide (from the CO_2 pump **[A]**) (at a concentration determined by

the gradient) as mobile phase. Each mobile phase was used with a 3.0 mL/min flow rate, a 50 °C column temperature, and 15 MPa outlet pressure. Separations were performed on the UC-Cyano column using isocratic and gradient elution. Isocratic runs were performed at 40, 20, and 10% modifier. Gradient runs were performed using the same 'generic screening gradient' used during column screening in previous development steps. The gradient program was as follows: Initial concentration of 5% was held for 1 minute (5% [B]; 0.00 – 1.00 min), before ramping to 40% over 6 minutes (5-40% [B]; 1.01 – 8.00 min), and held at 40% for 2 minutes (40%[B]; 8.01 – 10.00 min). No makeup flow was used.

The column was washed before and after each additive-type and equilibrated for each modifier used. The column was washed for a minimum of 30 minutes using 40% methanol with no additive before switching between mobile phase compositions. The column was allowed to equilibrate for at least 20 minutes (using 40%) with each mobile phase before an analysis was performed. Null injections were performed between each injection of target-analytes.

6.i.4.2. Methods for Evaluation of Effect of Modifier Concentration on Retention.

The mobile phase was composed of [B] MeOH + 5 mM ammonium formate (AmFo) in [A] CO_2. The flow rate used was 3.0 mL/min, with a 50 °C column temperature and 15 MPa outlet pressure [BPR_A]. Separations were performed on the UC-Cyano column, with isocratic elution, performed using 15, 7.5, 5, 2.5 and 1.5% modifier [B].

6.i.4.3. Methods for Evaluation of Effect of Secondary Parameters on Retention.

The mobile phase was composed of [B] MeOH + 5 mM ammonium formate (AmFo) in [A] CO_2. The flow rate used was 3.0 mL/min. Separations were performed on the UC-Cyano column, with isocratic elution, at two concentrations: low modifier concentration (5% [B]) and moderate modifier concentration (10% [B]). No makeup flow was used. To screen secondary parameters a total of 16 injections were repeated for each modifier concentration. Each injection utilized a different combination of column temperature (30, 40, 50, or 60 °C) and

system outlet pressure (11, 15, 20, and 25 MPa). Instrument equilibration after a change in pressure was 5 minutes and after a change in column temperature the instrument was allowed to equilibrate for 15 minutes.

6.i.4.4. Screening Gradients.

Eight screening gradients were used (**Table 27**). A flow rate of 3.0 mL/min was used with 15 MPa outlet pressure. All gradients were run using high (60 °C) and low (30 °C) column temperatures. SFC-MS injections (1.0 µL via the autosampler) of steroid mixture (AAS-mix) separated on a Shimadzu Corp., UC-Cyano (4.6 x 150 mm, 5.0 µm) column: using methanol (MeOH) + 5 mM ammonium formate (AmFo) as modifier in carbon dioxide (CO_2). Detection was via the MRM method described above.

Table 27. Screening Gradients Timetables: with Percent % [B] Methanol + 5 mM Ammonium formate in Carbon Dioxide.

SFC Time (min)	G[n]	G[o]	G[p]	G[q]	G[r]	G[s]	G[t]	G[u]	Step Duration (min)
0.0	2.0%	2.0%	2.0%	2.0%	5.0%	5.0%	5.0%	5.0%	0
2.0	2.0%	2.0%	2.0%	2.0%	5.0%	5.0%	5.0%	5.0%	2
8.0	10.0%	12.0%	15.0%	20.0%	10.0%	12.0%	15.0%	20.0%	6
9.0	30.0%	30.0%	30.0%	30.0%	30.0%	30.0%	30.0%	30.0%	1
15.0	30.0%	30.0%	30.0%	30.0%	30.0%	30.0%	30.0%	30.0%	6
	2-10	2-12	2-15	2-20	5-10	5-12	5-15	5-20	

6.i.4.5. Targeted Gradients for Group 1.

Three additional gradients (**Table 28**) were added later to attempt to improve resolution between the most difficult critical group. The first additional gradient (**G[x]**) involved an initial concentration of 4% (held for 2 minutes) and then ramped the modifier concentration to 7% (over 6 minutes). The second targeted gradient (**G[m]**) ramped the modifier concentration from 2% to 12.5% with no initial hold (0-8 min ramp). And the third additional gradient (**G[y]**) involved an initial concentration of 5% (held for 2 minutes) and then ramped the modifier concentration to 7.5% (over 6 minutes). All three gradients ramped sharply (over 1 minute) to 30%

modifier at 8 minutes. Each of the targeted gradients, were also ran at high (60 °C) and low (30 °C) column temperatures.

Table 28. Targeted Gradients Timetables: with Percent % [B] Methanol + 5 mM Ammonium formate in Carbon Dioxide.

SFC Time (min)	G[x]	Step Duration (min)	SFC Time (min)	G[y]	Step Duration (min)	SFC Time (min)	G[m]	Step Duration (min)
0.0	4.0%	0	**0.0**	5.0%	0	**0.0**	2.0%	0
2.0	4.0%	2	**2.0**	5.0%	2	**8.0**	12.5%	8
8.0	7.5%	6	**8.0**	7.5%	6	**9.0**	30.0%	1
9.0	30.0%	1	**9.0**	30.0%	1	**15.0**	30.0%	6
15.0	30.0%	6	**15.0**	30.0%	6	**-**	-	
	2-10			2-12			2-15	

6.i.4.6. Final SFC Method.

The mobile phase was composed of [B] MeOH + 5 mM ammonium formate (AmFo) in [A] CO_2. Separations were performed on the UC-Cyano column, using a flow rate of 2.5 mL/min, with a 60 °C column temperature and 15 MPa outlet pressure [BPR_A]. Gradient elution was used as follows: the initial starting concentration was 2 % [B] and ramped to 12.5 % [B] over 8 minutes (2-12.5% [B]; 0.00 – 8.00 minutes), followed by a second ramp to 30% over the next 1 minute (12.5 – 30% [B]; 8.01 – 9.00 min), which was held for 6 minutes until the end of the run (30% [B]; 9.01 – 15.00 min).

S_6. SUPPLEMENTARY MATERIALS

S_6.1. SUPPLEMENTAL: Effect of Modifier Concentration on Retention

S_Table 5. Resolution of Critical Pair Groups for Isocratic Runs using Methanol + Ammonium formate in Carbon Dioxide*.

Critical Group	AAS ID	Critical Group Resolution 40%	20%	15%	10%	7.5%	5%	2.5%	1.5%	% AmFo	
1	Elution Order	d/e/g	d/e/g	d, e, g	d, e, g	d, e, g	d, e/g	d, g, e	g/d, e	ADEN (d)	Group 1 Key
		<0.1	0.2	<0.1	0.6	1.5	2.5	2.2	<0.1	ETIO (e)	
		0.2	0.2	1.0	1.2	1.3	0.2	3.5	8.0	1DHEA (g)	
2	Elution Order	b, c/f/q/k/i	b, c, f, q, k, i	b, c, f, k/i/q	b, c, f, k, q/i	b, c, f, k/q, i	b, c, f, q, k, i	b/c, f, q, k, i	c, b, f, q, k, i	1STEN (b)	Group 2 Key
		0.5	1.3	1.9	2.1	1.7	2.0	0.7	2.2	MSAL (c)	
		<0.1	1.1	1.6	2.8	3.0	5.3	6.6	4.7	MSEL (f)	
		<0.1	1.4	2.2	3.6	4.8	5.1	3.3	1.6	MTHY (i)	
		0.1	0.2	0.5	0.8	0.5	2.0	3.4	5.4	MIBL (k)	
		0.1	<0.1	0.3	0.3	1.1	1.1	6.6	> 10.0	DNZL (q)	
2-B	MSAL : MSEL	<0.1	1.1	1.6	2.8	3.0	5.3	6.6	6.7		
2-C	MIBL : MTHY	0.1	0.2	0.5	1.1	1.5	2.0	3.4	5.4		
3	Elution Order	j/l/m/o, r	j, l, m/o, r	j, l, m/o, r	j, l, m/o, r	j, l, m/o, r	j, l, m/o, r	j, l, m/o, r	j, l/m/o, r	PRST (j)	Group 3 Key
		0.2	1.0	1.5	3.0	4.4	7.7	> 10.0	> 10.0	EPIT (l)	
		< 0.1	1.1	1.6	2.2	2.6	2.7	1.3	0.1	TSTO (m)	
		0.3	0.2	0.2	0.1	0.1	< 0.1	0.2	0.3	OXAN (o)	
		0.6	2.4	3.6	5.7	7.9	> 10.0	> 10.0	> 10.0	TRNB (r)	
3-D	PRST:TRNB	0.5	4.9	6.9	> 10.0	> 10.0	> 10.0	> 10.0	> 10.0		
3-E	EPIT:TSTO	< 0.1	1.1	1.6	2.2	2.6	2.7	1.3	0.1		
Non (mid-)	Elution Order	s/n/p	s/n/p	s/n/p	s, n/p	s, p/n	s, p/n	s, p, n	s, p, n	GSTN (s)	(mid-) key
		0.3	0.4	0.6	0.9	1.4	3.5	10.0	> 10.0	MTRB (p)	
		0.1	0.3	0.4	0.4	0.4	0.3	1.9	8.1	METD (n)	
Non (late-)	Elution Order	v, w	v, w	v, w	v/w	w, v	w, v	w, v	w, v	CLNB (w)	(late) ke
		6.9	> 10.0	5.9	0.1	7.8	> 10.0	> 10.0	> 10.0	ADAR (v)	

*Conditions: SFC-MS separations on UC-Cyano column, using methanol + 5 mM ammonium formate in carbon dioxide; 50° C column temperature and 15 MPa outlet pressure. 1.0 µL injections via autosampler of AAS-mix

S_6.2. SUPPLEMENTAL: Effect of Secondary Parameters on Retention

S_Table 6. Resolution of Critical Pair Groups during Secondary Parameters Screening using Low Modifier Concentration (5%)*.

		Critical Group Resolution									
Critical Group	Outlet Pressure	11	15	20	25	11	15	20	25	Mpa	
	Column Temperature	30	30	30	30	40	40	40	40	(°C)	
1	Elution Order	d, e, g	d, e, g	d, e, g	d, e, g	d, e, g	d, e, g	d, e, g	d, e/g	ADEN (d)	Group 1 Key
		0.9	0.8	0.5	0.3	1.1	1.0	1.0	0.8	ETIO (e)	
		1.2	0.9	0.8	0.5	1.4	0.9	0.7	0.4	1DHEA (g)	
2	Elution Order	b, c, f, k, q, i	b, c, f, k, q, i	b, c, f, k/q, i	b, c, f, q/k, i	b, c, f, k, l, q	b, c, f, k, i/q	b, c, f, k/q, i	b, c, f, q/k, i	1STEN (b)	Group 2 Key
		3.3	3.4	3.2	3.4	2.1	1.8	2.4	2.5	MSAL (c)	
		3.6	3.3	2.9	2.7	3.9	3.2	3.2	2.8	MSEL (f)	
		4.8	4.7	4.0	3.1	5.1	4.1	3.6	3.3	MTHY (i)	
		0.9	0.5	0.1	0.2	1.4	1.0	0.0	0.4	MIBL (k)	
		0.6	0.9	1.1	1.1	0.8	0.1	1.3	1.1	DNZL (q)	
2-B	MSAL : MSEL	3.6	3.3	2.9	2.7	3.9	3.2	3.2	2.8		
2-C	MIBL : MTHY	1.4	1.4	1.2	1.1	1.4	1.1	1.3	1.1		
3	Elution Order	j, l, o/m, r	j, l, o/m, r	j, l, o, m, r	j, l, o, m, r	j, l, o/m, r	j, l, o/m, r	j, l, o, m, r	j, l, o, m, r	PRST (j)	Group 3 Key
		5.1	4.6	4.6	3.7	5.9	4.6	4.4	3.8	EPIT (l)	
		2.6	1.8	1.7	1.2	3.0	2.2	1.5	1.2	TSTO (m)	
		0.3	0.4	0.5	0.7	0.1	0.3	0.5	0.7	OXAN (o)	
		8.4	6.9	6.7	5.9	9.4	7.9	6.9	6.4	TRNB (r)	
3-D	PRST:TRNB	17.0	13.4	13.0	11.4	18.7	14.7	13.0	12.2		
3-E	EPIT:TSTO	2.9	2.5	2.3	2.0	3.2	2.5	2.1	1.9		
Non (mid-)	Elution Order	s, n/p	s, n/p	s, p/n	s, p/n	n,p,s	s/n/p	s, n/p	s, n/p	GSTN (s)	(mid-) key
		0.8	1.0	1.2	1.2	0.5	0.3	1.1	1.3	MTRB (p)	
		0.1	<0.1	0.1	0.1	0.1	0.4	0.2	0.1	METD (n)	
Non (late-)	Elution Order	w, v	w, v	w, v	w, v	w, v	w, v	w, v	w, v	CLNB (w)	(late) key
		>10.0	>10.0	9.0	8.4	>10.0	>10.0	>10.0	10.0	ADAR (v)	

*__Conditions__: SFC-MS separations on UC-Cyano column, using 5% methanol + 5 mM ammonium formate in carbon dioxide. 1.0 µL injections via autosampler of AAS-mix

S_Table 6 (CON'T). Resolution of Critical Pair Groups during Secondary Parameters Screening using Low Modifier Concentration (5%)*.

Critical Group		Critical Group Resolution									
	Outlet Pressure	11	15	20	25	11	15	20	25	Mpa	
	Column Temperature	50	50	50	50	60	60	60	60	(°C)	
1	Elution Order	d, e, g	d, e, g	d, e, g	d, e/g	d, e, g	d, e, g	d, e/g	d, e/g	ADEN (d)	Group 1 Key
		1.4	1.3	1.0	1.0	0.7	2.0	1.6	1.2	ETIO (e)	
		1.5	0.9	0.6	0.3	0.9	1.0	0.2	0.2	1DHEA (g)	
2	Elution Order	b, c, f, k, l, q	b, c, f, k, i/q	b, c, f, k, q, i	b, c, f, q/k, i	b/c, f, k/l, q	b/c, f, k, i/q	b/c, f, k/q, i	b, c, f, q/k, i	1STEN (b)	Group 2 Key
		1.2	0.9	1.0	1.2	0.2	0.0	0.2	0.6	MSAL (c)	
		4.6	3.8	3.1	2.9	4.1	4.5	3.2	3.1	MSEL (f)	
		5.4	4.6	3.4	3.4	3.0	5.1	4.2	3.7	MTHY (i)	
		1.3	1.2	0.6	0.3	0.3	1.4	0.4	0.4	MIBL (k)	
		1.5	0.4	0.5	1.0	0.9	0.2	0.9	1.0	DNZL (q)	
2-B	MSAL : MSEL	4.6	3.8	3.1	2.9	4.1	4.6	3.2	3.1		
2-C	MIBL : MTHY	1.3	1.2	1.1	1.0	0.3	1.4	1.2	1.0		
3	Elution Order	j, l, m/o, r	j, l, m/o, r	j, l, o/m, r	j, l, o, m, r	j, l, m/o, r	j, l, m/o, r	j, l, o/m, r	j, l, o/m, r	PRST (j)	Group 3 Key
		6.0	5.5	4.2	4.0	2.1	6.2	5.1	4.4	EPIT (l)	
		3.2	2.6	1.6	1.1	2.0	3.0	1.8	1.2	TSTO (m)	
		0.3	0.2	0.4	0.6	0.4	0.3	0.3	0.4	OXAN (o)	
		9.3	8.8	7.2	7.0	6.2	9.8	8.3	7.0	TRNB (r)	
3-D	PRST:TRNB	19.1	16.4	12.8	12.7	11.5	19.8	15.7	12.5		
3-E	EPIT:TSTO	3.2	2.8	2.2	1.8	2.0	3.0	2.1	1.7		
Non (mid-)	Elution Order	n, p, s	n/s/p	s/n/p	s, n/p	p/n, s	n/s, p	s, n/p	s, n/p	GSTN (s)	(mid-) key
		0.6	0.1	0.4	1.2	0.3	0.1	0.9	1.3	MTRB (p)	
		0.6	0.4	0.4	0.3	0.7	0.5	0.4	0.4	METD (n)	
Non (late-)	Elution Order	w, v	w, v	w, v	w, v	w, v	w, v	w, v	w, v	CLNB (w)	(late) key
		>10.0	>10.0	>10.0	>10.0	>10.0	>10.0	>10.0	>10.0	ADAR (v)	

*Conditions: SFC-MS separations on UC-Cyano column, using 5% methanol + 5 mM ammonium formate in carbon dioxide. 1.0 µL injections via autosampler of AAS-mix

S_Table 7. Resolution of Critical Pair Groups during Secondary Parameters Screening using Moderate Modifier Concentration (10%)*.

		Critical Group Resolution									
Critical Group	Outlet Pressure	11	15	20	25	11	15	20	25	Mpa	
	Column Temperature	30	30	30	30	40	40	40	40	(°C)	
1	Elution Order	d/e, g	d/e, g	d/e, g	d/e/g	d/e, g	d/e, g	d/e, g	d/e/g	ADEN (d)	Group 1 Key
		< 0.1	< 0.1	< 0.1	< 0.1	< 0.1	< 0.1	< 0.1	< 0.1	ETIO (e)	
		1.3	1.0	0.9	0.4	1.1	0.7	0.6	0.4	1DHEA (g)	
2	Elution Order	b, c, f, k, l, q	b, c, f, k, l/q	b, c, f, k, l/q	b, c, f, k, q/l	b, c, f, k, l, q	b, c, f, k, l, q	b, c, f, k, l, q	b, c, f, k, q, l	1STEN (b)	Group 2 Key
		3.1	2.7	2.4	2.0	2.4	2.0	1.9	1.8	MSAL (c)	
		2.2	1.5	1.4	1.0	2.2	2.0	1.4	1.6	MSEL (f)	
		2.7	2.5	2.2	1.8	3.3	2.6	2.0	2.0	MTHY (i)	
		0.8	0.7	0.6	0.5	0.9	0.8	0.6	0.5	MIBL (k)	
		0.6	0.3	0.1	0.1	1.1	0.5	0.1	0.2	DNZL (q)	
2-B	MSAL : MSEL	2.2	1.5	1.4	1.0	2.2	2.0	1.4	1.6		
2-C	MIBL : MTHY	0.8	0.7	0.6	0.6	0.9	0.8	0.6	0.6		
3	Elution Order	j, l, m/o, r	j, l, m/o, r	j, l, o/m, r	j, l, o/m, r	j, l, m/o, r	j, l, m/o, r	j, l, o/m, r	j, l, o/m, r	PRST (j)	Group 3 Key
		2.5	2.3	1.9	1.7	2.8	2.3	2.0	1.8	EPIT (l)	
		2.0	1.7	1.4	1.4	2.7	1.9	1.7	1.4	TSTO (m)	
		0.3	0.1	< 0.1	0.1	0.3	0.1	0.1	0.2	OXAN (o)	
		4.1	3.9	3.7	3.4	5.1	4.5	4.1	3.7	TRNB (r)	
3-D	PRST:TRNB	8.5	7.9	7.2	6.8	10.4	8.5	7.8	7.1		
3-E	EPIT:TSTO	2.0	1.7	1.4	1.4	2.7	1.9	1.7	1.4		
Non (mid-)	Elution Order	s/n/p	s/n/p	s/n/p	s, n/p	n/s/p	s/n/p	s/n/p	s, n,p	GSTN (s)	(mid-) key
		< 0.1	0.3	0.4	0.5	0.4	0.2	0.4	0.5	MTRB (p)	
		0.3	0.2	0.1	0.2	0.2	0.3	0.3	0.3	METD (n)	
Non (late-)	Elution Order	v/w	v/w	v, w	v, w	w, v	w, v	w/v	v,w	CLNB (w)	(late) key
		0.2	1.0	1.9	2.5	3.7	1.4	0.4	1.3	ADAR (v)	

***Conditions**: SFC-MS separations on UC-Cyano column, using 5% methanol + 5 mM ammonium formate in carbon dioxide. 1.0 µL injections via autosampler of AAS-mix

S_Table 7 (CON'T). Resolution of Critical Pair Groups during Secondary Parameters Screening using Moderate Modifier Concentration (10%)*.

		Critical Group Resolution									
Critical Group	Outlet Pressure	11	15	20	25	11	15	20	25	Mpa	
	Column Temperature	50	50	50	50	60	60	60	60	(°C)	
1	Elution Order	d/e, g	d/e, g	d/e, g	d/e/g	d, e, g	d, e, g	d/e, g	d/e/g	ADEN (d)	Group 1 Key
		0.4	0.2	< 0.1	0.1	0.7	0.6	0.2	0.1	ETIO (e)	
		1.2	1.0	0.4	0.2	1.6	1.3	0.6	0.3	1DHEA (g)	
2	Elution Order	b, c, f, k, l, q	b, c, f, k, l, q	b, c, f, k, l/q	b, c, f, k/l/q	b, c, f, k/l, q	b, c, f, k, l, q	b, c, f, k/l/q	b, c, f, k/l/q	1STEN (b)	Group 2 Key
		1.6	1.7	1.6	1.2	1.5	0.9	0.9	1.0	MSAL (c)	
		2.4	2.2	2.0	1.8	5.0	3.0	2.4	2.1	MSEL (f)	
		4.2	2.9	2.5	1.9	3.3	3.3	2.4	2.0	MTHY (i)	
		0.9	0.8	0.6	0.4	0.2	0.8	0.5	0.4	MIBL (k)	
		1.9	0.8	0.3	< 0.1	2.0	1.4	0.5	< 0.1	DNZL (q)	
2-B	MSAL : MSEL	2.4	2.2	2.0	1.8	5.0	3.0	2.4	2.1		
2-C	MIBL : MTHY	0.9	0.8	0.6	0.4	0.2	0.8	0.5	0.4		
3	Elution Order	j, l, m/o, r	j, l, m/o, r	j, l, o/m, r	j, l, o/m, r	j, l, m/o, r	j, l, m/o, r	j, l, o/m, r	j, l, o/m, r	PRST (j)	Group 3 Key
		3.1	2.5	2.0	1.6	1.7	2.7	2.3	2.0	EPIT (l)	
		3.1	2.2	1.7	1.4	2.2	2.5	1.8	1.5	TSTO (m)	
		0.5	0.1	0.1	0.3	0.4	0.3	0.1	0.2	OXAN (o)	
		5.8	5.5	4.7	4.0	3.7	5.7	5.2	4.4	TRNB (r)	
3-D	PRST:TRNB	12.0	10.5	8.6	7.1	7.9	11.2	9.5	8.3		
3-E	EPIT:TSTO	3.1	2.2	1.7	1.4	2.2	2.5	1.8	1.5		
Non (mid-)	Elution Order	n, p/s	n/s/p	s/n/ p	s/n/p	n, p, s	n, p/s	n/s, p	s/n/p	GSTN (s)	(mid-) key
		0.6	0.2	0.2	0.3	0.5	0.6	0.2	0.3	MTRB (p)	
		0.4	0.4	0.4	0.3	1.1	0.3	0.5	0.4	METD (n)	
Non (late-)	Elution Order	w, v	w, v	w, v	w, v	w, v	w, v	w, v	w, v	CLNB (w)	(late) key
		8.1	4.8	2.8	1.2	> 10.0	> 10.0	7.2	3.9	ADAR (v)	

*Conditions: SFC-MS separations on UC-Cyano column, using 5% methanol + 5 mM ammonium formate in carbon dioxide. 1.0 µL injections via autosampler of AAS-mix

S_6.2. SUPPLEMENTAL: Effect of Screening Gradients on Retention

S_Table 8. Resolution of Critical Pair Groups for Screening Gradients using Low Column Temperature (30 °C).

Critical Group	AAS ID	Critical Group Resolution											Column	
		G(m)	G(n)	G(o)	G(p)	G(q)	G(r)	G(s)	G(t)	G(u)	G(x)	G(y)		
1	Elution Order	d, g/e	d, g, e	d, g/e	d, g/e	d, g/e	d, e, g	d, e, g	d, e, g	d, e/g	d, e, g	d, e, g	ADEN (d)	Group 1 Key
		1.5	2.0	1.8	1.4	1.5	1.2	1.2	1.1	1.2	1.1	0.8	ETIO (e)	
		0.2	0.4	0.2	< 0.1	< 0.1	0.6	0.4	0.7	0.6	0.7	0.9	1DHEA (g)	
2	Elution Order	b, c, f, q, k, i	b, c, f, q, k, i	b, c, f, q, k, i	b, c, f, q, k, i	b, c, f, q/k, i	b, c, f, q/k, i	b, c, f, q/k, i	b, c, f, q/k, i	b, c, f, q/k, i	b, c, f, q/k, i	b, c, f, k/q, i	1STEN (b)	Group 2 Key
		3.9	3.9	3.7	3.9	3.3	3.9	3.9	3.6	3.6	3.1	3.1	MSAL (c)	
		3.6	4.0	3.6	3.8	3.3	3.3	3.2	3.0	3.1	3.3	3.2	MSEL (f)	
		3.5	3.1	3.0	3.2	3.1	4.0	4.2	4.0	4.0	4.4	4.9	MTHY (i)	
		1.2	2.5	2.1	1.8	1.4	0.7	0.6	0.6	0.6	0.4	0.4	MIBL (k)	
		1.5	1.7	1.6	1.4	1.2	1.6	1.5	1.5	1.4	1.5	0.9	DNZL (q)	
2-B	MSAL : MSEL	4.8	5.7	5.1	5.0	4.5	4.6	4.8	4.5	4.5	4.6	4.4		
2-C	MIBL : MTHY	1.5	1.7	1.6	1.4	1.2	1.6	1.5	1.5	1.4	1.5	1.3		
3	Elution Order	j, l, o/m, r	j, l, o/m, r	j, l, o/m, r	j, l, o/m, r	j, l, o/m, r	j, l, o/m, r	j, l, o/m, r	j, l, o/m, r	j, l, o/m, r	j, l, m, o, r	j, l, o/m, r	PRST (j)	Group 3 Key
		6.0	7.5	7.0	6.3	5.4	5.8	5.3	5.4	5.2	6.1	4.6	EPIT (l)	
		1.8	1.6	1.6	1.6	1.5	1.9	1.9	1.9	1.8	1.7	1.9	TSTO (m)	
		0.3	0.4	0.4	0.3	0.2	0.3	0.3	0.3	0.3	0.6	0.4	OXAN (o)	
		6.4	6.7	6.1	5.9	4.8	6.9	6.2	5.8	5.8	7.0	6.4	TRNB (r)	
3-D	PRST:TRNB	13.7	15.8	14.1	13.6	11.7	16.1	14.6	13.1	13.3	14.6	12.2		
3-E	EPIT:TSTO	2.4	2.3	2.3	2.1	1.8	2.5	2.3	2.3	2.3	2.5	2.5		
Non (mid-)	Elution Order	s, p, n	s, p, n	s, p, n	s, p, n	s, p, n	s, p, n	s, p, n	s, p, n	s, p, n	s, p, n	s, p/n	GSTN (s)	(mid-) key
		1.8	2.5	2.2	1.9	1.7	1.9	1.6	1.6	1.4	1.4	0.9	MTRB (p)	
		0.4	0.5	0.5	0.4	0.3	0.3	0.3	0.2	0.3	0.2	<0.1	METD (n)	
Non (late-)	Elution Order	v, w	v, w	v, w	v, w	v, w	v, w	v, w	v, w	v, w	v/w	w, v	CLNB (w)	(late) key
		2.6	3.1	3.0	3.4	4.1	2.3	2.4	3.3	3.2	0.1	0.6	ADAR (v)	

S_Table 9. Resolution of Critical Pair Groups for Screening Gradients using High Column Temperature (60 °C).

Critical Group	AAS ID	Critical Group Resolution												
		G(m)	G(n)	G(o)	G(p)	G(q)	G(r)	G(s)	G(t)	G(u)	G(x)	G(y)	Column	
1	Elution Order	d, e, g	d, e/g	d, e/g	d, e/g	d, e, g	d, e, g	d, e, g	d, e, g	d, e, g	d, e/g	d, e, g	ADEN (d)	Group 1 key
		2.3	2.7	2.3	2.2	1.7	2.3	2.2	2.1	1.8	2.5	2.1	ETIO (e)	
		0.6	<0.1	0.3	0.3	0.5	0.8	0.8	0.8	0.9	0.3	0.8	1DHEA (g)	
2	Elution Order	b/c, f, k/q, i	c/b, f, q, k, i	c/b, f, q/k, i	b/c, f, q,/k, i	b/c, f, k/q, i	b/c, f, k/q, i	b/c, f, k, q, i	b/c, f, k, q, i	b/c, f, k, q/i	c/b, f, k, q, i	b/c, f, k, q/i	1STEN (b)	Group 2 Key
		0.3	0.5	0.3	0.1	0.1	0.4	0.3	0.5	0.3	0.3	0.2	MSAL (c)	
		4.7	4.6	4.5	4.5	3.8	4.5	5.1	4.5	4.6	5.3	5.0	MSEL (f)	
		5.2	4.8	5.0	5.0	4.7	6.0	6.2	5.9	5.7	7.0	6.0	MTHY (i)	
		0.1	0.6	0.3	0.1	0.4	0.4	0.6	0.7	0.8	0.6	1.1	MIBL (k)	
		1.3	1.6	1.4	1.2	0.8	1.1	0.7	0.6	0.4	1.0	0.3	DNZL (q)	
2-B	MSAL : MSEL	5.7	5.8	5.6	5.2	4.3	5.8	5.8	5.3	4.6	6.9	5.2		
2-C	MIBL : MTHY	1.4	1.6	1.4	1.3	1.2	1.6	1.4	1.4	1.3	1.7	1.5		
3	Elution Order	j, l, m/o, r	j, l, m/o, r	j, l, m/o, r	j, l, m/o, r	j, l, m/o, r	j, l, m/o, r	j, l, m/o, r	j, l, m/o, r	j, l, m/o, r	j, l, m/o, r	j, l, m/o, r	PRST (j)	Group 3 key
		6.3	6.8	6.0	5.5	4.9	6.5	5.9	5.5	4.7	7.2	6.2	EPIT (l)	
		2.6	2.5	2.5	2.4	2.1	2.8	2.8	2.6	2.4	2.7	2.8	TSTO (m)	
		0.3	0.3	0.3	0.3	0.3	0.2	0.2	0.2	0.2	0.2	0.2	OXAN (o)	
		7.3	6.4	6.8	6.4	5.7	8.0	7.3	7.1	6.0	12.1	7.8	TRNB (r)	
3-D	PRST:TRNB	17.4	20.0	14.7	14.1	13.7	18.4	15.9	15.7	13.3	27.9	17.0		
3-E	EPIT:TSTO	2.6	0.3	2.5	2.4	2.1	2.8	2.8	2.6	2.4	2.7	2.8		
Non (mid-)	Elution Order	s, n/p	s, n/p	s, n/p	s, n/p	s/n/p	s, n/p	s, n/p	s, n/p	s/n/p	s, n/p	s/n/p	GSTN (s)	(mid-) key
		1.0	1.2	1.0	0.8	0.5	0.9	0.7	0.6	0.4	0.6	0.3	MTRB (p)	
		0.4	0.2	0.3	0.4	0.4	0.4	0.4	0.4	0.4	0.4	0.5	METD (n)	
Non (late-)	Elution Order	v/w	v, w	v, w	v/w	v/w	w/v	w, v	w, v	w, v	w, v	w, v	CLNB (w)	(late) ke
		0.3	1.7	0.9	0.4	0.1	0.3	1.1	1.9	2.0	1.0	1.4	ADAR (v)	

S_6.3. SUPPLEMENTAL: Final SFC-MS Method Evaluations

S_Table 10. Peak Area and Retention Time Reproducibility, Elution Order and Resolution for Targeted Anabolic Agents for SFC Injections using Final Optimized SFC-MS Method.

Peak	Elution Order	AAS	ID	Critical Group	Retention Time (min)			Peak Area			Resolution
					Average	SD	%RSD	Average	SD	%RSD	
[*a*]	1	7-Keto-DHEA	KETO	n/a	2.25	0.01	0.3%	188,697,811	1,496,876	1%	-
[*b*]	2	Androstenedione	1STEN	2	3.03	0.01	0.5%	123,112,169	5,132,367	4%	4.7
[*c*]	3	Mestanolone	MSAL	2-C	3.38	0.01	0.2%	17,081,393	561,833	3%	2.4
[*f*]	4	Mesterolone	MSEL	2-C	3.95	0.01	0.3%	10,506,505	484,583	5%	4.0
[*d*]	5	Androsterone	ADEN	1	4.06	0.01	0.2%	33,003,927	1,463,598	4%	0.9
[*j*]	6	Prasterone (DHEA)	PRST	3-E	4.19	0.00	0.1%	2,596,139	127,528	5%	0.9
[*g*]	7	1-Androsterone	1DHEA	1	4.21	0.01	0.3%	3,206,237	118,244	4%	0.1
[*e*]	8	Etiocholanolone	ETIO	1	4.24	0.01	0.2%	14,544,547	609,332	4%	0.1
[*q*]	9	Danazol	DNZL	2	4.49	0.01	0.3%	48,140,406	1,553,669	3%	1.7
[*k*]	10	Methyltestosterone	MTHY	2-B	4.58	0.02	0.4%	158,059,580	964,871	1%	0.6
[*i*]	11	Mibolerone	MIBL	2-B	4.78	0.01	0.2%	104,069,594	2,568,685	2%	1.3
[*l*]	12	Epitestosterone	EPIT	3-D	4.95	0.01	0.2%	94,462,311	4,064,536	4%	1.2
[*o*]	13	Oxandrolone	OXAN	3	5.08	0.01	0.1%	111,737,657	4,906,363	4%	0.9
[*m*]	14	Testosterone	TSTO	3-D	5.18	0.01	0.2%	40,684,840	1,522,735	4%	0.7
[*s*]	15	Gestrinone	GSTN	NON (mid)	5.51	0.02	0.3%	135,914,574	2,610,076	2%	2.1
[*n*]	16	Metandienone	METD	NON (mid)	5.60	0.00	0.1%	33,107,881	911,888	3%	0.6
[*p*]	17	Metribolone	MTRB	NON (mid)	5.63	0.01	0.2%	167,061,821	2,984,541	2%	0.2
[*r*]	18	Trenbolone	TRNB	3-E	6.11	0.01	0.1%	2,318,317	115,802	5%	2.9
[*t*]	19	Zeranol	ZNRL	n/a	7.04	0.01	0.1%	598,248	27,331	5%	7.4
[*u*]	20	Stanozolol	STNZ	n/a	7.49	0.02	0.2%	51,146,116	2,525,721	5%	2.8
[*w*]	21	Clenbuterol	CLNB	NON (late)	8.62	0.01	0.2%	263,758,867	9,603,145	4%	4.7
[*v*]	22	Andarine	ADAR	NON (late)	9.48	0.00	0.1%	110,262,947	5,362,126	5%	4.3
[*h*]	-	Androstanolone	ADON	1	0.00	-	-	-	-	-	-

CHAPTER 7

SFE-OPTIMIZATIONS: ONLINE EXTRACTION OF AAS

CHAPTER 7
SFE-OPTIMIZATIONS: ONLINE EXTRACTION OF AAS
RESULTS & DISCUSSION

7.1. Extraction Optimization in SFE-SFC-MS Method Development

Online extractions have significant advantages, but complications of hyphenated method develop (MD) continues to hinder the techniques penetration into arenas where it could provide solutions for complicated sample preparations. Instrument advances provide new opportunity in online extractions via SFE-SFC-MS.

With online methods, the effects of instrument parameters can have widely different effects on the 'extractability' of compounds. These effects not only depend on the chemical specificities of the analytes targeted, but MD is further complicated due to synergistic effects between parameters. Systematic examples of observed effects provide a multitude of information, and provide indispensable insights into the mechanisms at play and help guide development of novel methods.[17] But these types of reports continue to be limited and little information is available to new users to guide development of novel online SFE-SFC-MS methods. Especially limited is information for the use of small volume (0.2-mL) extraction vessels, which are specifically designed for use with small sample sizes.

The goal of the current work is to add to the knowledge base by providing a simple, generic screening approach for systematic MD for online SFE-SFC-MS extraction. A pre-developed SFC-MS method is hyphenated with online SFE for a rapid evaluation of the effect of extraction-specific instrument parameters on the method performance (paying close attention to peak shapes and chromatographic reproducibility) and discussing the relative importance of each.

7.1.1. Overall MD Process for Online Extractions.

Method development (MD) for online extractions is a multistep process, involving four main steps:

1. **MS-based detection optimizations**
2. **SFC-based separation optimizations**
3. **SFE-based extraction optimizations**
4. **Matrix-specific optimizations**

The methods for detection (via MS, step 1) and separation (via SFC, step 2), used in the current work, were optimized in previous development steps of the online MD process. The work presented here, involves the SFE-based extraction optimizations (mainly step 3) in the development of a hyphenated method for the online extraction of anabolic agents from dried blood spots for anti-doping analysis. Online extractions are hyphenated with the pre-developed SFC-MS method to screen SFE extraction parameters (Figure 106).

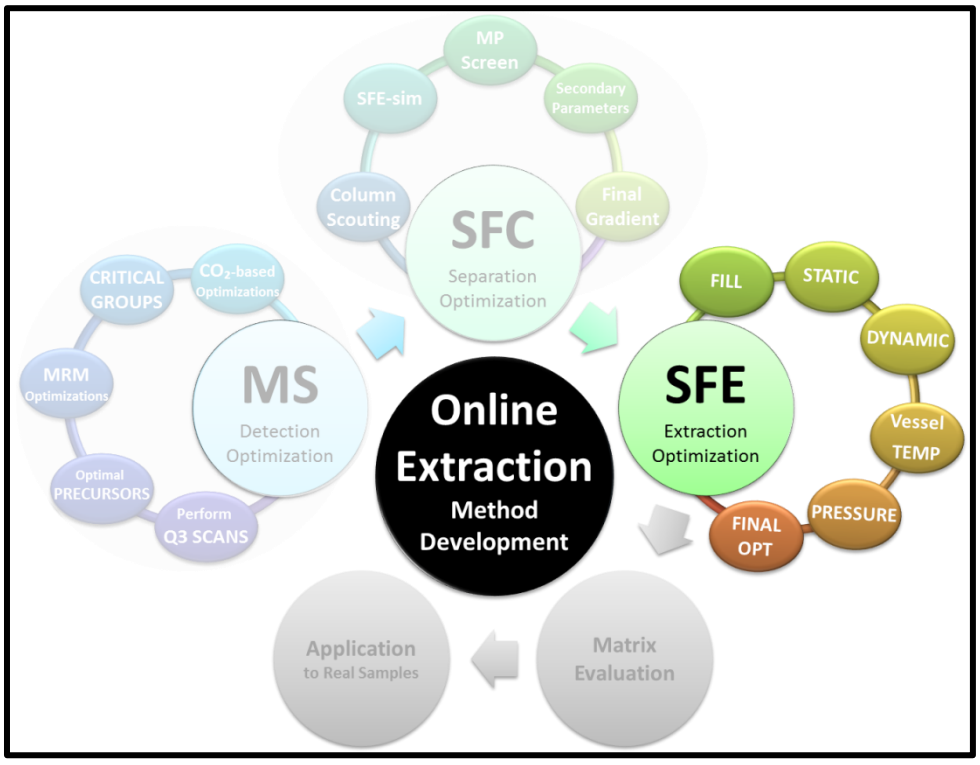

Figure 106. Online Extraction Method Development Focus for Chapter #7 SFE-Extraction Optimizations: Effect of Extraction Parameters.

7.1.2. Pre-developed MS-Detection method and Critical Pair Groups

Direct flow injection was used in ESI-positive and negative mode to create Q3 scans (120 – 1,200 m/z) for each steroid. Obtained spectra were compared to known precursors from literature. Optimal precursor and solution concentrations were chosen for each standard and used for further MRM optimization using the LabSolutions 'optimize MRM event from product ion search' function. Resulting Optimized MRM transitions are presented in **Table 29** and final MS conditions used in the current work are summarized in **Section 7.i.3.2. MS Method Parameters – MRM method.**

Structures for the 23 targeted anabolic agents are presented in **Figure 107**. Each of the standards were then individually reinjected using the newly optimized MRM method. Steroids that produced signal for two or more MRMs were investigated further for structural similarities and their Q3 scans compared. This identified five groups of compounds as 'critical pairs', where due to fundamental similarities in structure and/or molecular weight, make differentiation with MS-alone impossible, and therefore were flagged as requiring chromatographic separation in later development steps.

(detailed discussion of MS-optimizations can be found in previous chapters: Q3 scans and fragmentation patterns are discussed in **Chapter #3: MS-Detection: Q3 Scans** and MRM method optimizations discussed in **Chapter #4: MS-Detection: MRM Optimizations**).

Table 29. MRM Details for Targeted Anabolic Agents (AAS) listed by SFC Chromatographic retention order with critical ID groups

				Precursor			Product Ion							
				MW	+/-	(m/z)	Transition 1	(Q1/Q3 Bias, CE)	Transition 2	(Q1/Q3 Bias, CE)	Transition 3	(Q1/Q3 Bias, CE)	Transition 4	(Q1/Q3 Bias, CE)
Peak	Steroid	ID	Critical Group				(m/z)	([V]/[V], [eV])	(m/z)	([V]/[V], [eV])	(m/z)	([V]/[V], [eV])	(m/z)	([V]/[V], [eV])
[1]	7-Keto-DHEA	KETO	n/a	302.2	+	285	81	(-22/-32, -27)	79	(-20/-30,-44)	107	(-20/-20,-27)	149	(-20/-26,-21)
[2]	Mestanolone	MSAL	2-C	304.4	+	305	269	(-20/-28, -16)	229	(-20/-24,-20)	159	(-20/-34,-23)	187	(-20/-36,-22)
[3]	1-Androstenedione	1STEN	2	286.4	+	287	97	(-20/-20, -22)	109	(-22/-22,-24)	79	(-20/-30,-46)	109	(-20/-40,-35)
[4]	Androsterone	ADEN	1	290.4	+	273	255	(-20/-26, -14)	147	(-22/-32,-21)	199	(-22/-20,-21)	161	(-20/-36,-20)
[5]	Etiocholanolone	ETIO	1	290.4	+	273	255	(-20/-28, -12)	215	(-20/-42,-17)	105	(-20/-20,-35)	91	(-20/-38,-43)
[6]	Mesterolone	MSEL	2-C	304.4	+	305	269	(-22/-28, -17)	173	(-20/-40,-24)	287	(-22/-30,-16)	133	(-24/-22,-28)
[7]	1-Androsterone	1DHEA	1	290.4	+	291	273	(-20/-30, -10)	255	(-15/-26, -15)	135	(-20/-28,-20)	91	(-22/-36, -10)
[8]	Prasterone [DHEA]	PRST	3-E	288.2	+	271	253	(-20/-26, -12)	213	(-22/-46,-15)	213	(-20/-40,-17)	157	(-20/-32,-22)
[9]	Methyltestosterone	MTHY	2-B	302.5	+	303	109	(-22/-20, -28)	97	(-20/-20,-26)	97	(-22/-20,-27)	285	(-22/-30,-16)
[10]	Mibolerone	MIBL	2-B	302.5	+	303	271	(-22/-30, -12)	285	(-22/-20,-17)	121	(-22/-24,-25)	-	-
[11]	Epitestosterone	EPIT	3-D	288.4	+	289	109	(-20/-20, -24)	97	(-22/-38,-25)	79	(-22/-30,-44)	253	(-22/-26,-18)
[12]	Danazol	DNZL	2	337.5	+	338	148	(-24/-30, -25)	91	(-26/-32,-55)	120	(-24/-22,-28)	310	(-24/-32,-20)
[13]	Testosterone	TSTO	3-D	288.4	+	289	109	(-22/-20, -25)	97	(-22/-36,-22)	253	(-22/-28,-17)	79	(-22/-28,-46)
[14]	Oxandrolone	OXAN	3	306.4	+	307	289	(-22/-30, -12)	271	(-22/-30,-14)	121	(-22/-22,-24)	229	(-24/-24,-18)
[15]	Methandienone	METD	NON (mid)	300.4	+	301	121	(-22/-46, -28)	149	(-22/-26,-15)	283	(-22/-30,-11)	121	(-22/-22,-24)
[16]	Metribolone	MTRB	NON (mid)	284.4	+	285	227	(-22/-24, -23)	267	(-20/-28,-17)	198	(-22/-20,-30)	159	(-20/-30,-23)
[17]	Gestrinone	GSTN	NON (mid)	308.4	+	309	241	(-22/-26, -23)	199	(-24/-40,-32)	291	(-24/-20,-16)	262	(-22/-28,-21)
[18]	Zeranol	ZRNL	n/a	322.4	-	321	277	(34/28, 23)	303	(36.0/20,22)	259	(36.0/26,24)	235	(36.0/28,24)
[19]	Trenbolone	TRNB	3-E	270.4	+	271	253	(-20/-26, -19)	199	(-20/-20,-22)	165	(-20/-36,-56)	128	(-20/-26,-57)
[20]	Stanozolol	STNZ	n/a	328.5	+	329	81	(-24/-30, -51)	95	(-24/-20,-42)	121	(-24/-22,-37)	107	(-24/-20,-41)
[21]	Clenbuterol	CLNB	NON (late)	277.2	+	227	203	(-32/-36, -16)	259	(-20/-26,-10)	132	(-20/-24,-28)	168	(-20/-32,-28)
[22]	Andarine	ADAR	NON (late)	441.4	+	442	108	(-32/-20, -37)	208	(-32/-20,-21)	190	(-32/-20,-25)	148	(-32/-32,-31)
[-]	Androstanolone	ADON	1	290.4	+	291	255	(-11/-12, -16)	173	(-10/-18,-21)	227	(-10/-23,-10)	-	-

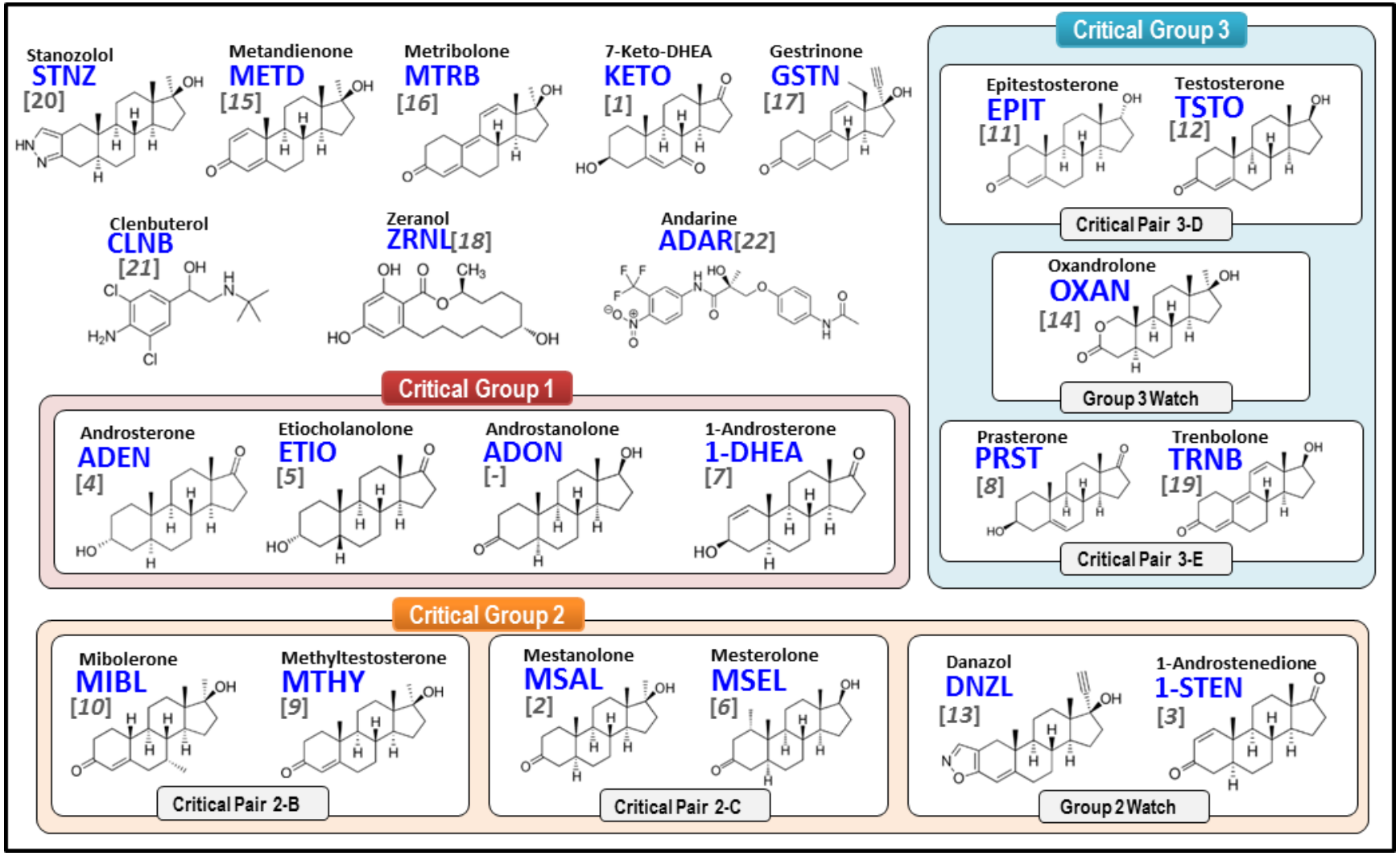

Figure 107. Structure of Targeted anabolic androgenic steroids and bio mimics, showing critical pair groups

7.1.3. SFC-MS Chromatographic Separation Optimization and SFE-simulation.

Fourteen stationary phases were originally screened. A Shimadzu Corp. UC-Cyano column was identified as the best performing column, based not only on its capability for resolution within and between critical groups of compounds, but also its ability to retain a sample plug during an SFE-simulation. SFC-specific parameters were then screened (including modifier concentration and additives, column temperature, and system backpressure), and optimal separation conditions were determined. The final optimized SFC-MS conditions are mirrored in **Section 7.i.3. Instrument Methods: Held Constant Throughout Method Screening**, which were used as the separation conditions throughout the current extraction optimization**.** For hyphenating for online extractions, a column wash was added to the end of the optimized SFC-MS gradient (30%[B] held for 5min), in anticipation of increased matrix complexity of real samples versus SFC-MS injections. The SFE-simulation performed during SFC column screening, identified a watch-list of compounds that could be potentially problematic during sample plug formation/retention, and included: MSAL, MSAL, TRNB, ZRNL and 1DHEA.

(Additional discussion can be found in previous chapters: Column screening/SFE-simulation was discussed in detail in **Chapter #5: Column Selection for Online Extractions** and Separation optimizations discussed in **Chapter #6: SFC-Separation Optimization**)

7.2. Hyphenated Instrument

7.2.1. System Configuration.

The Shimadzu Nexera UC^{TM} Online SFE-SFC-MS System shares a solvent delivery system. Sample is introduced to the system either via the online extraction loop or optionally can be used as a standard SFC-MS system (via automated liquid sampler/injector). The system is equipped with a column oven, and an additional solvent pump to facilitate delivery of the effluent for detection by a triple quadrupole mass spectrometer. In the current work, the instrument was used in SFE-SFC-MS mode for splitless online extractions for use with 0.2-mL extraction vessels (**Figure 108**). The sample is delivered via an online extraction loop, where facilitated by two switching valves, samples are extracted online and the resulting 'extract plug' is delivered to the column for online analysis.

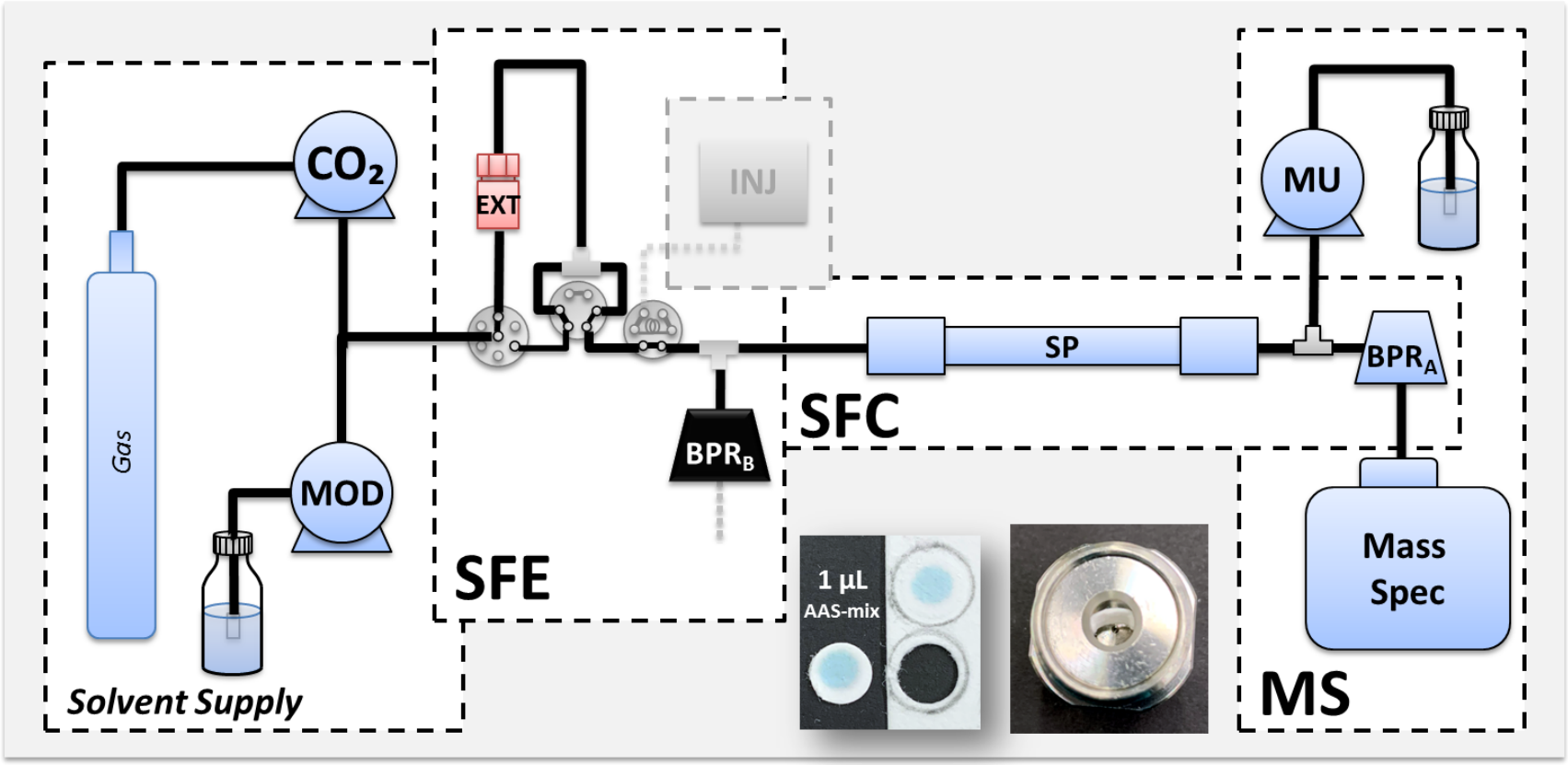

Figure 108. Nexera UC Online SFE-SFC-MS Instrument Configuration for splitless mode Online Extractions using 0.2-mL extraction vessels, showing PoMA core with 1.0 µL Methanolic AAS-mix spotted on Whatman Sample collection paper (with blue food dye added to show spread on card) and PoMA core loaded into a 0.2-mL Extraction vessel.

7.2.2. Online Extraction Process using 0.2-mL Vessels

The extraction process consists of four main steps in which are automated via the method timetable. Using 0.2-mL vessels, requires significantly less sample volume when compared to 5.0-mL vessels, and does not require system splitting, meaning BPR_B can be bypassed (or closed [set to 40 MPa]) throughout the duration of the extraction and analysis. This also means that BPR_A is responsible for all pressure regulation and that ultimately all system effluent will eventually pass through the column (i.e., splitless-mode extraction). The four major steps of an Online SFE-SFC-MS extraction are shown in **Figure 109** and include: Vessel Filling, Static and Dynamic Extractions and finally Analysis.

Pre-run. The specified rack is picked up by an automated arm and moved from the rack changer to the extraction module. The needle moves from the homeport into position connecting the specified vessel for extraction, and therefore completing the extraction loop. The vessel is heated (**Figure 109; A**), once the user specified temperature is reached, triggers the start of the run.

1. Vessel Filling (**Figure 109; orange**). The System flow is split between the extraction loop and the online SFC system. Mobile phase enters the extraction loop (**Figure 109; B**), and fills the empty ('solvent-less') vessel containing the sample (**Figure 109; C**). The extraction loop is 'dead-headed', which pushes excess flow over the column, to the system outlet. Once the vessel is filled with mobile phase system wide pressure stabilizes at a user defined outlet pressure (post-column [BPR_A]).

2. Static 'Passive' Extraction (**Figure 109; red**). The flow path does not change from vessel loading. The sample (now exposed to fill solvent), is left for a duration of time, allowing for 'passive' extraction (**Figure 109; D**). System effluent continues to flow through the column to the system outlet thru BPR_A.

3. Dynamic 'Active' Extraction (**Figure 109; blue**). The extraction valve (bottom) directs the system flow thru the extraction vessel (**Figure 109; E**). Note that post-vessel, the system flow now comes thru the extraction loop from the opposite direction. And at the tee, the flow is now deadheaded at the extraction valve. So just as in

static, all system effluent eventually flows through the column to the system outlet thru BPR_A. Since the MP flows thru the vessel, the solvent in the vessel that has been exposed to the sample (i.e., the extract plug) is pushed (carried) along with the system flow (**Figure 109; F**) and ultimately is delivered to the column with the system flow (**Figure 109; G**). For a duration of time (specified by the user in the method timetable), the flow continues thru the vessel, and over the column (**Figure 109; H**), allowing the MP solvent to continue 'actively' extracting from the sample (and therefore building [i.e., adding to] the extraction plug).

4. Analysis (**Figure 109; *green***). The two valves switch to bypass the vessel and extraction loop, directing all flow directly from the pump towards the column (**Figure 109; I**), and the chromatographic method is started (**Figure 109; J**).

Immediately proceeding the analysis, the extraction needle returns to the home port *(not pictured)* and the system completes a wash of the extraction loop and needle (via the homeport) and the system is reset for the next run.

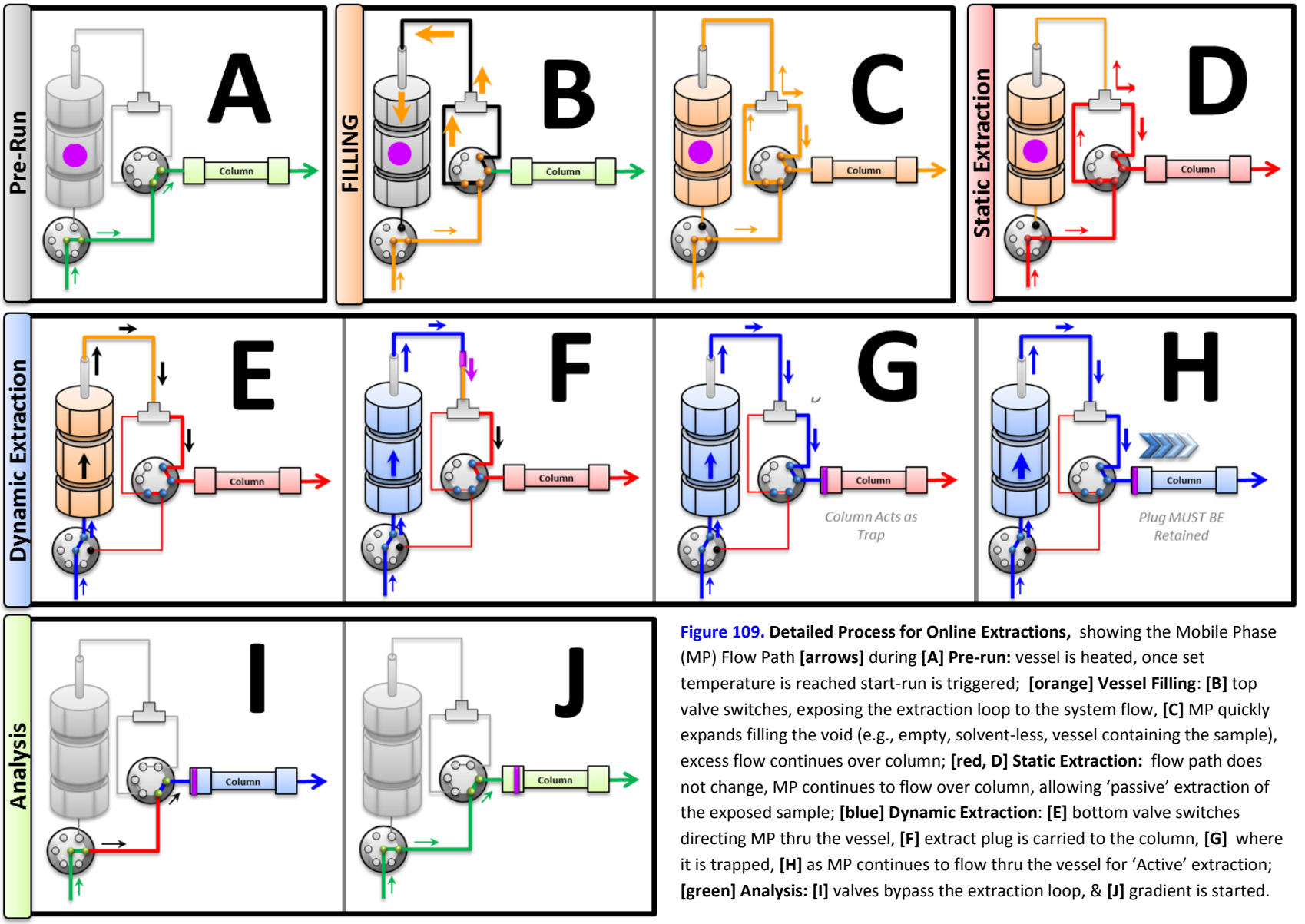

Figure 109. Detailed Process for Online Extractions, showing the Mobile Phase (MP) Flow Path **[arrows]** during **[A] Pre-run:** vessel is heated, once set temperature is reached start-run is triggered; **[orange] Vessel Filling**: **[B]** top valve switches, exposing the extraction loop to the system flow, **[C]** MP quickly expands filling the void (e.g., empty, solvent-less, vessel containing the sample), excess flow continues over column; **[red, D] Static Extraction:** flow path does not change, MP continues to flow over column, allowing 'passive' extraction of the exposed sample; **[blue] Dynamic Extraction**: **[E]** bottom valve switches directing MP thru the vessel, **[F]** extract plug is carried to the column, **[G]** where it is trapped, **[H]** as MP continues to flow thru the vessel for 'Active' extraction; **[green] Analysis: [I]** valves bypass the extraction loop, & **[J]** gradient is started.

7.3. Screening of Parameters for Online Extraction of Anabolic Agents.

Online SFE-SFC-MS extractions were performed on a single AAS-core using 0.2-mL extraction vessels. Effect of extraction-specific parameters were evaluated by performing online extractions on multiple vessels, each of which are extracted using a different setting for the targeted parameter.

7.3.1. Screened Extraction Parameters included:

- Vessel filling duration
- Vessel filling modifier concentration
- Static extraction duration
- Static modifier concentration
- Dynamic extraction duration
- Dynamic modifier concentration
- Vessel temperature
- Extraction pressure
- Flow rate during Extraction

7.3.2. Isolating the effect of One Extraction Parameter at a time

Synergistic effects can make systematic evaluations of the effect of individual extraction parameters extremely difficult. When applying more than one parameter change at a time (each with a known effect *[when used separately]*), will often produce unexpected results (i.e., the expected trends observed for individual parameters are not reflected, when used in combination). Frequently, when changing two parameters at once, it is nearly impossible to predict the outcome.

In an attempt to minimize possible synergistic effects across screened parameters, a single set of 'generic' settings were chosen as a 'base-method'. When screening a specific parameter (ex. Static extraction duration), only that

parameter was changed (variable) and all other generic settings were left unchanged (constant). Generic settings used low modifier concentrations and short durations to minimize overlapping effects from a different parameter than the desired screening objective at that time.

Each parameter was screened separately, while all other instrument parameters were held constant throughout (i.e., the same between each method) in the screening process. Instrument settings common to all SFE-screening methods are detailed in **Section 7.i.3. Parameters held constant throughout SFE-Extraction Method Screening.**

7.3.3. Evaluation of the Effect of Extraction Parameters.

Various instrument parameters were screened, and the resulting SFE-SFC-MS chromatograms were processed and peak areas for each compound compared. Peak area is the most helpful tool in evaluating extraction method performance, being analogous to extraction efficiency; more analyte extracted would produce a larger peak area for that analyte. Replicate vessels were extracted online for a single target-parameter. Each vessel was extracted a total of three consecutive times; the first extraction [EXT1], second extraction [EXT2] and third extraction [EXT3].

Detailed explanation of data processing approaches for SFE-SFC-MS are available in **Chapter #2; Materials and Methods: Section 2.9. General Data Processing Approaches**. The most relevant of which are mirrored in **Section 7.i.6. Data Processing Approaches used in the Evaluation of the Effect of Extraction Parameters.**

Effect of instrument parameters were assessed using the following evaluation criteria:

Visual comparison of chromatographic integrity. Chromatograms were visually compared to gain understanding of the effect of various extraction parameters on overall separation and chromatographic integrity. Qualitative comparisons were performed looking for any degradation to overall separation or peak symmetry, any increase to baseline noise, or any other signs of premature migration of the sample plug were noted. Normalized chromatograms proved more useful for identifying changes to peak shape and relative intensities produced by different groups of analytes (e.g., trends between early and late eluters). Comparing chromatograms at the same intensity were more useful for comparing extraction performance). Dotted lines coinciding with instrument

conditions were overlaid on chromatogram comparisons to aid in visualization of the changed parameter on the effect (especially helpful for evaluation of runtime and plug retention).

Retention time and peak area Comparisons. Multiple vessels were extracted for each screened parameter, each using a different (*'variable'*) setting. Vessels were treated as replicates for each screened parameter (n = # of vessels [i.e., # of settings for a given parameter]). Resulting retention times (Rt) and peak areas produced via online extraction were then compared for each targeted analyte. Reproducible retention times (≤ ± 0.02 minutes) and peak areas (≤ ± 15% RSD) indicated no change (i.e., no difference in effect of a given parameter within the screened range of settings). Alternatively, if the extractions were non-reproducible as replicates, differences in peak areas and/or retention times were evaluated for trends across/between extraction conditions.

Relative extractability can be investigated by comparing the percent extracted (of the total area) from each of three consecutive extractions [%EXT1 vs. %EXT2 vs. %EXT3]. For example, this is calculated by taking the area from the first extraction (EXT1) for a single vessel is divided by the total area extracted (T_{area}/vessel) for the same vessel. A higher %EXT1, indicates a quicker extraction. Comparing vessels extracted under different conditions, if there is no difference in the percent extracted per round (i.e., ≤ ± 1%), indicated no difference in extractability between extraction conditions.

Extraction performance was evaluated via comparison of the percent of the total area extracted in the first two extraction rounds [$\%EXT_{1+2}$] (calculated by combining the area for the first two extractions). Generally, $\%EXT_{1+2} \geq 85\%$ performance for online extractions are considered acceptable.

7.3.4. Sample Preparation and analysis workflow.

Ideally, online extraction evaluations are accomplished using a model sampling technique that could be applicable to a wide range of biological samples. This model must also provide blank material (contributing minimal background/matrix interference) in which targeted analytes can be spiked at known concentrations, in order to adequately evaluate developed methods.

Specifically, in the current work, online extractions are performed for the extraction of AAS, directly from **Whatman standard (cellulose-based) sample collection/preservation cards**. These cards can be used with urine, blood, plant, and tissue samples; they have a preservative which aids in the convenience of collection, preserving the sample for storage. The same steroid mixture was used in both the SFC and SFE screenings. In the SFC screening 1.0 µL injections were used, and therefore for SFE method development, 1.0 µL spots of the same standard mix was quantitatively applied to Whatman sample collection cards, dried, and cored using a standard single hole punch. Cored spots were placed directly into 0.2-mL vessels for extraction using the automated rack changer for Online SFE-SFC-MS analysis (**Figure 110**). Resulting chromatograms are used to evaluate and compare the effect of various extraction-specific parameters during online method development.

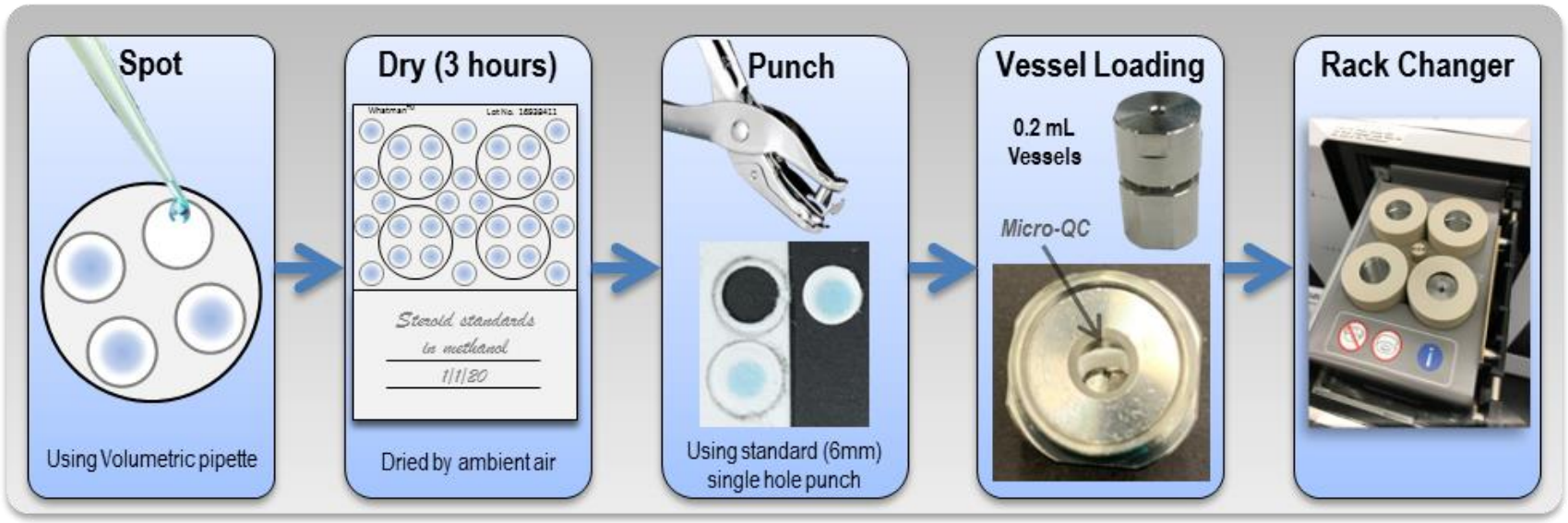

Figure 110. **Sample preparation workflow for online analysis**

7.4. Vessel Filling.

7.4.1. Minimum Duration of Vessel Filling

At the beginning of the extraction process, the vessel is initially empty (no solvent present); so naturally, the first step of extraction must be to expose the sample to mobile phase. Automated valves direct the system flow toward the extraction loop, which loads solvent into the (deadheaded) extraction chamber. Duration and modifier concentration during vessel filling are specified by the user into the programmed method timetable. Although for 5.0-mL vessels, as default, a one minute vessel filling duration using a 5.0 mL/min flow rate, is recommended. There are no recommended settings for vessel filling when using 0.2-mL extraction vessels, and little information is available for new users in regards to 'best practice' and/or expected effect on the extraction. In order to determine an appropriate optimal fill duration for 0.2-mL vessels, system pressure traces were monitored; using the CO_2 pump (pump A) and system outlet pressure (BPR_A) traces, extractions were performed using 0.2-mL vessels and compared to previous data (from another project) that utilized 5.0-mL extraction vessels.

Example traces are shown in **Figure 111**. A clear (and expected) pressure drop occurs immediately at the beginning of each run. This is indicative of the void volume of the 'empty' vessel and loop, which is now exposed to the flow path. The mobile phase quickly expands to fill the void and eventually the system stabilizes at the set 'extraction pressure' (the user defined [BPR_A] outlet pressure). The major difference between the two vessel sizes can be seen via the time required before the system stabilizes after vessel filling. Using the 5.0-mL vessels the fill time is just less than 1.0 minute, but alternatively the smaller, 0.2-mL vessels fill in less than half the time.

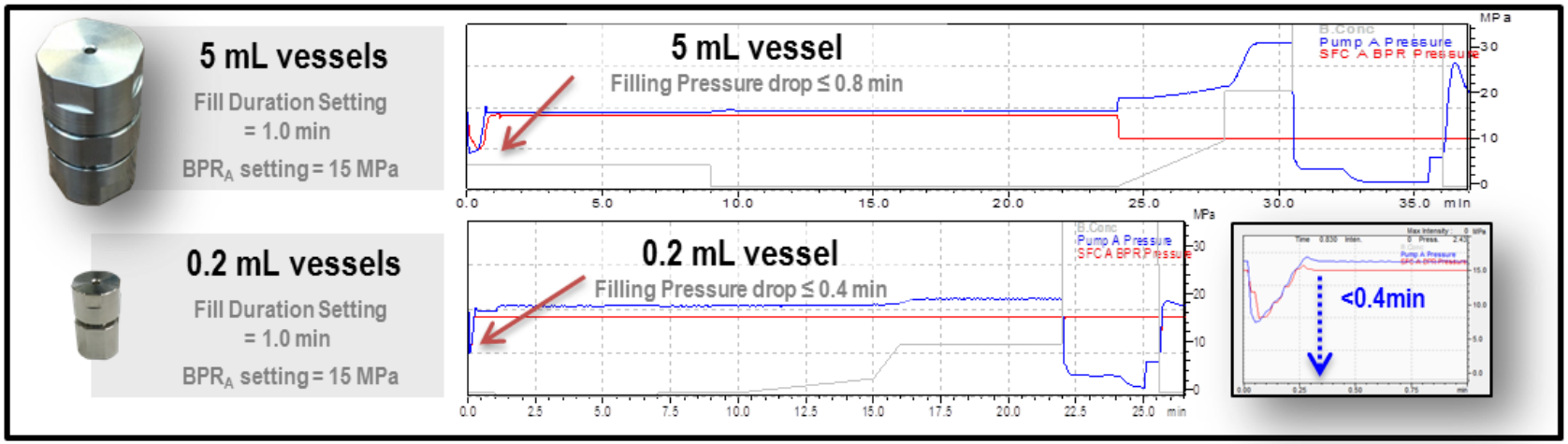

Figure 111. **System Pressure Traces During Online Extractions, showing vessel loading time using 5.0-mL [top] versus 0.2-mL [bottom] extraction vessels.** Displayed traces: **[red; *SFC A BPR Pressure*]** Back-pressure regulator (BPR_A) post-column outlet pressure control and **[blue; *Pump A Pressure*]** Carbon dioxide (CO_2) delivery module. **Fill duration setting:** 0.00 - 1.00 minutes. **BPRA Setting:** 15 Mpa. **Flow rate:** 5.0 mL/min for 5.0-mL vessels and 2.0 mL/min for 0.2-mL vessels.

7.4.2. Screening Conditions for Duration of Vessel Filling.

Effect of vessel filling duration was evaluated via four online extractions, each performed at a different fill duration: 0.5, 0.7, 1.0 or 1.3 minutes. Regardless of fill duration, vessel filling was performed at 2% modifier (2% [B]). All other parameters were the same between/throughout all screening methods.

*Complete method details are outlined in **Section: 7.i.4.1. Screening Conditions for Vessel Filling Duration**.*

7.4.3. Effect of Filling Duration.

The resulting SFE-SFC-MS chromatograms (**Figure 112**) were compared. Vessel filling had little effect on peak shape and the chromatographic resolution was maintained across all screened fill durations. Fill duration also had little effect on the total area extracted, producing reproducible areas between fill durations (%RSDs between 1 and 17%) for all targeted analytes. Furthermore, no change was seen in extraction performance (with 80-90% extracted in the 1st two extraction rounds [EXT_{1+2}]) regardless of fill duration used.

Ultimately, the greatest difference was only extending the overall runtime proportionally to the duration of vessel filling. Average retention times could not be compared, as the overall run time and most importantly the beginning of the analysis step changes proportionally on the duration of the vessel filling**.** As long as the minimum required fill time is reached to EQ system pressure. Vessel filling duration had little effect on the extraction and resulting separation and analysis.

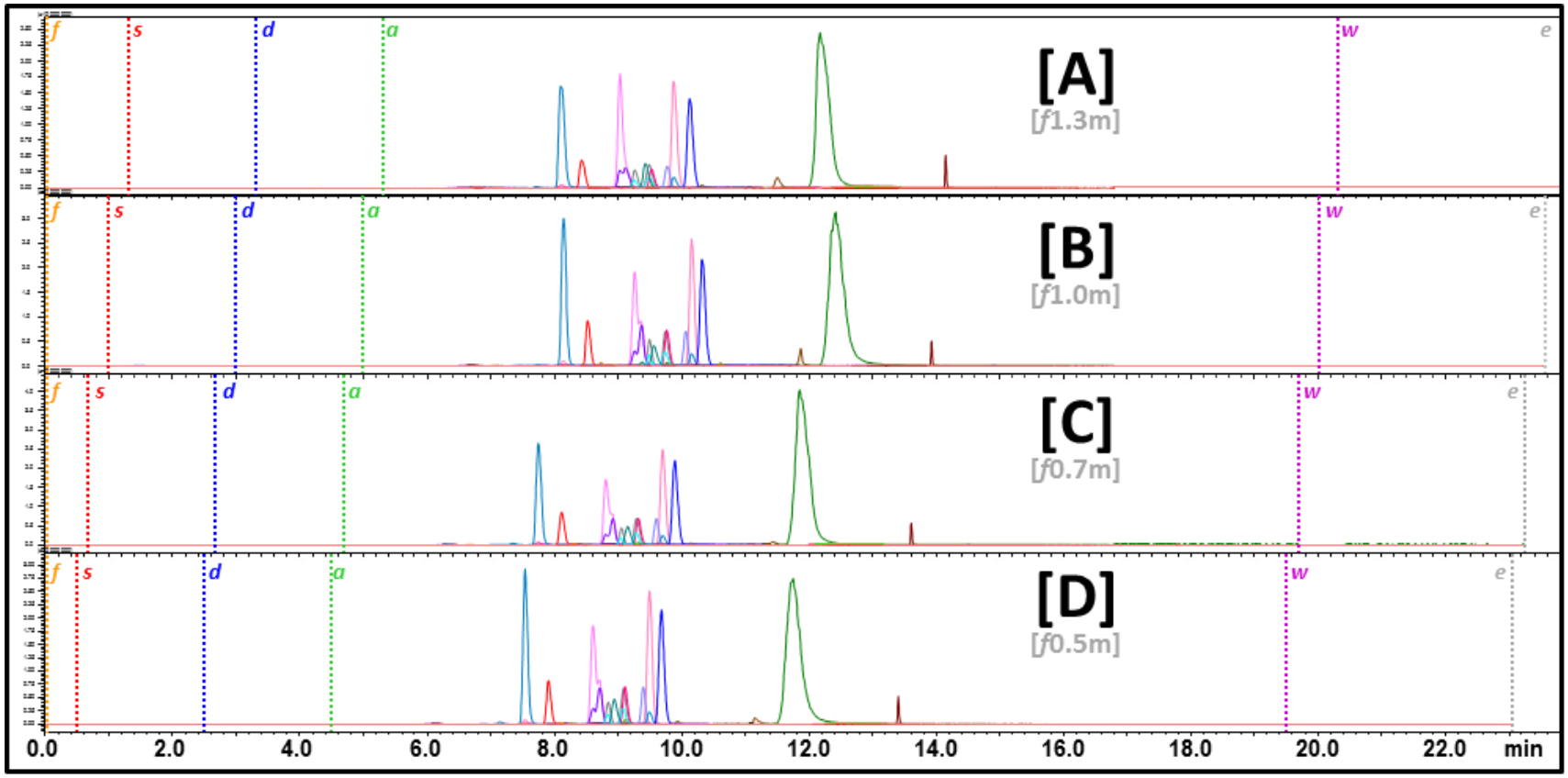

Figure 112. Overlaid SFE-SFC-MS Chromatograms for Online Extractions of Androgenic Anabolic Steroids (AAS) using Four Vessel Filling (*f*) Durations: [A] 1.3 minutes (min); [B] 1.0 min; [C] 0.7 min; and [D] 0.5 min. Chromatographic separations of the extraction plugs produced via online-SFE of spiked steroid standards (1.0 µL spot AAS-mix) from sample collection card (6 mm) core [AAS-QC]. Full runtime showing the start of each extraction step (*dotted lines*): vessel filling [***f***, *orange*]; static extraction [***s***, *red*]; dynamic extraction [***d***, *blue*]; analysis [***a***, *green*]; extraction loop wash [***w***, *purple*] and end of run [***e***, *gray*]. MRM-TIC chromatograms for targeted AAS: KETO [teal]; 1STEN [red]; MSAL [magenta]; ADEN [orange]; ETIO [blue]; MSEL [rose]; 1DHEA [pink]; MTHY [light pink); PRST [gold]; MIBL [purple]; TSTO [gray]; EPIT [cyan]; METD [lilac]; OXAN [hot pink]; MTRB [coral]; DNZL [turquoise]; TRNB [brown]; GSTN, [cobalt]; ZRNL [black]; STNZ [mocha]; CLNB [dark green] and ADAR [maroon]. *Normalized intensity scale.*

7.4.4. Screening Vessel Filling Concentration.

Effect of change in modifier concentration during the vessel filling step of online extraction was evaluated. Six extractions were performed using different fill concentrations (25, 15, 10, 5, 2 and 0%). Regardless of the fill concentration used, the fill duration was always 1.0 minute long. All other parameters were the same between/throughout all screening methods.

*Complete method details are outlined in **Section: 7.i.4.2. Vessel Fill Concentration Screening Conditions**.*

7.4.5. Effect of Modifier Concentration during Vessel Filling

The resulting SFE-SFC-MS chromatograms were compared for differences in peak shape & retention, and are shown in **Figure 113.** With lower modifier concentration during vessel filling, sample plug retention and peak shapes improved for all compounds, but peak areas for late eluting compounds decreased significantly due to the low polarity of the mobile phase.

Fill concentration appears to be very important while using 0.2-mL vessels, a compromise must be made between overall peak shapes (leading to reduced resolution and efficiency at high modifier fill concentration) and reduced peak area at low modifier fill concentration for late eluting (more polar) compounds.

The effect observed at higher filling concentration, looks similar to the sample plug representing a higher proportion of polar modifier (one could compare the effects to having a larger than optimal injection of a less concentrated solution on a standard analytical system, introducing a large concentration of the sample solvent).

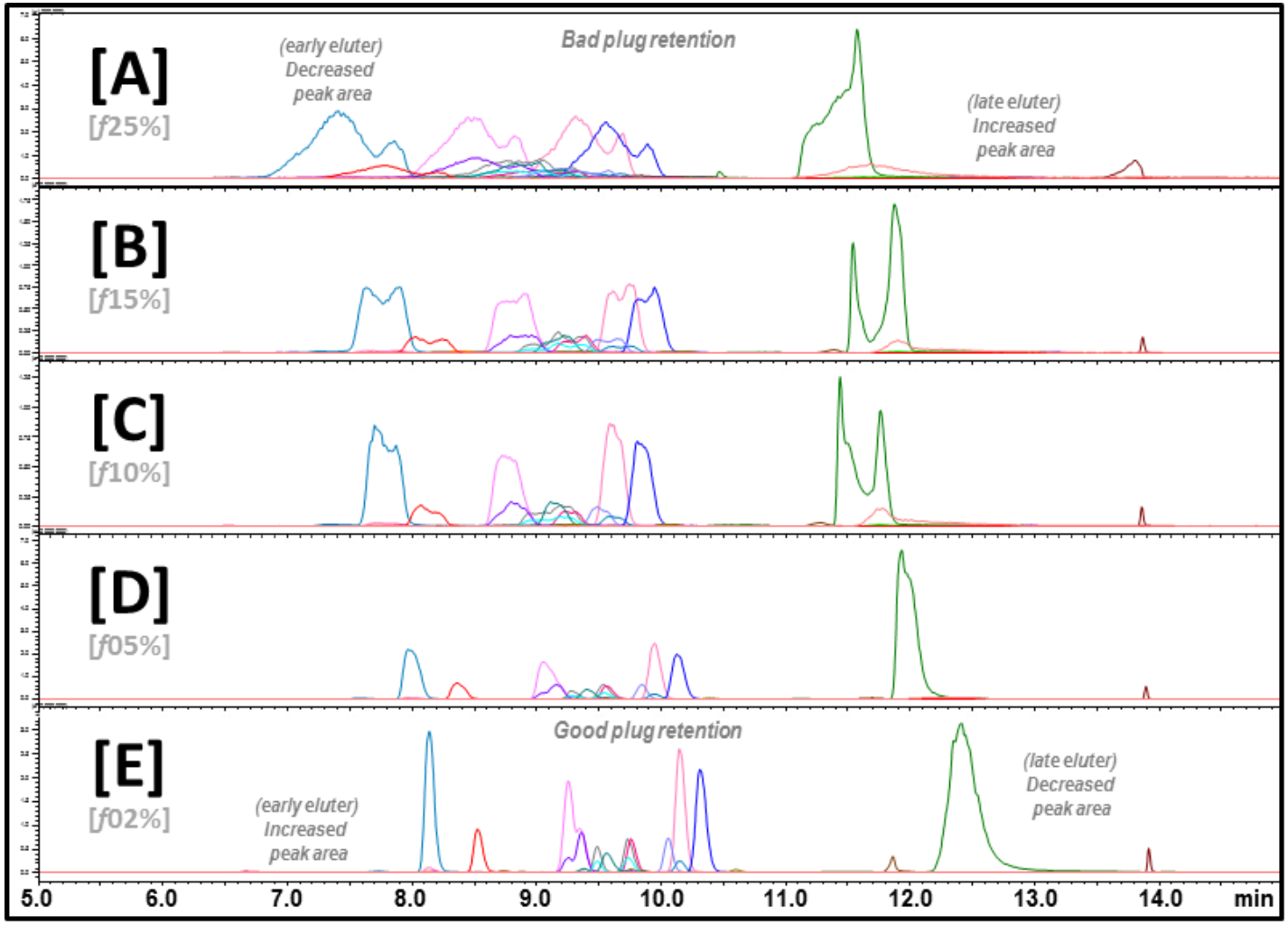

Figure 113. Overlaid SFE-SFC-MS Chromatograms for Online Extractions of Androgenic Anabolic Steroids (AAS) using Five Vessel Filling (*f*) Modifier Concentrations: [A] 25%; [B] 15%; [C] 10%; [D] 5%; and [E] 2% methanol + 5 mM ammonium formate in carbon Dioxide. Chromatographic separations of the extraction plugs produced via online-SFE of spiked steroid standards (1.0 µL spot AAS-mix) from sample collection card (6 mm) core [AAS-QC]. Overlaid MRM-TIC chromatograms zoomed on retention time range for targeted AAS: KETO [teal]; 1STEN [red]; MSAL [magenta]; ADEN [orange]; ETIO [blue]; MSEL [rose]; 1DHEA [pink]; MTHY [light pink); PRST [gold]; MIBL [purple]; TSTO [gray]; EPIT [cyan]; METD [lilac]; OXAN [hot pink]; MTRB [coral]; DNZL [turquoise]; TRNB [brown]; GSTN, [cobalt]; ZRNL [black]; STNZ [mocha]; CLNB [dark green] and ADAR [maroon]. *Normalized intensity scale.*

7.5. Static Extraction

7.5.1. Conditions for Screening the Duration of Static Extraction.

Effect of the duration of static extraction was evaluated via four online extractions performed using 1.0, 2.0, 4.0 or 6.0 minute static durations. Regardless of the static duration used, the static concentration was always 0% [B]. All other parameters were the same between/throughout all screening methods.

*Complete method details are outlined in **Section: 7.i.4.4. Static Extraction Duration Screening Conditions**.*

7.5.2. Effect of Static Extraction Duration.

The resulting SFE-SFC-MS chromatograms are compared in **Figure 114**. Inherently, overall runtime is increased proportionally with longer Static duration. Little effect on was seen on the chromatographic performance, with no deterioration in peak shapes were observed, indicating minimal effect on plug retention.

Alternatively, there was an effect of static duration on extractable peak areas, which was compound specific, showing a strong trend towards analyte polarity. For very early eluting compounds (those expected to be most non-polar), there was little difference in peak area regardless of static duration. Alternatively, mid- and late-eluting compounds, the effect of static duration was compound specific; decreasing for later eluting compounds (more polar) and increasing for early eluters (less polar) with longer static extraction. Longer Static extraction time was shown to improve peak area, with little negative effect on sample plug retention. A compromise between peak area and overall runtime should be considered.

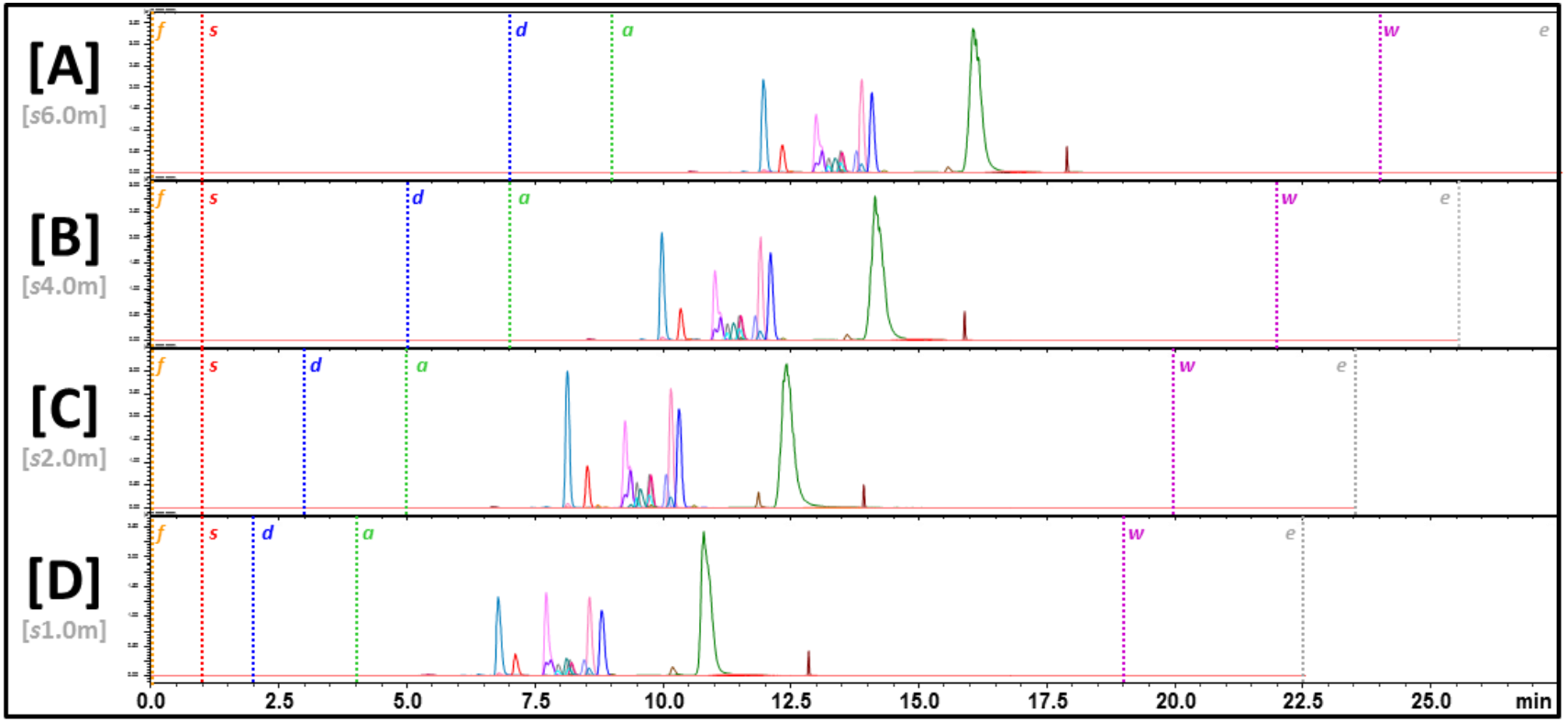

Figure 114. Overlaid SFE-SFC-MS Chromatograms for Online Extractions of Androgenic Anabolic Steroids (AAS) using Four Static Extraction (*s*) Durations: [A] 6.0 minutes (min); [B] 4.0 min; [C] 2.0 min; and [D] 1.0 min. Chromatographic separations of the extraction plugs produced via online-SFE of spiked steroid standards (1.0 µL spot AAS-mix) from sample collection card (6 mm) core [AAS-QC]. Full runtime showing the start of each extraction step (*dotted lines*): vessel filling [***f***, *orange*]; static extraction [***s***, *red*]; dynamic extraction [***d***, *blue*]; analysis [***a***, *green*]; extraction loop wash [***w***, *purple*] and end of run [***e***, gray]. MRM-TIC chromatograms for targeted AAS: KETO [teal]; 1STEN [red]; MSAL [magenta]; ADEN [orange]; ETIO [blue]; MSEL [rose]; 1DHEA [pink]; MTHY [light pink); PRST [gold]; MIBL [purple]; TSTO [gray]; EPIT [cyan]; METD [lilac]; OXAN [hot pink]; MTRB [coral]; DNZL [turquoise]; TRNB [brown]; GSTN, [cobalt]; ZRNL [black]; STNZ [mocha]; CLNB [dark green] and ADAR [maroon]. *Shown at normalized intensity.*

7.5.3. Modifier Concentration During Static Extraction

Effect of modifier concentration during the static extraction step was evaluated. Extractions were performed using 10, 5, 2, and 0% modifier during static extraction. Regardless of the static concentration used, the static duration was always 2.0 minute long. All other parameters were the same between/throughout all screening methods.

*Complete method details are outlined in **Section: 7.i.4.3. Static Extraction Concentration Screening Conditions**.*

7.5.4. Effect of Static Modifier Concentration

The resulting online SFE-SFC-MS chromatograms are compared in **Figure 115**. Peak shape deterioration (mainly in the form of tailing) likely due to decreased 'extraction plug' retention was seen with higher static modifier. Although this seems counter intuitive, since static extraction occurs previous to the 'extract plug', transport-to and loading-onto the column, and although the contents of the extraction vessel should be mostly isolated from the main flowpath; excess MP is continuously washing over the column. This could be thought of as a pre-conditioning step, where if a high modifier concentration is utilized, the phase is effectively being equilibrated with a high percentage of modifier just prior to loading of the plug. Since at the end of static extraction, the valves switch to dynamic, directing flow thru the vessel and out to over the column. This would make it harder to retain analytes (especially less polar compounds) at the head of the column. Ultimately the result is lower resolution, especially pronounced in the early to mid-eluting compounds, which include all the chromatographic critical groups.

Higher static concentration had an opposite effect on late versus early eluting compounds; peak areas increased for late eluting (more polar) compounds, but decreased for early eluting (less polar) compounds. Although overall extraction performance (%EXT_{1+2}) was above 82% for all compounds using any static concentration above 2%. Static modifier concentration did have a notable effect on the extractability of targeted analytes. This effect again had a trend related to analyte polarity (**Figure 116**). Where even with using low modifier concentration ([S] 2%), %EXT1 for early- and mid-eluting compounds, producing 80 - 92% of the total extractable area within the first

round extraction. Late eluters on the other hand, produced much lower %EXT1 when using low static concentrations, producing only less than 60% of the total extractable area in the first extraction round.

Alternatively, at 10% modifier, late-eluters greatly improved at 85-95% extracted in 1st round, but as modifier concentration is increased, early eluters (notably MSAL & 1DHEA) are lost down the column, being non-retained with the sample plug. A compromise would be needed to find a balance between early eluting peak shapes (thru better sample plug retention) at lower modifier and increased late eluting peak areas at higher modifier concentration (thru improved extractability with higher polarity mobile phase).

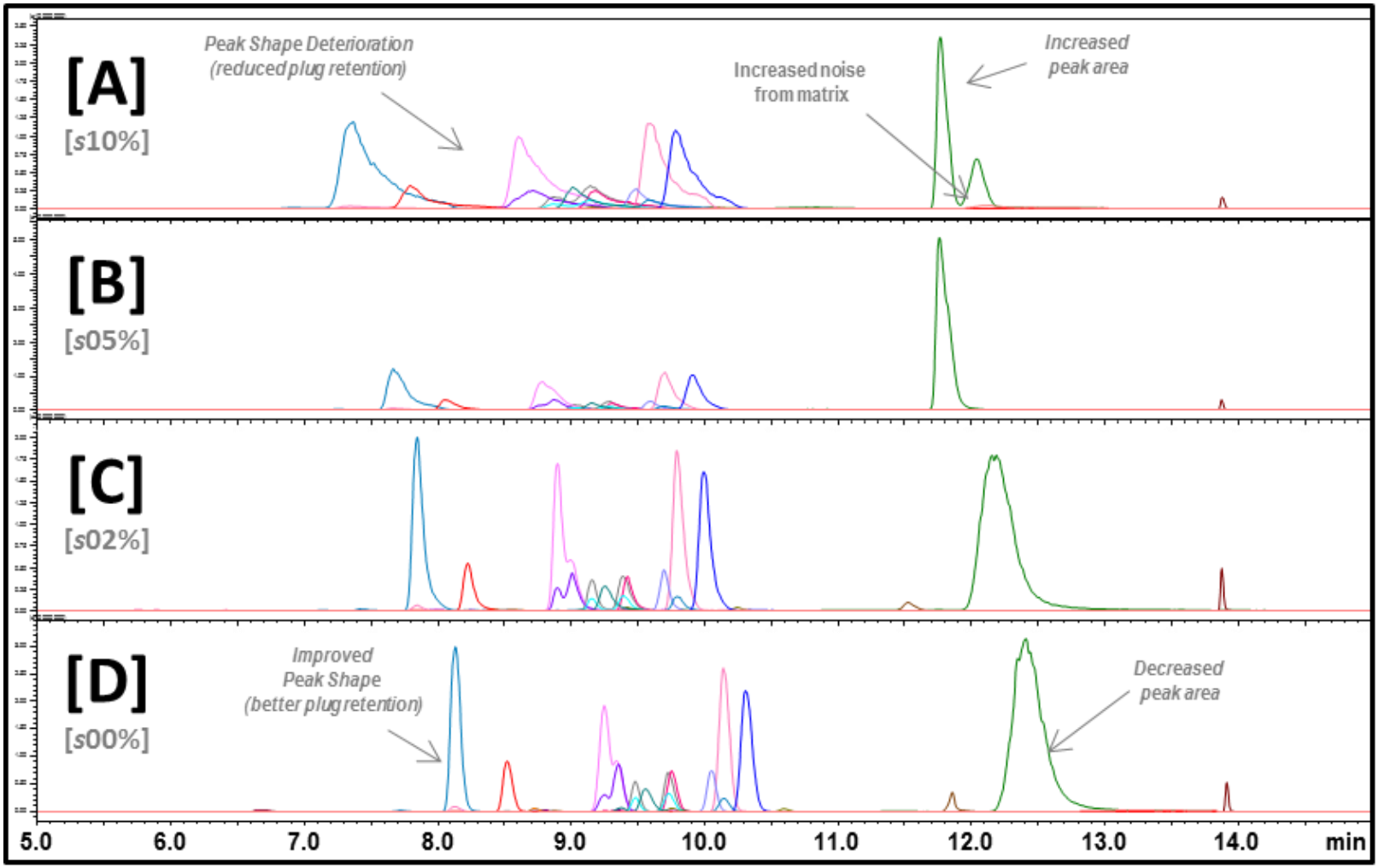

Figure 115. Overlaid SFE-SFC-MS Chromatograms for Online Extractions of Androgenic Anabolic Steroids (AAS) using Four Static Extraction (*s*) Modifier Concentrations: [A] 10%; [B] 5%; [C] 2%; and [D] 0% methanol + 5 mM ammonium formate in carbon Dioxide. Chromatographic separations of the extraction plugs produced via online-SFE of spiked steroid standards (1.0 µL spot AAS-mix) from sample collection card (6 mm) core [AAS-QC]. Overlaid MRM-TIC chromatograms zoomed to time retention range for targeted AAS: KETO [teal]; 1STEN [red]; MSAL [magenta]; ADEN [orange]; ETIO [blue]; MSEL [rose]; 1DHEA [pink]; MTHY [light pink); PRST [gold]; MIBL [purple]; TSTO [gray]; EPIT [cyan]; METD [lilac]; OXAN [hot pink]; MTRB [coral]; DNZL [turquoise]; TRNB [brown]; GSTN, [cobalt]; ZRNL [black]; STNZ [mocha]; CLNB [dark green] and ADAR [maroon]. *Normalized intensity scale.*

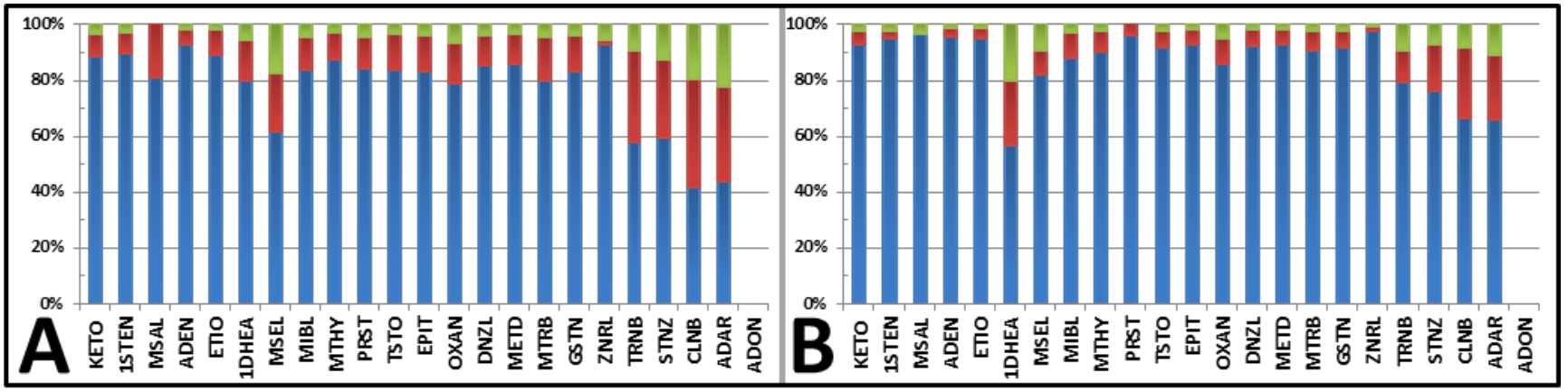

Figure 116. Extraction Performance Using Different Static Extraction (*s*) Modifier Concentrations: [A] 2%; and [B] 10% methanol +5 mM ammonium formate in Carbon Dioxide (CO_2). Showing percent of total area extracted for each targeted anabolic agent in three consecutive extraction rounds: **[blue]** first extraction (%EXT1); **[red]** second extraction (%EXT2); and **[green]** third extraction (%EXT3) for each vessel.

7.6. Dynamic Extraction

7.6.1. Screening Dynamic Extraction Duration

Effect of the duration of dynamic extraction was evaluated via four online extractions performed using 3.0, 2.0, 1.0 and 0.5 minute dynamic durations. Regardless of the dynamic duration used, the dynamic concentration was always 0% [B]. All other parameters were the same between/throughout all screening methods.

*Complete method details are outlined in **Section: 7.i.4.6. Conditions for Screening Dynamic Extraction Duration**.*

7.6.2. Effect of Dynamic Extraction Duration

Resulting SFE-SFC-MS online extractions are compared in **Figure 117**. Overall runtime was increased proportionally to longer dynamic durations. A mild increased total area was seen at higher dynamic duration, being between 0.9 – 1.5 times higher for the majority of the analytes using a 3.0 minute duration than the peak areas produced by the 0.5 minute dynamic extraction. A compound-specific 'optimum' was observed. Longer dynamic duration, above observed optimum, degrading peak shapes especially on early eluting (more non-polar) compounds, decreasing Rs between all critical pair groups. Dynamic duration had little effect on the extraction performance, even for early eluting compounds (which would be expected to be better extracted at longer 'active' extractions with the CO_2-based MP actively flowing over, extracting from the material, for a longer duration). But very little difference was observed in consecutive extractions between dynamic durations (**S_Figure 21**). An important note, that a significant increase in in background matrix noise on the 1DHEA-MRM (CARD-matrix) was also observed at high dynamic concentration.

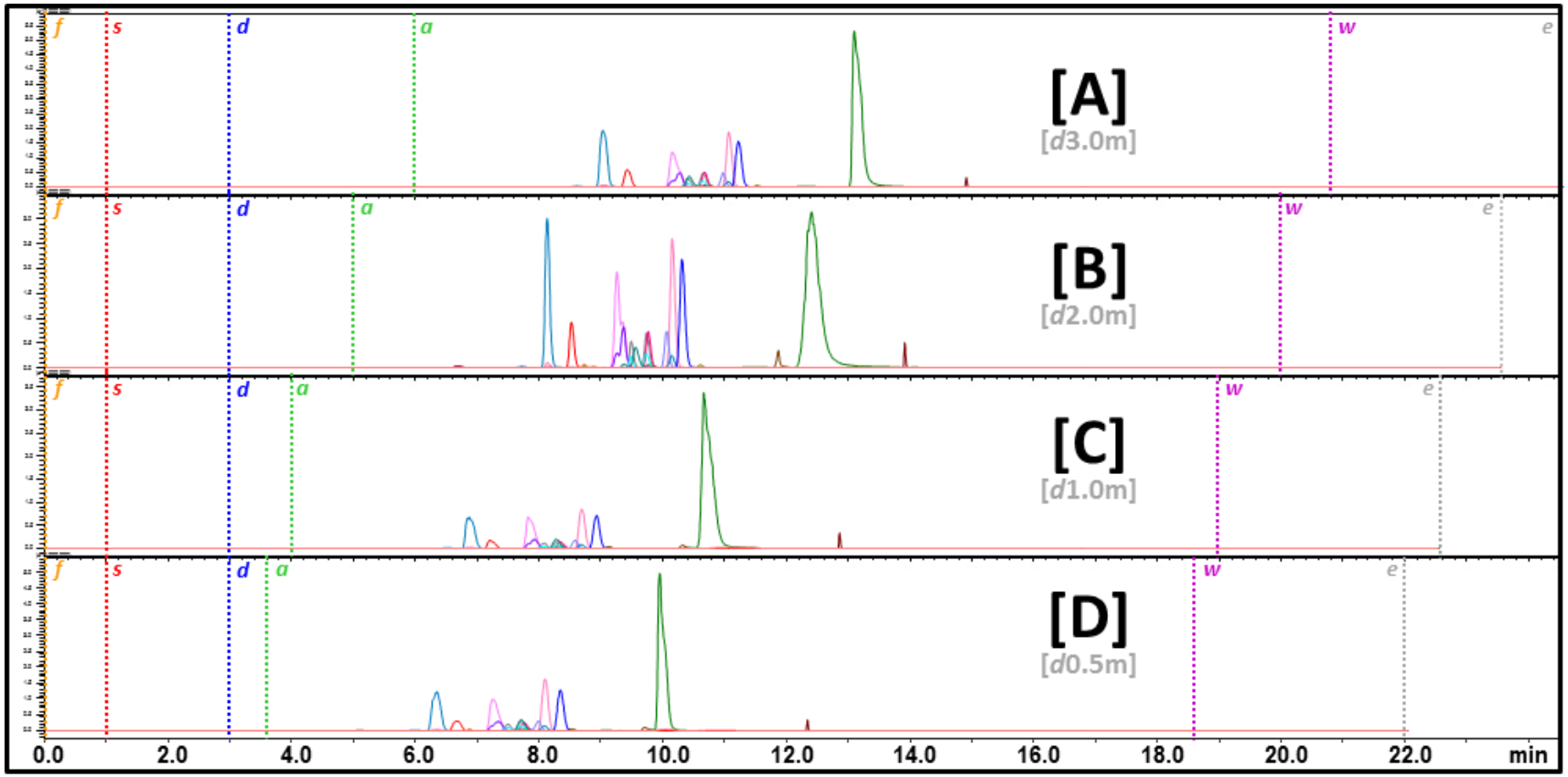

Figure 117. Overlaid SFE-SFC-MS Chromatograms for Online Extractions of Androgenic Anabolic Steroids (AAS) using Four Dynamic Extraction (*d*) Durations: [A] 3.0 minutes (min); [B] 2.0 min; [C] 1.0 min; and [D] 0.5 min. Chromatographic separations of the extraction plugs produced via online-SFE of spiked steroid standards (1.0 µL spot AAS-mix) from sample collection card (6 mm) core [AAS-QC]. Full runtime showing the start of each extraction step (*dotted lines*): vessel filling [***f***, *orange*]; static extraction [***s***, *red*]; dynamic extraction [***d***, *blue*]; analysis [***a***, *green*]; extraction loop wash [***w***, *purple*] and end of run [***e***, gray]. MRM-TIC chromatograms for targeted AAS: KETO [teal]; 1STEN [red]; MSAL [magenta]; ADEN [orange]; ETIO [blue]; MSEL [rose]; 1DHEA [pink]; MTHY [light pink); PRST [gold]; MIBL [purple]; TSTO [gray]; EPIT [cyan]; METD [lilac]; OXAN [hot pink]; MTRB [coral]; DNZL [turquoise]; TRNB [brown]; GSTN, [cobalt]; ZRNL [black]; STNZ [mocha]; CLNB [dark green] and ADAR [maroon]. *Normalized intensity scale.*

7.6.3. Screening Modifier Concentration during Dynamic Extraction.

Effect of modifier concentration during the dynamic extraction step was evaluated. Extractions were performed using 10, 5, 2, or 0% modifier during the dynamic extraction step. Dynamic extraction duration was 2.0 minutes regardless of the concentration used. All other parameters were the same between/throughout all screening methods.

*Complete method details are outlined in **Section: 7.i.4.5. Conditions for Screening Dynamic Extraction Concentration**.*

7.6.4. Effect of Dynamic Extraction Concentration.

The resulting SFE-SFC-MS chromatograms are compared in **Figure 118**. Higher dynamic concentration was accompanied by poor peak shapes and increased background noise, indicative of poor extract plug retention, and is due to analyte migration down the column before analysis begins. This can be clearly seen at the top of **Figure 118; A [*d*10%],** where several analytes have been eluted from the column and are detected before the start of the analysis step (**dotted green line**). This means that analytes are moving down the column during the time period, where dynamic extraction was still being actively performed (and therefore the sample plug is still being loaded onto the column). Alternatively using < 5% dynamic modifier, the polarity of mobile phase is sufficiently low enough to start promoting retention of the sample plug.

Total Extractable Areas. For the majority of the targeted analytes, increased dynamic concentration resulted in decreased peak areas (mainly due to the disruption of the sample plug). Comparing total area extracted with each dynamic concentration, a compound specific trend was observed. Where early eluting compounds (i.e., more non-polar) are effected more strongly in the presence of high modifier concentrations, producing very low peak areas due to migration across the column, where for example, in the most severe case, where only 6% of the total area extracted for KETO was accomplished using 10% dynamic concentration. Alternatively, late eluting compounds (i.e., more polar) are less effected where a significant decrease in peak area was not observed till much higher concentration.

Extraction Performance. Two compound specific trends can be observed when comparing the percent extracted during each of the three rounds. At low dynamic modifier concentration (**Figure 119; Left panel, A [0%D]**), nearly all compounds were still producing significant areas (> 5% of the total extractable area) in the third extraction round. But at high dynamic concentration (**Figure 119; right panel, B [5%D]**), only late eluting compound require more extraction rounds, producing less than 50% of the total extractable area in the first extraction. All early eluters were greater than 95% extracted in the first two rounds. Low dynamic modifier concentration expectedly was less efficient in extracting all compounds, regardless of analyte polarity. A strong compromise must be made between increased peak area for more polar compounds and the utmost importance of good sample plug retention.

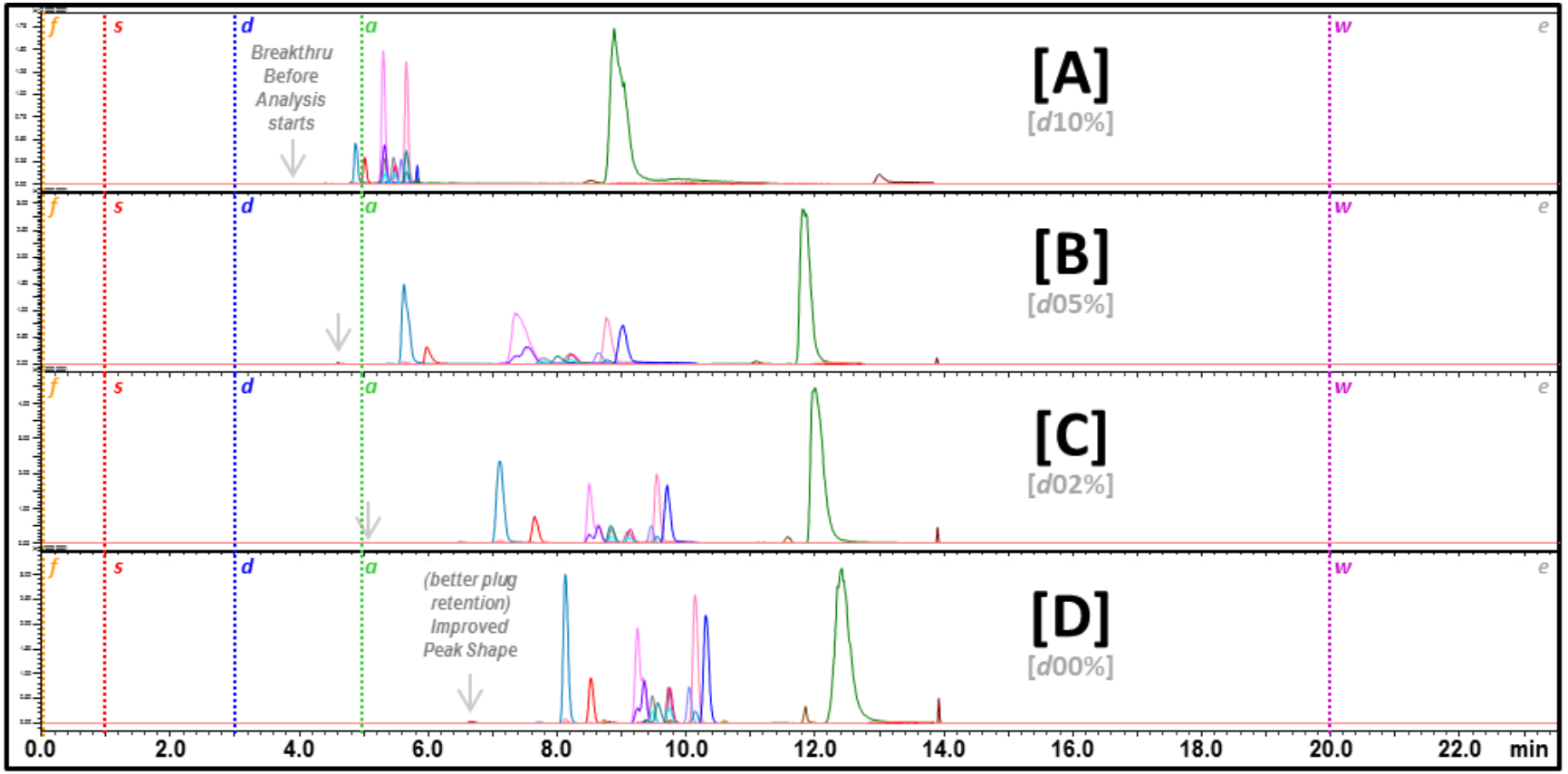

Figure 118. Overlaid SFE-SFC-MS Chromatograms for Online Extractions of Androgenic Anabolic Steroids (AAS) using Four Dynamic Extraction (*d*) Modifier Concentrations: [A] 10%; [B] 5%; [C] 2%; and [D] 0% methanol + 5 mM ammonium formate in carbon Dioxide. Chromatographic separations of the extraction plugs produced via online-SFE of spiked steroid standards (1.0 µL spot AAS-mix) from sample collection card (6 mm) core [AAS-QC]. Full runtime showing the start of each extraction step (*dotted lines*): vessel filling [***f***, *orange*]; static extraction [***s***, *red*]; dynamic extraction [***d***, *blue*]; analysis [***a***, *green*] and extraction loop wash [***w***, *purple*] and end of run [***e***, gray]. Overlaid MRM-TIC chromatograms for targeted AAS: KETO [teal]; 1STEN [red]; MSAL [magenta]; ADEN [orange]; ETIO [blue]; MSEL [rose]; 1DHEA [pink]; MTHY [light pink); PRST [gold]; MIBL [purple]; TSTO [gray]; EPIT [cyan]; METD [lilac]; OXAN [hot pink]; MTRB [coral]; DNZL [turquoise]; TRNB [brown]; GSTN, [cobalt]; ZRNL [black]; STNZ [mocha]; CLNB [dark green] and ADAR [maroon]. *Normalized intensity scale.*

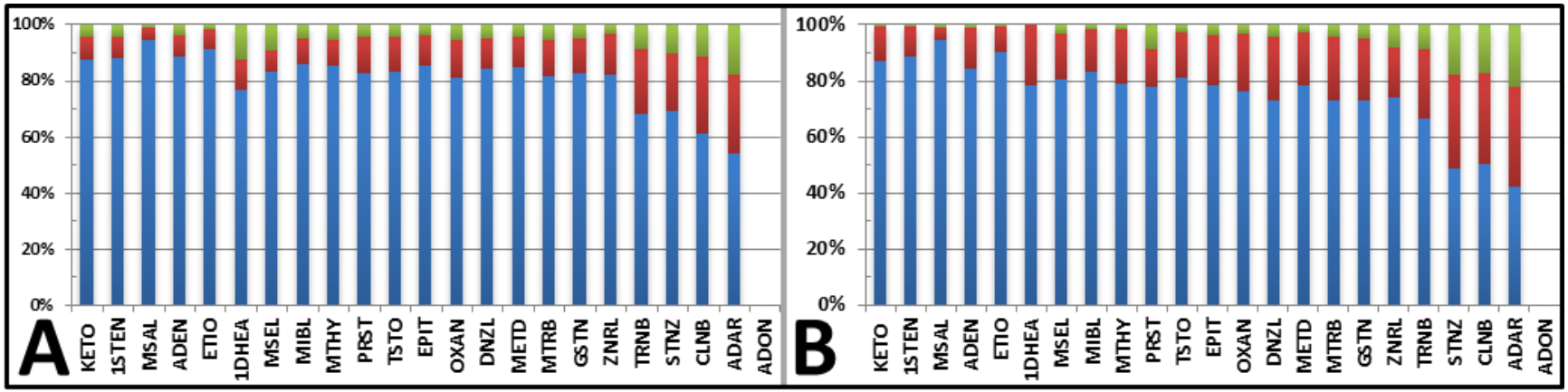

Figure 119. Extraction Performance Using Different Dynamic Extraction (*d*) Modifier Concentrations: [A] 0%; and [B] 5% methanol +5 mM ammonium formate in Carbon Dioxide (CO_2). Showing percent of total area extracted for each targeted anabolic agent in three consecutive extraction rounds: **[blue]** first extraction (%EXT1); **[red]** second extraction (%EXT2); and **[green]** third extraction (%EXT3) for each vessel.

7.7. Extraction Vessel Temperature during Online Extraction

7.7.1. Vessel Temperature Screening

Effect of vessel temperature during the dynamic extraction step was evaluated. Five extractions were performed, each using a different vessel temperature: 30, 35, 40, 60, or 80 °C. The rack changer held vessels (pre-extraction) constant at 20 °C. Each vessel was heated to the set (*'variable'*) temperature just moments prior to the start of the online extraction process. All other parameters were held constant for all screening methods.

Complete method details are outlined in ***Section: 7.i.4.7. Extraction Vessel Temperature Screening Conditions****.*

7.7.2. Effect of Vessel Temperature

The resulting SFE-SFC-MS online extractions are presented in **Figure 120.** There was very little effect on peak shape, retention, or resolution across all temperatures. Large changes in temperature were needed to see an effect on total peak area extracted (e.g., Less than ~40 °C change, produced minimal difference in total peak area extracted). Lower vessel temperature produced slightly larger total areas (T_{area}), but half the target analytes had T_{area} reproducible across all temperatures (%RSD = 4 - 14%), but the other half T_{area} was not reproducible (%RSD = 27 -57 %), with no apparent trend towards analyte polarity. Instead this, more interestingly, shows a trend towards the effect of vessel temperature on extraction performance. A strong trend was observed for all of the targeted analytes where significantly lower $\%EXT_{1+2}$ was seen at higher temperatures (**S_Figure 22**), indicating that the amount extracted in the third extraction round was higher at high temperatures (and therefore the extraction was not performing as well at higher temperatures in the first two rounds). **Figure 121** compares the three consecutive extractions for a vessel extracted at high (80 °C, A) and low (35 °C, B) vessel temperatures. A distinct difference can be seen between them, where all compounds required more extraction rounds at higher temperature. Stronger effect on late eluting, steroid mimics (TRNB, STNZ, CLNB & ADAR), producing significantly lower peak areas in the first extractions (< 50% = EXT1), and higher in the third extraction (> 20% = EXT3) when

using higher vessel temperature. Since these compounds (the most polar) are the hardest to extract, this effect is especially undesirable. Therefore lower vessel temperatures should be used to maximize the extractability of AAS.

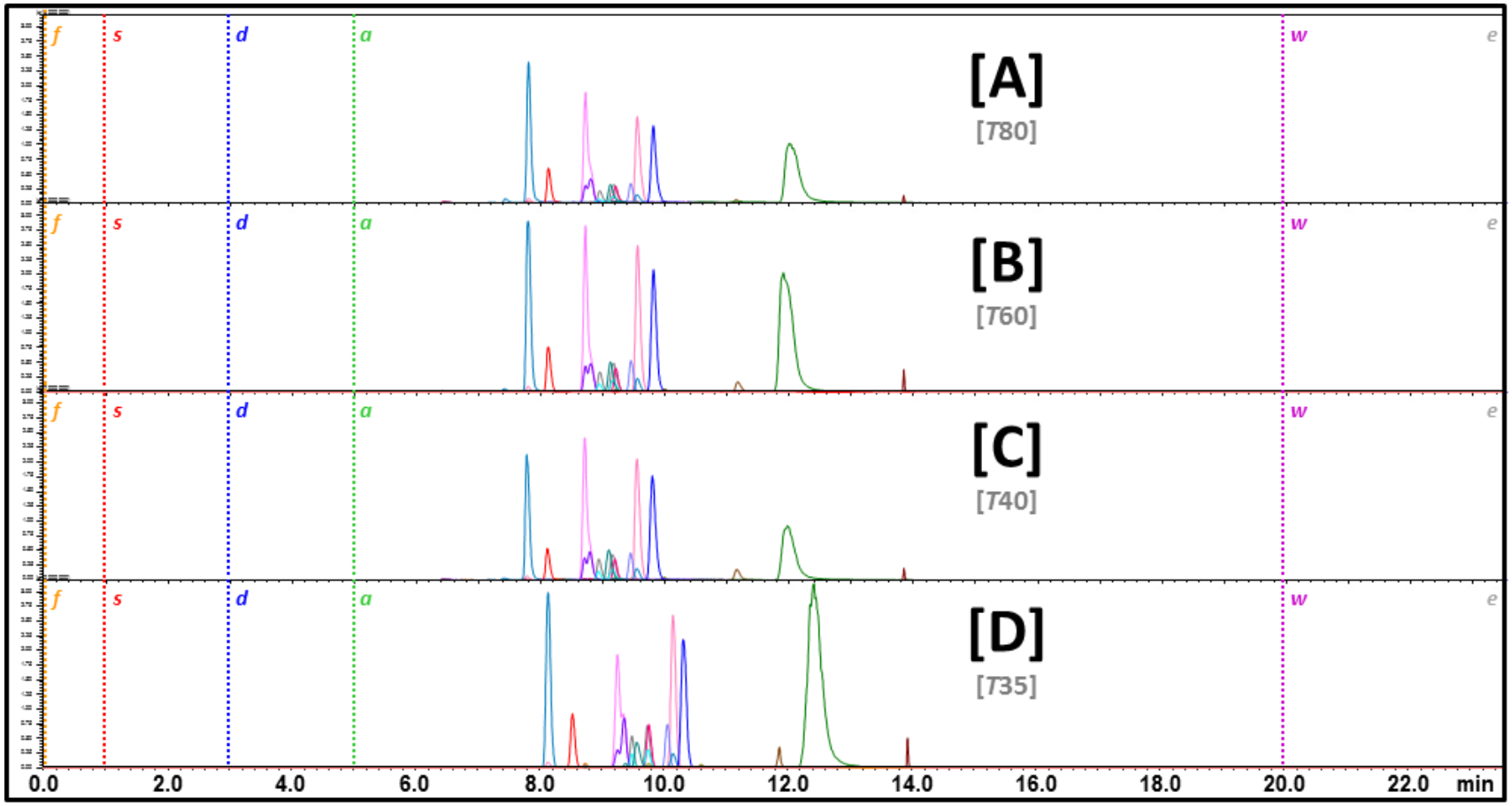

Figure 120. Overlaid SFE-SFC-MS Chromatograms for Online Extractions of Androgenic Anabolic Steroids (AAS) using Four Extraction Vessel Temperatures (*T*): [A] 35 °C; [B] 40 °C; [C] 60 °C; and [D] 80 °C. Chromatographic separations of the extraction plugs produced via online-SFE of spiked steroid standards (1.0 µL spot AAS-mix) from sample collection card (6 mm) core [AAS-QC]. Full runtime showing the start of each extraction step (*dotted lines*): vessel filling [***f***, *orange*]; static extraction [***s***, *red*]; dynamic extraction [***d***, *blue*]; analysis [***a***, *green*]; extraction loop wash [***w***, *purple*] and end of run [***e***, gray]. MRM-TIC chromatograms for targeted AAS: KETO [teal]; 1STEN [red]; MSAL [magenta]; ADEN [orange]; ETIO [blue]; MSEL [rose]; 1DHEA [pink]; MTHY [light pink); PRST [gold]; MIBL [purple]; TSTO [gray]; EPIT [cyan]; METD [lilac]; OXAN [hot pink]; MTRB [coral]; DNZL [turquoise]; TRNB [brown]; GSTN, [cobalt]; ZRNL [black]; STNZ [mocha]; CLNB [dark green] and ADAR [maroon]. *Shown at same intensity scale.*

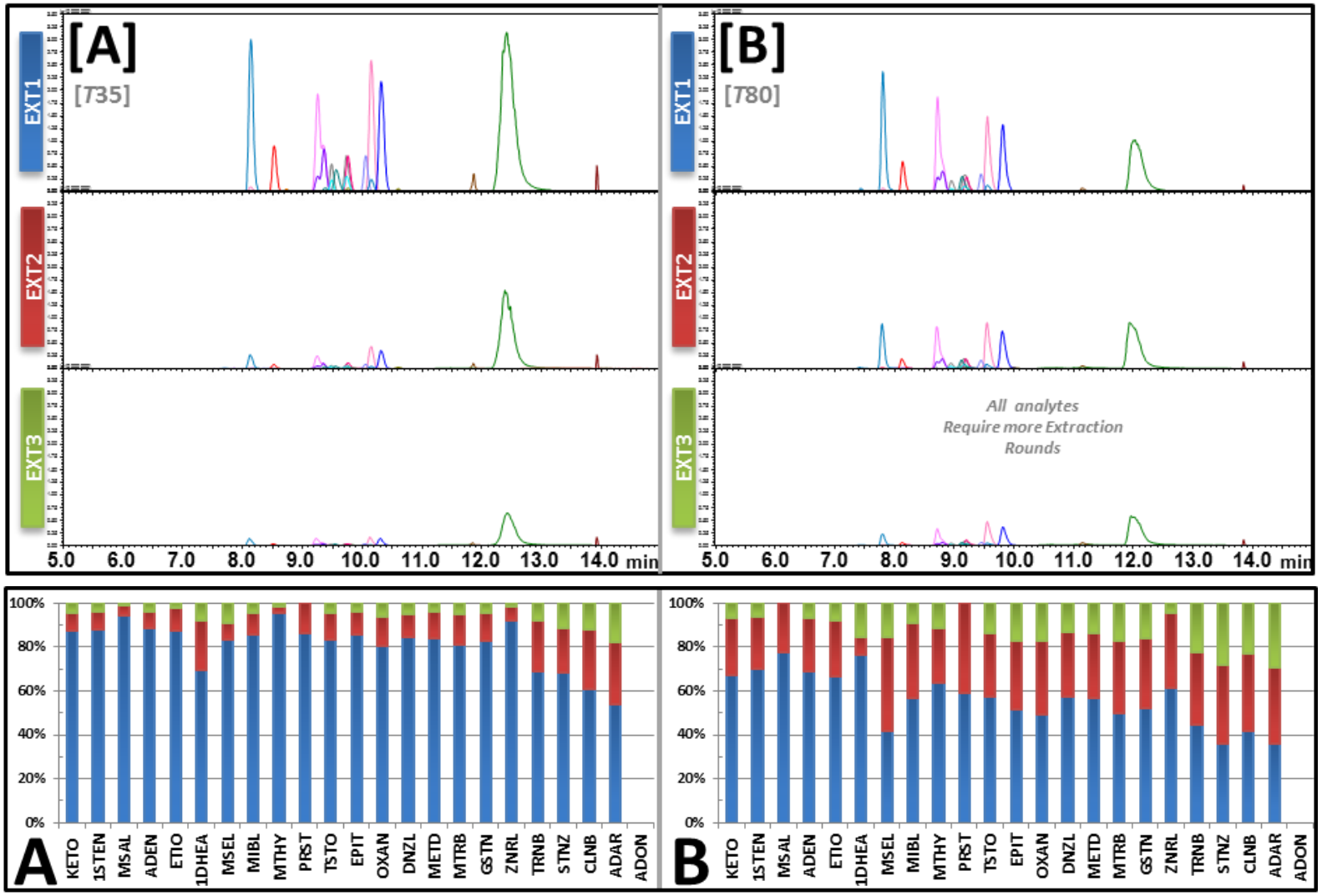

Figure 121. Extraction Performance Using Different Extraction Vessel Temperatures (*T*): [A] 35 °C; and [B] 80 °C. [bottom panel] bar graph showing percent of total area extracted for each targeted anabolic agent in three consecutive extraction rounds: **[blue]** first extraction (%EXT1); **[red]** second extraction (%EXT2); and **[green]** third extraction (%EXT3) for each vessel. **[top Panel] Overlaid SFE-SFC-MS Chromatograms for Online Extractions** targeted anabolic agent in three consecutive extraction rounds.

7.8. Extraction Pressure

7.8.1. Online extraction Pressure

The extraction vessel is not physically isolated during extraction, and there is no instrument component in which regulates pressure specifically for the extraction vessel (i.e., Separately from the rest of the system). Therefore, the vessel is exposed to the same pressure as the rest of the instrument (pre-column). In splitless extractions, the only regulation of system pressure, is via BPR_A. So instead, in practice, 'vessel pressure' refers to the setting for the system outlet pressure [BPR_A; post-column] regulator, during the online extraction process.

'Extraction pressure' is programmed in the method timetable, in the same way as the modifier concentration and flow rate. A different setting can be specified for each extraction step (i.e., A different pressure could be used for filling, static, dynamic and/or the analysis; -or- alternatively, could be held constant throughout all steps; -or- any combination therein).

In the current work, for simplification, 'extraction pressure' was held at one setting throughout the first three extraction steps (filling, static, and dynamic), independently of the last step, analysis. Therefore, the effect of extraction pressure was evaluated by screening variable outlet pressures, during the first three extractions steps-only. The outlet pressure for analysis was always held constant at 15 MPa.

7.8.2 Vessel Pressure during Extraction.

Effect of vessel pressure was evaluated, by performing online extractions using different outlet pressures [BPR_A], while holding all other parameters constant. Five extractions were performed, each using a different pressure: 10, 12.5, 15, 20, or 25 MPa. The outlet pressure was varied during extraction-only (i.e., one ***[variable]*** outlet pressure being applied and held constant during the 1st 3x extraction steps: filling, static and dynamic). After extraction (at the start of the analysis step) the outlet pressure (BPR_A) was always set to 15 MPa for chromatographic analysis (nomatter the extraction pressure used). All other parameters were held constant for

all screening methods. Complete method details are outlined in **Section: 7.i.4.8. Extraction Pressure Screening Conditions**.

7.8.3 Effect of Vessel Pressure during Extraction

Although overall runtime was un-effected by extraction pressure, retention times changed for all earlier eluting compounds, with increasing retention times, when moving from higher to lower pressure (**Figure 122.; top-to-bottom**). Later eluting compounds were much less affected, and the retention time of the latest eluting peak [ADAR; maroon] was unaffected producing reproducible runtimes across all four extraction pressures (Rt_{ADAR} = 13.89 ± 0.02 min). Surprisingly higher extraction pressure had a moderately negative effect on peak shape, especially for early eluting compounds. This points to a disruption of the 'extraction plug' at higher pressure. Generally, when using compressed fluids, higher pressures can mimic higher flow rates. Which could possibly physically push the sample plug prematurely down the column before analysis starts. Resulting band broadening, would be more noticeable for earliest eluters, and ultimately could be contributing to the negative effect on resolution and peak shapes at higher pressures.

Peak areas were significantly different between extraction pressures for all compounds. Higher pressure produced increased peak areas for almost all compounds, producing areas 1.1 - 3.8 times higher than those produced at lower extraction pressures. A negative effect on the extraction performance was observed for later eluting (more-polar) compounds, where more rounds were required to extract at higher pressures (**Figure 123**). Alternatively, although much less pronounced, the opposite trend, was observed for early eluters, which required less rounds to extract at higher pressures.

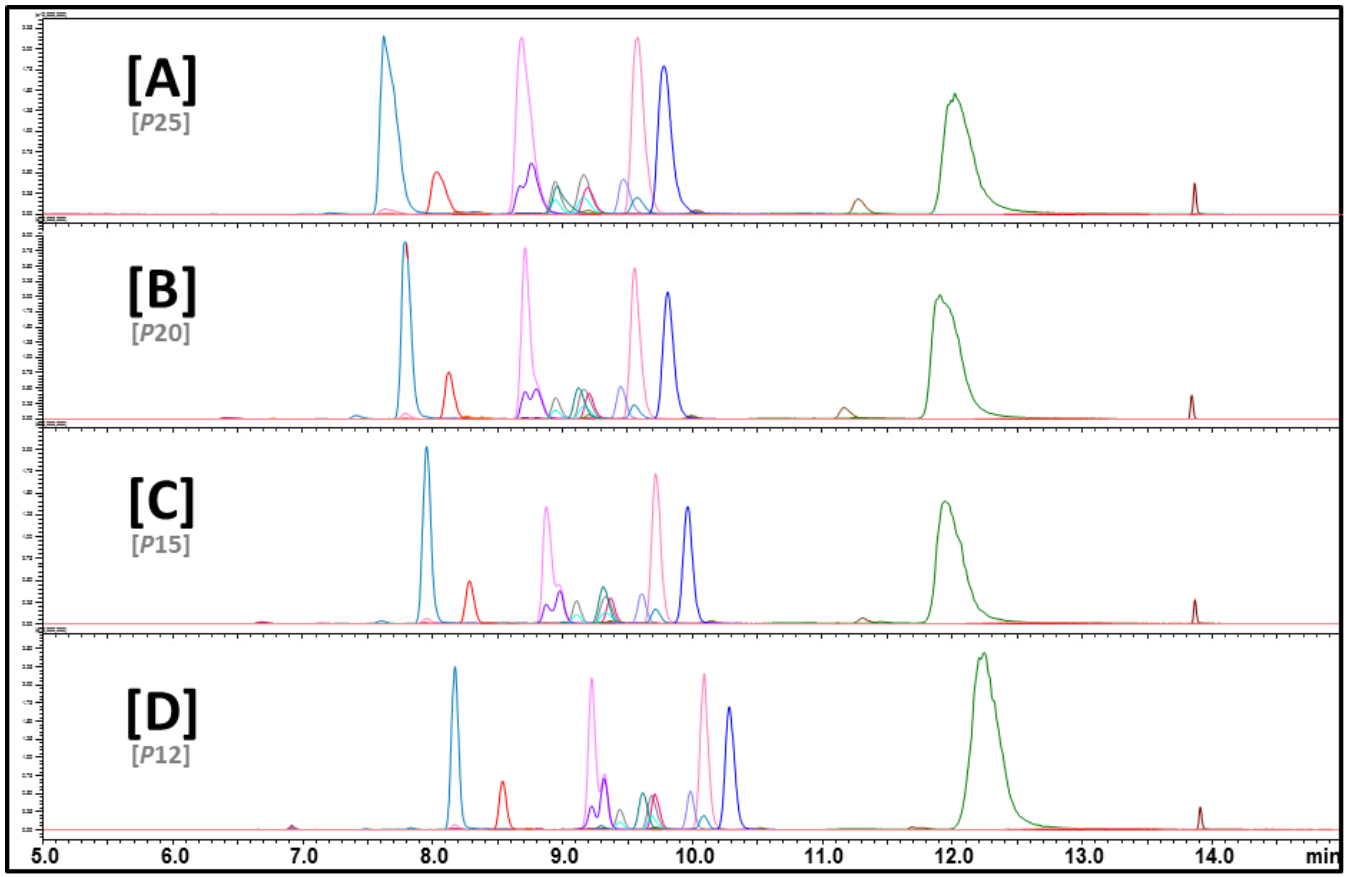

Figure 122. Overlaid SFE-SFC-MS Chromatograms for Online Extractions of Androgenic Anabolic Steroids (AAS) using Four Extraction Pressures (*P*): [A] 25 MPa; [B] 20 MPa; [C] 15 MPa; and [D] 12.5 MPa. Chromatographic separations of the extraction plugs produced via online-SFE of spiked steroid standards (1.0 µL spot AAS-mix) from sample collection card (6 mm) core [AAS-QC]. Overlaid MRM-TIC chromatograms zoomed to time retention range for targeted AAS: KETO [teal]; 1STEN [red]; MSAL [magenta]; ADEN [orange]; ETIO [blue]; MSEL [rose]; 1DHEA [pink]; MTHY [light pink); PRST [gold]; MIBL [purple]; TSTO [gray]; EPIT [cyan]; METD [lilac]; OXAN [hot pink]; MTRB [coral]; DNZL [turquoise]; TRNB [brown]; GSTN, [cobalt]; ZRNL [black]; STNZ [mocha]; CLNB [dark green] and ADAR [maroon]. *Normalized intensity scale.*

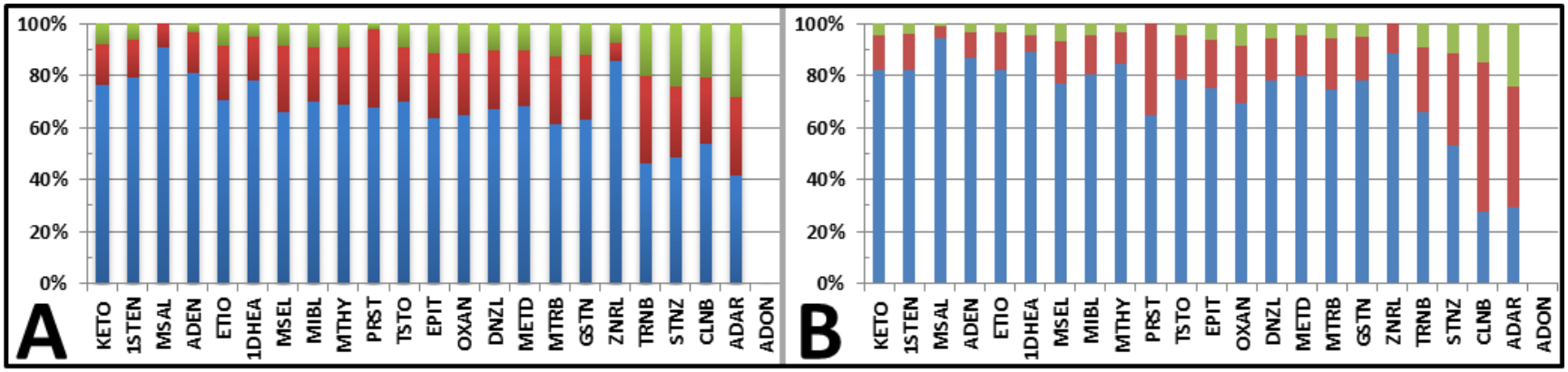

Figure 123. Effect of Extraction Pressure on Extraction Performance of Targeted Anabolic Agents at Low (12.5 MPa; [left]) and High (20 MPa; [right]) Pressure; showing percent (%) of total area extracted for each steroid in three consecutive extraction rounds for each vessel: [blue] first extraction (%EXT1); [red] second extraction (%EXT2); and [green] Third extraction (%EXT3).

7.9. Extraction Flow Rate

Care should be taken in regard to system flow rates to ensure compatibility with individual column specifications.

7.9.1 Screening Extraction Flow Rate.

Effect of flow rate on online extractions was evaluated by performing four extractions, each using a different flow rate: **[R2.0]** 2.0 mL/min; **[R2.5]** 2.5 mL/min; **[R3.0]** 3.0 mL/min; or **[R3.5]** 3.5 mL/min. The flow rate was varied during extraction-only (i.e., one (*'variable'*) flow rate being applied and held constant during the 1st 3x extraction steps: filling, static and dynamic). After extraction (at the start of the analysis step) the flow rate was then switched back to 2.5 mL/min for chromatographic analysis (no matter the extraction flow rate used). All other parameters were the same used in the other screening methods throughout the work.

Complete method details are outlined in **Section 7.i.4.9. Conditions for Screening Flow Rate during Extraction**.

7.9.2. Effect of Extraction Flow Rate.

Example SFE-SFC-MS chromatograms of online extractions using high (3.5 mL/min) and low (2.0 mL/min) flow rates are shown in **Figure 124**. Flow rate had no effect on total run time, having little effect on late eluting compounds. Retention times were the most changed for early eluting compounds. Where the same trend was observed, as seen with higher extraction pressure, producing degraded peak shapes and resolution, especially for early and mid-eluting compounds at higher flow rates.

Flow rate had minimal effect on peak areas, which were reproducible across all four flow rates used (%RSD = 5 - 17% for all compounds). Extraction performance was also quite similar between flow rates where 79 - 99 ± 1.0% of the total extractable area was accomplished within the first two rounds ($\%EXT_{1+2}$) for all compounds, with little change between using low and high flow rates.

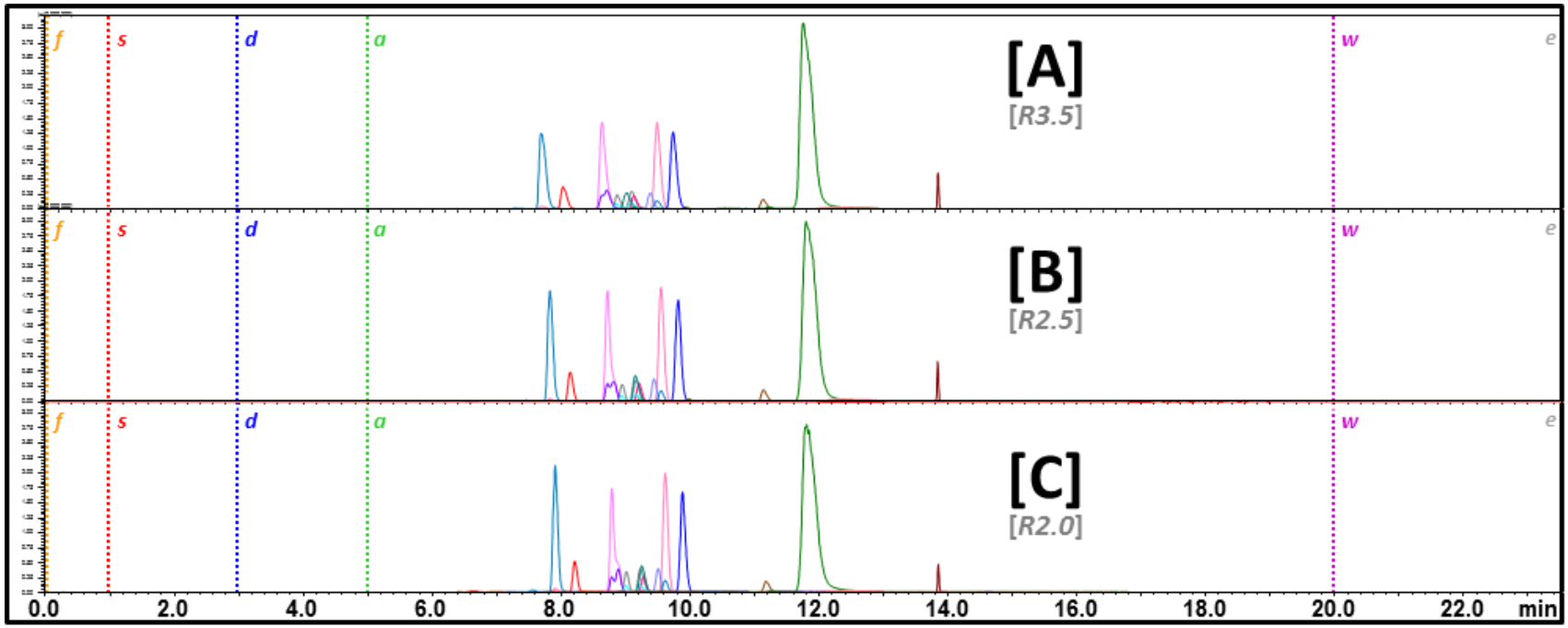

Figure 124. Overlaid SFE-SFC-MS Chromatograms for Online Extractions of Androgenic Anabolic Steroids (AAS) using Different Extraction Flow Rates (*R*): [A] 3.5 mL/min; [B] 2.5 mL/min; and [B] 2.0 mL/min. Chromatographic separations of the extraction plugs produced via online-SFE of spiked steroid standards (1.0 µL spot AAS-mix) from sample collection card (6 mm) core [AAS-QC]. Full runtime showing the start of each extraction step (*dotted lines*): vessel filling [***f***, *orange*]; static extraction [***s***, *red*]; dynamic extraction [***d***, *blue*]; analysis [***a***, *green*]; extraction loop wash [***w***, *purple*] and end of run [***e***, gray]. MRM-TIC chromatograms for targeted AAS: KETO [teal]; 1STEN [red]; MSAL [magenta]; ADEN [orange]; ETIO [blue]; MSEL [rose]; 1DHEA [pink]; MTHY [light pink); PRST [gold]; MIBL [purple]; TSTO [gray]; EPIT [cyan]; METD [lilac]; OXAN [hot pink]; MTRB [coral]; DNZL [turquoise]; TRNB [brown]; GSTN, [cobalt]; ZRNL [black]; STNZ [mocha]; CLNB [dark green] and ADAR [maroon]. *Shown at same intensity scale.*

7.10. Optimized SFE-SFC-MS Online Method

7.10.1. Final SFE-SFC-MS Method.

An example SFE-SFC-MS chromatogram using the final optimized extraction parameters, shown in **Figure 125**, produced extractions with a total runtime of 23 minutes. This includes a 1 min vessel loading at 2% Modifier, followed by a 4.0 minute static extraction (at 0% modifier) and 2.0 minute dynamic extraction (also at 0% modifier), and finally the 10 minute SFC-MS analysis via gradient elution. The online extraction and analysis is followed by a 5 minute column wash at 30% B along with a 3 minute wash of the extraction unit follows each extraction (detailed conditions are given at the end of this chapter in **Section 7.i.5. Instrument Methods: Optimized Online SFE-SFC-MS Extraction Method**).

Reduced Rs on critical pair groups: final resolutions were for critical group 1 ($Rs_{[4:6:7]}$ = 1.1, 0.4), critical group 2 ($Rs_{[2,3,5,9,10,12]}$ = 3.3, 2.3, 4.7, 0.8, 4.0, 10.4), and critical group 3 ($Rs_{[8,11,13,14,18]}$ = 4.9, 2.0, 1.0, 7.4). Very low signal was observed for MSAL and MSEL. At this point it was unclear if this was from reduced concentration from lower extractability, lower plug retentivity or alternatively from an effect of changes in ionization, as these were two of the analytes listed as suggested for qualitative comparisons only, due to vulnerabilities to changes in ionization based on differences in MP composition. Compounds problematic for extraction plug retention were successfully predicted by adding an additional step to the SFC column screening stage, and were helpful watch items for final online method optimizations.

Increased noise was observed in all extractions performed, especially notable on the 1-DHEA MRM and seems to be contributed by the card matrix. Detailed matrix evaluations will be need for application specific optimization (**Chapter #9**). Paper matrix could not be predicted and should be further investigated for effects contributing to background signals. Final method optimization should be performed, by profiling matrices relevant to final applications.

7.10.2. Online SFE-SFC-MS Method Performance.

Final method evaluations were implemented by performing extractions on three replicate vessels using the optimized SFE-SFC-MS method. The first extraction for each vessel are compared in S_Figure 23**; A**. Peak shapes and resolution are similar throughout all three first round extractions. Retention times and areas were evaluated for reproducibility and extraction performance (**Table 30**).

Reproducibility. The extractions produced reproducible retention times (±0.02 minutes) and peak areas (with %RSD between 1 – 13%) for all targeted anabolic agents.

Extraction Performance. Each of the three vessels were extracted three times consecutively (i.e., 1st extraction [EXT1], 2nd extraction [EXT2] and 3rd extraction [EXT3] on each vessel), example chromatograms of three consecutive extractions for a single vessels are shown in S_Figure 23**; B**. The total area extracted for each vessel was summed, for each round and the average percent (%) of the total extracted compared [**Figure 126**]. The av%EXT1 was between 53 - 98%; av%EXT2 was 5 - 29%; and av%EXT3 between 0 – 18%. The percent extracted in the first two rounds (av%EXT$_{1+2}$) was above 82% for all the targeted analytes. Average % total for the first two extractions (Round 1+2): although acceptable for all analytes, was much better for early and mid-eluting compounds where 95 -100% ± 0.1-0.7% extracted within the 1st two extraction rounds; but later eluting, more polar compounds, took more rounds to extract where only 82 -91% ± 0.3 – 1.3% in the first two rounds.

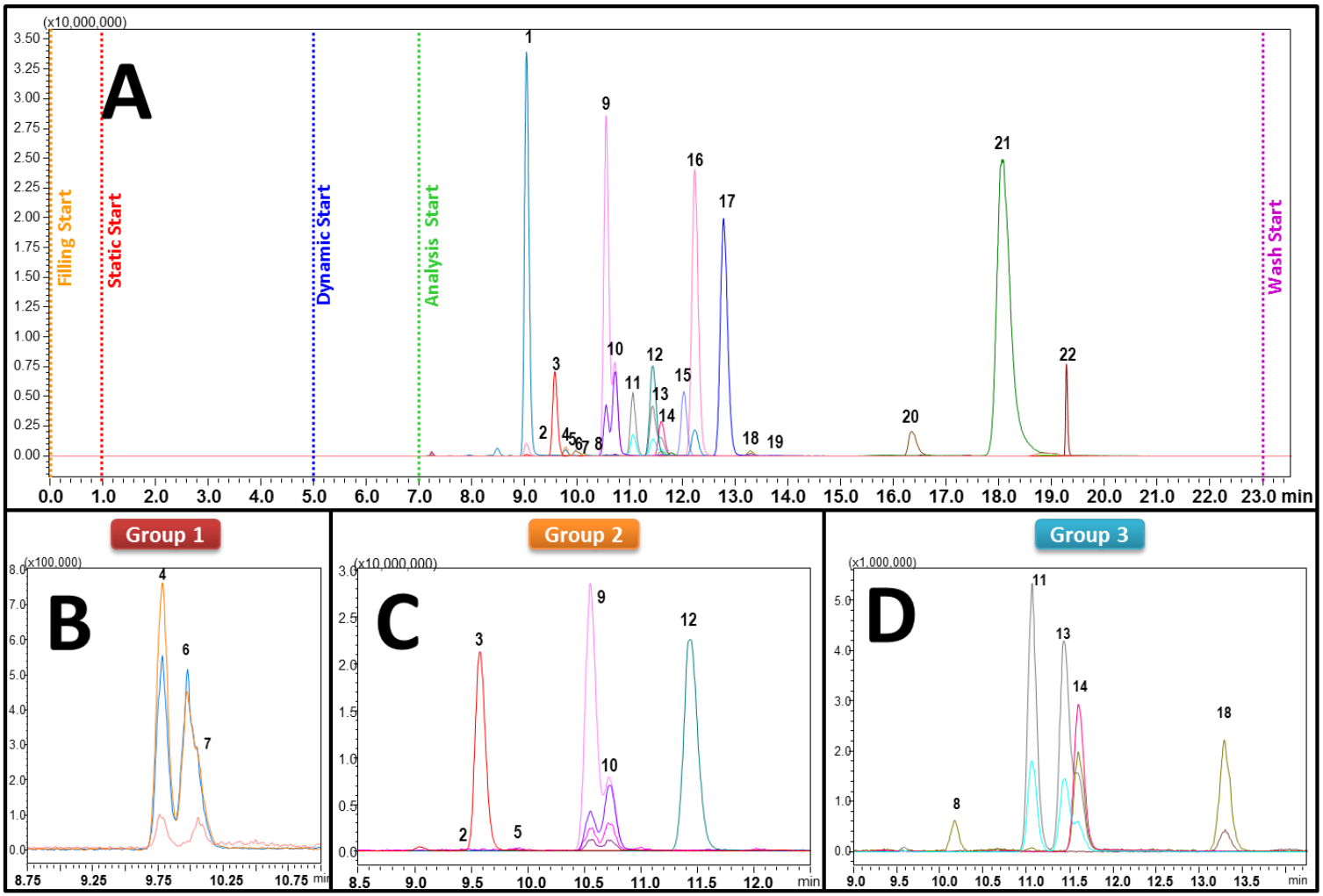

Figure 125. SFE-SFC-MS Chromatogram using Final Optimized Online Method for Extraction of Anabolic Agents using UC-Cyano Column. [A] MRM-overlays for all 22 anabolic agents, zoomed on elution timeframe for targeted analytes; [B] Critical Group 1 Analytes; [C] Critical Group 3 Analytes; [D] Critical Group 2 Analytes. Chromatographic separations of the extraction plugs produced via online-SFE of spiked steroid standards (1.0 µL spot AAS-mix) from sample collection card (6 mm) core [AAS-QC]. showing the start of each extraction step (*dotted lines*): vessel filling [***f***, *orange*]; static extraction [***s***, *red*]; dynamic extraction [***d***, *blue*]; analysis [***a***, *green*]; and extraction loop wash [***w***, *purple*]. MRM-TIC chromatograms for targeted AAS: KETO [**1**, teal]; MSAL [**2**, magenta]; 1STEN [**3**, red]; ADEN [**4**, orange]; MSEL [**5**, rose]; ETIO [**6**, blue]; 1DHEA [**7**, pink]; PRST [**8**, gold]; MTHY [**9**, light pink]; MIBL [**10**, purple]; EPIT [**11**, cyan]; DNZL [**12**, turquoise]; TSTO [**13**, gray]; OXAN [**14**, hot pink]; METD [**15**, lilac]; MTRB [**16**, coral]; GSTN [**17**, cobalt]; TRNB [**18**, brown]; ZRNL [**19**, black]; STNZ [**20**, mocha]; CLNB [**21**, dark green] and ADAR [**22**, maroon]. *Shown at same intensity scale.*

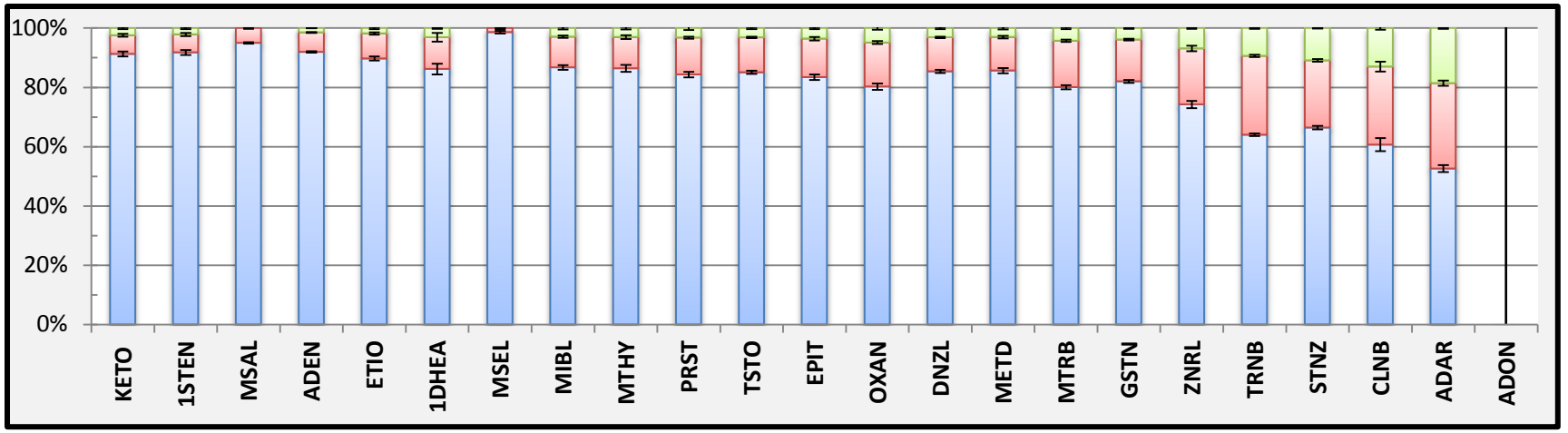

Figure 126. Extraction Performance of Targeted Anabolic Agents using the optimized SFE-SFC-MS method, showing average percent of total area extracted (n = 3) for each analyte in three consecutive extraction rounds for each vessel: [blue] first extraction (av%EXT1); [red] second extraction (av%EXT2); and [green] Third extraction (av%EXT3). Error bars = standard deviation (n=3).

Table 30. Retention time, Peak Area Reproducibility and Extraction Performance for Anabolic Agents Extracted Online from Spiked Whatman Paper Quality Controls [PøMA].

			PøMA (n=3)							
			Retention Time (min)		Total Peak Area		Extraction 1	Extraction 2	Extraction 3	Average
#	Analyte	ID	Average	%RSD	Average	%RSD	Average %	Average %	Average %	%EXT$_{1+2}$
1	7-Keto-DHEA	**KETO**	9.03 ± 0.01	0.16%	124,230,607	3%	91 ± 1.1%	6 ± 0.6%	2 ± 0.4%	98%
2	Mestanolone	**MSAL**	9.18 ± 0.02	0.18%	23,865	9%	95 ± 0.9%	5 ± 0.9%	0 ± 0.1%	100%
3	Androstenedione	**1STEN**	9.56 ± 0.01	0.15%	19,836,473	6%	92 ± 1.2%	6 ± 0.8%	2 ± 0.4%	98%
4	Androsterone	**ADEN**	9.77 ± 0.02	0.21%	2,575,012	9%	92 ± 0.7%	7 ± 0.5%	2 ± 0.2%	98%
5	Etiocholanolone	**ETIO**	9.96 ± 0.02	0.20%	2,223,012	7%	90 ± 0.8%	8 ± 0.6%	2 ± 0.3%	98%
6	Mesterolone	**MSEL**	9.87 ± 0.02	0.18%	35,926	7%	98 ± 1.5%	2 ± 1.5%	2 ± 0.0%	100%
7	1-Androsterone	**1DHEA**	10.05 ± 0.01	0.05%	212,287	9%	86 ± 1.8%	11 ± 1.5%	0 ± 0.4%	97%
8	Prasterone (DHEA)	**PRST**	10.14 ± 0.02	0.15%	476,552	4%	85 ± 0.9%	12 ± 0.3%	3 ± 0.7%	97%
9	Methyltestosterone	**MTHY**	10.53 ± 0.02	0.17%	78,131,703	4%	86 ± 1.5%	11 ± 1.0%	3 ± 0.6%	97%
10	Mibolerone	**MIBL**	10.69 ± 0.01	0.13%	31,015,546	7%	87 ± 1.2%	10 ± 0.7%	3 ± 0.5%	97%
11	Epitestosterone	**EPIT**	11.41 ± 0.02	0.19%	5,208,730	7%	85 ± 1.0%	12 ± 0.6%	3 ± 0.4%	97%
12	Danazol	**DNZL**	11.41 ± 0.01	0.08%	18,200,929	7%	85 ± 0.7%	11 ± 0.4%	3 ± 0.4%	97%
13	Testosterone	**TSTO**	11.04 ± 0.02	0.21%	18,653,405	5%	83 ± 1.4%	13 ± 1.0%	4 ± 0.4%	96%
14	Oxandrolone	**OXAN**	11.57 ± 0.02	0.18%	17,982,765	11%	80 ± 1.5%	15 ± 0.8%	5 ± 0.7%	95%
15	Metandienone	**METD**	12.00 ± 0.02	0.17%	15,661,055	11%	86 ± 1.1%	11 ± 0.6%	3 ± 0.5%	97%
16	Metribolone	**MTRB**	12.20 ± 0.01	0.12%	103,964,922	6%	80 ± 1.2%	16 ± 0.9%	4 ± 0.4%	96%
17	Gestrinone	**GSTN**	12.76 ± 0.02	0.19%	77,695,032	8%	82 ± 0.9%	14 ± 0.7%	4 ± 0.3%	96%
18	Zeranol	**ZNRL**	12.82 ± 0.01	0.11%	25,011	11%	94 ± 1.8%	6 ± 1.8%	0 ± 0.0%	100%
19	Trenbolone	**TRNB**	13.25 ± 0.02	0.18%	2,697,108	10%	64 ± 1.8%	26 ± 1.3%	9 ± 0.6%	91%
20	Stanozolol	**STNZ**	16.33 ± 0.01	0.06%	16,366,138	9%	66 ± 1.6%	23 ± 1.3%	11 ± 0.3%	89%
21	Clenbuterol	**CLNB**	18.02 ± 0.02	0.13%	344,068,966	1%	61 ± 5.1%	26 ± 3.8%	13 ± 1.3%	87%
22	Andarine	**ADAR**	19.28 ± 0.01	0.03%	17,234,595	13%	53 ± 2.3%	29 ± 1.9%	18 ± 0.4%	82%
23	Androstanolone	**ADON**	- -	-	-	-	- -	- -	- -	-

7.11. Summary

7.11.1. Summary of Effect of Instrument Parameters.

Minimum duration of Vessel filling summary. Since all system effluent flows thru the column, an appropriate flow rate must be used for the column. Although, as default a one minute vessel filling duration will certainly be sufficient to ensure a fully loaded vessel, and system pressure equilibration. If necessary, the duration for vessel filling can be optimized by monitoring system pressure traces; using the CO_2 pump (pump [A]) and system outlet pressure (BPR_A) traces, are sufficient to give the necessary information to determine the minimal time required to reach system re-equilibration.

Summary of Effect of Fill Duration and Concentration. As long as the minimum required fill time is reached to EQ system pressure, vessel filling duration has little effect on the extraction and resulting separation/analysis. Alternatively fill concentration has an effect on peak areas and can affect peak shapes at high modifier concentration. A compromise between peak area and peak shape needs to be made, finding a middle ground with lowest modifier which still gives adequate areas. Signs of exceeding the optimal fill concentration are peak fronting and splitting.

Summary of Effect of Static Extraction Duration and Concentration. The duration of Static extraction extends runtime proportionally, but has little effect on peak shapes. Static duration effect on peak area was compound specific, where little effect was seen on very early eluters (most non-polar), but significant for mid- and late-eluting compounds, and was compound specific. A compromise between peak area and overall runtime should be considered. Static Concentration on the other hand had a stronger effect on peak shapes for targeted AAS, especially above 10% modifier, degrading resolution. Due to the instrument flowpath during static extraction, the column is effectively equilibrated at high modifier concentration, just prior to extract plug delivery, reducing the ability of the phase to retain the plug at the head of the column. Not as strong of an effect as dynamic concentration, but requires a compromise between early eluting peak shapes (via better sample plug

retention) at lower modifier, and increased late eluting peak areas at higher modifier concentration (via improved extractability at higher polarity MP compositions). Early signs of exceeding the optimal static concentration involves peak shape deterioration mainly in the form of tailing.

Summary of Effect of Dynamic Extraction Duration and Concentration. Dynamic duration extends runtime proportionally. Having a mild effect on peak area across most of the targeted analytes but moderate effect on peak shape of early eluting compounds, leading to reduced resolution, at longer durations. Increased background matrix noise on the 1DHEA-MRM was also produced by longer static durations. In the current work, dynamic duration was mainly used to transport the sample plug from extraction chamber to the head of the column. Care was taken to limit the dynamic extraction time, but adequate time to load the entire sample plug was given. Dynamic Concentration had the strongest effect on the retention of the sample plug. A strong compromise was made between increased peak area for more polar compounds and the utmost importance of good sample plug retention, as the increase in area gained at higher concentrations, were not worth the negative effects on the chromatographic integrity. Early signs of exceeding the optimal dynamic concentration was mainly related to increased noise due to reduced plug retention. These peaks also tend to be asymmetric (mainly tailing). Peaks eluting before the start time for analysis is a tell-tale sign the dynamic concentration being used is too high.

Summary of Effect of Vessel Temperature. Little effect on peak shape was observed across all vessel temperatures used. Generally lower vessel temperature gave increased peak area. More strikingly, a strong effect on extractability was observed based on vessel temperature, where all compounds required more rounds to extract at higher temperature. This lower extractability (needing more rounds to extract) was most pronounced for the late eluting steroid mimics (TRNB, STNZ, CLNB & ADAR), which produced significantly lower peak areas with higher temperature.

Summary of Effect of Extraction Pressure. Generally higher vessel pressure gave increased peak areas, but late eluters, required more rounds to extract at higher pressures, while early eluters required less rounds to extract. Higher pressure had a mild effect on degraded peak shapes, especially for early eluters. The effect could

be related to mimicking higher than optimal flow rate. Compromise between higher peak areas at higher pressures and lower extractability and reduced resolution at high pressures was considered. Possibly investigating effect of pressure separately during each extraction step could be beneficial in the future to isolate negative effects during dynamic (e.g., while loading the extraction plug), would potentially isolate the effects to focus on effect on extraction.

Summary of Effect of Extraction Flow Rate. Negative effect on peak shape at higher than optimal flow rate was observed, giving reduced resolution for early and mid-eluting compounds. Flow rate had little effect on peak areas and/or extraction performance in the current work.

7.11.2. Summary of Extraction Optimization for Androgenic Steroids using Online SFE-SFC-MS

Modifier concentration during extraction had the strongest effect on peak areas, especially pronounced for later eluting, (more polar) analytes. The latest eluting compounds in the current work were CLNB and ADAR, two non-steroidal, anabolic agents. The dependence of more polar compounds was especially pronounced in vessel fill concentration, followed by static concentration and finally dynamic. As dynamic concentration did affect the peak area more strongly than static, but had a strong negative effect on peak shape due to a reduced capability of the column to retain the sample plug with higher modifier concentration (reducing peak areas above the optimum concentration).

Using the smaller extraction vessels seemed to amplify the effect of modifier concentration. Requiring much lower modifier concentrations than those found (in previous work) with the larger 5.0-mL vessels. It could be argued that this is application specific, but this observation was supported in the findings during method transfer in **Chapter #9: Microplastics**.

Overall, fill volume was used as the most significant factor in improving peak area, using a 2 % modifier concentration for 1 minute. Static extraction was run at 0% modifier to reduce the negative effect on peak shape

from higher static concentration. But static extraction time was utilized to maximize extraction, leaving the modifier sitting on the sample for an extended time (6 min). Dynamic time was utilized (also at 0% modifier, also to reduce negative effects on sample plug retention). Dynamic time was adjusted to ensure adequate delivery of the extraction plug onto the head of the column and limited to this time, to reduce negative effects on peak shape due to reduced sample plug retention of early eluting compounds.

7.i. Instrument Methods: SFE Extraction Optimizations

7.i.1. General Method Information.

Detailed information on materials and equipment used for SFE-based extraction optimizations performed in this study can be found in the following sections of **Chapter #2. Materials and Methods**:

7.i.1.1. Materials.

- Solvents used for mobile phases and dilution solutions can be found in **Section 2.1.1. Solvents**.
- Analytical standards information for targeted anabolic agents can be found in **Section 2.1.2. Analytical Standards; *Anabolic androgenic steroids (AAS)*** **and** **Table 1.**
- Sample collection paper details can be found in **Section 2.1.3. Dried Blood Spots (DBS) Materials: *Blood Spot Collection Materials.***

7.i.1.2. Instrumentation.

- The Instrumentation used is detailed in **Section 2.2.1. Instrumentation; *Nexera UC online SFE-SFC-MS***.
- Column details are given in **Section 2.2.2. Columns** and **Table 5.**
- Other equipment used is detailed in **Section 2.2.3. Other Equipment**:
    - ***Nitrogen Generator***
    - ***Analytical balances***

7.i.1.3. Solutions Preparation.

- Stock Solutions prep and storage detailed in **Section 2.3.1.1. AAS Stock Solutions** and **Table 6; Stock Solutions.**
- Injection solutions prep and concentrations are described in **Section 2.3.1.3. AAS Injection Solutions**; ***AAS Test Mixture [AAS-mix]*** and **Table 6**; ***AAS-mix*.**
    - ***AAS Test Mixture [AAS-mix]***

7.i.1.4. Sample Preparation.

- Sample preparation was accomplished using a micro sampling technique and is detailed in **Section 2.4.1. Sample Preparation: Micro-Dried Blood Spot (Micro-DBS); *Micro-DBS Sampling Technique*.**
- Sample preparation of micro-QCs is described in **Section 2.4.4. Micro-QCs for SFE Extraction Optimization**
    - ***AAS-QC spots [PøMA]***

During previous development steps, SFC injections (1.0 µL) were made of a mix of 23 androgenic anabolic agents [AAS-mix] in methanol. For extraction, the same AAS-mix was used, and spotted (applied in 1.0 µL aliquots) to Whatman® classic, cellulose based, sample collection/preservation cards. Spots were allowed to dry for at least 3 hours and cored using a standard (6mm) single hole punch. To enable rapid method screening, cored spots were placed inside 0.2-mL extraction vessel and set to the SFE automated rack changer for online extraction/analysis.

7.i.2. Instrument setup

The instrument setup utilized in the work presented was performed with the 'SFE Online Extraction Configuration using '***Splitless-mode' Extractions***' detailed in **Chapter #1. Hyphenated Instrumentation; Section 1.5.4: Instrument Configurations used for SFC Optimizations: 'Splitless-mode' Extractions**).

Sample Introduction. Online extractions were performed in splitless-mode, using 0.2-mL extraction vessels. Sample is placed in inside a small chamber and extracted online facilitated by two switching valves, an 'extraction plug is delivered to the head of the column for online analysis.

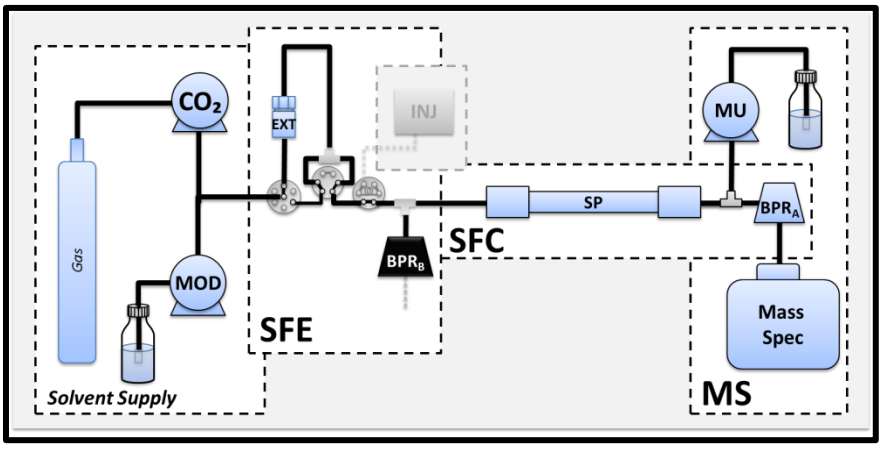

See Figure 17 in Chapter #1

7.i.3. Instrument Methods: Held Constant Throughout Method Screening

7.i.3.1. Mobile Phase (MP) and Stationary Phase (SP).

LCMS-grade methanol [MeOH] with 5 mM ammonium formate [AmFo] were utilized as modifier. For SFC mobile phases, up to 40% modifier was mixed with carbon dioxide ([CO_2] – Instrument grade) via the instrument solvent delivery pumps. Extraction steps (filling, static and dynamic) were performed at isocratic modifier concentrations, the analysis step always used gradient elution (utilizing the SFC-MS method gradient, detailed below). All online extractions and subsequent separations performed in the current work utilized a Shimadzu Corporation Shim-pack UC-Cyano 4.6 mm x 150 mm 5.0 µm column.

7.i.3.2. *MS Method Parameters – MRM method from Chapter #4*

Detection was achieved using an LCMS-8050 triple quadrupole mass spectrometer, equipped with an electrospray ionization (ESI-) source, operated in positive (+) and negative (-) ionization mode, using multiple reaction monitoring (MRM). MRM transitions are presented in **Table 29** including precursor and product ions, voltages and collision energies for each analyte. Interface voltages were set to 4.0 kV (for positive) and -3.0 kV (for negative mode) with an interface temperature of 300 °C. Nitrogen gas was used for both drying and nebulizing gas; with a flow rate of 3.0 L/min for nebulizing gas and 5.0 L/min for drying gas. Desolvation and DL temperatures were 602 °C and 350 °C respectively. Heat Block temperature was set to 500 °C, and heating gas used was dry air. Gas used for collision induced dissociation (CID) was argon at 270 kPa. DL Bias/Qarray Bias were both set as 0 V, and Q3 Pre-rod Bias at -15 V (for positive scan mode) and 15 V (for negative scan mode).

7.i.3.3. *SFC Method Parameters – optimized method from Chapter #6*

Gradient : 2.0 - 12.5% B (0-8 min), 12.5 - 30% B (8-10 min), 30% B (10-15 min).

Flow rate : 3.0 mL/min

Column Temp. : 60 °C

Outlet Pressure : (BPR_A) 15 MPa; (BPR_B) 40 MPa.

7.i.3.4. *SFE Method Details – used in all screening methods.*

Extraction Mode : Splitless-mode; (BPR_B) 40 MPa.

Final Wash : 100%B; 3.0 ml/min; 3.0 min duration.

Extraction Sample : Whatman™ FTA® classic sample collection card.

1.0µL spot (AAS-mix) applied; dried (≥ 3 hours) at room temperature.

6mm Core; placed directly into vessel.

Vessel Size : 0.2-mL vessels,

Vessel Filters : standard (non-sinter type) vessel filters.

Vessel Filler : None

Torque Wrench : 1.5 Nm (specific for 02 mL vessels)

7.i.3.5. *SFE Method Details – default settings for variable parameters.*

Vessel Filling	(duration; conc.)	:	1.0 min; 2% [B]
Static Extraction	(duration; conc.)	:	2.0 min; 0% [B]
Dynamic Extraction	(duration; conc.)	:	2.0 min; 0% [B]
Vessel Temperature		:	35 °C
Extraction Pressure		:	(BPR_A) 15 MPa
Extraction Flow Rate		:	2.0 mL/min

7.i.4. Instrument Methods: Screening Extraction Parameters

Methods used for screening Instrument parameters are summarized in **Table 31**, and described for each parameter in the below sections.

Table 31. Summary of Instrument Methods used for Extraction Parameter Screening Listing Systematic Approach for Investigation of Effect of Extraction-specific Parameters for Online Extraction Optimization.

	Vessel Filling [*f*]			Static Extraction [*s*]			Dynamic Extraction [*d*]			Vessel Temperature [*T*]		Vessel Pressure [*P*]		SFC Analysis				
Method ID	Conc. (%B)	Duration (min)	Flow Rate (mL/min)	Conc. (%B)	Duration (min)	Flow Rate (mL/min)	Conc. (%B)	Duration (min)	Flow Rate (mL/min)	Extraction *T* (°C)	Rack Changer (°C)	BPR_A (MPa)	BPR_B (MPa)	Gradient ID	BPRA (MPa)	BPRB (MPa)	Column (°C)	Flow Rate (mL/min)
***f*25**	25	1.0	2.0	00	2.0	2.0	00	2.0	2.0	35	20	15	40	G2-12.5%	15	40	60	2.0
***f*15**	15	1.0	2.0	00	2.0	2.0	00	2.0	2.0	35	20	15	40	G2-12.5%	15	40	60	2.0
***f*10**	10	1.0	2.0	00	2.0	2.0	00	2.0	2.0	35	20	15	40	G2-12.5%	15	40	60	2.0
***f*05**	05	1.0	2.0	00	2.0	2.0	00	2.0	2.0	35	20	15	40	G2-12.5%	15	40	60	2.0
***f*02 ***	02	1.0	2.0	00	2.0	2.0	00	2.0	2.0	35	20	15	40	G2-12.5%	15	40	60	2.0
***f*00**	00	1.0	2.0	00	2.0	2.0	00	2.0	2.0	35	20	15	40	G2-12.5%	15	40	60	2.0
***f*0.5m**	02	0.5	2.0	00	2.0	2.0	00	2.0	2.0	35	20	15	40	G2-12.5%	15	40	60	2.0
***f*0.7m**	02	0.7	2.0	00	2.0	2.0	00	2.0	2.0	35	20	15	40	G2-12.5%	15	40	60	2.0
f*1.0m	02	1.0	2.0	00	2.0	2.0	00	2.0	2.0	35	20	15	40	G2-12.5%	15	40	60	2.0
***f*1.3m**	02	1.3	2.0	00	2.0	2.0	00	2.0	2.0	35	20	15	40	G2-12.5%	15	40	60	2.0
***s*00**	00	1.0	2.0	00	2.0	2.0	00	2.0	2.0	35	20	15	40	G2-12.5%	15	40	60	2.0
s*00	02	1.0	2.0	00	2.0	2.0	00	2.0	2.0	35	20	15	40	G2-12.5%	15	40	60	2.0
***s*02**	02	1.0	2.0	02	2.0	2.0	00	2.0	2.0	35	20	15	40	G2-12.5%	15	40	60	2.0
***s*05**	02	1.0	2.0	05	2.0	2.0	00	2.0	2.0	35	20	15	40	G2-12.5%	15	40	60	2.0
***s*10**	02	1.0	2.0	10	2.0	2.0	00	2.0	2.0	35	20	15	40	G2-12.5%	15	40	60	2.0
***s*1.0m**	02	1.0	2.0	00	1.0	2.0	00	2.0	2.0	35	20	15	40	G2-12.5%	15	40	60	2.0
s*2.0m	02	1.0	2.0	00	2.0	2.0	00	2.0	2.0	35	20	15	40	G2-12.5%	15	40	60	2.0
***s*4.0m**	02	1.0	2.0	00	4.0	2.0	00	2.0	2.0	35	20	15	40	G2-12.5%	15	40	60	2.0
***s*6.0m**	02	1.0	2.0	00	6.0	2.0	00	2.0	2.0	35	20	15	40	G2-12.5%	15	40	60	2.0
d*00	02	1.0	2.0	00	2.0	2.0	00	2.0	2.0	35	20	15	40	G2-12.5%	15	40	60	2.0
***d*02**	02	1.0	2.0	00	2.0	2.0	02	2.0	2.0	35	20	15	40	G2-12.5%	15	40	60	2.0
***d*05**	02	1.0	2.0	00	2.0	2.0	05	2.0	2.0	35	20	15	40	G2-12.5%	15	40	60	2.0
***d*10**	02	1.0	2.0	00	2.0	2.0	10	2.0	2.0	35	20	15	40	G2-12.5%	15	40	60	2.0
***d*0.5m**	02	1.0	2.0	00	2.0	2.0	00	0.5	2.0	35	20	15	40	G2-12.5%	15	40	60	2.0
***d*1.0m**	02	1.0	2.0	00	2.0	2.0	00	1.0	2.0	35	20	15	40	G2-12.5%	15	40	60	2.0
d*2.0m	02	1.0	2.0	00	2.0	2.0	00	2.0	2.0	35	20	15	40	G2-12.5%	15	40	60	2.0
***d*3.0m**	02	1.0	2.0	00	2.0	2.0	00	3.0	2.0	35	20	15	40	G2-12.5%	15	40	60	2.0
T*35	02	1.0	2.0	00	2.0	2.0	00	2.0	2.0	35	20	15	40	G2-12.5%	15	40	60	2.0
***T*40**	02	1.0	2.0	00	2.0	2.0	00	2.0	2.0	40	20	15	40	G2-12.5%	15	40	60	2.0
***T*60**	02	1.0	2.0	00	2.0	2.0	00	2.0	2.0	60	20	15	40	G2-12.5%	15	40	60	2.0
***T*80**	02	1.0	2.0	00	2.0	2.0	00	2.0	2.0	80	20	15	40	G2-12.5%	15	40	60	2.0
***P*10**	02	1.0	2.0	00	2.0	2.0	00	2.0	2.0	35	20	10	40	G2-12.5%	15	40	60	2.0
***P*12**	02	1.0	2.0	00	2.0	2.0	00	2.0	2.0	35	20	12.5	40	G2-12.5%	15	40	60	2.0
P*15	02	1.0	2.0	00	2.0	2.0	00	2.0	2.0	35	20	15	40	G2-12.5%	15	40	60	2.0
***P*20**	02	1.0	2.0	00	2.0	2.0	00	2.0	2.0	35	20	20	40	G2-12.5%	15	40	60	2.0
***P*25**	02	1.0	2.0	00	2.0	2.0	00	2.0	2.0	35	20	25	40	G2-12.5%	15	40	60	2.0
***R*3.5**	02	1.0	2.0	00	2.0	2.0	00	2.0	2.0	35	20	15	40	G2-12.5%	15	40	60	2.0
***R*3.0**	02	1.0	2.0	00	2.0	2.0	00	2.0	2.0	35	20	15	40	G2-12.5%	15	40	60	2.0
***R*2.5**	02	1.0	2.0	00	2.0	2.0	00	2.0	2.0	35	20	15	40	G2-12.5%	15	40	60	2.0
R*2.0	02	1.0	2.0	00	2.0	2.0	00	2.0	2.0	35	20	15	40	G2-12.5%	15	40	60	2.0

***Same as Base-Method**

7.i.4.1. Screening Conditions for Vessel Filling Duration

Parameters used to evaluate effect of vessel filling duration on online extractions are summarized in (**Table 32**). Four extractions were performed: each using a different vessel filling (***f***) duration: 0.5 minutes **(*f*0.5)**; 0.7 minutes **(*f*0.7)**; 1.0 minute **(*f*1.0)**; or 1.3 minutes **(*f*1.3)**.

All other parameters were held constant between screening methods as follows: Pump B delivered methanol + 5 mM ammonium formate. Pump A delivers liquid carbon dioxide (CO_2). Extractions included a vessel filling using 2% modifier (2%B), followed by a 2.0 minute static extraction using 0% modifier (0%B), and a 2.0 minute dynamic extraction also using 0% modifier (0%B). The rack changer held the temperature of vessels constant at 20 °C until just prior to extraction where each vessel was heated to 35 °C. The outlet pressure (BPR_A) was set to 15 MPa and splitless-mode extractions were used, with BPR_B set to 40 MPa for the duration of the extraction and analysis. Extraction end occurred immediately at the end of the dynamic extraction (SFE-end; 5.01 min), and analysis was started using the SFC-MS method optimized in previous development steps (see above **Section 7.i.3. Instrument Methods: Held Constant Throughout Method Screening**).

Table 32. Screening Conditions for Vessel Filling Duration

Vessel Filling	(duration; conc.)	:	***Variable* (0.5, 0.7, 1.0 or 1.3 min);** 2% [B]
Static Extraction	(duration; conc.)	:	2.0 min; 0% [B]
Dynamic Extraction	(duration; conc.)	:	2.0 min; 0% [B]
Vessel Temperature		:	35 °C
Extraction Pressure	(BPR_A)	:	15 MPa
Extraction Mode	(BPR_B)	:	40 MPa ; Splitless
Extraction Flow Rate		:	2.0 mL/min

7.i.4.2. Vessel Fill Concentration Screening Conditions

Parameters used to evaluate effect of modifier concentration during vessel filling are summarized in (**Table 33**). Six extractions were performed, each using a different vessel filling (***f***) modifier concentration (% pump B, run isocratically): 0%B **(*f*0%)**; 2%B **(*f*2%)**; 5%B **(*f*5%)**; 10%B **(*f*10%)**; 15%B **(*f*15%)**; or 25%B **(*f*25%)**. Pump B delivered methanol + 5 mM ammonium formate. Pump A delivers liquid carbon dioxide (CO_2).

All other parameters were held constant between screening methods as follows: Pump B delivered methanol + 5 mM ammonium formate. Pump A delivers liquid carbon dioxide (CO_2). Extractions included a vessel filling duration of 1.0 minute (0.00 – 1.00 min; using a '*variable*' fill concentration as outlined above), followed by a 2.0 minute static extraction using 0% modifier (1.01 – 3.00 min; 0%B), and a 2.0 minute dynamic extraction also using 0% modifier (3.01 – 5.00 min; 0%B). The rack changer held the temperature of vessels constant at 20 °C until just prior to extraction where each vessel was heated to 35 °C. The outlet pressure (BPR_A) was set to 15 MPa and splitless-mode extractions were used, with BPR_B set to 40 MPa for the duration of the extraction and analysis. Extraction end occurred immediately at the end of the dynamic extraction (SFE-end; 5.01 min), and analysis was started using the SFC-MS method optimized in previous development steps (see above **Section 7.i.3. Instrument Methods: Held Constant Throughout Method Screening**).

Table 33. Screening Conditions for Modifier Concentration during Vessel Filling.

Vessel Filling	(duration; conc.)	:	1.0 min; ***Variable*** **(0, 2, 5, 10, 15, 25% [B])**
Static Extraction	(duration; conc.)	:	2.0 min; 0% [B]
Dynamic Extraction	(duration; conc.)	:	2.0 min; 0% [B]
Vessel Temperature		:	35 °C
Extraction Pressure	(BPR_A)	:	15 MPa
Extraction Mode	(BPR_B)	:	40 MPa ; Splitless
Extraction Flow Rate		:	2.0 mL/min

7.i.4.3. Static Extraction Concentration Screening Conditions

Parameters used to evaluate effect of modifier concentration during static extraction are summarized in (**Table 34**). Five extractions were performed, each using a different static extraction (***s***) modifier concentration (% pump B, run isocratically): 0%B **(*s*0%)**; 2%B **(*s*2%)**; 5%B **(*s*5%)**; or 10%B **(*s*10%)**.

All other parameters were held constant between screening methods as follows: Pump B delivered methanol + 5 mM ammonium formate. Pump A delivers liquid carbon dioxide (CO_2). Extractions included a 1.0 minute vessel filling using 2% modifier (0.00 – 1.00 min; 2%B), followed by a 2.0 minute static extraction (1.01 – 3.00 min; using a '*variable*' modifier concentration as outlined above), and a 2.0 minute dynamic extraction also using 0% modifier (3.01 – 5.00 min; 0%B). The rack changer held the temperature of vessels constant at 20 °C till just prior to extraction where each vessel was heated to 35 °C. The outlet pressure (BPR_A) was set to 15 MPa and splitless-mode extractions were used, with BPR_B set to 40 MPa for the duration of the extraction and analysis. Extraction end occurred immediately at the end of the dynamic extraction (SFE-end; 5.01 min), and analysis was started using the SFC-MS method optimized in previous development steps (see above **Section: 7.i.3. Instrument Parameters Held Constant; *SFC-MS Method***).

Table 34. Static Extraction Concentration Screening Conditions.

Vessel Filling	(duration; conc.)	:	1.0 min; 0% [B]
Static Extraction	(duration; conc.)	:	2.0 min; ***Variable*** **(0, 2, 5, or 10% [B])**
Dynamic Extraction	(duration; conc.)	:	2.0 min; 0% [B]
Vessel Temperature		:	35 °C
Extraction Pressure	(BPR_A)	:	15 MPa
Extraction Mode	(BPR_B)	:	40 MPa ; Splitless
Extraction Flow Rate		:	2.0 mL/min

7.i.4.4. Static Extraction Duration Screening Conditions

Parameters used to evaluate effect of the duration of static extraction are summarized in (**Table 35**). Four extractions were performed, each using a different static extraction (***s***) duration: 1.0 minute **(*s*1.0)**; 2.0 minutes **(*s*2.0)**; 4.0 minutes **(*s*4.0)**; or 6.0 minutes **(*s*6.0)** long.

All other parameters were held constant between screening methods as follows: Pump B delivered methanol + 5 mM ammonium formate. Pump A delivers liquid carbon dioxide (CO_2). Extractions included a 1.0 minute vessel filling using 2% modifier (0.00 – 1.00 min; 2%B), followed by a static extraction using 0% modifier for a '*variable*' duration as outlined above (1.01 min – *'variable'* min; 0%B), and a 2.0 minute dynamic extraction also using 0% modifier (0%B). The rack changer held the temperature of vessels constant at 20 °C till just prior to extraction where each vessel was heated to 35 °C. The outlet pressure (BPR_A) was set to 15 MPa and splitless-mode extractions were used, with BPR_B set to 40 MPa for the duration of the extraction and analysis. Extraction end occurred immediately at the end of the dynamic extraction, and analysis was started using the SFC-MS method optimized in previous development steps (see above **Section: 7.i.3. Instrument Parameters Held Constant; *SFC-MS Method***).

Table 35. Static Extraction Duration Screening Conditions

Vessel Filling	(duration; Conc.)	:	1.0 min; 2% [B]
Static Extraction	(duration; Conc.)	:	***Variable* (1.0, 2.0, 4.0, or 6.0 min)**; 0% [B]
Dynamic Extraction	(duration; Conc.)	:	2.0 min; 0% [B]
Vessel Temperature		:	35 °C
Extraction Pressure	(BPR_A)	:	15 MPa
Extraction Mode	(BPR_B)	:	40 MPa ; Splitless
Extraction Flow Rate		:	2.0 mL/min

7.i.4.5. Conditions for Screening Dynamic Extraction Concentration

Parameters used to evaluate effect of modifier concentration during dynamic extraction are summarized in (**Table 36**). Four extractions were performed: each using a different dynamic extraction (***d***) modifier concentration (% pump B, run isocratically): 0%B **(*d*0%)**; 2%B **(*d*2%)**; 5%B **(*d*5%)**; or 10%B **(*d*10%).**

All other parameters were held constant between screening methods as follows: Pump B delivered methanol + 5 mM ammonium formate. Pump A delivers liquid carbon dioxide (CO_2). Extractions included a 1.0 minute vessel filling using 2% modifier (0.00 – 1.00 min; 2%B), followed by a 2.0 minute static extraction using 0% modifier (1.01 – 3.00 min; 0%B), and finally a 2.0 minute dynamic extraction (3.01 – 5.00 min; using a '*variable*' modifier concentration as outlined above). The rack changer held the temperature of vessels constant at 20 °C till just prior to extraction where each vessel was heated to 35 °C. The outlet pressure (BPR_A) was set to 15 MPa and splitless-mode extractions were used, with BPR_B set to 40 MPa for the duration of the extraction and analysis. Extraction end occurred immediately at the end of the dynamic extraction (SFE-end; 5.01 min), and analysis was started using the SFC-MS method optimized in previous development steps (see above **Section: 7.i.3. Instrument Parameters Held Constant; *SFC-MS Method***).

Table 36. Conditions for Screening Dynamic Extraction Concentration.

Vessel Filling	(duration; conc.)	:	1.0 min; 0% [B]
Static Extraction	(duration; conc.)	:	2.0 min; 0% [B]
Dynamic Extraction	(duration; conc.)	:	2.0 min; ***Variable*** **(0, 2, 5, or 10% [B])**
Vessel Temperature		:	35 °C
Extraction Pressure	(BPR_A)	:	15 MPa
Extraction Mode	(BPR_B)	:	40 MPa ; Splitless
Extraction Flow Rate		:	2.0 mL/min

7.i.4.6. Conditions for Screening Dynamic Extraction Duration

Parameters used to evaluate effect of the duration of dynamic extraction are summarized in **Table 37**. Four extractions were performed: each using a different dynamic (***d***) extraction duration: 0.5 minutes **(*d*0.5)**; 1.0 minute **(*d*1.0)**; 2.0 minutes **(*d*2.0)**; or 3.0 minutes **(*d*3.0)** long.

All other parameters were held constant between screening methods as follows: Pump A delivers liquid carbon dioxide (CO_2). Pump B delivered methanol + 5 mM ammonium formate. Extractions included a 1.0 minute vessel filling using 2% modifier (0.00 – 1.00 min; 2%B), followed by a 2.0 minute static extraction using 0% modifier (1.01 – 3.00 min; 0%B), and finally a dynamic extraction using 0% modifier for a *'variable'* duration as outlined above (3.01 min – *'variable' min*; 0%B). The rack changer held the temperature of vessels constant at 20 °C till just prior to extraction where each vessel was heated to 35 °C. The outlet pressure (BPR_A) was set to 15 MPa and splitless-mode extractions were used, with BPR_B set to 40 MPa for the duration of the extraction and analysis. Extraction end occurred immediately at the end of the dynamic extraction, and analysis was started using the SFC-MS method optimized in previous development steps (see above **Section: 7.i.3. Instrument Parameters Held Constant; *SFC-MS Method***).

Table 37. Conditions for Screening Dynamic Extraction Duration

Vessel Filling	(duration; Conc.)	:	1.0 min; 2% [B]
Static Extraction	(duration; Conc.)	:	2.0 min; 0% [B]
Dynamic Extraction	(duration; Conc.)	:	***Variable*** **(0.5, 1.0, 2.0, or 3.0 min)**; 0% [B]
Vessel Temperature		:	35 °C
Extraction Pressure	(BPR_A)	:	15 MPa
Extraction Mode	(BPR_B)	:	40 MPa ; Splitless
Extraction Flow Rate		:	2.0 mL/min

7.i.4.7. Extraction Vessel Temperature Screening Conditions

Parameters used to evaluate the effect of vessel temperature on online extractions are summarized in **Table 38**. Five extractions were performed, each using a different vessel temperature (***T***): 30 °C **(*T*30)**; 35 °C **(*T*35)**; 40 °C **(*T*40)**; 60 °C **(*T*60)**; or 80 °C **(*T*80)**. The rack changer was set to 20 °C.

All other parameters were held constant between screening methods as follows: Pump A delivers liquid carbon dioxide (CO_2). Pump B delivered methanol + 5 mM ammonium formate. Extractions included a 1.0 minute vessel filling using 2% modifier (0.00 – 1.00 min; 2%B), followed by a 2.0 minute static extraction using 0% modifier (1.01 – 3.00 min; 0%B), and a 2.0 minute dynamic extraction also using 0% modifier (3.01 – 5.00 min; 0%B). The outlet pressure (BPR_A) was variable as discussed above. Splitless-mode extractions were used, with BPR_B set to 40 MPa for the duration of the extraction and analysis. Extraction end occurred immediately at the end of the dynamic extraction (SFE-end; 5.01 min), and analysis was started using the SFC-MS method optimized in previous development steps (see above **Section 7.i.3. Instrument Methods: Held Constant Throughout Method Screening**).

Table 38. Extraction Pressure Screening Conditions

Vessel Filling	(duration; Conc.)	:	1.0 min; 2% [B]
Static Extraction	(duration; Conc.)	:	2.0 min; 0% [B]
Dynamic Extraction	(duration; Conc.)	:	2.0 min; 0% [B]
Vessel Temperature		:	***Variable*** (30, 35, 40, 60, or 80 °C)
Extraction Pressure	(BPR_A)	:	15 MPa
Extraction Mode	(BPR_B)	:	40 MPa ; Splitless
Extraction Flow Rate		:	2.0 mL/min

7.i.4.8. Extraction Pressure Screening Conditions

Parameters used for the evaluation of effect of pressure on online extractions are summarized in **Table 39**. Five extractions were performed, each using a different outlet (BPR_A) pressure (***P***) during extraction: 10 MPa **(*P*10)**; 12.5 MPa **(*P*12)**; 15 MPa **(*P*15)**; 20 MPa **(*P*20)**; or 25 MPa **(*P*25)**.

All other parameters were held constant between screening methods as follows: Pump A delivers liquid carbon dioxide (CO_2). Pump B delivered methanol + 5 mM ammonium formate. Extractions included a 1.0 minute vessel filling using 2% modifier (0.00 – 1.00 min; 2%B), followed by a 2.0 minute static extraction using 0% modifier (1.01 – 3.00 min; 0%B), and a 2.0 minute dynamic extraction also using 0% modifier (3.01 – 5.00 min; 0%B). The rack changer held the temperature of vessels constant at 20 °C till just prior to extraction where each vessel was heated to 35 °C. The outlet pressure (BPR_A) was '*variable*' as discussed above. Splitless-mode extractions were used, with BPR_B set to 40 MPa for the duration of the extraction and analysis. Extraction end occurred immediately at the end of the dynamic extraction (SFE-end; 5.01 min), and analysis was started using the SFC-MS method optimized in previous development steps (see above **Section 7.i.3. Instrument Methods: Held Constant Throughout Method Screening**).

Table 39. Extraction Pressure Screening Conditions

Vessel Filling	(duration; Conc.)	:	1.0 min; 2% [B]
Static Extraction	(duration; Conc.)	:	2.0 min; 0% [B]
Dynamic Extraction	(duration; Conc.)	:	2.0 min; 0% [B]
Vessel Temperature		:	35 °C
Extraction Pressure	(BPR_A)	:	***Variable*** (10, 12.5, 15, 20 or 25 MPa)
Extraction Mode	(BPR_B)	:	40 MPa ; Splitless
Extraction Flow Rate		:	2.0 mL/min

7.i.4.9. Conditions for Screening Flow Rate during Extraction

Parameters used to evaluate effect of flow rate on online extractions are summarized in **Table 40**. Four extractions were performed, each using a different flow rate (***R***) during extraction: 2.0 mL/min **(*R*2.0)**; 2.5 mL/min **(*R*2.5)**; 3.0 mL/min **(*R*3.0)**; or 3.5 mL/min **(*R*3.5)**.

All other parameters were held constant between screening methods as follows: Pump A delivers liquid carbon dioxide (CO_2). Pump B delivered methanol + 5 mM ammonium formate. Extractions included a 1.0 minute vessel filling using 2% modifier (0.00 – 1.00 min; 2%B), followed by a 2.0 minute static extraction using 0% modifier (1.01 – 3.00 min; 0%B), and a 2.0 minute dynamic extraction also using 0% modifier (3.01 – 5.00 min; 0%B). The rack changer held the temperature of vessels constant at 20 °C till just prior to extraction where each vessel was heated to 35 °C. The outlet pressure (BPR_A) was set to 15 MPa and splitless-mode extractions were used, with BPR_B set to 40 MPa for the duration of the extraction and analysis. Extraction end occurred immediately at the end of the dynamic extraction (SFE-end; 5.01 min), and analysis was started using the SFC-MS method optimized in previous development steps (see above **Section 7.i.3. Instrument Methods: Held Constant Throughout Method Screening**).

Table 40. Conditions for Screening Flow Rates during Extraction

Vessel Filling	(duration; Conc.)	:	1.0 min; 2% [B]
Static Extraction	(duration; Conc.)	:	2.0 min; 0% [B]
Dynamic Extraction	(duration; Conc.)	:	2.0 min; 0% [B]
Vessel Temperature		:	35 °C
Extraction Pressure	(BPR_A)	:	15 MPa
Extraction Mode	(BPR_B)	:	40 MPa ; Splitless
Extraction Flow Rate		:	***Variable*** (2.0, 2.5, 3.0, or 3.5 mL/min)

7.i.5. Instrument Methods: Optimized Online SFE-SFC-MS Extraction Method

Detailed conditions for the final SFE-SFC-MS method are given below in **Table 41.**

Table 41. Conditions for Optimized Online Extraction of Anabolic Agents using 0.2-mL Vessels.

Mobile Phase	:	[A] carbon dioxide (CO_2);	[B] methanol + 5mM ammonium formate (AmFo).		
Column	:	Shimadzu Corp., Shim-pack, UC-Cyano (4.6 x 150mm, 5 µm)			
Online SFE Extraction					
SFE Vessel Size	:	0.2-mL			
Vessel Temp.	:	30 °C			
Rack Changer Temp.	:	20 °C			
Extraction Pressure	:	(BPR_A) 10 MPa			
Mode	:	(BPR_B) 40 MPa;	Splitless		
Filling	:	2.0 mL/min;	2% [B];	1.0 min;	(0.00 – 1.00 m).
Static Extraction	:	2.5 mL/min;	0% [B];	4.0 min;	(1.01 – 5.00 m).
Dynamic Extraction	:	2.5 mL/min;	0% [B];	2.0 min;	(5.01 – 7.00 m).
Analysis	:	2.0 mL/min;	*gradient**	16.0 min;	(5.01 – 21.00m).
Wash	:	2.5 mL/min;	100% [B];	3.0 min;	(21.01 – 24.00 m).
Re-Equilibration	:	2.5 mL/min;	2% [B];	0.5 min;	(24.01 – 24.50 m).
****SFC gradient***					
Column Temp.	:	60 °C			
Outlet Pressure	:	(BPR_A) 15 MPa			
Gradient	:	2 – 5% B;	9.0 min;	(5.01 - 14.00m),	
		5 – 12% B;	3.5 min;	(14.01 – 17.50m),	
		12 – 30% B;	3.0 min;	(17.51 – 19.50m),	
		30% B	1.5 min;	(19.51 – 21.00m).	

7.i.6. Data Processing Approaches **used in the Evaluation of the Effect of Extraction Parameters**

Area refers to the integrated area under the peak for an individual compound. Replicate vessels were extracted online for a single target-parameter. The number of vessels used reflects the number of settings screened for the given parameter being screened. Each replicate vessel, extracted using a different setting is referred to with a lower-case letter for clarity; the first replicate vessel [a], the second vessel [b], the third vessel [c], etc. Each vessel was extracted a total of three consecutive times; the first extraction [EXT1], second extraction [EXT2] and third extraction [EXT3]. Detailed explanation of data processing approaches for SFE-SFC-MS are available in **Chapter #2. Materials and Methods: Section 2.9. General Data Processing Approaches**.

7.i.6.1. *Peak area Comparisons.*

Total Area Extracted per vessel **[T_{Area}/vessel].** The summed area from all three extractions [EXT1 + EXT2 + EXT3] for a single vessel.

Total Area Extracted **[T_{area}].** The total area extracted per vessel (T_{Area}/vessel) is summed for all replicate vessels [ex. a + b + c] (n = 3).

Average Total Area Extracted **[Av_{total}].** The average and standard deviation (SD) are calculated using total area extracted per vessel (T_{area}/vessel) for all replicate vessels [ex. a : b : c] (n = 3).

7.i.6.2. *Extraction Performance Evaluations.*

Percent Total Area in the (for example) First Extraction per vessel **[%EXT1].** The area from the first extraction (EXT1) for a single vessel is divided by the total area extracted (T_{area}/vessel) for the same vessel.

Average Percent Total Area Extracted in the first Extraction [Av%EXT1]. The average and standard deviation are calculated for percent of the total area in the first extraction (%EXT1) for all replicates vessels [a : b : c] (n = 3).

Average Percent Total Area Extracted in the 1st Two Extractions [Av_{1+2}]. The average and standard deviation are calculated for percent of the total area in the first extraction (%EXT1) for all replicates vessels [a : b : c] (n = 3)

Average Percent Total Area Extracted /Round [Av%EXT#]. The area from *(for example)* the first extraction (EXT1) for a single vessel, is divided by the total area extracted (T_{area}/vessel) for the same vessel, giving the percent of the total area in the first extraction per vessel **[%EXT1]**. The average and standard deviation are calculated for [%EXT1] for all replicates vessels [a : b : c] (n = 3), which gives **[Av%EXT1]**.

Literature Cited:

FIRST CITED IN PREVIOUS CHAPTERS

[17] Wicker AP, Tanaka K, Nishimura M, Chen V, Ogura T, Hedgepeth W, Schug KA. (2020). "Multivariate approach to on-line supercritical fluid extraction supercritical fluid chromatography - mass spectrometry method development." *Analytica Chimica Acta*. **1127**: p282-294. https://doi.org/10.1016/j.aca.2020.04.068

S_7. SUPPLEMENTARY MATERIALS

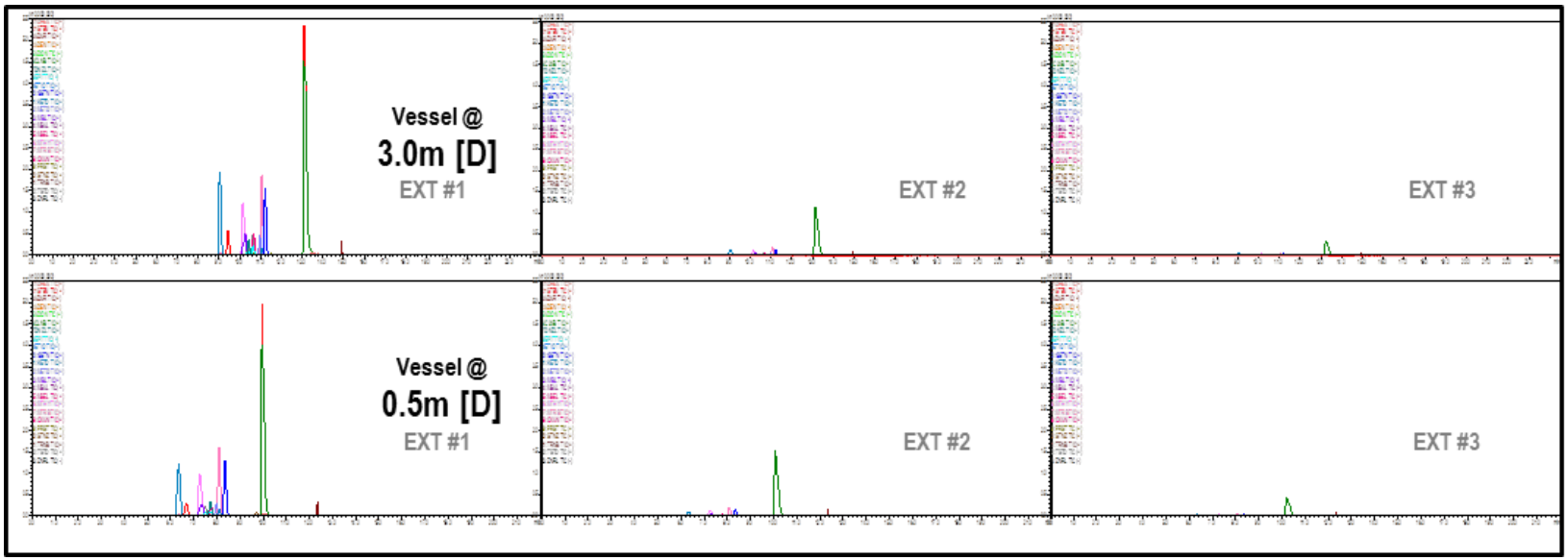

S_Figure 21. Extraction Performance Using Different Dynamic Extraction (d) Durations: [top] 3.0 minutes (min); and [bottom] 0.5 min. bar graph showing percent of total area extracted for each targeted anabolic agent in three consecutive extraction rounds: **[blue]** first extraction (%EXT1); **[red]** second extraction (%EXT2); and **[green]** third extraction (%EXT3) for each vessel. **[top Panel] Overlaid SFE-SFC-MS Chromatograms for Online Extractions** targeted anabolic agent in three consecutive extraction rounds.

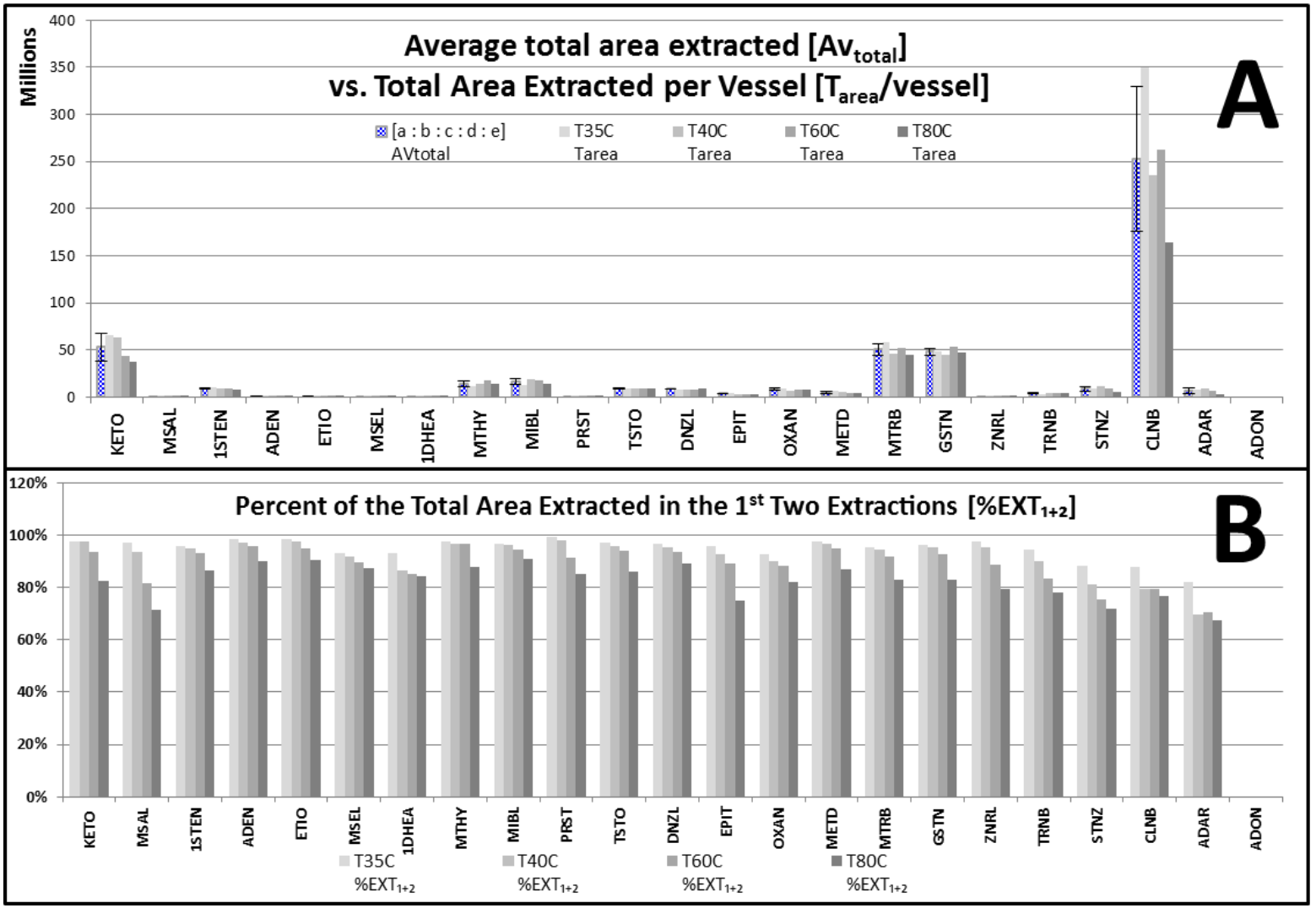

S_Figure 22. Bar Plots for Peak areas produced using different Extraction vessel temperatures, showing [A] Average total area extracted [Av_{total}, blue] vs. Total Area Extracted per Vessel (T_{area}/vessel, shades of gray; darkest 80 °C and lightest 35 °C). **[B]** Percent of the Total Area Extracted in the 1st Two Extractions [$\%EXT_{1+2}$; shades of gray corresponding to vessel temperature; darkest gray 80 °C].

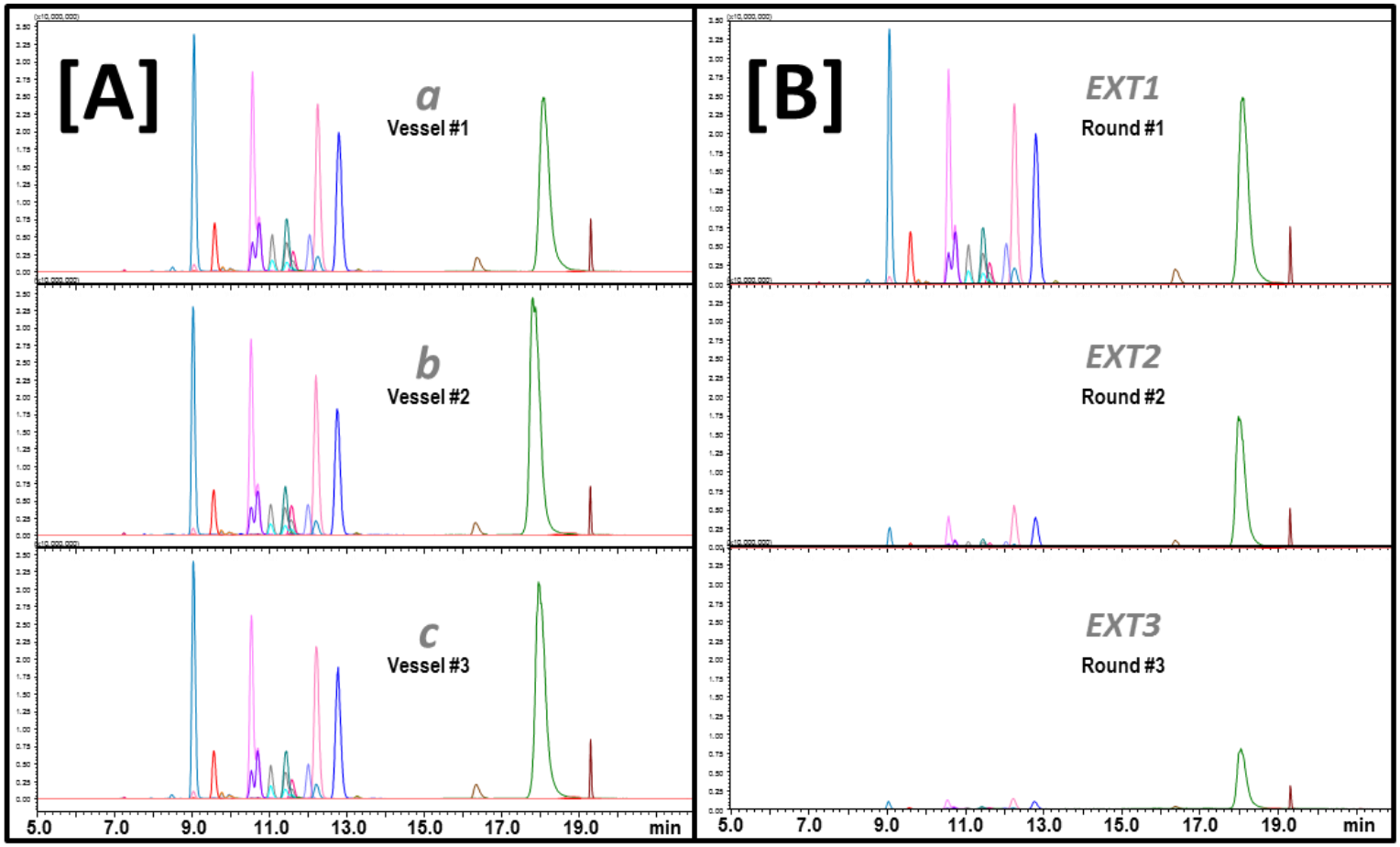

S_Figure 23. SFE-SFC-MS Chromatogram using Final Optimized Online Method for Extraction of Anabolic Agents using UC-Cyano Column. Showing zoomed on elution timeframe for 22 anabolic agents, **[A]** three replicate vessels: vessel #1 (a), vessel #2 (b), vessel #3 (c); **and [B]** Showing three consecutive extraction round for a single replicate vessel: extraction round #1 (EXT1), extraction round #2 (EXT2), and extraction round #3 (EXT3). **Chromatographic separations of the extraction plugs produced via online-SFE of spiked steroid standards (1.0 µL spot AAS-mix) from sample collection card (6 mm) core [AAS-QC].** MRM-TIC chromatograms for targeted AAS: KETO [**1**, teal]; MSAL [**2**, magenta]; 1STEN [**3**, red]; ADEN [**4**, orange]; MSEL [**5**, rose]; ETIO [**6**, blue]; 1DHEA [**7**, pink]; PRST [**8**, gold]; MTHY [**9**, light pink]; MIBL [**10**, purple]; EPIT [**11**, cyan]; DNZL [**12**, turquoise]; TSTO [**13**, gray]; OXAN [**14**, hot pink]; METD [**15**, lilac]; MTRB [**16**, coral]; GSTN [**17**, cobalt]; TRNB [**18**, brown]; ZRNL [**19**, black]; STNZ [**20**, mocha]; CLNB [**21**, dark green] and ADAR [**22**, maroon]. *Shown at same intensity scale.*

CHAPTER 8

RAPID ONLINE STEROID EXTRACTION IN ANTI-DOPING ANALYSIS WITH SFE-SFC-MS FROM MICRO-DRIED BLOOD SPOTS

CHAPTER 8
RAPID ONLINE STEROID EXTRACTION IN ANTI-DOPING ANALYSIS WITH SFE-SFC-MS FROM MICRO-DRIED BLOOD SPOTS

8.1. Anti-Doping Analysis Introduction.

Drug doping remains a prevalent and potent form of drug cheating among elite athletes.[85] Consistent anti-doping policies and regulations within sport organizations and governments across the world are of ongoing importance. At the core is the ever evolving need for rapid, accurate and sensitive techniques to detect abuse of established and newly regulated substances in a time-sensitive and reliable manner. Currently, using standard methods of analysis, significant challenges exist due to the excessive time required for method validation and extensive sample preparation. On-line supercritical fluid extraction coupled with supercritical fluid chromatography - mass spectrometry (SFE-SFC-MS/MS) is a quickly developing analytical technique providing extraction, separation, and detection in a single, rapid, analysis. Being ideal for investigation of steroids in complex matrices, it gives a highly specific, sensitive chemical analysis, while eliminating extensive sample preparation

8.1.1. Androgenic Anabolic Steroids (AAS) in Doping.

Biological samples, being complex isomeric mixtures, tend to present unique challenges for analytical processing and analysis. Anti-doping challenges extend past the presence of endogenous, naturally occurring isomers, where designer drugs, synthesized specifically to circumvent abuse controls also contribute to making the determination of 'doped' levels hard to establish. The World Anti-Doping agency (WADA) produces a yearly list of restricted compounds.[19] The list of target analytes for the current work is sourced from Category S1: Anabolic Agents, where 23 Androgenic steroids were chosen; includes endogenous and exogenous steroids and synthetic mimics

8.1.2. Anti-Doping: Blood vs Urine.

In anti-doping the debate of Blood versus urine is ongoing. Urine due to ease of collection gained early traction over blood. Blood being considered more invasive, requires international medical guidelines to be followed, limiting sample availability versus urine which does not need to follow the same rules. But with advancements in instrumentation and data processing over the years, urines simplicity now limits the possibilities. A new push towards overcoming the analysis and collection issues associated with blood has been fueled because only blood offers the possibility for a biological signature of doping, only blood contains the information and potential for use in -omics type studies, to offer a true bio fingerprint for genuine monitoring.

A major drawback of blood sampling remains, a hematocrit (Hct)-based volumetric difficulties having compound-specific impacts on quantitative analysis and presents a difficult challenge. Specifically, the analysis of Dried Blood Spots (DBS) has been well investigated via HPLC and GC through offline extraction techniques and Online SFE-SFC has been shown to be a legitimate alternative for the analysis of disease biomarkers in dried serum spots and potential for use in large-scale screening.[86]

8.1.3. Method Development for Online Extractions.

Method development (MD) for online extractions is a multistep process, involving four main steps:

1. **MS-based detection optimizations**
2. **SFC-based separation optimizations**
3. **SFE-based extraction optimizations**
4. **Matrix-specific optimizations**

The methods used in the current work, for detection (via MS, step 1), chromatographic separation (via SFC, step 2), and extraction (via online SFE, step 3), were optimized in previous development steps of the online MD process. The work presented in this chapter, involves the matrix-specific extraction optimizations (mainly step 4) in the development of a hyphenated method for the online extraction of anabolic agents from dried blood spots for anti-doping analysis (**Figure 127**). Online extractions are performed using the pre-developed SFE-SFC-MS method to

evaluate the complexities of the sample matrix. Targeted anabolic agents were extracted online from bovine and human whole blood. Single donor whole blood was sampled using a micro-spotting technique. Whole micro-dried blood spots (micro-DBS) were directly analyzed via online SFE-SFC-MS extractions performed using 0.2-mL extraction vessels.

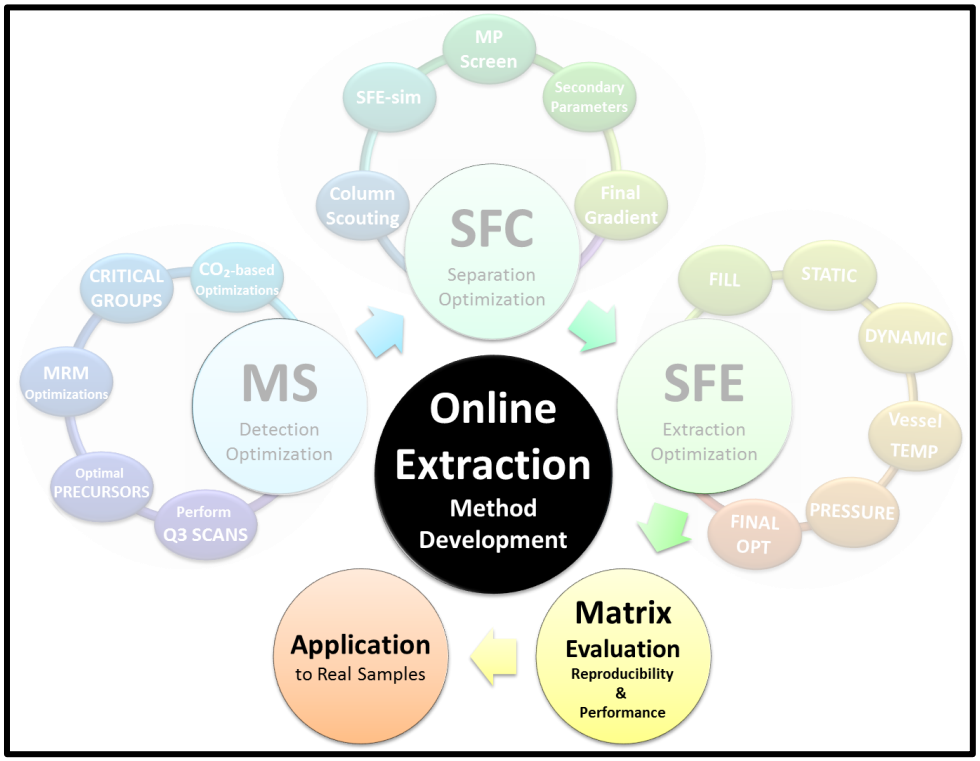

Figure 127. Online Extraction Method Development Focus for Chapter #8 Matrix-Specific Optimizations using Application Specific Quality Controls Relevant to Direct Comparisons with Real Samples.

8.2. System Configuration.

The Shimadzu Nexera UC™ Online SFE-SFC-MS System shares a solvent delivery system. Sample is introduced to the system either via the online extraction loop or optionally can be used as a standard SFC-MS system (via automated liquid sampler/injector). The system is equipped with a column oven, and an additional solvent pump to facilitate delivery of the effluent for detection by a triple quadrupole mass spectrometer. In the current work, the instrument was used in SFE-SFC-MS mode for splitless online extractions for use with 0.2-mL extraction vessels (**Figure 128**). The sample is delivered via an online extraction loop, where facilitated by two switching valves, samples are extracted online and the resulting 'extract plug' is delivered to the column for online analysis.

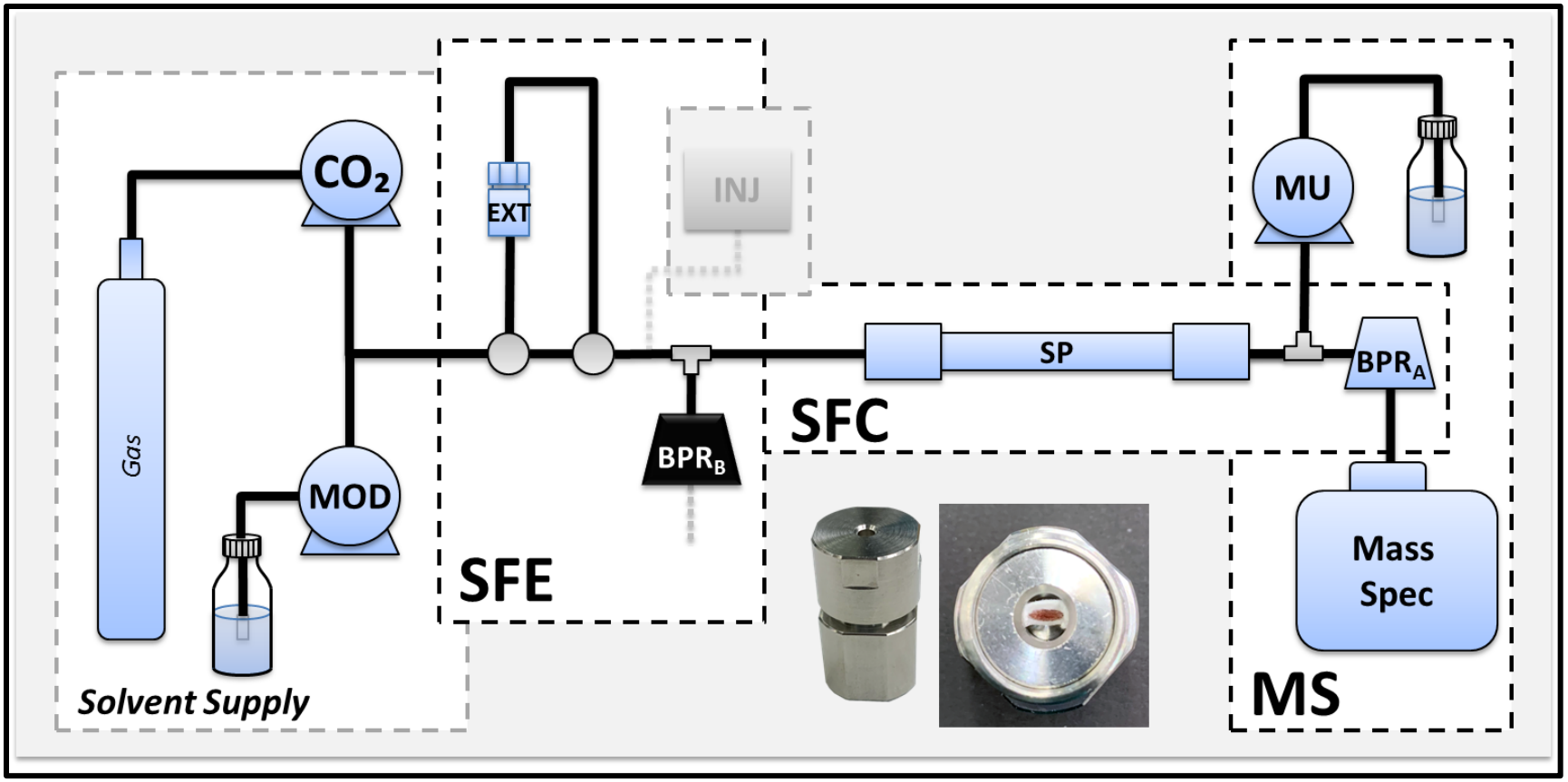

Figure 128. Nexera UC SFE-SFC-MS Instrument Configuration for Splitless-mode Online Extractions using 0.2-mL Vessels.

8.2.1. Automated Sampling for Online Extractions.

The extraction unit can be equipped with a rack changer to allow for the automatic processing of up to 48 samples. The use of 0.2-mL vessels adds flexibility to the extraction method development process, allowing for split or splitless delivery of the extraction plug onto the column. Requiring a much smaller sample volume, having all effluent being delivered directly on column provides high sensitivity analysis. Samples are loaded directly into vessels without the need for an additional filling medium. Although care should be taken when using fine powders. Supplementary filters are available to work with these more challenging samples. The Nexera UC online SFE-SFC-MS is well suited for dried blood spot analysis, allowing rapid screening or method expansion for newly regulated steroids in anti-doping analysis

8.2.2. Online Extraction Process; Loading of the sample Plug.

Using 0.2-mL vessels, requires significantly less sample volume when compared to 5.0-mL vessels, and does not require system splitting. A sample is loaded into a small the vessel and extracted online. The four major steps of an Online SFE-SFC-MS method are shown in **Figure 129**, and include: Vessel Filling, Static extraction, Dynamic Extraction and finally Analysis.

1. Vessel Filling. Mobile phase enters the extraction loop and fills the empty (i.e., 'solvent-less') vessel containing the sample, exposing it to the extraction solvent.

2. Static 'Passive' Extraction. The flow path does not change from vessel loading. The sample (now exposed to fill solvent), is left for a duration of time, allowing for 'passive' extraction.

3. Dynamic 'Active' Extraction. The extraction valves direct the system flow directly thru the extraction vessel. As solvent flows thru, the 'extract plug' is carried along with the system flow being delivered to the column. The MP is allowed to continue to flow thru the vessel for a period of time, 'actively' extracting from the sample and adding to the 'extract plug' retained at the head of the column.

4. Analysis. A extraction valves bypass the extraction loop, directing all system flow on column and the chromatographic method is started.

Immediately proceeding each analysis the system vents the pressure to complete a wash of the extraction loop before the system is reset for the next run.

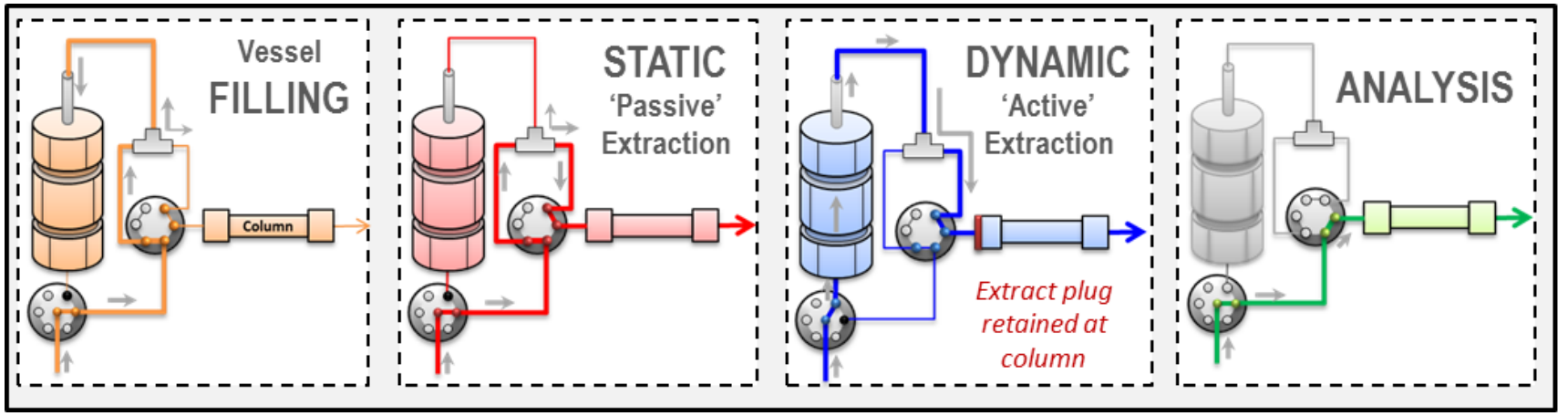

Figure 129. Extraction Process using 0.2-mL Vessels

8.3. Pre-developed SFE-SFC-MS Method.

8.3.1. MRM Optimization & Critical MS-Groups.

Individual stock solutions were used for MRM optimizations, using the LabSolutions 'optimize MRM event from product ion search' function. Resulting Optimized MRM transitions are presented in **Table 42** and optimal detection conditions are mirrored at the end of this chapter in **Section 8.i.3.2. MS Method Parameters –MRM method**. Targeted analytes were individually reinjected using the optimized MRM method. Structures for each analyte are given in **Figure 130**. Steroids that produced signal for two or more MRMs were grouped as 'critical pairs', which would require chromatographic separation. Resolution of critical pairs are used throughout the work presented to evaluate chromatographic method performance.

(detailed discussion of MS-optimizations are presented in **Chapter #3. MS-Detection: MRM Optimizations** and **Chapter #4. MS-Detection: Q3 Scans**).

8.3.2. Pre-Optimized SFC-MS Method for AAS separation.

Fourteen stationary phases were screened. Various separation parameters were evaluated for the two best performing columns, with SFC injections using 1.0 µL of a steroid mixture (AAS-mix). Screened parameters included modifier concentration and additives, column temperature and system backpressure. (optimal separation conditions are mirrored at the end of this chapter in **Section 8.i.3.3. SFC Method Parameters – optimized method**) .

(Detailed discussion can be found in previous chapters: Column screening/SFE-simulation was discussed in detail in **Chapter #4. Column Selection for Online Extractions** and Separation optimizations discussed in **Chapter #5. SFC-Separation Optimization**)

8.3.3. Pre-Optimized Method for Online Extraction of AAS

Various extraction parameters were screened using analytical standards of targeted analytes spiked on to blank Whatman sample collection/preservation cards. The same mixture of anabolic agents was used for SFE-optimizations as used in all previous work. A 1.0µL aliquot of the AAS-mix was applied to the paper, allowed to dry

and cored using a standard hole punch (producing a 6mm core). SFE Screened parameters included modifier concentration during vessel filling and static extraction, Static and dynamic extraction duration, extraction vessel temperature, pressure and flow rate. The final optimized method produced extractions with a total runtime of 26.5 minutes. This includes a 1 min vessel loading at 10% Modifier, followed by a six minute static extraction (at 0% modifier) and 0.8 minute dynamic extraction (also at 0% modifier), and finally the 10 minute SFC-MS analysis via gradient elution. The online extraction and analysis is followed by a 5 minute column wash at 40% B along with a 3 minute wash of the extraction unit follows each extraction (optimal extraction conditions are mirrored at the end of this document in **Section 8.i.3.5. Instrument Methods: Optimized Online SFE-SFC-MS Extraction Method**).

(Detailed discussion of screened extraction parameters and optimal conditions can be found in the previous **Chapter #6. SFE-Optimization for Online Extraction of AAS).**

Table 42. MRM Details for the Online Extraction of Targeted Anabolic Agents (AAS) listed by Peak elution order

			Precursor			Product Ion							
			MW	+/-	(m/z)	Transition 1	(Q1/Q3 Bias, CE)	Transition 2	(Q1/Q3 Bias, CE)	Transition 3	(Q1/Q3 Bias, CE)	Transition 4	(Q1/Q3 Bias, CE)
Peak	Steroid	ID				(m/z)	([V]/[V], [eV])	(m/z)	([V]/[V], [eV])	(m/z)	([V]/[V], [eV])	(m/z)	([V]/[V], [eV])
[1]	7-Keto-DHEA	KETO	302.2	+	285	81	(-22/-32, -27)	79	(-20/-30,-44)	107	(-20/-20,-27)	149	(-20/-26,-21)
[2]	Mestanolone	MSAL	304.4	+	305	269	(-20/-28, -16)	229	(-20/-24,-20)	159	(-20/-34,-23)	187	(-20/-36,-22)
[3]	1-Androstenedione	1STEN	286.4	+	287	97	(-20/-20, -22)	109	(-22/-22,-24)	79	(-20/-30,-46)	109	(-20/-40,-35)
[4]	Androsterone	ADEN	290.4	+	273	255	(-20/-26, -14)	147	(-22/-32,-21)	199	(-22/-20,-21)	161	(-20/-36,-20)
[5]	Etiocholanolone	ETIO	290.4	+	273	255	(-20/-28, -12)	215	(-20/-42,-17)	105	(-20/-20,-35)	91	(-20/-38,-43)
[6]	Mesterolone	MSEL	304.4	+	305	269	(-22/-28, -17)	173	(-20/-40,-24)	287	(-22/-30,-16)	133	(-24/-22,-28)
[7]	1-Androsterone	1DHEA	290.4	+	291	273	(-20/-30, -10)	255	(-15/-26, -15)	135	(-20/-28,-20)	91	(-22/-36, -10)
[8]	Prasterone [DHEA]	PRST	288.2	+	271	253	(-20/-26, -12)	213	(-22/-46,-15)	213	(-20/-40,-17)	157	(-20/-32,-22)
[9]	Methyltestosterone	MTHY	302.5	+	303	109	(-22/-20, -28)	97	(-20/-20,-26)	97	(-22/-20,-27)	285	(-22/-30,-16)
[10]	Mibolerone	MIBL	302.5	+	303	271	(-22/-30, -12)	285	(-22/-20,-17)	121	(-22/-24,-25)	-	-
[11]	Epitestosterone	EPIT	288.4	+	289	109	(-20/-20, -24)	97	(-22/-38,-25)	79	(-22/-30,-44)	253	(-22/-26,-18)
[12]	Danazol	DNZL	337.5	+	338	148	(-24/-30, -25)	91	(-26/-32,-55)	120	(-24/-22,-28)	310	(-24/-32,-20)
[13]	Testosterone	TSTO	288.4	+	289	109	(-22/-20, -25)	97	(-22/-36,-22)	253	(-22/-28,-17)	79	(-22/-28,-46)
[14]	Oxandrolone	OXAN	306.4	+	307	289	(-22/-30, -12)	271	(-22/-30,-14)	121	(-22/-22,-24)	229	(-24/-24,-18)
[15]	Methandienone	METD	300.4	+	301	121	(-22/-46, -28)	149	(-22/-26,-15)	283	(-22/-30,-11)	121	(-22/-22,-24)
[16]	Metribolone	MTRB	284.4	+	285	227	(-22/-24, -23)	267	(-20/-28,-17)	198	(-22/-20,-30)	159	(-20/-30,-23)
[17]	Gestrinone	GSTN	308.4	+	309	241	(-22/-26, -23)	199	(-24/-40,-32)	291	(-24/-20,-16)	262	(-22/-28,-21)
[18]	Zeranol	ZRNL	322.4	-	321	277	(34/28, 23)	303	(36.0/20,22)	259	(36.0/26,24)	235	(36.0/28,24)
[19]	Trenbolone	TRNB	270.4	+	271	253	(-20/-26, -19)	199	(-20/-20,-22)	165	(-20/-36,-56)	128	(-20/-26,-57)
[20]	Stanozolol	STNZ	328.5	+	329	81	(-24/-30, -51)	95	(-24/-20,-42)	121	(-24/-22,-37)	107	(-24/-20,-41)
[21]	Clenbuterol	CLNB	277.2	+	227	203	(-32/-36, -16)	259	(-20/-26,-10)	132	(-20/-24,-28)	168	(-20/-32,-28)
[22]	Andarine	ADAR	441.4	+	442	108	(-32/-20, -37)	208	(-32/-20,-21)	190	(-32/-20,-25)	148	(-32/-32,-31)
[-]	Androstanolone	ADON	290.4	+	291	255	(-11/-12, -16)	173	(-10/-18,-21)	227	(-10/-23,-10)	-	-

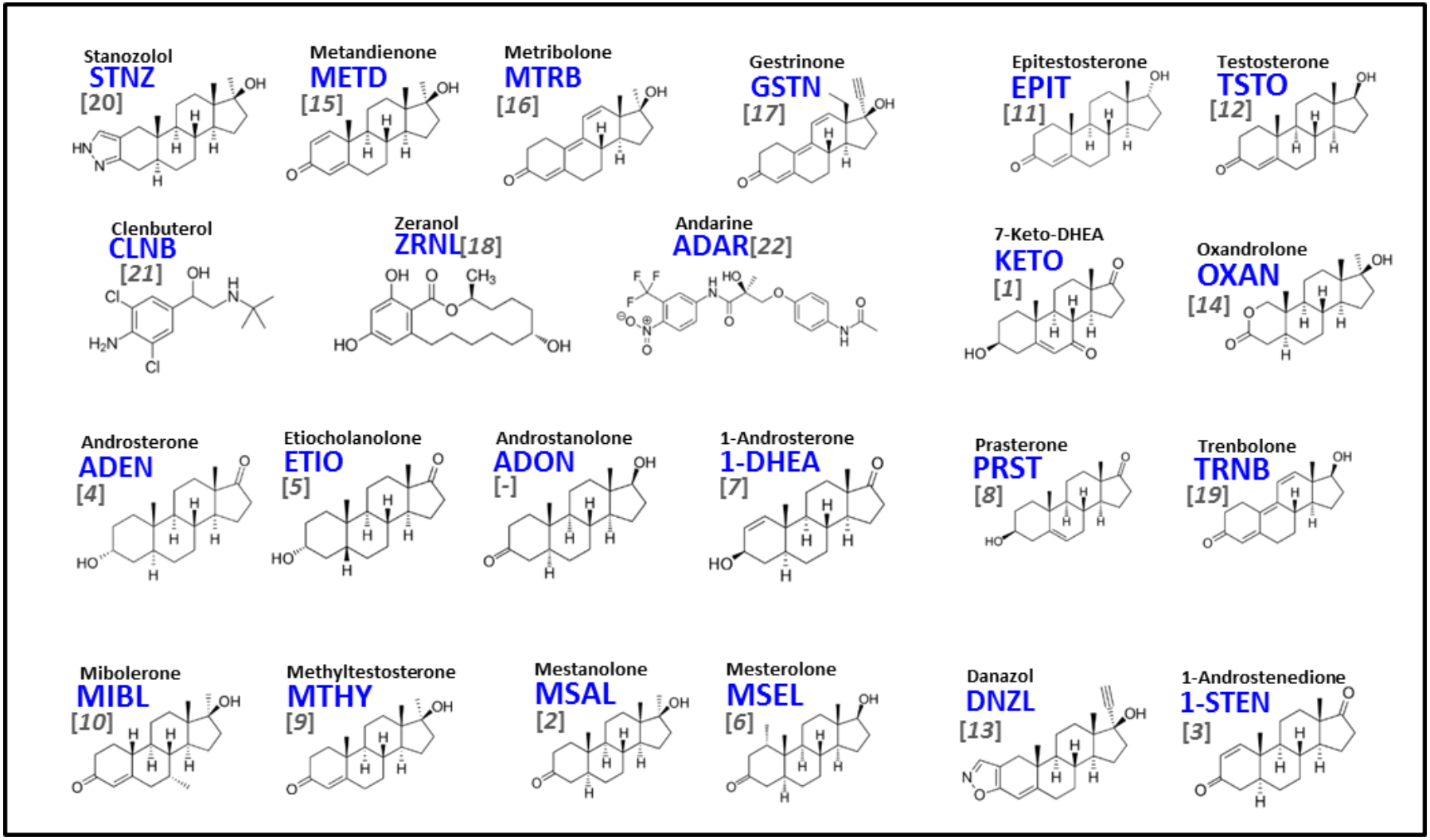

Figure 130. Structure of Targeted Anabolic Agents (AAS) numbered according to elution Order

8.4. Blood Sampling and Hematocrit Issues.

The whole concept of dried blood spots (DBS) is meant to be 'convenience'. Blood is collected in the field, and applied to a sample collection card, where it is preserved, and can later be sampled in an appropriate laboratory setting. Unfortunately, that seems to be where the convenience ends, as current standard methods of analysis, tend to be elaborate multi-step processes, riddled with complications and issues.

Since online extractions minimize sample preparation, no sample cleanup pre-analysis is performed. So for online extractions, to ensure evaluations are relevant when applied to real samples, it's important to understand the sample matrices and what challenges are faced specific to each application. Therefore, for online methods, there is more emphasis on the need for relevant reference materials and controls. As in many applications, considerations extend beyond the complexity of the sample matrix, and the collection materials need to also be considered. In DBS, blood sampling is commonly accomplished via cellulose-based collection cards. These cards are chemically treated and contain a preservative. These chemicals protect samples from oxidation and UV damage, lyse cells, denature proteins and protect nucleic acids from nucleases. Whatman FTA cards rapidly inactivate organisms, prevent the growth of bacteria and other microorganisms, allowing for long-term storage/archiving of samples.

It is important to understand not only how well the online method can extract from this material, but also what kind of background this will contribute. Therefore, the overall goal was to get a blank matrix, for optimization of the extraction of the analytes, by directly spiking the standard solutions. This also introduces the solvents the standards are dissolved in, which can also contribute and/or have secondary effects on the extractions. So not only do relevant controls need to be developed to effectively evaluate the methodologies, but also need to make sure that these are appropriate, to enable direct comparison to real samples. To accomplish this the challenges inherent to the sample matrix must be understood. In the case of DBS, there are hematocrit-based sampling issues, that introduce bias and make sampling non-volumetric. Hematocrit (Hct) refers to the volume of red blood cells in the total volume of blood. There are two types of Hct based biases: area bias and matrix bias.

Area bias is a physical consequence of blood viscosity, from whole blood spreading over cellulose-based cards. Where lower hematocrit spreads more across the card, giving less concentrated samples.

Matrix bias. two samples of different hematocrit levels can be considered as different matrices leading to recovery and precision effects (e.g., lower recovery at higher Hct).

Overall, the impact of Hct-bias is compound specific and internal standards (IS) are ineffective in correcting for these issues and ultimately Hct-adapted volume factors are mandatory for analytical analysis of DBS.[87],[88] Many solutions have been proposed; spray-on IS, plasma isolation, quantitative cards, and volumetric application plus coring, among the most common.[89] Isolation is the preferred industry method for blood testing, due to simplicity of non-volumetric whole blood collection in the field. But this utilizes plasma isolation cards, which quantitatively filter a set amount of plasma from the applied blood thru a membrane. These cards are very expensive, costing around $8.50 per spot, which makes them impractical for method development purposes.

On the other hand, Whatman cellulose-based sample collection cards, cost only $2.50 per blood spot. Additionally, each spot can be cored multiple times, being very cost efficient for the development of methods. Furthermore, cellulose-based cards have a wider applicability range, and can be used with urine, blood, plant and tissue samples. Meaning, developed methods for the extraction of a specific set of analytes from these cards could be applied to multiple biological applications.

Two approaches can be taken for sampling of blood with cellulose-based collection cards. In one approach, blood is applied non-volumetrically, and using a 1.2 mm punch, a small portion of the card is volumetrically obtained. The non-volumetric blood application appeals to the testing industry, but area bias is clear, take for example the compressed spot shown in **Figure 131**, a core from the center would give lower concentration versus sampling from the outer more concentrated ring. The alternative is volumetric blood application. Although unpopular on the blood collection side in the industry, this method is more common to lab-based studies. One form of volumetric application involves the miniaturization of spots. By utilizing smaller volumes we developed a micro-sampling technique.

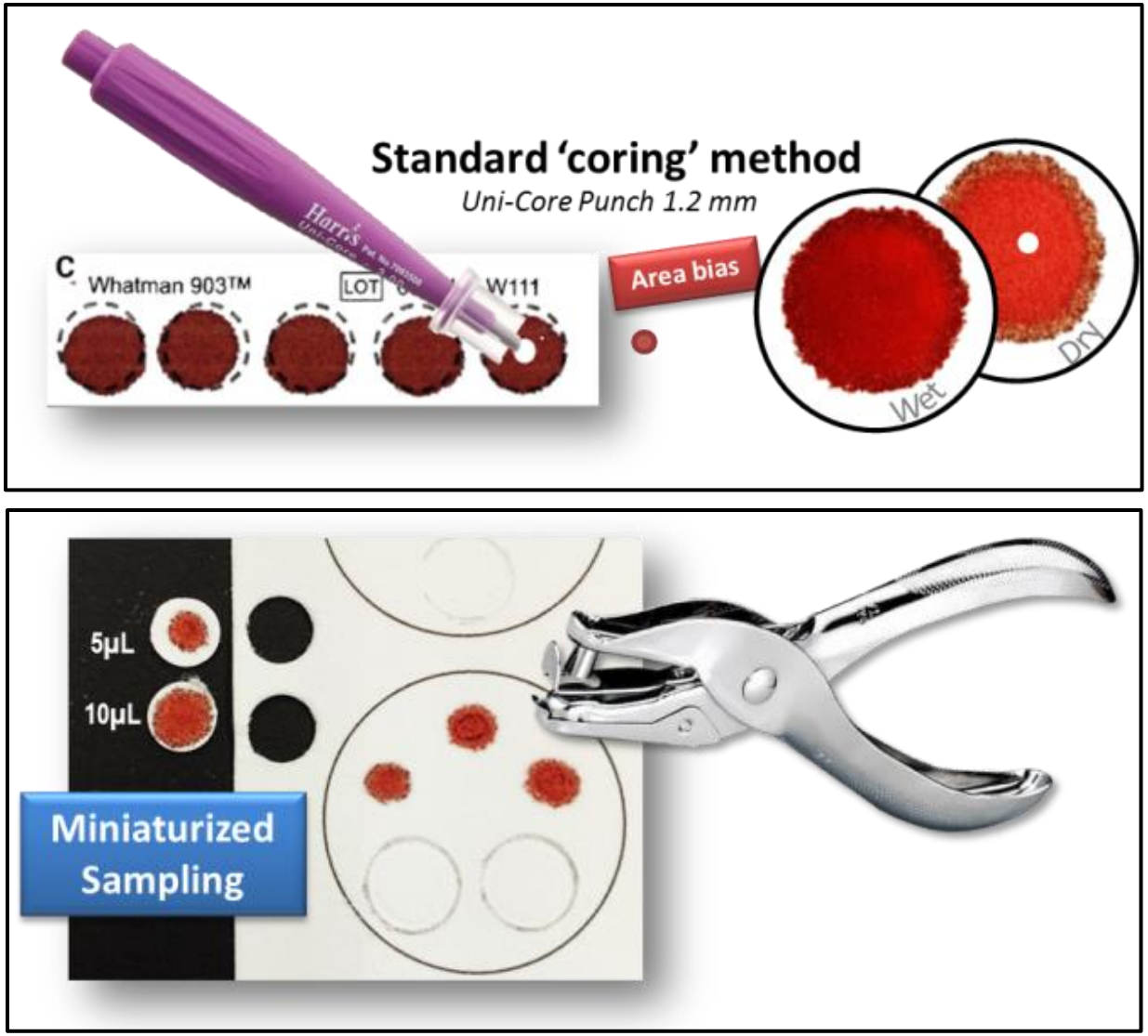

Figure 131. Blood application techniques for Cellulose-based cards. (top) Standard blood spots on Whatman collection card (reproduced from Wilhelm, den Burger & Swart, 2014 [90]), pictured with 1.2 mm Corer and standard-DBS pre- [wet] and post-drying (produced during spot volume testing in the current work); and **(bottom) Miniaturized blood spots**, volumetric application and coring used in the current work.

8.5. Sample Preparation: Micro-DBS Sampling Technique.

For blood sampling, a micro-spotting technique was implemented. This was beneficial in overcoming the variability inherent to blood sampling due to differences in hematocrit between donors. As the entire sample (whole spot) was excised from the card and placed directly into an extraction vessel. Using a standard single hole punch, produces 6 mm cores of the entire miniaturized dried blood spot (micro-DBS) and allows quantitate application and collection. Further Volume tests using the solvents (*pictured in some figures with red or blue food coloring added for visualization of solvent spread on the card*), allows verification that the QCs will also be within the diameter for the punch. Using this technique has an added benefit, since both the samples (micro-DBS) and QCs (micro-QCs) can be applied to the same card, which allows for confirmation of inter- and intra-card reproducibility.

8.5.1. Determination of Spotting Volume.

An added benefit of this technique is that samples and QCs can be applied and collected from a single card. As long as the diameter of the spot did not exceed the diameter of the hole puncher (a standard 6mm single hole punch was used in the work presented here), volumes could later be calculated directly from the volumetric application. Blood was applied at 1, 2, 5, 8, 10 and 25 µL aliquots to cellulose-based standard sample collection/preservation cards (**Figure 132**). The largest volume that created a spot with diameter < 6 mm was chosen. Both 10 µL and 5 µL of blank blood did not exceed the 6 mm punch size. But MeOH was observed to spread farther on the card than blood (methanol shown with red food dye added to show spread on card). Therefore, a 5 µL blood spotting volume was chosen, enabling ample excess blank paper to surround each spot, so that when MeOH was added (for spiked and blank quality controls) it would not exceed the punch size sampling area.

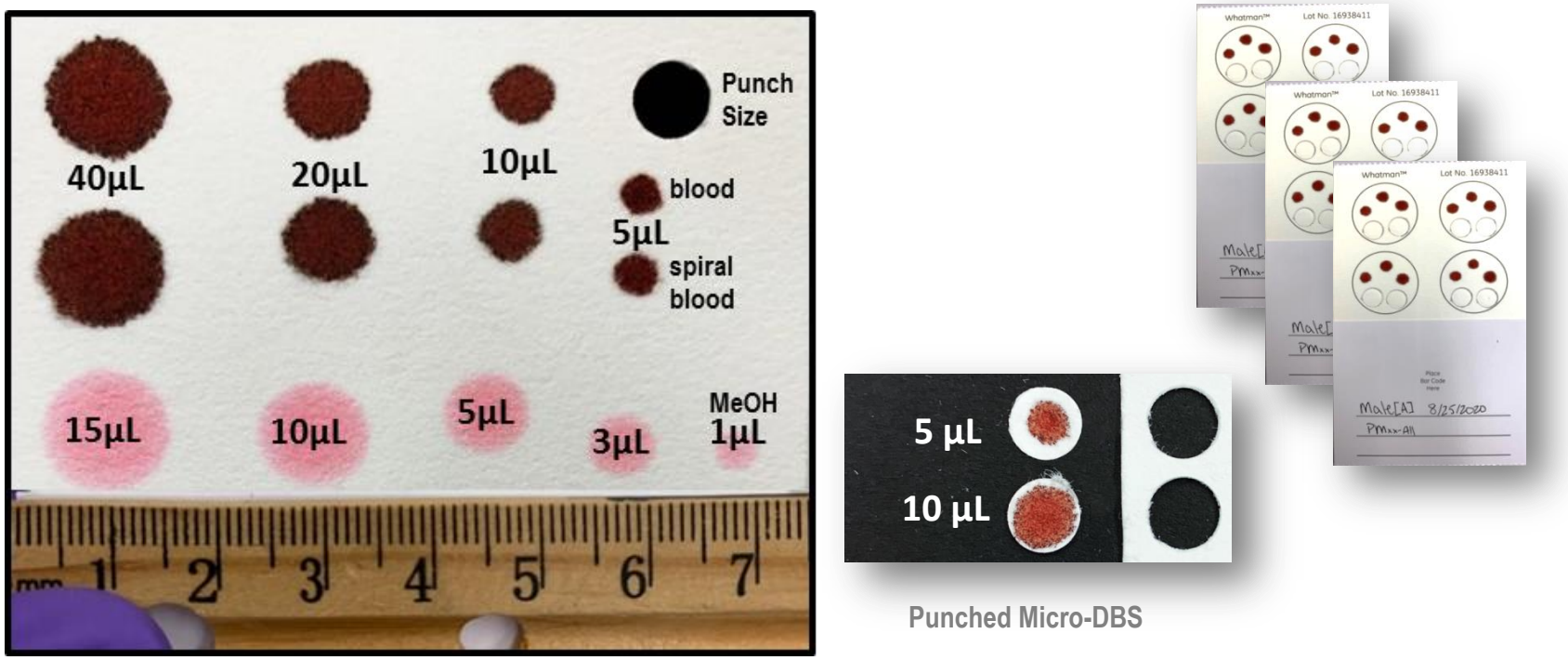

Figure 132. **Determination of spot application volume** ***(shown after 24 hours drying, methanol shown with Red food coloring added)***

8.5.2. Sampling Approach.

Whole Blood: Single donor, human (male and female), and bovine (Grade US origin) was used. All blood the same anticoagulant was requested from the vendor. Sample Collection cards used were Whatman FTA Classic /preservation cards. Three types of single donor, whole blood were used: bovine (Grade US origin [**PB**]), human female [**PF**] and human male [**PM**]. Three replicate cards were created for each blood (Card **A**, **B** and **C** for bovine; Cards **D**, **E**, and **F** for male; and Cards **G**, **H**, and **I** for female). On each card, four replicate spots (spot **a**, **b**, **c**, & **d**) were applied for each spot-type. Six spot-types were used (**Pøøø, PøMø, PøMA, PXøø, PXMø** and **PXMA**). One spot was extracted per vessel.

8.5.3. Spot Types: Quality Controls and Blanks

Blood collection cards contain a preservative, to evaluate potential matrix effects, a blank portion of each card was cored in triplicate (Pøøø) and analyzed for comparison. Additionally, quality control spots (micro-QCs) were prepared in triplicate on each collection card; using 1.0 µL blank methanol with no blood (PøMø), and 1.0 µL of the AAS-mix spiking solution (PøMA). Blanks of each type of blood (PXøø) and blank blood with blank methanol (PXMø) were also used to evaluate potential interferences (**Table 43**).

Spot Types. All spots were collected ('cored') using a standard single hole punch, which produced a 6mm diameter core. The entire spot was excised.

8.5.4. Micro-DBS Analysis Workflow

Dried, punched, micro-DBS and micro-QCs were placed /dropped directly into 0.2-mL extraction vessels and loaded into the automated rack changer for online SFE-SFC-MS analysis (**Figure 133**). The longest step of the sample processing was allowing the blood to dry (at least 3 hours). Blood could be applied to pre-punched spots, allowing immediate processing of applied samples, this would shorten prep time to less than 5 minutes.

Table 43. **Sample Spot Types used for Matrix Optimizations.**

(#) Spot Type	Short Description	Picture**	ID
(0) Null	N/A *(empty vessel)*	-	**øøøø**
(1) Blank Paper QC	6mm Core Blank Paper		**Pøøø**
(2) Solvent Blank QC	1.0µL Blank MeOH applied		**PøMø**
(3) Steroid Standards	1.0µL steroid mix in MeOH (AAS-mix)		**PøMA**
(4) Blood	5.0µL whole Blood		**Pxøø**
(5) Blood : Solvent QC	5.0µL Blood + 1.0µL Blank MeOH*		**PXMø**
(6) Spiked Blood	5.0µL Blood + 1.0µL AAS-mix*		**PxMA**

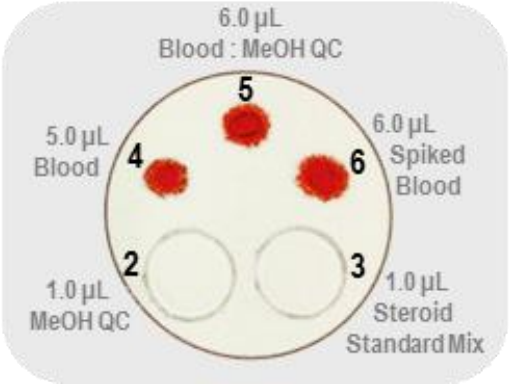

* Spiked spot volume = 6µL = Total volume applied to card of mixture

Mixture = [5:1 Blood:MeOH], 40µL AASmix (in MeOH) in 200 µL Blank Blood

** spot (2) & (3) pictured with ood coloring added for visualization of the spread of the solvent across the spot, to the methanol before being spiked onto the paper

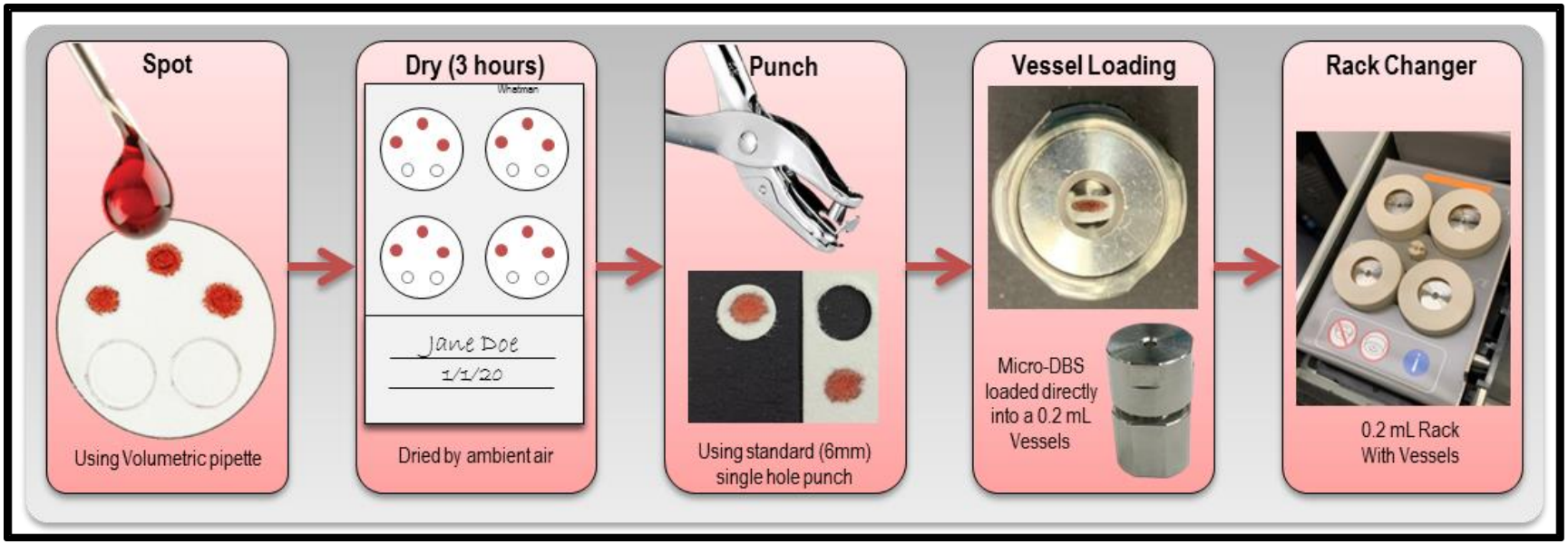

Figure 133. **Micro-DBS Analysis Workflow**

8.6. Results and Discussion: Matrix Evaluations

Micro- Sampling. Three separate cards were prepared for each type of blood (human male, human female and unknown bovine origin). Four spots were applied for each spot type. Cards were allowed to dry for at least 3 hours, before spots were excised, placed into 0.2-mL extraction vessel and loaded into the automated rack changer for online SFE-SFC-MS analysis. Micro-DBS and micro-QCs were compared looking for interfering signals.

8.6.1. Blank-QCs: Blank Paper vs. Blank Methanol Spike (Pøøø vs. PøMø)

To evaluate the background contribution of the sampling materials, cores of the blank paper [Pøøø] were compared to cores spiked with blank-MeOH [PøMø]. Example chromatograms are presented in **Figure 134.**

Extraction of the blank paper produced a characteristic profile. The addition of Solvent had little effect and contributed no additional background signals. Although the card does contribute to nearly every MRM transition being monitored, when overlaying extractions of replicate cores from a single card, little difference across each card was observed, and moreover, overlaying replicate cores from 3x different cards, was also nearly the same across all cards. This means that a single evaluation of the blank-QCs can be applicable to a large sample set.

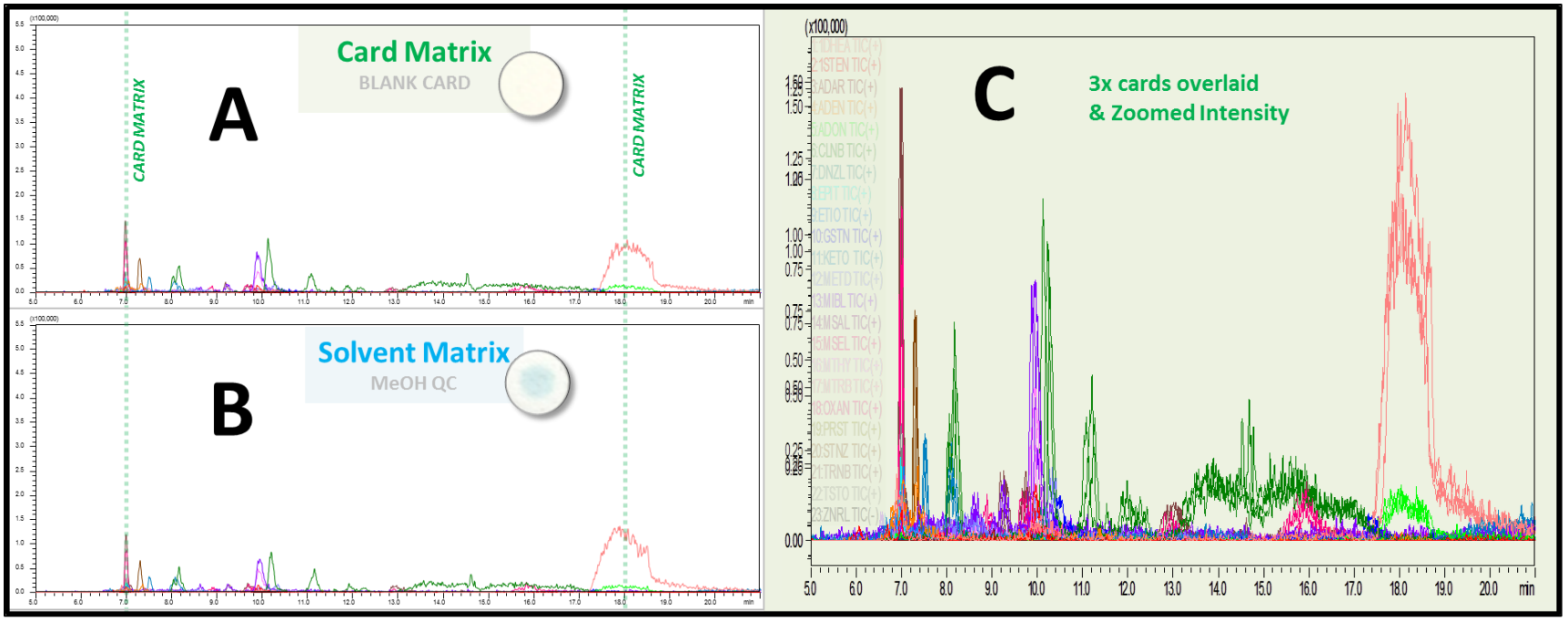

Figure 134. SFE-SFC-MS Online Extractions of Micro-DBS Quality Controls (QCs): [A] Blank Card (6mm core Whatman card, [PøøØ], green]; **[B] MeOH-QC** (6mm Core with 1.0 µL Blank Methanol, [PøMØ], blue); **[C] Overlaid Replicates** Blank Card (3x replicate spots each from a different collection card). **[green dotted lines] highlighting major profile contribution from card matrix.** Chromatograms in A&B displayed at same intensity; C displayed at max intensity.

8.6.2. Background Contribution from the Addition of Blood (PFøø vs. PFMø)

Comparing the blank card cores (above) to cores with blood applied (**Figure 135; A,** Blank Blood [PFøø]), the background contribution from the collection card, as expected, is still present (***green dotted lines***). But the presence of Blood during the extraction, certainly also contributed a background profile specific to the blood ***(red dotted lines)***. Comparing the methanol QC (**B,** Blood:MeOH-QC, [PFMø]), now with the solvent added to the blood, again the solvent had little effect on the extraction profile for the blood. Allowing the focus to be mainly be on the blood extraction. Although very reproducible, even across cards (**C,** [PFøø]). These signals are a quite a bit more significant and so needed to be monitored during further analyses, to ensure they do not interfere with the analysis by comparing each signal to the standards.

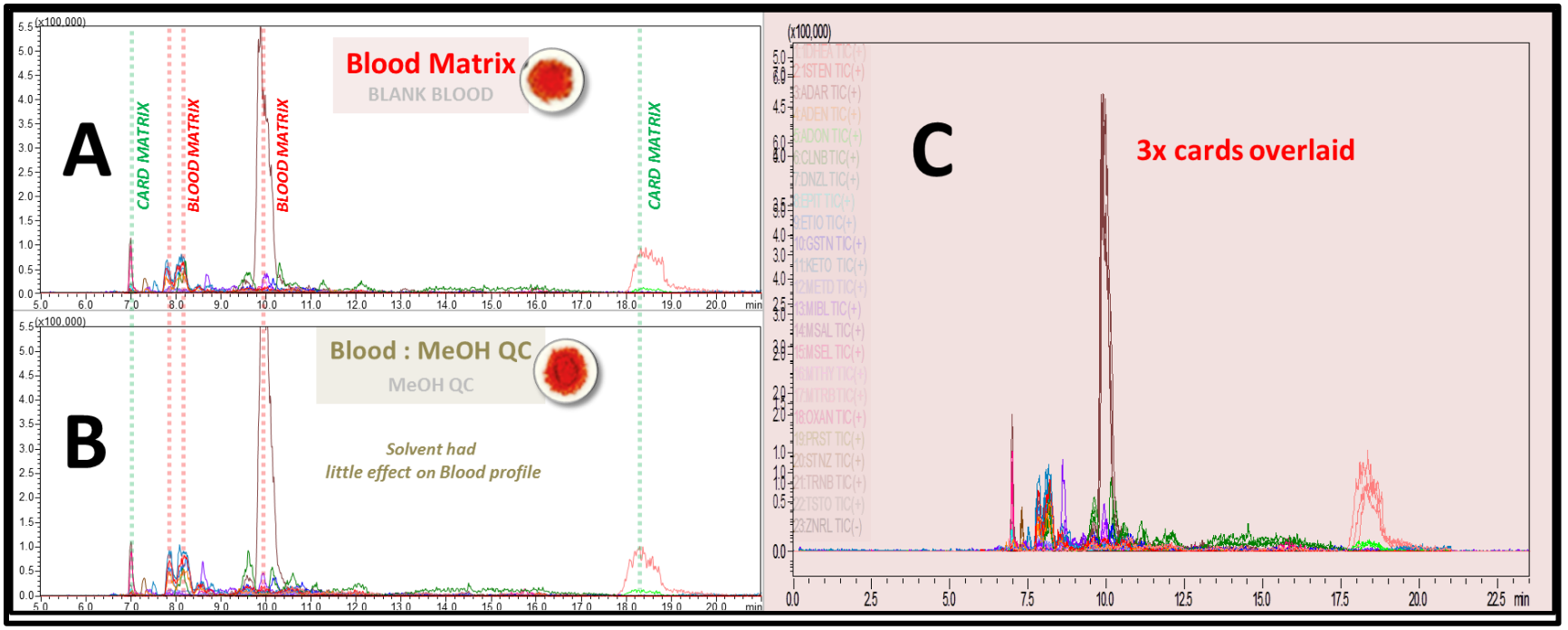

Figure 135. SFE-SFC-MS Online Extractions of Micro-Dried Blood Spots (micro-DBS) Quality Controls (QCs): [A] whole blood Micro-DBS (6mm core Whatman card + 5.0 µL whole Blood, [PFøø], red]; **[B] Blood:MeOH-QC** (6mm Core + 5.0 µL Blood + 1.0µL Blank MeOH, [PøMø], brown); **[C] Overlaid Replicates** PFøø (3x replicate spots each from a different collection card). **Highlighting major profile contributions: from card matrix [green dotted lines] and blood matrix [red dotted lines].** Chromatograms in A&B displayed at same intensity; C displayed at max intensity.

8.6.3. Spiked Standards (PFMA vs. PøMA) Profile

Comparing the spiked blood samples (PFMA) with the spiked standards with no blood (PøMA), overall inter- and intra-card repeatability was quite good. Three replicate spots, each from a different collection card are shown overlaid in **Figure 136; right panel,** for each spot type. Peak area Reproducibility was evaluated by summing the average total area extracted and % RSDs compared for each analyte. Peak area %RSDs ranged from 5 and 15% for PoMA spots and 3- 14% for PFMA spots for intra-card reproducibility (**S_Figure 24**). Both spiked samples, have 1.0 µL of the same steroid mixture (AAS-mix) applied, and therefore theoretically should give the same areas for each analyte when extracted using the same instrument method. But if the MRM overlays are normalized to our standards (**Figure 136; left panel**), a distinct difference can be seen between the spiked standards, and the spiked blood. Where the presence of blood during the extraction, producing lower peak areas.

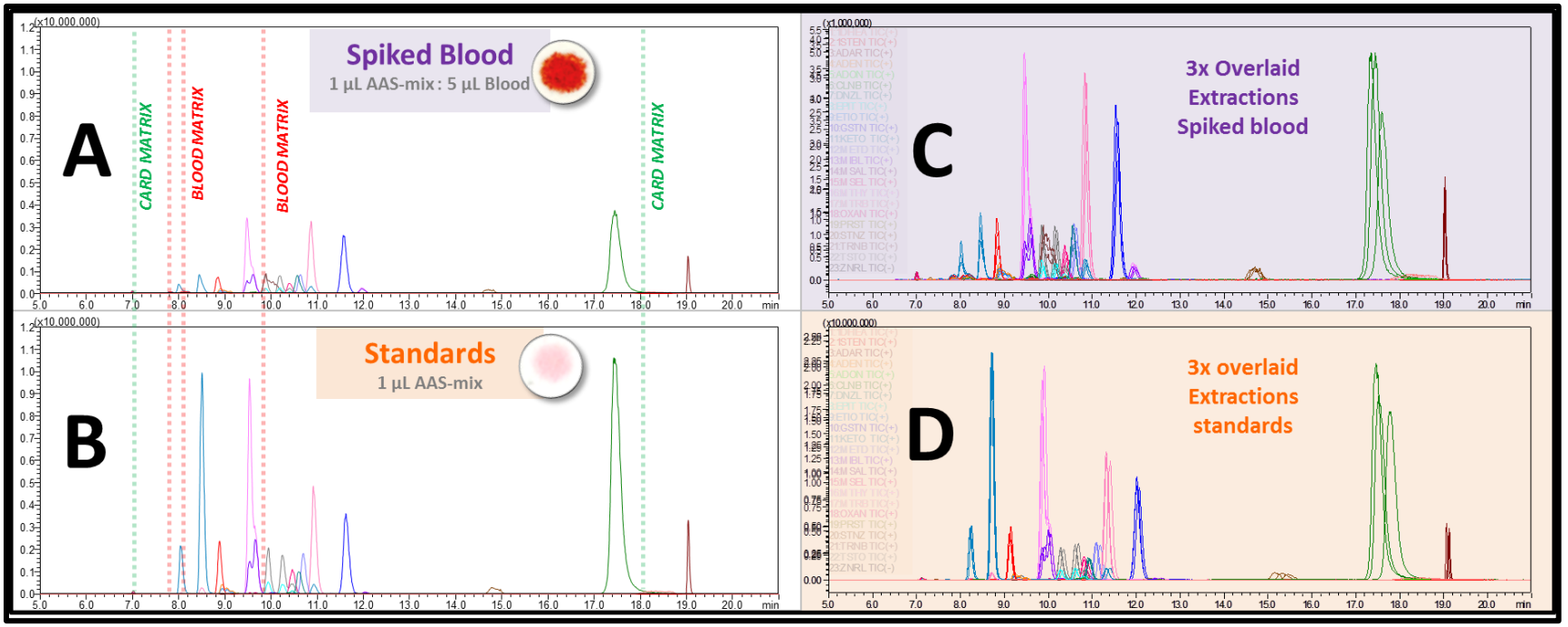

Figure 136. SFE-SFC-MS Online Extractions of Micro-Dried Blood Spots (micro-DBS) Quality Controls (QCs): [A] Spiked Micro-DBS (6mm core Whatman card + 5.0 µL whole Blood + 1.0 µL AAS-mix, [PFMA] **using [PF3A] Human (female); whole blood**, purple]; **[B] Spiked Standards** (6mm Core + 1.0 µL AAS-mix, [PøMA], orange); **[right panel] Overlaid Replicates** (3x replicate spots each from a different collection card) for **[C]** PFMA and **[D]** PoMA.

Total Area Extracted. Direct comparison of the average total area extracted (AV_{total}), lower areas were produced when blood was present for all compounds except STNZ which was not affected by the presence of blood. The majority of the targeted analytes produced 50-90% lower AV_{total} areas when being extracted from blood (**Figure 137**). Four steroids produced less than 50% of the area produced by PoMA: KETO, MSAL, CLNB, and ZRNL. KETO was the only analyte where the presence of blood reduced the extractability below 25% of the standards-alone.

Extraction Performance. Extraction performance was evaluated by extracting each vessel three times, sequentially. Comparing the percent of the total extracted per extraction round (%EXT1 vs. %EXT2 vs. %EXT3), reveals differences in the 'extractability' between materials when extracted under the same conditions. The percent of the total for each extraction round are compared in **Figure 138,** for the spiked standards QC (**[PøMA]; panel A**) and Spiked:blood-QC for female human blood (**[PFMA]; panel B**) from a single collection card.

in extractions of PøMA spots (standards with no blood), percent total extracted was compound specific. Over 85% of the total extractable area (**black dotted line**), was achieved within the first 2x extraction rounds, for all targeted analytes (with the exception of ZRNL). Due to the low concentration and high cost of the initial standard solution, ZRNL was difficult to evaluate at this stage due to dilution. ZRNL will need to be evaluated separately at a later stage. For early eluting compounds over 70% of the total was extracted in the first round extraction, but the addition of blood (spiked standards in whole blood), there was an effect on the extraction performance. Where more extraction rounds are required to extract the same percentage of the total area. About half of the compounds were below 85% extracted in the first two rounds in the spiked blood. So not only less overall is extracted, also the compounds are harder to extract as quickly when the blood is present.

Taking the difference in the percent extracted in the first two rounds (%EXT1+2) between the two sample types we can more clearly see the how much less is extracted (in the 2x extractions) when blood is present (**S_Figure 25**). In percent of the total represented by the first two rounds of extraction ($\%EXT_{1+2}$) for the majority of the steroids, was only 10% less when blood was present. A trend was observed where the more polar compounds % total extracted was even lower being between 10-15% less, which would be expected.

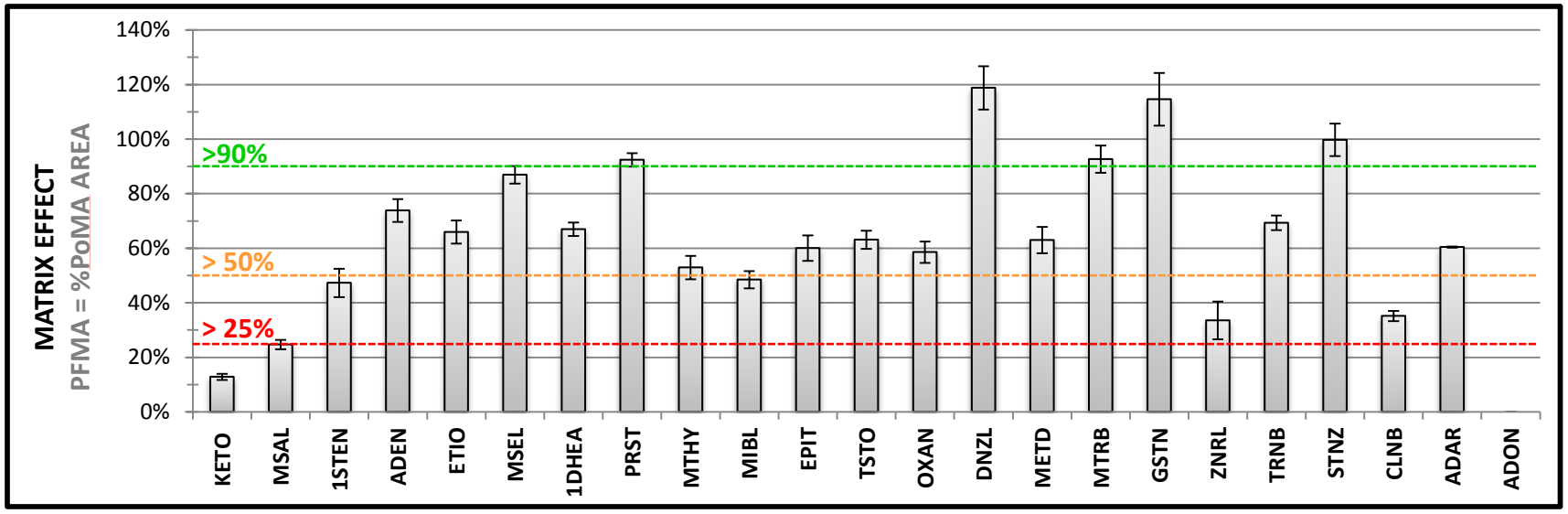

Figure 137. Percent Average Total Area Extracted for Spiked Human (Female) Blood [PFMA] of the Average Total Area Extracted from Standards with no blood present [PoMA]. (n = 3). **Standards [PoMA] spots** with 1.0 µL AAS-mix spotted on whatman collection cards**; versus Spiked Blood [PFMA] 1.0 µL AAS-mix in 5.0 µL of [PF3A] Human (female); whole blood**.

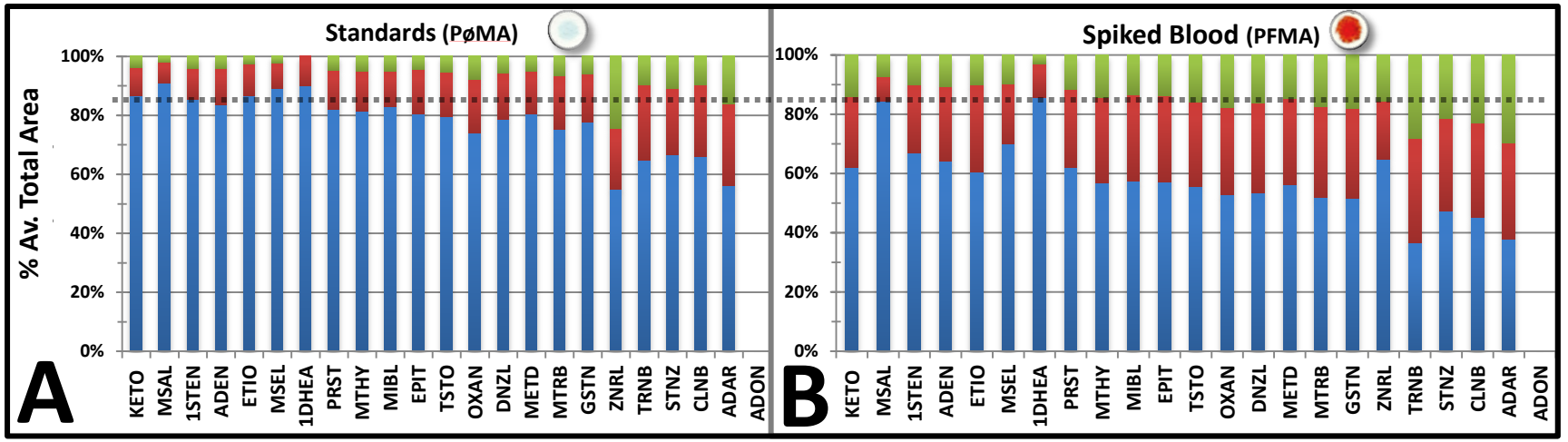

Figure 138. Extraction Performance for Anabolic Agents Extracted Online from Micro-DBS Quality Control Spots (QCs): [A] Spiked Human Female Whole Blood (Spiked:Blood QC, PFMA) **and [B] Spiked Standards with no blood** (AAS-mix QC, PøMA). Showing percent of average total area (AV_{total}) extracted for targeted anabolic agent in three consecutive extraction rounds for each vessel (n=3): **[blue]** first extraction (%EXT1); **[red]** second extraction (%EXT2); and **[green]** third extraction (%EXT3). Black Dotted line = Highlights 85% of the total area extracted.

8.6.4. Investigation for Interfering Signals.

An investigation for interfering signals was performed, comparing online extractions of micro-DBS and micro-QCs, using the spiked blood and the standards as reference. With the signals still normalized to the blank blood, the background profile from the card, and the blood, could be clearly tied to each matrix. All four sample types (Pøøø, PFøø, PBMA, and PøMA), were compared for each individual MRM. Four examples are given in (**Figure 139**). Example signal comparison Ⅲ, shows a relatively large peak on the TRNB-MRM. This peak was observed in extractions from spots that contained blood (i.e., blood matrix), this signal did not coincide with the elution time of the standard, so therefore was determined to be non-interfering.

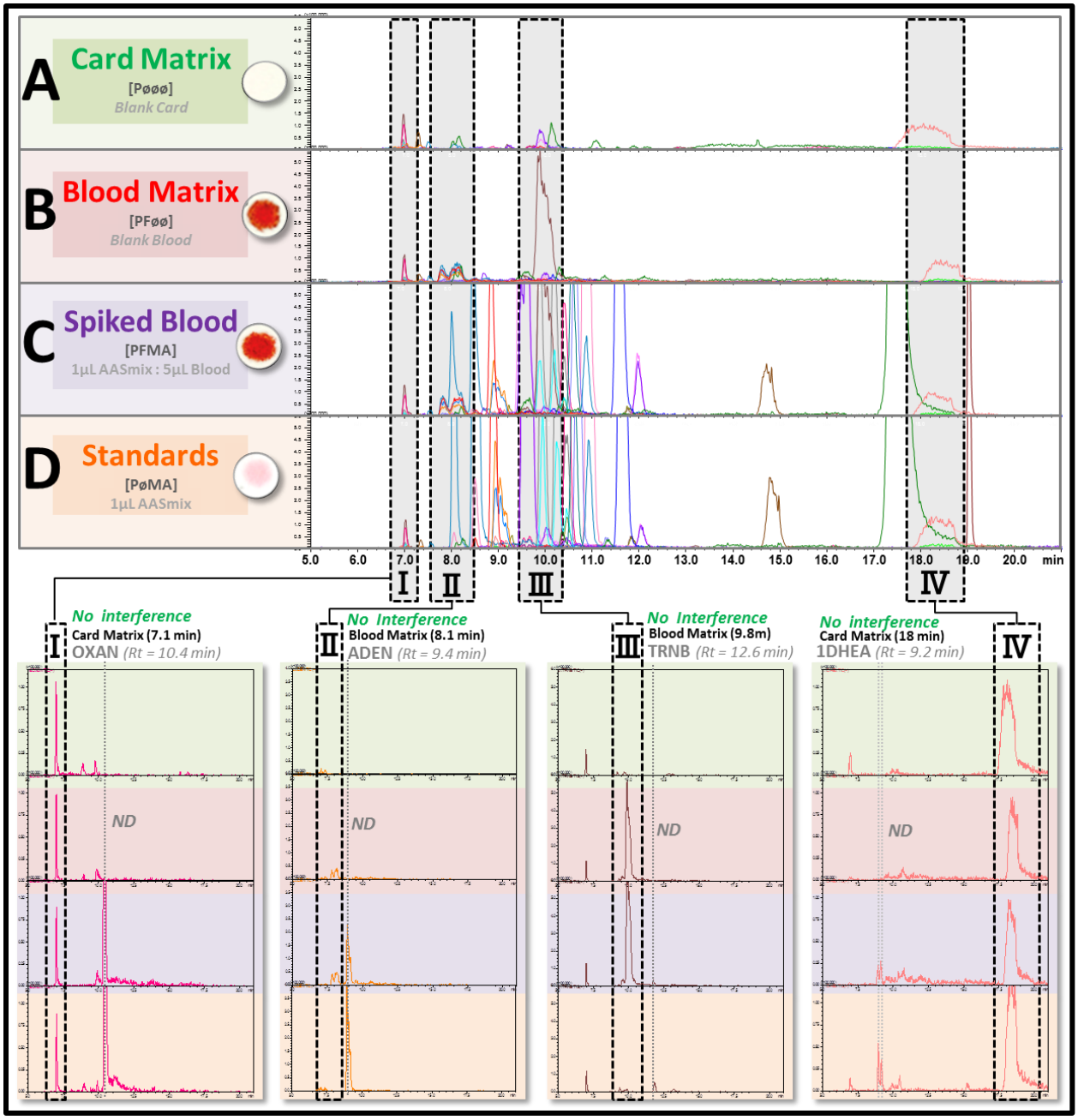

Figure 139. SFE-SFC-MS Online Extractions of Micro-Dried Blood Spots (micro-DBS) Examples of Investigation for Interfering Signals, Comparing Online Extractions of Micro-DBS and Micro-QCs: [A] Card Matrix, Blank Card ([Pøøø], green); **[B] Blood Matrix,** 5.0 µL Blank Blood ([PFøø], red); **[C] Spiked Blood,** 5.0 µL Blood : 1.0 µL AASmix ([PFMA], purple); **[D] Spiked Standards,** AAS-mix ([PøMA], orange) **.**

[Ⅰ] Signal comparison example 1: OXAN-MRM (hot pink), Peak corresponding to Card matrix (7.1 min), OXAN analytical standard (Rt = 10.4 min);

[Ⅱ] Signal comparison example 2: ADEN-MRM (Orange), Peak corresponding to Blood matrix (8.1 min), ADEN analytical standard (Rt = 9.4 min);

[Ⅲ] Signal comparison example 3: TRNB-MRM (Brown), Peak corresponding to Blood matrix (9.8 min), TRNB analytical standard (Rt = 12.6 min);

[Ⅳ] Signal comparison example 4: 1DHEA-MRM (light pink), Peak corresponding to Card matrix (18 min), 1DHEA analytical standard (Rt = 9.2 min).

8.6. Online Extraction of AAS from Dried Blood Spots (micro-DBS).

Triplicate cores were used and three consecutive extractions were performed on each type of spot (i.e., three replicate spots of each type were analyzed [n = 3]).

8.6.1. Bovine Micro-DBS

Extractions were performed on micro-DBS made with bovine blood using the original extraction method. Online extractions are presented in **Figure 140** for spiked (PBMA) and blank (PBøø) bovine blood.

Background Matrix-based Observations for Bovine Blood.

Paper Matrix. A marked increase in background noise was observed on the 1DHEA-MRM, which appears to come from the Whatman paper. Specifically the artifact pk at 17.0 min for 1DHEA-MRM, was seen in all extractions, except the vessel blank. All analytes that give signal for this MRM elute much earlier between 12.0 & 13.0 min and therefore seems unlikely to interfere.

Blood Matrix. A large peak at 12.75 min for TRNB-MRM was seen in all extractions where blood was present. Of the 23 target analytes only TRNB gives signal for its own MRM. TRNB elutes earlier than this artifact at 11.22min.

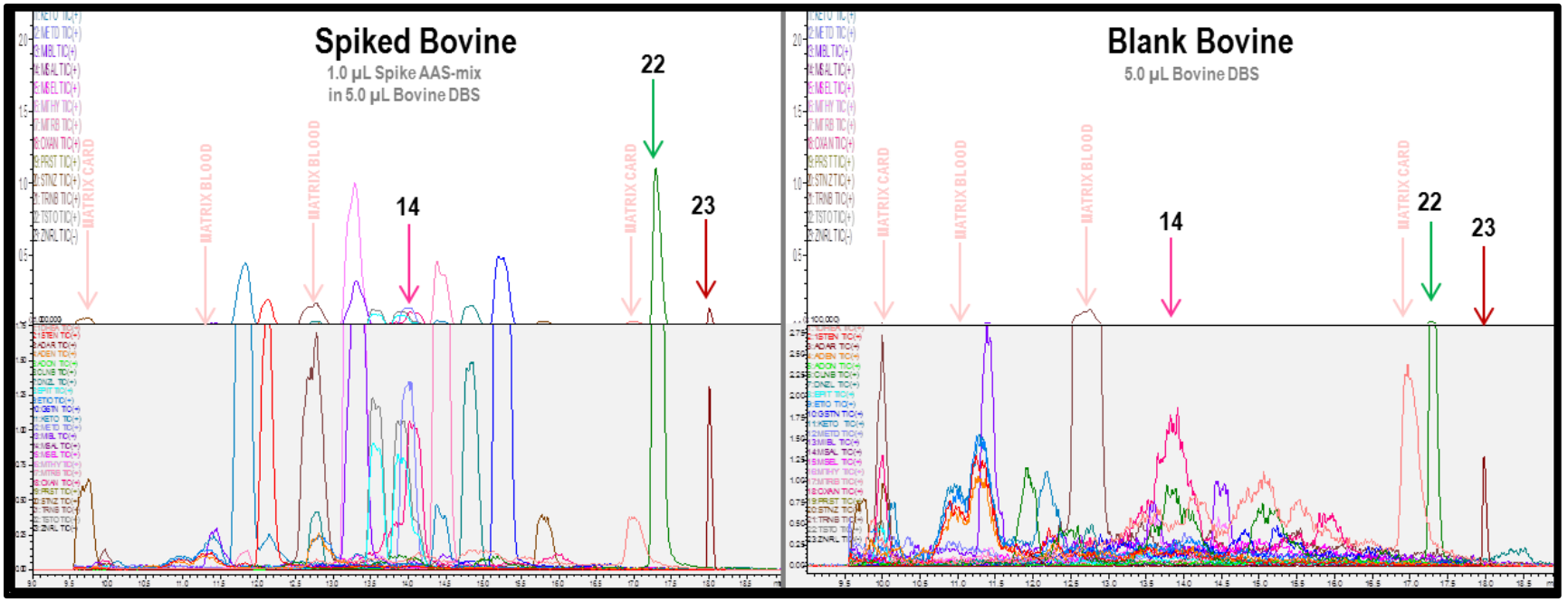

Figure 140. Zoomed SFE-SFC-MS Chromatograms for Online Extractions of Bovine (US-grade) whole blood comparing blank blood to Quality Controls: [A] Spiked bovine blood (6.0 µL spiked blood [1:5 AAS-mix:Blood], PBMA); and [B] Bovine micro-DBS (5.0 µL blank blood, PBøø). (top) Intensity normalized to standard mixture, showing low relative intensity of signal contribution from the card and blood matrices; (bottom) baseline zoomed/normalized to blank card, showing similar signal contribution from card in all extractions. (PB3A).

Spiked bovine blood vs standards alone. All compounds were successfully extracted from spiked bovine blood, except ZRNL was not observed due to the low concentration of the standard. Comparison of % total extracted for three consecutive extraction rounds is compared in **Figure 141.** Percent total extracted in the first two extraction rounds was compound specific and ranged between 66-92%.

Blank Bovine blood. Peaks coinciding with OXAN, CLNB and ADAR were found in the Blank Bovine Blood. Although all three compounds have been reported in bovine blood in the literature. Later, during data processing, issues with the original method become clear that there was an intermittent carryover issue that potentially affected most of the bovine samples. The carry-over issue has been resolved. Further investigation to verify either the presence or absence of these compounds in the blank blood are planned, but have not yet been performed.

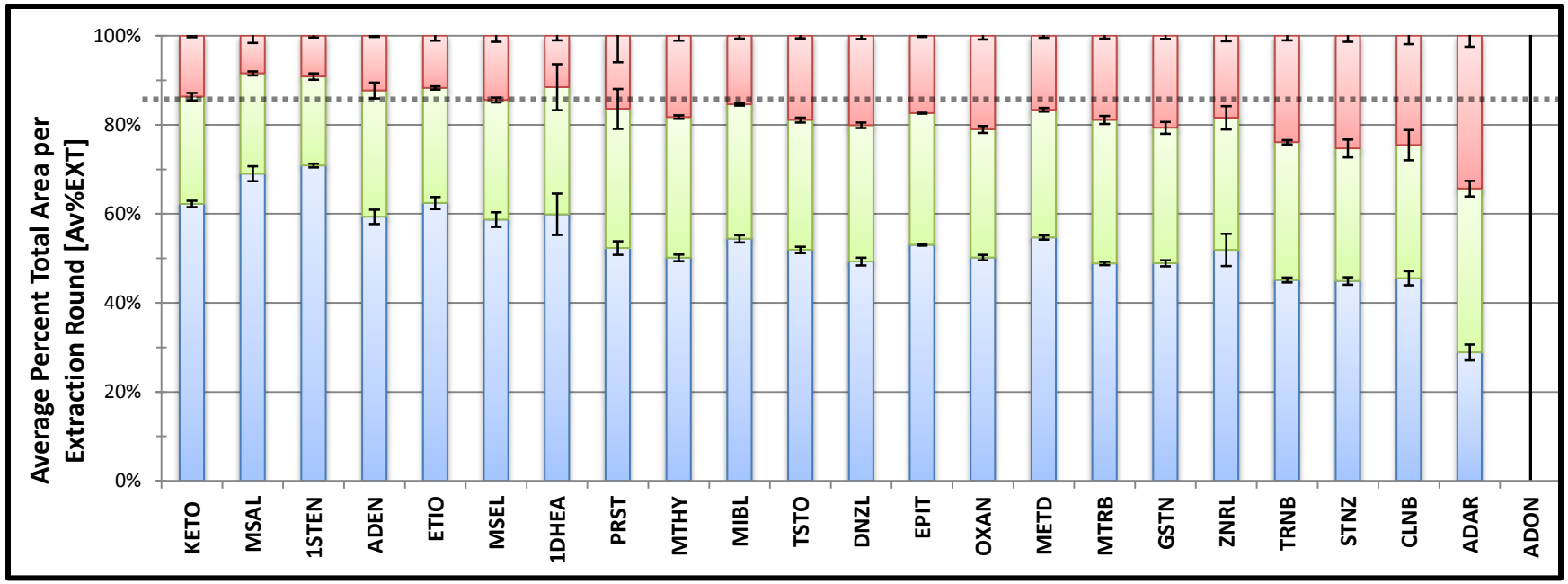

Figure 141. Extraction Performance for Anabolic Agents Extracted Online from Spiked Bovine Micro-DBS: [A] Spiked Bovine Whole Blood (Spiked:Blood QC, PBMA). Showing percent of average total area (AV_{total}) extracted for targeted anabolic agents in three consecutive extraction rounds for three replicate vessels [n = 3]: **[blue]** average produced by the first extraction ($Av\%EXT_1$); **[red]** second extraction ($Av\%EXT_2$); and **[green]** third extraction ($Av\%EXT_2$). Error bars = standard deviation (n = 3). Black Dotted line = Highlights 85% of the total area extracted.

8.6.2. Human (Female) Micro-DBS.

Extractions were performed on micro-DBS made with female human blood using the final matrix optimized extraction method. Online extractions are presented in **Figure 142** for spiked (PFMA) and blank (PFøø) female blood.

Spiked Female Blood vs Steroid Standards. All compounds were successfully extracted from spiked human (female) blood, except ZRNL was not observed due to the low concentration of the standard.

Blood Matrix. Data processing is currently under way, but has not been fully completed at this time.

8.6.3. Human (Male) Micro-DBS.

Extractions were performed on micro-DBS made with male human blood using the final matrix optimized extraction method. Online extractions are presented in **Figure 143** for spiked (PMMA) and blank (PMøø) male blood.

Spiked Male Blood vs Steroid Standards. All compounds were successfully extracted from spiked human (male) blood, except ZRNL was not observed due to the low concentration of the standard.

Blood Matrix. Data processing is currently under way, but has not been fully completed at this time.

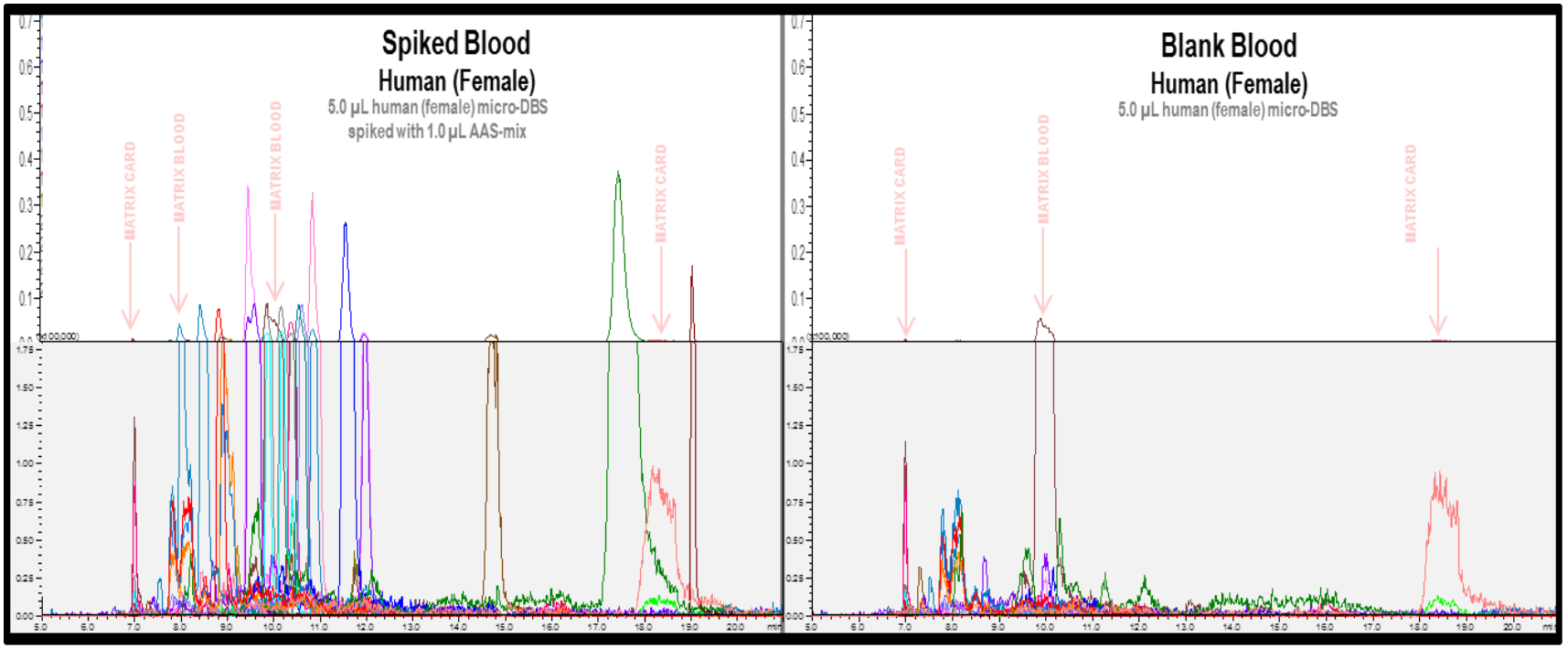

Figure 142. Zoomed SFE-SFC-MS Chromatograms for Online Extractions of Female Human whole blood comparing blank blood to Quality Controls: [A] Spiked female blood (6.0 µL spiked blood [1:5 AAS-mix:Blood], PFMA); and [B] Female micro-DBS (5.0 µL blank blood, PFøø). (top) Intensity normalized to standard mixture, showing low relative intensity of signal contribution from the card and blood matrices; (bottom) baseline zoomed/normalized to blank card, showing similar signal contribution from card in all four extractions and blood matrix. [single donor female whole blood = Black female, 35 years of age **(PF3A)**].

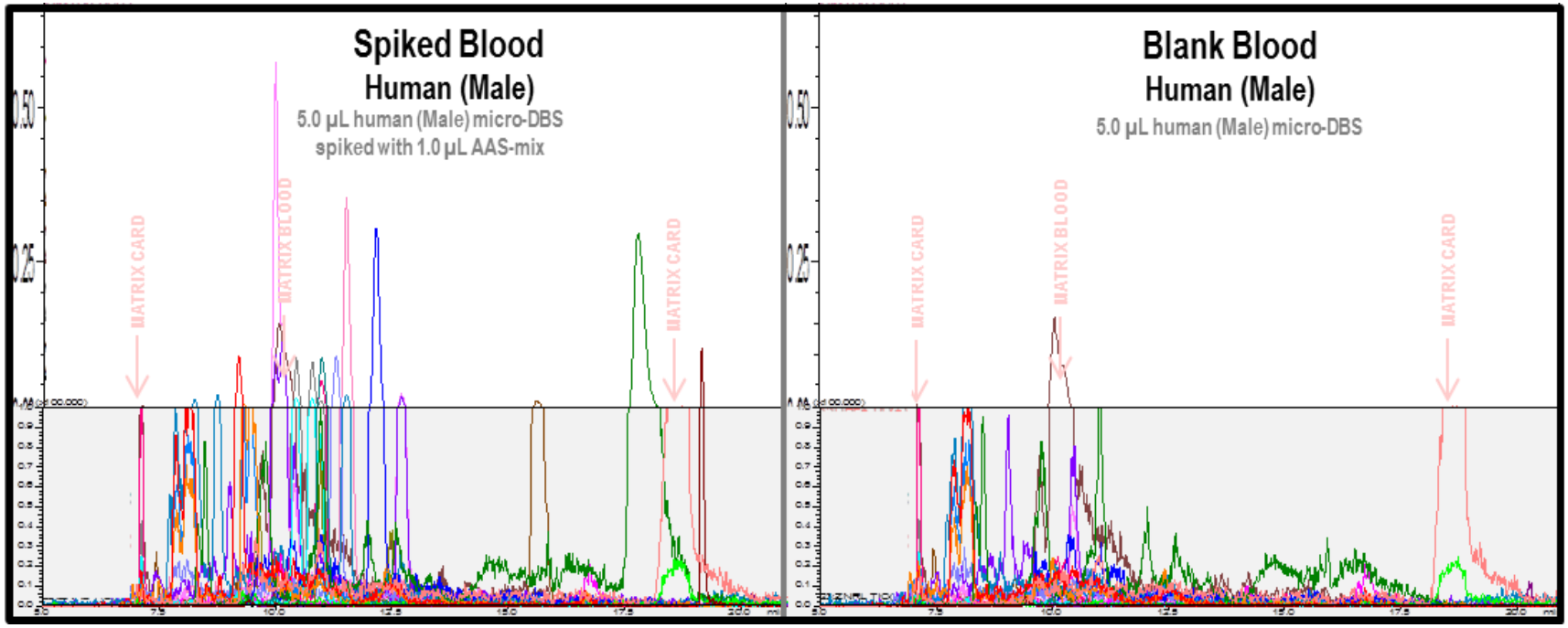

Figure 143. Zoomed SFE-SFC-MS Chromatograms for Online Extractions of Human Male Donor whole blood comparing blank blood to Quality Controls: [A] Spiked male blood (6.0 µL spiked blood [1:5 AAS-mix:Blood], PMMA); and [B] Male micro-DBS (5.0 µL blank blood, PMøø). (top) Intensity normalized to standard mixture, showing low relative intensity of signal contribution from the card and blood matrices; (bottom) baseline zoomed/normalized to blank card, showing similar signal contribution from card in all four extractions and blood matrix. [single male donor whole blood = Hispanic male, 37 years of age **(PM3A)**].

8.7. Preliminary Evaluation of Detection Levels

Naturally occurring steroid levels can change depending on gender, age, health, and activity/lifestyle, and in many cases can be quite low. Therefore level of detection and quantitation will be important during validation. Extraction of testosterone was selected as the target to demonstrate proof-of-concept. Approximate ranges of naturally occurring testosterone expected in humans ranges from 0.1 – 0.70 ng/mL for females and 2.8 – 13.2 ng/mL.[91] For women testosterone can spike to the high side of the range during menstruation, but generally should be expected to be very low. For men, age is the biggest factor, where males between 18-24 are expected to have much higher naturally occurring levels than males outside this age range.

A pre-test was performed as an initial evaluation of detection levels for the online extractions. In consideration of the lower edge of the range expected for males, in anticipation of the lowest calibration point for validation, our testosterone pre-test concentration was set at 2.0 ng/mL. Bovine blood (US origin, **[PB4B])** was spiked with a testosterone spiking solution **[TSTO_c002]** at 2 ng/mL of testosterone **[PBMTv002],** for comparison with whole blood obtained from male donors of various ages: Donor #1 was 37 years of age (Hispanic male, **[PM3A]**); Donor #2 was 18 years of age (Black male, **[PM4B]**); and Donor #3 was 20 years of age (Caucasian male, **[PM5C]**). Triplicate spots were created, cored, and extracted online using the same SFE-SFC-MS method.

(Detailed in **Chapter #2. Materials & Methods: Section 2.5.3. Micro-DBS fortified 'Doped' Blood: Testosterone Pre-test [TSTO_c002]**).

(Detailed in **Chapter #2. Materials & Methods: Section 2.1.3. Dried Blood Spot (DBS) Materials: *Biological Fluids***).

Example extractions are presented in supplemental figure, **S_Figure 26.** Extractions from the blank male blood samples produced average total areas (**Figure 144**) between 1 and 5 times higher than the spiked bovine blood (at 2 ng/mL). The areas produced by the blood samples correlated with the age of the donor. The blood extractions from the youngest male donor produced the highest areas for testosterone and the oldest donor produced the lowest areas. This preliminary test shows promise that the method should be able to achieve sensitivity with high relevance for natural samples, during method validation.

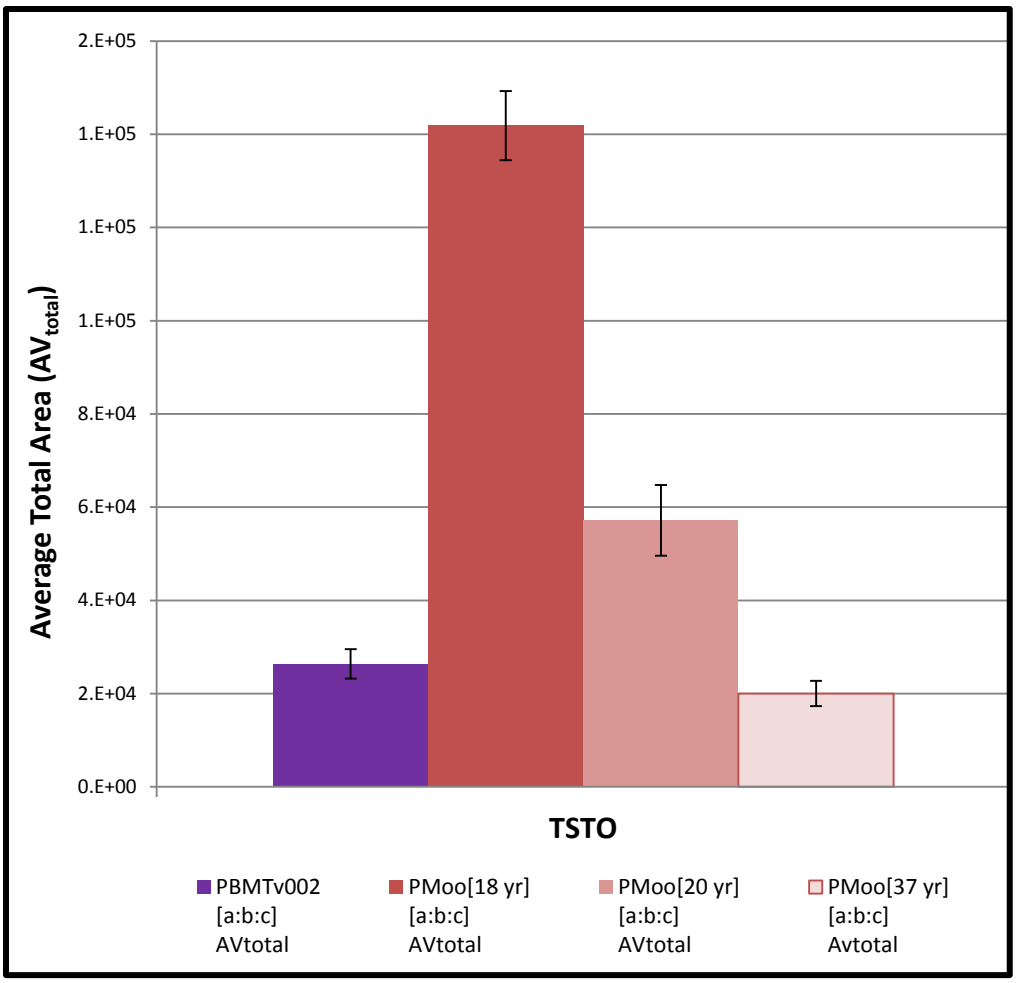

Figure 144. **Total Average Area Extracted for Testosterone Pre-Test For Three Male donors of Various Ages**: 18 years ([**PM4B]**, dark red); 20 years ([**PM5C**], red); and 37 years ([**PM3A**], light red] of age comparing to Spiked Bovine blood (2.0 ng/mL, [PBMTv002], purple). **Error bars = standard deviation (n = 3).**

8.7. Summary.

In summary an optimized hyphenated method was developed for the online extraction of Anabolic agents from dried blood spots using SFE-SFC-MS. By first performing initial optimizations for the MS detection and SFC-separation of Androgenic steroids. This SFC-MS method was hyphenated for online extraction optimizations. which involved the development of a micro-DBS sampling technique, which also provided quality controls relevant for comparison with final samples. Matrix evaluations produced no interfering signals at corresponding retention times to the targeted analytes. But Matrix effects were observed, resulting in lower extractable areas. preliminary evaluation of method sensitivity shows promise for validity for natural steroids. The work in this chapter is only partially completed. Extractions have been performed but data analysis has yet to be completely processed. Data Evaluations and final method validation are currently in progress.

8.i. Instrument Methods: Matrix-Specific Optimizations

8.i.1. General Method Information.

Detailed information on materials and equipment used for the matrix optimizations performed in this study can be found in the following sections of **Chapter #2. Materials and Methods**:

8.i.1.1. Materials.

- Solvents used for mobile phases and dilution solutions can be found in **Section 2.1.1. Solvents**.
- Analytical standards information for targeted anabolic agents can be found in **Section 2.1.2. Analytical Standards; *Anabolic androgenic steroids (AAS)*** **and** **Table 1.**
- Sample collection materials are detailed in **Section 2.1.3. Dried Blood Spots (DBS) Materials: *Blood Spot Collection Materials.***
- Details for biological fluids in **Section 2.1.3. Dried Blood Spot (DBS) Materials: *Biological Fluids*** and **Table 3**.
    - **[PB3A]** Bovine; whole blood (WB) #3; US Origin.
    - **[PB4B]** Bovine; whole blood (WB) #4; US Origin.
    - **[PF3A]** Human (female); whole blood (WB) #3; single donor (female; 35 yrs).
    - **[PM3A]** Human (male); whole blood (WB) #3; single donor (male; 37 yrs)
    - [**PM4B]** Human (male); whole blood (WB) #3; single donor (male; 18 yrs)
    - [**PM5C**] Human (male); whole blood (WB) #3; single donor (male; 20 yrs)

8.i.1.2. Instrumentation.

- The Instrumentation used is detailed in **Section 2.2.1. Instrumentation; *Nexera UC online SFE-SFC-MS***.
- Column details are given in **Section 2.2.2. Columns** and **Table 5.**
- Other equipment used is detailed in **Section 2.2.3. Other Equipment**:
    - ***Nitrogen Generator***
    - ***Analytical balances***

8.i.1.3. Solutions Preparation.

- Stock Solutions prep and storage detailed in **Section 2.3.1.1. AAS Stock Solutions** and **Table 6; Stock Solutions.**
- Injection and Spiking solutions prep and concentrations are described in **Section 2.3.1.3. AAS Injection and Spiking Solutions** and **Table 6.**
    - ***AAS Test Mixture [AAS-mix]***
    - ***AAS Initial Calibration Mixture [AASc1,000]*** and ***AAS Calibration Solutions.***
    - ***Testosterone Pre-test Spiking solution [TSTO_c002]***

8.i.1.4. Sample Preparation.

Sample preparation was accomplished using a micro sampling technique and is detailed in **Section 2.4.1. Sample Preparation: Micro-Dried Blood Spot (Micro-DBS); *Micro-DBS Sampling Technique*.**

- Quality Control and Blanks Approach is described in **Section 2.4.2. Quality Controls and Blanks**
- Micro-QCs Spot Types are described in **Section 2.4.3. Micro-QCs for SFE Extraction Optimization;**
    - ***AAS-QC spots*: [Pøøø], [PøMø], [PøMA], [PXøø], [PXMø], [PXMA]**

      (key: X = whole blood: [B] = Bovine; [F] = Female; [M] = Male).
- Sample preparation of micro-QCs is described in **2.4.6. Micro-DBS sets for Matrix-specific optimizations.**
- Validation spots are is described in **Section 2.5. DBS Validation; 2.5.1. Micro-DBS sets for Validation.**
    - ***Matrix Spots***
- Validation spots are is described in **Section 2.5.3. Micro-DBS fortified 'Doped' Blood.**
    - **Testostosterone Pre-Test Spiked Bovine Spots [PBMTv002]**

During previous development steps, SFC injections (1.0 µL) were made of a mix of 23 androgenic anabolic agents [AAS-mix] in methanol. For extraction, the same AAS-mix was used, and spotted (applied in 1.0 µL aliquots) to Whatman® 904 FTA®, classic, cellulose based, sample collection/preservation cards. Spots were allowed to dry for atleast 3 hours and cored using a standard (6mm) single hole punch. To enable rapid method screening, cored spots were placed inside 0.2-mL extraction vessel and set to the SFE automated rack changer for online extraction/analysis.

8.i.1.5. General Vessel Preparation.

General Workflows for online extractions and approaches to the use of the extraction vessels are detailed in **Section 2.8. General Workflow for Online Extractions**.

8.i.1.6. Data Processing.

General data processing approaches are detailed in **Section 2.9. General Data Processing Approaches**.

8.i.2. Instrument setup

The instrument setup utilized in the work presented was performed with the 'SFE Online Extraction Configuration using '***Splitless-mode' Extractions***' detailed in **Chapter #1: Hyphenated Instrumentation: SFE-SFC-MS**; **Section 1.5.4: Instrument Configurations used for SFC Optimizations: 'Splitless-mode' Extractions**).

Sample Introduction. Online extractions were performed in splitless-mode, using 0.2-mL extraction vessels. Sample is placed in inside a small chamber and extracted online facilitated by two switching valves, an 'extraction plug is delivered to the head of the column for online analysis.

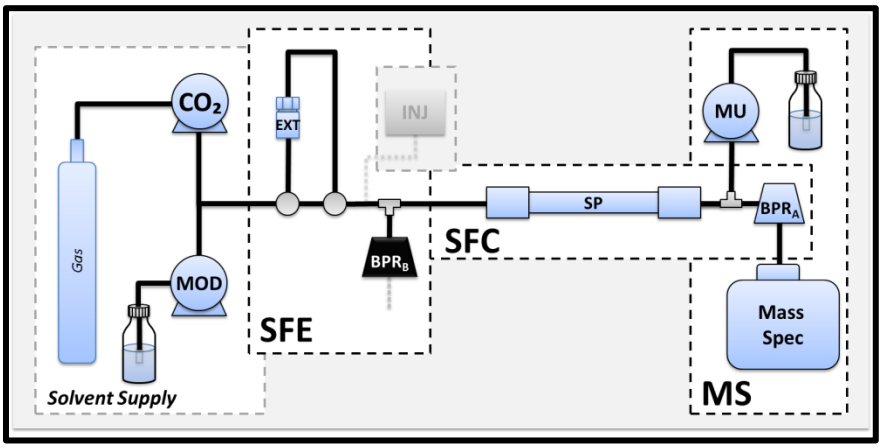

See Figure 17 in Chapter #1

8.i.3. Instrument Methods:

8.i.3.1. Mobile Phase (MP) and Stationary Phase (SP).

LCMS-grade methanol [MeOH] with 5 mM ammonium formate [AmFo] were utilized as modifier. For SFC mobile phases, up to 40% modifier was mixed with carbon dioxide ([CO_2] – Instrument grade) via the instrument solvent delivery pumps. All online extractions and subsequent separations performed in the current work utilized a Shimadzu Corporation Shim-pack UC-Cyano 4.6 mm x 150 mm 5.0 µm column.

8.i.3.2. *MS Method Parameters –MRM method from Chapter #4*

Detection was achieved using an LCMS-8050 triple quadrupole mass spectrometer, equipped with an electrospray ionization (ESI-) source, operated in positive (+) and negative (-) ionization mode, using multiple reaction monitoring (MRM). MRM transitions are presented in **Table 42** including precursor and product ions, voltages and collision energies for each analyte. Interface voltages were set to 4.0 kV (for positive) and -3.0 kV (for negative mode) with an interface temperature of 300 °C. Nitrogen gas was used for both drying and nebulizing gas; with a flow rate of 3.0 L/min for nebulizing gas and 5.0 L/min for drying gas. Desolvation and DL temperatures were 602 °C and 350 °C respectively. Heat Block temperature was set to 500 °C, and heating gas used was dry air. Gas used for collision induced dissociation (CID) was argon at 270 kPa. DL Bias/Qarray Bias were both set as 0 V, and Q3 Pre-rod Bias at -15 V (for positive scan mode) and 15 V (for negative scan mode).

8.i.3.3. *SFC Method Parameters – optimized method from Chapter #6*

Gradient	:	2.0 - 12.5% B (0-8 min), 12.5 - 30% B (8-10 min), 30% B (10-15 min).
Flow rate	:	3.0 mL/min
Column Temp.	:	60 °C
Outlet Pressure	:	(BPR_A) 15 MPa; (BPR_B) 40 MPa.
Injection	:	*(when applicable)* 1.0 µL partial loop (AAS-mix) [5.0µL external loop]

8.i.3.4. *Extraction Vessel Details*

Extractions were performed using 0.2-mL extraction vessels, equipped with the standard (non-sinter type) screen-type filters. Samples were placed directly into vessels with no added filler. Vessels were closed using the appropriate Torque wrench (1.5 N-m). Splitless-mode extractions were used where BPRB was either physically plumbed out of the system flow path or shut (i.e., set to 40 MPa).

Summary of Vessel-specific Details

Extraction Mode	:	Splitless-mode; (BPR_B) = 40 MPa.
Final Wash	:	100%B; 3.0 ml/min; 5.0 min duration.
Extraction Sample	:	Whatman™ FTA® classic sample collection card. Spots applied to card; dried (≥ 3 hours) at room temperature. 6mm Core; placed directly into vessel.
Vessel Size	:	0.2-mL vessels,
Vessel Filters	:	standard (non-sinter type) vessel filters.
Vessel Filler	:	None
Torque Wrench	:	1.5 Nm (specific for use with 0.2-mL extraction vessels).

8.i.3.5. Instrument Methods: Optimized Online SFE-SFC-MS Extraction Method

The final optimized online extraction method was finalized in **Chapter #7** and the final hyphenated online extraction method is detailed below in **Table 44**.

Table 44. Conditions for Optimized Online Extraction of Anabolic Agents using 0.2-mL Vessels.

Mobile Phase	:	[A] carbon dioxide (CO_2);	[B] methanol + 5mM ammonium formate (AmFo).		
Column	:	Shimadzu Corp., Shim-pack, UC-Cyano (4.6 x 150mm, 5 µm)			
Online SFE Extraction					
SFE Vessel Size	:	0.2-mL			
Vessel Temp.	:	30 °C			
Rack Changer Temp.	:	20 °C			
Extraction Pressure	:	(BPR_A) 10 MPa			
Mode	:	(BPR_B) 40 MPa;	Splitless		
Filling	:	2.0 mL/min;	2% [B];	1.0 min;	(0.00 – 1.00 m).
Static Extraction	:	2.5 mL/min;	0% [B];	4.0 min;	(1.01 – 5.00 m).
Dynamic Extraction	:	2.5 mL/min;	0% [B];	2.0 min;	(5.01 – 7.00 m).
Analysis	:	2.0 mL/min;	*gradient**	16.0 min;	(5.01 – 21.00m).
Wash	:	2.5 mL/min;	100% [B];	3.0 min;	(21.01 – 24.00 m).
Re-Equilibration	:	2.5 mL/min;	2% [B];	0.5 min;	(24.01 – 24.50 m).
****SFC gradient***					
Column Temp.	:	60 °C			
Outlet Pressure	:	(BPR_A) 15 MPa			
Gradient	:	2 – 5% B;	9.0 min;	(5.01 - 14.00m),	
		5 – 12% B;	3.5 min;	(14.01 – 17.50m),	
		12 – 30% B;	3.0 min;	(17.51 – 19.50m),	
		30% B	1.5 min;	(19.51 – 21.00m).	

Literature Cited:

FIRST CITED IN PREVIOUS CHAPTERS

[19] World Anti-Doping Agency. International Standard Prohibited List, 2021. Resources. https://www.wada-ama.org/sites/default/files/resources/files/2021list_en.pdf. (Accessed January 03 2021).

NEW TO THIS CHAPTER

[85] Handelsman DJ, Bermon S. (2019). "Detection of testosterone doping in female athletes." *Drug Testing and Analysis*. **11**(10): p1566–1571. https://doi.org/10.1002/dta.2689

[86] Suzuki M, Nishiumi S, Kobayashi T, Sakai A, Iwata Y, Uchikata T, Izumi Y, Azuma T, Bamba T, Yoshida M. (2017). "Use of on-line supercritical fluid extraction-supercritical fluid chromatography/tandem mass spectrometry to analyze disease biomarkers in dried serum spots compared with serum analysis using liquid chromatography/tandem mass spectrometry." *Rapid Communications in Mass Spectrometry.* **31**(10): p886–894. https://doi.org/10.1002/rcm.7857

[87] Ramsthaler F, Schlote J. Wagner C, Fiscina J, Kettner M. (2015). "The ring phenomenon of diluted blood droplets." *International Journal of Legal Medicine*. **130**: p731-736. https://doi.org/10.1007/s00414-015-1304-1

[88] George RS, Moat SJ. (2016). "Effect of Dried Blood Spot Quality on Newborn Screening Analyte Concentrations and Recommendations for Minimum Acceptance Criteria for Sample Analysis. Clinical Chemistry." *Clinical Chemistry*. **62**(3): p466–475. https://doi.org/10.1373/clinchem.2015.247668

[89] Velghe S, Delahaye L, Stove CP. (2018). "Review: Is the hematocrit still an issue in quantitative dried blood spot analysis?" *Journal of Pharmaceutical and Biomedical Analysis*. **163**: p188–196. https://doi.org/10.1016/j.jpba.2018.10.010

[90] Wilhelm AJ, den Burger JCG, Swart EL. (2014). "Therapeutic drug monitoring by dried blood spot: progress to date and future directions." *Clinical Pharmacokinetics*. **53**(11): p961-973. https://doi.org/10.1007/s40262-014-0177-7

[91] Chang W C-W, Cowan DA, Walker CJ, Wojek N, Brailsford AD. (2020). "Determination of anabolic steroids in dried blood using microsampling and gas chromatography-tandem mass spectrometry: Application to a testosterone gel administration study." Journal of Chromatography A. 1627: e461445. https://doi.org/10.1016/j.chroma.2020.461445

S_8. SUPPLEMENTARY MATERIALS:

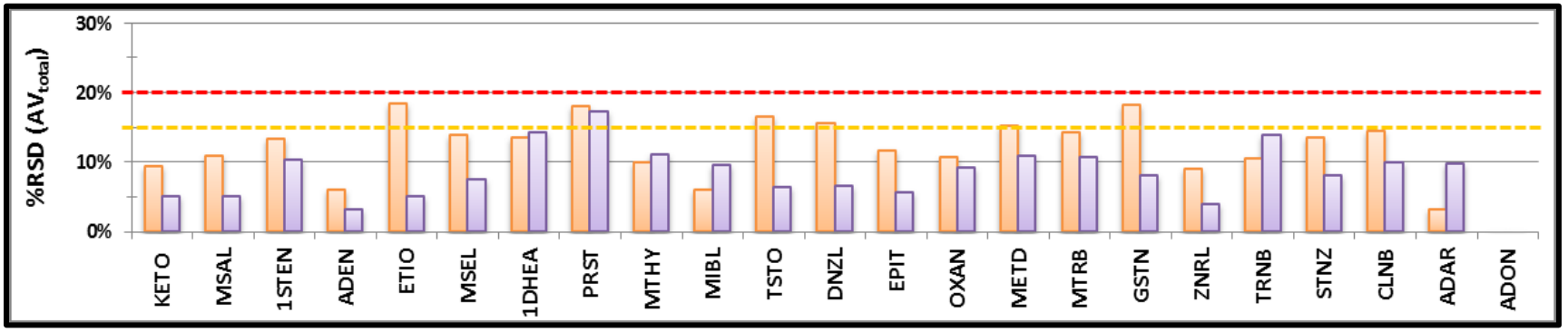

S_Figure 24. Intra-Card Reproducibility for Spiked Female Blood (PBMA, Purple) and Spiked Paper (PoMA, orange) showing percent residual standard deviation (%RSD) for Average Total Area Extracted for replicate cored Micro-DBs (n=3).

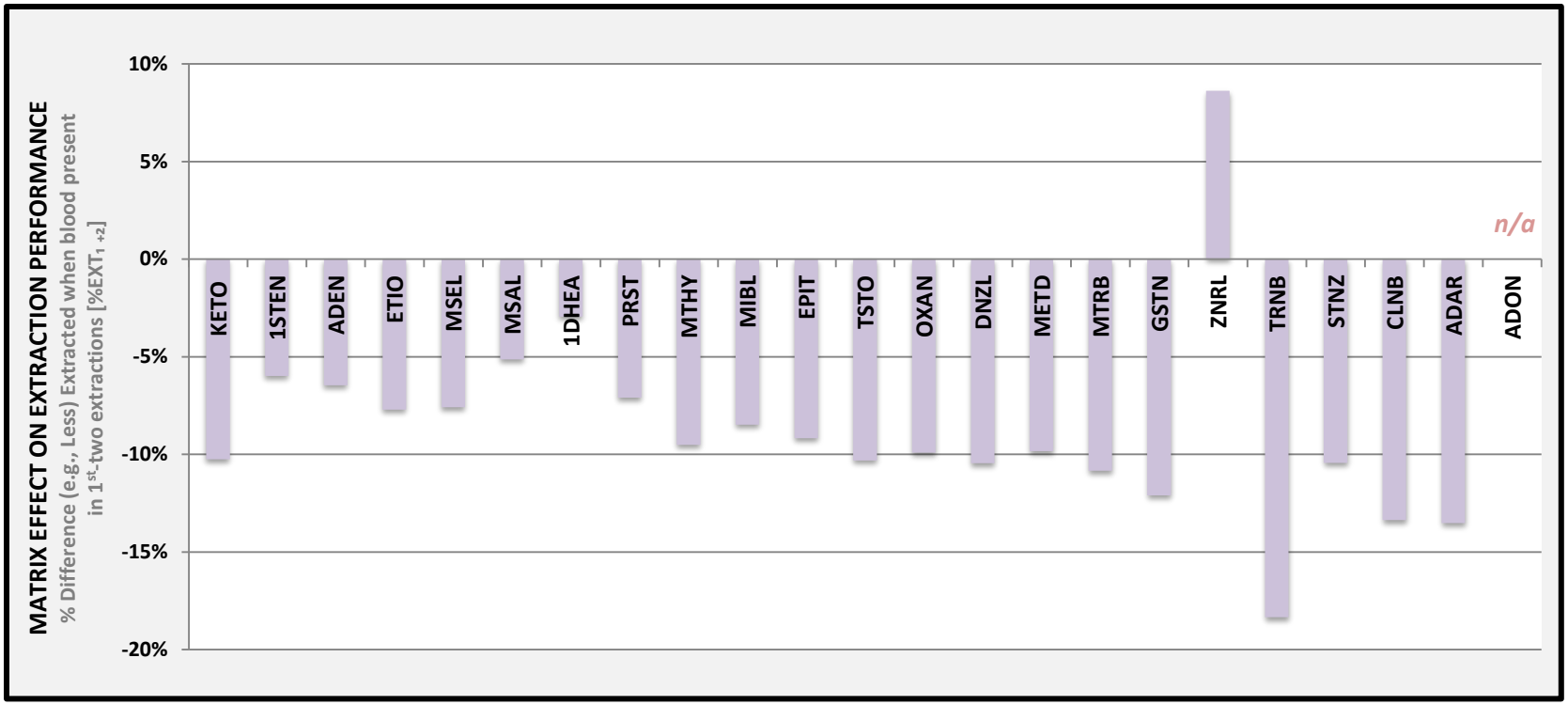

S_Figure 25. Matrix Effect on Extraction Performance showing Percent Difference (e.g., Less [-] or More [+]) Extracted (in the 1st-Two Extractions [%EXT_{1+2}]) for Each Anabolic Agent When Blood is Present. Difference between Av%EXT_{1+2} for Spiked Bovine Blood [PFMA] versus spiked standards with no blood present [PoMA]. Data Set = PF

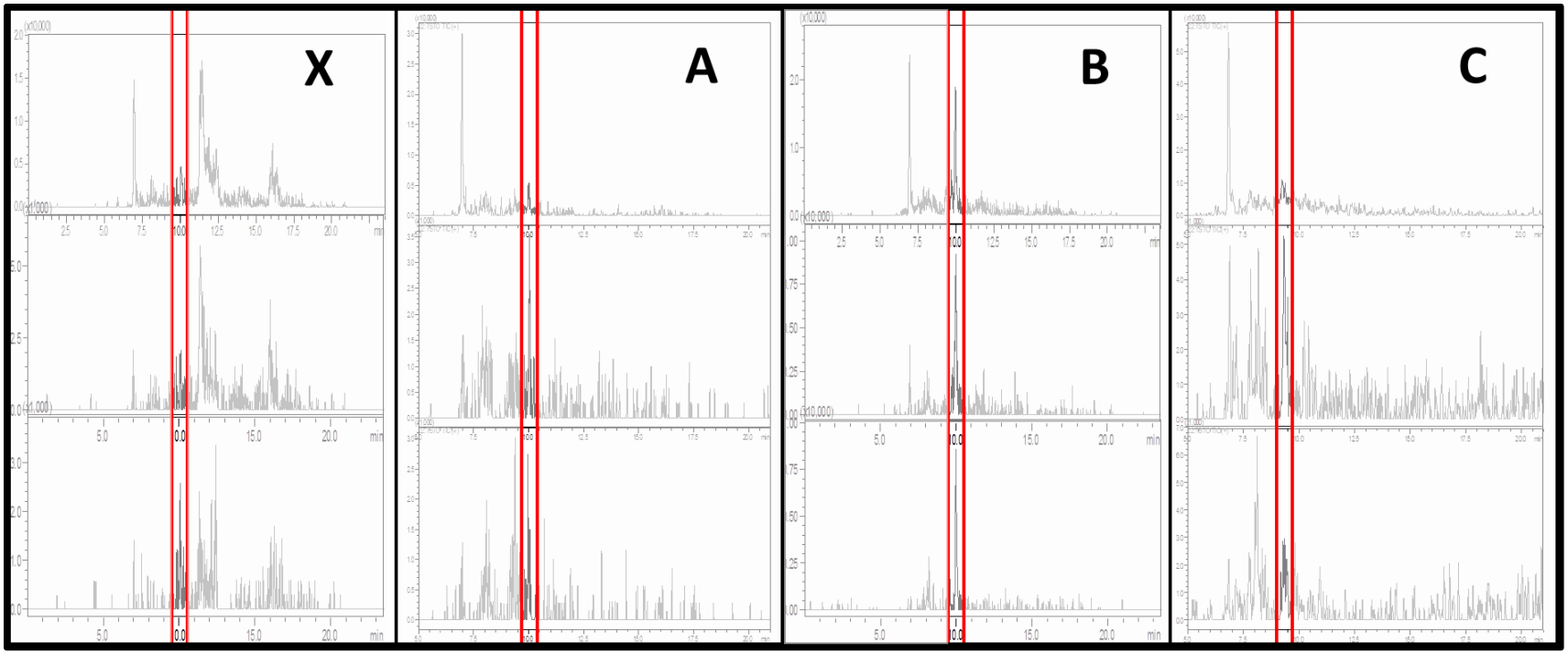

S_Figure 26. SFE-SFC-MS Chromatograms for Testosterone Pre-test: showing Testosterone (TSTO) MRM-TIC for [X] Spiked Bovine Blood [PBMTv002], spiked at 2ng/mL testosterone **[A] Blank Male Blood Donor #1, 18 years old** (PMoo_PM3-A); **[B] Blank Male Blood Donor #2, 20 years old** (PMoo_PM3-A); and **[C] Blank Male Blood Donor #3, 37 years old** (PMoo_PM3-A).

CHAPTER 9

ONLINE EXTRACTION OF ENVIRONMENTAL CONTAIMINANTS FROM MICROPLASTICS

CHAPTER 9

ONLINE EXTRACTION OF ENVIRONMENTAL CONTAIMINANTS FROM MICROPLASTICS

9.1. Microplastics Introduction.

9.1.1. Microplastics (µPs): An emerging environmental concern.

In 2015, 407 million tons of plastics were produced worldwide. A 26% recycling rate suggests the majority of these products end up entering the environment via landfills and other means. It is estimated that nearly 13 million metric tons of land-based plastic waste enter the oceans every year.[92],[93] Classes of plastics commonly encountered in the environment (% fraction of global plastics production in 2018): LDPE (18%), HDPE (12%), PP (19%), PVC (10%) PET (8%), and Polystyrene (6%).[94],[95] The majority of consumable products are made of polyethylene terephthalate (PETE) and high- or low-density polyethylene (HDPE and LDPE, respectively).[96],[97] Microplastics (µPs) also come directly from waste- and storm-water, industrial and residential sources (**Figure 145**), entering waterbodies through discharge from treatment plants and in sewage used in agriculture.[98],[99]

Examples of direct sources of microplastics include: Industrial microbeads from cleaning products and abrasives; Residential sources such as microbeads in personal care items, cleaning products and fibers from textiles (e.g., it is estimated that up to 1,900 fibers could be released per wash load from garmets made of synthetic materials); and stormwater type sources from road abrasions. Ultimately a major source of plastics in the environment come directly from garbage or directly enter the environment through carelessness, such as littering or poor waste management (e.g., wind blown debris). [100],[101]

-.

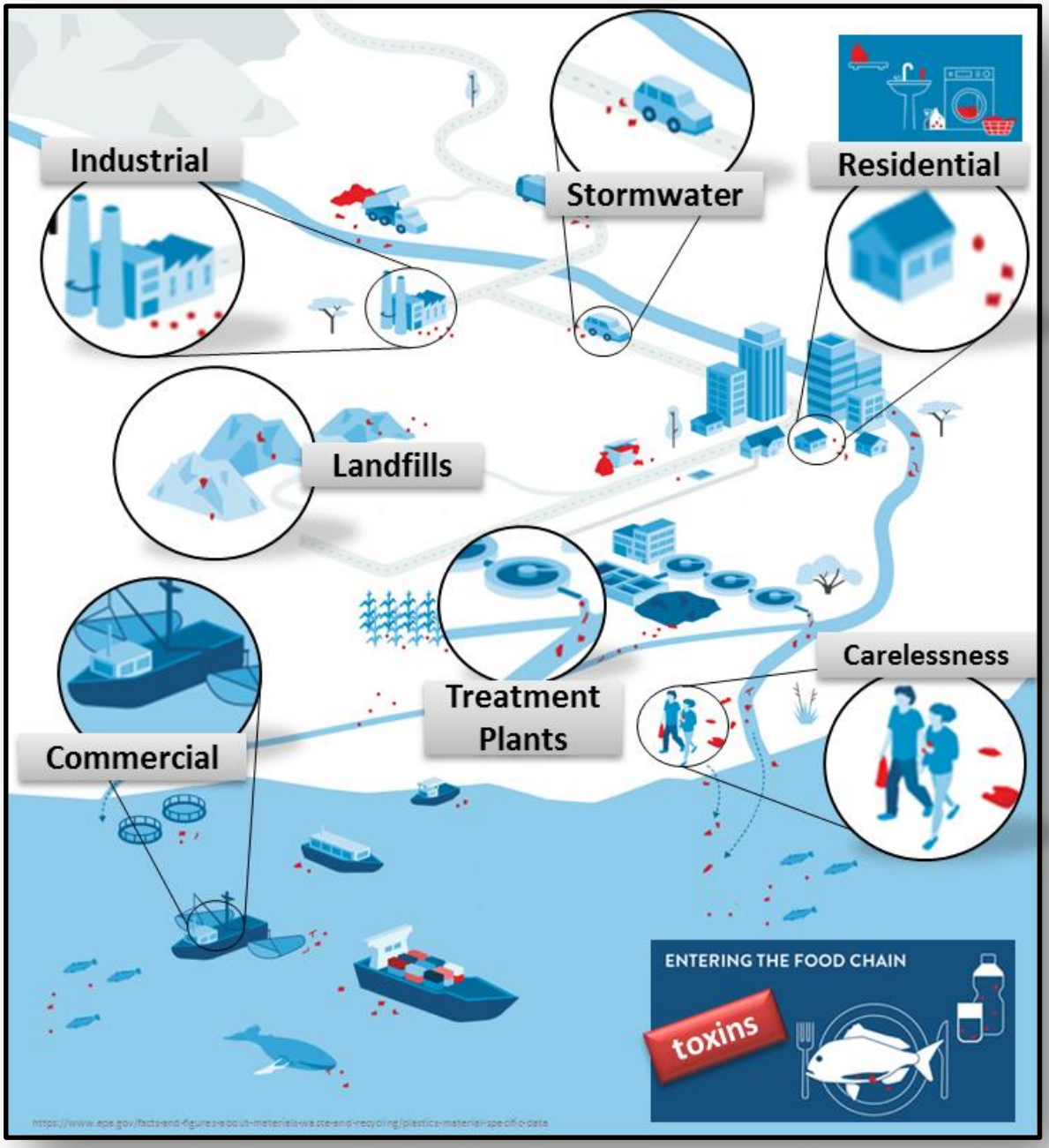

Figure 145. **Common Sources of Plastic Debris as Waste and Pathways of introduction into the Ocean.** (Figure modified from the New Zealand Royal Society – Evidence Summary, 2019[101])

Degradation of plastics to smaller particles is attributed to a variety of factors. Physical forces (such as photodegradation, hydrolysis, mechanical, thermal and biodegradation), environmental conditions (e.g., temperature, sunlight and oxygen), material properties and polymer type (e.g., crystallinity, chemical composition, molecular weight, hydrophobicity and morphology, functionalization, production method and additives) are all considered to play a role. Mechanical degradation as well as exposure to ultra violet light play major roles in the breaking down of plastics in the environment. Larger plastics tend to break down through mechanical degradation, from the surface inward, but µPs on the other-hand, having small fissures and increased surface area, allow oxygen, water and UV light to permeate through the particle, leading to further cracking and bulk degradation (**Figure 146**).[102],[103] Plastic particles, between 5mm and 1.0 µm are classified as 'microplastics' (**Figure 147**).[104],[105]

Once in the environment, µPs can be ingested by organisms, introducing associated toxins into the food chain.[101],[106] Plastics have been found in organisms across nearly every trophic level.[107],[108],[109] Micro/nano particles size, are very similar to the size of phytoplankton, which are the staple diet of zooplankton (ex. Pacific Krill).[95] Fish feed thru sediment (which is the main sink for microplastic sized debris). Birds ingest larger plastic particles. As plastics degrade to smaller particles, the possibility it will infiltrate food webs becomes more likely.[110],[111]

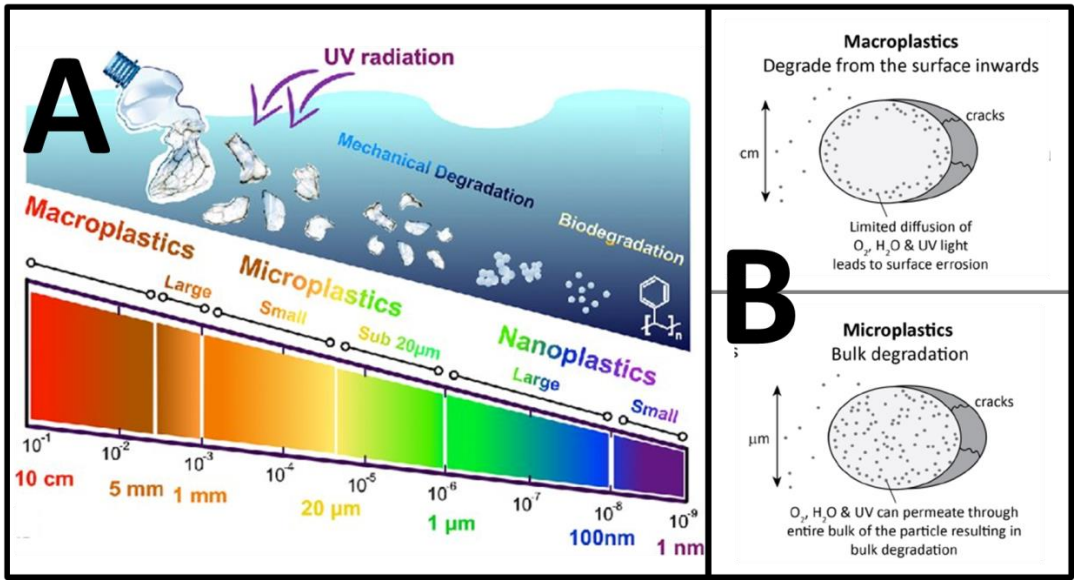

Figure 146. Degradation of larger plastics to smaller particles. [A] Figured modified from Gilibert et. al. 2019 [103]; [A] Figured modified from Booth et. al., 2017[102].

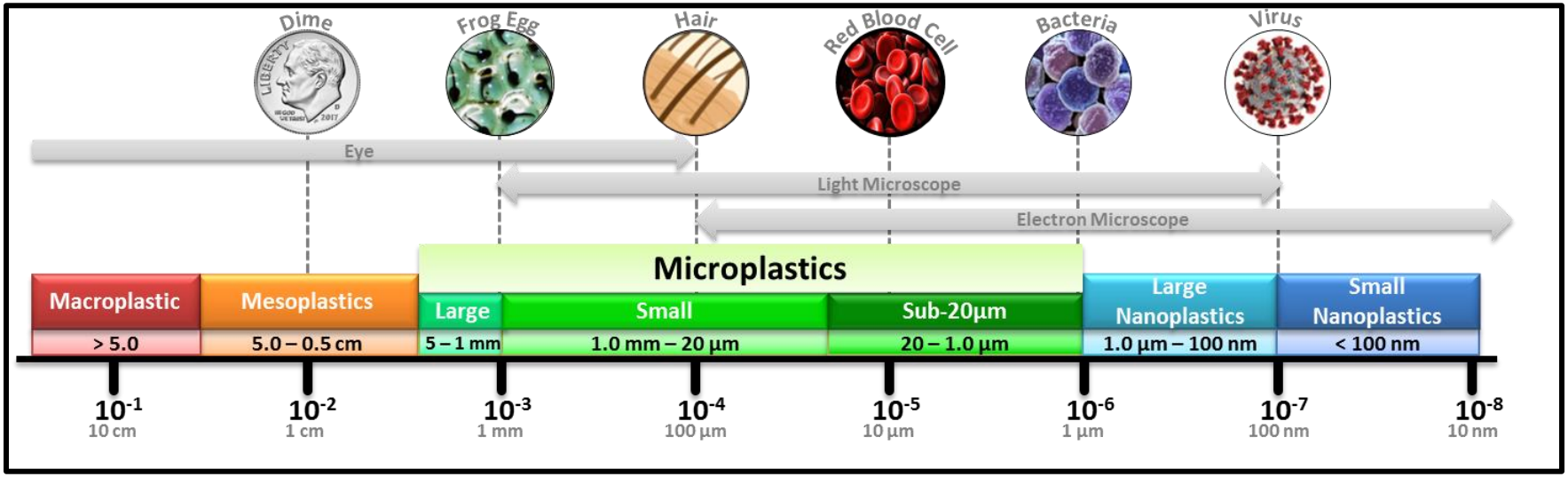

Figure 147. Common Classifications of Particles Sizes for Small Plastics, with Comparison to Common Objects.

9.1.2. Chemicals Associated with Microplastics.

Plastic debris contains two types of chemicals: those inherent to the polymer (e.g., created during manufacturing or additive-derived) and those sorbed from the surrounding seawater (e.g., hydrophobic chemicals). Plastics act as a sink for many hydrophobic pollutants, such as PAHs and other hazardous chemicals listed as priority pollutants in many countries. Some µPs have been found containing concentrations of hazardous materials orders of magnitude higher than those found in sediments and in sea water.[110],[112],[113],[114],[115],[116],[117]

The sorption of chemicals onto plastics is dependent on the chemical and physical properties of each polymer (e.g., composition, surface area, diffusivity and crystallinity). Polymers with heteroatoms in the main chain (e.g., PET, PU, and PA) have an increased stability compared to polymers with a C-C backbone. PETE (Polyethylene terephthalate), has a density of 1.4 g/cm^3, and sinks. When ethylene is polymerized (PE) the result is relatively straight polymer chains. From the main chain they can branch out. We get different kinds of polyethylene's from the varying degree of branching in their molecular structure. HDPE has minimal branching of its polymer chains, is denser, more rigid and less permeable than LDPE. This causes the low density to have a less compact molecular structure. LDPE Low-density polyethylene has a density of, 0.910 - 0.925 g/cm^3.

Environmental Contaminants. Environmentally persistent organic pollutants (ePoPs) are compounds resistant to chemical, biological, and photolytic degradation. Being stable and persistent, bioaccumulative and biomagnifiable in the food chain, these compounds are of high environmental concern. Often ePOPs data related to occurrence or impact are inadequate due to analytical difficulties and /or lack of proper methods.[118]

Polycyclic Aromatic Hydrocarbons (PAHs) originate from incomplete combustion of fossil fuels and organic matter. They are of environmental concern due to their carcinogenic and mutagenic properties.[119] Some PAHs found in marine plastic debris (hydrophobic organic compounds sorbed from seawater), showed a petrogenic signature, suggesting the sorption from oil slicks.[115] EPA method 8310 (1986) identifies 16 PAHs as priority pollutants in ground water and wastes.[20] An online SFE-SFC-MS method has been developed for the extraction of PAHs from soil.[120]

9.1.3. Issues of applicability of Plastics – exposure in a Lab environment

Most laboratory studies have used virgin plastics as obtained from the manufacturer, without any degradation. Comparison of plastics found in a marine environment to controlled-exposure experiments in a laboratory setting can have limited applicability to the quantification of chemical pollutants in marine plastic debris.[121],[122]

The main factors responsible for these limitations stem directly from the lack of knowledge of the specific forces environmentally-exposed plastics experience, such as the degree of mechanical degradation, chemical degradation and photo-degradation, all having significant effects on increasing surface area of plastic debris. In addition, one must also consider the unknown exposure time and the multitude of changing environmental conditions (e.g., In temperature, salinity, and light) a plastic experiences in the environment. There is also the likelihood of local effects such as specific pollution sources. All of these factors lead to greater surface area and therefore greater sorption of contaminants over time in marine exposed plastics,[95],[123] all of which are extremely difficult to simulate in a lab-setting.

In the current work, one major environmental factor was simulated: the mechanical degradation of plastics. Using a cryomill, virgin plastics were subjected to mechanical degradation to emulate the surface area of environmentally produced microplastics. This allowed laboratory and field experiments to be performed on the same more appropriate materials. This study focuses on the sorption of environmentally persistent organic pollutants (ePOPs), specifically polycyclic aromatic hydrocarbons (PAHs), to the five most commonly mass produced plastics.

9.2. Microplastics Reference Material

9.2.1. CryoMilling of Plastic Pellets.

Mechanical degradation gives a rough surface and texture to the particles that dramatically increases the available surface area, increasing the adsorption capacity for environmental contaminants.[124],[125] The generally accepted size range for micro-plastics,[104] is between 5 mm and 1.0 µm. Virgin pellets made of nine different plastic types: PETE, HDPE, LDPE, PPrp, ABSt, TPUr, HIPS, PETG, and PCrb were obtained and CryoMilled to a fine powder (as described **in Chapter #2. Materials and Methods, Section 2.6.2. Milling of Microplastics**).

Virgin plastic materials were used in the current work, being easier to work with versus fragments collected in the field, as they are well defined chemically, widely available, and do not contain dyes.[123] Although the original pellets are already small enough (~5 mm) to be small meso-plastics to large micro-plastics, it has been cautioned, making comparison between results obtained in a lab setting, using pre-production pellets to real world environmental samples.[121],[126] Pellets used in manufacturing, are made of virgin materials, which makes them smooth on the outer surface (**Figure 148**). This smooth outer surface provides significantly lower surface area than would be expected on environmentally exposed plastic debris.

One intent in this work was to create micro-plastics reference materials [µPs-RM], which more closely mimic the surface area of environmental samples. A CryoMill is perfectly suited for this task, using liquid nitrogen. The materials are effectively pre-embriddled, by the liquid nitrogen, allowing a milling ball to pulverize them to fine powders (**S_Figure 27**). The resulting micro-particles (**Figure 149**) fall into the category of a small to sub-micron micro-plastic with the rough texture associated with mechanical degradation.

Figure 148. Virgin Plastic Pellets: Pre-CryoMilling 20 pellets shown with a dime for sizecomparison: Comparing example photos of nine different types of plastic; [A] LDPE; [B] HDPE; [C] PPrp; [D]TPUr ; [E] HIPS ; [F] PETE; [G] PETG; [H] PCRb; and [I] ABSt particles.

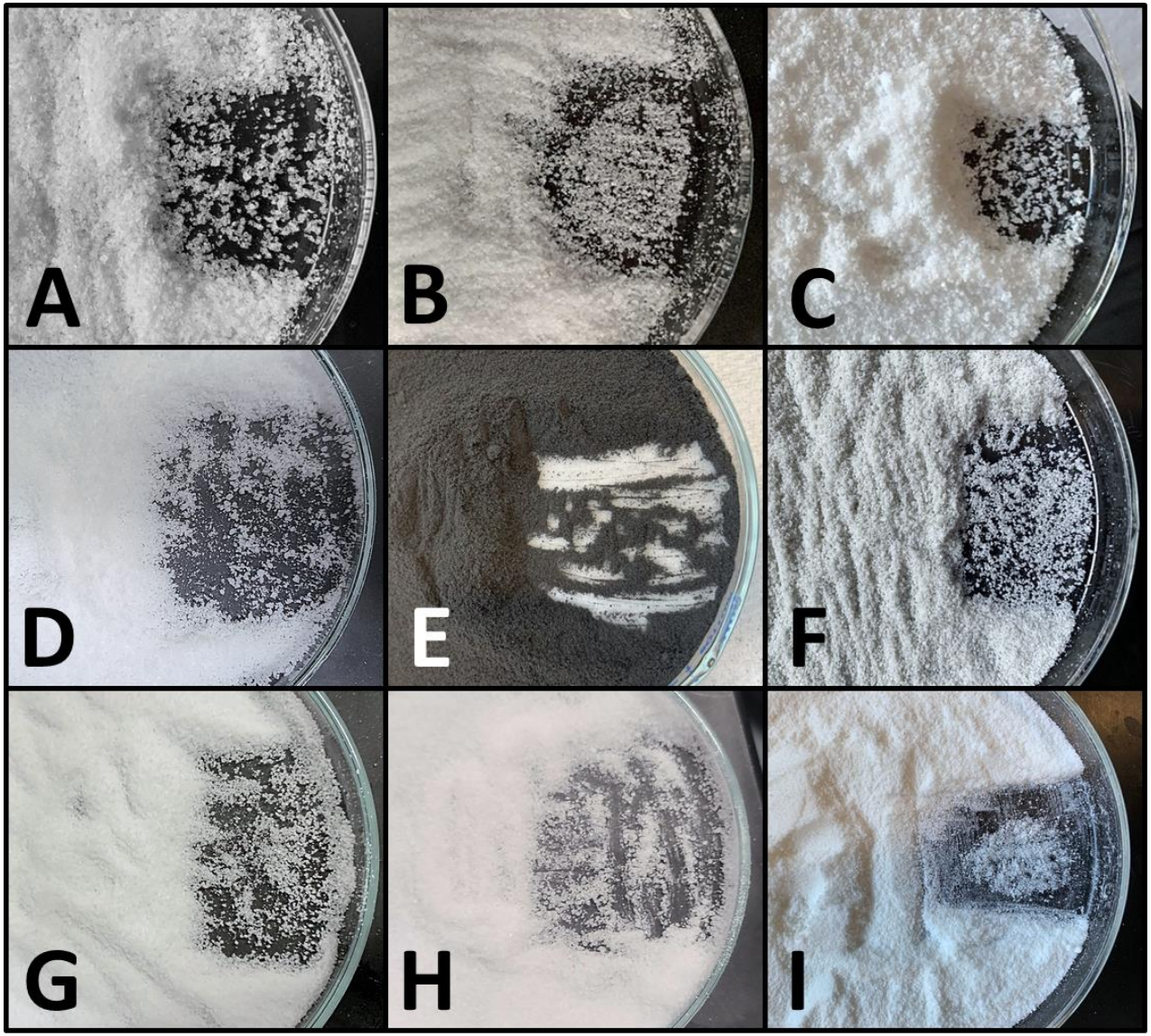

Figure 149. Plastic Powder: Post-CryoMill Particles showing contents of a single milling Jar spread on a petri Dish**:** Comparing example photos of nine different types of plastic; [A] LDPE; [B] HDPE; [C] PPrp; [D]TPUr ; [E] HIPS ; [F] PETE; [G] PETG; [H] PCRb; and [I] ABSt particles.

9.2.2. Achieving a Homogenized Stock

Tensile strength of the plastics proved to be the most significant factor. During CryoMilling, auto pre-cooling functions were used. This allows internal-sensors to determine the duration of the initial cryogenic cooling. Grinding only began once the entire system had been sufficiently cooled. The final milling method included 3 cryo-cycles in order to effectively pre-embriddle the materials. Although, this allowed for efficient cryogenic treatment of the sample pre-grinding, it was found that, for effective milling, a consistent, specific amount of plastic pellets needed to be added to the milling jar each time to obtain a homogenous particle size.

Generally, the lower amount added to the jar, the finer the resulting powder. Considering the large amount of stock that would be needed for the planned experiments, a compromise was needed between final particle size achieved (e.g. less plastic per milling round) and the overall throughput (total material produced). Therefore an optimal milling weight was determined for each type of plastic and ranged from 6.0 – 12.0 g per jar depending on the plastic (**S.Table_11; Optimal Milling Weight**).

9.2.3. Particle Size Analysis

Initial attempts using a particle size analyzer were unsuccessful, as the presence of particles above 800 µm easily resulted in saturating the detector. Therefore alternatively, the milled powders were then compared for size range and distribution under magnification via light microscope. Microscope analysis was performed to determine approximate smallest, largest and average diameter particle (mm), as well as a visual modal (range 1-10), and are given in supplementary table **S_Table 11; Microscope Size Analysis.**

(for specific method details see **Chapter #2. Materials & Methods; Section 2.6.3. Size Analysis via Light Microscope**).

Clear differences between the plastics were observed, including dramatic differences in size, shape, texture, and size distribution. It was also clear that the milling was successful in achieving a much rougher texture, matching more closely what one would expect from a micro-plastic produced through mechanical degradation in the

environment. Particle sizes ranged from 10 µm to over 800 µm in size, depending on the plastic. Example photos from each type of plastic are shown in **Figure 150**.

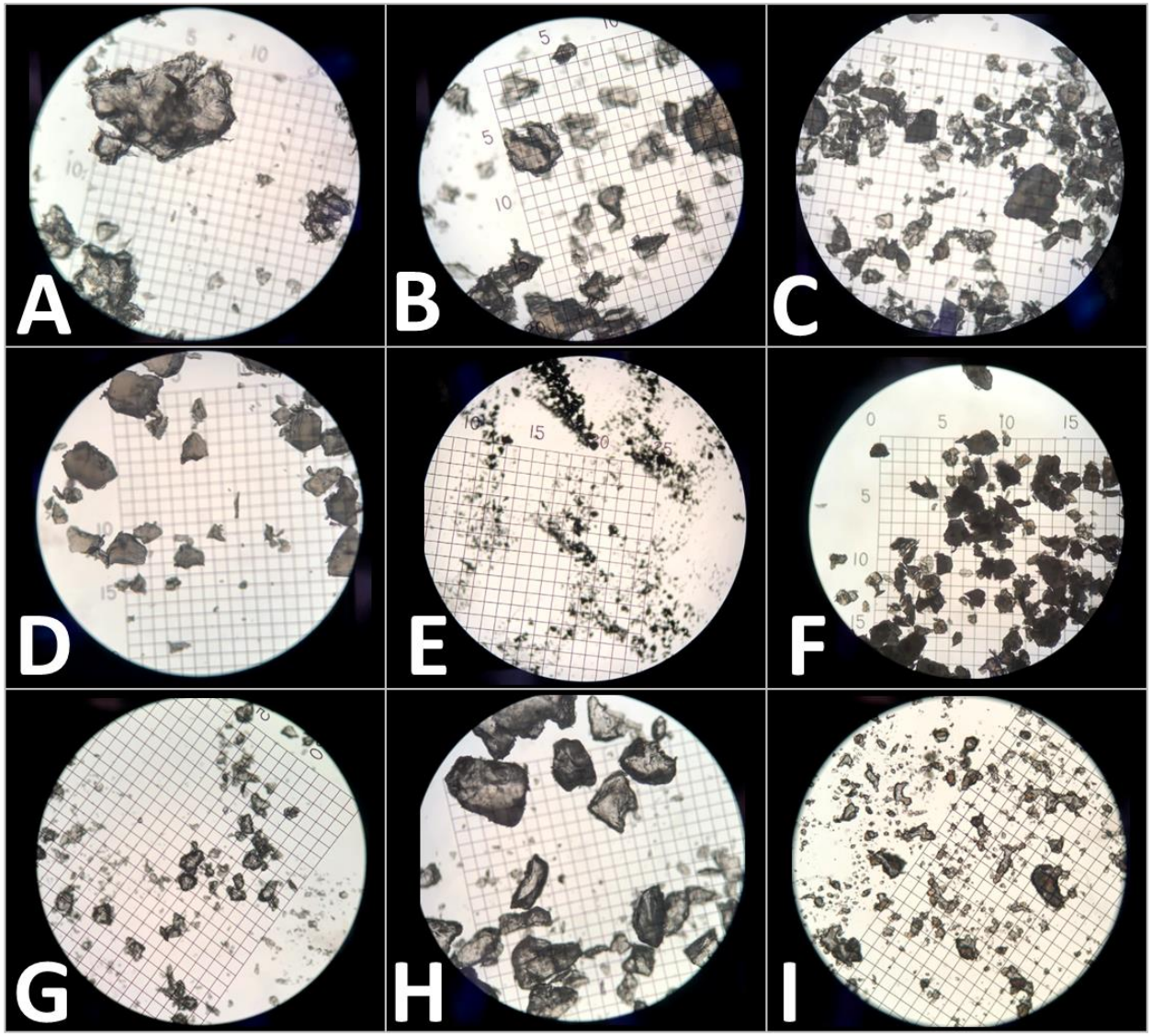

Figure 150. CryoMilled Plastic Particle Size Analysis via Light Microscope: Comparing example photos resulting particles of nine different types of plastic; **[A]** Low-density polyethylene (LDPE); **[B]** High-density polyethylene (HDPE); **[C]** Polypropylene (PPrp); **[D]** Thermoplastic polyurethane (TPUr) ; **[E]** High impact polystyrene (HIPS) ; **[F]** Polyethylene terephthalate (PETE); **[G]** Polyethylene terephthalate glycol (PETG); **[H]** Polycarbonate (PCRb); and **[I]** Acrylonitrile butadiene styrene (ABSt). *All shown on Grid 1 (0.05 mm²) under 4x magnification.*

9.2.4. Microplastics Reference Materials Discussion.

During CryoMilling, HIPS, PETG and ABSt, all resulted in a very fine powder, regardless of the jar input volume. This was supported by the particle size analysis, where the average particle diameter was ≈ 20 µm for PETG and ABSt. HIPS produced the smallest diameter with an average particle of ~ 5.0 µm. These fine powders were ruled out for further use at a very early stage for practical sampling reasons. (how to contain them yet expose them to a realistic aqueous environment). Alternatively, TPUr , proved difficult to produce a consistent, smaller than original particle size, normally producing only large fractured chunks, and an optimal milling weight could not be found. Similarly PCRb, also proved difficult to determine an optimal milling weight, also producing large chunks of the original pellets, but unlike TPUr, the PCRb chunks would be mixed in with a very fine powdered dust, adjustment of the milling weight only produced more dust-like particles with very little intermediate sized particles, and therefore was also ruled out for further processing. LDPE, HDPE, PETE, and PPrp all produced usable ranges of particle size and were chosen for use in further sample testing. They were processed in bulk to create homogenized stocks of each plastic, and were evaluated further for texture and consistency:

PETE particles clumped together easily, making it hard to separate when dry, and therefore required the viewing solvent for all size determinations. The tendency to clump tightly was so strong that size was initially hard to determine, as once a particle of largest diameter would be manipulated/moved into position, more often than not the particle would fall apart into smaller pieces. Ultimately, the largest particle diameter was determined to be 200 µm, which was the smallest for all of the plastics chosen for analysis. This also gave PETE the smallest range in particle size having only 0.18 mm difference between the largest and smallest particle.

LDPE. had the largest bi-modal range of particles, where the majority were either very large (~550 µm) or very small (~60 µm) in size, with very few particles between. Additionally LDPE had the largest diameter range, with the largest particle being ~490 µm larger than the smallest, but less than 5% of the particles present were on the end of the size range. The largest size of LDPE was believed to be the result of the high elasticity of the material, requiring the lowest optimal milling weight (6.0 g) compared to the other plastics, in order to achieve a powder.

The resulting particles were also visually very rough in appearance, as if they were ripped apart, versus a sharp fracturing seen in some of the other plastics.

HDPE also had a high clumping tendency, but would clump in much less dense chunks when compared to PETE, possibly due to the larger average size of the particles which was the most moderate of the plastics chosen for analysis. Average particle size was approximately 450 µm, with a 220 µm range between the largest and smallest particle. HDPE represented the largest visual modal, where the particle size distribution was evenly spread across the entire size range. Similarly to LDPE, HDPE also required the lowest optimal milling weight of 6.0 g of pellets, but was much easier to attain a homogenous particle size, possibly due to the its higher density.

9.3. Microplastics Instrument Methods

9.3.1. Original SFE-SFC-MS Method for Online Extraction of PAHs from Soil using 5.0-mL Vessels from Wicker et. al., 2018.[120]

Original MRM-Detection method. PAHs are commonly studied using LCMS and GCMS, and APCI ionization is common to the detection of PAHs.[127],[128] The MRM method used in this work was a previously developed method from **Wicker et. al., 2018**[120] and was not modified for the current work. Details of the method are provided at the end of this chapter in **Section 9.i.3.2. Original Method for Soil: *Original MS Parameters*.** In short, the Shimadzu LabSolutions optimization program was used with flow injection analysis to determine optimal MRM transitions and collision energies for each of the targeted PAH compounds. Resulting MRM transitions are given in **Table 45,** for all 16 PAH standards and the 5 internal standards**.** Both the protonated molecular species $[M+H]^+$ and the molecular radical cations $[M]^{\bullet+}$ were monitored for the targeted analytes**.** Using an APCI source, charge transfer dominated ion formation for the majority of the PAHs, producing the $[M]^{\bullet+}$ ion as the predominant precursor; with the exception of IDPY & BGPY, having six-membered ring structures, alternatively ionized by proton transfer.

Table 45. Multiple Reaction Monitoring (MRM) Parameters of 16 Polycyclic Aromatic Hydrocarbons (PAHs) and 5 Internal Standards.

Elution Order	Critical Group	Analyte	ID	Monoisotopic Mass (g/mol)	Precursor (m/z)	+/-	Product (m/z)	Q1 Pre Bias (V)	Collision Energy (V)	Q3 Pre Bias (V)
1	-	Naphthalene	**NAPL**	128.06	128.3	+	102.0	-24	-26	-10
2	-	Acenaphthylene	**ANPY**	125.06	152.2	+	150.1	-11	-37	-14
3	-	Acenaphthene	**ACEN**	154.08	154.0	+	152.0	-10	-38	-14
4	-	Fluorene	**FLUR**	166.08	166.0	+	164.0	-15	-33	-16
5	A	Phenanthrene	**PHNR**	178.08	178.3	+	151.2	-13	-41	-26
6	A	Anthracene	**ANRN**	178.08	178.3	+	151.2	-14	-41	-15
7	B	Fluoranthene	**FLAT**	202.08	202.1	+	150.1	-20	-68	-15
8	B	Pyrene	**PYRN**	202.08	202.1	+	150.2	-28	-65	-30
9	C	Benzo(a)anthracene	**BARC**	228.09	228.3	+	200.2	-21	-57	-21
10	C	Chrysene	**CHSY**	228.09	228.4	+	200.2	-16	-52	-20
11	D	Benzo(b)fluoranthene	**BBFA**	252.09	252.0	+	250.2	-18	-45	-28
12	D	Benzo(k)fluoranthene	**BKFA**	252.09	252.0	+	250.2	-22	-46	-24
13	D	Benzo(a)pyrene	**BAPY**	252.09	252.0	+	250.2	-20	-46	-24
14	-	Dibenzo(a,h)anthracene	**DBAR**	278.11	278.3	+	276.2	-14	-44	-28
15	E	Indeno(1,2,3-cd)pyrene	**IDPY**	276.09	277.3	+	276.3	-30	-33	-25
16	E	Benzo(g,h,i)perylene	**BGPY**	276.09	277.3	+	276.2	-19	-33	-13
17	-	Acenaphthene-d_{10}	**A-d10**	136.11	136.1	+	108.3	-24	-33	-10
18	-	Benzo[e]pyrene-d_{12}	**B-d12**	164.14	164.0	+	162.0	-12	-20	-15
19	-	Chrysene-d_{12}	**C-d12**	212.14	212.2	+	156.2	-25	-59	-14
20	-	Fluoranthene-d_{10}	**F-d10**	240.17	240.0	+	236.0	-18	-47	-25
21	-	Naphthalene-d_8	**N-d8**	264.17	264.2	+	232.3	-23	-70	-11

Targeted PAHs & Critical pairs. Structures for the 16 PAHs are shown in **Figure 151**. Five groups of isomers were identified as 'critical groups', having such similar masses and ion transitions, that chromatographic separation would be required: group A (ANRN & PHNR); group B (FLAT & PYRN); group C (BARC & CHSY); group D (BAPY, BBFA & BKFA) and group E (IDPY & BGPY).

Original Method for Online Extraction of PAHs from Soil. The original method was developed and validated to extract, separate and analyze all 16 PAHs in less than 30 minutes from soils, such as clay, sand and sediment, and was demonstrated successfully at levels below the practical quantitation limits set by the EPA. Details of the original method are given at the end of this chapter in **Section 9.i.3.2. Original Method for Soil: *Original SFC Separation Parameters*** and ***Original SFE Extraction Parameters.*** This method utilized gradient elution, with acetonitrile as modifier. Separation was achieved on a Cosmosil Cholester column (4.6 x 250 mm, 5 µm d_p), using a 3.0 mL/min flow rate with a 50 °C column temperature and 15.0 MPa backpressure during chromatographic separation. These parameters were also optimal for the separation of PAHs in the current work and therefore were not modified. Extractions utilized a 40 °C vessel temperature and and 15 MPa outlet pressure during extraction, with a 1.0 minute (min) filling, 6.0 min Static and 5.0 min dynamic extraction (all at 10% ACN).

In the original method, extractions utilized 5.0-mL vessels with a BPR split configuration (see **Chapter #1: Hyphenated Instrumentation; Section 1.5.4. 'Split' versus 'Splitless' Extraction Modes**). In short, in 'Split-mode' configuration, the duel BPRs are operated so that there is a delta pressure pre- and post- column. This delta pressure results in a condition where during extraction (and consequently during 'sample plug' loading) the majority of the effluent (from the extraction loop) is forced out to waste, reducing the volume of extract loaded onto the chromatographic column. This allowed for large capacity of starting materials (i.e., 1 gram of soil loaded into the large capacity, 5.0-mL vessels), specifically this method was optimized for 1.0 g of starting materials. In the current work, 0.2-mL extraction vessels are indicated, due to the limited availability of microplastics sample material, and therefore it was necessary to transfer and further develop the method for use with smaller volume extractions chambers.

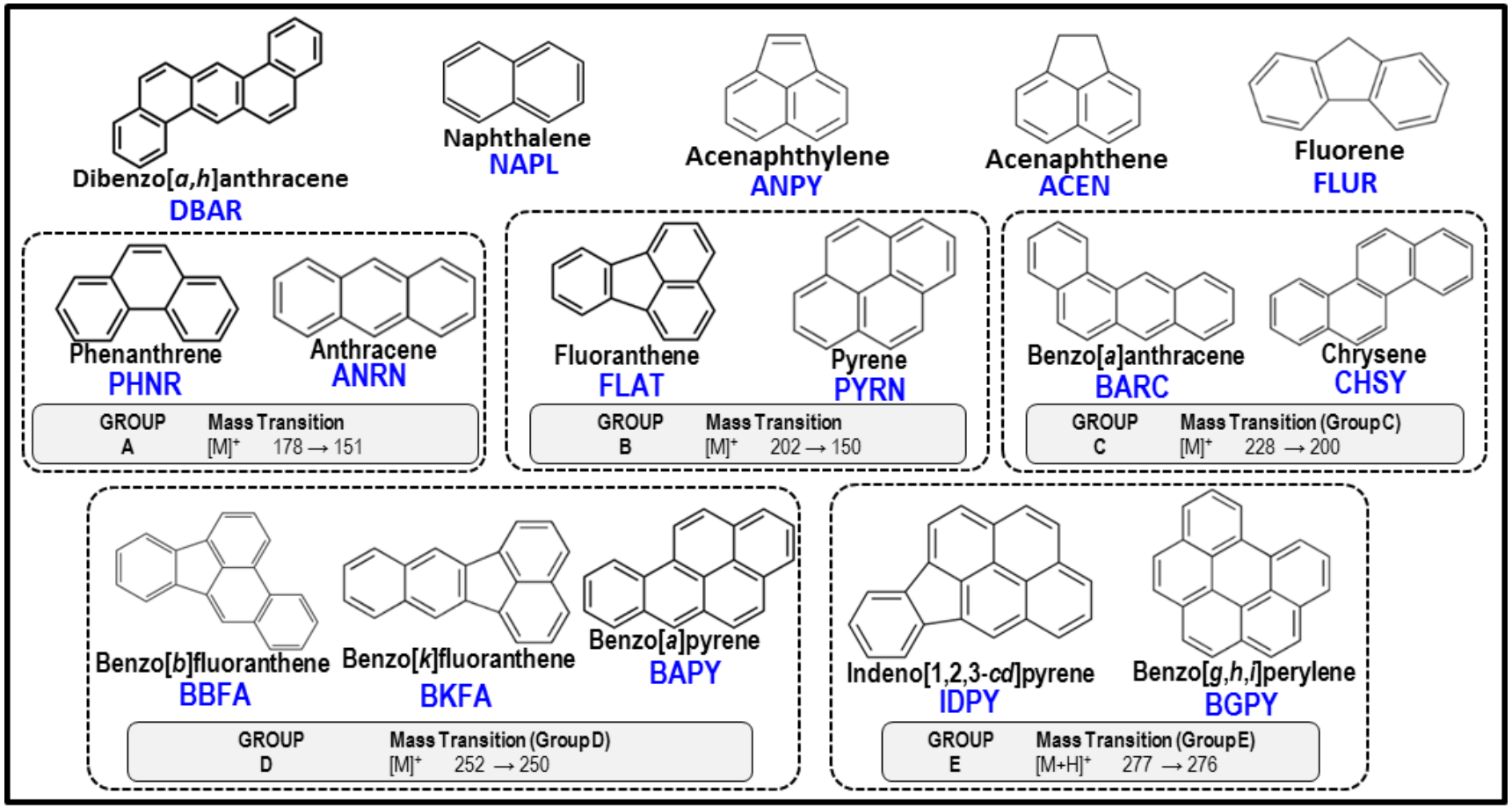

Figure 151. Critical Pair Groups showing structure and (similar) MRM Transitions identified during MRM optimization.

9.3.2. Direct Application of Original method to Microplastics.

An example SFE-SFC-MS chromatogram of an online extraction from soil using the previously developed method is provided in supplementary figure S_Figure 28**; [A]**, showing the separation between critical groups. Initially the method was directly applied to microplastics spiked with 11 PAHs and the results are shown in supplementary figure S_Figure 28**; [B].** Using the original method, applied directly to 0.2-mL extractions, all 11-spiked PAHs were successfully extracted. Signal intensity was lower, which would be expected in consideration that 1/100th of the materials were present (1 g in clay versus 10 mg for microplastics). However, peaks begin to elute during dynamic extraction step (i.e., before the "start" of the run), since the gradient does not begin until after 5 pks have already traveled thru the column and had been detected. There was also a marked decrease in resolution between critical pairs in group A (pk 5 & 6, green). This indicates some modification to the method would be necessary to transfer the method for 0.2-mL vessels.

9.4. Method Transfer for 0.2-mL Vessels

9.4.1. SFE-SFC-MS Re-optimization: Extraction Parameter Screening

Extraction parameters screened for optimization for 0.2-mL vessels are given at the end of this chapter in **Section 9.i.3.3. SFE-SFC-MS Method Transfer for 0.2-mL Vessels: *Extraction Parameter Screening***. The duration was shortened and modifier concentration decreased to 0%, for dynamic extraction. The duration was determined by the retention time of the first peak in in supplementary figure S_Figure 28**; [B],** which resulted in a 1.0 minute dynamic extraction time. These changes resulted in improved 'extraction plug retention', evidenced by a large increase in area for peak 1 (NAPL), and lowered noise for the earliest eluting peaks (pk 1-4). Peak shape, especially for NAPL was still poor, and therefore a change to 0% modifier on the static extraction step was needed. This produced improved peak shape, and little to no change in peak area for all the analytes (i.e., lower modifier present during "static extraction" did not have a negative observable effect on extractability at these conditions). To try to further improve 'plug retention', the dynamic time was then decreased further from 1.0 minutes to 0.5

minutes. This resulted in a decrease in peak area for peaks (1-7), apparently due to incomplete sample plug delivery to the column before vent valve switching. Increasing the dynamic duration to 0.8 minutes, allowed sufficient time for plug loading, and the peak area was restored to original values. This was determined to be the optimal extraction parameters which are outlined in **Section 9.i.3.5. Final SFE-SFC-MS Method for Online Extraction of PAHs from Microplastics**.

9.4.2. SFE-SFC-MS Re-optimization: Gradient Screening

Gradients were screened with the intent to improve Rs between critical pairs. Instrument parameters used during gradient screening are provided in **Section: 9.i.3.4. SFE-SFC-MS Method Transfer for 0.2-mL Vessels: Gradient Screening Parameters; *Gradient Screening Parameters***. Full baseline resolution (Rs) was maintained for all members of critical groups B, C and E (**S_Table 12**). More than adequate resolution could be attained between the two later eluting members of group D; BKFA and BAPY, with minimum resolution > 8 for all screened gradients. The earlier eluting pair, BBFA: BKFA, proved harder to separate, with Rs ranging from near baseline (1.42) separation, to a minimum Rs of 1.26. However, the lowest resolution was achieved for critical group A (PHNR and ANRN, Rs = 1.22 – 1.41). Ultimately a compromise in resolution between groups A and B was required.

Gradient 6, was determined to provide the best compromise and overall best separation, additionally producing a small increase in resolution between peaks 2-4, which gives the final optimized SFE-SFC-MS method for PAH extraction with 0.2-mL vessels (**Section: 9.i.3.5. Final SFE-SFC-MS Method for Online Extraction of PAHs from Microplastics**).

9.4.3. Optimized SFE-SFC-MS Method for 0.2-mL vessels.

In the end, method transfer required minimal time, the original method being quite applicable in many respects, with only small changes needed to the chromatographic gradient to compensate for the lower volume of the extraction chamber. The stationary phase, column temperature and outlet pressure during separation were all directly transferable and, therefore, were not modified. Extraction parameters were modified more heavily, which

was required to produce adequate sample plug retention, and is believed to directly stem from the lower vessel volume (no packing material to saturate, etc.). These results exhibits the importance of investing in the development of robust, highly sensitive methods, and the ease of method transfer between similar applications.

The resulting final re-optimized method for use with 0.2-mL extraction vessels. Minimal modification to the chromatographic method was necessary, where lengthening the gradient by 1 minute gave nearly the same resolution achieved in the original method. The method also required the extraction durations to be shortened, and the percent modifier to be lowered, due to the lower volume of the extraction chamber, resulting in a 1.0 minute vessel filling (10% B), followed by a 6 minute static extraction and 0.8 minute dynamic extraction (both at 0% B). The total runtime was 25 minutes for extraction, separation and analysis. Final re-optimized method details are given in **Section 9.i.3.5. Final SFE-SFC-MS Method for Online Extraction of PAHs from Microplastics**, and a representative chromatogram is shown in **Figure 152.**

Extractions were performed using the re-optimized method to evaluate reproducibility of retention times and peak areas. Online extractions gave reproducible retention times (± 0.03 minutes) and peak areas (RSD ≤ 14%) for all target analytes (**Table 46** for LDPE; **Table 47** for HDPE; and **Table 48** for PETE type plastics).

Full baseline resolution (Rs) was maintained for three of the five critical MRM groups: Group B (FLAT : PYRN, [pks 7 & 8], $Rs_{[7:8]}$ = 5.3); Group C (BARC : CHSY, [pks 9 & 10], $Rs_{[9:10]}$ = 4.0); and group E (IDPY : BGPY, [pks 15 & 16] $Rs_{[15:16]}$ = 4.6). More than adequate resolution could be attained for two of the members of group D (BKFA : BAPY, [pks 12 & 13], $Rs_{[12:13]}$ = 7.6), but a compromise between the remaining two critical compounds (BBFA: BKFA, [pks 11 & 12],$Rs_{[11:12]}$ = 1.48) and the remaining critical group A (PHNR : ANRN, [pks 5 & 6], $Rs_{[5:6]}$ = 1.26) resulted in near baseline resolution for both pairs.

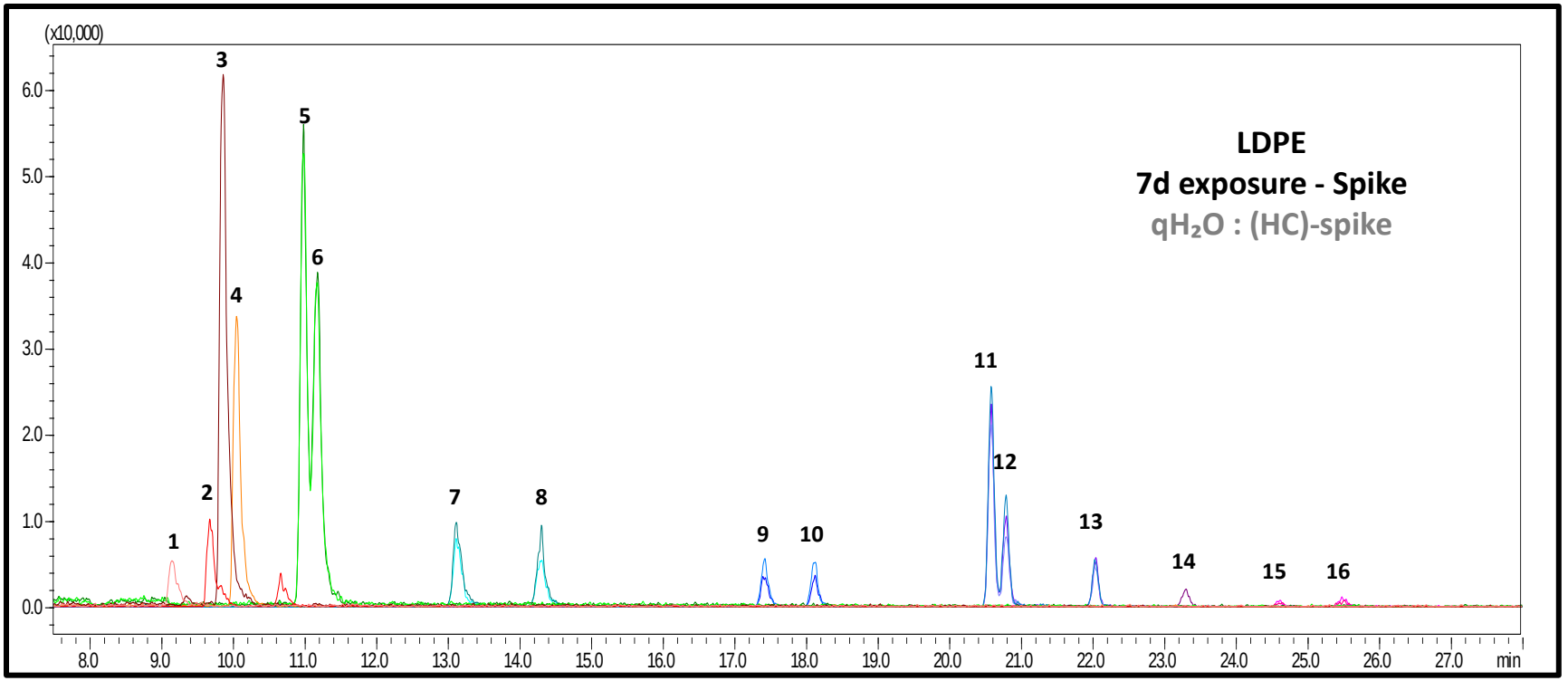

Figure 152. Modified SFE-SFC-MS Method for 0.2-mL Vessel Online Extraction of 16 PAHs from Microplastics. Showing representative chromatogram for LDPE microplastics reference materials after 7 days of exposure to Milli-Q water spiked with PAHs (1250 ng/g). Peak order: [1] NAPL, naphthalene (pink); [2] ANPY, acenaphthylene (red); [3] ACEN, acenaphthene (maroon); [4] FLUR, fluorene (orange); [5] PHNR, phenanthrene (green); [6] ANRN, anthracene (dark green); [7] FLAT, fluoranthene (torquoise); [8] PYRN, pyrene (cyan); [9] BARC, benzo(*a*)anthracene (blue); [10] CHSY, chrysene (cobalt); [11] BBFA, benzo(*b*)fluoranthene (teal); [12] BKFA, Benzo(*k*)fluoranthene (lilac); [13] BAPY, benzo(*a*)pyrene (purple); [14] DBAR, dibenzo(*a*,*h*)anthracene (magenta); [15] IDPY, indeno(1,2,3-*cd*)pyrene (rose); [16] BGPY, benzo(*g*,*h*,*i*)perylene (hot pink). Zoomed baseline for 'Analysis' = 7.5 – 28.0 minutes.

Table 46. Low-Density Polyethylene (LDPE) Microplastics Reference Materials (µPs-RMs) Exposed to Milli-Q Water Spiked with 11 Polycyclic Aromatic Hydrocarbons (PAHs) at High Concentration (qH_2O : HC-spike, 1250 ng/g). **Data in Process**

					1 day Exposure (n =3)			7 day Exposure (n =3)			14 day Exposure (n = 2)		
			Retention Time (min)		Total Peak Area		Av%EXT	Total Peak Area		Av%EXT	Total Peak Area		Av%EXT
#	Analyte	ID	Average	%RSD	Average	%RSD	[1+2]	Average	%RSD	[1+2]	Average	%RSD	[1+2]
1	Naphthalene	NAPL	9.13 ± 0.02	0.23%	67,290	2%	87%	62,889	4%	83%	97,801	2%	90%
2	Acenaphthylene	ANPY	9.63 ± 0.02	0.24%	99,395	6%	87%	114,663	9%	86%	170,385	1%	88%
3	Acenaphthene	ACEN	9.82 ± 0.02	0.18%	333,278	5%	87%	667,108	12%	87%	520,749	2%	88%
4	Fluorene	FLUR	10.00 ± 0.02	0.24%	149,108	7%	87%	320,995	9%	88%	238,834	1%	89%
5	Phenanthrene	PHNR	10.93 ± 0.03	0.25%	324,106	7%	87%	477,950	10%	88%	650,982	2%	88%
6	Anthracene	ANRN	11.12 ± 0.02	0.22%	320,256	9%	89%	397,490	10%	89%	577,766	4%	88%
7	Fluoranthene	FLAT	13.08 ± 0.02	0.19%	83,902	8%	89%	108,341	10%	88%	199,641	2%	87%
8	Pyrene	PYRN	14.23 ± 0.03	0.19%	52,174	10%	89%	64,437	10%	89%	125,182	4%	86%
9	Benzo(a)anthracene	BARC	17.38 ± 0.02	0.14%	40,142	8%	92%	45,481	9%	89%	139,062	1%	87%
10	Chrysene	CHSY	18.08 ± 0.02	0.11%	ns	ns	ns	29,039	5%	91%	ns	ns	ns
11	Benzo(b)fluoranthene	BBFA	20.58 ± 0.01	0.01%	ns	ns	ns	175,713	9%	90%	ns	ns	ns
12	Benzo(k)fluoranthene	BKFA	20.78 ± 0.01	0.03%	46,075	5%	92%	67,405	5%	89%	150,900	5%	87%
13	Benzo(a)pyrene	BAPY	22.05 ± 0.01	0.03%	50,059	6%	92%	42,669	8%	92%	119,180	10%	88%
14	Dibenzo(a,h)anthracene	DBAR	23.31 ± 0.02	0.08%	ns	ns	ns	15,090	14%	92%	ns	ns	ns
15	Indeno(1,2,3-cd)pyrene	IDPY	24.63 ± 0.01	0.02%	ns	ns	ns	2,569	14%	94%	ns	ns	ns
16	Benzo(g,h,i)perylene	BGPY	25.48 ± 0.02	0.06%	ns	ns	ns	9,771	13%	91%	ns	ns	ns

ns = 'not-spiked', standard not included in original test;

Table 47. High-Density Polyethylene (HDPE) Microplastics Reference Materials (µPs-RMs) Exposed to Milli-Q Water Spiked with 11 Polycyclic Aromatic Hydrocarbons (PAHs) at High Concentration (qH_2O : HC-spike, 1250 ng/g). **Data in Process**

				1 day Exposure (n =3)			7 day Exposure (n =1)			14 day Exposure (n =0)		
			Retention Time (min)	Total Peak Area		Av%EXT	Peak Area		%EXT	Peak Area		Av%EXT
#	Analyte	ID	Average	Average	%RSD	[1+2]	Total	%RSD	[1+2]	Av. Total	%RSD	[1+2]
1	Naphthalene	NAPL	9.09 ± 0.02	0.22%	156,735	5%	93%	165,844	n/a	92%	-	-	-
2	Acenaphthylene	ANPY	9.60 ± 0.02	0.19%	263,935	14%	93%	151,658	n/a	91%	-	-	-
3	Acenaphthene	ACEN	9.78 ± 0.02	0.21%	1,092,042	13%	91%	532,489	n/a	90%	-	-	-
4	Fluorene	FLUR	9.97 ± 0.02	0.24%	609,786	14%	92%	245,790	n/a	90%	-	-	-
5	Phenanthrene	PHNR	10.90 ± 0.02	0.16%	783,321	14%	92%	647,825	n/a	89%	-	-	-
6	Anthracene	ANRN	11.08 ± 0.02	0.18%	783,414	6%	92%	603,863	n/a	91%	-	-	-
7	Fluoranthene	FLAT	13.08 ± 0.02	0.15%	242,574	14%	91%	181,275	n/a	89%	-	-	-
8	Pyrene	PYRN	14.24 ± 0.02	0.15%	150,967	13%	91%	122,110	n/a	90%	-	-	-
9	Benzo(a)anthracene	BARC	17.41 ± 0.02	0.09%	131,335	13%	92%	119,596	n/a	89%	-	-	-
10	Chrysene	CHSY	ns ± ns	ns	ns	ns	ns	ns	ns	ns	-	-	-
11	Benzo(b)fluoranthene	BBFA	ns ± ns	ns	ns	ns	ns	ns	ns	ns	-	-	-
12	Benzo(k)fluoranthene	BKFA	20.82 ± 0.01	0.03%	148,791	7%	91%	120,491	n/a	87%	-	-	-
13	Benzo(a)pyrene	BAPY	22.08 ± 0.00	0.00%	96,179	15%	92%	101,036	n/a	87%	-	-	-
14	Dibenzo(a,h)anthracene	DBAR	ns ± ns	ns	ns	ns	ns	ns	ns	ns	-	-	-
15	Indeno(1,2,3-cd)pyrene	IDPY	ns ± ns	ns	ns	ns	ns	ns	ns	ns	-	-	-
16	Benzo(g,h,i)perylene	BGPY	ns ± ns	ns	ns	ns	ns	ns	ns	ns	-	-	-

ns = 'not-spiked', standard not included in original test; **n/a** = not applicable

Table 48. Polyethylene terephthalate (PETE) Microplastics Reference Materials (µPs-RMs) Exposed to Milli-Q Water Spiked with 11 Polycyclic Aromatic Hydrocarbons (PAHs) at High Concentration (qH_2O : HC-spike, 1250 ng/g). **Data in Process**

					1 day Exposure (n =3)			7 day Exposure (n =1)			14 day Exposure (n =0)		
			Retention Time (min)		Total Peak Area		Av%EXT	Peak Area		%EXT	Peak Area		%EXT
#	Analyte	ID	Average	%RSD	Average	%RSD	[1+2]	Total	%RSD	[1+2]	Total	%RSD	[1+2]
1	Naphthalene	NAPL	9.12 ± 0.02	0.23%	143,736	9%	94%	140,055	n/a	97%	-	-	-
2	Acenaphthylene	ANPY	9.65 ± 0.01	0.08%	32,643	10%	99%	39,103	n/a	99%	-	-	-
3	Acenaphthene	ACEN	9.84 ± 0.02	0.20%	277,440	13%	99%	195,827	n/a	99%	-	-	-
4	Fluorene	FLUR	10.06 ± 0.02	0.15%	171,509	8%	99%	112,927	n/a	99%	-	-	-
5	Phenanthrene	PHNR	10.99 ± 0.02	0.18%	219,263	11%	99%	228,964	n/a	99%	-	-	-
6	Anthracene	ANRN	11.13 ± 0.01	0.10%	178,507	14%	99%	132,904	n/a	98%	-	-	-
7	Fluoranthene	FLAT	13.09 ± 0.02	0.15%	87,322	8%	99%	60,979	n/a	99%	-	-	-
8	Pyrene	PYRN	14.30 ± 0.02	0.17%	55,726	10%	100%	35,019	n/a	98%	-	-	-
9	Benzo(a)anthracene	BARC	17.41 ± 0.01	0.07%	53,953	11%	98%	31,792	n/a	99%	-	-	-
10	Chrysene	CHSY	ns ± ns	ns	ns	ns	ns	ns	ns	ns	-	-	-
11	Benzo(b)fluoranthene	BBFA	ns ± ns	ns	ns	ns	ns	ns	ns	ns	-	-	-
12	Benzo(k)fluoranthene	BKFA	20.83 ± 0.02	0.11%	113,336	11%	97%	44,716	n/a	97%	-	-	-
13	Benzo(a)pyrene	BAPY	22.10 ± 0.01	0.06%	56,906	14%	97%	22,465	n/a	99%	-	-	-
14	Dibenzo(a,h)anthracene	DBAR	ns ± ns	ns	ns	ns	ns	ns	ns	ns	-	-	-
15	Indeno(1,2,3-cd)pyrene	IDPY	ns ± ns	ns	ns	ns	ns	ns	ns	ns	-	-	-
16	Benzo(g,h,i)perylene	BGPY	ns ± ns	ns	ns	ns	ns	ns	ns	ns	-	-	-

ns = 'not-spiked', standard not included in original test; **n/a** = not applicable

9.4.4. Microplastics Analysis Workflow

The final method utilized 10.0 mg of sample material per extraction. This is especially beneficial in studies such as that for microplastics where sample availability can be quite limited. Ten milligrams of microplastics were weighed accurately on weigh paper, transferred directly into pre-assembled 0.2-mL extraction vessels, closed, and loaded into the automated rack changer for online analysis (**Figure 153**). A note should be made about the importance of using compatible vessel filters (Sinter-type) for samples that contain small particle (**S_Figure 29**). These filters are not the standards filters for 0.2-mL vessels and may require to be purchased separately.

Additionally, to prevent the particles from falling between the parts, extraction vessels were pre-assembled to ensure the bottom filter was efficiently seated into the body, then re-opened (i.e., only the vessel lid and top filter removed) just prior to sample loading. Once the sample was loaded, the top filter and lid were replaced.

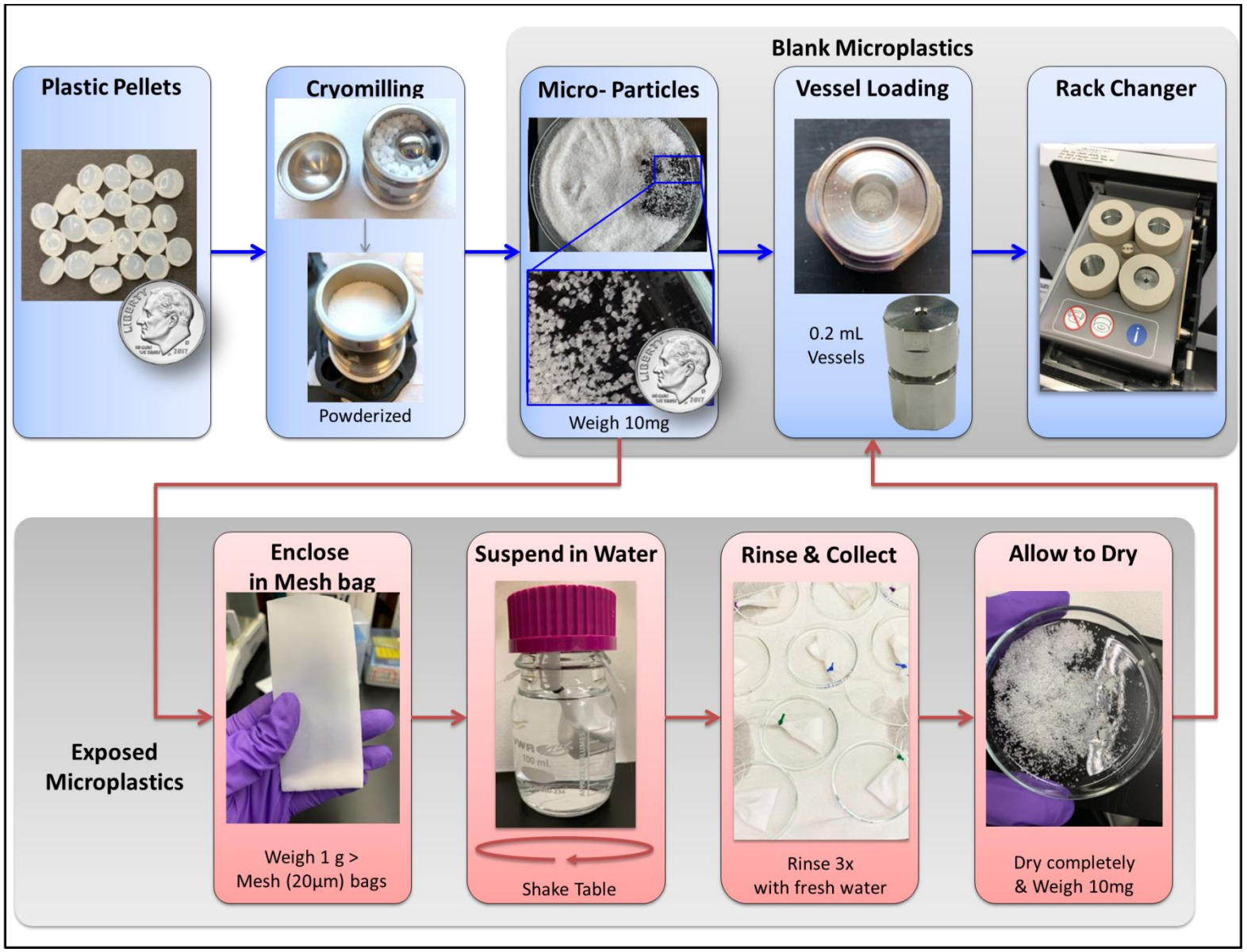

Figure 153. Microplastics Cryomilling and Sampling Workflow.

9.5. Online Extractions - Initial Matrix Evaluation *Lab Blanks and Spiked Lab QCs*

9.5.1. Lab Controls

Laboratory exposed-microplastics were limited to three types of plastics due to practical limitations. Therefore controls were created for LDPE, HDPE and PETE only. Laboratory control sets were created for each plastic type as described in **Chapter #2. Materials and Methods; Section: 2.7.5. Sample Prep: *Exposed-µPs; Lab Control Test-Sets,*** exposed to either blank or spiked water and shaken for 1, 7 and 14 days. The shake table conditions were set to mimic the temperature and motion of tidal water circulation. Low and high spike concentrations were chosen based on literature values reported for PAHs in marine waters.

Lab Blank - ***Online Extractions*** **[qH_2O : Blank].** Extractions were performed, on the lab blank (no-spike) QC for each plastic (**Figure 154; top**). These materials were exposed for 1-day, to blank- Milli-Q water [qH2O:Blank]. The presence of PAHs were detected in the lab blanks for all three types of plastic. Not all the target compounds were observed, but when detected, the PAHs present, were dependent on polymer-type (**Table 49** for LDPE; **Table 50** for HDPE; and **Table 51** for PETE type plastics).

Prep Control Exposed Sampling Bags: Extractions are planned but have not yet been performed, on portions of sample bags used in exposure tests.

Spiked Samples – Online Extractions **[qH_2O : HC-Spike]**. After exposure to Milli-Q water spiked with 11 PAHs at high QC (1250 ng/g µPs-RMs), a marked increase in peak areas were observed for all spiked analytes in all three plastics (**Table 46** for LDPE; **Table 47** for HDPE; and **Table 48** for PETE type plastics). Differences in peak areas were seen between plastic types and between exposure durations for both total area extracted and extraction performance.

9.5.2. Initial Matrix Evaluation

Blank Matrix Evaluation: Blank controls are compared to spiked samples in **Figure 154.** Due to the low intensity of the detected PAHs in the blanks, Zoomed chromatograms for blank controls are also provided in supplementary figure **S_Figure 30**. Six of the targeted PAHs were detected in at least one of the blank plastics. NAPL (pk 1), FLUR (pk 4) and PHNR (pk 5) were detected in all three plastics: FLUR was only seen at very low levels, representing < 2% of the total area for the equivalent 1day spiked samples for each plastic. NAPL was also very low in HDPE and LDPE lab blanks, representing less than 6 and 9% respectively, of the average total area in the equivalent exposure spiked sample, but significant area was observed for NAPL in lab blank for PETE, representing 40% of the total area extracted from the equivalent spiked PETE sample. The level of PHNR was moderate in all plastics, giving areas between 4 and 12% of the equivalent exposure spiked sample. Interestingly, PHNR being one of the two compounds in critical group A, was found in all the plastics, but the other member of this group, ANRN (pk 6), was only detected in one of the plastics, LDPE (11% spike area), but was not detected in the HDPE or PETE lab blanks. FLAT was detected in both the LDPE and PETE blanks (3% and 2% respectively of the equivalent exposure lab samples). Other notable features of the blank matrix would include a significant artifact on the ANPY-MRM [red], at 10.8 min. This artifact peak does not coincide with any of the target analytes, as ANPY (pk 2) elutes much earlier at 9.6 minutes, and was not detected in any of the lab blanks, therefore this signal was not considered to be interfering but is consistently present between pks 3 and 4, especially in the LDPE and HDPE samples.

The presence of PAHs in the blanks, are not unexpected. PAHs are associated with plastics as ingredients and/or byproducts of manufacturing. Especially low molecular weight PAHs are known to originate directly from petrogenic sources, as byproducts formed during the manufacturing process.[129],[130] Therefore the presence of PAHs in virgin plastics, should be expected, since they are associated with petroleum, the raw material of plastics. Although no quantitation was performed, generally the amount present could be considered low compared to the areas observed in the spiked samples for 6 of the 7 PAHs found in the blanks.

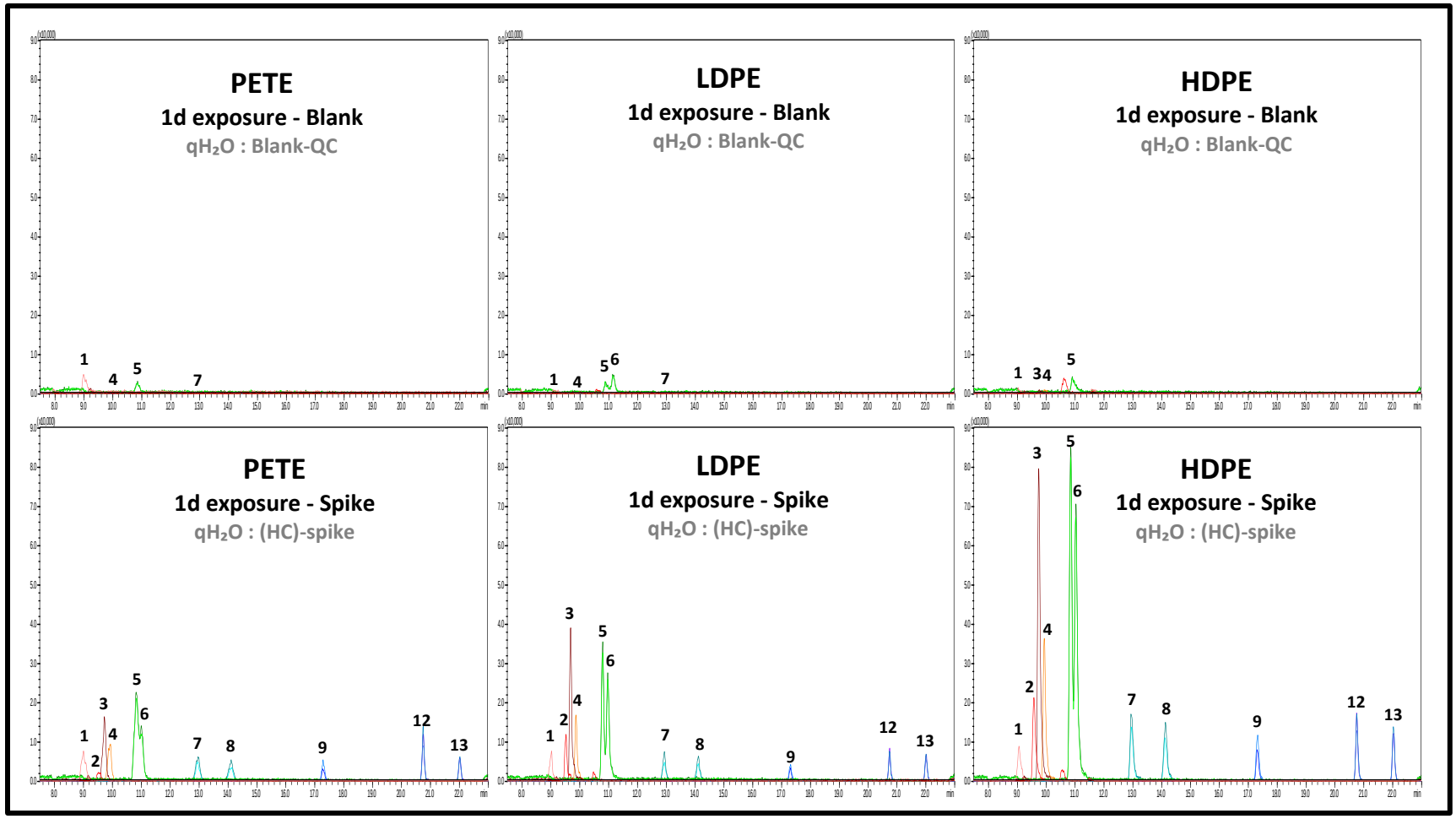

Figure 154. SFE-SFC-MS Chromatograms for Online Extractions µPs-RMs After 1-Day Exposure to Milli-Q Water (*qH₂O*): PETE (left), LDPE (middle), and HDPE (right); Comparing [top] Blank Quality Controls (*Blank-QCs*); and [bottom] High Concentration Polycyclic Aromatic Hydrocarbons Spike Mixture (*PAH-(HC)-spike*, 1250 ng/g). **Peak order: [1] NAPL, naphthalene (pink); [2] ANPY, acenaphthylene (red); [3] ACEN, acenaphthene (maroon); [4] FLUR, fluorene (orange); [5] PHNR, phenanthrene (green); [6] ANRN, anthracene (dark green); [7] FLAT, fluoranthene (torquoise); [8] PYRN, pyrene (cyan); [9] BARC, benzo(*a*)anthracene (blue); *[10] CHSY, chrysene (cobalt); * [11] BBFA, benzo(*b*)fluoranthene (teal); [12] BKFA, Benzo(*k*)fluoranthene (lilac); [13] BAPY, benzo(*a*)pyrene (purple); * [14] DBAR, dibenzo(*a*,*h*)anthracene (magenta); * [15] IDPY, indeno(1,2,3-*cd*)pyrene (rose); * [16] BGPY, benzo(*g*,*h*,*i*)perylene (hot pink). All Chromatograms *Displayed at the same intensity; and baseline zoomed on 'analysis-step' = 7.50 – 23.00 minutes.* *peaks 10, 11, 13, 15 & 16 were not spiked in the original test.**

Table 49. Low-Density Polyethylene (LDPE) Microplastics Reference Materials (µPs-RMs) Exposed to Blank Quality Control Milli-Q Water (qH₂O : Blank).

Data in Process

#	Analyte	ID	Retention Time (min) (min)		%RSD	1 day Exposure (n =1) Total Peak Area Total	%RSD	S/N	Av%EXT [1+2]	% HC-Spike	7 day Exposure (n =0) Peak Area Average	%RSD	%EXT [1+2]	14 day Exposure (n =0) Peak Area Average	%RSD	Av %EXT [1+2]
1	Naphthalene	**NAPL**	9.08	±	**n/a**	4,843	**n/a**	1.9	74%	9%	-	-	-	-	-	-
2	Acenaphthylene	**ANPY**	ND		ND	ND	ND	ND	ND	ND	-	-	-	-	-	-
3	Acenaphthene	**ACEN**	ND		ND	ND	ND	ND	ND	ND	-	-	-	-	-	-
4	Fluorene	**FLUR**	9.99	±	**n/a**	3,451	**n/a**	3.2	94%	2%	-	-	-	-	-	-
5	Phenanthrene	**PHNR**	10.88	±	**n/a**	21,240	**n/a**	4.5	93%	8%	-	-	-	-	-	-
6	Anthracene	**ANRN**	11.14	±	**n/a**	34,252	**n/a**	7.1	8%	11%	-	-	-	-	-	-
7	Fluoranthene	**FLAT**	13.06	±	**n/a**	2,978	**n/a**	2.5	100%	3%	-	-	-	-	-	-
8	Pyrene	**PYRN**	ND		ND	ND	ND	ND	ND	ND	-	-	-	-	-	-
9	Benzo(a)anthracene	**BARC**	ND		ND	ND	ND	ND	ND	ND	-	-	-	-	-	-
10	Chrysene	**CHSY**	ND		ND	ND	ND	ND	ND	ND	-	-	-	-	-	-
11	Benzo(b)fluoranthene	**BBFA**	ND		ND	ND	ND	ND	ND	ND	-	-	-	-	-	-
12	Benzo(k)fluoranthene	**BKFA**	ND		ND	ND	ND	ND	ND	ND	-	-	-	-	-	-
13	Benzo(a)pyrene	**BAPY**	ND		ND	ND	ND	ND	ND	ND	-	-	-	-	-	-
14	Dibenzo(a,h)anthracene	**DBAR**	ND		ND	ND	ND	ND	ND	ND	-	-	-	-	-	-
15	Indeno(1,2,3-cd)pyrene	**IDPY**	ND		ND	ND	ND	ND	ND	ND	-	-	-	-	-	-
16	Benzo(g,h,i)perylene	**BGPY**	ND		ND	ND	ND	ND	ND	ND	-	-	-	-	-	-

-' = No data currently available; **ND** = Not Detected; **n/a** = not applicable (i.e., insufficient replicates)

Table 50. High-Density Polyethylene (HDPE) Microplastics Reference Materials (µPs-RMs) Exposed to Blank Quality Control Milli-Q Water (qH_2O : Blank).

Data in Process

			1 day Exposure (n =1)						7 day Exposure (n =0)			14 day Exposure (n =0)		
			Retention Time (min)		Total Peak Area				Peak Area			Peak Area		
#	Analyte	ID	(min)	%RSD	Total	%RSD	S/N	Av%EXT [1+2]	% HC-Spike	Average	%RSD	%EXT [1+2]	Average	%RSD	Av %EXT [1+2]
1	Naphthalene	**NAPL**	9.04 ±	**n/a**	5,990	**n/a**	4.9	93%	6%	-	-	-	-	-	-
2	Acenaphthylene	**ANPY**	ND	ND	ND	ND	ND	ND	ND	-	-	-	-	-	-
3	Acenaphthene	**ACEN**	9.77 ±	**n/a**	7,357	**n/a**	4.0	100%	1%	-	-	-	-	-	-
4	Fluorene	**FLUR**	9.94 ±	**n/a**	6,034	**n/a**	5.6	87%	1%	-	-	-	-	-	-
5	Phenanthrene	**PHNR**	10.86 ±	**n/a**	26,663	**n/a**	5.7	98%	4%	-	-	-	-	-	-
6	Anthracene	**ANRN**	ND	ND	ND	ND	ND	ND	ND	-	-	-	-	-	-
7	Fluoranthene	**FLAT**	ND	ND	ND	ND	ND	ND	ND	-	-	-	-	-	-
8	Pyrene	**PYRN**	ND	ND	ND	ND	ND	ND	ND	-	-	-	-	-	-
9	Benzo(a)anthracene	**BARC**	ND	ND	ND	ND	ND	ND	ND	-	-	-	-	-	-
10	Chrysene	**CHSY**	ND	ND	ND	ND	ND	ND	ND	-	-	-	-	-	-
11	Benzo(b)fluoranthene	**BBFA**	ND	ND	ND	ND	ND	ND	ND	-	-	-	-	-	-
12	Benzo(k)fluoranthene	**BKFA**	ND	ND	ND	ND	ND	ND	ND	-	-	-	-	-	-
13	Benzo(a)pyrene	**BAPY**	ND	ND	ND	ND	ND	ND	ND	-	-	-	-	-	-
14	Dibenzo(a,h)anthracene	**DBAR**	ND	ND	ND	ND	ND	ND	ND	-	-	-	-	-	-
15	Indeno(1,2,3-cd)pyrene	**IDPY**	ND	ND	ND	ND	ND	ND	ND	-	-	-	-	-	-
16	Benzo(g,h,i)perylene	**BGPY**	ND	ND	ND	ND	ND	ND	ND	-	-	-	-	-	-

'-' = No data currently available; **ND** = Not Detected; **n/a** = not applicable (i.e., insufficient replicates)

Table 51. Polyethylene terephthalate (PETE) Microplastics Reference Materials (µPs-RMs) Exposed to Blank Quality Control Milli-Q Water (qH₂O : Blank).

Data in Process

						1 day Exposure (n =1)					7 day Exposure (n =0)			14 day Exposure (n =0)		
			Retention Time (min)			Total Peak Area			Av%EXT	% HC-	Peak Area		%EXT	Peak Area		Av %EXT
#	Analyte	ID	(min)		%RSD	Total	%RSD	S/N	[1+2]	Spike	Average	%RSD	[1+2]	Average	%RSD	[1+2]
1	Naphthalene	**NAPL**	9.00	± **n/a**	**n/a**	38,736	**n/a**	11.2	91%	43%	-	-	-	-	-	-
2	Acenaphthylene	**ANPY**	ND	ND	ND	ND	ND	ND	ND	ND	-	-	-	-	-	-
3	Acenaphthene	**ACEN**	ND	ND	ND	ND	ND	ND	ND	ND	-	-	-	-	-	-
4	Fluorene	**FLUR**	9.97	± **n/a**	**n/a**	3,119	**n/a**	3.1	95%	2%	-	-	-	-	-	-
5	Phenanthrene	**PHNR**	10.87	± **n/a**	**n/a**	19,401	**n/a**	3.8	96%	12%	-	-	-	-	-	-
6	Anthracene	**ANRN**	ND	ND	ND	ND	ND	ND	ND	ND	-	-	-	-	-	-
7	Fluoranthene	**FLAT**	12.99	± **n/a**	**n/a**	2,080	**n/a**	1.9	100%	2%	-	-	-	-	-	-
8	Pyrene	**PYRN**	ND	ND	ND	ND	ND	ND	ND	ND	-	-	-	-	-	-
9	Benzo(a)anthracene	**BARC**	ND	ND	ND	ND	ND	ND	ND	ND	-	-	-	-	-	-
10	Chrysene	**CHSY**	ND	ND	ND	ND	ND	ND	ND	ND	-	-	-	-	-	-
11	Benzo(b)fluoranthene	**BBFA**	ND	ND	ND	ND	ND	ND	ND	ND	-	-	-	-	-	-
12	Benzo(k)fluoranthene	**BKFA**	ND	ND	ND	ND	ND	ND	ND	ND	-	-	-	-	-	-
13	Benzo(a)pyrene	**BAPY**	ND	ND	ND	ND	ND	ND	ND	ND	-	-	-	-	-	-
14	Dibenzo(a,h)anthracene	**DBAR**	ND	ND	ND	ND	ND	ND	ND	ND	-	-	-	-	-	-
15	Indeno(1,2,3-cd)pyrene	**IDPY**	ND	ND	ND	ND	ND	ND	ND	ND	-	-	-	-	-	-
16	Benzo(g,h,i)perylene	**BGPY**	ND	ND	ND	ND	ND	ND	ND	ND	-	-	-	-	-	-

'-' = No data currently available; **ND** = Not Detected; **n/a** = not applicable (i.e., insufficient replicates)

9.6. Lab-Exposed Microplastics: (1-day Exposure)

9.6.1. Plastic-type Comparison: Total Area Extracted.

When the average total area extracted for each compound is compared between all three plastics (**Figure 155**): a compound specific difference between all three types of plastics can be seen. NAPL was not significantly different between any of the spiked plastics. The areas observed in the blank plastics could explain this, as PETE having the lowest areas for all other low MW PAHs, but produced the highest blank area for NAPL. Extractions from HDPE produced significantly larger areas, compared to the other two plastics, for all other spiked-PAHs. For LDPE and PETE the areas produced were compounds specific for early eluting, smaller MW, spiked-PAHs (ANPY, ACEN, FLUR, PHNR and ANRN). Extractions from LDPE produced the second highest areas. For ANPY, ACEN, FLUR, PHNR and ANRN = 3 ring, small MW PAHs. For mid-eluting compounds (FLAT, PYRN and BARC): LDPE and PETE produced equivalent areas. Interestingly the trend between LDPE and PETE, reverse for the latest eluting compounds, where LDPE produced the lowest areas, for BKFA and BAPY.

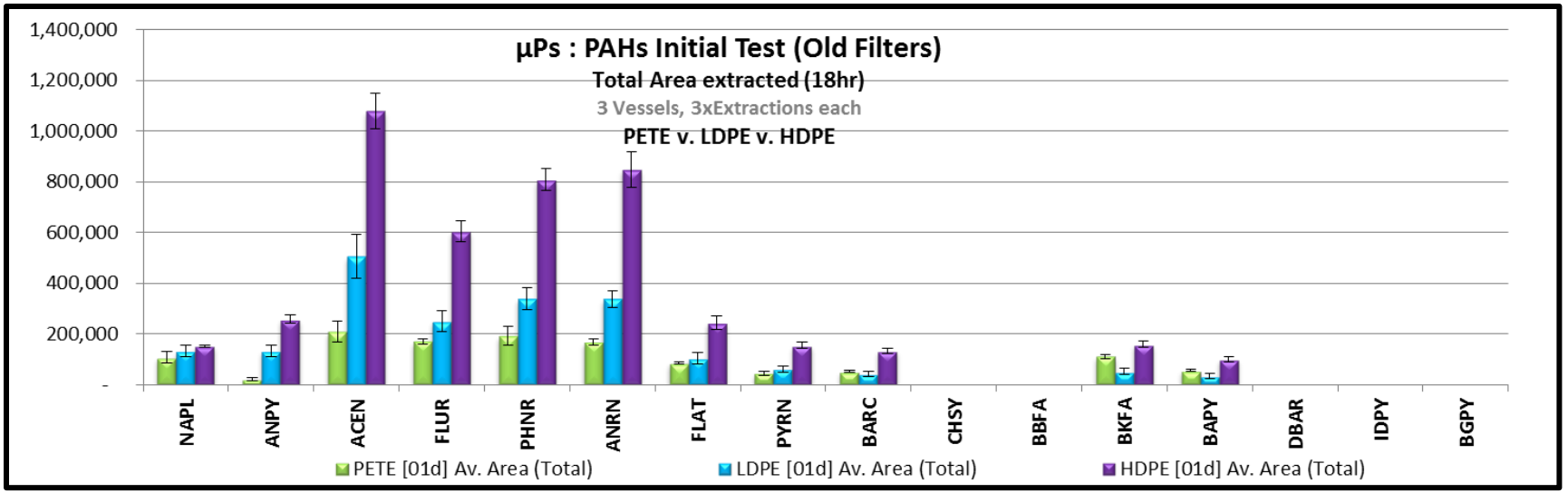

Figure 155. Average Total Area Extracted for Microplastics Exposed for 1-day to Spiked Milli-Q water (HC-Spike; 1250 ng/g); comparing 3 plastic types: PETE [green]; LDPE [blue]; and HDPE [purple]. **Error bars = standard deviation (n=3).**

9.6.2. Plastic-type Comparison: Extraction Performance.

Each vessel was extracted a total of three consecutive times, taking the average of the total amount extracted, and comparing the percent (%) of the total area per extraction round gives a visual representation of how easily extractable a material is, and is especially useful when comparing differences between sample types extracted using the same online SFE-SFC-MS method. As the instrumental conditions have not changed, any difference in proportionality shows relative differences in the extractability of the materials. Bar graphs showing the extraction performance are presented in **Figure 156** for all three plastics.

PETE - ***Extraction Performance***. The average percent of the total area per extraction round for PETE is presented in **Table 54** and is shown in the top panel of **Figure 156; green**. In consecutive online extractions PETE (1d-spike), 97-100% of the total extracted area was in the first two extractions (T_{1+2}). In fact, all spiked analytes (except NAPL, BKFA and BAPY), more than 93% of the total area was extracted in the 1st extraction (%EXT1) alone. The only compound where the first extraction was not statistically the same as the total area extracted was NAPL (Av%EXT1 = 84 ± 3.1%), but the 1st two extractions were the same as the total area (AV%EXT_{1+2} = 94 ± 4.2%).

HDPE - Extraction Performance. The average percent of the total area per extraction round for HDPE is presented in **Table 53** and is shown in the middle panel of **Figure 156; purple**. The area from the 1st two extractions was lower for HDPE (1d-spike), producing between 91 and 93% percent of the total area for each compound, where all compounds required more rounds to extract, with the 1st extraction representing at the highest 81% of the total extractable area for each PAH. The area represented by the second (%EXT2 = 17-20%) and third (%EXT3 = 7-9%) extractions were much higher than in PETE, but lower than LDPE.

LDPE- ***Extraction Performance.*** The average percent of the total area per extraction round for HDPE is presented in **Table 52** and is shown in the bottom panel of **Figure 156; blue**. The area produced in consecutive extractions of LDPE (1d-spike) were more compound specific than in PETE and HDPE. The 1st two extractions (%1+2) produced the smallest proportion, out of the three plastics, representing only 87 to 92% of the total

extractable area for LDPE. Additionally with LDPE a trend can be seen where earlier eluting (lower MW) PAHs needed more rounds to extract, being between 66-68% extracted in the first extraction (%EXT1), when compared to later eluting (higher MW) PAHs where over 75% of the total area was represented in the first extraction. Moreover the second (%EXT2 = 16 -22%) and third extractions (%EXT3 = 8-13 %) represented the highest proportions of the total area seen in all three plastic types.

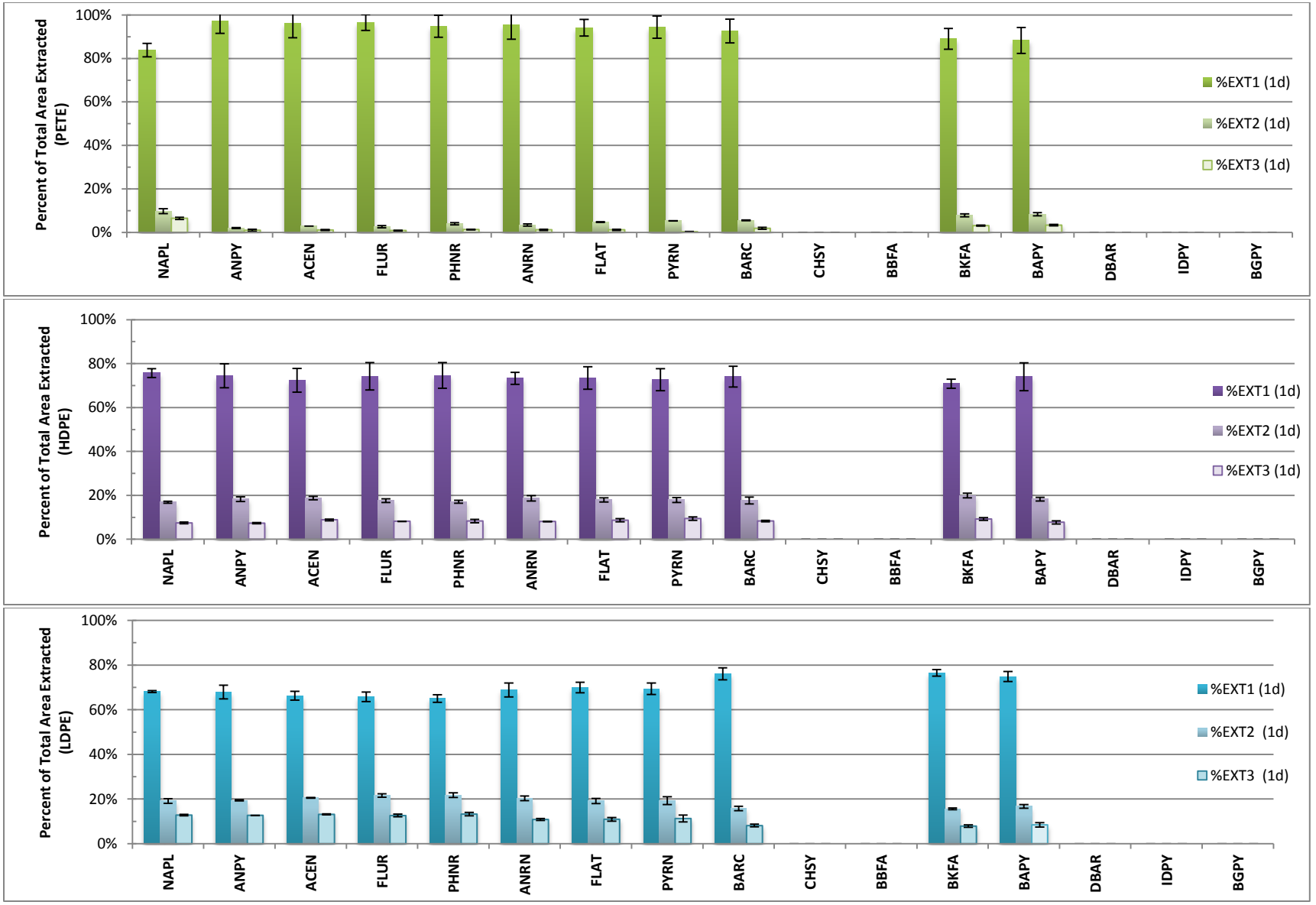

Figure 156. Percent of the Total Area per Extraction Round for Microplastics Exposed for 1-day to Milli-Q water Spiked with 11 Polycyclic Aromatic Hydrocarbons (PAHs) at High Concentration (HC-Spike; 1250 ng/g); comparing 3 plastic types: PETE [green, top]; HDPE [purple, middle]; and LDPE [blue, bottom]. **Error bars = standard deviation (n=3).**

Table 52. Online Extraction Performance (Average Percent of the Total Area per Extraction Round) for LDPE µPs-RMs Exposed to Milli-Q Water HC-Spike with PAHs at 1250 ng/g (qH₂O : HC-spike). **Data in Process**

			1 day Exposure (n =3)			7 day Exposure (n =3)			14 day Exposure (n =2)		
			Extraction 1	Extraction 2	Extraction 3	Extraction 1	Extraction 2	Extraction 3	Extraction 1	Extraction 2	Extraction 3
#	Analyte	ID	Average %	Average %	Average %	Average %	Average %	Average %	Average %	Average %	Average %
1	Naphthalene	NAPL	68 ± 0.4%	19 ± 1.1%	13 ± 0.3%	57 ± 1.5%	26 ± 2.4%	17 ± 1.5%	68 ± 1.5%	21 ± 0.3%	10 ± 0.3%
2	Acenaphthylene	ANPY	68 ± 3.1%	19 ± 0.3%	13 ± 0.1%	65 ± 3.0%	21 ± 1.9%	14 ± 0.6%	67 ± 0.2%	21 ± 0.2%	12 ± 0.1%
3	Acenaphthene	ACEN	66 ± 2.0%	21 ± 0.2%	13 ± 0.2%	64 ± 3.8%	23 ± 1.6%	13 ± 0.7%	67 ± 1.0%	21 ± 0.1%	12 ± 0.1%
4	Fluorene	FLUR	66 ± 2.2%	22 ± 0.8%	13 ± 0.6%	64 ± 3.1%	23 ± 1.1%	12 ± 0.3%	68 ± 0.8%	21 ± 0.2%	11 ± 0.0%
5	Phenanthrene	PHNR	65 ± 1.7%	22 ± 1.1%	13 ± 0.8%	67 ± 3.9%	21 ± 0.8%	12 ± 0.3%	67 ± 0.5%	21 ± 0.2%	12 ± 0.3%
6	Anthracene	ANRN	69 ± 3.2%	20 ± 1.0%	11 ± 0.4%	69 ± 3.7%	20 ± 0.9%	11 ± 0.3%	68 ± 1.3%	20 ± 0.2%	12 ± 0.3%
7	Fluoranthene	FLAT	69 ± 2.4%	19 ± 1.2%	11 ± 0.8%	68 ± 2.9%	20 ± 1.2%	12 ± 0.7%	64 ± 0.5%	23 ± 0.2%	13 ± 0.2%
8	Pyrene	PYRN	69 ± 2.6%	19 ± 1.7%	11 ± 1.5%	68 ± 3.6%	21 ± 0.8%	11 ± 0.8%	63 ± 1.6%	23 ± 0.0%	14 ± 0.4%
9	Benzo(a)anthracene	BARC	76 ± 2.7%	16 ± 1.0%	8 ± 0.6%	71 ± 3.3%	18 ± 0.9%	11 ± 0.2%	65 ± 1.2%	22 ± 0.6%	13 ± 0.3%
10	Chrysene	CHSY	ns ns	ns ns	ns ns	73 ± 1.7%	18 ± 0.9%	9 ± 0.2%	ns ns	ns ns	ns ns
11	Benzo(b)fluoranthene	BBFA	ns ns	ns ns	ns ns	71 ± 3.2%	19 ± 0.9%	10 ± 0.5%	ns ns	ns ns	ns ns
12	Benzo(k)fluoranthene	BKFA	76 ± 1.5%	16 ± 0.4%	8 ± 0.5%	67 ± 3.0%	23 ± 0.7%	11 ± 0.4%	65 ± 3.1%	22 ± 0.2%	13 ± 0.4%
13	Benzo(a)pyrene	BAPY	75 ± 2.2%	17 ± 0.8%	8 ± 1.0%	68 ± 3.7%	22 ± 1.1%	10 ± 0.6%	64 ± 4.5%	23 ± 0.3%	12 ± 0.3%
14	Dibenzo(a,h)anthracene	DBAR	ns ns	ns ns	ns ns	71 ± 5.0%	21 ± 1.7%	8 ± 0.1%	ns ns	ns ns	ns ns
15	Indeno(1,2,3-cd)pyrene	IDPY	ns ns	ns ns	ns ns	80 ± 7.1%	14 ± 1.5%	6 ± 0.4%	ns ns	ns ns	ns ns
16	Benzo(g,h,i)perylene	BGPY	ns ns	ns ns	ns ns	69 ± 2.2%	21 ± 2.9%	9 ± 1.5%	ns ns	ns ns	ns ns

"-" = Never ran; **ns** = 'not-spiked' standard not included in original test; **ND** = Not Detected; **n/a** = not applicable

Table 53. Online Extraction Performance (Average Percent of the Total Area per Extraction Round) for HDPE µPs-RMs Exposed to Milli-Q Water HC-Spike with PAHs at 1250 ng/g (qH_2O : HC-spike). **Data in Process**

			1 day Exposure (n =3)			7 day Exposure (n =1)			14 day Exposure (n =0)		
			Extraction 1	Extraction 2	Extraction 3	Extraction 1	Extraction 2	Extraction 3	Extraction 1	Extraction 2	Extraction 3
#	Analyte	ID	Average %	Average %	Average %	Average %	Average %	Average %	Average %	Average %	Average %
1	Naphthalene	NAPL	76 ± 2.0%	17 ± 0.5%	7 ± 0.4%	76 %	16 %	8 %	- -	- -	- -
2	Acenaphthylene	ANPY	74 ± 5.5%	18 ± 1.1%	7 ± 0.3%	74 %	17 %	9 %	- -	- -	- -
3	Acenaphthene	ACEN	72 ± 5.4%	19 ± 0.8%	9 ± 0.4%	69 %	20 %	10 %	- -	- -	- -
4	Fluorene	FLUR	74 ± 6.3%	18 ± 0.8%	8 ± 0.0%	69 %	21 %	10 %	- -	- -	- -
5	Phenanthrene	PHNR	75 ± 5.9%	17 ± 0.7%	8 ± 0.8%	69 %	20 %	11 %	- -	- -	- -
6	Anthracene	ANRN	73 ± 2.7%	19 ± 1.2%	8 ± 0.1%	72 %	19 %	9 %	- -	- -	- -
7	Fluoranthene	FLAT	73 ± 5.1%	18 ± 1.0%	9 ± 0.7%	67 %	22 %	11 %	- -	- -	- -
8	Pyrene	PYRN	73 ± 5.0%	18 ± 1.1%	9 ± 0.8%	70 %	20 %	10 %	- -	- -	- -
9	Benzo(a)anthracene	BARC	74 ± 4.7%	18 ± 1.6%	8 ± 0.3%	66 %	23 %	11 %	- -	- -	- -
10	Chrysene	CHSY	ns ns	ns ns	ns ns	ns ns	ns ns	ns ns	- -	- -	- -
11	Benzo(b)fluoranthene	BBFA	ns ns	ns ns	ns ns	ns ns	ns ns	ns ns	- -	- -	- -
12	Benzo(k)fluoranthene	BKFA	71 ± 2.0%	20 ± 1.1%	9 ± 0.6%	67 %	20 %	13 %	- -	- -	- -
13	Benzo(a)pyrene	BAPY	74 ± 6.4%	18 ± 0.8%	8 ± 0.7%	62 %	25 %	13 %	- -	- -	- -
14	Dibenzo(a,h)anthracene	DBAR	ns ns	ns ns	ns ns	ns ns	ns ns	ns ns	- -	- -	- -
15	Indeno(1,2,3-cd)pyrene	IDPY	ns ns	ns ns	ns ns	ns ns	ns ns	ns ns	- -	- -	- -
16	Benzo(g,h,i)perylene	BGPY	ns ns	ns ns	ns ns	ns ns	ns ns	ns ns	- -	- -	- -

"-" = Never ran; **ns** = 'not-spiked' standard not included in original test; **ND** = Not Detected; **n/a** = not applicable

Table 54. Online Extraction Performance (Average Percent of the Total Area per Extraction Round) for PETE µPs-RMs Exposed to Milli-Q Water HC-Spike with PAHs at 1250 ng/g (qH_2O : HC-spike). **Data in Process**

			1 day Exposure (n =3)			7 day Exposure (n =1)			14 day Exposure (n =0)		
			Extraction 1	Extraction 2	Extraction 3	Extraction 1	Extraction 2	Extraction 3	Extraction 1	Extraction 2	Extraction 3
#	Analyte	ID	Average %	Average %	Average %	Average %	Average %	Average %	Average %	Average %	Average %
1	Naphthalene	NAPL	84 ± 3.1%	10 ± 1.1%	6 ± 0.5%	91 %	6 %	3 %	- -	- -	- -
2	Acenaphthylene	ANPY	97 ± 5.5%	2 ± 0.2%	1 ± 0.4%	97 %	3 %	1 %	- -	- -	- -
3	Acenaphthene	ACEN	96 ± 6.5%	3 ± 0.0%	1 ± 0.2%	96 %	3 %	1 %	- -	- -	- -
4	Fluorene	FLUR	97 ± 3.7%	3 ± 0.5%	1 ± 0.2%	95 %	4 %	1 %	- -	- -	- -
5	Phenanthrene	PHNR	95 ± 5.1%	4 ± 0.5%	ND ND	94 %	5 %	1 %	- -	- -	- -
6	Anthracene	ANRN	95 ± 6.7%	3 ± 0.5%	1 ± 0.3%	93 %	5 %	2 %	- -	- -	- -
7	Fluoranthene	FLAT	94 ± 3.8%	5 ± 0.0%	1 ± 0.3%	94 %	5 %	1 %	- -	- -	- -
8	Pyrene	PYRN	94 ± 5.1%	5 ± 0.1%	ND ND	93 %	5 %	2 %	- -	- -	- -
9	Benzo(a)anthracene	BARC	93 ± 5.5%	5 ± 0.2%	2 ± 0.4%	94 %	5 %	1 %	- -	- -	- -
10	Chrysene	CHSY	ns ns	ns ns	ns ns	ns ns	ns ns	ns ns	- -	- -	- -
11	Benzo(b)fluoranthene	BBFA	ns ns	ns ns	ns ns	ns ns	ns ns	ns ns	- -	- -	- -
12	Benzo(k)fluoranthene	BKFA	89 ± 4.8%	8 ± 0.7%	3 ± 0.2%	89 %	8 %	3 %	- -	- -	- -
13	Benzo(a)pyrene	BAPY	88 ± 6.0%	8 ± 0.8%	3 ± 0.3%	90 %	9 %	1 %	- -	- -	- -
14	Dibenzo(a,h)anthracene	DBAR	ns ns	ns ns	ns ns	ns ns	ns ns	ns ns	- -	- -	- -
15	Indeno(1,2,3-cd)pyrene	IDPY	ns ns	ns ns	ns ns	ns ns	ns ns	ns ns	- -	- -	- -
16	Benzo(g,h,i)perylene	BGPY	ns ns	ns ns	ns ns	ns ns	ns ns	ns ns	- -	- -	- -

"-" = Never ran; **ns** = 'not-spiked' standard not included in original test; **ND** = Not Detected; **n/a** = not applicable

9.6.3. Plastic-type Comparison: Discussion.

Directly comparing total area extracted for each plastic type, showed a compound specific difference between all three types of plastics. Although at this stage it cannot be determined whether the areas produced are directly related to 'extractability' between the types of plastics (e.g., the Largest area directly tied to easiest material to extract from), as adsorption of the compounds to the plastic must inherently play a large role. But the trends observed at this early stage are promising, as they are corroborated by trends observed in literature:

Lab-Exposed PETE Produced the Lowest Total Area Extracted. The polymeric structure of PETE being smooth,[131] and glassy,[132] suggests smaller surface area[126] and therefore faster saturation would be expected for PET versus PE, since lower surface area would not facilitate diffusion into the material that would be expected alternatively for HDPE, and LDPE.[21],[132] Alternatively, HDPE and LDPE are considered to have rubbery-type textures, especially when compared to the more glassy type of polymers, such as PET.[132] Rubbery texture would be expected to demonstrate greater diffusion, permeability and greater free volume compared to glassy-type polymers. This was suggested by **Rochman et. al., 2013**[121] in the first long-term controlled field experiment designed to measure sorption of several priority pollutants (including PAHs), in the marine environment, who reported, HDPE, LDPE to consistently sorb greater concentrations of PAHs than did PET; with all sorbed PAHs at orders of magnitudes higher concentrations than PET.

PETE is the most dense polymer (1.4 g/cm^3) used in the present work, the same 10.0 mg portion would represent a smaller volume of exposed materials, which could have also played a role. Additionally, Polymers with heteroatoms (such as PET) are known to have increased stability, and would be expected not to crack easily, and instead to readily fracture (i.e., into shards). This would produce greater outer surface area, but consequently, the fragments would have a less porous surface texture and therefore less overall surface area when compared to fragments of a more porous type material (such as the rubbery type PE polymers). So ultimately, although milling of PETE produced the smallest particles, its polymeric structure, density and stability could have played significant roles in either producing lower the lowest total area extracted for spiked PAHs.

Lab-Exposed HDPE & LDPE Produced the Highest Total Area Extracted. Regardless of the source of the higher observable areas (e.g., 'Sorptivity' vs 'extractability'), LDPE should be expected to have greater sorptive capacity and/or extractability over HDPE due to greater distance between the polymeric chains (due to branching) giving greater surface area, making it less dense (i.e., more diffusivity),[133] but an observed opposite trend, with HDPE appearing to be the most 'extractable'.

If consideration is given to the particle size achieved for each plastic, which may explain the trends observed here, perhaps the density of the material is directly related to increased cracking during the Cryomilling (increased surface area for adsorption). Particle size was easier to achieve with smaller fragments, versus LDPE (very elastic), which was much harder to effectively pulverize (i.e., it fought back). The most average particle size distribution was achieved for HDPE, where, the amount of particles/surface area ratio was higher in the same 1 g portion (in-bag) of particles, which would support the idea that HDPE would have the most surface area (i.e., available sites for sorption) where compounds could adhere (aka higher adsorption > higher concentration of PAHs available to be extracted).

Compound-specific interactions in the polymer phase are also important, greater affinity for the type of plastic could play a role. PETE's chemical structure is a heteroatom. Cleavage at carboxyl end, would give a more polar surface. Extractions from PETE did have nearly the same area for later eluting compounds. SFC being a normal phase technique, it is generally accepted that later eluting compounds would tend to be more polar or having a larger π-electron cloud as in PAHs (requiring more polar modifier for elution). PE is essentially long hydrocarbon chains and therefore would be expected to be most similar to a C18 type stationary phase. A combination of earlier eluters being more apt to adsorb to a non-polar surface (especially in an aqueous environment), could support the increased adsorption (i.e., Higher concentration present for extraction) for LDPE and HDPE.

9.7. Exposure-duration *[1d vs. 7d vs. 14d Exposure to Spiked MilliQ Water (1250 ng/g)]*

9.7.1. Exposure-duration: Effect on Total Area Extracted (Av_{total})

LDPE. Comparing average total area extracted (Av_{total}) for 1 day exposure to 14 days exposure, a compound specific increase was observed, producing between 34% [NAPL] and 244% [BARC] higher av. total area from microplastics exposed for 14 days (**Figure 157**). Although, the overall trend was also the same for each round of extraction (total area increasing with exposure duration (S_Figure 31), the ratio (% change) was different between extraction rounds, additionally pointing to a difference in extraction performance (i.e., extractability) between exposure durations.

HDPE and PETE. Data still needs to be obtained for 7-day exposure and 14-d exposure sets for both HDPE and PETE type plastics.

9.7.2. Exposure-duration : Effect on Extraction Performance (S_Figure 32).

LDPE. The average percent of the total area in the 1st two extractions [Av%1+2] ranged between 87 and 92% of the total area extracted for all spiked PAHs for all three exposure durations. Although the average of the first two rounds was nearly the same, later eluting compounds (higher MW) PAHs, trended slightly lower with longer exposure duration.

HDPE and PETE. Data still needs to be obtained for 7-day exposure and 14-d exposure sets for both HDPE and PETE type plastics.

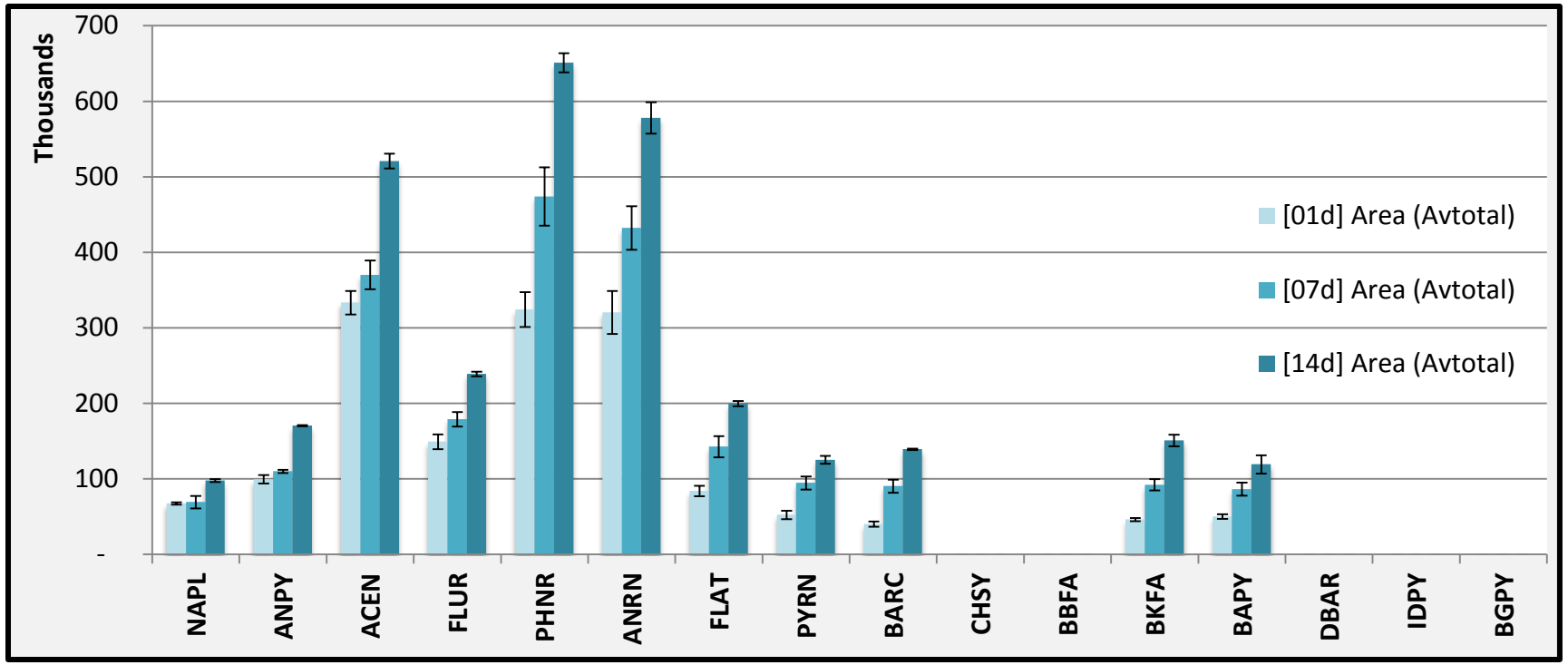

Figure 157. Average Total Area Extracted (Av_{total}) for LDPE-type Microplastics exposed for 1, 7 and 14 days to Milli-Q Water Spiked with 11 PAHs (HC-Spike; 1250 ng/g). *1-day exposure ([01d], light blue); 7-days exposure ([07d], blue); and 14 days exposure ([14d], dark blue); Error bars = standard deviation (n=3).*

9.7.3. Exposure-duration: Effect per Extraction Round (Figure 158)

LDPE. Comparing the effect of exposure duration on Av%EXT (the average percent of total area for each extraction round), a compound specific trend emerges, where: Av%EXT1, was lower for 14 days-exposure, for late eluting (larger MW) compounds but nearly the same for early eluting (lower MW) compounds regardless of exposure duration. Alternatively, both Av%EXT2 and Av%EXT3, was higher for late eluting PAHs for 14 days-exposure, when compared to microplastics exposed for a shorter duration. Furthermore, only in the third extraction, can a significant, opposite trend for some of the earliest eluting compounds [NAPL, ANPY, ACEN, FLUR and PHNR] be seen; where Av%EXT3 for materials exposed for 14-days was a lower proportion of the total extractable area, when compared to materials exposed for a shorter duration.

HDPE and PETE. Data still needs to be obtained for 7-day exposure and 14-d exposure sets for both HDPE and PETE type plastics.

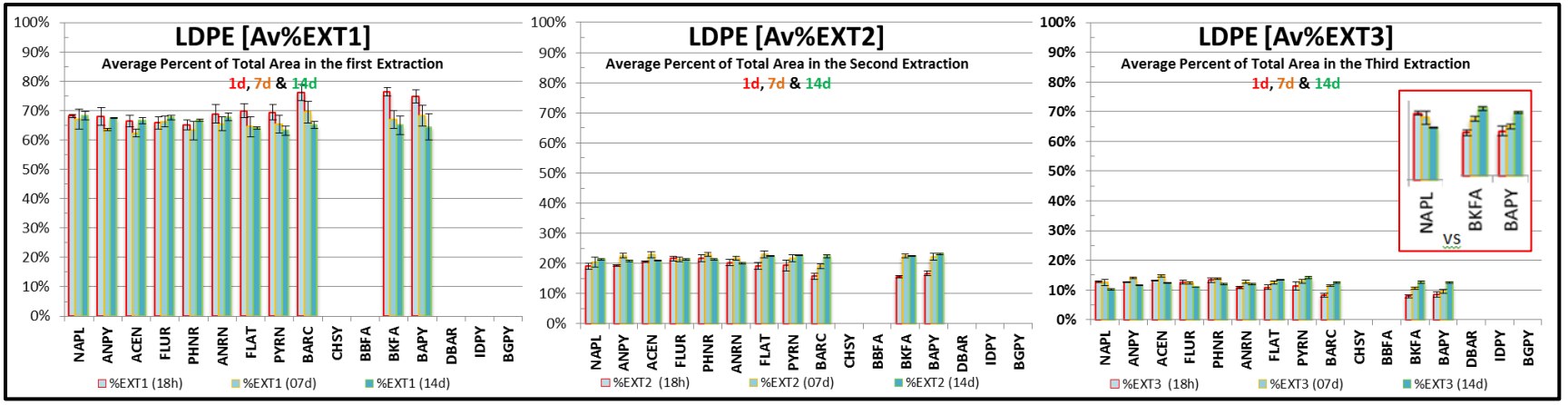

Figure 158. **Average Percent of Total Area per Extraction Round for LDPE-type Microplastics Exposed to MilliQ Water Spiked with HC-PAH-Spike (1250 ng/g) for three durations: 1 day [red]; 7 days [orange]; and 14 days [green] of Exposure.** Comparing Extraction Round 1 ([Av%EXT1], left); Extraction Round 2 ([Av%EXT2], middle); and Extraction Round 3 ([Av%EXT3], right). *Error Bars = Standard deviation (n = 3).*

9.7.4. Discussion : Effect of Exposure Duration.

Effect of Exposure Duration on Total Area Extracted. Average total area extracted (Av_{total}) was significantly higher with longer exposure duration for LDPE-type plastics. This is corroborated **Rochman et. al., 2013**[121] reported a concentration equilibrium for HDPE, LDPE and PP that was reached by 6 months of exposure, followed by slower sorption over the following months, and suggested diffusion into the polymeric matrix as support to the rapidly increasing concentrations observed in the first months (i.e., adsorption) and the slow tapering off thereafter (i.e., absorption) towards the concentration equilibrium**.** In the same work, they also reported PAH concentrations to change very little over time for PET in field sorption experiments.

Effect of Exposure Duration on %EXT. Later eluters, should generally need more polar modifier for not only elution, but also for extraction. A trend towards lower extractable areas in the first round of extraction in combination with simultaneous higher extractable area in the third round points towards a stronger/deeper association of the analyte with the sample matrix.

Compound specific adsorption should be expected, being often driven by hydrophobicity (octanol-water partition coefficient [$logK_{ow}$]) in combination with the molecular weight (MW) of individual PAHs ($logK_{ow}$ and MW are provided in **Table 2** in **Chapter #2. Materials and Methods**).[21],[22],[23] Chemicals with lighter MW and lower hydrophobicity would be expected to reach saturation faster, and alternatively chemicals with heavier MW and higher hydrophobicity would be expected to reach saturation slower (i.e., take longer to reach max sorbed concentration).[134],[135]

This implies the longer the µPs-RMs are exposed to PAHs the stronger the adsorption /deeper into the cracks/fissures. The observed trend in this work is more prominence of the later eluting compounds, which are also PAHs with heavier MW and higher hydrophobicity (which would be expected to take longer to reach saturation), supports these findings.

9.8. Conclusions

Virgin pellets of multiple plastics were successfully CryoMilled to closely mimic the mechanical degradation associated with environmentally exposed plastics. However, there was no UV or chemical degradation. Field experiments are partially completed and under way for the same materials.

The method originally optimized for soil was successfully transferred, and optimized for use with 0.2-mL extraction vessels for small sample sizes. The final method utilized 1/100th the starting materials used in the original method for 5.0-mL vessels.

Some of the CryoMilled micro-plastics were successfully sorbed with some amount of the POPs (PAHs) to LDPE, HDPE and PET type plastic materials. The PAHs were then successfully extracted from both blank and exposed/'sorbed' plastics materials. A difference in peak areas was demonstrated between plastic types, exposure duration, and *(possibly)* between particle size. A difference in "extractability" was demonstrated, where a compound specific change was seen w/ correlation to exposure time. This could point to the greater association/deeper (greater adsorption) over-time, previously only seen in field experiments. (normally lab experiments hit saturation after 24 hours, whereas in our plastics the concentration was still increasing.)

The work in this chapter is only partially completed. Prep Control Exposed Sampling Bags, 7-day exposure and 14-d exposure sets, data still needs to be obtained. Extractions are planned but have not yet been performed.

9.i. Instrument Methods: Microplastics Lab Exposure Sets

9.i.1. General Method Information.

Detailed information on the materials and equipment used in this study can be found in the following sections of **Chapter #2. Materials and Methods**:

9.i.1.1. Materials.

- Solvents used for mobile phases, stock, dilution and spiking solutions can be found in **Section 2.1.1. Solvents**.
- PAH analytical standards in **Section 2.1.2. Analytical Standards: *Environmental pollutants*** and **Table 2.** Sixteen polycyclic aromatic hydrocarbons (PAHs) were chosen from EPA method 8310.[20]
- Virgin Plastic Pellets details in **Section 2.1.4. Microplastics Materials: *Virgin Plastic Pellets*** and **Table 4**.
- Sampling Materials in **Section 2.1.4. Microplastics Materials: *Microplastics Exposure/Sampling Materials***.

9.i.1.2. Instrumentation.

The instrument used in all presented work was the Shimadzu Nexera UC Online SFE-SFC-MS.

- The Instrumentation and software used is detailed in **Section 2.2.1. Nexera UC online SFE-SFC-MS**.
- Column details are given in **Section 2.2.2. Columns** and **Table 5**.
- Information on other equipment used can be found in **Section 2.2.3. Other Equipment:**
    - ***Nitrogen Generator***
    - ***Cryogenic Grinder***
    - ***Particle Analyzer***
    - ***Light Microscope***
    - ***Large-capacity Shaker Table***
    - ***Analytical Balances***

9.i.1.3. Solutions Preparation.

Solutions Preparation for Microplastics work is detailed in **Section 2.3.2. Solutions for Microplastics:**

- Stock Solutions in **Section 2.3.2.1. PAHs Stock Solutions** and **Table 8; Stock concentrations.**
- Spiking solutions prep and final concentrations are described in **Section 2.3.2.2. PAHs Spiking Solutions for Microplastics Exposure solutions.**
    - ***High concentration Spiking solution ([HC:PAHs]; 1,250 ng/g).***
    - ***Low concentration Spiking solution ([LC:PAHs]; 50 ng/g).***

9.i.1.4. Sample Preparation.

Preparation of exposed-microplastics is detailed in **Section 2.7. Sample Preparation: Exposed-Microplastics.**

- Sampling bag prep in **Section 2.7.1. Microplastics sample bags.**
- Marine-exposed µPs-RMs in **Section 2.7.2. Marine-Exposed Microplastics [µPs:Marine].**
    - ***Sample Deployment*** (**Figure 19** and **Table 9**).
    - ***Field collected control water***.
    - ***Ambient Conditions.***
- Lab-exposed µPs-RMs in **Section 2.7.3. µPs:PAHs Laboratory-exposed Blanks and QCs.**
- Lab exposure solutions prep in **Section 2.7.4. Laboratory control Exposure Solutions.**
    - ***Laboratory Control Water [qH$_2$O].***
    - ***Field Control Water*** **[Sea-H$_2$O]** and **Figure 19**.
- Test-Sets for laboratory exposure controls in **Section 2.7.5. Lab Control Test-Sets.**
    - ***Lab Null (1x/test-set).***
    - ***Lab Blank*** **([qH$_2$O:Blank]; 1x/test-set).**
    - ***Field Blank*** **([SeaH$_2$O:Blank]; 1x/test-set).**
    - ***High Concentration Laboratory Control samples*** **([qH$_2$O:HC], 3x/test-set).**
    - ***High Concentration Field Control samples*** **([SeaH$_2$O:HC], 3x/test-set).**
    - ***Low Concentration Laboratory Control samples*** **([qH$_2$O:LC], 3x/test-set).**
    - ***Low Concentration Field Control samples*** **([SeaH$_2$O:LC], 3x/test-set).**
    - ***Bag QC Check (1x/plastic)***.

9.i.1.5. General Microplastics Workflow for Online Extractions

Information on the general workflow can be found in Section **2.8. General Workflow for Online Extractions**

- ***2.8.1. Vessel filters***
- ***2.8.2. Vessel cleaning***
- ***2.8.3. Vessel assembly***

9.i.1.6. Data Processing.

General data processing approaches are detailed in **Section 2.9. General Data Processing Approaches .**

9.i.2. Instrument setup

The instrument setup utilized in the work presented was performed with the 'SFE Online Extraction Configuration using '***Splitless-mode' Extractions***' detailed in **Chapter #1: Hyphenated Instrumentation: SFE-SFC-MS**; **Section 1.5.4: Instrument Configurations used for SFC Optimizations: *'Splitless-mode' Extraction***.

Sample Introduction. Online extractions were performed in splitless-mode, using 0.2-mL extraction vessels. Sample is placed in inside a small chamber and extracted online facilitated by two switching valves, an 'extraction plug is delivered to the head of the column for online analysis.

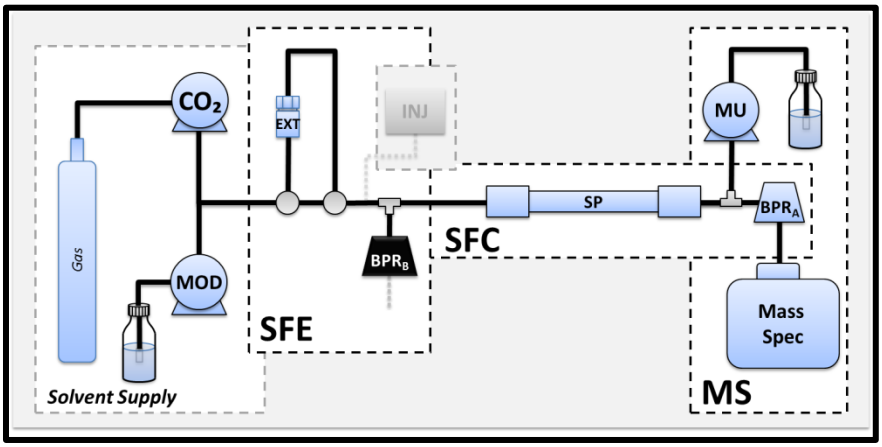

See Figure 17 in Chapter #1

9.i.3. Instrument Methods:

9.i.3.1. Mobile Phase (MP) and Stationary Phase (SP).

Several parameters originate from the previously optimized method for soil by **Wicker et. al., 2018**.[120] and remained unchanged throughout the entirety of the work.

Cholester Column. The same column was used in all presented work and was a CHROMOSIL, cholester (4.6 x 150mm, 5.0 µm) column from Nacalai Tesque, Inc.

Mobile phase. The same mobile phase components were used for all microplastics work presented, and consisted of [A] liquid carbon dioxide (CO_2) modified with [B] acetonitrile (ACN).

MS Detection Parameters. No modification was performed to the original MRM-method, and therefore all presented work used the same conditions given in **Section 9.i.3.1. Original MS parameters**.

9.i.3.2. Original SFE-SFC-MS Method for Extraction of PAHs from Soil.

All 'original' methods used in this work (which are detailed below) originated from a previously developed method from **Wicker et. al., 2018**.[120]

Original MS Parameters. Detection was achieved using an LCMS-8050 triple quadrupole mass spectrometer, equipped with an APCI source, and operated in positive (+) ionization mode. Interface voltage and temperature were set to 4.5 kV and 300 °C, respectively. Nitrogen gas was used for both drying and nebulizing gas; with flow rate of 4.0 L/min for nebulizing gas and 15.0 L/min for drying gas. Desolvation and DL temperatures were 526 °C and 300 °C respectively. Heat Block temperature was set to 300 °C, and heating gas used was dry air. Gas used for collision induced dissociation (CID) was argon at 270 kPa. MRM-optimization was performed using the LabSolutions software, with Q1 and Q3 resolution set to Unit. The resulting MRM transitions for 21 events (event time of 0.017 sec) with one channel each, were used with a loop time of 0.357 sec and dwell time of 14.0 msec applied to every channel.

***Original SFC Separation Parameters*.** Separation was achieved using the chromosil, cholester column, using gradient elution at 3.0 mL/min. The column temperature was set to 50 °C and system outlet pressure set to 15 MPa. The original gradient program is as follows: 0.00 - 5.00 min, 10% [B]; 5.01 - 9.00 min, 10 - 20% [B]; 9.01 - 10.00 min, 20 - 40% [B]; 10.01 – 16.00 min, 50% [B].

Original SFE Extraction Parameters. For online extractions, 5.0-mL vessels were used, which were heated to 40 °C just prior to extraction. The BPR_B pressure was also set to 15.0 MPa giving system operation in split-mode, with the majority of the system flow being pushed out to waste pre-column during extraction.

The original method extraction program was as follows:

0.00-1.00 min,	10% [B],	*(1 min vessel filling)*;
1.01 – 7.00 min,	10% [B],	*(6 min static extraction)*;
7.01 – 12.00 min,	10% [B],	*(5 min dynamic extraction);*
12.01 min,	End SFE;	
12.02 – 17.00 min,	10% [B],	*(analysis start, 5 min initial gradient hold);*
17.01 – 21.00 min,	10 - 20% [B];	*(gradient, first ramp, 4 min)*;
21.01 – 25.00 min,	20 – 40% [B];	*(gradient, second ramp, 4 min)*;
25.01 – 26.00 min,	40% [B];	*(gradient hold, 1 min)*;
26.01 – 32.00 min,	50% [B].	*(gradient step, then hold, 6 min)*;

Followed by an 8.00 minute system wash (32.01 – 40.00 min, 100% [B])

9.i.3.3. SFE-SFC-MS Method Transfer for 0.2-mL Vessels: Extraction Parameter Screening.

Screened Extraction Parameters. Static extraction concentration was screened and included 10, 5 and 0% [B]. Dynamic concentration and durations were screened, using 10, 5 and 0% B and 5.0, 1.0, 0.8 and 0.5 minutes, respectively. All other instrument parameters were held constant.

Parameters held constant during extraction screening. The mobile phase composition was liquid CO_2 modified with Acetonitrile, using a flow rate of 3.0 mL/min. Extraction vessels were 0.2-mL size, equipped with sinter-type filters, and an extraction temperature of 40 °C was used. Extraction mode was splitless, holding BPR [B] at 40 MPa throughout the duration for the extraction and analysis. System outlet pressure was also the same in both extraction and analysis, and was set to 15 MPa. During the extraction process; the vessel filling step was always 1.0 minute long using 10% [B]; and the static extraction duration was always 6.0 minutes. Separation was achieved via the CHROMOSIL, cholester (4.6 x 150mm, 5.0 µm) column. During Analysis the same gradient was used starting with a 5.0 minute hold at 5.0% [B], followed by an increase to 20% [B] over 4.0 minutes, next a 1.0 minute increase to 40% [B] and finally a step to 50% [B] over 0.01 minute which was then held for 6.0 minutes at 50% [B]. The column temperature was set to 50 C.

9.i.3.4. SFE-SFC-MS Method Transfer for 0.2-mL Vessels: Gradient Screening Parameters

Gradient Screening (**Table 55**)***.*** Six gradients were screened: Gradient 1[g1] started at 8% [B] and ramped to 18% [B]; Gradient 2 (g2) started at 6% [B] and ramped to 16% [B]; Gradient 3 (g3) started at 5% [B] and ramped to 20% [B]; Gradient 4 (g4) started at 2.5% [B] and also ramped to 20% [B]; Gradient 5 (g5) also started at 2.5% [B] but ramped to 15% [B]; Gradient 6 (g6) had no hold to start and instead had a three step gradient, starting at 2.5% [B], then ramped to 5.0% [B], before goint to 20% [B] before the final ramp to 40% [B]. The step duration remained the same for all gradients.

Table 55. Percent Acetonitrile (ACN) in Carbon Dioxide (CO_2) for Screening Gradients used During Method Transfer to 0.2-mL Extraction Vessels for Online Extraction of PAHs from Microplastics.

SFE Time (min)	g1	g2	g3	g4	g5	g6	Gradient Time (min)	Step Duration (min)
7.82	8.0%	6.0%	5.0%	2.5%	2.5%	2.5%	0.00	0
12.80	8.0%	6.0%	5.0%	2.5%	2.5%	5.0%	5.00	5
16.80	18.0%	16.0%	20.0%	20.0%	15.0%	20.0%	9.00	4
20.80	40.0%	40.0%	40.0%	40.0%	40.0%	40.0%	13.00	4
21.80	40.0%	40.0%	40.0%	40.0%	40.0%	40.0%	14.00	1
21.81	50.0%	50.0%	50.0%	50.0%	50.0%	50.0%	14.01	0.01
27.81	50.0%	50.0%	50.0%	50.0%	50.0%	50.0%	20.00	6
	8-18 (Long)	6-16	5-20	2-20	2-5	2-5-20		

Parameters held constant during Gradient Screening. The separation was preceded by an online extraction, parameters of which were held constant, using a 1.0 minute vessel filling, at 10% [B]; a 6.0 minute static extraction and 0.8 minute dynamic extraction, both using 0% [B]; the flow rate was 3.0 mL/min, the column temperature was 50 °C, the outlet pressure BPR_A set to 15 MPa, and splitless instrument-mode, with a BPR_B set to 40 MPa, throughout extraction as well as the separation. Vessels were heated to 30 C just prior to each extraction.

9.i.3.5. Final SFE-SFC-MS Method for Online Extraction of PAHs from Microplastics.

The MS method remained unchanged from the original method for Soil (**Section 9.i.3.1. Original MS parameters)** MRM transitions used are provided in **Table 45** (in **Section 9.3.1**) in the main text. Separation was achieved using the CHROMOSIL, cholester column (4.6 x 150mm, 5.0 µm, Nacalai Tesque, Inc) using gradient elution at 3.0 mL/min. The column temperature was set to 50 C and system outlet pressure set to 15 MPa.

Microplastics were analyzed by accurately weighing 10.00 mg µPs-RMs and transferring directly to 0.2-mL extraction vessels, no additional packing material was added to the vessel. Sinter-type vessel filters were used for compatibility with small particle type samples. Vessels were closed using a torque wrench, set to 1.5 N-m for compatibility with 0.2-mL extraction vessels and placed directly into the automated rack changer.

For online extractions, the flow rate was held constant throughout the entire process (vessel filling, static and dynamic extraction and analysis). The system was operated in split-less mode, where BPR_B was set to 40 MPa at all times. The system outlet pressure was also the same for both extraction and analysis, with BPR_A set to 15 MPa.

<u>The time program for online extractions was as follows</u>

0.00 - 1.00 min,	10% [B],	*(1 min vessel filling)*;
1.01 – 7.00 min,	0% [B],	*(6 min static extraction)*;
7.01 – 7.80 min,	0% [B],	*(0.8 min dynamic extraction)*;
7.81 min,	End SFE;	
7.82 – 12.80 min,	8% [B],	*(analysis start, 5 min initial gradient hold)*;
12.81 – 16.80 min,	8 - 18% [B],	*(gradient, first ramp, 4 min)*;
16.81 – 20.80 min,	18 - 40% [B],	*(gradient, second ramp, 4 min)*;
20.81 – 21.80 min,	40% [B]	*(gradient hold, 1 min)*;
21.81 – 25.81 min,	50% [B]	*(gradient step, then hold, 4 min)*;
25.33 min	SFE Wash;	*(100% [B], 6 min)*
31.36 min	EQ	*(Column Equilibration, initial gradient settings, 1 min)*.

Literature Cited:

FIRST CITED IN PREVIOUS CHAPTERS

[20] U.S. Environmental Protection Agency, Office of Research and Development, National Center for Environmental Assessment. *Method 8310: Polycyclic aromatic hydrocarbons in ground water*. Washington, DC, 1986.

[21] Lohmann R. (2012). "Critical review of low-density polyethylene's partitioning and diffusion coefficients for trace organic contaminants and implications for its use as a passive sampler." *Environmental Science and Technology*. **46**(2): p606-618. https://doi.org/10.1021/es202702y

[22] Ministry of Environment, Lands and Parks Province of British Columbia. "*Ambient Water Quality Criteria For Polycyclic Aromatic Hydrocarbons (PAHs). February 1993*." Approved Water Quality Guidelines, Technical Reports, Polycyclic Aromatic Hydrocarbons (PAHs), Technical Appendix. K_{OW}'s from https://www2.gov.bc.ca/assets/gov/environment/air-land-water/water/waterquality/water-quality-guidelines/approved-wqgs/pahs/pahs-tech.pdf (accessed August 25 2021).

[23] Hansch C, Leo A, Hoekman D. (1995). "Exploring QSAR - Hydrophobic, Electronic, and Steric Constants." In: S.R. Heller (ed.). ACS professional reference books, vol 2. American Chemical Society: Washington, DC. ISBN 0-8412-2993-7

NEW TO THIS CHAPTER

[92] Jambeck JR, Geyer R, Wilcox C, Siegler TR, Perryman M, Andrady A, Narayanet R, Law KL. (2015) "Marine pollution. Plastic waste inputs from land into the ocean." *Science*. **347**(6223): p768–771. https://doi.org/10.1126/science.1260352

[93] Borrele S, Rochman CM, Liboiron M, Bond AL, Lusher A, Bradshaw H, Provencher JF. (2017). "Why we need an international agreement on marine plastic pollution." *Proceedings of the National Academy of Sciences.* **114**(38): p9994–9997. https://doi.org/10.1073/pnas.1714450114

[94] PlasticsEurope. Plastics—the Facts 2019: An analysis of European plastics production, demand and waste data for 2018. https://www.plasticseurope.org/en/resources/publications/1804-plastics-facts-2019. (accessed August 25 2021).

[95] Andrady AL. (2011). "Microplastics in the marine environment." *Marine Pollution Bulletin.* **62**(8): p1596-1605. https://doi.org/10.1016/j.marpolbul.2011.05.030

[96] Geyer R, Jambeck JR, Law KL. (2017). "Plastics: Production, use, and fate of all plastics ever made." *Science Advancements.* **3**(7): e1700782. https://doi.org/10.1126/sciadv.1700782

[97] United States Environmental Protection Agency: Office of Land and Emergency Management. (EPA 530-F-20-009) *"Advancing Sustainable Materials Management: 2018 Fact Sheet. Assessing Trends in Materials Generation and Management in the United States."* U.S. Environmental Protection Agency Web site. https://www.epa.gov/sites/production/files/2018-03/documents/methodolgy_document_for_selected_municipal_solid_waste_products.pdf (accessed February 02, 2021).

[98] McIlwraith HK, Lin J, Erdle LM, Mallos N, Diamond M, Rochman CM. (2019). "Capturing microfiber – marketed technologies reduce microfiber emissions from washing machines." *Marine Pollution Bulletin.* **139**: p40-45. https://doi.org/10.1016/j.marpolbul.2018.12.012

[99] Rochman CM. (2018). "Microplastics research: from sink to source." *Science.* **360**(6384): p28-29. https://doi.org/10.1126/science.aar7734

[100] McIlwraith HK, Lin J, Erdle LM, Mallos N, Diamond M, Rochman CM. (2019). "Capturing microfiber – marketed technologies reduce microfiber emissions from washing machines." *Marine Pollution Bulletin.* **139**: p40-45. https://doi.org/10.1016/j.marpolbul.2018.12.012

[101] New Zealand Royal Society Te Aparangi. "*Plastics in our Environment – Evidence Summary, 2019*." [Online ISBN: 978-1-877264-39-9]. NZ Royal Society Website. https://www.royalsociety.org.nz/assets/Uploads/Plastics-in-the-Environment-evidence-summary.pdf (accessed February 06 2021).

[102] Booth AM, Kubowicz S, Beegle-Krause C, Skancke J, Nordam T, Landsem E, Throne-Holst M, Jahren S. (M-918) *Microplastic in Global and Norwegian Marine Environments: Distributions, Degradation Mechanisms and Transport, 2017*. Norwegian Environment Agency website. https://www.miljodirektoratet.no/globalassets/publikasjoner/M918/M918.pdf (accessed February 08, 2021).

[103] Gillibert R, Balakrishnan G, Deshoules Q, Tardivel M, Magazzu A, Donato MG, Marago OM, de La Chapelle ML, Colas F, Lagarde F, Gucciardi PG. (2019). "Raman Tweezers for Small Microplastics and Nanoplastics Identification in Seawater." *Environmental Science and Technology*. **53**(15): p9003-9013. https://doi.org/10.1021/acs.est.9b03105

[104] Rochman CM, Brookson C, Bikker J, Djuric N, Earn A, Bucci K, Athey S, Huntington A, McIlwraith H, Munno K, De Frond H, Kolomijeca A, Erdle L, Grbic J, Bayoumi M, Borrelle SB, Wu T, Santoro S, Werbowski LM, Zhu X, Giles RK, Hamilton BM, Thaysen C, Kaura A, Klasios N, Ead L, Kim J, Sherlock C, Ho A, Hung C. (2019). "Rethinking microplastics as a diverse contaminant suite." *Environmental Toxicology and Chemistry*. **38**(4): p703-711. https://doi.org/10.1002/etc.4371

[105] Klein S, Dimzon IK, Eubeler J, Knepper TP. (2017). "Analysis, occurrence, and degradation of microplastics in the aqueous environment." In: M. Wagner & S. Lambert (Eds.). The Handbook of Environmental Chemistry, vol 58. *Freshwater Microplastics: emerging environmental contaminants?* (pp.51-67). Springer, Cham. https://doi.org/10.1007/978-3-319-61615-5_3

[106] Ali SS, Elsamahy T, Koutra E, Kornaros M, El-Sheekh M, Abdelkarim EA, Zhu D, Sun J. (2020). "Degradation of conventional plastic wastes in the environment: A review on current status of knowledge and future perspectives of disposal." *Science of the Total Environment*. **771**: e144719. https://doi.org/10.1016/j.scitotenv.2020.144719

[107] Provencher JF, Ammendolia J, Rochman CM, Mallory ML. (2019). "Assessing plastic debris in aquatic food webs: what we know and don't know about uptake and trophic transfer." *Environmental Reviews*. **27**(3): p304-317. https://doi.org/10.1139/er-2018-0079

[108] Rochman CM, Parnis JM, Serrato S, Browne MA, Reiner EJ, Robson M, Young T, Diamond ML, Teh SJ. (2017). "Direct and indirect effects of different types of common microplastics in a freshwater foodchain." *PLoS ONE*. **12**(11): e0187664. https://doi.org/10.1371/journal.pone.0187664

[109] Smith M, Love DC, Rochman CM, Neff RA. (2018). "Microplastics in seafood and implications for human health." *Current Environmental Health Reports.* **5**(3): p375-386. https://doi.org/10.1007/s40572-018-0206-z

[110] Rochman CM, Browne M A, Halpern BS, Hentschel BT, Hoh E, Karapanagioti HK, Rios-Mendoza LM, Takada H, Teh S, Thompson RC. (2013). "Classify plastic waste as hazardous." *Nature* . **494**: p169-171. https://doi.org/10.1038/494169a

[111] Gassel M, Rochman CM. (2019). "The complex issue of chemicals and microplastic pollution: A case study in North Pacific Lanternfish." *Environmental Pollution.* **248**: p1000-1009. https://doi.org/10.1016/j.envpol.2019.03.002

[112] De Frond HL, van Sebille E, Parnis JM, Diamond ML, Mallos N, Kingsbury T, Rochman CM. (2019). "Estimating the mass of chemicals associated with ocean plastic pollution to inform mitigation efforts." *Integrated Environmental Assessment and Management*. **15**(4): p596-606. https://doi.org/10.1002/ieam.4147

[113] Hong SH, Shim WJ, Hong L. (2017). "Methods of analyzing chemicals associated with microplastics: a review." *Analytical Methods.* **9**: p1361-1368. https://doi.org/10.1039/c6ay02971j

[114] Ogata Y, Takada H, Mizukawa K, Hirai H, Iwasa S, Endo S, Mato Y, Saha M, Okuda K, Nakashima A, Murakami M, Zurcher N, Booyatumanondo R, Zakaria MP, Dung LQ, Gordon M, Miguez C, Suzuki S, Moore C, Karapanagioti HK, Weerts S, McClurg T, Burres E, Smith W, Van Velkenburg M, Lang JS, Lang RC, Laursen D, Danner B, Stewardson N, Thompson RC. (2009). "International pellet watch: Global monitoring of persistent organic pollutants (POPs) in coastal waters. 1.

Initial phase data on PCBs, DDTs, and HCHs." *Marine Pollution Bulletin.* **58**(10): p1437–1446. https://doi.org/10.1016/j.marpolbul.2009.06.014

[115] Hirai H, Takada H, Ogata Y, Yamashita R, Mizukawa K, Saha M, Kwan C, Moore C, Gray H, Laursen D, Zettler ER. (2011). "Organic micropollutants in marine plastics debris from the open ocean and remote and urban beaches." *Marine Pollution Bulletin.* **62**(8): p1683–1692. https://doi.org/10.1016/j.marpolbul.2011.06.004

[116] Van A, Rochman CM, Flores EM, Hill KL, Vargas E, Vargas SA, Hoh E. (2011). "Persistent organic pollutants in plastic marine debris found on beaches in San Diego, California." *Chemosphere*. **86**(3): p258-263. https://doi.org/10.1016/j.chemosphere.2011.09.039

[117] Rochman CM. (2013). "Plastics and priority pollutants: a multiple stressor in aquatic habitats." *Environmental Science and Technology.* **47**(6): p2439-2440. https://doi.org/10.1021/es400748b

[118] Lorenzo M, Campo J, Pico Y. (2018). "Analytical challenges to determine emerging persistent organic pollutants in aquatic ecosystems." *Trends in Analytical Chemistry*. **103**: p137-155. https://doi.org/10.1016/j.trac.2018.04.003

[119] Mastral AM, Callen MS. (2000). "A Review on Polycyclic Aromatic Hydrocarbon (PAH) Emissions from Energy Generation." *Environmental Science and Technology.* **34**(15): p3051-3057. https://doi.org/10.1021/es001028d

[120] Wicker AP, Carlton DD, Tanaka K, Nishimura M, Chen V, Ogura T, Hedgepeth W, Schug KA. (2018). "On-line supercritical fluid extraction—supercritical fluid chromatography mass spectrometry of polycyclic aromatic hydrocarbons in soil." *Journal of Chromatography B.* **1086**: p82-88. https://doi.org/10.1016/j.jchromb.2018.04.014

[121] Rochman CM, Hoh E, Hentschel BT, Kaye S. (2013). "Long-term field measurement of sorption of organic contaminants to five types of plastic pellets: Implications for plastic marine debris." *Environmental Science and Technology*. **47**(3): p1646-1654. https://doi.org/10.1021/es303700s

[122] Karakolis EG, Nguyen B, You JB, Rochman CM, Sinton D. (2019). "Fluorescent dyes for visualizing microplastic particles and fibers in laboratory-based studies." *Environmental Science and Technology Letters.* **6**(6): p334-340. https://doi.org/10.1021/acs.estlett.9b00241

[123] Fotopoulou KN, Karapanagioti HK. (2012). "Surface properties of beached plastic pellets." *Marine Environmental Research*. **81**: p70-77. https://doi.org/10.1016/j.marenvres.2012.08.010

[124] Mato Y, Isobe T, Takada H, Kenehiro H, Ohtake C, Kaminuma T. (2001). "Plastic Resin Pellets as a Transport Medium for Toxic Chemicals in the Marine Environment." *Environmental Science and Technology.* **35**(2): p318–324. https://doi.org/10.1021/es0010498

[125] Karapanagioti HK, Klontza I. (2008). "Testing phenanthrene distribution properties of virgin plastic pellets and plastic eroded pellets found on Lesvos island beaches (Greece)." *Marine Environmental Research*. **65**(4): p283-290. https://doi.org/10.1016/j.marenvres.2007.11.005

[126] Teuten EL, Rowland SJ, Galloway TS, Thompson RC. (2007). "Potential for Plastics to Transport Hydrophobic Contaminants." *Environmental Science and Technology.* **41**(22): p7759–7764. https://doi.org/10.1021/es071737s

[127] Airiau CY, Brereton RG, Crosby J. (2000). "High-performance liquid chromatography/electrospray tandem mass spectrometry of polycyclic aromatic hydrocarbons." *Rapid Communications in Mass Spectrometry*. **15**(2): p135-140. https://doi.org/10.1002/1097-0231(20010130)15:2<135::AID-RCM204>3.0.CO;2-Z

[128] Jjunju FPM, Maher S, Li A, Badu-Twiah AK, Taylor S, Cooks RG. (2015). "Analysis of Polycyclic Aromatic Hydrocarbons Using Desorption Atmospheric Pressure Chemical Ionization Coupled to a Portable Mass Spectrometer." *Journal of the American Society for Mass Spectrometry.* **26**: p271-280. https://doi.org/10.1007/s13361-014-1029-2

[129] Rochman CM, Manzano C, Hentschel BT, Massey Simonich SL, Hoh E. (2013). "Polystyrene Plastic: A Source and Sink for Polycyclic Aromatic Hydrocarbons in the Marine Environment." *Environmental Science and Technology.* **47**(24): p13976-13984. https://doi.org/10.1021/es403605f

[130] Schonlau C, Larsson M, Lam MM, Engwall M, Glesy JP**,** Rochman CM, Karrman A. (2019). "Aryl hydrocarbon receptor-mediated potencies in field-deployed plastics vary by type of polymer." *Environmental Science and Pollution Research.* **26**: p9079-9088. https://doi.org/10.1007/s11356-019-04281-4

[131] Loakeimidis C, Fotopoulou KN, Karapanagioti HK, Geraga M, Zeri C, Papathanassiou E, Galgani F, Papatheodorou G. (2016). "The degradation potential of PET bottles in the marine environment: An ATR-FTIR based approach" *Nature Scientific Reports*. **6**: e23501. https://doi.org/10.1038/srep23501

[132] Pascall MA, Zabik ME, Zabik MJ and Hernandez RJ. (2005) "Uptake of Polychlorinated Biphenyls (PCBs) from an Aqueous Medium by Polyethylene, Polyvinyl Chloride, and Polystyrene Films." *Journal of Agricultural and Food Chemistry*. **53**(1): p164-169. https://doi.org/10.1021/jf048978t

[133] Fries E, Zarfl C. (2012). "Sorption of polycyclic aromatic hydrocarbons (PAHs) to low and high density polyethylene (PE)." *Environmental Science and Pollution Research*. **19**: p1296–1304. https://doi.org/10.1007/s11356-011-0655-5

[134] Smedes F, Geertsma RW, van der Zande T, Booij K. (2009). "Polymer−Water Partition Coefficients of Hydrophobic Compounds for Passive Sampling: Application of Cosolvent Models for Validation." *Environmental Science and Technology.* **43**(18): p7047–7054. https://doi.org/10.1021/es9009376

[135] Booij K, Hofmans HE, Fischer CV, Van Weerlee EM. (2003). "Temperature-Dependent Uptake Rates of Nonpolar Organic Compounds by Semipermeable Membrane Devices and Low-Density Polyethylene Membranes." *Environmental Science and Technology.* **37**(2): p361–366. https://doi.org/10.1021/es025739i

S_9. SUPPLEMENTARY MATERIALS:

S_9.1. SUPPLEMENTARY MATERIALS: Microplastics Reference Material.

S_Table 11. Microplastics Reference Materials: milling weights, Particle Size, Stock, and Sample bags.

		Single Pellet			Total Stock Milling (µPs: Reference Materials Created)				Microscope Size Analysis				Sample Bags		
SMP ID	PLASTIC	Average Weight (mg)	%RSD	Optimal Milling Weight (g)	# Jars processed	Average Weight per Jar (g)	%RSD	Total Amount Milled (g)	Approx. Smallest Diameter Particle (mm)	Approx. Largest Diameter Particle (mm)	Approx. Average Diameter Particle (mm)	Visual Modal (1-10)	Sample Bags Created	Average weight per bag (g)	% RSD
LDPE	Low-Density Polyethylene	24.90 ± 0.15	0.7%	6.0	(n=33)	6.017 ± 0.012	0.20%	199	0.060	0.550	0.235	7 - 9	(n=189)	1.000 ± 0.003	0.32%
HDPE	High-Density Polyethylene	26.82 ± 0.17	1.0%	6.0	(n=36)	6.045 ± 0.165	2.73%	212	0.120	0.345	0.450	4 - 8	(n=189)	1.000 ± 0.012	1.17%
PPrp	Polypropylene	22.96 ± 0.15	0.6%	9.5	(n= 6)	9.517 ± 0.016	0.17%	57	0.025	0.240	0.080	4 - 6	(n=57)	1.001 ± 0.003	0.28%
TPUr	Thermoplastic Polyurethane	18.67 ± 0.26	0.6%	8.0	(n=1)	10.005 -	-	10	0.010	0.290	0.210	6 - 8	-	- -	-
HIPS	High Impact Polystyrene	23.97 ± 0.12	0.3%	10.0	(n=1)	7.900 -	-	8	0.005	0.050	0.005	1 - 4	-	- -	-
PETE	Polyethylene terephthalate	32.01 ± 0.10	1.4%	8.0	(n=24)	7.862 ± 0.263	3.35%	189	0.020	0.200	0.075	2 - 6	(n=189)	1.000 ± 0.013	1.28%
PETG	Polyethylene terephthalate glycol	18.98 ± 0.06	0.5%	8.0	(n=1)	8.008 -	-	8	0.015	0.185	0.100	2 - 4	-	- -	-
PCrb	Polycarbonate	16.42 ± 0.26	0.3%	8.0	(n=1)	8.005 -	-	8	0.010	0.425	0.225	7 - 9	-	- -	-
ABSt	Acrylonitrile Butadiene Styrene	20.75 ± 0.20	1.6%	12.0	(n=7)	9.045 ± 0.016	0.17%	63	0.010	0.160	0.020	2 - 3	-	- -	-

S_Figure 27. Cryomill used to process Virgin Plastics to Fine Powder showing milling jar with plastic pellets.

S_9.2. SUPPLEMENTARY MATERIALS: Microplastics Instrument Methods.

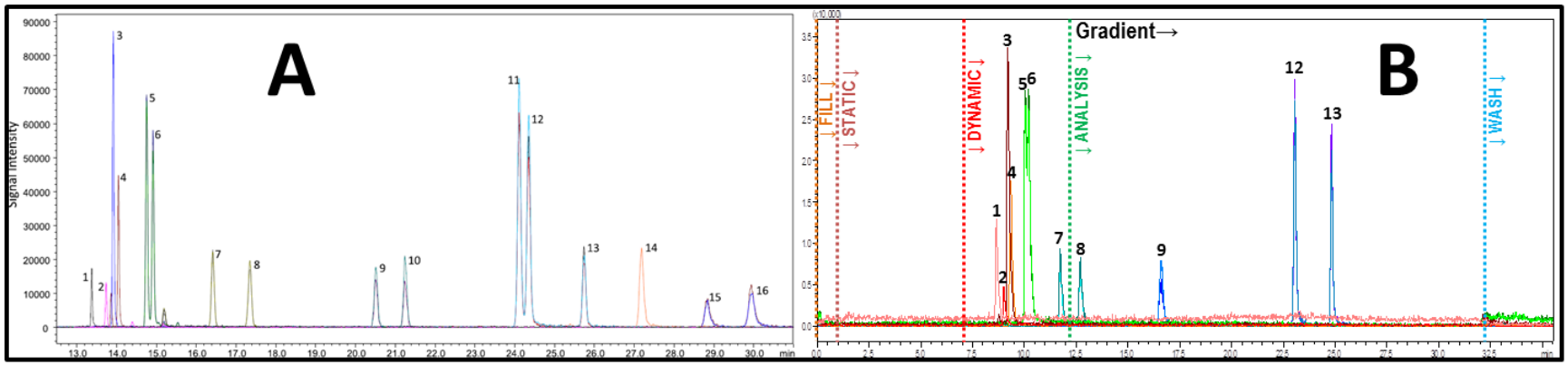

S_Figure 28. SFE-SFC-MS Chromatograms of Online Extractions Using the Original Method for PAHs in Soil, Comparing Extractions from [A*] Soil Sample in 5.0-mL Extraction Vessel and [B] Microplastics in 0.2-mL Extraction Vessel.** *[A] Reproduced with the permission of the author from **Wicker et. al., 2018**[120]: shows extraction from 1 g CRM clay spiked with 16 PAHs at low QC (50 ng) packed with hydroprotect; zoomed baseline for 'Analysis' in [A] = 12.5 – 31.0 minutes. **[B] Result of the current work shows extraction from 10 mg microplastics exposed for 1-day to Milli-Q water spiked with 11 PAHs at high QC (1250 ng/g); Full runtime shown in [B], showing peaks eluding pre-analysis (green dotted line). **Peak order: [1] NAPL, naphthalene; [2] ANPY, acenaphthylene; [3] ACEN, acenaphthene; [4] FLUR, fluorene; [5] PHNR, phenanthrene; [6] ANRN, anthracene; [7] FLAT, fluoranthene; [8] PYRN, pyrene; [9] BARC, benzo(*a*)anthracene; [10] CHSY, chrysene; [11] BBFA, benzo(*b*)fluoranthene; [12] BKFA, Benzo(*k*)fluoranthene; [13] BAPY, benzo(*a*)pyrene; [14] DBAR, dibenzo(*a*,*h*)anthracene; [20] IDPY, indeno(1,2,3-*cd*)pyrene; [16] BGPY, benzo(*g*,*h*,*i*)perylene.**

S_9.3. SUPPLEMENTARY MATERIALS: Method Transfer for 0.2-mL Extraction Vessels.

S_Table 12. **Resolution of Critical Pair Groups during Gradient Screening.**

Critical MRM Group	PAH ID	Critical Group Resolution						Gradient
		g1	g2	g3	g4	g5	g6	
A	PHNR	-	-	-	-	-	-	
	ANRN	1.23	1.26	1.26	1.22	1.41	1.26	
B	FLAT	-	-	-	-	-	-	
	PYRN	5.57	5.38	5.52	4.80	5.44	5.05	
C	BARC	-	-	-	-	-	-	
	CHSY	4.05	3.62	3.44	3.46	3.43	3.57	
D	BBFA	-	-	-	-	-	-	
	BKFA	1.34	1.34	1.42	1.33	1.26	1.48	
	BAPY	8.18	7.83	9.48	8.18	7.73	7.97	
E	IDPY	-	-	-	-	-	-	
	BGPY	4.56	9.61	6.81	7.91	5.31	5.12	

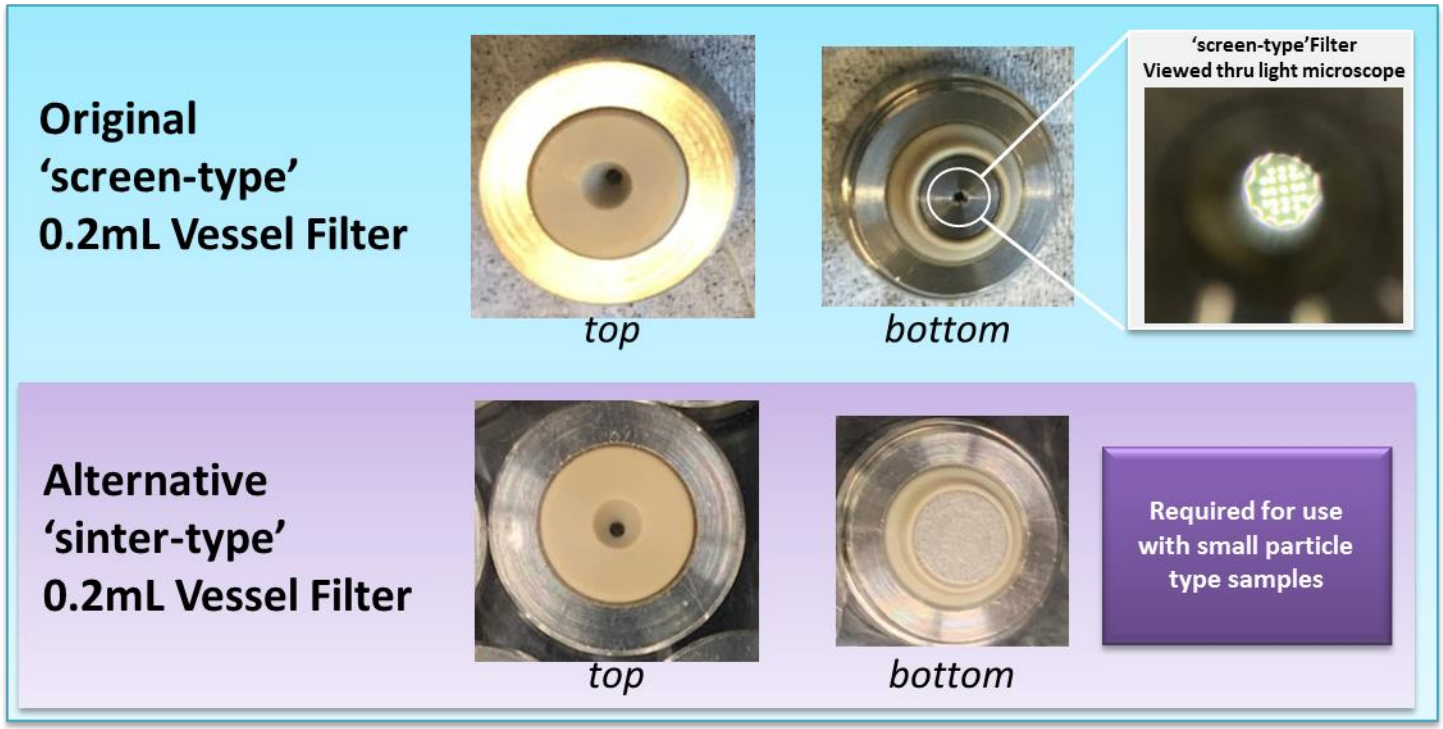

S_Figure 29. Comparison of Filter Types for 0.2-mL Extraction vessels. Showing (top; blue) Original 'Screen'-type filters [SSI part #: 228-59264-84] and (bottom; purple) Alternative 'Sinter'-type Filters [SSI part #: 228-59264-81] required for fine particles (*purchased separately*).

S_9.4. SUPPLEMENTARY MATERIALS: Initial µPs-RMs Matrix Evaluation.

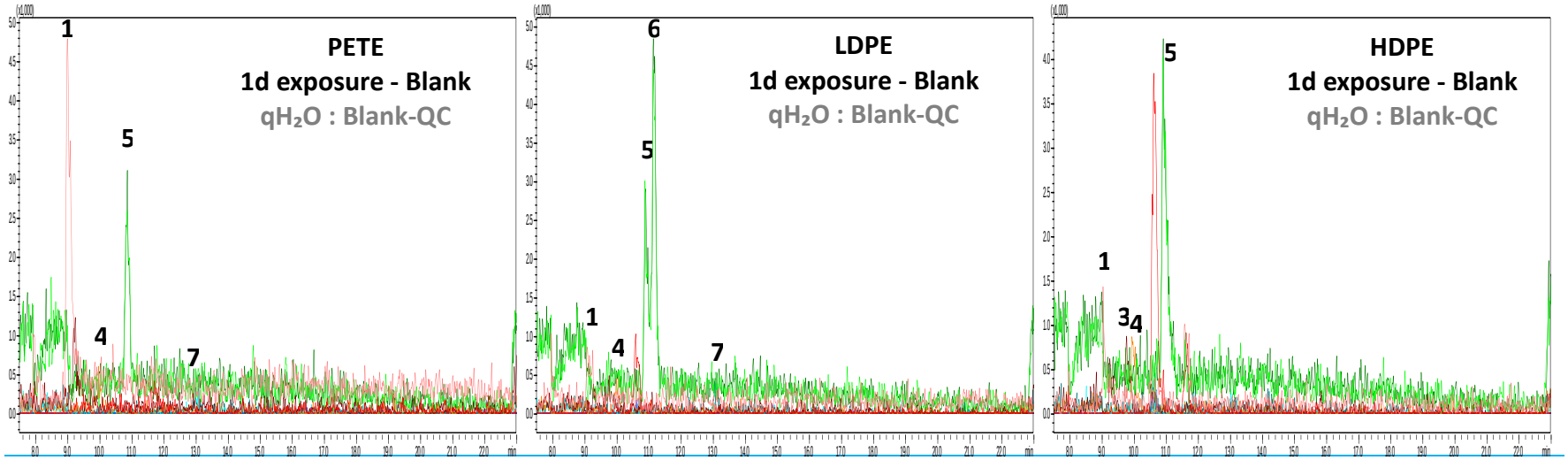

S_Figure 30. Zoomed SFE-SFC-MS Chromatograms for Online Extractions of µPs-RMs Blank QCs for PETE (left), LDPE (middle), and HDPE (right); showing One (**1**)-Day Exposure to Blank Milli-Q Water (qH2O:*Blank-QCs*). **Peak order: [1] NAPL, naphthalene (pink); [3] ACEN, acenaphthene (maroon); [4] FLUR, fluorene (orange); [5] PHNR, phenanthrene (green); [6] ANRN, anthracene (dark green); [7] FLAT, fluoranthene (torquoise).** ***Displayed intensity = Normalized for all chromatograms; and baseline zoomed on 'analysis-step' = 7.50 – 23.00 minutes.***

S_9.5. SUPPLEMENTARY MATERIALS: Exposure Duration.

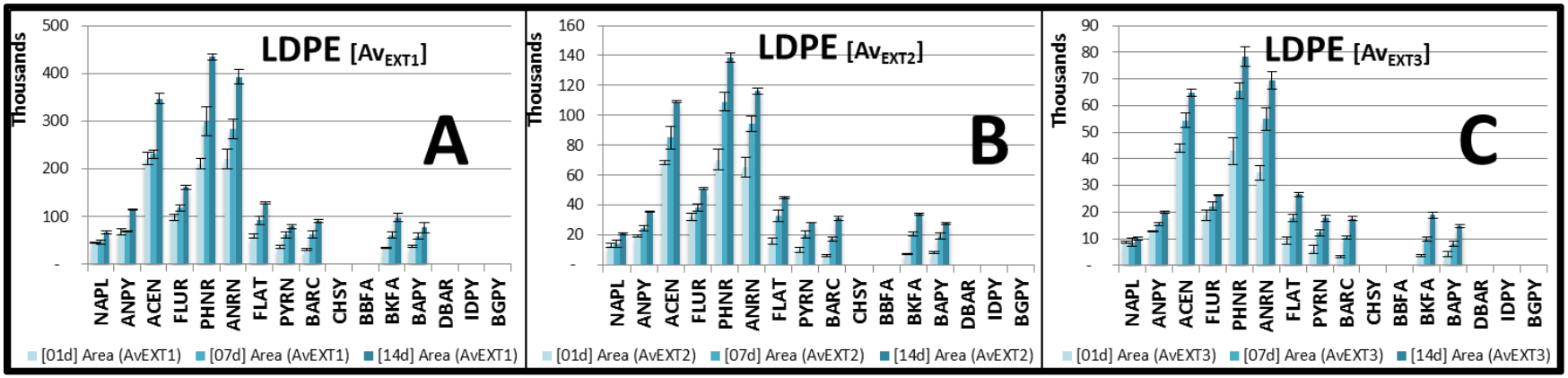

S_Figure 31. Average Total Area per Extraction Round (Av_{total}/EXT) for LDPE Microplastics exposed for 1 [light blue], 7- [blue] and 14 Days [dark blue] to Spiked Milli-Q water (1250 ng), comparing: [A] Av_{total} in Extraction 1 (Av_{EXT1}); [B] Av_{total} in Extraction 2 (Av_{EXT2})[middle]; and [C] Av_{total} in Extraction 3 (Av_{EXT3}). *1-day exposure ([01d], light blue); 7-days exposure ([07d], blue); and 14 days exposure ([14d], dark blue). Error bars = standard deviation (n=3).*

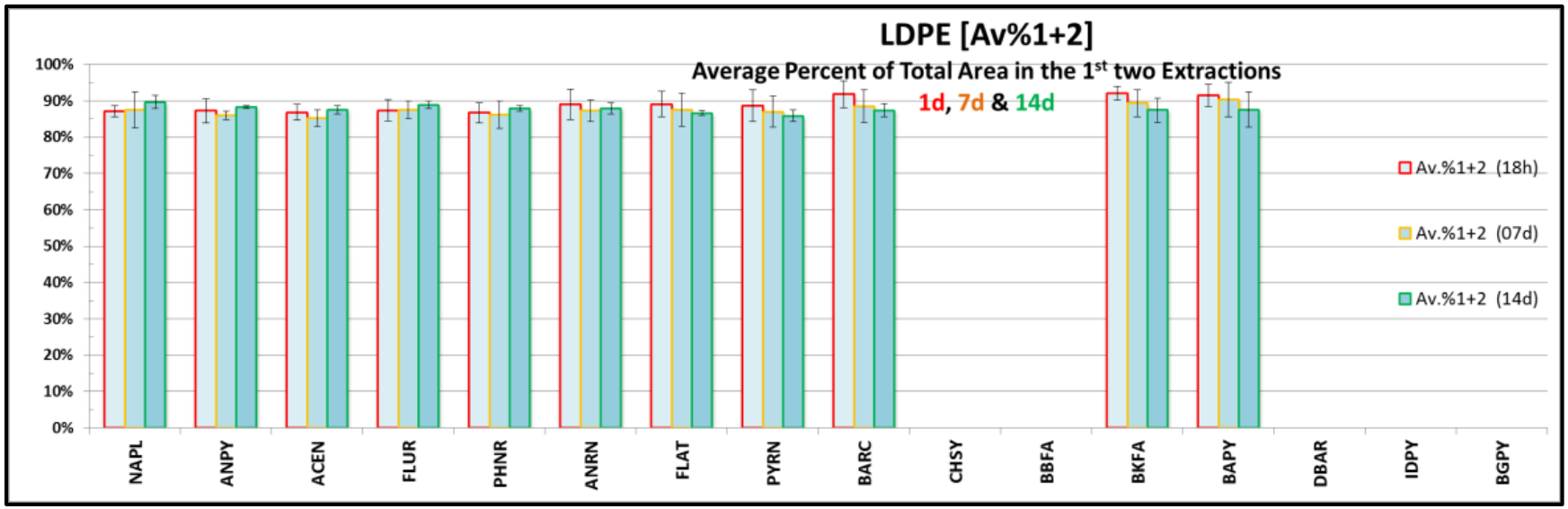

S_Figure 32. Average Percent of Total Area in the First Two Extractions for LDPE-type Microplastics Exposed to MilliQ Water Spiked with HC-PAH-Spike (1250 ng/g). Comparing for three durations: 1 day [red outline]; 7 days [orange outline]; and 14 days [green outline] of Exposure. *Error Bars = Standard deviation (n = 3).*

APPENDIX A

LIST OF FIGURES

APPENDIX A

LIST OF FIGURES

APPENDIX B

SUPPLEMENTAL
LIST OF FIGURES

APPENDIX B

SUPPLEMENTAL

LIST OF SUPPLEMENTAL FIGURES

APPENDIX C

LIST OF TABLES

APPENDIX C

LIST OF TABLES

APPENDIX D

SUPPLEMENTAL
LIST OF TABLES

APPENDIX D

SUPPLEMENTAL LIST OF TABLES

LITERATURE CITED

[1] Berger TA. (2015). "Supercritical fluid chromatography" Primer series; publication number 5991-5509EN; Agilent Technologies, USA. https://www.agilent.com/cs/library/applications/5991-8554EN_SFC_appcompendium_LR.pdf

[2] Berger TA. (1991). "Density of Methanol-Carbon Dioxide Mixtures at Three temperatures: Comparison with Vapor Liquid Equilibria Measurements and Results obtained from Chromatography." *Journal of High Resolution Chromatography.* **14**(5): p312–316. https://doi.org/10.1002/JHRC.1240140504

[3] Berger TA. (1995). "Packed Column SFC." *RCS Chromatography Monographs Series*; R. M. Smith (Eds.).; The Royal Society of Chemistry: Cambridge, UK. ISBN: 0-85404-500-7

[4] Bolanos B, Greig M, Ventura M, Farrell W, Aurigemma CM, Li H, Quenzer TL, Tivel K, Bylund JMR, Tran P, Pham C, Phillipson D. (2004). "SFC/MS in drug discovery at Pfizer, La Jolla." *International Journal of Mass Spectrometry.* **238**(2): p85-97. https://doi.org/10.1016/j.ijms.2003.11.021

[5] Tarafder A. (2016). "Metamorphosis of supercritical fluid chromatography to SFC: An Overview." *Trends in Analytical Chemistry.* **81**: p3–10. http://dx.doi.org/10.1016/j.trac.2016.01.002

[6] Maftouh M, Granier-Loyaux C, Chavana E, Marini J, Pradines A, Vander Heyden Y, Picard C. (2005). "Screening approach for chiral separation of pharmaceuticals Part III. Supercritical fluid chromatography for analysis and purification in drug discovery." *Journal of Chromatography A.* **1088**(1-2): p67-81. https://doi.org/10.1016/j.chroma.2004.12.038

[7] White C. (2005). "Integration of supercritical fluid chromatography into drug discovery as a routine support tool Part I. Fast chiral screening and purification." *Journal of Chromatography A.* **1074**(1-2): p163-173. https://doi.org/10.1016/j.chroma.2005.03.073

[8] Berger TA, Berger BK, Fogelman K. (2012). "8.18 Chromatographic Separations and Analysis: Supercritical Fluid Chromatography for Chiral Analysis and Semi-Preparative Purification." In: E.M. Carreira & H. Yamamoto (Eds.). Comprehensive Chirality (pp.354-392). Elsevier: Amsterdam, Netherlands. https://doi.org/10.1016/B978-0-08-095167-6.00836-3

[9] Berger, TA. Guest Speaker Lecture on Introduction to Packed Column Supercritical Fluid Chromatography (SFC). Presented at University of Texas at Arlington, Arlington, TX, USA, September 20, 2020.

[10] Chowdhury, SM. CHEM 5324 Lecture on Mass Spectrometry (MS) Background. Presented at University of Texas at Arlington, Arlington, TX, USA, January 22, 2020.

[11] Chowdhury, SM. CHEM 5324 Lecture on Mass Spectrometry; Sources; Electrospray Ionization (ESI). Presented at University of Texas at Arlington, Arlington, TX, USA, February 7, 2020.

[12] Chowdhury, SM. CHEM 5324 Lecture on Mass Spectrometry; Sources; Atmospheric Pressure Chemical Ionization (APCI). Presented at University of Texas at Arlington, Arlington, TX, USA, February 5, 2020.

[13] Chowdhury, SM. CHEM 5324 Lecture on Mass Spectrometry; Analyzers; Quadrupole Mass Analyzers. Presented at University of Texas at Arlington, Arlington, TX, USA, February 26, 2020.

[14] del Pilar Sanchez-Camargo A, Parada-Alfonso F, Ibanez E, Cifuentes A. (2017). "On-line coupling of supercritical fluid extraction and chromatographic techniques." *Journal of Separation Sciences.* **40**(1): p213–227. https://doi.org/10.1002/jssc.201601040

[15] Taylor LT. (2013). "Analytical Supercritical Fluid Extraction Goes Back to the Future." *LC/GC special Issues*. **31**(11): p10–13.

[16] del Pilar Sanchez-Camargo A, Parada-Alfonso F, Ibanez A, Cifuentes A. (2019). "Recent applications of on-line supercritical fluid extraction coupled to advanced analytical techniques for compounds extraction and identification." *Journal of Separation Sciences.* **42**(1)**:** p243–257. https://doi.org/10.1002/jssc.201800729

[17] Wicker AP, Tanaka K, Nishimura M, Chen V, Ogura T, Hedgepeth W, Schug KA. (2020). "Multivariate approach to on-line supercritical fluid extraction - supercritical fluid chromatography - mass spectrometry method development." *Analytica Chimica Acta*. **1127**: p282-294. https://doi.org/10.1016/j.aca.2020.04.068

[18] Sakai M, Hayakawa Y, Funada Y, Ando T, Fukusaki E, Bamba T. (2017). "Development of a split-flow system for high precision variable sample introduction in supercritical fluid chromatography." *Journal of Chromatography A.* **1515**: p218-231. https://doi.org/10.1016/j.chroma.2017.07.077

[19] World Anti-Doping Agency. International Standard Prohibited List, 2021. Resources. https://www.wada-ama.org/sites/default/files/resources/files/2021list_en.pdf. (Accessed January 03 2021).

[20] U.S. Environmental Protection Agency, Office of Research and Development, National Center for Environmental Assessment. *Method 8310: Polycyclic aromatic hydrocarbons in ground water.* Washington, DC, 1986.

[21] Lohmann R. (2012). "Critical review of low-density polyethylene's partitioning and diffusion coefficients for trace organic contaminants and implications for its use as a passive sampler." *Environmental Science & Technology.* **46**(2): p606-618. https://doi.org/10.1021/es202702y

[22] Ministry of Environment, Lands and Parks Province of British Columbia. **"***Ambient Water Quality Criteria For Polycyclic Aromatic Hydrocarbons (PAHs). February 1993*." Approved Water Quality Guidelines, Technical Reports, Polycyclic Aromatic Hydrocarbons (PAHs), Technical Appendix. K_{OW}'s from https://www2.gov.bc.ca/assets/gov/environment/air-land-water/water/waterquality/water-quality-guidelines/approved-wqgs/pahs/pahs-tech.pdf (accessed August 25 2021).

[23] Hansch C, Leo A, Hoekman D. (1995). "Exploring QSAR - Hydrophobic, Electronic, and Steric Constants." In: S.R. Heller (ed.). ACS professional reference books, vol 2. American Chemical Society: Washington, DC. ISBN 0-8412-2993-7

[24] van Eenoo P, Delbeke FT. (2006). "Metabolism and excretion of anabolic steroids in doping control—New steroids and new insights." *The Journal of Steroid Biochemistry and Molecular Biology*. **101**(4-5): p161–178. https://doi.org/10.1016/j.jsbmb.2006.06.024

[25] Handelsman DJ,Bermon S. (2019). "Detection of testosterone doping in female athletes." *Drug Testing and Analysis.* **11**(10): p1566–1571. https://doi.org/10.1002/dta.2689

[26] Fragkaki AG, Angelis YS, Koupparis M, Tsantili-kakoulidou A, Kokotos G, Georgakopoulos C. (2009). "Structural characteristics of anabolic androgenic steroids contributing to binding to the androgen receptor and to their anabolic and androgenic activities applied modifications in the steroidal structure." *Steroids*. **74**(2): p172–197. https://doi.org/10.1016/j.steroids.2008.10.016

[27] de Kock N, Acharya, SR, Ubhayasekera SJKA, Bergquist J. (2018). "A Novel Targeted Analysis of Peripheral Steroids by Ultra-Performance Supercritical Fluid Chromatography Hyphenated to Tandem Mass Spectrometry." *Nature Scientific Reports*. **8**: e16993. https://doi.org/10.1038/s41598-018-35007-0

[28] Teubel J, Wüst B, Schipke CG, Peters O, Parr MK. (2017). "Methods in endogenous steroid profiling – A comparison of gas chromatography mass spectrometry (GC–MS) with supercritical fluid chromatography tandem mass

spectrometry (SFC-MS/MS)." *Journal of Chromatography A.* **1554**: p101-116. https://doi.org/10.1016/j.chroma.2018.04.035

[29] Thevis M, Kuuranne T, Geyer H. (2020). "Annual banned-substance review: Analytical approaches in human sports drug testing 2019/2020." *Drug Testing and Analysis.* **13**(1): p8–35. https://doi.org/10.1002/dta.2969

[30] World Anti-Doping Agency. 2018 anti-doping testing figures; 2019. https://www.wada-ama.org/sites/default/files/resources/files/2018_testing_figures_report.pdf (accessed on 06 July 2021).

[31] Thevis M, Kuuranne T, Geyer H. (2019). "Annual banned-substance review – Analytical approaches in human sports drug testing." *Drug Testing and Analysis.* **12**(1): p7–26. https://doi.org/10.1002/dta.2735

[32] Thevis M, Schanzer W. (2006). "Mass spectrometry in sports drug testing: structure characterization and analytical assays." *Mass Spectrometry Reviews*. **26**(1): p79-107. https://doi.org/10.1002/mas.20107

[33] Schanzer W, Thevis M. (2015). "human sports drug testing by mass spectrometry." *Mass Spectrometry Reviews.* **36**(1): p16–46. https://doi.org/10.1002/mas.21479

[34] Cha E, Kim S, Kim HJ, Lee KM, Kim KH, Kwon O-S, Lee J. (2015). "Relationships between structure, ionization profile and sensitivity of exogenous anabolic steroids under electrospray ionization and analysis in human urine using liquid chromatography–tandem mass spectrometry." Biomedical Chromatography. **30**(4): p555-65. https://doi.org/10.1002/bmc.3583

[35] Pozo OJ, Van Eenoo P, Deventer K, Delbeke FT. (2017). "Development and validation of a qualitative screening method for the detection of exogenous anabolic steroids in urine by liquid chromatography-tandem mass spectrometry." *Analytical and Bioanalytical Chemistry.* **389**: p1209–1224. https://doi.org/10.1007/s00216-007-1530-6

[36] Pozo OJ, Van Eenoo P, Deventer K, Delbeke FT. (2007). "Ionization of anabolic steroids by adduct formation in liquid chromatography electrospray mass spectrometry." *Journal of Mass Spectrometry.* **42**(4): p497-516. https://doi.org/10.1002/jms.1182

[37] Berger T. (1997). "Review: Separation of polar solutes by packed column supercritical fluid chromatography." *Journal of Chromatography A.* **785**: p3-33. https://doi.org/10.1016/S0021-9673(97)00849-2

[38] Desfontaine V, Guillarme D, Francotte E, Novakova L. (2015). "Review: Supercritical fluid chromatography in pharmaceutical analysis." *Journal of Pharmaceutical and Biomedical Analysis.* **113**: p56–71. http://dx.doi.org/10.1016/j.jpba.2015.03.007

[39] Quanson JL, Stander MA, Pretorius E, Jenkinson C, Taylor AE, Storbeck KH. (2016). "High-throughput analysis of 19 endogenous androgenic steroids by ultra-performance convergence chromatography tandem mass spectrometry." *Journal of Chromatography B.* **1031**: p131-138. https://doi.org/10.1016/j.jchromb.2016.07.024

[40] Teubel J, Wust B, Schipke CG, Peters O, Parr MK. (2018). "Methods in endogenous steroid profiling – A comparison of gas chromatography mass spectrometry (GC–MS) with supercritical fluid chromatography tandem mass spectrometry (SFC-MS/MS)." *Journal of Chromatography A.* **1554**: p101-116. https://doi.org/10.1016/j.chroma.2018.04.035

[41] Joseph JF, Parr MK. (2020). "I.5. Techniques for identifying and quantifying drugs and metabolites: Application of SFC for bioanalysis." In S. Ma & S.K. Chowdhury (Eds.). Identification and Quantification of Drugs, Metabolites, Drug Metabolizing Enzymes, and Transporters (Second Edition) (pp.354-392). Amsterdam, Netherlands: Elsevier.

[42] Akbal L, Hopfgartner G. (2020). "Hyphenation of packed column supercritical fluid chromatography with mass spectrometry: where are we and what are the remaining challenges?" *Analytical and Bioanalytical Chemistry*. **412**: p6667–6677. https://doi.org/10.1007/s00216-020-02715-4

[43] Gurst JE, Djerassi C. (1964). "Mass Spectrometry in Structural and Stereochemical Problems. LIX. Mechanism of the formal loss of acetone from 2-oxo-5α-steroids." *Journal of the American Chemical Society.* **86**(24): p5542 – 5547. https://doi.org/10.1021/ja01078a029

[44] Ma Y-C, Kim H-Y. (1997). "Determination of Steroids by Liquid Chromatography/Mass Spectrometry." *Journal of the American Society for Mass Spectrometry.* **8**(9): p1010-1020. https://doi.org/10.1016/S1044-0305(97)00122-0

[45] Thevis M, Schanzer W. (2005). "Mass Spectrometric Analysis of Androstan-17ß-ol-3-one and Androstadiene-17ß-ol-3-one Isomers." *Journal of the American Society for Mass Spectrometry.* **16**(10): p1660–1669. https://doi.org/10.1016/j.jasms.2005.06.007

[46] Verheyden K, Bizec BL, Coutheyn D, Mortier V, Vandewiele M, Gillis W, Vanthemsche P, De Brabander HF, Noppe H. (2006). "Mass spectrometric detection of and similarities between 1-androgens." *Analytica Chimica Acta.* **586**(1-2): p57–72. https://doi.org/10.1016/j.aca.2006.10.058

[47] Thevis M, Guddat S, Schanzer W. (2009). "Doping control analysis of trenbolone and related compounds using liquid chromatography–tandem mass spectrometry." Steroids. **74**(3): p315-321. https://doi.org/10.1016/j.steroids.2008.10.004

[48] Guan F, Soma LR, Luo Y, Uboh CE, Peterman S. (2006). "Collision-Induced Dissociation Pathways of Anabolic Steroids by Electrospray Ionization Tandem Mass Spectrometry." *Journal of the American Society for Mass Spectrometry.* **17**(4): p477–489. https://doi.org/10.1016/j.jasms.2005.11.021

[49] Schanzer W. (1996). "Metabolism of anabolic androgenic steroids." *Clinical Chemistry.* **42**(7): p1001-1020. https://doi.org/10.1093/CLINCHEM/42.7.1001

[50] Williams TM, Kind AJ, Houghton E, Hill DW. (1999). "Electrospray Collision-induced Dissociation of Testosterone and Testosterone Hydroxy Analogs." *Journal of Mass Spectrometry.* **34**(3): p206-216. https://doi.org/10.1002/(SICI)1096-9888(199903)34:3<206::AID-JMS785>3.0.CO;2-1

[51] Schanzer W, Thevis M. (2017). "human sports drug testing by mass spectrometry." *Mass Spectrometry Reviews.* **36**(1): p16–46. https://doi.org/10.1002/mas.21479

[52] Cha E, Kim S, Kim HJ, Lee KM, Kim KH, Kwon O-S, Lee J. (2015). "Sensitivity of GC-EI/MS, GC-EI/MS/MS, LC-ESI/MS/MS, LC-Ag+CIS/MS/MS, and GC-ESI/MS/MS for analysis of anabolic steroids in doping control." *Drug Testing and Analysis.* **7**(11-12): p1040–1049. https://doi.org/10.1002/dta.1906

[53] Pozo OJ, van Eenoo, Deventer K, Lootens L, Grimalt S, Sancho JV, Hernandez F, Delbeke FT. (2008). "General guidelines for the CID fragmentation of 3-keto-anabolic steroids." In: W Schänzer, H Geyer, A Gotzmann, U Mareck (eds.) Recent Advances In Doping Analysis (16). Sport und Buch Strauß - Köln 2008. pp. 131. https://www.dshs-koeln.de/fileadmin/redaktion/Institute/Biochemie/PDF/Proceedings/Proceedings_16/16_pp_131-140.pdf

[54] Karliner J, Budzikiewicz H, Djerassi C. (1966). " Mass Spectrometry in Structural and Sterochemical Problems. XCI. The electron Impact induced Elimination of Water from 3-Hydroxy Steroids." *The Journal of Organic Chemistry.* **31**(3): p710–713. https://doi.org/10.1021/jo01341a015

[55] Thevis M, Makarov AA, Horning S, Schanzer W. (2005). "Mass spectrometry of stanozolol and its analogues using electrospray ionization and collision-induced dissociation with quadrupole-linear ion trap and linear ion trap-

orbitrap hybrid mass analyzers." *Rapid Communications in Mass Spectrometry.* **19**(22): p3369–3378. https://doi.org/10.1002/rcm.2204

[56] Pozo OJ, van Eenoo P, Deventer K, Grimalt S, Sancho JV, Hernandez F, Delbeke FT. (2008). "Collision-induced dissociation of 3-keto anabolic steroids and related compounds after electrospray ionization. Considerations for structural elucidation." *Rapid Communications in Mass Spectrometry.* **22**(24): p4009–4024. https://doi.org/10.1002/rcm.3823

[57] Thevis M, Fubholler G, Geyer H, Rodchenkov G, Mareck U, Sigmund G, Koch A, Thomas A, Schanzer W. (2006). "Detection of Stanozolol and Its Major Metabolites in Human Urine by Liquid Chromatography-Tandem Mass Spectrometry." *Chromatographia*. **64**: p441-446. https://doi.org/10.1365/s10337-006-0043-3

[58] Thevis M, Beuck S, Hoppner S, Thomas A, Held J, Schafer M, Oomens J, Schanzer W. (2012). "Structure Elucidation of the Diagnostic Product Ion at *m/z* 97 Derived from Androst-4-en-3-One-Based Steroids by ESI-CID and IRMPD Spectroscopy." *Journal of the American Society for Mass Spectrometry.* **23**(3): p537-546. https://doi.org/10.1007/s13361-011-0308-4

[59] Thevis M, Bommerich U, Opfermann G, Schanzer W. (2005). "Characterization of chemically modified steroids for doping control purposes by electrospray ionization tandem mass spectrometry." *Journal of Mass Spectrometry.* **40**(4): p494–502. https://doi.org/10.1002/jms.820

[60] Verhayden K, Le Bizec B, Courtheyn D, Mortier V, Vandewiele M, Gillis W, Vanthemsche P, De Brabander HF, Noppe H. (2007). "Mass spectrometric detection of and similarities between 1-androgens." *Analytica Chimica Acta.* **586**(1-2): p57–72. https://doi.org/10.1016/j.aca.2006.10.058

[61] Shapiro RH, Williams DH, Budzikiewicz H, Djerassi C. (1964). " Mass Spectrometry in Structural and stereochemical problems. LIII. Fragmentation and Hydrogen Transfer Reactions of a Typical 3-Keto Steroid, 5α-Androstan-3-one." *Journal of the American Chemical Society.* **86**(14): 2837-2845. https://doi.org/10.1021/ja01068a016

[62] Shapiro RH, Djerassi C. (1964). "Mass Spectrometry in Structural and stereochemical problems. L. Fragmentation and hydrogen migration Reactions of α,ß-Unsaturated 3-Keto Steroids." *Journal of the American Chemical Society.* **86**(14): p2825–2832. https://doi.org/10.1021/ja01068a014

[63] Kochnova E, Sobolevsky T, Sizoi V, Rodchenkov G. (2009). "Calibration issue for the quantitative determination of endogenous steroids: the comparison of 6 matrices." In: Schanzer W, Geyer H, Gotzmann A, Mareck U (eds.). Recent Advances in Doping Analysis (17), Köln, pp. 47-62. https://www.dshs-koeln.de/fileadmin/redaktion/Institute/Biochemie/PDF/Proceedings/Proceedings_17/17_pp_253-256.pdf

[64] Putz M, Piper T, Thevis M. (2020). "Identification of Trenbolone Metabolites Using Hydrogen isotope Ratio Mass Spectrometry and Liquid Chromatography/High Accuracy/High Resolution Mass Spectrometry for Doping Control Analysis." *Frontiers in Chemistry.* **8**: p435. https://doi.org/10.3389/fchem.2020.00435

[65] Schanzer W, Geyer H, Donike M. (1999). "Metabolism of Metandienone in man: Identification and Synthesis of conjugated excreted urinary metabolites, determination of excretion rates and gas chromatographic-mass spectrometric identification of bis-hydroxylated metabolites." *The Journal of Steroid Biochemistry and Molecular Biology.* **38**(4): p441-464. https://doi.org/10.1016/0960-0760(91)90332-Y

[66] Thevis M, Piper T, Horning S, Juchelka D, Schanzer W. (2013). "Hydrogen isotope ratio mass spectrometry and high-resolution/high-accuracy mass spectrometry in metabolite identification studies: Detecting target compounds for sports drug testing." *Rapid Communications in Mass Spectrometry.* **27**(17): p1904–1912. https://doi.org/10.1002/rcm.6648

[67] Martinez-Brito D, de la Torre X, Colamonici C, Curcio D, Botre F. (2019). "7-ketoDHEA metabolism in humans. Pitfalls in interpreting the analytical results in the antidoping field." *Drug Testing and Analysis.* **11**(11-12): p1629-1643. https://doi.org/10.1002/dta.2734

[68] Budzikiewicz H, Djerassi C. (1962). "Mass Spectrometry in Structural and Stereochemical Problems. I. Steroid Ketones." *Journal of the American Chemical Society.* **84**(8): p1430–1439. https://doi.org/10.1021/ja00867a019

[69] Musharraf SG, Ali A, Khan NT, Yousuf M, Chaudhary MI, Rahman A. (2013). "Tandem mass spectrometry approach for the investigation of the steroidal metabolism: Structure–fragmentation relationship (SFR) in anabolic steroids and their metabolites by ESI-MS/MS analysis." *Steroids*. **78**(2): p171-181. https://doi.org/10.1016/j.steroids.2012.10.017

[70] Egger H, Spiteller G. (1966). "Massenspektren und stereochemie von hydroxyverbindungen, 1. Mitt.: Hydroxysteroide." *Mh Chem* **97**: p579–601. https://doi.org/10.1007/BF00905276

[71] Leinonen A, Kuuranne T, Kotiaho T, Kostianinen R. (2004). "Screening of free 17-alkyl-substituted anabolic steroids in human urine by liquid chromatography-electrospray ionization tandem mass spectrometry." *Steroids*. **69**(2): p101-109. https://doi.org/10.1016/j.steroids.2003.10.007

[72] Gorityala S, Yang S, Montano MM, Xu Y. (2018). "Simultaneous determination of dihydrotestosterone and its metabolites in mouse sera by LC-MS/MS with chemical derivatization." *Journal of Chromatography B.* **1090**: p22–35. https://doi.org/10.1016/j.jchromb.2018.05.008

[73] Schanzer W, Thevis M. (2015). "human sports drug testing by mass spectrometry." *Mass Spectrometry Reviews*. **36**(1): p16–46. https://doi.org/10.1002/mas.21479

[74] Yan Z, Wu M, He G, Dong Y, Ouyang G, Wu Y, Lu J, Yang S, Xu Y, Wang X. (2013). "An Improved LC-MS-MS method for the determination of Clenbuterol in Human Urine." *LCGC North America*. **31**(3): p240-247.

[75] Thevis M, Opfermann G, Schanzer W. (2003). "Liquid chromatography/electrospray ionization tandem mass spectrometric screening and confirmation methods for ß2-agonists in human or equine urine." *Journal of Mass Spectrometry.* **38**(11): p1197–1206. https://doi.org/10.1002/jms.542

[76] Biancotto G, Angeletti R, Piro RDM, Favretto D, Traldi P. (1997). "Ion Trap High-performance Liquid Chromatography/Multiple Mass Spectrometry in the Determination of $ß_2$-Agonists in Bovine Urines." *Journal of mass spectrometry*. **32**(7): p781-784. https://doi.org/10.1002/(SICI)1096-9888(199707)32:7<781::AID-JMS532>3.0.CO;2-5

[77] Cai J, Henion J. (1997). "Quantitative multi-residue determination of ß-agonists in bovine urine using on-line immunoaffinity extraction-coupled column packed capillary liquid chromatography-tandem mass spectrometry." *Journal of Chromatography B*. **691**(2): p357-370. https://doi.org/10.1016/S0378-4347(96)00433-1

[78] Thevis M. (2009). "Detection of the arylpropionamide-derived selective androgen receptor modulator (SARM) S-4 (Andarine) in a black-market product." *Drug Testing and Analysis.* **1**(8): p387–392. https://doi.org/10.1002/dta.91

[79] Thevis M, Schanzer W. (2008). "Mass Spectrometry of selective androgen receptor modulators." *Journal of Mass Spectrometry.* **43**(7): p865-876. https://doi.org/10.1002/jms.143

[80] Thevis M, Volmer DA. (2018). "Mass spectrometric studies on selective androgen receptor modulators (SARMs) using electron ionization and electrospray ionization/collision-induced dissociation." European Journal of Mass Spectrometry. **24**(1): p145–156. https://doi.org/10.1177/1469066717731228

[81] Thevis M, Thomas A, Fubholler G, Beuck S, Geyer H, Schanzer W. (2010). "Mass spectrometric characterization of urinary metabolites of the selective androgen receptor modulator andarine (S-4) for routine doping control purposes." *Rapid Communications in Mass Spectrometry.* **24**(15): p2245–2254. https://doi.org/10.1002/rcm.4637

[82] Launay FM, Young PB, Sterk SS, Blokland MH, Kennedy DG. (2004). "Confirmatory assay for zeranol, taleranol and the Fusarium spp. toxins in bovine urine using liquid chromatography-tandem mass spectrometry." *Food Additives and Contaminants*. **21**(1): p52–62. https://doi.org/10.1080/02652030310001636930

[83] Jodlbauer J, Zollner P, Lindner W. (2000). "Determination of Zeranol, Taleranol, Zearalenone, α- and ß-Zearalenol in Urine and Tissue by High-Performance Liquid Chromatography-Tandem Mass Spectrometry." *Chromatographia*. **51**: p681-687. https://doi.org/10.1007/BF0250540

[84] Thevis M, Fubholler G, Schanzer W. (2011). "Zeranol: doping offence or mycotoxin? A case-related study." *Drug Testing and Analysis.* **3**(11/12): p777–783. https://doi.org/10.1002/dta.352

[85] Handelsman DJ, Bermon S. (2019). "Detection of testosterone doping in female athletes." *Drug Testing and Analysis*. **11**(10): p1566–1571. https://doi.org/10.1002/dta.2689

[86] Suzuki M, Nishiumi S, Kobayashi T, Sakai A, Iwata Y, Uchikata T, Izumi Y, Azuma T, Bamba T, Yoshida M. (2017). "Use of on-line supercritical fluid extraction-supercritical fluid chromatography/tandem mass spectrometry to analyze disease biomarkers in dried serum spots compared with serum analysis using liquid chromatography/tandem mass spectrometry." *Rapid Communications in Mass Spectrometry.* **31**(10): p886–894. https://doi.org/10.1002/rcm.7857

[87] Ramsthaler F, Schlote J. Wagner C, Fiscina J, Kettner M. (2015). "The ring phenomenon of diluted blood droplets." *International Journal of Legal Medicine*. **130**: p731-736. https://doi.org/10.1007/s00414-015-1304-1

[88] George RS, Moat SJ. (2016). "Effect of Dried Blood Spot Quality on Newborn Screening Analyte Concentrations and Recommendations for Minimum Acceptance Criteria for Sample Analysis. Clinical Chemistry." *Clinical Chemistry*. **62**(3): p466–475. https://doi.org/10.1373/clinchem.2015.247668

[89] Velghe S, Delahaye L, Stove CP. (2018). "Review: Is the hematocrit still an issue in quantitative dried blood spot analysis?" *Journal of Pharmaceutical and Biomedical Analysis*. **163**: p188–196. https://doi.org/10.1016/j.jpba.2018.10.010

[90] Wilhelm AJ, den Burger JCG, Swart EL. (2014). "Therapeutic drug monitoring by dried blood spot: progress to date and future directions." *Clinical Pharmacokinetics*. **53**(11): p961-973. https://doi.org/10.1007/s40262-014-0177-7

[91] Chang W C-W, Cowan DA, Walker CJ, Wojek N, Brailsford AD. (2020). "Determination of anabolic steroids in dried blood using microsampling and gas chromatography-tandem mass spectrometry: Application to a testosterone gel administration study." Journal of Chromatography A. 1627: e461445. https://doi.org/10.1016/j.chroma.2020.461445

[92] Jambeck JR, Geyer R, Wilcox C, Siegler TR, Perryman M, Andrady A, Narayanet R, Law KL. (2015) "Marine pollution. Plastic waste inputs from land into the ocean." *Science*. **347**(6223): p768–771. https://doi.org/10.1126/science.1260352

[93] Borrele S, Rochman CM, Liboiron M, Bond AL, Lusher A, Bradshaw H, Provencher JF. (2017). "Why we need an international agreement on marine plastic pollution." *Proceedings of the National Academy of Sciences.* **114**(38): p9994–9997. https://doi.org/10.1073/pnas.1714450114

[94] PlasticsEurope. Plastics—the Facts 2019: An analysis of European plastics production, demand and waste data for 2018. https://www.plasticseurope.org/en/resources/publications/1804-plastics-facts-2019. (accessed August 25 2021).

[95] Andrady AL. (2011). "Microplastics in the marine environment." *Marine Pollution Bulletin.* **62**(8): p1596-1605. https://doi.org/10.1016/j.marpolbul.2011.05.030

[96] Geyer R, Jambeck JR, Law KL. (2017). "Plastics: Production, use, and fate of all plastics ever made." *Science Advancements.* **3**(7): e1700782. https://doi.org/10.1126/sciadv.1700782

[97] United States Environmental Protection Agency: Office of Land and Emergency Management. (EPA 530-F-20-009) *"Advancing Sustainable Materials Management: 2018 Fact Sheet. Assessing Trends in Materials Generation and Management in the United States.*" U.S. Environmental Protection Agency Web site. https://www.epa.gov/sites/production/files/2018-03/documents/methodolgy_document_for_selected_municipal_solid_waste_products.pdf (accessed February 02, 2021).

[98] McIlwraith HK, Lin J, Erdle LM, Mallos N, Diamond M, Rochman CM. (2019). "Capturing microfiber – marketed technologies reduce microfiber emissions from washing machines." *Marine Pollution Bulletin.* **139**: p40-45. https://doi.org/10.1016/j.marpolbul.2018.12.012

[99] Rochman CM. (2018). "Microplastics research: from sink to source." *Science.* **360**(6384): p28-29. https://doi.org/10.1126/science.aar7734

[100] McIlwraith HK, Lin J, Erdle LM, Mallos N, Diamond M, Rochman CM. (2019). "Capturing microfiber – marketed technologies reduce microfiber emissions from washing machines." *Marine Pollution Bulletin.* **139**: p40-45. https://doi.org/10.1016/j.marpolbul.2018.12.012

[101] New Zealand Royal Society Te Aparangi. "*Plastics in our Environment – Evidence Summary, 2019*." [Online ISBN: 978-1-877264-39-9]. NZ Royal Society Website. https://www.royalsociety.org.nz/assets/Uploads/Plastics-in-the-Environment-evidence-summary.pdf (accessed February 06 2021).

[102] Booth AM, Kubowicz S, Beegle-Krause C, Skancke J, Nordam T, Landsem E, Throne-Holst M, Jahren S. (M-918) *Microplastic in Global and Norwegian Marine Environments: Distributions, Degradation Mechanisms and Transport, 2017*. Norwegian Environment Agency website. https://www.miljodirektoratet.no/globalassets/publikasjoner/M918/M918.pdf (accessed February 08, 2021).

[103] Gillibert R, Balakrishnan G, Deshoules Q, Tardivel M, Magazzu A, Donato MG, Marago OM, de La Chapelle ML, Colas F, Lagarde F, Gucciardi PG. (2019). "Raman Tweezers for Small Microplastics and Nanoplastics Identification in Seawater." *Environmental Science and Technology.* **53**(15): p9003-9013. https://doi.org/10.1021/acs.est.9b03105

[104] Rochman CM, Brookson C, Bikker J, Djuric N, Earn A, Bucci K, Athey S, Huntington A, McIlwraith H, Munno K, De Frond H, Kolomijeca A, Erdle L, Grbic J, Bayoumi M, Borrelle SB, Wu T, Santoro S, Werbowski LM, Zhu X, Giles RK, Hamilton BM, Thaysen C, Kaura A, Klasios N, Ead L, Kim J, Sherlock C, Ho A, Hung C. (2019). "Rethinking microplastics as a diverse contaminant suite." *Environmental Toxicology and Chemistry.* **38**(4): p703-711. https://doi.org/10.1002/etc.4371

[105] Klein S, Dimzon IK, Eubeler J, Knepper TP. (2017). "Analysis, occurrence, and degradation of microplastics in the aqueous environment." In: M. Wagner & S. Lambert (Eds.). The Handbook of Environmental Chemistry, vol 58. *Freshwater Microplastics: emerging environmental contaminants?* (pp.51-67). Springer, Cham. https://doi.org/10.1007/978-3-319-61615-5_3

[106] Ali SS, Elsamahy T, Koutra E, Kornaros M, El-Sheekh M, Abdelkarim EA, Zhu D, Sun J. (2020). "Degradation of conventional plastic wastes in the environment: A review on current status of knowledge and future perspectives of disposal." *Science of the Total Environment*. **771**: e144719. https://doi.org/10.1016/j.scitotenv.2020.144719

[107] Provencher JF, Ammendolia J, Rochman CM, Mallory ML. (2019). "Assessing plastic debris in aquatic food webs: what we know and don't know about uptake and trophic transfer." *Environmental Reviews*. **27**(3): p304-317. https://doi.org/10.1139/er-2018-0079

[108] Rochman CM, Parnis JM, Serrato S, Browne MA, Reiner EJ, Robson M, Young T, Diamond ML, Teh SJ. (2017). "Direct and indirect effects of different types of common microplastics in a freshwater foodchain." *PLoS ONE.* **12**(11): e0187664. https://doi.org/10.1371/journal.pone.0187664

[109] Smith M, Love DC, Rochman CM, Neff RA. (2018). "Microplastics in seafood and implications for human health." *Current Environmental Health Reports.* **5**(3): p375-386. https://doi.org/10.1007/s40572-018-0206-z

[110] Rochman CM, Browne M A, Halpern BS, Hentschel BT, Hoh E, Karapanagioti HK, Rios-Mendoza LM, Takada H, Teh S, Thompson RC. (2013). "Classify plastic waste as hazardous." *Nature* . **494**: p169-171. https://doi.org/10.1038/494169a

[111] Gassel M, Rochman CM. (2019). "The complex issue of chemicals and microplastic pollution: A case study in North Pacific Lanternfish." *Environmental Pollution.* **248**: p1000-1009. https://doi.org/10.1016/j.envpol.2019.03.002

[112] De Frond HL, van Sebille E, Parnis JM, Diamond ML, Mallos N, Kingsbury T, Rochman CM. (2019). "Estimating the mass of chemicals associated with ocean plastic pollution to inform mitigation efforts." *Integrated Environmental Assessment and Management*. **15**(4): p596-606. https://doi.org/10.1002/ieam.4147

[113] Hong SH, Shim WJ, Hong L. (2017). "Methods of analyzing chemicals associated with microplastics: a review." *Analytical Methods.* **9**: p1361-1368. https://doi.org/10.1039/c6ay02971j

[114] Ogata Y, Takada H, Mizukawa K, Hirai H, Iwasa S, Endo S, Mato Y, Saha M, Okuda K, Nakashima A, Murakami M, Zurcher N, Booyatumanondo R, Zakaria MP, Dung LQ, Gordon M, Miguez C, Suzuki S, Moore C, Karapanagioti HK, Weerts S, McClurg T, Burres E, Smith W, Van Velkenburg M, Lang JS, Lang RC, Laursen D, Danner B, Stewardson N, Thompson RC. (2009). "International pellet watch: Global monitoring of persistent organic pollutants (POPs) in coastal waters. 1. Initial phase data on PCBs, DDTs, and HCHs." *Marine Pollution Bulletin.* **58**(10): p1437–1446. https://doi.org/10.1016/j.marpolbul.2009.06.014

[115] Hirai H, Takada H, Ogata Y, Yamashita R, Mizukawa K, Saha M, Kwan C, Moore C, Gray H, Laursen D, Zettler ER. (2011). "Organic micropollutants in marine plastics debris from the open ocean and remote and urban beaches." *Marine Pollution Bulletin.* **62**(8): p1683–1692. https://doi.org/10.1016/j.marpolbul.2011.06.004

[116] Van A, Rochman CM, Flores EM, Hill KL, Vargas E, Vargas SA, Hoh E. (2011). "Persistent organic pollutants in plastic marine debris found on beaches in San Diego, California." *Chemosphere*. **86**(3): p258-263. https://doi.org/10.1016/j.chemosphere.2011.09.039

[117] Rochman CM. (2013). "Plastics and priority pollutants: a multiple stressor in aquatic habitats." *Environmental Science and Technology.* **47**(6): p2439-2440. https://doi.org/10.1021/es400748b

[118] Lorenzo M, Campo J, Pico Y. (2018). "Analytical challenges to determine emerging persistent organic pollutants in aquatic ecosystems." *Trends in Analytical Chemistry*. **103**: p137-155. https://doi.org/10.1016/j.trac.2018.04.003

[119] Mastral AM, Callen MS. (2000). "A Review on Polycyclic Aromatic Hydrocarbon (PAH) Emissions from Energy Generation." *Environmental Science and Technology.* **34**(15): p3051-3057. https://doi.org/10.1021/es001028d

[120] Wicker AP, Carlton DD, Tanaka K, Nishimura M, Chen V, Ogura T, Hedgepeth W, Schug KA. (2018). "On-line supercritical fluid extraction—supercritical fluid chromatography mass spectrometry of polycyclic aromatic hydrocarbons in soil." *Journal of Chromatography B.* **1086**: p82-88. https://doi.org/10.1016/j.jchromb.2018.04.014

[121] Rochman CM, Hoh E, Hentschel BT, Kaye S. (2013). "Long-term field measurement of sorption of organic contaminants to five types of plastic pellets: Implications for plastic marine debris." *Environmental Science and Technology*. **47**(3): p1646-1654. https://doi.org/10.1021/es303700s

[122] Karakolis EG, Nguyen B, You JB, Rochman CM, Sinton D. (2019). "Fluorescent dyes for visualizing microplastic particles and fibers in laboratory-based studies." *Environmental Science and Technology Letters.* **6**(6): p334-340. https://doi.org/10.1021/acs.estlett.9b00241

[123] Fotopoulou KN, Karapanagioti HK. (2012). "Surface properties of beached plastic pellets." *Marine Environmental Research*. **81**: p70-77. https://doi.org/10.1016/j.marenvres.2012.08.010

[124] Mato Y, Isobe T, Takada H, Kenehiro H, Ohtake C, Kaminuma T. (2001). "Plastic Resin Pellets as a Transport Medium for Toxic Chemicals in the Marine Environment." *Environmental Science and Technology.* **35**(2): p318–324. https://doi.org/10.1021/es0010498

[125] Karapanagioti HK, Klontza I. (2008). "Testing phenanthrene distribution properties of virgin plastic pellets and plastic eroded pellets found on Lesvos island beaches (Greece)." *Marine Environmental Research*. **65**(4): p283-290. https://doi.org/10.1016/j.marenvres.2007.11.005

[126] Teuten EL, Rowland SJ, Galloway TS, Thompson RC. (2007). "Potential for Plastics to Transport Hydrophobic Contaminants." *Environmental Science and Technology*. **41**(22): p7759–7764. https://doi.org/10.1021/es071737s

[127] Airiau CY, Brereton RG, Crosby J. (2000). "High-performance liquid chromatography/electrospray tandem mass spectrometry of polycyclic aromatic hydrocarbons." *Rapid Communications in Mass Spectrometry*. **15**(2): p135-140. https://doi.org/10.1002/1097-0231(20010130)15:2<135::AID-RCM204>3.0.CO;2-Z

[128] Jjunju FPM, Maher S, Li A, Badu-Twiah AK, Taylor S, Cooks RG. (2015). "Analysis of Polycyclic Aromatic Hydrocarbons Using Desorption Atmospheric Pressure Chemical Ionization Coupled to a Portable Mass Spectrometer." *Journal of the American Society for Mass Spectrometry.* **26**: p271-280. https://doi.org/10.1007/s13361-014-1029-2

[129] Rochman CM, Manzano C, Hentschel BT, Massey Simonich SL, Hoh E. (2013). "Polystyrene Plastic: A Source and Sink for Polycyclic Aromatic Hydrocarbons in the Marine Environment." *Environmental Science and Technology.* **47**(24): p13976-13984. https://doi.org/10.1021/es403605f

[130] Schonlau C, Larsson M, Lam MM, Engwall M, Glesy JP**,** Rochman CM, Karrman A. (2019). "Aryl hydrocarbon receptor-mediated potencies in field-deployed plastics vary by type of polymer." *Environmental Science and Pollution Research.* **26**: p9079-9088. https://doi.org/10.1007/s11356-019-04281-4

[131] Loakeimidis C, Fotopoulou KN, Karapanagioti HK, Geraga M, Zeri C, Papathanassiou E, Galgani F, Papatheodorou G. (2016). "The degradation potential of PET bottles in the marine environment: An ATR-FTIR based approach" *Nature Scientific Reports*. **6**: e23501. https://doi.org/10.1038/srep23501

[132] Pascall MA, Zabik ME, Zabik MJ and Hernandez RJ. (2005) "Uptake of Polychlorinated Biphenyls (PCBs) from an Aqueous Medium by Polyethylene, Polyvinyl Chloride, and Polystyrene Films." *Journal of Agricultural and Food Chemistry*. **53**(1): p164-169. https://doi.org/10.1021/jf048978t

[133] Fries E, Zarfl C. (2012). "Sorption of polycyclic aromatic hydrocarbons (PAHs) to low and high density polyethylene (PE)." *Environmental Science and Pollution Research*. **19**: p1296–1304. https://doi.org/10.1007/s11356-011-0655-5

[134] Smedes F, Geertsma RW, van der Zande T, Booij K. (2009). "Polymer−Water Partition Coefficients of Hydrophobic Compounds for Passive Sampling: Application of Cosolvent Models for Validation." *Environmental Science and Technology.* **43**(18): p7047–7054. https://doi.org/10.1021/es9009376

[135] Booij K, Hofmans HE, Fischer CV, Van Weerlee EM. (2003). "Temperature-Dependent Uptake Rates of Nonpolar Organic Compounds by Semipermeable Membrane Devices and Low-Density Polyethylene Membranes." *Environmental Science and Technology.* **37**(2): p361–366. https://doi.org/10.1021/es025739i